University of Salford MANCHESTER

A COMPARISON OF FIXED TUBE CURRENT (FTC) AND AUTOMATIC TUBE CURRENT MODULATION (ATCM) CT METHODS FOR ABDOMINAL SCANNING: IMPLICATIONS ON RADIATION DOSE AND IMAGE QUALITY

MAILY J. ALROWILY

PhD. Thesis **2018**

A COMPARISON OF FIXED TUBE CURRENT (FTC) AND AUTOMATIC TUBE CURRENT MODULATION (ATCM) CT METHODS FOR ABDOMINAL SCANNING: IMPLICATIONS ON RADIATION DOSE AND IMAGE QUALITY

Maily J. Alrowily

School of Health Sciences

College of Health and Social Care

University of Salford, Manchester, UK

Submitted in Partial Fulfilment of the Requirements of the

Degree of Doctor of Philosophy (PhD)

April 2018

Supervision and research area information

A Comparison of Fixed Tube current (FTC) and Automatic Tube Current Modulation (ATCM) CT methods for abdominal scanning: implications on radiation dose and image quality

Research area: Radiography sciences / image quality / Dosimetry/ Medical physics/ CT scan

1. Professor Peter Hogg/ First Supervisor **Sign……**

Professor of Radiography,

Director, Centre for Health Sciences Research,

Research Dean, School of Health Sciences

University of Salford

Room L608, Allerton Building,

University of Salford, Salford, M5 4WT

Telephone: +44 (0) 161 295 2492

Email: P.Hogg@Salford.ac.uk

2. Dr. Andrew England / Co-Supervisor **Sign……**

Senior Lecturer, Health Sciences Research Center

Directorate of Radiography

L613, Allerton Building, University of Salford, Salford, M5 4WT

Telephone: +44 (0) 161 295 0703

Email: a.england@salford.ac.uk

3. Mr. Andrew K. Tootell / Supervisory team member **Sign…….**

Lecturer, Health Sciences Research Center

Directorate of Radiography

L617, Allerton Building, University of Salford, Salford, M5 4WT

Email: A.K.Tootell@salford.ac.uk

Table of Contents

List of Tables

Chapter 2

Chapter 3

Chapter 4

Chapter 5

Chapter 6

Chapter 7

List of Figures

Chapter 1

Chapter 2

Chapter 3

Chapter 4

Chapter 5

Chapter 6

List of publications, Book chapter, conferences paper and poster

Title	Note
Comparison of radiation dose and image quality for Fixed Tube current (FTC) and Automatic Tube Current (ATC) CT methods for abdominal scanning; **M Alrowily**, A England, P Hogg; Presented in the United Kingdom Radiology Congress (UKRC); Liverpool 2016	**Poster**
Effective dose comparison between fixed tube current FTC and automatic tube current ATC methods for abdominal CT examinations; **M Alrowily**, A England, P Hogg; Presented in the European Congress of Radiology(ECR) ;Vienna 2017	**Conferences paper and poster**
Visual image quality assessment methods(review).In P. Hogg, C. Blakeley, C. Buissink Multicultural team-based research in radiography, a holistic educational approach (Eds).OPTIMAX 2015; M Hussien ; **M Alrowily**; 2016	**Book Chapter**
Impact fixed tube current (FTC) and automatic tube current modulation (ATCM) objective and subjective evaluation of image quality in CT examinations of the abdomen; **M Alrowily**, A England, A Tootell, P Hogg; Presented in the Presented in the United Kingdom Radiology Congress (UKRC); Liverpool 2018	**Poster Presentation**
MTHODS FOR DIRECT MEASURMENT OF RDIATION DOSE: TLD and MOSFET. In P Hogg, R H Thompson , C Buissink Optimising image quality for medical imaging (Eds).OPTIMAX 2016;R Ali , **M Alrowily**, M Benhalim, A Tootell; 2017	**Book Chapter**
Comparative analysis of effective risk for fixed tube current (FTC) and automatic tube current modulation (ACTM) during abdominal CT imaging; **M Alrowily**, A England, L Walton, A Tootell P Hogg; Presented in the European Congress of Radiology(ECR) ;Vienna 2018	**Poster**
An investigation into the impact of image viewing parameter settings (magnification and window parameters) on the performance of 2.4 MP color monitor in visualizing low contrast detail using the CDRAD phantom; S Al-Murshedi, P Hogg, M Benhalim, **M Alrowily**, A England; Presented in the European Congress of Radiology(ECR); Vienna 2018(*Additional work*)	**Conferences paper**
THINKING OUTSIDE THE BOX the effects of collimation and dose reduction; N Muscroft, N Coller, **M Alrowily**, A England; Presented in the United Kingdom Radiology Congress (UKRC); Liverpool 2016(*Additional work)*	**Poster**

List of Training Sessions

Date	Sessions name	Hours
15-04-2015	Completing a Learning Agreement & the PhD Progression Points	2
24-04-2015	Excel Basic	2
4-05-2015	CT- scan and x-ray machines training.	6
07-05-2015	Excel – Analysing Data	2
18-05-2015	Thermoluminescent Dosimeters (TLDs) training	12
20-05-2015	Intro to Endnote X7	2.5
21-05-2015	Doing a Literature Review	2
27-05-2015	Power point Academic poster	2
25-05 -2015	SPARC Conference	6
10-06-2015	Electronic Resources for researchers	2
22-06-2015	Google Scholar for research	1.5
23-06-2015	Time Management and Procrastination	2
24-06-2015	Visual assessment of image quality 2AFC software training.	6
26-06-2015	Referencing & Information Ethics for Research	1.5
15-07-2015	Tackling Literature Reviews	2
22-07-2015	Referencing your work APA (Harvard) style	2
04-08-2015	Writing the thesis	2
10-08-2015	Critical and Analytical Skills	2
23-09-2015	Search the academic way	1
15-04-2015	Completing a Learning Agreement & the PhD Progression Points	2
24-04-2015	Excel Basic	2
29-10-2015	Introduction to SPSS	3
18-11-2015	T-TEST, ANOVA and repeated measures	2
30-11-2015	Organizing and synthesising your work	2

16-12-2015	Seminars for the PGR PhD milestones ethics applications, interim and internal assessments etc.)	2
10-02-2016	Seminars for Controversial issues in breast cancer diagnosis using full field digital mammography	2
13-14-02-2016	9th Saudi Student Conference in Birmingham, UK	10
07-03-2016	Translating our diagnostic imaging research into practice	2
21-03-2016	MOSFETs training course – Day 1	6
24-03-2016	MOSFETs training course – Day 2	6
08-04-2016	Presentation Skills	2
15-04-2016	Reflective writing	2
25-04-2016	PGR Presentation Practise Session	2
18-05-2016	Critical Thinking and Critical Writing at Doctoral Level	12
01-04-2016	RESEARCH SEMINAR Direct X-Radiation Dose Measurements in Human Phantom	2
6-8-06-2016	Poster at UKRC 2016	1
15-06-2016	ImPACT training	2
14-09-2016	Pressure Ulcers, a joint research seminar	2
18-10-2016	Endnote Basics for Researchers	2
10-11-2016	Developing Critical Writing for PhD Science Students (Being Critical)	2
17-11-2016	Developing Critical Writing for PhD Science Students (Building the Argument)	2
24-11-2016	Developing Critical Writing for PhD Science Students (Methods)	2
01-12-2016	Developing Critical Writing for PhD Science Students (Results)	6
08-12-2016	Developing Critical Writing for PhD Science Students (Discussion)	2
15-12-2016	Developing Critical Writing for PhD Science Students (Conclusions)	2
19-01-2017	Advanced SPSS	2
15-11-2017	Health sciences PGR seminar	2
06-12-2017	Health sciences PGR seminar	2
10-01-2018	Health sciences PGR seminar	2

Acknowledgements

Firstly. I would like to thank deepest appreciation to my supervisors, **Professor Peter Hogg and Dr Andrew England,** for their help, guidance and encouragement during my journey to completing my PhD, and for evoking so much excitement and interest in their teaching. Words would not be enough to express my feelings for their tremendous help and support.

I am also grateful to **Dr Katy Szczepura, Dr Lucy Walton, Dr John Thompson, Mr Andrew Tootell and Mr Christopher Beaumont**, who have been great advisors to me for their sharing expertise about radiography and medical physics and giving valuable guidance.

Finally, I would like to take the opportunity to thank my mother and father for their support, encouragement and attention. Also, I am also grateful to my wife for her support, kindness and patience as she accompanied me along this PhD journey. I am also grateful to my children: **Sanad, Bader, Yara, Salman and Basmah**. In addition, I would like to thank my brothers, sisters and friends for their support throughout all my PhD studies. I would also like to express my upmost gratitude to all who supported me to complete my PhD thesis.

List of Abbreviations

2AFC	2-Alternative Force Choice
3D	Three dimension
4D	Four dimension
AAPM	American Association for Physicist in Medicine
ABM	Active Bone Morrow
ACR	American College of Radiology
ACS	Automatic Current Selection
AEC	Automatic Exposure Control
AIDR	Adaptive Iterative Dose Reduction
AL	Aluminium
ALARA	As-Low-As-Reasonably-Achievable
AP	Antero-Posterior
ASIR	Adaptive Statistical Iterative Reconstruction
ATCM	Automatic Tube Current Modulation
ATCM- corrected data	Automatic Tube Current Modulation corrected radiation dose by equivalent equation from ATCM raw data
ATCM- uncorrected data	Automatic Tube Current Modulation main radiation dose raw data
$CDTI_W$	Computed Tomography Dose Index Weighted
CEC	Commission of the European Community
CFs	calibration factors
CNR	Contrast-to-Noise Ratio
CR	Contrast Resolution
CR	Contrast Resolution
CT	Computed Tomography
CTDI	Computed Tomography Dose Index
CTDIvol	Computed Tomography Dose Index Volume
DICOM	Digital Imaging and Communications in Medicine
DLP	Dose Length protected
DOM	DoseRight dose modulation
E.C	Exposure Control
ED	Effective Dose
ER	Effective risk
FBP	Filtered Back Projection
FDA	Food and Drug Administration
FROC	Free-response ROC
FTC	Fixed-Tube Current
GE	General Electric
HP	Helical Pitch
HU	Hounsfield unit
IAEA	International Atomic Energy Agency
IC	Image Criteria
ICRP	International Commission on Radiation Protection
IEC	International Electrotechnical Commission
IPEM	Institute of Physics and Engineering in Medicine
IR	Iterative Reconstruction
IRIS	Iterative Reconstruction in Image Space
kVp	Kilo voltage
LLQ	Left Lower Quadrant
LROC	Localization ROC
LSS	Life Span Study
LUQ	Left Upper Quadrant

mA	milliAmperes
M-AFC	Multi Alternative Forced Choice
MBIR	Model-Based Iterative Reconstruction
MDCT	Multi Detector CT
MeV	mega electron volts
mm	millimetre
MOS	Mean Opinion Score
MOSFET	Metal Oxide Semiconductor Field Effect Transistor
MRMC	Multiple-Reader Multiple-Case
mSv	MilliSieverts
NAS	National Academy of Sciences
NCRP	National Council on Radiation Protection
PFs	Pitch Factors
PMMA	Poly(methyl methacrylate)
QC	Quality Control
RLQ	Right Lower Quadrant
ROC	Receiver Operator Characteristics
ROI	Region Of Interest
RUQ	Right Upper Quadrant
SAFIRE	Sinogram Affirmed Iterative Reconstruction
SD	Stander Deviation
SKE	Signal-Known-Exactly
SNR	Signal-to-Noise Ratio
SR	Spatial Resolution
TLD	ThermoLuminescence Dosimeter
UNSCEAR	United Nations Scientific Committee on the Effects of Atomic Radiation
V	Voltage
VGA	Visual Grading Analysis
VGAS	Visual Grading Analysis Score
VGASabs	Visual Grading Analysis Score (absolute)
VGASrel	Visual Grading Analysis Score (relative)

Abstract

PURPOSE: There has been a huge increase in the use of abdominal CT scanning in recent years. This has contributed to an increase in radiation dose administered to patients. Abdominal CT scans generally require higher exposure factors when compared to other anatomical regions. This drives a need for urgent optimisation of the radiation dose and image quality for abdominal CT examinations. The aim of this thesis is to evaluate Fixed Tube Current (FTC) and Automatic Tube Current Modulation (ATCM) on image quality and radiation dose during abdominal CT examinations across a range of scanning parameters.

MATERIALS AND METHODS: Using a Toshiba Aquilion 16 CT scanner (120 kVp, 0.5 seconds tube rotation), an adult ATOM dosimetry and abdominal anthropomorphic phantom were exposed to a series of FTC and ATCM CT protocols with variations in tube current as follows: FTC - 100, 200, 250, 300 and 400mA; ATCM - low dose+, low dose, standard, quality and high quality. The pitch factors evaluated included were 0.688, 0.938 & 1.438 and the detector configurations included were 0.5×16 mm, 1.0×16 mm and 2.0×16 mm. Radiation doses for nine abdominal organs were directly measured using the Metal Oxide Semiconductor Field Effect Transistors (MOSFET). Effective dose (ED) was measured and estimation comprised of three methods: mathematical modelling with k-factors and dose length product DLP, direct with MOSFET and indirectly with Monte Carlo simulation (ImPACT). Effective risk (ER) was estimated using MOSFET data and Brenner's equations / BEIR VII 2006 report. The raw data for ATCM radiation dose was corrected using an equivalence equation. The ATCM corrected and uncorrected data were compared against FTC. Image quality was assessed using SNR (five abdominal organs) and a relative visual grading analysis (VGA) method (five different axial images). Image quality evaluation was performed by the researcher after testing agreement between against five different observers.

RESULTS: There were no significant differences in the mean radiation doses between FTC and corrected ATCM across a range of acquisition protocols ($P>0.05$). This was with the exception of the 300mA/quality protocols, and for a fast pitch factor with 0.5×16mm detector configurations. These had significantly lower doses for FTC ($P<0.05$). These differences were up to 13% for the mean abdominal organ doses, effective doses and the effective risk. In addition, for all acquisition parameters, the mean radiation dose was significantly higher ($P<0.05$; 17%-23%) for uncorrected ATCM when compared to FTC. In terms of image quality, there were no differences in SNR values between FTC and ATCM for the majority of acquisition protocols, excepting the higher mean SNR value ($P<0.05$) for the FTC at

100mA/low dose + and 200 mA/ low dose (pancreas, left and right kidneys). Conversely, the mean SNR values were significantly higher ($P<0.05$) for the ATCM scans for 300mA/quality and fast pitch factor (1.438) (liver, spleen and pancreas) than FTC. Finally, relative VGA scores for both FTC and ATCM demonstrated no significant difference, except for 'quality' ATCM scans (image # 1, image # 2) and a fast pitch factor (1.438) for image #2 and #3.

CONCLUSION: FTC and corrected ATCM were generally similar in terms of radiation dose and image quality except for some acquisition parameters; 300mA/quality tube current and fast (1.483) pitch factor FTC was lower than the corrected ATCM. However, the uncorrected ATCM produced higher radiation dose when compared with FTC techniques. In addition, FTC and ATCM generally produced similar SNR, again with the exception of some protocols. The SNR was higher for FTC than ATCM at lower tube current (pancreas, left and right kidneys), at 300mA/quality and fast pitch factor (1.438) SNR values for ATCM higher than FTC (liver and spleen). However, the ATCM technique is able to produce higher mean relative VGA scores for upper and middle abdominal organs. Further investigation of image quality and radiation dose difference between FTC and ATCM is required.

Chapter One: Introduction

1.1 Introduction

The clinical applications of CT have increased in recent years due to rapid technological developments and innovations in this imaging field. CT provides an opportunity to study the body's anatomy, and diagnose and investigate diseases. Advances in technology have led to improved image quality and the ability to gain added diagnostic information that can benefit patients (Kachelrie ß & Noo, 2017). There are notable risks associated with the use of ionising radiation, one of which is the induction of cancer. This risk arises not only from higher radiation dose techniques, but also from the increased uptake of imaging. As with all fields of medicine, CT imaging's risks should be adequately understood and balanced against its benefits. The risk of radiation induced cancer would linearly increase in the absence of a 'safe' threshold. Therefore, the ultimate goal of CT imaging is to minimise radiation exposure whilst maintaining optimum image quality for diagnosis (Russell et al., 2008).

In 2010, the United Nations Scientific Committee on the Effects of Atomic Radiation (UNSCEAR) estimated the contribution of CT to total global collective radiation dose at about 43% (UNSCEAR, 2010). In the United Kingdom, CT accounted for 60% of the total radiology collective effective dose between 2005 and 2006 (Hall & Brenner, 2008). In Germany, the contribution of CT was slightly higher for public hospitals (60%) than private practice (43%) (Brix et al., 2009). In the United States, CT accounted for up to 67% of the collective radiation dose, despite comprising of only 11 - 13% of all diagnostic ionising radiation examinations (Mazonakis et al., 2007). The increase in the collective radiation doses from CT has raised concerns about the potential risks from diagnostic radiation. Therefore, it is important to optimise the doses administered to patients in line with the as-low-as-reasonably-achievable (ALARA) principle. The need to minimise radiation dose has led to increased medical, regulatory and public scrutiny. A 2011 report estimated that the typical effective doses for common CT examinations in the UK were 20% higher for CT head and up to 400% higher for high-resolution chest CT, compared with 2003 estimates (Shrimpton, Jansen & Harrison, 2015).

Radiation dose during CT imaging can be quantified in terms of scanner radiation output, absorbed dose (organ dose), effective dose (ED) and effective risk (ER). The radiation dose can be directly measured using Thermoluminescent dosimeters (TLDs) and Metal Oxide Semiconductor Field Effect Transistor (MOSFETs), as well as other methods that are based on organ dose estimates that explicitly use tissue-weighting coefficients as specified by the

International Commission on Radiological Protection (ICRP) (Christner, Kofler, & McCollough, 2010). Indirect estimation can also be carried out using mathematical methods, which are simpler and are based on dose length product (DLP) and conversion coefficients (k factors). Another method of estimating radiation dose in CT scan is the ImPACT method, which estimates organ and tissue doses based on Monte Carlo simulations. The simulations account for many variables, including scanner geometry, bowtie filtration, beam collimation, tube potential, and current as well as the CT dose index (CTDI). Several CT-specific dose descriptors have also been developed to quantify CT radiation dose. The CT volume dose index (CTDIvol) describes the radiation output of the scanner. It is measurable by using head and body CT phantoms and a pencil ionisation chamber. Dose measurements are normally made at the core and periphery of these phantoms. The measured values are combined to give a weighted average CT dose index (CTDIw) which represents a single estimate of radiation dose to the phantom.

Within CT, image quality has always been a concern for the medical physics community; clinically acceptable image quality has become even more of an issue as a strategy to reduce radiation dose. Several metrics have been used to describe image quality. These include physical methods such as image noise, which describes the variation of CT numbers in a physically uniform region; contrast resolution, which quantifies the minimum size of contrast object that can be resolved; and spatial resolution, which quantifies the minimum size of contrast object that can be differentiated from the background. Spatial resolution is related both to the contrast of the material and the noise-resolution properties of the system (Acquah et al., 2014). Other common metrics include: contrast-to-noise ratio (CNR) and signal-to-noise ratio (SNR) (Yu et al., 2009). In order to complement the physical measurements of image quality, visual image quality assessments can be made with the receiver operating characteristic (ROC) or Visual Grading Analysis (VGA) traditionally being used. ROC is time consuming, requiring a large sample of images to obtain precise results but provides excellent information about lesion detection performance. The VGA method can be relative or absolute. It is relatively fast to conduct and it provides more information on the acceptability of the appearance (i.e. image noise level) of the clinical images and how the anatomical structures are visualised. It also provides a context for the interpretation of physical metrics.

CT scan parameters such as tube current, tube potential, pitch factors, rotation time and detector configuration impact directly on the radiation dose and image quality. In particular, tube current is an important factor for both radiation dose and image quality in CT examinations. With other parameters constant, the radiation dose is linearly proportional to the current-time value.

Within CT, radiation dose can be reduced by utilising either Fixed Tube Current (FTC) or Automatic tube current modulation (ATCM). The ATCM adjusts the tube current to provide a constant level of image noise on the basis of patient size, attenuation profile, and the other acquisition parameters. The mAs automatically decreases for regions with lower attenuation and increases the radiation dose for the higher attenuation regions. Only a few studies have compared radiation dose and image quality for FTC and ACTM during CT imaging. (Su et al., 2010; Kalra et al., 2004a; Lee et al., 2009). In clinical practice, knowledge of the effect of FTC and ATCM on image quality and radiation dose is also limited. Therefore, the purpose of this thesis is to compare FTC and ATCM during adult abdominal CT examinations and determine their effect on radiation dose and image quality.

1.2 Rationale

Risks associated with the use of ionising radiation are a major concern in medical imaging. Organ dose measurements from CT scans are often 10 times higher than that of conventional x-ray examinations and may range from 2 to 35 mSv depending on various factors including the number of scans, acquisition parameters and patient specific factors (e.g. body habitus) (Brenner, 2010& Smith-Bindman et al., 2015). CT scans are increasingly being used within healthcare due to a number of potential factors, such as the requirements for follow-ups of cancer patients and the increase in assessment of traumatic injuries in the Emergency Department. The increasing use of CT scans therefore underscores the need to minimise patient risks. A critical component of radiation protection during CT scanning is the careful selection of the acquisition factors (optimisation). Optimisation is necessary because any reduction in the radiation dose for an examination may compromise the image quality. Dose reduction generally reduces the number of photons carrying specific anatomical information to the imaging detector. Therefore, decreases in the radiation dose should be balanced against the required image quality level (Sezdi, 2011).

For abdominal CT examinations there is a greater need for radiation dose minimisation since the abdomen is a radiosensitive region and it contains a number of critical organs (e.g. stomach and colon), which are located within the primary CT radiation field (ICRP 103, 2007). Furthermore, abdominal CT has the highest reported effective dose (ED) for all CT examinations (e.g. head = 2.0 mSv, chest = 7 mSv and abdomen = 10 to 35 mSv (Dougeni, Faulkner & Panayiotakis., 2012). The abdominal region is also a low-contrast area containing organs with different densities and atomic numbers (bone, soft tissue, air and water), and this results in variation in the absorption of radiation by the organs as well as differences in the quality of the images produced. The abdomen is, therefore, the ideal region to test any method aimed at radiation-dose reduction and image-quality optimisation (McCollough et al., 2009).

Several authors have sought to optimise CT examinations of the abdomen by calculating the indirect effective dose using DLP with K factors when comparing between FTC and ATCM techniques (e.g. Su et al., 2010; Kalra et al., 2004a; Lee et al., 2009; Lee et al., 2011b). However, no studies have compared the radiation dose from abdominal CT between FTC and ATCM using direct radiation dose measurement (organ doses from either TLDs or MOSFETs). As such there is a clear need to fill this gap. For the purposes of this thesis, there will be a comparison of radiation doses between FTC and ATCM using direct and indirect dose

measurements together with image quality assessments across a range of acquisition parameters.

One method of evaluating image quality between FTC and ATCM is based on an absolute visual grading analysis (VGA) (Kalra et al., 2004a; Rizzo et al., 2006; Su et al 2010; Lee et al., 2011b). Another is through the use of physical image quality metrics for liver abdominal CT scans (Su et al., 2010). There is therefore a need to produce combined physical and visual image quality comparison data for FTC and ATCM techniques.

1.3 Thesis aims

The aims of this thesis are to compare the radiation dose and image quality between FTC and ATCM techniques during abdominal CT scanning. This will involve investigating a number of different acquisition factors such as tube current, pitch factor and detector configuration. The primary research aim is the comparison of the radiation dose for FTC and ATCM using corrected and uncorrected data. These will be measured and estimated directly (MOSFET) and indirectly (ImPACT software / DLP and k factors). The second aim is the comparison of image quality obtained with FTC and ATCM techniques, using the physical (SNR) and the relative VGA methods.

1.4 Objectives of the thesis

1. To investigate the radiation dose (organ dose, effective dose and effective risk) variation between FTC and ATCM (corrected and uncorrected) for abdominal CT examinations by making use of different dose measurements and estimation methods (i.e. DLP, ImPACT and MOSFETs).

2. To study the physical image quality differences between FTC and ATCM for abdominal CT examinations, by calculating SNR values across a range of abdominal organs.

3. To study the visual image quality differences between FTC and ATCM for abdominal CT examinations using a relative VGA method for five different abdominal slices.

4. To determine the optimum CT technique- FTC or ATCM- for reducing the radiation dose whilst producing acceptable image quality.

1.5 Overview of the thesis and structure

The structure of PhD thesis is divided into seven chapters**: See Figure 1-1**

Chapter One - introduces the key issues and provides an overview of the thesis. This chapter includes the following sections: introduction, rationale for the thesis, thesis aim, and the objectives.

Chapter Two - includes a brief history of CT; a description of different CT parameters and how they can affect the radiation dose and image quality; abdominal CT acquisition protocols; details of the FTC and ATCM CT techniques used by the different manufactures; and the rationale for the comparison between FTC and ATCM.

Chapter Three - provides an overview of medical radiation dose; including CT dose parameters, types of CT dosimetry and radiation dose indices (absorbed dose, effective dose and effective risk). It also includes a literature review of the common radiation dose methods to compare FTC and ATCM techniques.

Chapter Four - provides an overview of the image quality evaluation methods, including physical methods and visual image quality methods. It also includes a literature review of the common methods for comparing FTC and ATCM techniques during abdominal CT.

Chapter Five - provides a description of the materials and methods utilised for the two main experiments. The first experiment compares radiation dose (nine abdominal organ doses, effective dose and effective risk) between FTC and ATCM using MOSFET, DLP and ImPACT methods and the CRIS ATOM phantom. The second compares image quality between FTC and ATCM using SNR and relative VGA using an anthropomorphic abdomen phantom. This section also includes an assessment of observer performance in the rating of CT visual image quality.

Chapter Six - provides all of the results for radiation dose including the organ dose (MOSFET method), effective dose (MOSFET, DLP and ImPACT methods) and effective risk (MOSFET method), with a comparison between FTC and ATCM. In addition, this section provides all of the results for the image quality assessments including SNR and relative VGA.

Chapter Seven - provides an overall discussion on the comparison of radiation dose and image quality between FTC and ATCM techniques during abdominal CT. Additionally, final conclusions of this thesis will be reported together with the novelty of the thesis, limitations and areas for future work.

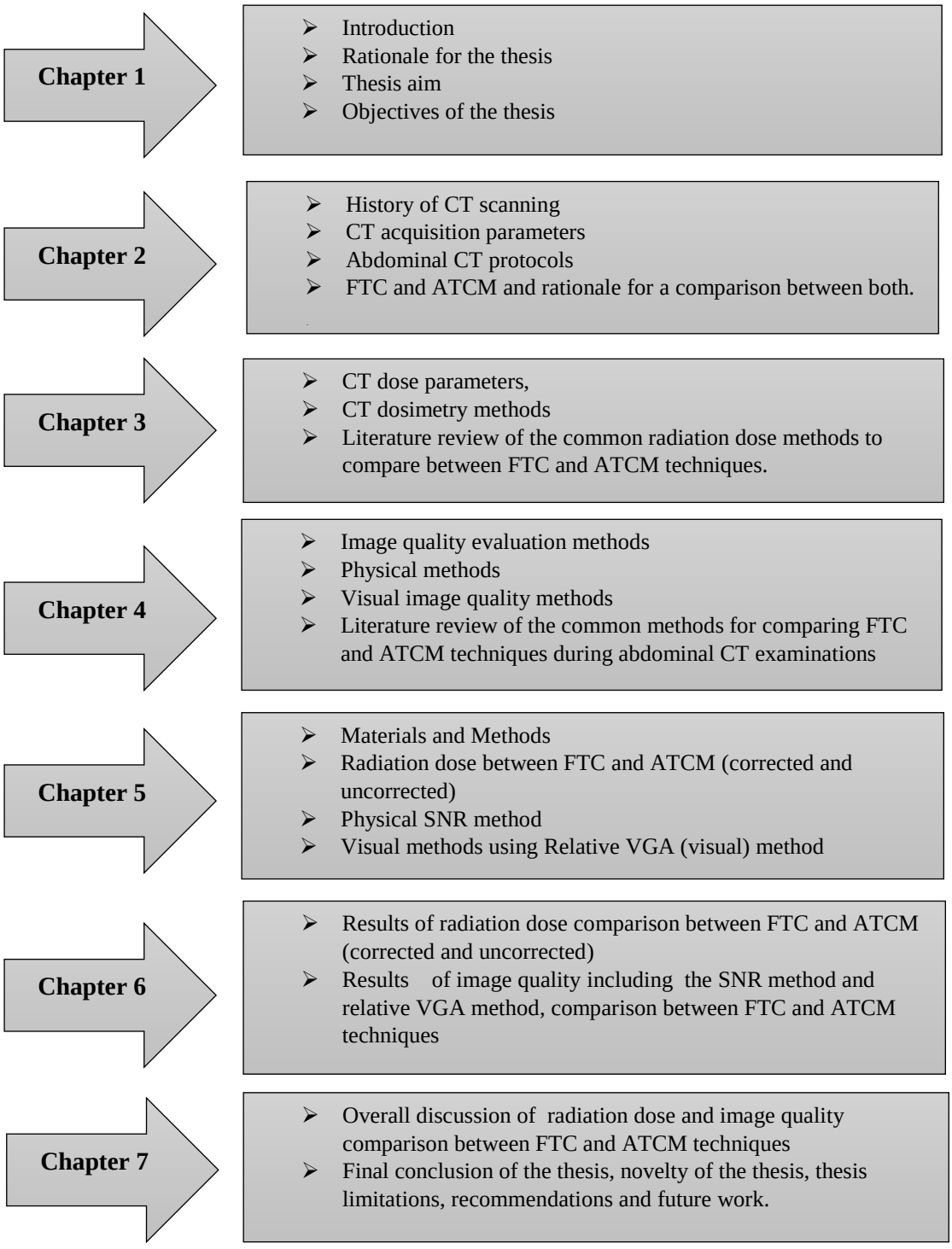

Figure 1- 1: Schematic diagram illustrating the main structure of this thesis

Chapter Two: Background - CT scanning, Fixed Tube Current (FTC) and Automatic Tube Current Modulation (ATCM) techniques

2.1 Chapter Overview

The development of the CT scanner was credited to Allan MacLeod Cormack and Godfrey Newbold Hounsfield. Cormack was a theoretical physicist, who worked on image reconstruction methods for X-ray projection data. Sir Godfrey Hounsfield was an engineer at the THORN EMI Central Research Laboratories in the United Kingdom and worked independently of Cormack on the construction of the first CT scanner. Both men were awarded the Nobel Prize for Physiology and Medicine in 1979 for their work. The first CT scan of a patient with a suspected brain tumour was successfully undertaken in October 1971. By the end of 1973, the EMI CT 1000 became the first commercially marketed CT scanner with a total of six being sold in the first year. These initial scanners were capable of generating an image in about 20 seconds with an image quality of 320 x 320 pixels; contemporary scanners of today can scan in a few hundred milliseconds with much greater resolution (2048 x 2048 pixels) (Cierniak, 2011).

The aim of this chapter is to provide a detailed background regarding general knowledge of CT equipment and image formation principles. Additionally, fixed tube current (FTC) and automatic tube current modulation (ATCM) techniques will be discussed along with the wider CT acquisition parameters including tube-voltage, pitch and detector configuration. The focus of this thesis will be CT techniques for examinations of the abdomen clinical protocols, based on both FTC and ATCM.

2.2 History of Computed Tomography

Medical imaging literature makes reference to CT scanner generations. The generations used for CT scan examinations are discussed in this chapter (**Figure 2-1)** and are based on the X-ray beam geometry and the detector array. These are: first generation (pencil beam), second generation (small fan beam), third generation (fan beam with revolving detector array) and fourth generation (fan beam with a motionless (static) 360^{o} detector array). The third-generation design has had great success and is currently the preferred scanner design. It is fitted with slip ring technology which permits constant revolution of the X-ray tube and detector array around the patient. (Cierniak, 2011). The successive scanner generations differ in the number of detectors and have shown a trend in decreasing the overall scan time.

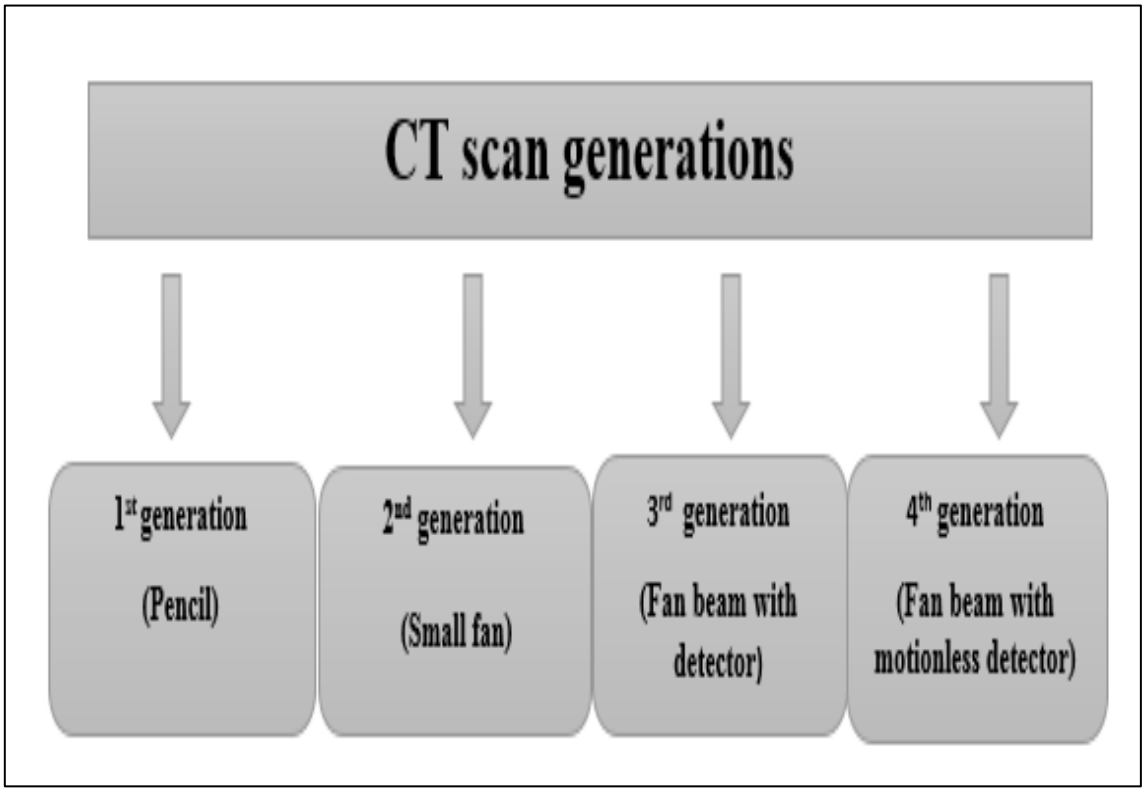

Figure 2- 1: Schematic diagram illustrating the CT scan different generations.

2.2.1 First and second generation CT scanners

First generation CT scanners employed a solitary thin pencil shaped X-ray beam which was concentrated on one or two points. The width of the beam determined the thickness of the slice of the image produced (slice thickness). This generation of CT imaging imaged the patient into a series of axial slices (Mohan, Singh& Gundappa., 2011) **(Figure 2-2)**. 1st generation CT scanners had only a single detector; this was rigidly linked to the X-ray tube and the images were acquired through a translate-rotate motion (Goldman, 2007). The translate-rotate motion refers to the linear transverse path of the X-ray tube and detector across the patient. During the combined translation-rotation motion, the detector measures the X-ray transmission through the subject at several locations. One degree of incremental rotation of the tube-detector assembly occurs after each translation. This sequence of movement is repeated until the tube and detector are 180 degrees from the starting position. A major drawback of these scanners was the prolonged scanning time, which lasted up to 5 minutes and was primarily reserved for head scanning (Cunningham & Judy, 2014).

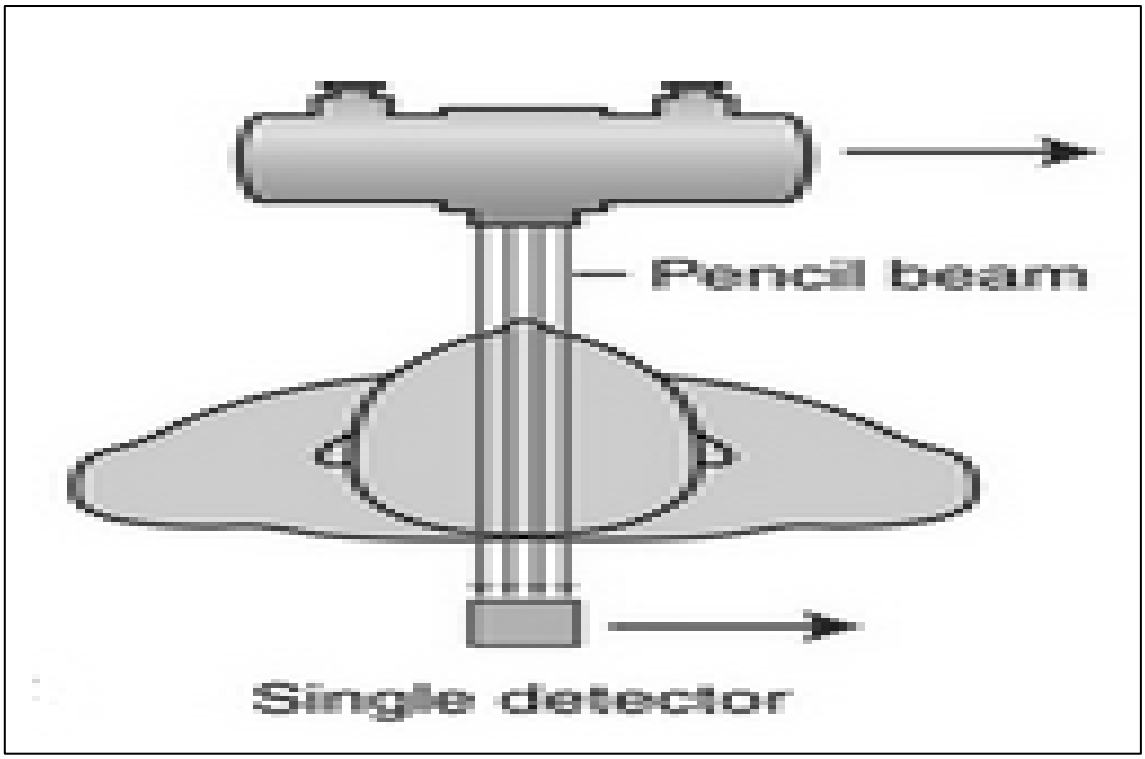

Figure 2- 2: Schematic diagram illustrating the 1st generation CT scanner (Saunders and Ohlerth, 2011)

In 1975, the second-generation of CT scanners were introduced and these were based on small fan beam geometry. Such systems utilised multiple radiation beams and detectors (up to 30 detectors) and, like 1st generation scanners, they also made use of a translate-rotate movement **(Figure 2-3)**. This generation of CT scanner brought with it a significant decrease in scanning time by increasing the degree of rotation from 1 to 30 degrees (Cunningham & Judy, 2014). However, the low image quality was often related to patient motion, which was caused by the significant amount of time required to acquire the CT images (Goldman. 2007).

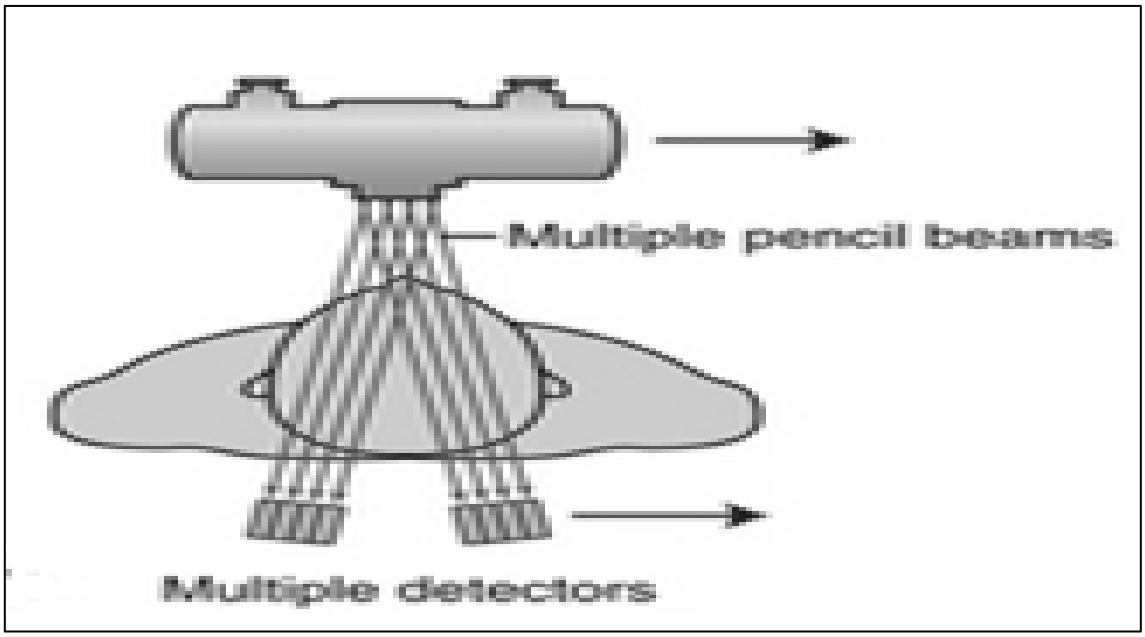

Figure 2- 3: Schematic diagram illustrating the 2nd generation of CT scan (Saunders and Ohlerth 2011)

2.2.2 Third and fourth generation CT scanners

The third-generation of CT scans was introduced in 1976. Within these systems there are rotating x-ray tubes and detector assemblies. The X-ray tube produces a wide fan beam and multiple detectors are installed in a curvilinear array (**Figure 2-4)**. Depending on the location of the detector in the array, they each measure the rays passing only at a specific distance from the centre of rotation (Kalender, 2011). The broad fan beam is sufficiently broad to encompass the entire patient in one exposure. This enables scanning time to be reduced to almost one second per image; image quality is also sufficiently maintained for diagnosis (Mohan et al., 2011).

A major drawback of 3rd generation CT scanners was the presence of ring artefacts; these were caused by errors in detector calibration relative to other detectors. The detector gives a consistently false reading at each angular position thereby resulting in circular artefacts (Nagarajappa, Dwivedi & Tiwari., 2015). Ring artefacts on 3rd generation CT images are never completely removed, even with very minimal inaccuracies in calibration (up to 0.1%) they can still generate ring artefacts. Such artefacts can be minimised by daily calibrations, selecting the correct scan field of view and a high-quality detector design (Kalender, 2011). Furthermore, ring artefacts can be removed from CT images by utilising image processing algorithms (Goldman, 2007).

The 3rd generation CT scanner design is the most widely used today and is present on the Toshiba Aquillion scanner used in this thesis in order to compare FTC and ATCM techniques. Third generation CT scanners include a large array of detectors (300-700 detectors) and generally sub-second tube rotation times which makes body scanning quick and easy for patients to tolerate. Within these systems the reduction in scan times have also led to reductions in the radiation dose for patients and improvement in detector and data acquisition technology which has improved image quality; image reconstruction is significantly faster than 1st or 2nd generation systems (Nagarajappa, Dwivedi & Tiwari., 2015).

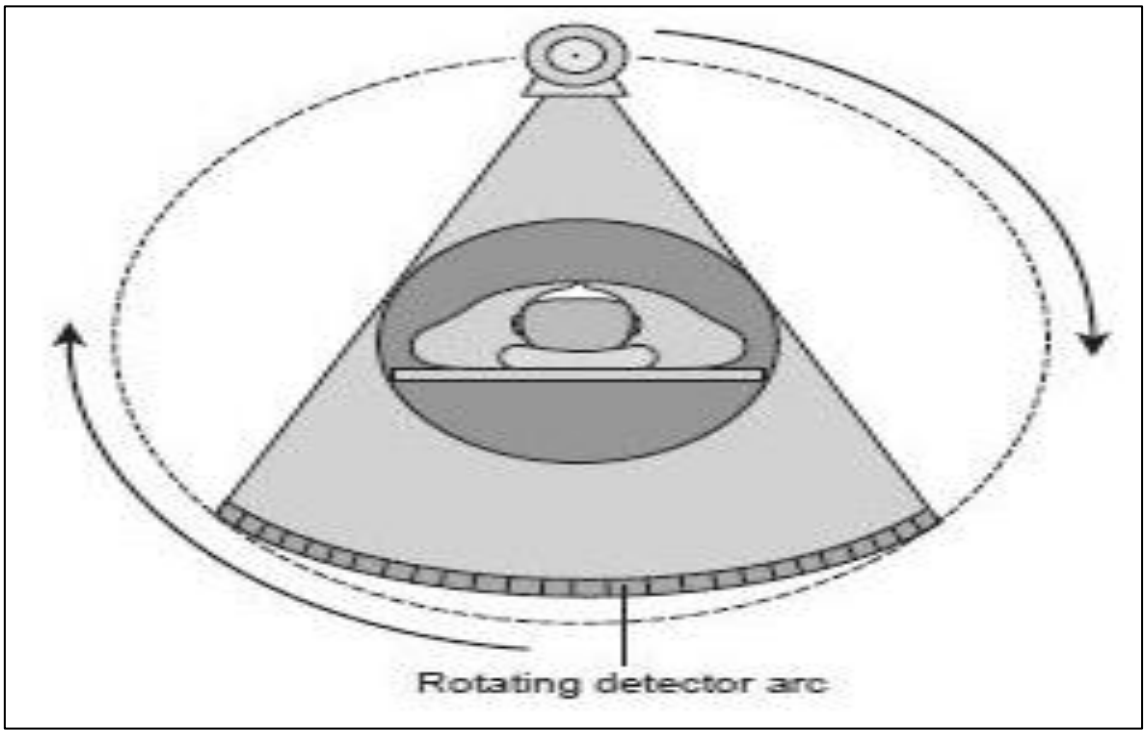

Figure 2- 4: Schematic diagram illustrating the 3rd CT scanner generation (Saunders and Ohlerth, 2011)

Fourth generation CT scanners were developed in the same year as third generation scanners. These scanners were designed to incorporate a large stationary ring of detectors (360^{o} array), with only the x-ray tube rotating around the patient. As many as 2,000 detectors were utilised in this scanner design, which is much greater than the 500 detectors accommodated in 3rd generation units **(Figure 2-5)**. Images can be acquired in between 2 to 10 seconds (Cunningham & Judy, 2014). Unlike third-generation detectors, the detectors can be dynamically calibrated and, therefore, ring artefacts do not occur.

However, a major problem with fourth generation CT scanners was the presence of scatter. The scatter-absorbing septa utilised in third-generation scanners were not usable in fourth generation technology. Septa would preferentially transmit scatter rather than primary x-rays as the tube rotated inside the detector ring (Goldman, 2007). Despite the technical advantages of the fourth-generation CT scanners, they are very expensive (limiting their clinical utility). Consequently, most of the commercially available CT scanners today are third generation.

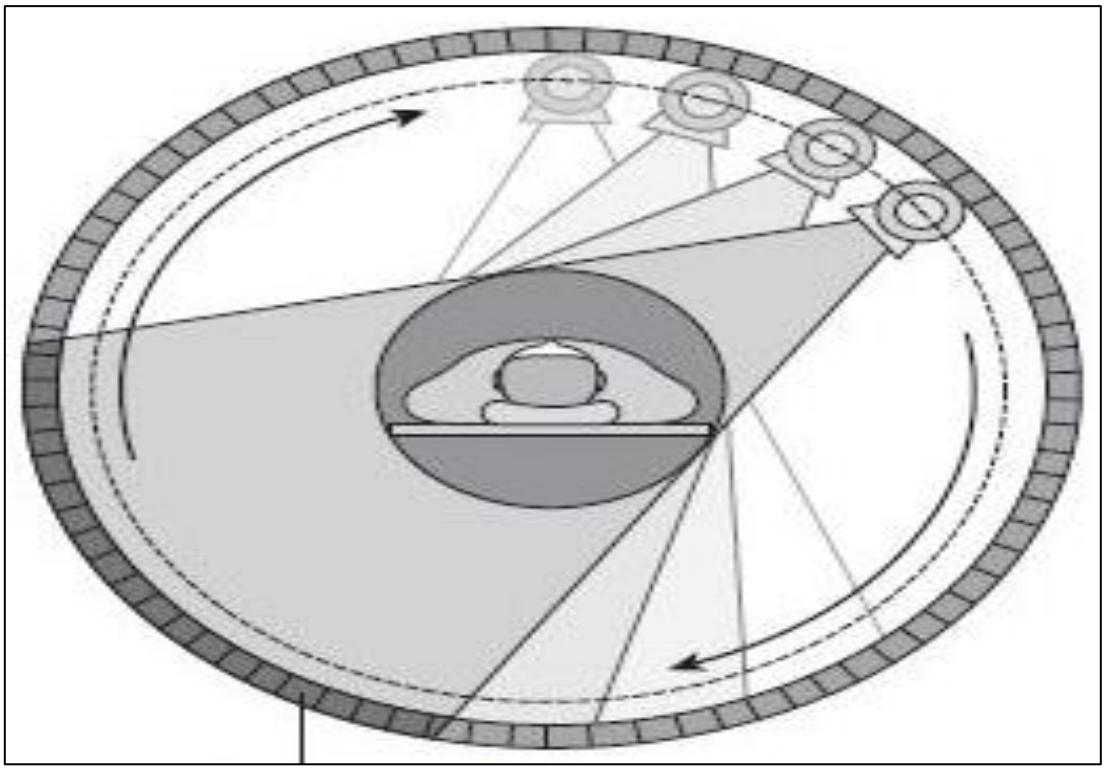

Figure 2- 5: Schematic diagram illustrating the fourth generation of CT technology (Saunders and Ohlerth, 2011)

2.3 Helical and Multidetector CT (MDCT)

Development of CT technology saw the introduction of helical CT into clinical practice during the early 1990s. The name "helical" refers to the pattern in which the X-ray tube and detectors rotate around the patient. A helical path is traced by the tube and detectors relative to the patient, as the table on which the patient lies is smoothly moved though the gantry whilst the x-ray tube continuously rotates around the patient. Helical pitch is a term which describes how fast the table slides through the gantry relative to the rotation time and slice thicknesses of the images being acquired **(Figure 2-6)**.

The greatest advantage of helical CT, compared with previous technological advantages, was the shorter scan period and the potential to reduce the radiation dose. For example, less than one minute is required to carry out a chest or abdomen CT scan which can be achieved within a single breath-hold. In addition, the inter-scan delay that was experienced in earlier CT generations has been solved using slip ring technology that has replaced the older CT scanner cable technology. This allows the X-ray tube and detectors to spin continuously around the patient and ultimately reduces the total scan duration (Kalender, 2011).

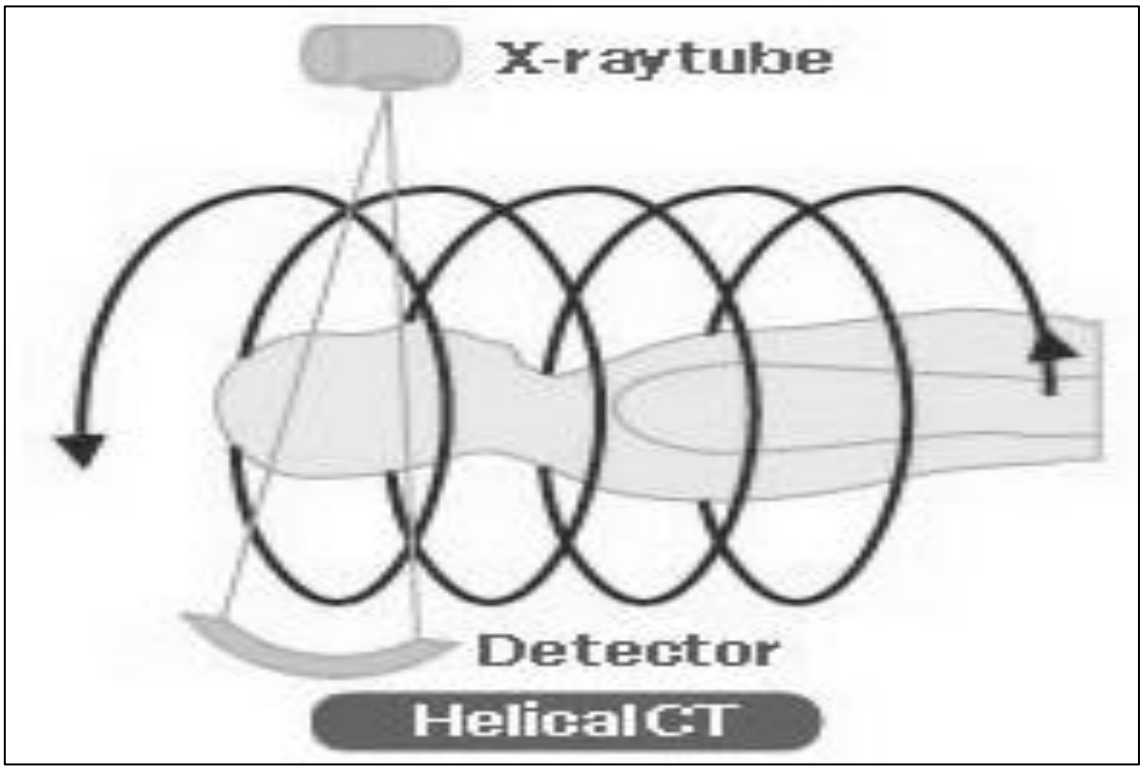

Figure 2- 6: Schematic diagram illustrating helical CT scanning (Hsieh, 2009).

In 1998, multi detector CT (MDCT) was introduced and quickly received acceptance from the international radiological community (Prokop & Galanski, 2003). The MDCT is a CT system designed with multiple rows of CT detectors in the z-axis. When combined with helical scanning, this produced images made up of multiple slices per rotation. MDCT has enhanced the performance of CT in terms of image quality. It produces thinner slices/sections and reduces the time taken for examinations **(Figure 2-7)**. MDCT systems are available with 2, 4, 8, 16, 32 and 64 rows of detectors. A 640 slice system was recently introduced from Toshiba (Toshiba, 2017).

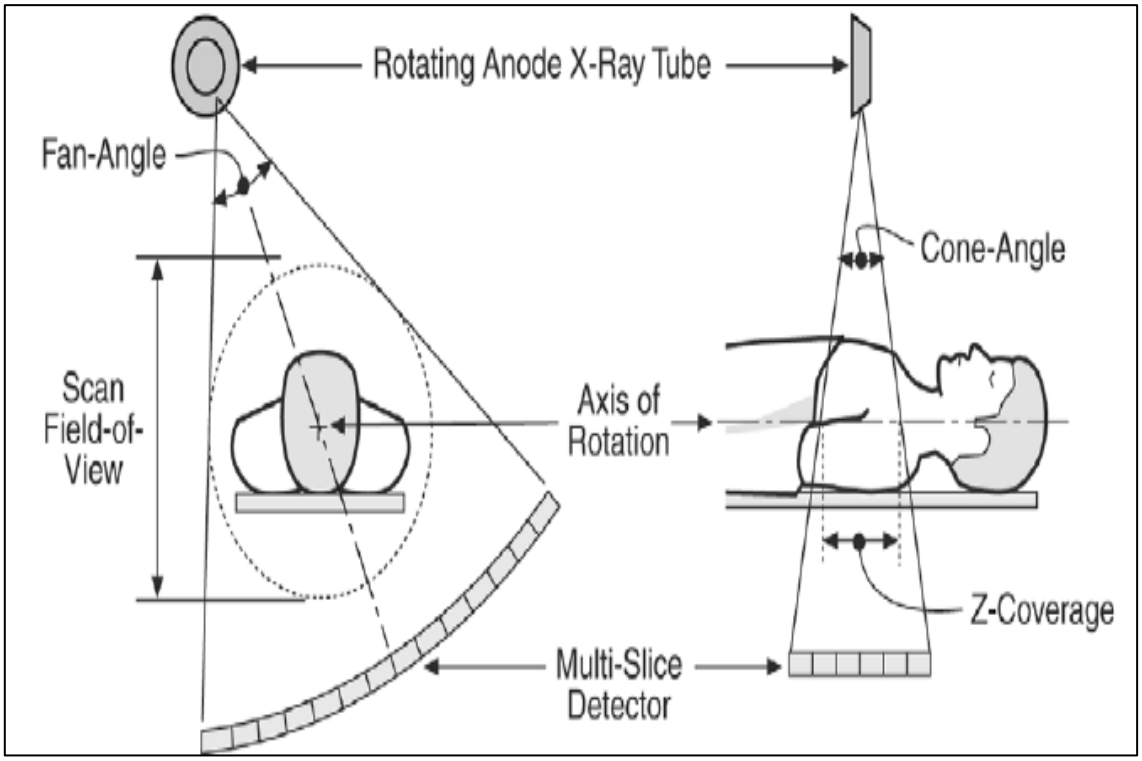

Figure 2- 7: Schematic diagram illustrating the multi-detector CT scanners (Hsieh, 2009)

A major advantage of MDCT over helical CT is its ability to attain high image quality over a long scan range. This is achieved by acquiring multiple simultaneous slices with multiple rows of detectors and utilising a higher speed of rotation. Other advantages include shorter scan time, which is especially useful in paediatrics and acutely ill patients (Pontone et al., 2015). However, MDCT allows for the reformatting of acquired images into different planes and enables the detection of smaller lesions due to the thin slice acquisitions (Saba and Suri, 2013).

On the other hand, MDCT also has other advantages including reduced artefacts and that the number of active detector rows is generally lower than the actual number of detector rows. This is called the 'detector configuration' and is dependent on the collimation setting and the type of CT examination (Prokop, 2005). Faster scanning times can minimise radiation exposure and also reduce the potential need for repeat scanning due to motion artefacts (Baert, Heuck &Youker, 2012). A drawback of MDCT is the markedly increased data load, with as much as one thousand images produced per body area scanned. The volume of images available to the radiologist has been cited as a burden since more time is needed to interpret images and this can result in delays to diagnosis (e.g. cancer) (Raman et al., 2015). Finally, **Table 2-1** shows a summary of CT scanner development from 1971 until 201

Table 2- 1:summary CT scan development up to 2009 (Brornan & Stoel, 2009, Toshiba 2017)	
Years	**Events**
1971	G.N. Hounsfield: technological advances
1971	First scanner for human head
1974	First scanner for full human body
1975	2nd generation
1976	3rd generation
1977	4th generation
1979	Nobel prize awarded to A.M. Cormack and G.N. Hounsfield
1980	5th generation by Andrew Castagnin (Electron Gun that produce a focused electron beam and generate a rotating x-ray fan beam)
1983	Dynamic spatial reconstruct
1987	Scanners with continuously rotating tube
1989-1990	6th generation Helical CT and Slip-Ring Technology
1991	Dual-slice helical CT
1991	CT angiograph
1995	Real-time reconstruction
1997	Automatic tube current modulation ATCM development
1998	Multi-slice CT (4 detector rows
1999	Multi-slice cardiac imaging
2001-2002	Multi-slice CT (8/16 detector rows)
2004-2008	7th generation Multiple detector array (64 slice CT)
2009	Cone beam CT (180- 265 detector rows) and advances in micro-CT
2010	Developing a CT detectors slice up to 330-340 slice imaging system based on synchrotron X-rays
2011	Dual-energy CT, developed Iterative Reconstruction in Image Space (IRIS) Siemens, Adaptive Iterative Dose Reduction (AIDR) Toshiba and developed iDose Philips.
2010-2017	Developing ATCM techniques and Iterative Reconstruction to reduced radiation dose also CT detectors slice up to 640 slices with Toshiba medical groups.

2.4 CT scan parameters

Various factors influence the radiation dose administered to the patient and the resultant image quality. These include the geometry of the CT scanner, slice thickness, pitch, rotation time, detector type, peak kilovoltage (kVp) and milliampere-seconds (mAs). There is a complex relationship between image quality and the radiation dose imparted to the patient. Coursey and Frush (2008) assert that it is impossible to employ similar scan parameters with such variations in patient size (i.e. small / large), if diagnostic images are to be acquired. The application of size and weight-based procedures within an ATCM technique have been observed to reduce the radiation dose administered to patients during examination (Coursey &Frush, 2008). An intricate relationship exists between image quality and the administered dose of radiation. Contrast and spatial resolution are the factors that determine the acceptability of image quality in CT

The tube current mainly affects the image quality whilst peak kilovoltage (kVp) influences the contrast as well as the spatial resolution (Alsleem et al., 2013). The main determinants of image quality and radiation dose to a patient in a CT examination are a result of similar elements: energy of the x-ray beam (controlled by the peak kilovoltage) and the intensity of the x-ray beam or the amount of x-ray photons produced (controlled by the output of the tube current and time) (Paterson & Frush, 2007).

Within the next thesis subsection, the main CT acquisition parameters factors that influence radiation dose and image quality will be discussed.

2.4.1 Tube current (mA)

The primary scan parameter used to optimise radiation dose is the tube current (McCollough et al 2009). Tube current is measured in milliamperes (mA) which is a measure of the rate at which electrons flow through the x-ray tube. mA is usually reported by some manufactures with respect to time, i.e. milliampere-seconds or effective milliampere seconds; while some manufactures simply use mA (Frey, 2014). Effective mAs is used by Siemens while Philips uses mAs per slice, both essentially are the same (Patersona & Frush, 2007). Effective mAs is defined as the product of average tube current gantry rotation time (milliampere-second) divided by the pitch. It is the total mA for all slices divided by number of slices. It is the simplest and most convenient parameter for the adjustment of the radiation dose. It was introduced by some manufacturers because table advance (movement) in CT is often not the same as the total nominal beam width. It is also used by manufacturers to highlight the fact that as the pitch increases so does image noise, as a result Siemens and Philips' scanners software proportionately raise the tube current. This compensatory increase is automatic on these two machines (Tawfik et al., 2011). Raising the tube current or the product of tube current and scan time (mAs) will improve image quality and lower image noise, but will also raise radiation dose exposure (Raman et al., 2013).

As seen in **Figure 2-8,** there is a directly proportional relationship between tube current and radiation dose. Thus, an increase in the current (mA) will result in a proportionate increase in the radiation dose and vice versa (Patersona & Frushb, 2007). For example, up to 50% reduction in radiation dose can be achieved by reducing tube current by half, however, this will result to an increase in the image noise - low mAs produces fewer photons causing more image noise (Aweda & Arogundade, 2007).

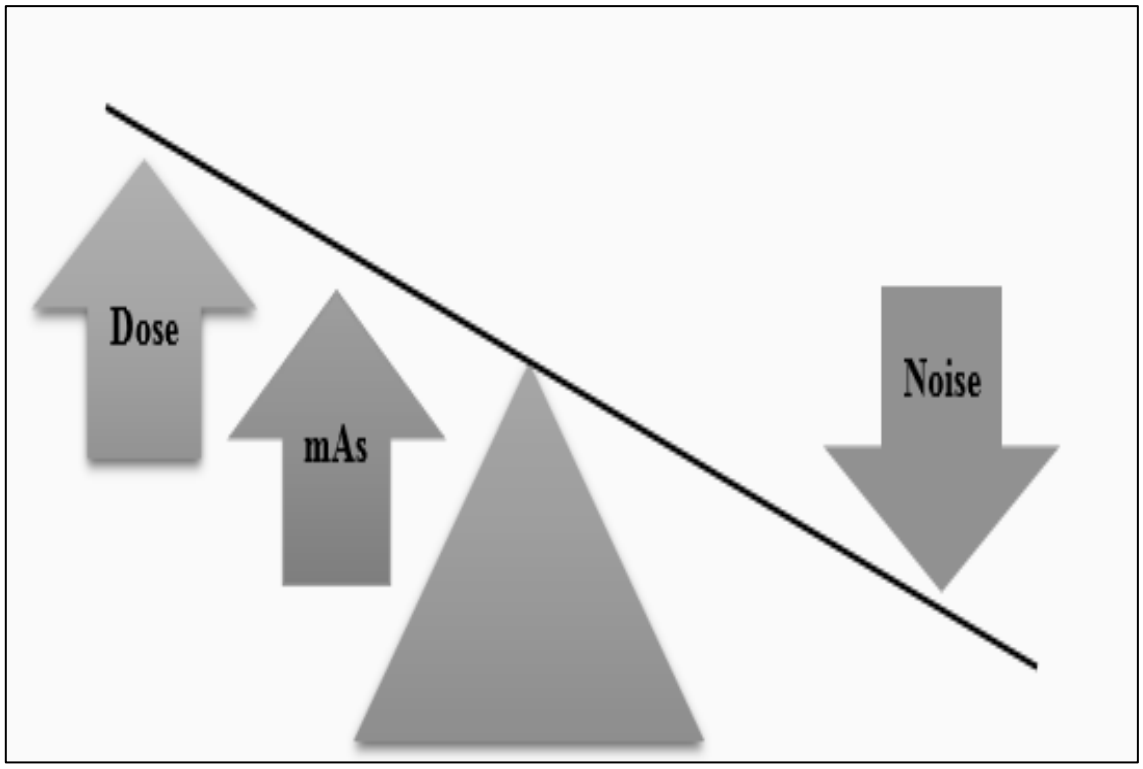

Figure 2- 8: Schematic diagram illustrating the relationship between mAs, noise and radiation dose.

Slim patients and low attenuation body regions such as the chest require lower tube current settings for CT scanning. However, larger patients and higher attenuating body regions like the abdomen and shoulders should be scanned at higher tube current settings (Kalra, Sodickson & Smith, 2015). Lower tube current can also be used for the assessment of high contrast regions for some clinical indications such as kidney stones. These areas are less affected by image noise unlike low contrast tissues such as the liver and pancreas, which generally require high tube currents (Kalra et al., 2015). Kalra et al. (2005) showed that kidney stones ≤2.5 mm can be adequately depicted at higher noise levels while achieving up to 77% reduction in radiation dose. Another study by Jin et al. (2010) showed that reduction of tube current from 100mA to 30 mA did not affect the detection of renal stones, however patient radiation dose exposure was reduced by up to 70 %.

Although some studies have claimed that it is possible to reduce the tube current without having any adverse effect on image quality (Lee et al., 2011a; Kalra et al., 2004b), such reductions should be made with caution, especially for low contrast region scans (particularly abdominal scans), which are susceptible to image noise. Image noise degrades image quality, which reduces the diagnostic value of such images. Tube current for general abdomen CT scans for adult patients are generally around 100–500 mA (Rizzo et al., 2006, Lee et al., 2009 and Padole

et al., 2016), while other studies have supported a reduction in tube current for abdominal CT scans. Lee et al., 2011b, Padole et al., 2016, Su et al., 2010 and Beeres et al., 2014). Ultimately, any alteration of the tube current is still the main controller of radiation dose reduction in abdominal CT scans (Sodickson, 2012 & Kalra et al., 2004c).

2.4.2 X-ray tube-voltage (kVp)

Tube-voltage is an electrical potential applied across the anode and cathode of the x-ray tube. This attracts the electrons from the cathode to the anode of the x-ray tube. It is quantified as kilovoltage (kV) and it influences the energy of electrons liberated from the cathode and consequently the penetrating power of the x-ray beam (Ramirez-Giraldo, Primak, Grant, Schmidt& Fuld, 2014). Unlike a change in tube current, a change in voltage is associated with a change in CT numbers. This number is related to the liner attenuation coefficient value of water and liner attenuation coefficient value for tissue HU. For water, this is equal to 0 HU and 1000HU for air. At all tube energies, the HU number measurements allow for a quick and simple method for the characterisation of certain tissue types on abdominal CT images, images-**see Equation 2-1** (Lamba et al., 2014 & Kalra, Sodickson & Smith, 2015).

$$\text{CT numbers} = \frac{100 \times (\mu t - \mu w)}{\mu w} \quad \text{.....Equation (2-1)}$$

Where μt is the liner attenuation coefficient for tissue in pixel, μw is the liner attenuation coefficient for water.

Traditionally, 120 kV is the most commonly used tube potential for adult CT examinations (IAEA, 2009). This is considered optimal for soft-tissue imaging (Kaza et al., 2014). The availability of high beam X-ray tubes on contemporary MDCT scanners has, however, led to a reduced kV, particularly with contrast-enhanced CT wherein the noise could be overcome by the improved image contrast. When an X-ray tube voltage is increased, the tube output and the effective energy of the X-ray beam are also increased. This results in better penetrating power of the beam and lower image noise.

An increase in tube voltage also increases radiation dose. However, the relationship between radiation dose and tube potential is not linear. Studies have shown an exponential relationship which varies according to specific circumstances. Reducing the peak kilovoltage can result in a substantial reduction in the radiation dose (**Figure 2-9)**. This is in contrast with tube current, which has a linear relationship with radiation dose. The effective dose will rise by approximately 50% if the kilovoltage is increased from 120 kV to 140 kV at a constant tube

current; effective dose decreases by about 65% if the kilovoltage is reduced from 120 kV to 80 kV at constant tube current (Kaza et al., 2014). A study by Huda and colleagues (2002) demonstrated a four-fold decrease in the radiation dose when the tube potential was reduced from 140 kVp to 80 kVp for paediatric or small adult size patients when using head CT protocols (Huda, Ravenel & Scalzetti, 2002).

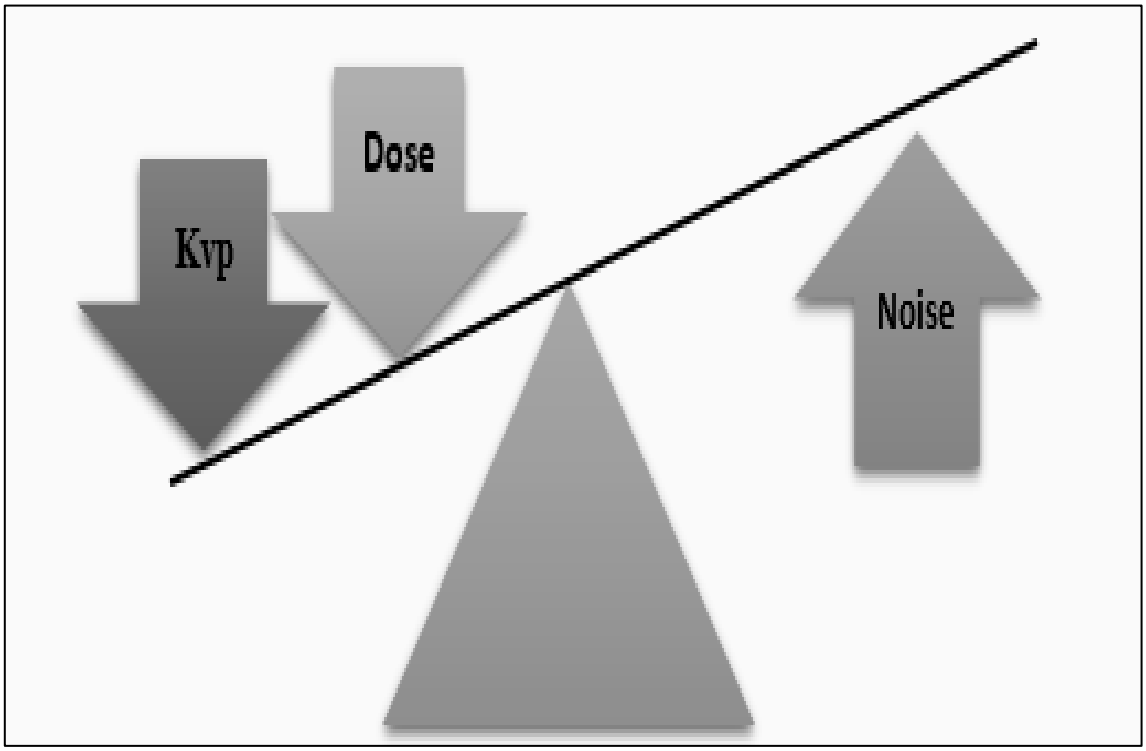

Figure 2- 9: Schematic diagram illustrating the relationship between Kvp, noise and radiation dose.

For CT image quality, Kaza et al. (2014) reported a more complex relationship with tube potential, as both image noise and tissue contrast are influential. They reported that any increase in the peak voltage will raise the contrast-to-noise ratio (CNR) for all tissues; the biggest differences are seen in soft and fat tissues. In addition, when the kilovoltage is increased to compensate for the energy of the X-ray beam required to achieve adequate tissue penetration, there is resultant excessive noise and reduction in image quality. Finally, when using iodinated contrast enhancement during examination, a lower kV is recommended, 120 kV to 100 kV or even 80 kV is ideally suitable for medium and small-sized patients. This tube potential reduction is however not suitable for larger patients because, the magnitude of increase in image noise following a reduction in kilovoltage is higher for larger patients than for smaller patients. This is because x-ray beam penetration is reduced in larger patients. Although contrast is better for larger patients with low tube potential, this potential advantage is negated by an

increase in noise, leading to an overall reduction in kilovoltage (Kaza et al., 2014). Therefore, to optimise radiation dose and image quality, high-voltage (120 kVp) intensities should be used for routine abdominal scans in large patients, while lower voltages (100 kvp) are required for children and small adults. Iodinated structures have higher HU values at lower kilovoltage and this results in pseudo enhancement, therefore characterisations of lesions with lower tube potentials (80-100Kv) are suitable for CT angiography and procedures that use contrast-enhancement iodine (Huda et al., 2002, Nagel 2007, Kaza et al., 2014; Kalra et al, 2015; Lira, Padole, Kalra & Singh., 2015).

2.4.3 Pitch (p)

In helical CT scanners, the pitch is defined as the feed-rate of the table through the gantry (z-axis) in relation to the rotational speed. For these scanners, the patient passes through the CT gantry at a constant speed, thus the CT slice will have a rough screw head shape rather than a disc shape. The pitch value is therefore the ratio of CT table movement (or displacement per 360º of the revolution) to the thickness of the slice (Tobergte & Curtis, 2006). For example, with a slice thickness of 5 mm and a table movement of 7.5 mm per rotation, pitch would be 1.5 (Zhang et al., 2015). Helical pitch (p) is calculated as **Equation 2-2**

$$P = \frac{\text{Table travel per rotation}}{\text{slice width}} \quad \text{..... Equation (2-2)}$$

With MDCT scanners, pitch can be defined as the table travel for each rotation divided by beam collimation (Nagel, 2007). For example, the pitch of a 4-slice MDCT helical scan with 15 mm of table movement per rotation and a 20-mm-wide x-ray beam (to acquire four 5-mm slices) is calculated as: pitch = table movement per rotation/(n × T) = 15 mm/(4 × 5 mm) = 0.75. Where n is the number of slices, T is the slice thickness and n × T is the total width (Goldman 2007). If the pitch is <1, it suggests an overlap between adjacent acquisitions; while a pitch >1 suggests that there are gaps between adjacent acquisitions. A pitch that is equal to 1 implies that acquisitions neither overlap nor have gaps i.e. x-ray beams from adjacent rotations are contiguous (Raman et al., 2013).

With other parameters remaining constant, an increase in pitch reduces radiation dose proportionately and vice versa. For example, when the pitch is low, i.e. with increased overlap of anatomy or owing to increased sampling at each location, radiation dose exposure increases.

Conversely, a larger pitch suggests gaps in the slices and hence lower radiation dose (Verdun et al., 2015) **Figure 2-10.** However, in scanners that use effective mAs, the effect of pitch on dose is cancelled by automatic proportionate change in the tube current thus maintaining similar image noise.

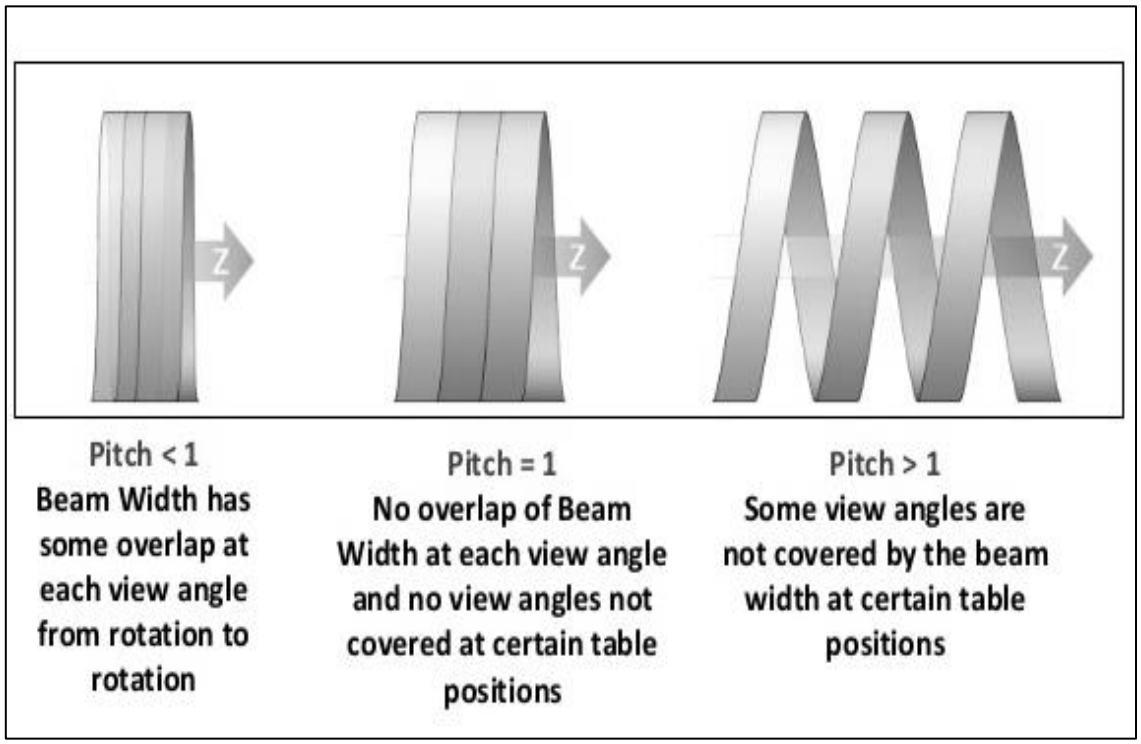

Figure 2- 10: Schematic diagram illustrating different pitch values (Tobergte & Curtis, 2006)

A pitch >1 is often used for routine body CT protocols. This value produces generally acceptable images. A pitch >1.5 however can cause interpolation artefacts with high image noise (Schindera et al 2007). Low-pitch provides better image quality with less image noise. Helical artefacts are generally reduced at low pitch settings. Therefore, some scanners allow the settings of a limited number of pitch values. Where motion artefacts are of concern, such as with most cardiac CT scans, slower pitch values (<0.5) are usually used because faster gantry rotations are required in order to avoid discontinuities in anatomic coverage of the heart between reconstructed images from consecutive cardiac cycles. The clinical implication of this is that in cardiac helical MDCT, faster rotation times results in an improved image quality. However, a higher radiation dose will be necessary to achieve similar image quality. There are three modes of helical pitch (HP) or pitch factor (PF) used on the Toshiba Aquillion 16 CT scanner used in this thesis: detail (0.688), standard (0.938) and fast PF (1.438).

Yu-ChunL et al (2002) suggested that abdominal CT can be carried out with helical pitches 1.0, 1.3 and 1.5. This was applicable for single-detector helical CT. With the employment of a helical pitch above 1, clinicians and patients can benefit from the increased scan coverage in over shorter period of time that employs less radiation than may be attained using standard helical pitch (1.0 procedures). Further studies are required to determine the optimal scan pitch with MDCT during abdominal CT. Several CT applications require both good image quality and fast volume coverage speed (Yu-Chun Lin et al., 2002). In addition, Lell et al. (2011) suggested that using high-pitch chest CT is a method to provide the highest image quality and low radiation dose values during paediatric CT examination when using sedation or controlled ventilation for the examination of infants, small or uncooperative children. However, Lell et al. (2009) and Hetterich, Wirth, Johnson & Bamberg (2013) both studied pitch factors for patient's using ATCM techniques and their results showed high-pitch scan mode has a very low radiation exposure.

CT scanners are associated with increased radiation dose at lower pitch, and lower radiation dose at a higher pitch with dual source MDCT scanners in which use of higher pitch factors (>1.5:1) is associated with a reduction in radiation dose (Singh et al., 2014). Therefore, it becomes very important to understand how pitch affects the radiation dose and image quality during abdominal CT examination during FTC and ATCM techniques in order to obtain lower radiation dose with acceptable image quality.

2.4.4 Detector Configuration

MDCT systems are equipped with two or more parallel detector arrays and utilise third-generation CT technology. Apart from the dual detector systems, all MDCT scanners have five or more detector-rows so as to achieve more than one collimation setting (Prokop, 2003). This is done by collimation and summation of the signals of the neighbouring detector rows. Detector configuration refers to the number of detector rows and the width of each detector row. The detector arrangement establishes the collimation or width of the X-ray beam. There are two types of detector arrays. These are the matrix detectors and adaptive array detectors. The former consists of parallel rows of equal thickness, while the latter has rows of varying thickness. **Figure 2-11** shows different detector configurations (8-slice matrix detector (GE), a 16-slice adaptive array detector (Philips/ Siemens) and a 16-slice hybrid detector (Toshiba Aquilion-16). There are three different detectors configuration modes used on the Toshiba Aquillion 16 CT scanner which are used in this thesis: 0.5×16mm, 1.0×16mm and 2.0×16mm

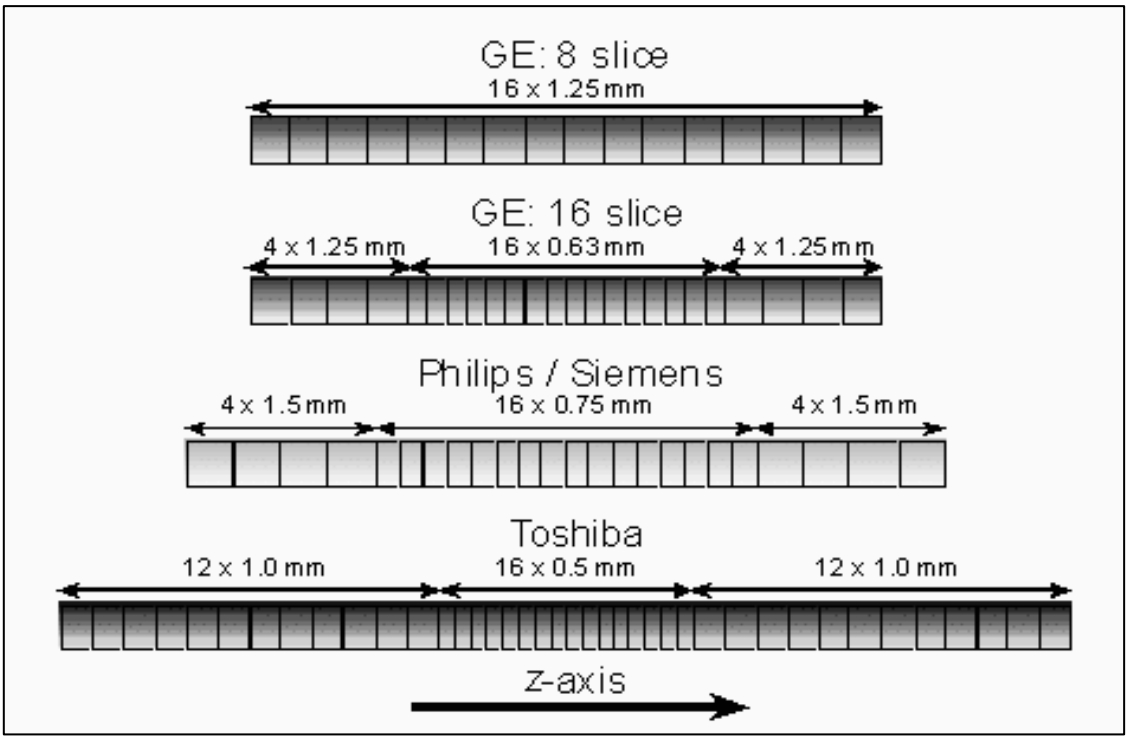

Figure 2- 11: Schematic diagram illustrating the examples of an 8-slice matrix detector (GE), a 16-slice adaptive array detector (Philips/ Siemens), and a 16-slice hybrid detector (Toshiba Aquilion-16) (Kalra et al., 2015).

The third type (hybrid detectors) has smaller detector rows in the middle and larger ones towards the periphery of the detector array (Kalra et al., 2015). When similar tube current settings were used to compare MDCT with helical CT scanners of the same vendors, radiation dose exposure was markedly increased for MDCT. Generally, increasing detector configuration leads to lower dose per scan as well as a decrease in image noise. Decreasing the detector configuration, whilst keeping the noise constant, results in a higher radiation dose (Lewis & Edyvean, 2014). A study by Nagel (2007) reported that increases radiation dose at the detector array came with an increase in tube potential when the tube potential increased from 120 kV to 140 kV (Nagel 2007). Using thinner collimation will significantly increase image noise, which may be partially offset by increasing tube current and thus raising radiation dose (Ulzheimer, 2005). While a higher image noise can be tolerated with thin sections/slices, thick sections/slices require reconstructing to avoid this increase in radiation dose. Guimarães et al., 2010 illustrated that a 14 × 1.2 mm detector configuration produces images of significantly better quality than with a 64 × 0.6-mm configuration. There were large image quality variations at four anatomic structures between the 14×1.2-mm and 64 × 0.6-mm detector configuration for abdominal dual-energy CT- results show the image quality was better than that obtained with the 64 × 0.6-mm.

Also, radiation dose was affected by detector configuration for scanners with 16 slice detector rows. The choice of detector width may depend on the need for body sections. For example, a detector collimation of 1.5 ×16 mm gives a higher radiation dose than 0.75 ×16-mm beam collimation for a 16-channel MDCT (Singh et al., 2014).

3.5 Abdominal organs and regions

The abdominal CT examination is among the most common CT examination carried out in the radiology department. Various CT techniques may be employed depending on the indications for the examination. The main abdominal viscera included within the scan volume are the terminal part of the oesophagus, stomach, intestines, spleen, pancreas, liver, gallbladder, kidneys and the adrenals glands. For general clinical descriptions, the abdomen can be divided into four quadrants: right upper quadrant (RUQ), left upper quadrant (LUQ), right lower quadrant (RLQ) and left lower quadrant (LLQ) (**Figure 2-12)** (Moore et al., 2010). In fact, several CT examinations specifically scan the upper abdomen and pelvis together. The abdomen extends from the dome of the diaphragm to the iliac crest.

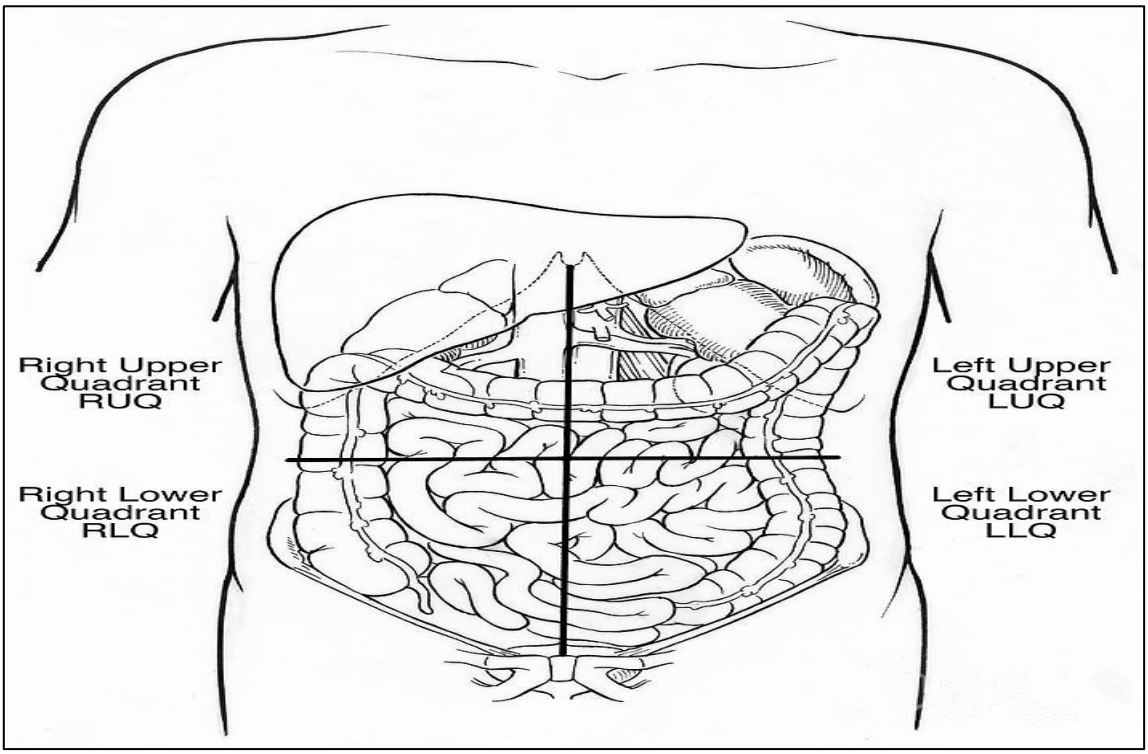

Figure 2- 12: Four abdominal major quadrants regions (Moore et al., 2010).

2.6 Abdominal CT protocols

Procedures for abdominal CT scanning are entrenched in the protocols of new CT scanners. The operator is allowed to automatically select appropriate parameters to be used within CT scans for these procedures. kVp, mAs, table speed as well as slice thickness are several of the scan parameters that can be varied during abdominal CT examinations. They are subjected to manual changes to account for patient size, the primary scanned organ and the clinical state of the patient. A number of standard procedures can be used for different parameters (Kalra et al., 2015). With the introduction of new hardware and software technologies, there is now a surplus of scanning parameters that are automatically selected or manually set for each protocol. This can become a complex problem in that several scanner manufacturers assign different proprietary names to similar parameters (Singh et al., 2014)

Typically, abdominal CT imaging involves the pelvis and upper abdomen and imaging tends to occur during inspiration to reduce internal motion. Normally, the X-ray tube potential ranges from 120–140 kVp and the tube current varies from 100 to 550 mA, based on patient size and the clinical question (Sodickson, 2012). In addition to these, there are other scanning parameters which must be optimised. The selection of slice collimation can vary from 5–8 mm and the pitch from 0.689-1.5 (Hara, Wellnitz, Paden, Pavlicek & Sahani, 2013). When the focus of CT scan is individual organs, such as the kidney or pancreas, the slice thickness can range from 2–5 mm, allowing for the detection of small lesions. In the case of image reconstruction, a decreased slice thickness could be used to improve image detail (Jin et al., 2010). A pitch of 1 or lower is essential in regular CT to produce enhanced detail in the sagittal or coronal reconstructed images. Pitches over 1 could cause misregistration, and some reconstruction might be irregular and impact the accuracy of diagnosis (Kalra et al., 2015). However, abdominal abnormalities (e.g. lesions within the spleen, liver and pancreas) usually produce a reduced image contrast compared to raised-contrast of chest CT images.

Finally, a disproportionate decrease in the radiation dose within the abdomen may increase the image noise and artefacts, which then might influence the conspicuousness of several low-contrast lesions. Thus, abdominal procedures must be stratified cautiously on the basis of the patient's clinical signs and reduced dose CT protocols should be used in moderation. Such dose reduction is generally achieved with a reduction in tube current through suitable modification of ATCM techniques or FTC (Moore et al., 2015). Multiphase examinations of the abdomen should be restricted to appropriate clinical situations. For example, acquisition of non-enhanced images before contrast-enhanced routine abdominal CT should be avoided. Delayed images should be acquired only when they may help in evaluation of an abnormality. Reduction of scanning range for one or more phases to the specific region of interest can help reduce radiation dose substantially and improve acceptable image quality. (Kalra et al., 2015).

2.7 Tube current modulation techniques in CT

Studies have demonstrated that radiation dose and image quality to the population has increased significantly over the last few decades (Hendee & O'Connor, 2012). The increased number of CT scan examinations to patients is one cause of this increase (National Council on Radiation Protection (NCRP), 2009). In order to reduce radiation exposure, scanning methods have to be modified to achieve optimal image quality at the lowest possible radiation dose (optimisation). One of the most important modifiable factors for CT dose optimisation is the tube current. This can be controlled during the scan by fixing the tube current (FTC) or using automatic tube current modulation (ATCM). Both techniques have the ability to produce a large volume of images and this has helped make CT scanning one of the most important abdominal radiological diagnostic tools (Siemens AG Medical Solutions, 2010). Both tube current selection methods are now available across all commercially available CT systems. The ATCM modulation method is a significant technological advancement, the intention of which is to enable the optimization of image quality and radiation dose as the scan progress throughout the patient. However, questions have arisen as to which tube current selection method (FTC or ATCM) provides radiation dose reduction whilst maintaining a consistent (diagnostic) image quality (Lee et al., 2011b).

Within the next thesis subsection of this chapter there will be a discussion on both FTC and ATCM techniques types, including their advantages and disadvantages.

2.7.1 Fixed tube current (FTC)

The tube current and tube potential determine photon flux and beam energy and have traditionally been determined manually by operators. The photon flux and beam energy determines the image quality and radiation dose for the examination. When tube current is reduced, image noise increases and the radiation dose is lowered (Lohan, 2015). With FTC techniques, the tube current remains constant for the entire region scanned (Kalra, et al. 2005). Manual adjustment of the tube tends to be currently based on patient weight or dimensions, and these factors can aid in establishing an appropriate balance between image noise and radiation exposure **(see Figure 2-13)**. However, these adjustments do not guarantee constant image quality throughout the examination. For example, in CT scanning of the chest the choice of a fixed tube current does not account for differences in beam attenuation between the shoulder region and mid chest region, or between anteroposterior and lateral cross-sectional dimensions (McCollough et al., 2009). As a result, there are likely to be areas which are both over- and under-exposed and this generates moral, ethical and legal issues from the examination.

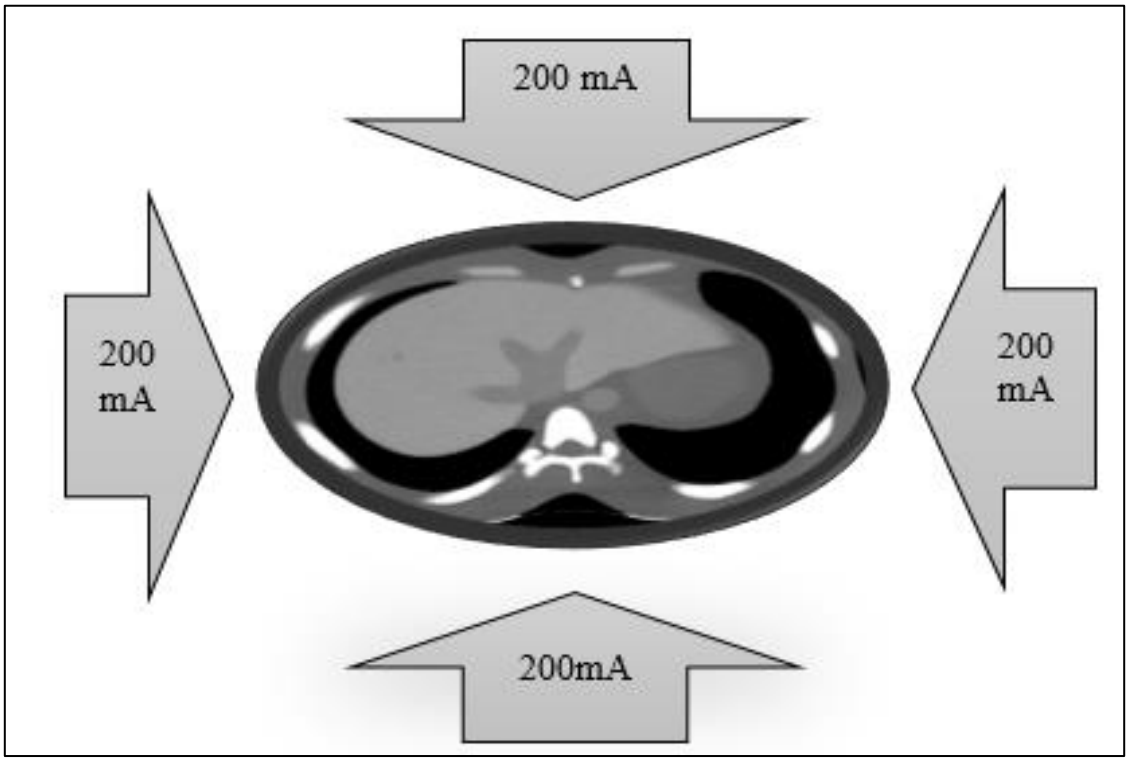

Figure 2- 13: Schematic diagram illustrating the process of using a FTC

2.7.2 Automatic tube current modulation (ATCM)

The automatic tube current modulation technique (or automatic exposure control [AEC]), allows for the automatic adjustment of the tube current during the CT scan. Current ATCM algorithms can be classified into three groups: 1) x, y plane angular modulation, 2) z-axis modulation (longitudinal modulation), and 3) integrated (z-axis and x, y) modulation (Martin & Sookpeng, 2016) **(see Figure 2-14)**. This adjustment is based on the attenuation and size of the patients' scanned area of the body. This implies that the tube current (mA) is increased in the area of the body with the greatest attenuation- e.g. through the shoulders or hips- and decreased in areas of low attenuation- e.g. through the abdomen and thorax. (Raman et al. 2013) Although the principles behind most of the ATCM techniques are similar, some differences still exist among the different vendors (Linton and Mettler, 2003). Some vendors allow the operator to choose a mA range within which dose modulation is desirable. Others allow control of the modulation strength for patients who are smaller or larger than a 'reference patient' (Singh, Kalra, Thrall & Mahesh, 2011).

X-Y modulation or angular modulation lowers the selected tube current in the x-y plane, resulting in less attenuation, while z axis modulation modifies the tube current from section to section. When switching from FTC to ATCM, protocols should be age-defined. i.e. separate protocols should be used for adults and children. However, ATCM systems, in the majority of instances, minimise the radiation dose when an operator selects an image quality level, and then the system can adjust the tube current. This results in a reduced radiation dose of between 10 and 50%, in the absence of any visual reduction of image quality (Söderberg, 2008). ATCM has also been evaluated by Raman et al. (2013a) for a range of vendors; the results showed the radiation dose reduced between 40% and 50% with different vendor's systems. The radiation dose reduced by up to a half when using different ATCM software provided by different vendors (Raman et al. 2013a).

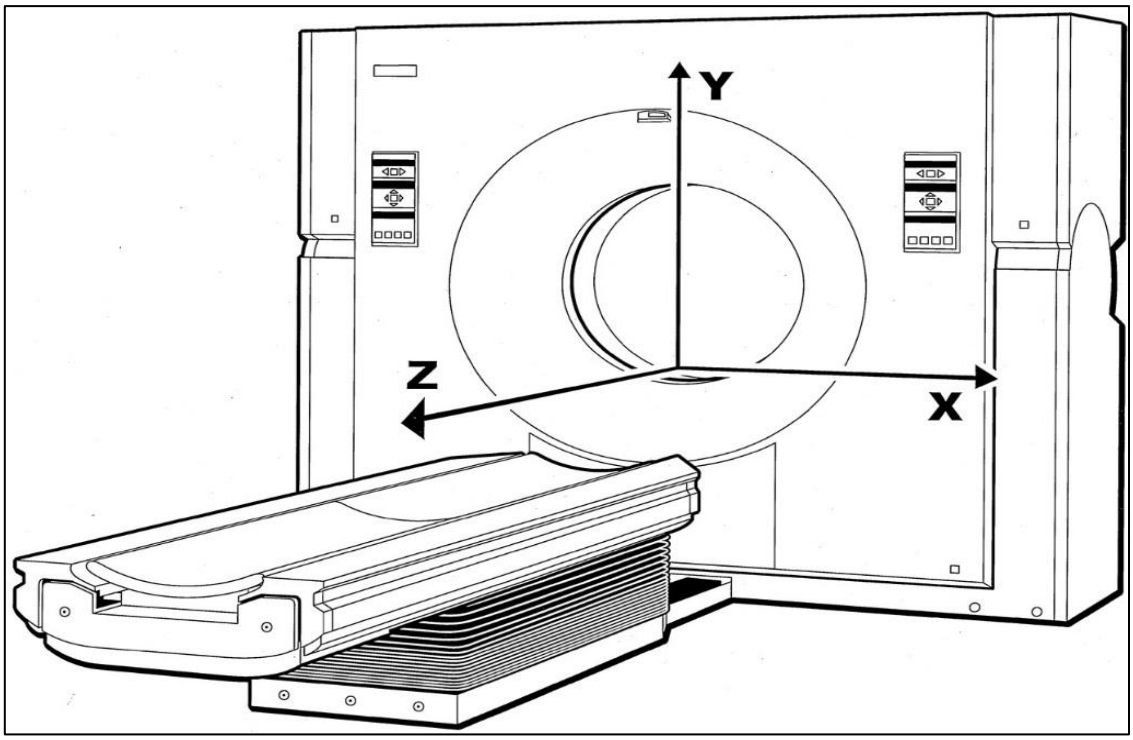

Figure 2- 14: Schematic diagram illustrating x, y and z-axis modulation in CT scan (Martin & Sookpeng, 2016).

2.7.2.1 Angular modulation (x, y planes)

This technique was introduced in 1994. It involves the modification of the tube current during X-ray tube rotation between anteroposterior and lateral projections. The radiographer selects an initial tube current which is modulated upward or downward within a period of one gantry rotation or selected maximum/minimum image quality level values (McCollough et al., 2009). The tube current varies as the square root of the measured attenuation and is usually reduced in the anteroposterior direction, which is the direction of the lower attenuation projection (Lohan, 2015) **(see Figure 2-15**). For example, in an asymmetric body region (e.g. shoulder or hip) there is less attenuation of the x-ray beam in the anteroposterior projection compared with the lateral direction. Furthermore, when the lateral scan projections pass through a thick bony asymmetric body region, starvation (streaking) artefacts may emerge. These artefacts are the result of photon deficiency (Ramirez-Giraldo, Fuld, Grant, Primak, & Flohr, 2015). Current modulation minimises radiation exposure in the anteroposterior projection without compromise to image quality. In areas where the patient is more homogenous and circular (e.g. head), less tube current modulation is required (Lohan, 2015).

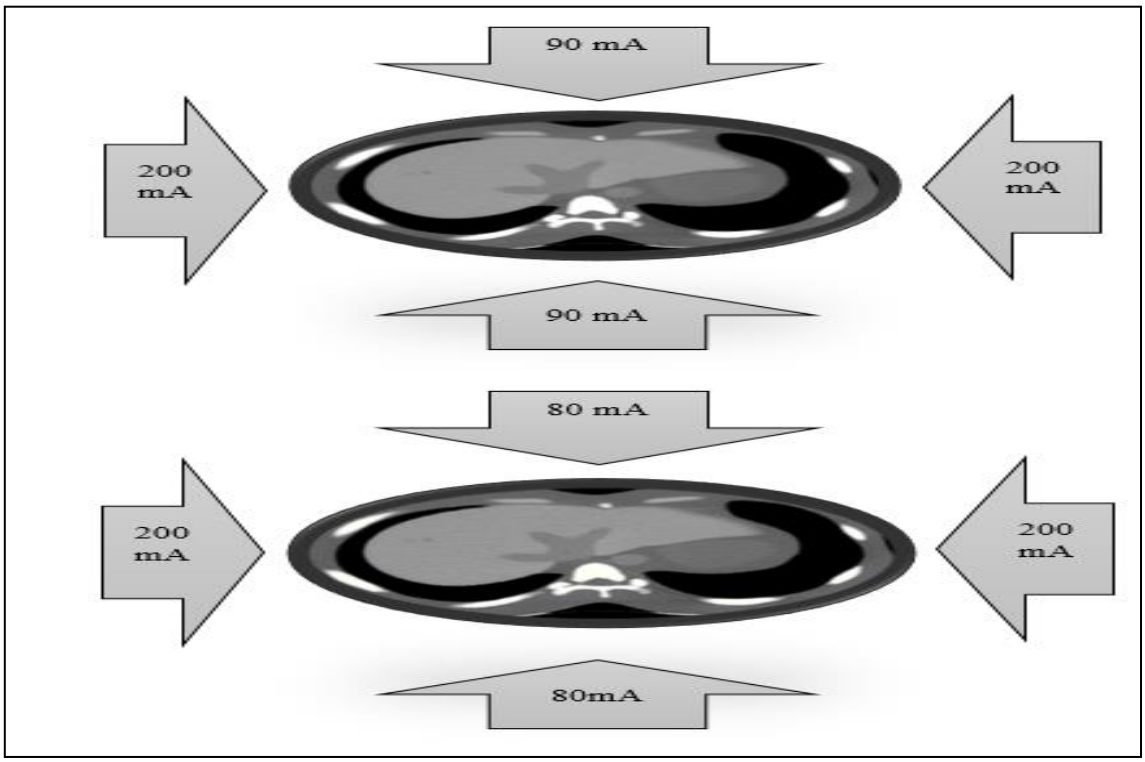

Figure 2- 15: Schematic diagram illustrating the process of using angular modulation (in the x, y plane)

To determine the attenuation, anteroposterior and lateral scanograms are typically performed. Using the attenuation measurements from these scanograms a sinusoidal sequence is fitted to the data acquired from these two projections (Ramirez-Giraldo et al., 2015). This ATCM method can be found in machines manufactured by Siemens Medical Solutions (CARE Dose), Philips Medical Systems (DoseRight dose modulation (DOM)) and Toshiba Medical Systems (SureExposure – which is used in this thesis). The CARE Dose technique has the added value of using real-time CT attenuation data from the beam attenuation acquired in the preceding 180° rotations; this is used to adapt the tube current for the subsequent 180° rotations. However, a study by Abou-Issa, Elganayni & AL-Azzazy. 2011 evaluated radiation dose for coronary CT angiography (CCTA) protocols using angular modulation ATCM. The results demonstrated a radiation dose reduction between 40% and 60% with low contrast objects detectable between 100kV and 120 kV (Abou-Issa et al., 2011). Similarly, the DoseRight system has been shown to reduce radiation dose by up to 40% by adapting the tube current from the preceding 180 to 360° tube rotation for the subsequent 360° (Kalra, et al., 2005).

2.7.2.2 Longitudinal modulation (z-axis)

This technique adapts tube current along the direction of scanning for each slice. The adaptation is based on the size, shape, and attenuation of the region of the body that is being scanned. This technique differs from angular modulation since the tube current is adapted so that a user-specified quantum image noise is maintained (Kalra et al., 2005). The aim of z-axis modulation is the reduction radiation dose and reduction in the variation of image quality (Singh et al., 2011) **(see Figure 2- 16).**

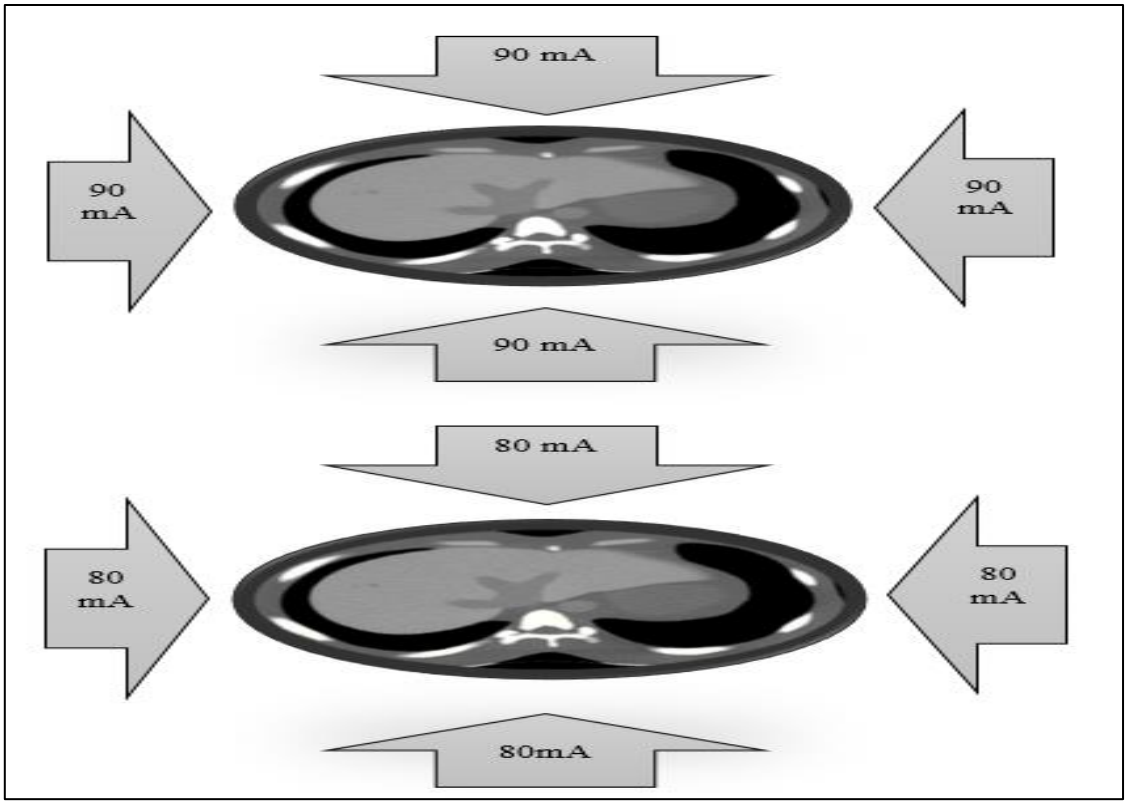

Figure 2- 16: Schematic diagram illustrating the process of using longitudinal modulation (in the z-plane).

The tube current in this system, which is set within an acceptable range, is determined by the projection data collected from the topogram and is empirically determined from noise prediction coefficients. These noise prediction coefficients are obtained from using a reference technique (Lee et al., 2008). Only a single topogram (scout view) is required to determine the tube current required to produce images with the required noise level (Ramirez et al., 2015). The topogram enables the system to compute the photon fluency necessary for the maintenance of the user-defined level of noise within the reconstructed image (Singh et al., 2011). By setting a minimum value for tube current, excessive reduction in tube current for small patients is

avoided. Furthermore, errors from very high noise indices are also avoided. Setting a maximum mA limit avoids excessive tube current increase while trying to maintain radiation dose (Kalra et al., 2005). While the tube current is variable within the set range on the z-axis, it remains constant on the x-axis (Soderberg and Gunnarsson, 2010).

2.7.2.3 Combined modulation (x-, y- and z-axes)

A combined tube current modulation technique is currently the method of choice for all major CT scanner manufacturers (Soderberg and Gunnarsson, 2010; Lohan, 2015). This technique involves the combination of angular and longitudinal (x, y, z) mA modulation to alter the tube current. The variation in tube current is achieved both during rotation and along the z axis of the patient. The modulation of the tube current occurs during every gantry rotation for every slice. However, the operator must still specify the required quality of image by either of the two methods (McCollough et al., 2009). The first method takes two scout views—an antero-posterior (AP) view to determine modulation along the z-axis, followed by a lateral projection to determine the x-y modulation of the image acquisition. **(Figure 2-17).**

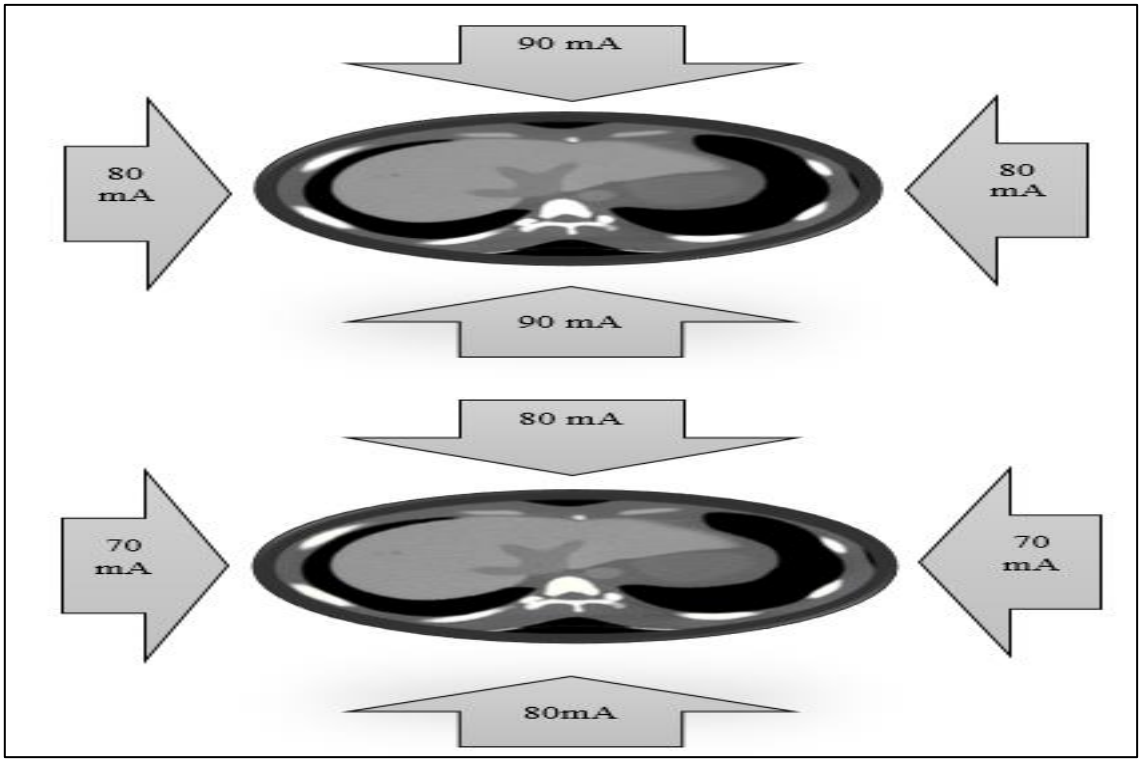

Figure 2- 17: Schematic diagram illustrating the process of using combined modulation (z, x and y plane)

The second method involves taking two simultaneous scout views (AP and lateral), from which both the z-axis and x-y axis changes to the tube current are determined. This combined method results in dose reductions higher than either angular or z-axis ATCM alone (Lee et al., 2009; Rizzo et al., 2006). The combined modulation method is the most comprehensive method for CT dose reduction, as the radiation dose is modified in line with the patient attenuation in three planes (Soderberg and Gunnarsson, 2010). A study by Mulkens et al. (2005) compared the effect of the combined modulation and angular modulation on dose reduction; the combined modulation was shown to significantly reduce radiation dose exposure for all body regions: thorax, 20% and 14%, respectively; abdomen-liver, 38% and 18%, respectively; abdomen-pelvis, 32% and 26%, respectively; lumbar spine, 37% and 10%, respectively; and cervical spine, 68% and 16%, respectively. No significant difference in image noise and mean image quality scores, between the two methods, were reported. However, one exception (cervical spinal examinations) demonstrated significance ($P<0.001$), wherein the examinations with angular modulation resulted in better image quality scores (Mulkens et al., 2005). However, another study compared image quality and radiation dose for abdominal-pelvic CT examination between combined modulation and angular modulation with FTC constant tube current (Rizzo et al., 2006). The result demonstrated the combined modulation reduction in radiation dose was approximately 42%-44%, with acceptable noise and image quality better than both angular modulation and FTC techniques (Rizzo et al., 2006).

2.8 ATCM techniques used within current CT systems

Each CT scanner manufacturer has developed different ATCM techniques and application capabilities (Söderberg, 2008). **Table 2-2** outlines the ATCM methods which have been overviewed in the previous section. The main purpose of all ATCM techniques is the adaptation of the tube current to be consistent with the x-ray beam attenuation for the patient anatomical structures (**Table 2-2**). The most common systems are discussed below.

Table 2- 2:ATCM systems used by different CT vendors

Manufacturer	ATCM system	Method to set level of image quality
Toshiba	SureExposure 3D	Image quality level/standard deviation
Siemens	CARE Dose 4D DoseRight	Quality reference mAs Reference
GE	AutomA 3D	Noise index
Philips	DoseRight	Reference image Noise

2.8.1 Toshiba ATCM – Sure Exposure 3D

A Toshiba CT scanner was used in this thesis for all experimental work. Toshiba Medical Systems employs an integrated modulation structure, referred to as Sure Exposure 3D. The method provides the operator with two techniques for setting the necessary image standard: standard deviation of CT digits and image quality extent. Both techniques are based on the quantification of the standard deviation (SD) of pixel values determined from a patient-equivalent water phantom (Toshiba, 204). The operator begins by setting the SD of the required image noise as well as setting the minimum and maximum tube current. A greatly decreased tube current may result in increased image noise as well as very poor quality images. High tube currents result in increased radiation exposure and less image noise, thus improving image quality (Angel & Zhang, 2012) (**Figure 2-18)**.

Figure 2- 18: Schematic diagram illustrating the AP and lateral scout views which in combination with SD values aid the determination of tube current values for CT scans of the abdomen. (Nievelstein, Van Dam, & Van Der Molen, 2010)

The SureExposure 3D process begins by acquiring one frontal as well as one lateral CT scout view of the patient. Data from the scout views are subsequently employed to map the chosen image standard to the estimated values of tube current. SureExposure 3D utilizes the frontal and lateral diameters of the patient and attenuation data from the detectors to modify the tube current (modulation) for every gantry rotation (American Association for Physicist in Medicine (AAPM), 2008). This attenuation data is gathered and employed to pre-compute the map of the tube current for the forthcoming CT slices. The real values of tube current are established through a specified target standard deviation image quality metric, which establishes the standard deviation for pixel values within the reconstructed image. The Toshiba ATCM 'Sure Exposure 3D' technique modulates the tube current through patient size and level of attenuation. The modulation of the tube current is performed along the longitudinal (z-direction) and axial (x, y) planes. Sure Exposure3D will initially alter the tube current towards the z-direction, but if a dual AP and lateral scout views are employed then Sure Exposure3D will alter the tube current in all three directions as the tube revolves around the patient (Toshiba, 2017).

For modulation along the z-axis, the water phantom equivalent diameter at every level of the patient is computed and contrasted with the greatest feasible attenuation. The tube current necessary for attaining the selected standard deviation for the ultimate water equivalent diameter is implemented (McCollough, Bruesewitz & Kofler, 2006). Tube current is subsequently altered to obtain the target standard deviation all through the scan range. The level of the image quality can be placed automatically for the specific clinical question. These are associated with the choice of various predetermined levels of image noise; a) Low dose+ (SD 12.50HU), b) Low dose (SD 7.50HU), c) Standard (SD 5.00HU), d) Quality (SD 3.00 HU), e) High Quality SD 1.00 HU) (Toshiba. 2014). The ATCM algorithm additionally permits the user to manually select any standard deviation of pixel value (using HU) as well as a minimum and maximum range for the tube current. The Toshiba Aquilion ONE Sure Exposure 3D intends to reduce the dose by approximately 40%, when in comparison with ATCM SD and FTC, and sustain a standard level of image quality. (Angel, 2009).

2.8.2 Siemens ATCM – CARE Dose 4D

Siemens employs an integrated tube current modulated process referred to as CARE Dose 4D. The ATCM process considers the size and shape of the patient as well as real-time, online, managed tube current modulation within every tube rotation. Again subject to data from the scout views, lateral or anterior-posterior attenuation profiles (size, anatomical shape and attenuation at every position down the long axis (z-axis) of the patient) are quantified in the orientation of the projection and approximated for the perpendicular orientation with a mathematical algorithm. From the approximation of these attenuation profiles, values of axial tube current are established (Söderberg, 2016).

The association of attenuation profiles and tube current is established by an analysis of slice position in the z-axis. The tube current is modified in relation to the size of the patient and attenuation profile (longitudinal modulation). ATCM with CARE Dose 4D is based on the operator selecting an image quality reference mAs, and it is meant to maintain the necessary image quality. According to the axial tube current profiles (AP and lateral), the ATCM process carries out modulation of tube current within every tube rotation (angular modulation). The ATCM process further employs feedback from the prior rotations to place the tube current in line with the angular attenuation profile of the patient's size at various angles of the projections (SIEMENS, 2010 & Sookpeng, Cheebsumon, Pengpan & Martin, 2014b).

The image quality determined during CARE Dose 4D, chosen by the operator, has to be based on the diagnostic needs of the clinical image acquisition protocol wherein different options are available. For every kind of CT examination, the quality reference mAs signifies the mean efficient mAs (tube current-time product/pitch). A characteristic value is chosen by the operator, signifying a reference patient, which is described as an adult comprising an estimated weight of between 70 and 80kg. For paediatric procedures, the effective mAs has to be chosen for a regular child comprising a weight of 20kg (McCollough et al., 2006). Finally, research using CARE Dose 4D has illustrated that when compared to FTC, a 20-40% decrease in radiation dose can be achieved resulting from observation of anatomical area and patient shape, with an enhanced quality of images (Söderberg, 2016).

2.8.3 General Electric ATCM - AutomA 3D

General Electric (GE) employs an integrated ATCM process referred to as AutomA 3D. This consists of two elements: AutomA, which offers longitudinal AEC, and SmartmA, which offers rotation AEC. It is feasible to employ AutomA on its own as well as in collaboration with SmartmA. AutomA employs a single scout view to establish patient size, anatomical form as well as attenuation features in which to alter the tube current for every slice position down the long axis of the patient (Söderberg & Gunnarsson, 2010).

With SmartmA, the tube current is different for various projection angles inside every X-ray tube rotation change. For every rotation, the ATCM process computes every x and y mA value from information on the long and short axis of the patient, subject to the scout image. To employ AutomA 3D, the operator has to stipulate a noise index value, minimum and maximum mA range. The noise index permits the user to set a stipulated image quality and it is referenced to the image noise (the SD of pixel values within the central area of an image of an even water phantom) (General Electric (GE), 2008). The attenuation values of the patient are mapped in a lookup table as quantified on the scout image into mA values for every gantry rotation in line with GE's proprietary algorithm. The algorithm is meant to sustain the same extent of image noise as the attenuation values differ between one attenuation index and the next. The chosen minimum and maximum values of tube current stipulate the range of where the modulation of tube current is preferred. Researchers have illustrated the possibility of a 60% reduction of dose using the AutomA 3D method within abdomen/ pelvis CT scanning and, combined with automatic tube current modulation, allows for the CT radiation dose to be reduced by 44.7% without losing image quality in pelvic scans (McCollough et al., 2006; Wang et al., 2013).

2.8.4 Philips ATCM – DoseRight

The Philips DoseRight ATCM system consists of three components: Automatic Current Selection (ACS) which offers patient base ATCM, D-Dom which offers angular ATCM and Z-DOM which offers longitudinal ATCM. Presently, the use of all three dose modulation instruments simultaneously is not feasible, although ACS may be paired with Z-DOM or D-DOM to avoid the increasing the radiation dose to the patient. Philips employs a reference image to set the necessary standard of image quality (Kalra et al., 2005). The data is stored as a reference image for comparison with a CT projection radiograph, in addition to data acquired from other patients in scans for a similar clinical study. The predetermined reference values are regarded to be for a regular patient size (33 centimetres in diameter). The regular patient size is employed as a benchmark for ACS when it suggests particular mA values for every patient, determined by a proprietary algorithm (Wood, Moore, Stephens, Saunderson & Beavis, 2015).

The proposed mA values are intended to attain a consistent level of image noise if the patient is larger than the reference set (standard patient). Using the scout view, mA values are computed for the actual patient in order to attain similar image quality across all slices. With advancement in the scanning procedure, the Z-DOM mAs values alter and modification is subject to absorption differences in the scanning orientation, as opposed to adjustment based on anatomical shape of patients. However, a study by Wood et al. (2015), which evaluated Philips DoseRight 2 CT automatic exposure control system AEC, demonstrated excellent dose and image quality when using this technique (Wood et al., 2015).

2.9 Rationale - abdominal CT scan comparison between FTC and ATCM radiation dose and image quality

When ATCM is used there are several distinct advantages. There is the possibility of dose reduction by means of an optimised modulation of the tube current subject to patient size/density in all three planes. Employing too high tube current on smaller patients is avoided, as the necessary level of quality has been previously established (Martin & Sookpeng, 2016). Longitudinal modulation addresses the challenge of some areas receiving either higher than required doses of radiation or too high image noise. Angular radiation renders it feasible to minimize the tube current for projections comprising of reduced attenuation without too high an increase in image noise. Using ATCM, even more consistent image quality is generated (Keat, 2005). Unlike FTC, which requires users to select tube current settings for patients of different sizes, and for different clinical conditions, ATCM only requires user defined adjustment for different indications while automatically adapting the current for different sizes of patients. An additional advantage is that most ATCM techniques are programmed to maintain similar radiation dose when scanning parameters- e.g. pitch, slice thickness and kV are modified (Singh et al., 2011).

One of the disadvantages of ATCM is the heterogeneity of commercially available solutions from each manufacturer. This makes it difficult to carry out universal standardisation for various scanning procedures across a range of CT systems. For instance, owing to undefined optimal image quality with ATCM, it is difficult to translate a reference mA value into a standard deviation (SD) noise value. Another limitation is the need to change tube current for some ATCM systems in small or large patients to reduce the radiation dose. (McCollough Cody, Edyvean& Geise, 2008; Gutierrez et al., 2007).

Prior studies have reported significant dose reduction with ATCM than FTC. For abdomino-pelvic CT, Lee et al. (2011b) reported a statistically significant (42%) reduction in radiation dose exposure during CT of the abdomen and pelvis with ATCM when compared with FTC (Lee et al., 2011b). This was also similar to the findings of an earlier study by Rizzo et al (2006), which also reported a substantial reduction (42-44%) in radiation dose with acceptable image noise and diagnostic performance- again during CT abdomen and pelvis. A cadaver study investigating radiation dose from CT, using ATCM and FTC, also showed a two-fold increase in dose when using FTC when compared to ATCM following abdomino-pelvic CT scanning (Padole et al., 2016). For head CT, Namasivayam, Kalra, Pottala, Waldrop, & Hudgins (2006) reported that z axis ATCM significantly decreased radiation dose when compared to

FTC. Russell et al. (2008) also reported a 34% decrease in radiation dose when using a noise index of 20.2 with ATCM when compared with FTC (Russell et al., 2008). For CT abdomen-liver, between 38% and 18% radiation dose reductions with ATCM have been reported (Kalra et al., 2005; Singh et al., 2011; Mulkens et al., 2005). Another study by Lee et al. (2009) also showed no significant difference in visual image quality parameters between the FTC and combined ATCM techniques during cranio-cervical CT angiograms and reduction radiation dose with the ATCM technique (Lee et al., 2009). **Table 2-3** demonstrates the radiation dose and image quality relationship summary between ATCM and FTC techniques using with different CT scan examination and different manufacturers from 2004 up to 2017.

Table 2- 3:Summary general comparison between ATCM and FTC techniques using different CT scan examination and different manufacturer's from 2004 up to 2017

Author	Year	CT system	Body part	Sample	Finding	Comments
Sookpeng & Butdee	**2017**	128 slices MDCT Siemens	Lens of the eye and the other nearby organs from the CT brain scan	Adult anthropomorphic phantom	ATCM decrease in the dose to the lens of the eye while reduced signal-to-noise ratio image quality when compare FTC	ATCM/ mAs Value 300 and 400 FTC/effective mAs 250 and 330
Papadakis , Perisinakis & Damilakis	**2016**	Simulated on a 64-slice CT scanner	Routine head, thorax, and abdomen/pelvis CT	92 Pediatric patients	The percent difference organ dose between FTC and ATCM acquisitions was *10%* for eyes in head, *26%* for thymus in thorax, and *76%* for kidneys in abdomen/pelvis	ATCM 109–167mA
Padole et al	**2016**	128-slice, dual-source	Abdominal organs CT scan	Human cadaver	The differences among the estimated organ doses were higher for AEC technique compared to the FTC	No image quality evaluation
Mayer et al	**2014**	CARE Dose4D , Siemens Healthcare	Contrast enhanced chest or abdominal CT	617 patients	ATCM radiation dose reduction 18.4% when using with automatic tube voltage selection (ATVS) with maintaining adequate image quality	ATCM (CARE Dose4D0 with 120 kVp

Kishimoto, Sakou & Ohta	**2013**	CT-AEC	Cardiac CT	65 patients	AEC provided consistent image noise for cardiac CT when compare FTC	image noise only
Park et al	**2013**	128-slice dual source CT Siemens	Vascular enhancement CT scan	100 patients	ATCM acceptable image quality and low radiation dose more than *59%*, compared with the with the control setting FTC 120mA	FTC 120Ma only
Kim at al	**2013**	128 slices MDCT Siemens	Myocardial perfusion CT protocols	330 consecutive patients	ATCM resulted in a *36 %* reduction compared with FTC. image quality with FTC reduced image noise and high visual scores compared with ATCM myocardial perfusion CT	ATCM; CAREDose4D
Angel & Zhang	**2012**	Toshiba Aquilion ONE CT	Phantom study (brain CT scan)	Two acquisitions	ATCM techniques reduced CT dose by *38%* compared to FTC, image noise was equivalent (3% increase with ATCM)	SURE Exposure SD
Lee et al	**2011b**	16 slice MDCT Siemens	Abdomen and pelvis CT scan	100 patients	ATCM for CT of the abdomen and pelvis reduced radiation dose *45.25%* compare with FCT and no difference in image noise and image quality between two techniques	FTC OF 165 mAs only with ATCM range 75–142 mAs
Su et al	**2010**	16 slices Auto mA GE	Liver CT scan	182 patients between 2006 and 2007 (contrast medium)	averaged tube current and effective dose liver scan of ATCM *6.2% and 35.9%* lower than FTC but the image quality no difference between both techniques	FTC 350mA and ATCM 10 – 380 mA with different kVp 100 and 120
Lee et al	**2009**	64-section MDCT SURE Exposure 3D	Craniocervical CT angiography performed CT scan	50 consecutive adult patients	Combined ATCM technique reduction in radiation dose *18%* compare with FTC and no difference	FTC of 300 mA only with ATCM technique range 101–300 mA

		Toshiba			subjective image quality between techniques.	
Namasivayam et al	**2006**	16-section MDCT GE	Neck CT scan	52 consecutive subjects	ATCM reduction radiation dose between *21% and 33%* when compare with FTC and similar image quality (diagnostic image quality and image noise)	FTC of 300mA with ATCM range 150–440mA
Rizzo et al	**2006**	16-MDCT scanner Siemens CARE Dose 4D	Abdomen and pelvis CT scan	152 patients	Combined modulation ATCM technique reduction *(42–44%)* in radiation dose with compare FTC. Also similar image quality scores and lower image noise with ATCM	Effective mA (FTC 160and 200mA) and (ATCM 160–200mA)
Russell et al	**2008**	64-slices GE Healthcare	Clinical Applications of Neck Volume CT	84 patients underwent neck CT	ATCM reduction radiation dose *34%* when compare with FTC and statistical significance with visual image quality was small average scores	FTC of 400 and 650mA only compare with ATCM rang 100 to 750 mA
Mulkens et al	**2005**	Care Dose 4D; Siemens review from 2003	Thorax, abdomen-pelvis, abdomen-liver, lumbar spine, and cervical spine CT scan	200 patients	Combined modulation ATCM reduced radiation dose when compare with Angular modulation ATCM abdomen-liver, *38% and 18%* and no different image quality	Effective mAs (Combined ATCM 30–118mA and Angular ATCM 63–89)
Kalra et al	**2004a**	16-slices GE	Abdomen and pelvis CT scan	62 consecutive subjects (mean	ATCM reduction radiation dose *54%* when compare with FTC and similar image noise and image quality	FTC of 200 and 300mA only compare with ATCM rang 10–380 mA

2.10 Chapter Summary

In conclusion, the utilisation of ATCM for abdominal CT scan imaging can result in an increase in radiation dose, if the maximum permitted tube current is not properly set (Gutierrez et al., 2007). Most of the new scanners have the option of both FTC and ATCM techniques, while some low-dose scanning protocols still operate with FTC. Radiation dose from CT examinations continues to increase. In the last five years, radiation dose increased from 10% to 36%- also 59% with iodinated contrast medium. A fairly recent study comparing between both techniques for abdominal pelvic CT scan (Lee et al., 2011b) only reported ATCM radiation dose reduction of about 45%. The study was carried out using 165 mAs FTC with rang tube current from ATCM and there was no difference in image noise and image quality between both techniques.

All the studies considered in this chapter have some limitations, since they compared abdominal pelvic CT examinations only, and did not compare different protocols and parameters for the same patients. In addition, they also used different weights, ages and cross-sectional dimensions for the patients. It is difficult to compare between any techniques for radiation dose and image quality because the results are not sufficiently accurate for the evaluation for both techniques. The CTDIvol and DLP methods have value for radiation dose estimation as they are based on the standard parameters used. However, image quality grading also uses the common method absolute VGA 5-point scale for image quality evaluation which might not be more accurate for the comparison for both techniques for patients with various clinical conditions.

There is a need to further investigate and develop methods for the measurement and evaluation of radiation dose and image quality. Particularly, more studies are required to evaluate the abdominal CT examinations differences between FTC and ATCM with various parameters. In order to avoid the limitations of the previous studies. The review of the literature confirmed that no studies have compared radiation dose and image quality with different methods for abdominal CT scans between FTC and ATCM and there is an absence of research investigating different main acquisition parameters.

Chapter Three: CT scan dosimetry methods and radiation dose

3.1 Chapter Overview

A significant proportion of the radiation dose generated from medical procedures is due to CT scanning. This is a result of the increasing utilisation of CT in medical practice over the past decade and advances in scanner technology which have provided increased imaging opportunities (Mathews et al., 2013). For example, Gibson, Moorin, Semmens, & Holman (2014) evaluated changes in the number of radiology examinations in Australia between 2006/07 and 2011/12. The number of CT examinations had increased by an average of 36% and the annual radiation dose per patient was reported as being almost double. The study concluded that CT is the largest contributor to patient dose in radiology (Gibson et al., 2014) and this is a feature emulated in the majority of developed countries around the world.

Generally, radiation dose can be estimated using the Computed Tomography Dose Index volume ($CTDI_{vol}$), Dose Length Product (DLP) and Monte Carlo simulation. CTDIvol is generally said to underestimate patient dose (Strauss & Goske, 2011). In 2011 a report estimated the typical effective doses for common CT examinations in the UK to be 20% higher for CT head (using DLP) and up to 400% higher for high-resolution chest CT, compared with 2003 estimates (Shrimpton, Jansen & Harrison, 2015). Furthermore, an increase of up to 90% was reported for abdominal CT DLP. Based on CTDIvol, the level of increase was approximately 10% for head, chest and abdomen. The Monte Carlo simulation method (e.g. ImPACT) is a fast statistical simulation technique that is widely used to estimate effective dose from CT examinations. However, the simulation uses previously obtained raw data and makes certain assumptions regarding CT unit design. Changes in CT design limits the accuracy of computer simulated dosimetry and introduces the potential for significant error in the estimated doses. Using direct measurement radiation dose with TLD or MOSFET and an anthropomorphic phantom is labour intensive work, but more accurate for measuring radiation dose (Shrimpton, Hillier, Meeson & Golding, 2005).

In this chapter, various CT dosimetry concepts will be introduced, such as CTDI and DLP. Alternative methods of CT dosimetry will also be discussed. Areas discussed will include TLD and MOSFET for direct dose measurements, mathematical methods (DLP) and simulation methods (ImPACT). Additionally, the radiation dose, including absorbed dose (organ dose), effective dose and effective risk, will be discussed. Finally, this review of the literature will also discuss the common methods used for assessing the radiation dose for studies involving abdominal CT examinations. It is also essential to demonstrate the knowledge gap for CT

dosimetry methods and their role in the comparison of radiation dose during abdominal CT scans, with FTC and ATCM (theoretical and practical) techniques.

3.2 CT scan dosimetry

Radiation dose for patients undergoing CT examinations can be estimated using CT dosimetry. The computed tomography dose index (CTDI) is a parameter displayed on the CT scanner and is derived using CT quality control (QC) phantoms. The absorbed dose from a CT scan can be estimated using the CTDI for each CT slice. Effective dose from a CT scan can only be estimated by multiplying the CTDI and the scan length to generate the dose length product (DLP). The DLP is then used together with a series of coefficients in order to estimate effective dose. The CTDI is influenced by a range of scan parameters.

3.2.1 CTDI

The main CT scan dosimetry measurement concept is the CTDI, which is expressed in the unit of Gy. The CTDI comprises of the integrated dose profile on the z-axis, inside the scan volume. It is adjusted to the smallest slice area (signifying the average absorbed dose). CTDI is the absolute dose of radiation and is one of the main dose parameters recorded by CT manufacturers (McCollough et al., 2011). CTDI is a concept employed to recognise the absorbed dose of radiation from CT. Following the introduction of CTDI, considerable differences have been identified in CTDI estimates between different CT manufacturers. The description of the CTDI in mathematical terms is the sum of the dose contribution down a line parallel to the scanner's axis of rotation (z-axis) (Food and Drug Administration (FDA), 2006).

The CTDI includes CTDI air, weighted CTDIw, $CTDI_{100}$ and volume $CTDI_{vol}$. All of these CT dose parameters utilise a polymethyl methacrylate (PMMA) dose phantom, employing a pencil ion chamber of length 100mm (Abdallah & Salih, 2013) **(Figure 3-1).** The CTDIw comprises the average dose within a PMMA phantom slice at varying positions. This value provides an estimate of the radiation dose from each CT scan. The alternative CT dose parameters are obtained from it, such as the DLP (International Atomic Energy Agency (IAEA), 2009).

The quantification of CTDI for an axial CT scan is based on the radiation dose from the primary beam in addition to the scatter from nearby slices from one single CT slice within a PMMA phantom. Phantoms are available in two diameters (16 cm and 32 cm) to simulate the head and body, respectively (American Association of Physicists in Medicine (AAPM), 2011).

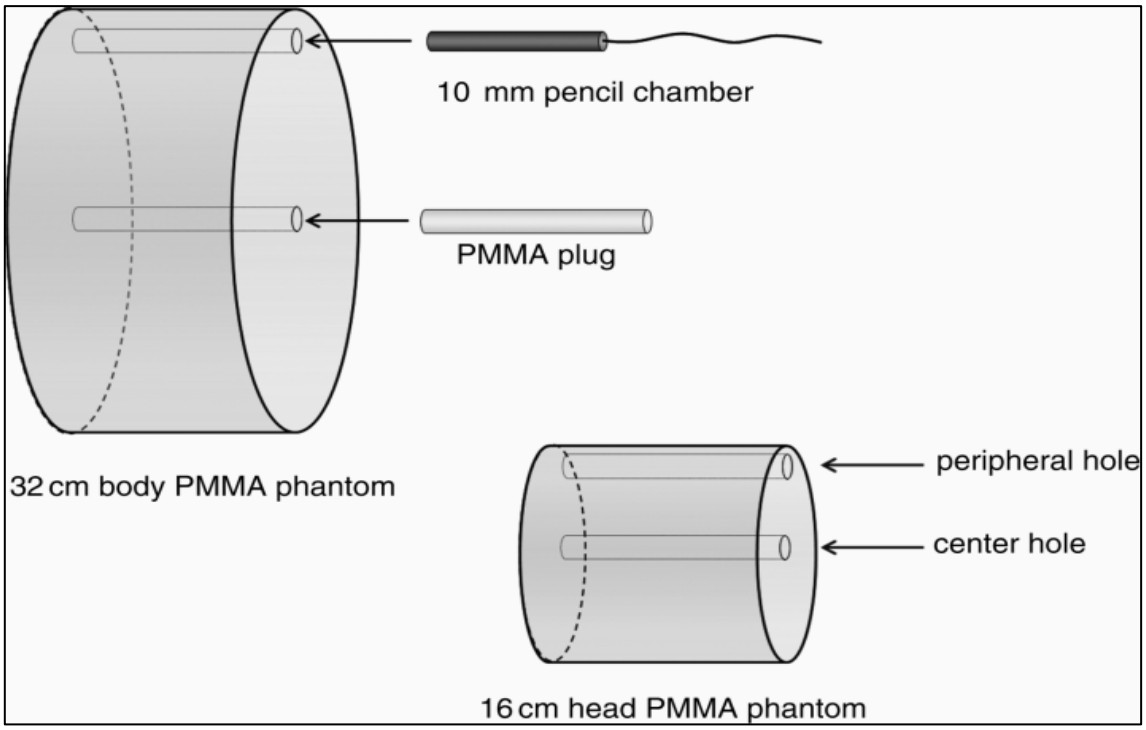

Figure 3- 1: Schematic diagram illustrating the PMMA dosimetry phantom (head-16cm and body-32cm diameters (AAPM, 2011)

3.2.2 $CTDI_{100}$

$CTDI_{100}$ (mGy) is a more practical measure of radiation dose. It is carried out with a fixed-length (100 mm) pencil ionization chamber and the result is divided by the nominal beam width. It can be measured within phantoms or in air. It is the integral of the dose profile along a line perpendicular to the tomographic plane divided by the product of the nominal tomographic section thickness and the number of tomograms produced in a single axial scan (Sookpeng et al., 2016). It is represented by the formula below **Equation 3-1:**

$$CTDI_{100} = \frac{1}{nT}\int_{-50}^{+50} D(Z)dz \quad \text{.....Equation (3-1)}$$

Where: **z** = position along a line perpendicular to the tomographic plane.

D (z*)* = dose in air at position *z* of the dosimetry phantom.

T = nominal tomographic section thickness.

n = number of tomograms produced in a single scan

There are several assumptions for this formula. The first is that the dose profile is centred on z=0. The second assumption is that air serves as a reference medium while the polymethyl

methacrylate (PMMA) serves as the actual material matrix within which measurements are made. Finally, for a repeated CT scan, the scan increment between adjacent scan settings is assumed to be nT. When this increase is not equal to nT, an adjustment should be made and this should be included in the user information (FDA, 2006).

The 100 mm fixed length of CTDI implies that only 14 sections of 7-mm thickness can be measured with a chamber. Therefore, in order to measure CTDI for thinner sections, lead sleeves are occasionally used to cover the part of the chamber that exceeds 14 section widths. This limitation to 14 sections has been overcome with the introduction of $CTDI_{100}$, which allows the calculation of the index for 100 mm along the length of an entire pencil ionization. The $CTDI_{100}$ is measurable for the centre of the phantom as well as at least one of the peripheral positions (10mm below the surface) within the phantom. For slice thickness between 2mm and 10mm, $CTDI_{100}$ values are larger than CTDI values by factors between 2.6-1.0, respectively (McNitt-Gray, 2002).

3.2.3 Weighted CTDI ($CTDI_w$)

CTDIw was created to address the shortcoming of $CTDI_{100}$. While $CTDI_{100}$ is dependent on the position within the scan plane, $CTDI_w$ calculates the weighted average of the centre ($CTDI_{100}$) and peripheral (1 cm below the surface ($CTDI_{100,p}$) contributions to radiation dose within the scan plane. $CTDI_w$ estimates the average dose over a single slice for every nominal slice thickness setting, while assuming that dose in a particular phantom reduces linearly with radial position from the surface to the centre (Sookpeng et al., 2016). It can be assessed by **Equation 3-2** as shown below:

$$CTDI_W = \frac{1}{3} CTDI_{100,C} + \frac{2}{3} CTDI_{100,P} \quad \text{.....Equation (3-2)}$$

Where: **$CTDI_{100,C}$** = average of measurements at different locations around the central of the phantom

$CTDI_{100,p}$ = average of measurements at different locations around the periphery of the phantom.

3.2.4 Volumetric CT Dose Index ($CTDI_{VOL}$)

The $CTDI_{vol}$ describes the mean absorbed radiation dose over the x, y and z orientations (McCollough et al, 2008). In the past two decades, $CTDI_{vol}$ has increased by approximately 50% and 90% respectively for head and body phantoms, respectively (Elojeimy, Tipnis & Huda, 2010). For specific CT examinations, $CTDI_{vol}$ provides details of the radiation intensity

used. It differs by a factor of two for similar radiographic techniques, i.e. techniques with the same kVp and mAs. The differences in CTDI with identical radiographic techniques is caused by variations in x-ray tube designs and tube filtration (Huda & Mettler, 2011b). Altering kVp and/or mAs results in variations in CTDI. For example, a reduction in kV for abdominal CT scan from 140 to 120 could result in a 20%-40% decrease in the radiation dose to a patient. It can be calculated as $CTDI_{vol}$ through **Equation 3-3** as shown below:

$$CTDI_{vol} = \frac{CTDI_W}{pitch} \quad \text{.....Equation (3-3)}$$

3.2.5 Limitations of the CTDI

One of the limitations of CTDI is that measurements are obtained from a regular, homogenous, cylindrical phantom, which is dissimilar to the human body. It is thus questionable whether CTDI represents the radiation dose to the human body (Bauhs, Vrieze, Primak, Bruesewitz & McCollough, 2008). Another limitation is that it uses the radiation dose to air as an indication of the radiation dose to tissue (McCollough, 2008). Although there are techniques for approximating organ doses using various human dimensions, the body length of 14-cm represented by $CTDI_{100}$ phantom does not adequately compare with the length of the human torso (Boone, 2007). Furthermore, the 100-mm combination length may be inadequate for beam breadths over 10 mm, although Boone (2007) reported that the $CTDI_{100}$ measurement efficiency did not significantly change as the collimated x-ray beam width increased from 10mm to 40 mm (Boone, 2007). Finally, the radiation dose received by each patient is not quantifiable by $CTDI_{vol.}$ Rather it describes the intensity of radiation received by the patient. CTDIvol is fixed and not dependent on patient size or scan length (Laghi & Paolantonio, 2006).

3.2.6 Dose Length Product (DLP)

The DLP, measured in milligray-centimetres, is a measure of the total amount of radiation incident on a patient. It is calculated from the product of $CTDI_{vol}$ and scan length (cm). DLP reflects the total energy absorbed during a CT scan. Owing to the role of scan length on DLP, the DLP of a CT scan of the abdomen and pelvis is greater than the DLP of abdominal CT alone (McCollough et al., 2011). The DLP refers to radiation dose received by patient during an entire scan. It also gives some indication as to the possible biological effects of the radiation. The DLP is calculated based on scan length for CT scan examinations. For helical CT, data interpolation from two points must be carried out for all angles of projection. Therefore, the images at the start and end of a helical CT scan require data from x-axis throughout the scan

length (i.e. the start and end of the anatomic range over which images are required) (Smith, Dillon, Gould& Wintermark, 2007). For DLP measurements the milligray per centimetre (mGy x cm) is used as the physical unit see **Equation 3-4**

$$DLP(mGy\ x\ cm)(= CTDI_{vol(}(mGy) \times scanlength(cm) \text{ .....} \textbf{Equation (3-4)}$$

DLP allows estimation of the effective dose. Therefore, the ratio of effective dose to DLP can be utilised as a conversion factor for DLP to effective dose (Huda & Mettler, 2011b). The conversion factors (also known as k-factors) are only appropriate for specific scan types (e.g. abdominal or chest CT) in normal sized adult patients. For example, the conversion factors for head and body CT in a new-born have been reported to be approximately five-times higher than those for a normal-sized adult (Huda, Sterzik & Tipnis, 2009). Other factors such as phantom size, International Commission on Radiological Protection (ICRP) weighting factors, x-ray tube voltage and tube current can influence the conversion factor (Huda & Mettler, 2011b).

The conversion factor can also be highly variable for highly radiosensitive organs, such as the stomach, small intestine, breast, ovaries during different test locations under CT scan length. For example, a variability factor of up to 30 with the long-axis location (z-axis) of a patient has been reported. DLP data are quantified in a cylindrical phantom of either 16 cm or 32 cm diameter. Therefore, the DLP and the conversion factor must be based on data from the same phantom size (i.e. 16cm or 32 cm) (Huda, Ogden & Khorasani, 2008). This is because a reduction of phantom size by half from 32cm to 16 cm halves the conversion factor and doubles the DLP data.

3.3 Alternative CT scan dosimetry methods

Several CT based dosimetry methodologies have been suggested. The most frequently used methods for measuring and estimating patient radiation dose in diagnostic imaging include ionization chambers, thermoluminescent dosimeters (TLDs), metal-oxide semiconducting field effect transistors (MOSFETs), diodes, optically-stimulated luminescence (OSL) and Monte Carlo simulation ImPACT (Tootell, Szczepura, & Hogg, 2014a). In diagnostic imaging dosimetry, especially for in-phantom measurements, an ideal dosimeter, according to (Koivisto, Wolff, Kiljunen, Schulze & Kortesniemi, 2015), should have the following characteristics: -

- Similar effective atomic number to that of human tissue
- Uniform energy response
- Linear response to measured radiation doses
- High sensitivity
- Excellent reproducibility
- Small size
- In situ readability (real-time readings)
- Possibility of simultaneous measurement
- Low cost.

Not all dosimetry methods can satisfy all situations. The choice of the most suitable method depends on the clinical or research situation in which the measurements are required. The above methods are all suitable for the evaluation of dose distribution, effective dose, organ dose and effective risk in CT scanning (Lemoigne & Caner, 2011).

3.3.1 Metal Oxide Semiconductor Field Effect Transistor (MOSFET)

The use of MOSFETs as radiation dosimeters was proposed as far back as 1974. However, MOSFETs have only been applied within the past ten years as a clinical dosimeter. One of the main advantages of MOSFET is that they are capable of providing almost real-time dosimetry measurements. MOSFETs are able to measure cumulative radiation dose by relating the charge accumulated by the MOSFET sensors to the dose of radiation received.

A MOSFET dosimeter is made up of four levels, which are the source, drain, gate and body. The source and drain are separated by about 1µm, and metalised contacts are linked to the source as well as to the drain, which is normally made of aluminium. The remainder of the substrate area is encompassed by a thin oxide layer- usually around 0.05µm in thickness. The gate electrode is placed over the insulating oxide level and the body electrode is attached to this (Koivisto et al., 2015). The physical measurements of the detectors are 3 mm wide and 3 mm thick and they are enclosed within water to generate a layer similar to tissue surrounding the detector (**Figure 3-2)**.

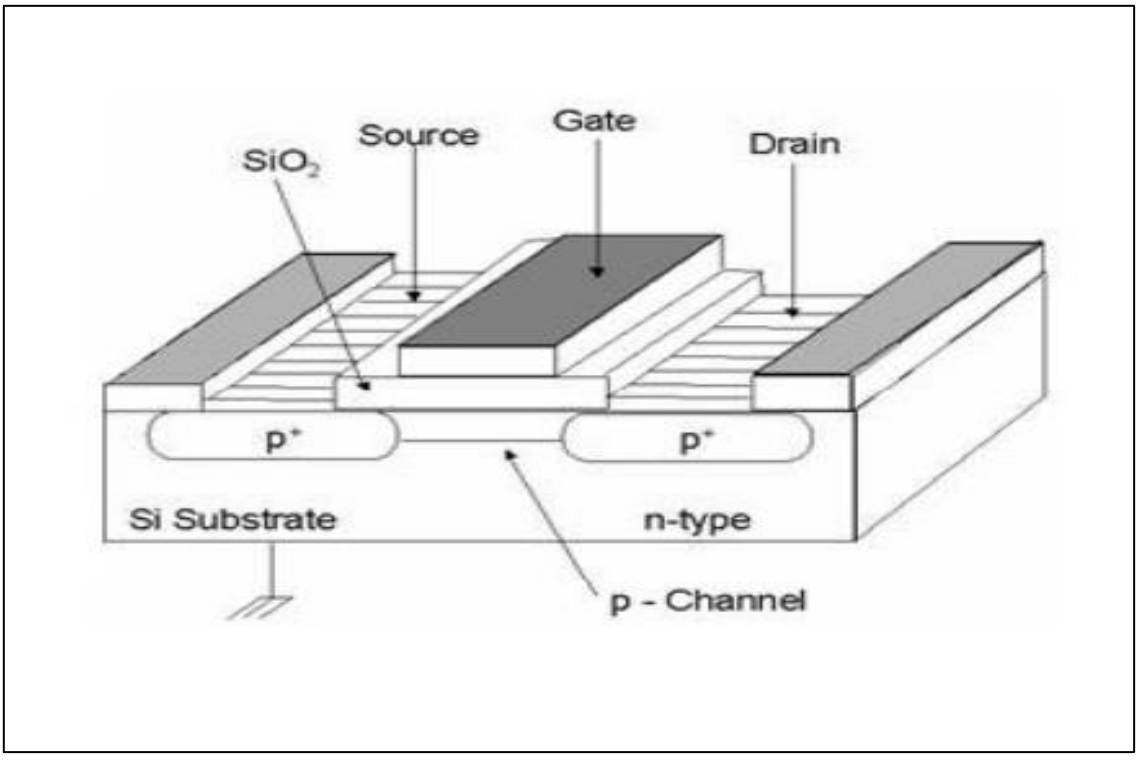

Figure 3- 2: Basic structure of a MOSFET dosimeter (Koivisto et al., 2015).

The types of MOSFET gate can be split into two categories, which depend on the polysilicon material used (N-type or P-type). Normally, the N-type trench power MOSFET comprises of a reduced gate resistance compared to P-type as a result of reduced sheet resistance from N type in situ doped polysilicon and more sensitivity **(Table 3-1)** (Baliga, 2010).

Table 3- 1:Main types of MOSFET are the N-channel and P-channel

PARAMETER	N-CHANNEL	P-CHANNEL
Source / drain material	N-Type	P-Type
Channel material	P-Type	N-Type
Threshold voltage V_{th}	negative	doping dependent
Substrate material	P-Type	P-Type
Inversion layer carriers	Electrons	Holes

3.3.1.1 Comparison between P- and N-channel MOSFETs

When employed as a high side switch, the source voltage from an N-channel MOSFET will be at a raised potential. Therefore, to move the charge from an N-channel MOSFET, a separate gate or a pulse converter must be employed. A power supply is required, while the transformer may at times generate different conditions. This is not true of the P-channel (Tamma, 2013; Pejović, 2016). For N-channel MOSFET it is simple to push a P-channel elevated side switch using a much uncomplicated level shifter circuit. Carrying this out eases the circuit and usually decreases the cost of the detector. The P-channel chip has to be 2 to 3 times bigger than the N-channel. Due to the greater chip size, the P-channel instrument will have a reduced thermal resistance and a raised current rating although its dynamic performance will be influenced in proportion to the chip size. Therefore, an appropriate P-channel MOSFET has to be chosen meticulously, accounting for the gate charge. There are benefits of using a P-channel MOSFETs, these include the use of low-voltage drives and non-isolated point of loads. These parameters become more important depending on the switching frequency (Tamma, 2013).

3.3.1.2 Principles of MOSFET

The main idea behind the operation of a MOSFET detector is the charging of the gate. The build-up of charge is produced by exposure to ionising radiation. If a MOSFET encounters ionising radiation, the formation of electron-hole pairs is brought about within the insulating layer of silicon dioxide. A number of the electrons will move towards the gate, and some will reintegrate with the holes. The holes that have not reintegrated with the electrons will flow towards the oxide-substrate interface, where a number of them will be held

The additional interface values will result in a shift in the negative voltage that has to be employed amid the source terminals and the gate to form the conducting channel, and to achieve the same current flow as before the irradiation, as seen in **Figure 3-3**. This difference in the threshold voltage (ΔVth), from before irradiation to after, ΔVth, is proportional to the quantity of the radiation dose supplied to the MOSFET (Koivisto, Kiljunen, Wolff & Kortesniemi, 2013).

The sensitivity of a MOSFET detector may be enhanced by raising the number of holes at the interface. This could be achieved through employing a positive gate bias during irradiation, which raises the amount of electrons gathered at the gate, reducing the quantity of recombination and thus raising the amount of positive holes remaining at the oxide-substrate interface. Furthermore, the constructive gate bias drives the holes in the direction of the oxide interface. An alternative technique is to reduce the breadth of the oxide layer, which raises the amount of electron-hole pairs formed within irradiation; this enhanced sensitivity reduces the life span of the detector (Manninen, Kotiaho, Nikkinen & Nieminen, 2015).

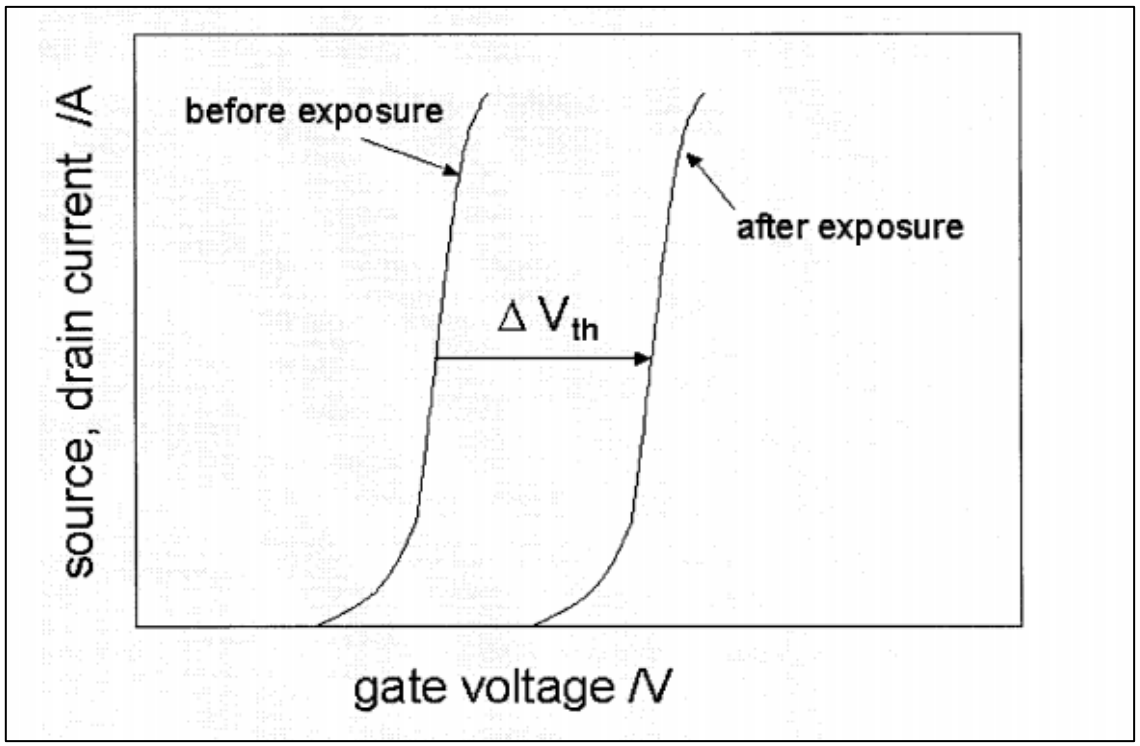

Figure 3- 3: Change in threshold voltage with exposure to radiation (Koivisto et al., 2013)

3.3.1.3 Advantages and disadvantages of MOSFET

Over the last few years some of the current dosimetry technology has been subjected to evaluation with regard to their verification and application. This work includes the evaluation of MOSFETS using tissue-equivalent adult anthropomorphic phantoms. In brief, organ doses provided by MOSFET technology may be implemented to establish an effective dose assessment for CT scanning of the abdomen. MOSFETs are suitable for *in vivo* measurements so that they can be used with phantoms to measure the radiation dose at different organ / tissue depths during abdominal CT scanning. In this application, MOSFET technology is said to be precise and reliable in comparison to alternative methods used in CT (Trattner et al., 2014). The benefit of the MOSFET technology is that it permits a real-time dose analysis; data are conveyed automatically to a laptop computer (Frush & Yoshizumi, 2006).

MOSFET dosimeters comprise several relevant practical features including excellent linearity and reproducibility which make it a good candidate for CT dosimetry use within the dose range to be analysed. In addition, the higher radiation doses responsd to MOSFET dosimetry because MOSFET high sensitivity for over wide range dose. Generally, the average sensitivity value of 29.2 mV/Gy is less than 1% for individual sensor calibration or around 5% for collective sensor calibration (Koivisto et al., 2015). An advantage of MOSFET is that they may be read directly after exposure, and, unlike TLDs, there is no requirement for annealing or any kind of post-processing following exposure and reading. Furthermore, the dose data history is maintained within the dosimeter as a result of the accumulation of the charge (Ali, Alrowily, Benhalim, & Tootell, 2016a). MOSFETs is a high input resistance, voltage controlled, simple to use, single polar device majority carrier. It is also a fast switching and voltage decrease comprising constructive temperature coefficient, and is simple to employ in parallel with radiation dose (Zhao, Zhang, Zhou, Li & Wang, 2015).

The main drawback, however, with MOSFET is the lack of uniformity in reaction to different energies. This is often seen with other dosimeters as well. Other disadvantages include their higher atomic number than human tissue, notable angular reliance, and elevated saturation voltage- usually above 20,000mV. Also, MOSFET dosimeters should always be calibrated in the clinical settings for the beam geometry (Koivisto, Schulze, Wolff & Rottke, 2014)
Many studies have used MOSFET for radiation dose measurement during CT scan dosimetry analyses. Table **3-2** shows a summary of some studies which have used MOSFET for measurement radiation dose for CT studies.

Table 3- 2:summary of studies using MOSFET for measuring radiation dose during CT scan examinations (2009 -2017)

Author	Year	CT scan examinations	Radiation dose measurement method	Finding
Sharma et al	**2012**	Phantom study (head)	MOSFET dosimeters	The MOSFET dosimeter can be a suitable choice for routine dose verification.
Kim et all	**2009**	5-y-old paediatric anthropomorphic phantom (abdomen)	Monte Carlo and MOSFET	The radiation dos (effective dos and organ dose) from Monte Carlo simulations were comparable to the MOSFET measurements and easily applied to CT scan dosimetry
Kumar et al	**2015**	Phantom study	MOSFET dosimeters	The response of the MOSFET dosimeter for radiation dose at 3 cm depth in tissue equivalent phantom.
Kaasalainen et al	**2015**	Phantom study	MOSFET dosimeters and simulations to estimate organ and effective doses	The simulations method supported the findings with MOSFET measurements radiation dose.
Koivisto et al	**2013**	PMMA phantom	MOSFET dosimeters	MOSFET dosimeters always be calibrated in the clinical settings for the beam geometry
Mattison et al	**2016**	Phantom study (abdomen/pelvis)	MOSFET dosimeters	The effective dose for the abdomen/pelvis CT scans were with MOSFET and DLP method no statistically significant difference.

Kelaranta et all	**2017**	Adult female anthropomorphic phantom	Monte Carlo simulations and MOSFET dosimeter	Monte Carlo simulations showed good correlation with the MOSFET measurement at the measured radiation dose different locations in CT abdomen-pelvis scan

3.3.2 Thermoluminescent dosimeters (TLDs)

Since 1954, when Daniels first proposed the application of thermoluminescent phosphors within patient dosimetry (*in vivo* dosimetry), the use of TLDs for measuring radiation dose has successfully been carried out on many occasions. Within *in vivo* dosimetry (where dose measurement is performed immediately within anthropomorphic phantoms or on the patient's body), the dose received by the patient during diagnostic radiology (or radiotherapy) is assessed either through measurement of entrance dose, measurement of exit dose, intra cavity dose measurement or measurement of organ dose (Puchalska & Bilski, 2008).

TLDs are employed broadly in space dosimetry due to their small size, lack of power supply requirements and their not being affected by any environmental conditions. TLDs are available in circular rods, chips, square rods, disks and powder form. Lithium Fluoride is the most commonly used material used in TLD (100) chips, these are doped with magnesium (Mg) and titanium (Ti) (LiF: Mg, Ti). This type of TLD can measure radiation doses at wide ranges from 10 µGy to 10 Gy and they have a linear response from 0.1 mGy to 10 mGy. TLD 100H (LiF: Mg, Ti) chips have a higher sensitivity than TLD100 chips and can measure radiation doses of 1µGy to 20 Gy. The thermal fading of TLD 100H is negligible- about 3% per year. TLDs provide the opportunity to determine the radiation received, this is normally achieved by employing the high thermal range (HTR) and a high-temperature peak ratio technique or the ratio of reactions of various kinds of TLDs. The result from the HTR technique is reliant on the LET (linear energy transfer) as well as on the ion species depositing its energy within the TLD crystal (Berger, Reitz, Hajek & Vana, 2006).

Overall, a number of features are necessary for optimum TLDs: linearity, referring to the linear reaction with absorbed dose covering a broad energy range; sensitivity, the quantity of light generated for every unit of dose absorbed; independence of energy autonomy from radiation

energy; satisfactory mechanical stability and fixed chemical method; and reduced charge fading (Rottke, Grossekettler, Sawada, Poxleitner & Schulze, 2013). Due to their appropriate dosimetric features, TLDs are employed in many clinical and research applications. Within medicine, TLDs are implemented in various areas. For diagnostic radiology, for instance, TLDs are used to assess the radiation dose in general X-ray examinations, CT scans, positron emission tomography (PET) and nuclear medicine (Rottke et al., 2013).

3.3.2.1 Principles of TLDs

TLDs are constructed from various crystal substances which exhibit thermoluminescence properties when they encounter radiation. The TLD crystal absorbs a portion of the incident radiation energy and maintains it within its lattice; if the crystal is subsequently heated then part of this energy may be emitted as visible light. The TLD quantifies the radiation dose from exposure to ionising radiation in relation to the light concentration discharged by the detector's crystal when heated. Two types of TLD substances are common - calcium fluoride and lithium fluoride; several impurities are used to generate trap states for energetic electrons (Rottke et al., 2013). When the TLD crystal is exposed to radiation, some atomic electrons jump into higher energy levels, in which they remain trapped. As a result of heating, these electrons fall back to their ground condition, emitting a photon of energy equivalent to the energy difference between the trap state and the ground state as demonstrated by **Figure 3-4.** Additionally, the electrons may drop back to their ground condition following an extended time period due to an effect known as fading. This is reliant on the incident radiation energy as well as innate features of the TLD material (Koivisto et al., 2014).

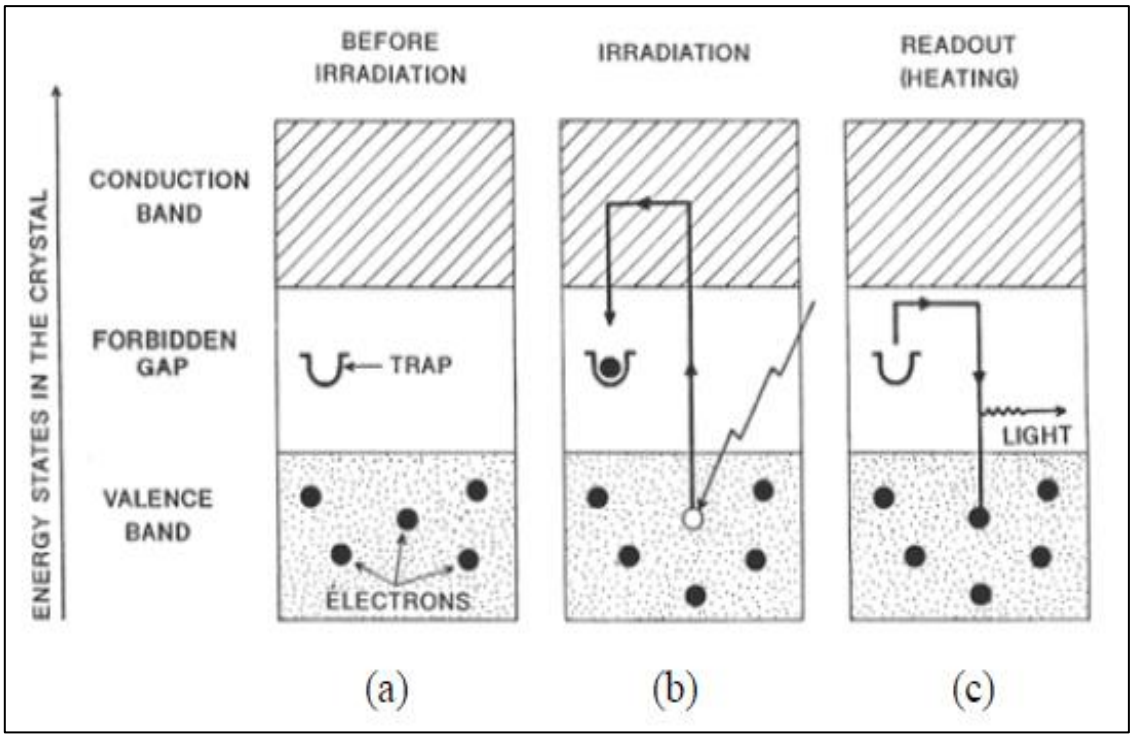

Figure 3- 4: Schematic diagram illustrating the TL process (Koivisto et al., 2014)

3.3.2.2 Advantages and disadvantages of (TLDs)

TLDs have many benefits and disadvantages. The key benefit of TLDs is their reliability and accuracy. The small physical dimensions, the availability in various forms as well as their tissue equivalency render TLDs appropriate for *in vivo* dose analysis. Accordingly, they may be employed with phantoms to quantify the dose of radiation in various organs. Furthermore, TLDs are easy to use but must be handled carefully in order to avoid contamination. A further significant feature of TLD detectors is that they are independent of radiation direction within their efficiency and as a result the back scatter is encompassed within their readings (Rottke et al., 2013). In spite of the previously stated benefits, there are many disadvantages of the TLDs. Primarily, they cannot provide immediate measurements due to the protracted procedures of readout and calibration. Secondly, TLDs only permit one time reading within heating as the signal is erased within the readout process. Thirdly, the storage signal may diminish over time as a result of the impact of light or temperature in some kinds of TLDs (Bostani et al., 2015). However, many studies have used TLDs for radiation dose measurement during CT scan examination. **Table 3-3** shows a summary of some studies which have used TLDs for measurement radiation dose for CT studies

Table 3- 3:summary of studies using TLDs for measuring radiation dose for CT scan examinations (2007 -2015)

Author	Year	CT scan examinations	Radiation dose measurement method	Finding
Bostani et al	**2015**	Patients study	TLD dosimeters and Monte Carlo simulation	The radiation dose very good agreement between simulated method and TLD method undergoing CT examinations
Yoshizumi et al	**2007**	Phantom study 20 organ locations	TLD and MOSFET dosimeters	The good agreement between the results with the MOSFET and TLD methods for CT organ dose easily applied to CT scan dosimetry
Gardner et al	**2012**	Animal models	TLD and MOSFET dosimeters	The radiation dose measured on the with TLDs averaged 5% less than the MOSFET
Koivisto et al	**2014**	Phantom study	TLD and MOSFET dosimeters	The effective doses using MOSFET dosimeters the good agreement with using TLD

3.3.3 Optically Simulated Luminescence Dosimeters (OSLD)

The development of OSLDs occurred during the late 1990s. The operating procedure for these dosimeters is comparable to TLDs, as the luminescence procedure is prompted by a laser light beam as opposed to heat. These detectors are constructed of aluminium oxide ($A1_2O_3$) which discharge visible light. The quantity of light discharged is in proportion to the radiation dose taken up by the detector. For the purposes of occupational radiation observation, the OSLD is preferable to TLDs (Bushong, 2013; Zhang et al, 2013b).

An advantage of OSLD is that it does not have to be totally discharged to obtain a significant signal. Furthermore, it gives one the choice of reading and retaining the data for future analysis. The signal decay is stable for up to 2.5 days however stability of up to 100 days has even been reported. In order to avoid the wait time that is required before reading the OSLD, it is expected that the future design of readers could incorporate a low-intensity, red light pre-read cycle that could optically empty the low-level traps and not deplete the higher energy dosimetric traps (Jursinic, 2007). Compared with TLD, OSLD does not require carefully controlled temperature changes to read; hence, thermal annealing is less complicated. However, TLDs have an advantage of several years of proven utilisation for *in vivo* dosimetry (Jursinic, 2007). Kadir et al, (2013) showed that the OSLD yielded a better high-energy response performance compared with the TLD -100H dosimeter. However, for low-energy response, OSLD was seen to be less superior than the TLD-100H (Kadir, Priharti, Samat, & Dolah, 2013).

3.3.4 Dose Modelling in CT

The Monte Carlo simulation survey was first performed in 1989. The National Radiological Protection Board (NRPB), a UK public authority on x-ray spectra within a regular adult hermaphrodite mathematical phantom, used CT (ImPACT Scan Working Group, 2013) to establish the CTDOSE group, employing 23 sets of data using NRPB SR-250 for CT scanners available at that point in time. The SR-250 data offers regularized organ doses for different CT scanners generated from a mathematical phantom (**Figure 3-5).**

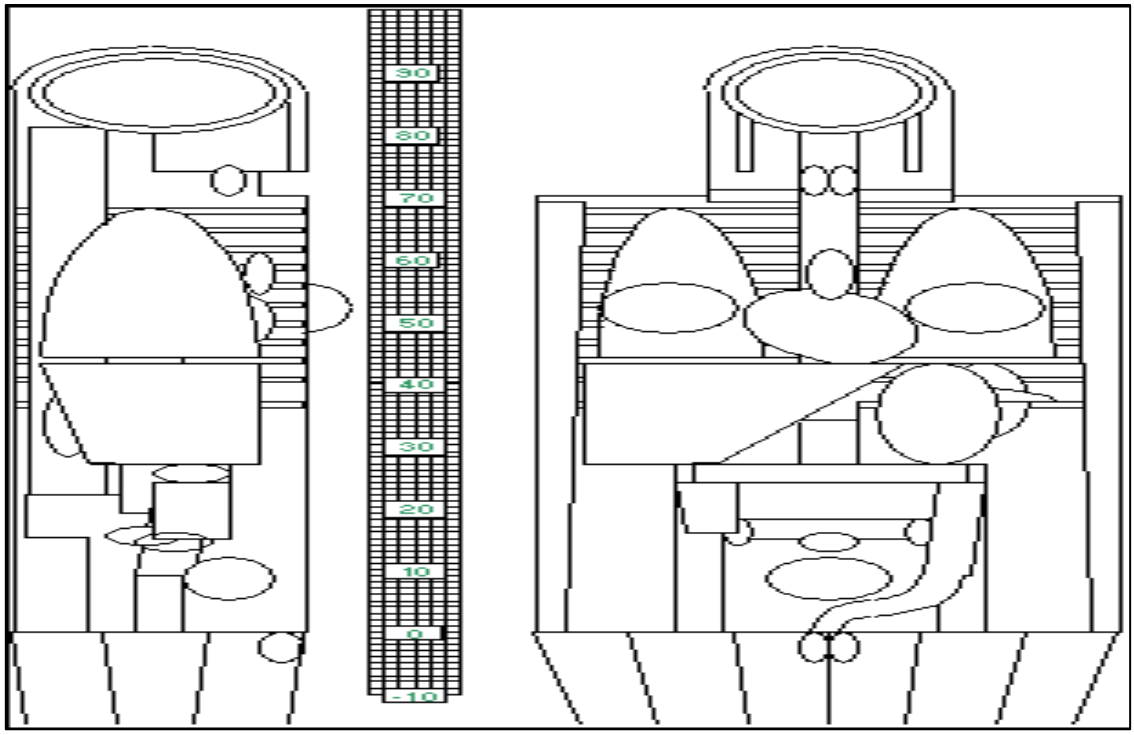

Figure 3- 5: Schematic diagram illustrating the NRPB mathematical CT phantom (ImPACT Scan Working Group, 2013)

The key challenge in employing these data sets is that they were last updated in 1993, which only encompassed CT scanners employing axial scanning as well as non-angled gantries. They are specific for helical CT scan. Therefore, the NRPB established a procedure to match contemporary scanners with the previous NRPB data sets. These novel downloadable datasets may be acquired from NRPB and employed using the free software - ImPACT CT Patient Dosimetry Calculator (available on their website). The user enters the CT machine model and manufacturer, beam energy, tube current, pitch, anatomical scan region and the scan length. The program outputs scan dosimetry estimates: CTDIVOL, (DLP) (Huda et al, 2008), and organ absorbed doses and effective dose shown in **Figure 3-6.**

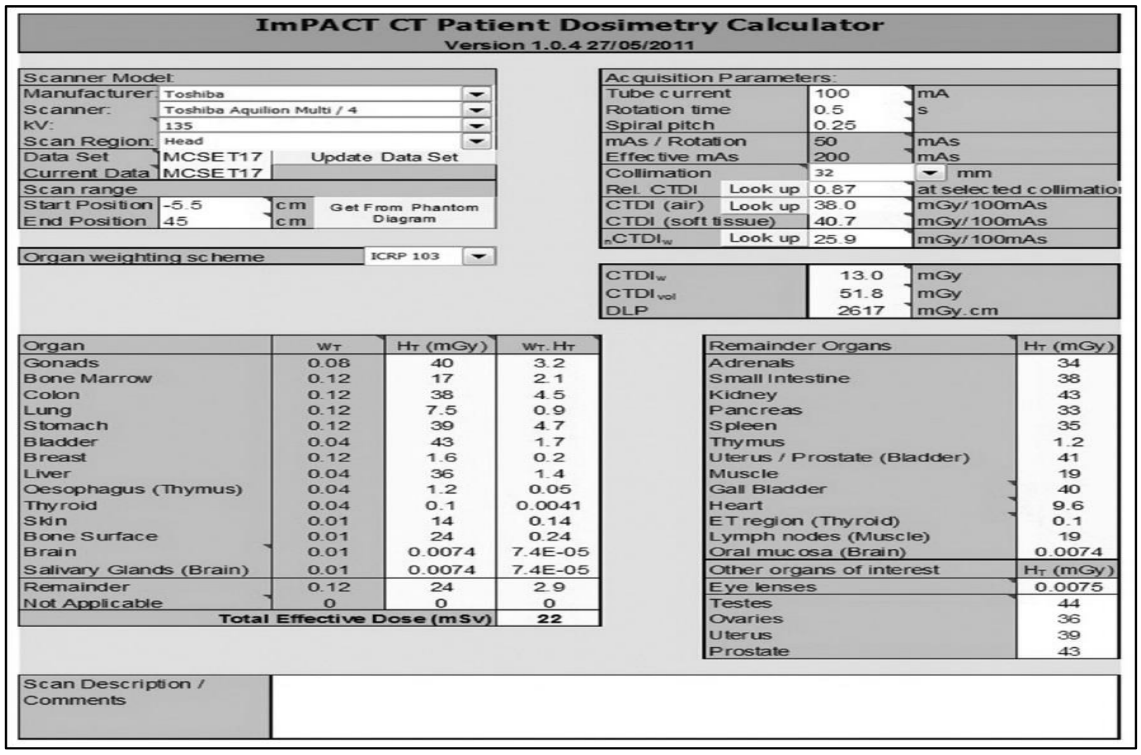

Figure 3- 6: Schematic diagram illustrating the ImPACT CT patient dosimetry calculator input parameters and output data

A restriction of the ImPACT spreadsheet is that it does not consider whether patient size differs from the mathematical phantom. This limitation is not actually a challenge for effective dose estimates, as effective dose is only relevant for a population of average size. However, organ doses differ greatly due to changes in the ImPACT phantom size. Thus, alterations have to be proposed to the ImPACT organ doses in order to employ them for dosimetry use. The ImPACT method for estimation is produced from radiation dose, underestimating CT doses in the range of between 18 and 40% with comparisons between other simulation dosimetry methods (Tootell, et al., 2014). The geometrical limitation of human body mathematical phantoms using Monte Carlo simulation is another cause. The resultant organ dose overestimation by Monte Carlo is due to the geometrical limitation of the mathematical phantom.

Many studies used ImPACT for radiation dose estimation in CT. **Table 3-4** shows a summary of some studies that have used ImPACT for estimating radiation dose in CT studies

Table 3- 4: Summary of studies using ImPACT simulation for estimating radiation dose for CT scan examinations.

Author	Year	CT scan examinations	Radiation dose estimation method	Finding
Bahadori et al	**2015**	organ doses from DICOM data	Monte Carlo simulations	The Monte Carlo method radiation dose calculation using patient specific anatomies from CT images may provide more accurate and reduces the time for a large number of patients.
Gu et al	**2012**	Phantom study	Monte Carlo simulations (ImPACT)	ImPACT improve the accuracy of CT radiation dose calculation for pregnant patients
Zhang et al	**2013b**	Phantom study	Monte Carlo simulations (ImPACT)	The ImPACT tool also overestimated radiation dose to eye lenses and still useful dose for CT neuroperfusion studies.
Matsunaga et al	**2017**	Phantom study	Monte Carlo simulations (ImPACT) and TLD	The difference in the radiation doses between the TLD measurement and simulation software estimation was 23 % in CT scan examinations

3.4 Radiation dose from Computed Tomography

The clinical use of CT scanning has increased rapidly over the last 30 years. Data from the last UK survey of radiation doses to patients highlighted than CT scan examinations made up 60% of the collective radiation dose from medical diagnostic exposures (Hart, Wall, Hillier & Shrimpton, 2010). Detrimental effects of ionizing radiation are a cause for concern in medical imaging (Desouky, Ding, & Zhou, 2015). Radiation dose from CT scans have been known to have adverse population health effects (Brenner, 2010; Kim et al., 2009; Hall & Brenner, 2008). Therefore, it is important to quantify the radiation dose from CT examinations. The radiation dose to a patient can be defined as the amount of energy absorbed in the body from radiation interactions. The radiation dose in CT does have a dependence on the type of acquisition techniques used (e.g. FTC and ATCM) and the variations in MDCT geometry and filtration. Because of large doses from CT examinations, manufacturers, radiologists, radiographers and physicists have been invited to collaborate in order to find mechanisms to decrease patient dose in accordance with the ALARA principle.

ATCM has been identified by ICRP as one method that could reduce the radiation dose from CT examinations (ICRP 2007). However, to fully understand the impact of ATCM and the possibility of reducing radiation dose to patients when compared with FTC, detailed investigations are necessary.

3.4.1 Absorbed Dose (D)

Absorbed dose (D) is also referred to as the organ dose and is the energy deposited for each unit mass of substance (measured in Grays or rads). One Gray is equal to one joule of energy absorbed for every kilogram of substance (joule per kilogram); 100 rad = 1 Gray. Absorbed dose does not describe where the specific radiation dose is absorbed nor to which tissue type. When X-rays pass through the human body they lose energy. Different organs and soft tissues will absorb different amounts of energy depending on their tissue types and location. For example, the tissues closer to the surface will have a higher dose absorbed than deeper tissues (ICRP, 2007).

The organ or tissue absorbed doses are the most relevant metrics for assessing radiation exposure. Absorbed dose can be determined experimentally by utilising direct dosimeters (e.g. TLD / MOSFET) placed in a phantom that has a similar shape and size to the human body. In addition to the similarity in physical characteristics, the dosimetry phantom will also have equivalent tissue properties to the human body (Simkó, Nosske, & Kreyling, 2014). **Table 3-5 shows** a summary of some studies that have used a range of methods for the measurement and estimation of organ dose in CT.

Table 3- 5:Summary of some studies which have used measurement and estimation of organ dose in CT

Author	Year	CT scan examinations	Organs dose estimation method	Finding
Kost et al	**2015**	40 patients chest-abdomen-pelvis	Monte Carlo simulation model	The Monte Carlo simulation model agree method for patient organs dose estimation
Lechel et al	**2009**	Phantom study	Monte Carlo simulations CT-EXPO and TLD	The both methods product provide reliable measurement and estimates of the organs dose
Lee et al	**2011a**	Phantom study	Monte Carlo simulations	The organs dose estimation method readily provides organ doses for a reference adult

				male and female for different CT scan
Hurwitz et al	**2007a**	Phantom study	MOSFET	Organ doses measurement from MOSFET method total body higher than for MDCT clinical body imaging protocols.
Hoang et al	**2012**	Phantom study	MOSFET	The organ dose from MOSFET method based CT scan modulation educe the thyroid organ dose
Koivisto et al	**2012**	Phantom study neck	MOSFET and Monte Carlo simulations	The MOSFET dosimeter head phantom gave results similar organs dose to Monte Carlo simulations. MOSFET dosimeters constitute a feasible method for dose assessment of CT scan examinations

In the literature, there are only a small number of studies providing information on organ and tissue absorbed doses for general CT examinations (Angel et al., 2009; Kost et al., 2015; Brenner & Hall, 2007; Hoang, et al., 2012; Kawaguchi et al., 2014). According to research conducted by Padole et al., (2016) they discussed various abdominal organ dose methods for comparing FTC and ATCM in abdominal CT examinations. They compared radiation dose-tracking (RDT) software to directly measure organ dose. The results demonstrated that most CT organ dose estimates using the simulation software were higher compared to ionization chamber directly measured doses using the ATCM technique. This is because a geometric software effect occurs when the angular dose profile is adapted to the slice profile during angular ATCM. Therefore, the measurement of organ doses may not be adequate to describe the effect of ATCM when compared with FTC. However, TLD or MOSFET provide a more adequate way to compare between FTC and ATCM.

A study conducted by Sabarudin, Mustafa, Nassir, Hamid & Sun, (2014) compared the radiation dose in thoracic and abdomen–pelvic CT scans, with and without use of tube current modulation (ATCM), on phantoms. The absorbed doses were measured in selective radiosensitive organs using TLDs for ATCM and an FTC of 300 mA. The results showed reduction in organ dose when using ATCM. However, no study has measured the specific abdominal organ dose to compare between FTC and ATCM techniques by direct dosimetry using MOSFET dosimeters. One of the aims of this thesis is, therefore, to measure and compare the 'main' abdominal organ doses in order to compare between FTC and ATCM.

3.4.2 Effective dose (ED)

Effective dose (ED) is a concept reflecting the stochastic risk, such as cancer or genetic defect induction that may occur as result of radiation exposure (Christner et al., 2010). Cancer induction risk from an equivalent dose depends on the irradiated organ; therefore, effective dose is a measure that allows for a comparison of the risks when different organs are irradiated. It designed to compare the risks of exposure to different fields of radiation. It is a weighted average of organ doses. It considers the entire quantity of the absorbed dose provided and averages these amounts to provide an entire body effective dose (Brenner, 2012). Unlike absorbed dose, it takes into account the location of the absorbed radiation dose and reflects the absorption of non-uniform radiation from partial body exposure relative to the whole-body radiation dose exposure (Brenner, 2012). It also reflects estimates of individual or collective patient risk and biological effects (McCollough et al., 2009). ED takes into consideration not only the nature of the incoming radiation but also the sensitivities of the body organs affected to provide a dose relevant for the entire body (Costa, Yoshimura, Nersissian & Melo, 2016). Patient factors such as body mass, abdominal circumference and body mass index influence the effective dose to the abdomen (Rodrigues, Abrantes, Ribeiro, & Almeida, 2012). In addition, radiation dose to abdominal organs can also affected by obesity because of the greater absorption of radiation dose by the subcutaneous and visceral fat (Schindera et al., 2007).

The unit used for reporting the effective dose is the Sievert (Sv) or Millisievert (mSv) (Sabarudin et al., 2013). The effective dose can be calculated using the following **Equation 3-5**.

$$\text{Effective Dose } (ED) = \sum W_T \times H_T \quad \text{.....Equation (3-5)}$$

Where: **ED** = is the effective radiation dose

W_T = is the tissue weighting factor for tissue, as seen in **Table 3-6** (ICRP, 2007).

H_T = is the absorbed dose of tissue T

Table 3- 6:Tissue weighting factors according to ICRP 103 (ICRP 2007)

Tissue	Tissue weighting factor wT
Bone-marrow	0.12
colon	0.12
lung	0.12
stomach	0.12
breast	0.12
remaining tissues	0.12
Gonads	0.08
Bladder	0.04
Oesophagus	0.04
liver	0.04
thyroid	0.04
Bone surface	0.01
Brain	0.01
Salivary glands	0.01
Skin	0.01

Effective dose not merely signify quantification of a radiation dose. It comprises an average in radiation detriment spanning age and gender and is usually articulated even though there are several restrictions to its employment; the quantification of effective dose facilitates the contrasting of risks related to various imaging techniques (Tootell, Szczepura & Hogg, 2014b). Two widespread techniques are employed in the quantification of effective dose for a CT scan. One technique is by direct measurement of organ dose elements of tissue-weighting, employing an anthropomorphic phantom and dosimeters, for instance TLD and MOSFET. The second is indirect measurement or mathematical estimation and includes the use of the Monte Carlo simulation, for instance DLP combined with k factors (McCollough, Christner & Kofler, 2010).

3.4.2.1 Direct effective dose calculations using organ dose measurements and tissue-weighting factors

This technique involves the quantification of organ doses using dosimeters such as MOSFETs or TLDs. After the organ doses have been estimated, ED is calculated using the ICRP 60 or 103 tissue-weighting factors. These are the two versions of the relative radiation sensitivities of different organs recommended by the International Commission on Radiation Protection (ICRP). ICRP 60 was recommended in 1991 and ICRP 103 more recently in 2007. Differences in ICRP tissue-weighting factors (wT) result in differences in the radiation doses calculated for CT examinations on the same patient (Christner et al., 2010). Christner et al. (2010) reported a 7% difference between the effective dose calculated for abdominal and pelvic CT examinations using organ dose estimates and ICRP 103 tissue-weighting factors and ICRP 60 values. A much higher percentage difference (39%) has been reported for head CT examinations in the same study. For example, Huda and colleagues (2011a) showed that using the ICRP 103 instead of ICRP 60 weighting factors increases the effective doses for head, chest and pelvic CT scans by approximately 11%, 20% and 25% respectively. Hence, when a value of ED is reported, it is important to also report the relevant ICRP article used in the calculation (e.g. ICRP 60 or ICRP 103).

The quantification of organ dose requires the use of physical dosimetry phantoms, such as the CIRS ATOM phantom. The weighted equivalent doses for every tissue and organ are added together to obtain an estimate of the ED (McCollough et al., 2009). The numerical values of wT are selected based on epidemiological data on radiation detriments. This will account for the variation in the sensitivity to radiation (ICRP, 2007). Phantoms are utilised for scanning in order to generate results that are similar to real patients. The dosimeters are placed inside pre-cut holes within each phantom at measurement locations representing different organs. An ideal phantom should:

Be similar in size to real patients and should also have similarly sized organs and anatomic structures to real patients. Owing to the differences between patients, the phantoms are modelled to match reference percentile values for each body organ based on the ICRP 103. (Zhang et al., 2013a).

Constructed using tissue-equivalent materials. Most phantoms comprise of three tissue equivalent materials: soft tissue, lung and bone equivalent (Hyer, Fisher & Hintenlang, 2009). The direct measurement and quantification of effective dose requires enormous resources including trained staff, equipment and time, thus they are difficult to implement in clinical

radiology departments (Brady et al., 2013). In order to avoid these challenges, indirect or computational methods provide a suitable alternative.

Within this thesis, the selections of direct measurement radiation dose by MOSFETs for abdominal organ dose estimations were based on the human tissue equivalency of the MOSFETs. This was done due to their high sensitivity; their suitability for high dose measurement in abdominal CT scanning; and that a large number of them can be used for dose measurement in different body organs at the same time. However, the main disadvantages of using MOSFETs include that they have a saturation voltage at 200V and are associated with small percent of error and a constantly changing calibration factor, which requires repeated calibration (Trattner et al., 2014). In addition, MOSFET dosimetry can used for different protocol development in the MDCT scanner examinations (Yoshizumi et al., 2007).

3.4.2.2 Indirect estimates of effective dose using DLP and k coefficients

The DLP has already been discussed in this **Chapter 3, Section 3.2.6**. Typically, the irradiation length is increased by about one and half times the total nominal beam width. These values vary according to the model of the scanner, the manufacturer and the image quality required. It is worth noting that changing the technique (mAs/rotation) alters the CTDIvol and consequently the DLP. Altering the acquisition length (using the same technique) is also reflected in the DLP (McCollough et al., 2008).

DLP is one of the two measures of CT radiation dose that are available on CT consoles. It is the product of the CTDIvol and the scan length. The scan length is the product of the slice thickness and the number of slices, in centimetres. It varies along with the desired image quality and type of scanner. It can also vary as result of differences in technique. Such differences include a variation in the patient thickness and scan parameters like kVp and mAs (Christner et al., 2010).

ED from the CT machine can be calculated using DLP. It is the product of the DLP (mGy.cm) and specific conversion coefficients (K factors) (mSv mGy-1 cm-1) see **Equation 3-6** below.

$$\text{Effective Dose } (ED) = K \times DLP \quad \text{.....Equation (3-6)}$$

Where the values of "k" are dependent only on the region of the body, being scanned (head, neck, chest, abdomen, and pelvis**. (Table 3-7).** (Christner et al., 2010)

Table 3- 7:Conversion coefficients (K- factors) for adults patients (Christner et al., 2010 from ICRP 103 ,2007)	
Region of body	**Normalised effective dose, EDLP (mSv $mGy^{-1}cm^{-1}$)**
Head	0.0023
Neck	0.0054
Chest	0.017
Abdomen	0.015
Pelvis	0.019

Some have criticised the use of k coefficents because they are based on old technology and old data (Christner et al., 2010). They are generally based on data from scanners that were in use around the 1990s. The K- factors for adult patients used in the calculation also updated from ICRP 60. This method is also limited by the possibility of underestimating the CT dose due to the differences in beam geometry between physical phantoms and the computer simulation software. The use of computer software relies on the use of correct CT units and the calculations based on the properties of each unit such as the radiation quality and field geometry (Tootell, Szczepura, & Hogg, 2013).

Groves at al., 2004 demonstrated a marked difference between effective dose measured by computer simulation and TLDs. For various organs, differences in measurements ranged between 20% for the bladder and 100% for the skin. For all organs, effective dose was higher for TLD than simulated by computer software. The difference between the mean effective dose obtained using both methods was 18% **(Table 3-8).** Because, the geometrical limitation of human body mathematical phantoms using Monte Carlo simulations organ dose was overestimated by Monte Carlo compared to the measured (TLD) dose, due to the geometrical limitation of the mathematical phantom, has previously been reported by Tootell et al (2014a)

Table 3- 8:Comparison of weighted organ doses and effective doses using both TLD and computer simulations (Groves ,et al. 2004)

Organ	Computer simulation (mGy)	TLD measurements (mGy)	Percentage difference %
Gonad	3.6	5.3	47
Bone marrow	1.8	2.2	22
Colon	2	2.5	25
Lung	1.7	2.3	35
Stomach	2.3	2.9	26
Bladder	1	1.2	20
Breast	0.4	0.7	75
Liver	0.9	1.3	44
Skin	0.1	0.2	100
Effective dose mSv	18.8	22.2	15.3

DLP cannot provide a true estimate of effective dose or detrimental cancer risk to individual patients, because the k coefficients are for standard sized patients (Brenner, 2008). The accuracy of such ED calculations are also limited when applied to individual patients because the weighting factors utilised are from population averages and do not reflect the known dependence of radiation sensitivity on a patient's age or gender (Sodickson, 2012). Another limitation is the possibility of underestimating effective dose for helical scanning. This may result from the typical scan length exceeding the prescribed scan length, however this is not reflected in the calculations (McCollough et al., 2009). Tootell et al., (2014b) compared effective dose estimates, obtained by DLP and TLD (EDLP and ETLD) and showed significant differences between the two methods. Most modern CT scanners calculate and display the values of DLP, with a scan range less than 100mm.

Many studies have evaluated image quality for different radiation doses using the TLD method Tootell et al., (2014a) & Hurwitz et al., (2007b). In a study by Tootell et al. (2014a), the organ doses were measured and effective dose calculated by TLDs and DLP from CT attenuation correction (CTAC) acquisitions. A Hurwitz et al., 2007 study evaluated four commonly used gamma camera single photon emission SPECT/CT systems. The dosimetry data from various manufacturers included GE Healthcare's Infinia™ Hawkeye™ (GE Healthcare, Buckinghamshire, UK) -four and single-slice systems, Siemens Symbia™ T6 (Siemens Health- care, Erlangen, Germany) and the Philips Precedence (Philips Healthcare, Amsterdam, Netherlands), as shown in **Table 3-9**. Large differences in effective dose using TLD and DLP can be seen, and range between 13% and 85% across different CT scan manufacturers.

Table 3- 9:Effective dose using DLP CT- chest k conversion Coefficient, mSv .mGy 21cm where k 0.017.(Hurwitz et al., 2007b)			
Manufacturers	**Calculated effective dose (E/DLP) (mSv)**	**Measured effective dose (E/TLD) (mSv)**	**Percentage difference (%)**
GE (single slice)	0.83	1	13.5
GE (four slice)	0.78	1.2	46.3
Siemens Symbia	0.36	0.9	85.7
Philips Precedence	0.71	1.5	71.5

A study by Tyan, Tsai, Hung, Lia, & Chen, (2008), which evaluated radiation doses using TLDs within an anthropomorphic phantom, reported variations in effective dose using ATCM. Their study showed that in-plane dose varied between 16.8 and 50.5 mSv, while out-of-plane surface doses were 1.1-8.0 mSv and 1.4-9.6 mSv. Aldrich et al. (2006) reported institutional variations in CT dose. Abdominal CT doses from 18 Canadian radiology departments (using the DLP method) varied between 3.6 and 25.6mSv (mean=10.1), while abdominal-pelvic CT varied between 7.3 and 31.5mSv (mean=16.3mSv).

Other studies have also estimated differences in radiation dose using the DLP (Su et al., 2010, Lee et al., 2009, Lee et al., 2011b; Rizzo et al., 2006). However, a systematic review by Dougeni et al. (2012) showed that most of the mean ED from several published studies were below the European (EU) diagnostic reference values. The report considered effective dose within regular CT scan assessments in adults as well as paediatric patients. The differences are associated with the selected length of the area requiring scanning, tube rotation velocity, helical pitch, collimation, patient weight as well as filtration (Dougeni et al., , 2010; Sodickson, 2012). The values of effective dose for adult abdominal scans acquired from different dosimetry measurements and estimation methods are described within **Table 3-10.**

Table 3- 10:Effective doses from CT scanning in adults for abdomen showing different dosimetry methods that have been used (review period 2003-2017)		
Reference(CT abdomen)	**Effective dos mSv/scan or patients**	**ED dosimeter method**
Papadimitriou et al. 2003	6.4–14.8	DLP- k
Heggie 2005	3.6- 13.3	DLP- k
Moss and McLean 2006	7.7–13.3	DLP- k
Origgi et al. 2006	2.4–21.2	DLP- k
Ngaile et al. 2006	15.3	DLP- k
Shrimpton et al. 2006	5.3	DLP- k
Fujii et al 2007	7.6–18	DLP- k
Tyan et al 2008	20.6–34.6	DLP- k
Fujii et al. 2009	10.3–20.7	DLP- k
Kharuzhyk et al 2010	3.1–9.7	DLP- k
Suliman et al 2011	6.6	DLP- k
Chan et al 2012	10.3	DLP- k
Kortesniemi et al 2012	7.3 14.5	Monte Carlo simulations
Tsapaki et al 2014	10	DLP- k
Mayer et al 2014	8.7-10.7	DLP- k
Sabarudin et al 2014	6.0- 17.30	DLP- k
Suliman et al 2014	7.5 - 11.6	Monte Carlo simulations
Yeh et al 2016	8.3-20.1	DLP- k
Vilar-Palop et al 2016	5.6–8	DLP- k
Tootell et al 2017(practical)	13-15	ImPACT method
	8.74	MOSFET
Wichmann et al 2017	5.3-8.8	DLP- k
Shirazu et al 2017	4.7-7.7	DLP- k

The effective dose was calculated by DLP with the k value method of CT scan examinations. The DLP method provides only large determination of effective dose for standard sized patients. Effective dose calculations done in this way are independent of age, weight, gender and scanner model because the k coefficient values is derived using ICRP 103 2007, based on the region of the body for standard sized patients only. Further limitations of this method include the possible underestimation in CT dose from differences in beam geometry between physical phantoms and the computer simulation software (Kalender, 2014).

For this thesis, indirect estimations of effective dose by DLP k factors and ImPACT along with direct measurements by MOSFET have been used to compare results for FTC and ATCM.

3.4.3 Effective risk (ER)

For diagnostic radiology, the radiation doses from routine examinations are generally low enough not to cause deterministic fatal effects such as death and malformation. However, the risk of probabilistic stochastic effects such as cancer induction must be considered during CT scan examinations (Linet et al., 2012). Some authors have advocated the use of effective risk (ER) or lifetime attributable risk of cancer instead of ED (Brenner, 2008), considering that the utilisation of ED as a measure of radiobiological detriment has its limitations. A common limitation is the use of tissue weighting factors, which are highly subjective and change regularly. Another limitation is that ED is independent of age at exposure, contrary to the fact that radiation risk is dependent on age. Unlike ED however, ER calculation takes tissue type, age and gender into account (Committee to Assess Health Risks from Exposure to Low Levels of Ionizing Radiation, 2006). A further limitation of ED is that it is often confused with equivalent dose, which refers to the dose to a given tissue, as both measured in Sieverts (Bankier & Kressel, 2012).

Risk is an epidemiological term used to indicate association. It can be described in two ways: relative and absolute risk. For example, the ratio of the cancer incidence rate in an exposed population to that in an unexposed population is the relative risk; while the simple rate of cancer incidence in a specific population is the absolute risk (National Academy of Sciences (NAS), 2006). The lifetime attributable risk (LAR) estimates the incidence of cancer over a study period. The ICRP recommends the use of LAR (ICRP, 2007) to assess the risk of radiation-induced cancer in different ages and gender **Table 3-11**. Using the following formula effective risk (R) can calculated see **Equation 3-7** below:

$$R = \sum rT \times HT \quad \text{.....Equation (3-7)}$$

Where: **R**= is the effective risk

rT= is the Lifetime-attributable tissue specific cancer risk (LAR) per unit equivalent dose to tissue T.

HT= is the equivalent absorbed dose for tissue T

Table 3- 11:Lifetime attributable risk (LAR) of radiation induced cancer for organs tissues for each decade of female and male age (from 20 to 70) as listed from Table 12-1D - BEIR VII phase 2 (NAS, 2006).

Tissue female and male	Risk coefficient (cases /1000,000 persons /Gy) at different ages					
	20	**30**	**40**	**50**	**60**	**70**
Males /Stomach	40	28	27	25	20	14
Colon	173	125	122	113	94	65
Liver	30	22	21	19	14	8
Lungs	149	105	104	101	89	65
Prostate	48	35	35	33	26	14
Bladder	108	79	79	76	66	47
Other	312	198	172	140	98	57
Thyroid	21	9	3	1	0.3	0.1
Females / Stomach	52	36	35	32	27	19
Colon	114	82	79	73	62	45
Liver	14	10	10	9	7	5
Lungs	346	242	240	230	201	147
Breasts	429	253	141	70	31	12
Uterus	26	18	16	13	9	5
Ovary	50	34	31	25	18	11
Bladder	109	79	78	74	64	47
Other	323	207	181	148	109	68
Thyroid	113	41	14	4	1	0.3
NOTE: Number of cases per 1000,000 persons exposed to a single dose of 0.1 Gy.						

Cancer risk estimates based on BEIR VII modelling has its limitations as well. First, there are uncertainties of deriving cancer risk by utilising the Life Span Study LSS data. This has been used since 1950 to derive radiation induced cancer risk. Furthermore, the LSS study data can only be used for low dose and dose rate exposure situations. The variability of sampling in the model parameter estimates can affect risk modelling despite these limitations, however cancer risk estimation based on the BEIR VII radiation risk models is still very useful. The cancer mortality risk estimates based on the BEIR VII models are generally in consonance with those of other scientific bodies: ICRP and UNSCEAR (ICRP, 2007; UNSCEAR, 2010).

Figure 3-7, as presented by Brenner D. J. and Hall E. J., (2007), shows the corresponding estimated lifetime percent risk of death from cancer that is attributable to radiation from a single CT scan. The mean risks were determined for male and female patients. The risks are highly age dependent, given that dose and risks per unit dose are age-dependent. Owing to the sensitivity of the digestive organs to radiation-induced cancer, the risks are higher for abdominal scans. (Brenner and Hall 2007).

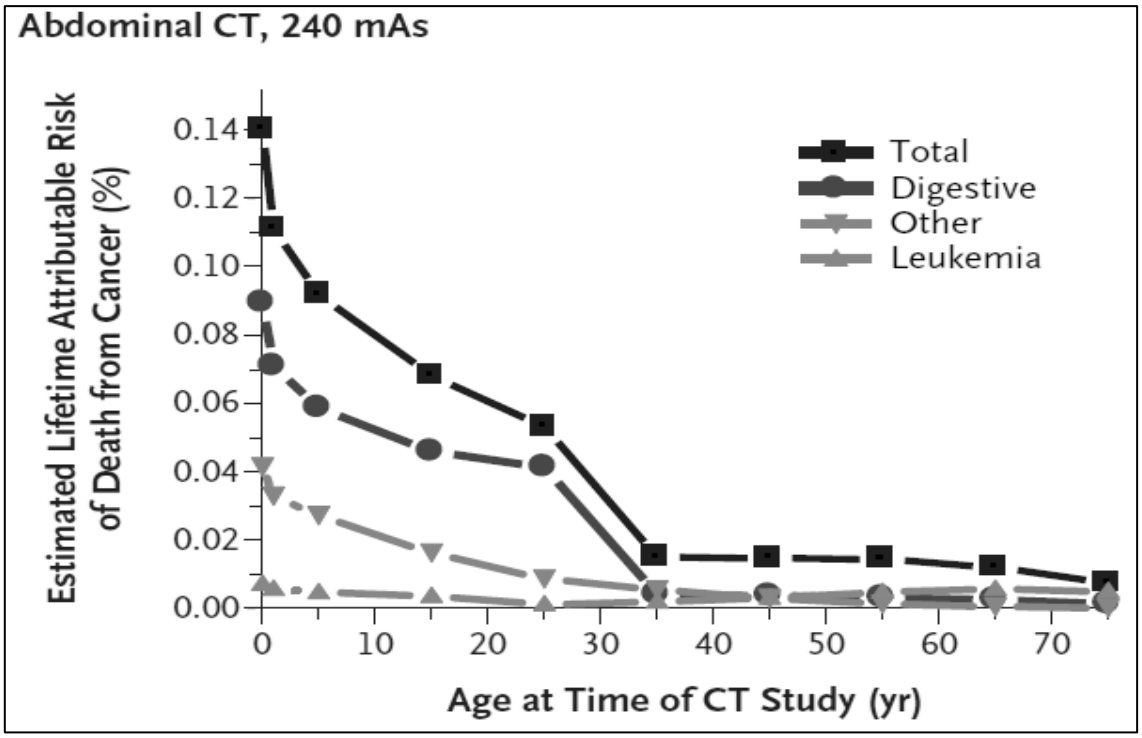

Figure 3- 7: Estimated lifetime cancer risks from typical single CT Scans of the Abdomen (Brenner & Hall, 2007).

ER estimates based on the BEIR VII Phase 2 report (NAS, 2006) reflect the combined detriment from the risk for each age and gender from 0-80 years. ER calculations are relatively easy and are no more difficult than the ED calculations to undertake. They have the added benefit of taking an individuals' age and gender into account, and generating data which are more understandable to the public. In other words, for the general public it is easier to understand the radiation risk of abdominal CT scan in terms of cancer cases per million. The derived number of cancer incidence cases using the BEIR VII Phase 2 report indicates a substantially higher lifetime attributable risk (LAR) of cancer incidence in females compared with males, and also in younger patients. The ER for different CT scans acquired from different dosimetry estimation methods based on the BEIR VII Phase 2 report 2006 are described within **Table 3-12**.

Table 3- 12:Effective risk based on BEIR VII Phase 2 report 2006 from CT scanning in adults for clinical with different dosimetry methods			
Reference	**CT body part /age**	**ER method**	**Finding**
González et al 2011	CT colonography 50 to 80 years men and women	BEIR VII Phase 2 report / Monte Carlo simulation estimate risks methods	Radiation risks based on these models the benefits for CT screening
Koral et al 2012	CT head 1.3- 2 old year	BEIR VII Phase 2 report / Monte Carlo ImPAC estimate risks methods	The ER increased with decrease patients age using CT head examinations
Lahham et al 2017	CT chest examination 15-80 female old years	BEIR VII Phase 2 report / Monte Carlo simulation estimate risks methods	The ER decreases remarkably with patient's age.
Wylie et al 2018	CT hip 10- through 60-year	BEIR VII Phase 2 report / Monte Carlo simulation estimate risks methods	The ER 5-17 times of cancer compared with radiographs hip also decreases with increasing age.

No large-scale epidemiologic studies of cancer risk or average ER for different ages of men and women found within the literature have compared FTC and ATCM for abdominal CT examinations. In this thesis, one of the key aims is to report such novel ER data for adult male and female patients, aged from 20 to 70 years old using direct measurement by MOSFET when undergoing abdominal CT.

3.5 Radiation dose comparison between FTC and ATCM using different dosimetry methods

The radiation dose comparison between FTC and ATCM for abdominal CT scan is based on effective dose. It is an essential radiation dose quantity. CT of the abdomen has a characteristically greater effective dose in contrast to CT scans that can be performed on other body parts **(Table 3-7)** (Smith-Bindman et al., 2015**).** This is reliant on the age and gender of the patient and considers the comparative radio-sensitivity of the different organs within the scanned area.

Table 3- 13:Typical effective doses for different CT examinations (Smith-Bindman et al ., 2015)

CT Examinations	Typical Effective dose(mSv)
Head CT	2-4
Chest CT	9-18
Abdominal CT	10-22

According to research conducted by Vilar-Palop ae al ., (2016), different CT examinations using ATCM, where the mean effective dose ranged from 5.6 to 8 mSv for abdominal CT scan examinations, haven't been updated since 2007 using the DLP method. The dose range reported was slightly lower than the 11.7mSv recommended by Commission of the European Community CT examinations (CEC) (CEC, 2000). The results from Vilar-Palop et al., (2016) were slightly similar abdominal mean effective dose (5.3-8.8 mSv) analysed for 200 patients by Wichmann et al., (2017).

Similarly, Lee et al. (2009) reported an 18% reduction in effective dose (during cranio-cervical CT angiography) with an ATCM method compared with FTC. However, in a study conducted by Lee et al., (2011b) compared the radiation dose between FTC and ATCM using a percentage dose reduction by (CTDIvol and DLP); their results demonstrated a reduced radiation dose with ATCM. However, different DLP and CTDI values between both techniques existed. Schindera et al., 2007 performed research which intended to evaluate the effect of different CT machines on six abdominal organs using ATCM. Their study measured organ dose using MOSFETs and an anthropomorphic adult phantom. They found variable estimates of organ doses between 10% and 15% from typical abdominal CT scanning.

Teeuwisse et al. (2007) reported effective dose of 0.1-2.4 mSv, 0.4-13.7 mSv 2.8-40.8 mSv for head, chest and abdominal CT examinations in a Dutch survey using ATCM. Very high mean

dose values for abdominal CT examinations were attributed to a protocol used by some hospitals for patients with metastases. Furthermore, Rizzo et al. (2006) compared the radiation dose between FTC and ATCM using both DLP and CTDIvol. This study showed that the radiation dose with ATCM was substantially reduced (by approximately 42–44%), when compared with FTC.

A study by Su et al. (2010) involving 182 patients referred for dual-phase contrast-enhanced CT to assess liver tumours compared radiation exposure between FTC and ATCM for liver MDCT. Participants were divided into four groups based on different scanning parameters. Radiation dose measurements were generated automatically by the CT unit using the DLP- k factors. The results showed that the average tube current with the ATCM was 23% lower than FTC and the mean effective dose in the ATCM group was 36% lower than the FTC.

Angel & Zhang (2012) compared the CT dose difference between two FTCs (165 mAs) and an ATCM in a head phantom. CT dose difference was calculated using DLP and CTDIvol values. They showed that the ATCM reduced CT dose by up to 38%. The differences depended upon the dosimetry method, DLP values and average tube current for FTC and ACTM. Kim at al. (2013) compared radiation dose for different adenosine stress dynamic myocardial perfusion CT protocols. Two different techniques- FTC (330 mA) and ATCM (CAREDose4D range, effective tube current 350 mA) - were compared. Radiation dose was estimated using the DLP-k factor. ATCM resulted in a 36 % overall reduction in mean effective radiation dose (7.7 mSv ± 2.5), compared with FTC (12.1 mSv ± 1.6.).

Park et al. (2013) compared the vascular enhancement, image quality and radiation dose of a 128-slice dual source CT in 100 venography patients. They compared between a setting of 120 kVp with low pitch (and 120mA FTC) and 100 kVp with high pitch (with ATCM). Effective dose was estimated using the DLP- k factors. The radiation dose was reduced by 26% with the ATCM, compared with the FTC. Padole et al, (2016), used a human cadaver (88 years old, male, 68 kg) to evaluate organ doses in six abdominal/pelvic organs, namely, liver, stomach, colon, left kidney, small intestine, and urinary bladder. The cadaver was scanned according to routine abdomen pelvis protocol on a 128-slice MDCT scanner using both ATCM with three average reference mAs of 100 (58 mAs), 200 (118 mAs), and 300 (188 mAs) and FCT with three different mAs of 100, 200, and 300. Organ doses were estimated with the Monte Carlo simulation and direct measurement by ionization chambers. The authors reported a mean of

12.3 mGy for the six organs with ATCM and 24mGy with FTC. The ATCM method reduced abdominal /pelvic organ dose by 49% compared with FTC.

Finally, Sookpeng et al. (2017) estimated radiation dose to the lens of the eye and other nearby organs (mandibles, temporal bones, thyroid and the base of skull) from the CT brain scan using ATCM. Gafchromic film XR-QA2 was used to measure the absorbed dose of the organs. Compared with FTC, ATCM resulted in dose reductions of 22–24% to the lens and 16–36% for other organs. FTC and ATCM comparison is usually not a like for like comparison, because the average tube current with ATCM is generally lower than the average tube current with FTC. **Table 3-14** shows a summary of clinical radiation dose comparisons between FTC and ATCM for a number of CT scan examinations using a range of dosimetry methods.

Table 3- 14: Summary - clinical radiation dose comparison between FTC and ATCM different CT scan examinations with different dosimetry methods.

Reference (CT abdomen)	CT body part /age	Radiation dose (FTC and ATCM)	Dosimetry method
Kalra et al 2004a	CT Thorax, abdomen/pelvis	ATCM decreasing radiation dose ~38%	DLP- K factor
Rizzo et al 2006	CT Abdomen/ pelvis	ATCM decreasing radiation dose ~ (42–44%)	DLP- K factor
Russell et al 2008	CT neck	ATCM decreasing radiation dose ~34%	DLP- K factor
Lee et al 2009	CT Craniocervical	ATCM decreasing radiation dose ~18%	DLP- K factor.
Su et al 2010	Liver CT scan	ATCM decreasing radiation dose ~35.9%	DLP- K factor.
Lee et al 2011b	CT Abdomen/ pelvis	ATCM decreasing radiation dose ~45.25%	DLP- K factor
Angel et al 2012	CT Brain	ATCM decreasing radiation dose ~38%	DLP- K factor
Kim at al 2013	CT Myocardial perfusion	ATCM decreasing radiation dose ~36 %	DLP- K factor

Park et al 2013	CT Vascular enhancement	ATCM decreasing radiation dose ~26 %	DLP- K factor
Padole et al 2016 (Cadaver Study)	CT Abdominal/pelvis (organs dose)	ATCM decreasing radiation dose ~48.7 %	Ionization chambers and Monte Carlo simulation
Papadakis et al 2016	CT head, thorax, and abdomen/pelvis (organs dose)	ATCM decreasing radiation dose ~76% for abdomen/pelvis	Monte Carlo simulation
Sookpeng et al 2017	CT Brain	ATCM decreasing radiation dose ~ 2–24% for the eye lens and 16–36% for the other organs	Gafchromic film

3.6 Chapter Summary

In conclusion, the radiation dose from CT examinations can be estimated using a number of different methods. Until recently, the DLP method used in most studies and ED variations varied between 3.1 and 34 mSv. Studies evaluating radiation dose differences between FTC and ATCM during abdominal CT examinations are rare. Most studies adopt a mathematical dose estimation (DLP) method and this has accepted limitations. Major publications have failed to consider the added effects of changes in pitch and detector configuration, which would result from using different FTC / ATCM options. There is no evidence of using all dosimetry methods in CT to measure or estimate the radiation dose between FTC and ATCM techniques for abdominal CT examinations. Furthermore, no large-scale epidemiologic studies of specific abdominal organ doses and effective risk, determined by direct dosimetry, for different ages and genders when comparing between FTC and ATCM techniques have been reported. Therefore, this thesis addresses a major literature gap by investigating the dosimetric consequences of using ATCM and FTC techniques for abdominal CT.

Chapter Four: CT image quality

4.1 Chapter Overview

Assessment of image quality in CT scanning is essential in order to facilitate an effective diagnosis. Measures of image quality (metrics) can be used in three ways. Firstly, they are employed for the quality control of imaging techniques or system performance (e.g. for comparison of FTC or ATCM techniques). Secondly, for dose optimisation of CT examinations. Thirdly, because quality control can be employed as a benchmark in the selection of suitable image processing post processing algorithms (Sezdi, 2011).

As previously identified, CT has become increasingly common; thus it is essential to be conscious of radiation safety in order to keep the radiation dose as-low-as-reasonably-achievable (ALARA). It is equally important to keep in mind the need for good image quality for diagnostic purposes. It is well known that a specific level of image quality is required to answer a specific clinical question (Russell et al., 2008). The growing application of CT in clinical practice has raised concerns about the increasing incidence of cancer from radiation exposure. Therefore, reducing the radiation dose without compromising diagnostic imaging quality is increasingly becoming the subject of much research (Wang et al., 2013).

A common method for maintaining consistent image quality during a CT scan is through the use of ATCM. In this process, the tube current is altered automatically in order to keep noise and therefore image quality at a standard level throughout the scan length. ATCM facilitates standardised image quality through the automatic alteration of the tube current in different planes (x-y and z). Tube current changes are determined by the size of the patient and the attenuation of the region of the body scanned (Lee et al., 2011).

Establishing optimal image quality is an intricate task requiring quantitative objective physical measures together with visual observer studies (Zarb, McEntee, & Rainford, 2015). These physical and visual methods of assessing CT image quality will be discussed in this chapter. It is essential to understand the knowledge gap for CT image quality methods when comparing FTC and ATCM techniques for abdominal CT scanning.

4.2 Methods of CT image quality evaluation

A number of methods are available for the assessment of CT image quality. These methods can be categorised according to the type of information obtained, ranging from higher to lower order tasks. Those comprising low order tasks could quantify exposure factors, equipment features, and assess radiographic technique. By comparison, those tasks of high order would explore the quality of images. These two methods encompass the assessment of technical elements (physical as well as psychophysical) in addition to diagnostic performance (e.g. observer performance) (Zarb, Rainford &McEntee, 2010). Details of these methods will be described, and the advantages and disadvantages of each method will be considered in relation to CT scan examinations and the wider aims of this thesis **(see Figure 4-1)**.

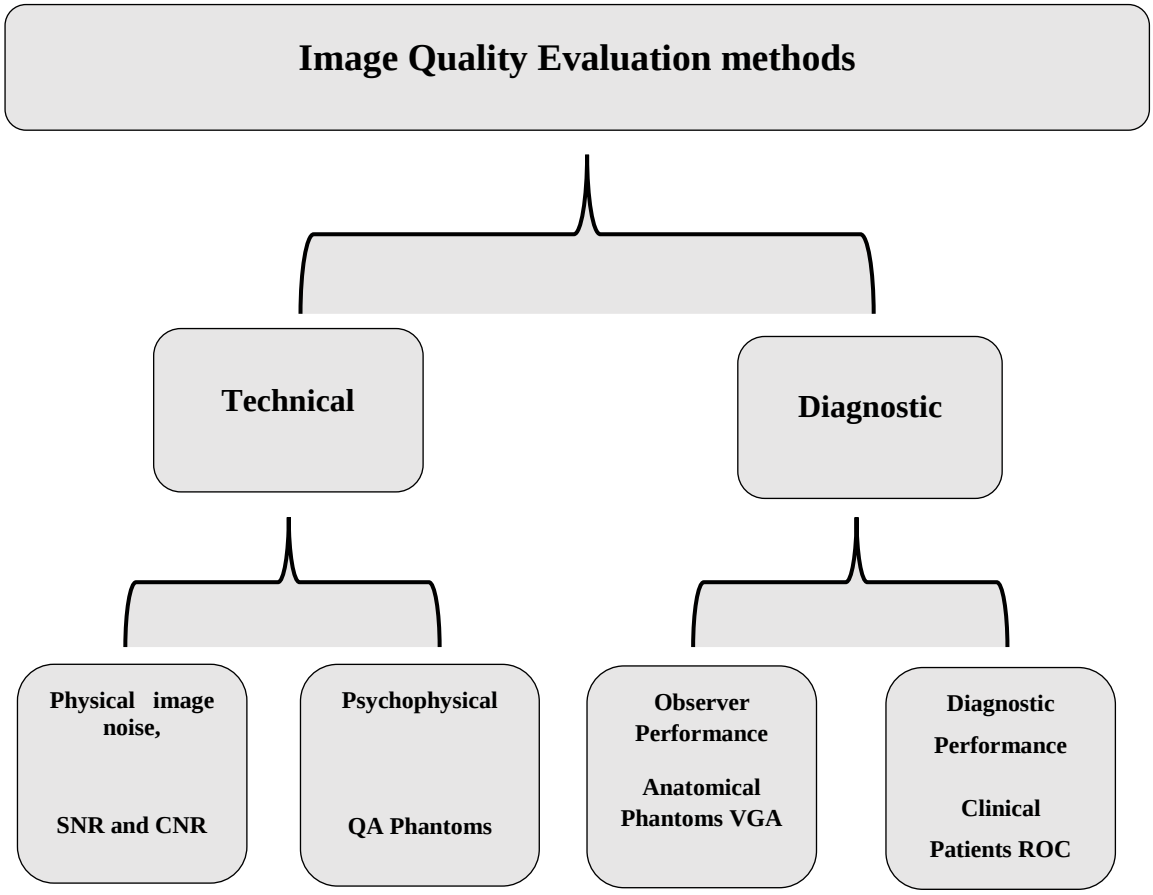

Figure 4- 1: Methods of evaluating image quality in CT scan (Zarb et al., 2010)

4.2.1 Physical methods

The phrase ‘physical measurements’ refers to the depiction of the physical aspects of image quality. A description of image quality within CT makes reference to how accurately the technique (CT image) portrays the three-dimensional attenuation distribution of the x-ray beam. Specific image control quality appraisals performed regularly establish that the CT unit dose does not deviate from accepted quality levels, assuring uniformity of the structure with time (Verdun et al., 2015). Expressions of the quality of CT images concerning physical aspects have been proposed by the International Electrotechnical Commission (IEC, 1994). Such physical measures include image noise, spatial resolution (SR), contrast to noise ratio (CNR), signal to noise ratio (SNR) as well as contrast resolution (CR) (Månsson, 2000; Zarb, Rainford, & McEntee, 2010).

Image resolution is an essential feature of image quality. It refers to the ability of the medical imaging process to discriminate between two objects in the image. Good image resolution clarifies accurate anatomical structures and detail within the image (Bourne 2010). Within this section of the chapter image noise, SR, CNR, SNR and CR will be discussed.

4.2.1.1 Image noise for CT scan

In CT, noise is defined as the "variation of CT numbers from a mean value in a defined area in the image of a uniform substance. The magnitude of noise is indicated by the standard deviation (SD) of the CT numbers of a uniform substance in the region of interest (ROI)’’ (IAEA, 2012). Noise should not be too large so as not to impact adversely on the resultant image. In CT, noise is related to the quantity of x-ray photons incident on the detectors; quantum noise occurs when insufficient photons reach the detectors. This results in a reduction of image quality. The SD of the attenuation values is measured through the use of ROI in different structures within the image, which are often regarded to be objective measures (Zaehringer et al., 2016). Quantum noise is quantified by calculating the SD from the mean HU over a region 10% of the cross-sectional area of a test object. A standard range of quantum noise for helical CT scanners comprises 4HU (McNitt-Gray, 2006). This is particularly important for using FTC and ATCM techniques during abdominal CT imaging wherein low contrast structures are being imaged- see **Chapter 1 Section 1.2**. In abdominal CT imaging, when kV is reduced, the image noise needs to be considered carefully (Yu et al., 2009). A study by Zaehringer et al. (2016) reported twice as much noise when using 100 kVp compared to 120 KVp when imaging the spleen. Similarly, higher image-noise levels were observed between 100 KVp and 120 kVp for images of both the right and left kidneys. Noise was, however, shown to be lower at 120 KVp within

regions of the aorta and liver. However, Söderberg& Gunnarsson (2010) evaluated image noise using ATCM and FTC from four different CT scanner manufacturers. The results demonstrated differences in image noise, with it being lower when using the ATCM compared with FTC (Söderberg& Gunnarsson, 2010).

CT techniques using ATCM produce a consistent level of image noise based on noise index (NI) value in addition to SD. The tube current is altered in relation to the attenuation profile of the patient, as established from the scout image, to acquire images which have constant noise nearer to the set NI. Choosing a higher NI permits more noise on subsequent images; thus, a reduced tube current which results in a lower radiation dose. Alternatively, choosing a reduced NI causes delivery of a higher dose of radiation (Kaza et al., 2014). The subsequent equation may be employed to calculate the radiation dose for varying noise indices- **Equation 4-1**:

$$\frac{Dose_2}{Dose_1} = \left[\frac{NI_1}{NI_2}\right]^2 \quad \text{.....Equation (4-1)}$$

Where $Dose_2$ and $Dose_1$ are the radiation doses for conditions 2 and 1, respectively,

$NI_1$and NI_2 are the corresponding noise indices.

An experiment by Van der Molen, Joemai & Geleijns. (2012) evaluated image noise by comparing between ATCM and FTC with different noise levels. The experiment was carried out using a phantom and a Toshiba CT scanner with SURE Exposure 3D. The study reported that ATCM showed more constant image noise compared to FTC. The implementation of ATCM led to more homogeneous image quality compared to FTC, with the authors reporting good adaptation to phantom (patient) size (Molen et al., 2012).

4.2.1.2 Spatial Resolution

The level of detail seen on an image is known as the spatial resolution (SR). SR should be routinely monitored in CT. It determines the ability of the system to resolve close high contrast small sized objects (Lin & Alessio, 2016). The closer the objects are to each other, provided the image still shows them as separate, the better the SR. Several parameters determine the SR, these include: the reconstruction matrix; detector width; slice thickness; object to detector distance; focal spot and matrix size (Bushberg, et al, 2012). There are two methods of evaluating high contrast resolution- direct measurement or by calculation. A line pair phantom (a module inside a Catphan 600 phantom made up of closely space metal strips embedded in it) is used for direct measurement. Each bar and the adjacent space is regarded as a line pair. In principle, the phantom is scanned and the number of visible strips is counted. (Goldman, 2007)

The modulation transfer function (MTF) describes the resolution properties of an imaging system. It refers to the percentage of an object's contrast that is recorded by the imaging system as a function of its size (spatial frequency). MTF calculations during routine QC tests are too complicated, thus direct estimation with appropriate test phantoms such as the Catphan series of phantoms (Zard, 2010) is recommended.

There are two types of spatial resolution on CT scan images, namely in-plane resolution (the X/Y plane) and longitudinal or cross- plane resolution (the Z plane). In-plane spatial resolution is the resolution in the X and Y directions. This can be affected by scanner geometry and the reconstruction algorithm (Hsieh, 2009). The x-ray focal spot size and shape, the distance between the source and the isocenter, the distance between the detectors and the source, and the detector cell size are the main physical influences on in plane spatial resolution. The isocenter is the point where the x-ray beams intersect while the gantry is rotating during beam-on. In order to acquire CT images with proper spatial resolution and noise performance, it is essential to have selected appropriate geometric parameters (Seeram, 2009). Other influences like the interpolation reconstruction algorithms, reconstruction intervals, the size of the detector element and pitch can also determine spatial resolution (Mahesh, 2009). Current CT scanners have a spatial resolution of 0.5–0.625 mm in the z-axis, and approximately 0.5 mm in the x- to y-axes (Lin & Alessio, 2016)

4.2.1.3 Contrast to noise ratio (CNR)

CNR is another physical image quality measure; it is often used to see how well the object of interest is differentiated from its surrounding background. CNR, therefore, offers a suitable metric concerning the ability of the imaging modality to visualise the anatomical structures, pathological lesions as well as abnormities with a given image (Dhawan, 2011). Within this context, it has been proposed that within certain circumstances, CNR provides helpful information about lesion contrast on a CT scan.

CNR measures the quality of an image based on contrast rather than the raw signal. It is the difference between the mean attenuation coefficient of a defined structure in the ROI and the mean attenuation coefficient of the image background surrounding this structure divided by the standard deviation of the background noise (Grant et al., 2014). CNR can be determined by following **Equation 4-2**:

CNR_ (A and B) = (S_ (mean A)-S_ (mean B)) / N_ (SD B) ……. **Equation (4-2)**

Where CNR A and B = is the contest noise ratio between two organs A and B

S mean A = is the mean signal from organ A

S mean B = is the mean signal from organ B

NSD B = is the SD (noise background) from organ B

The image quality depends on the image contrast detectability. This is due to the fact that an image with high SNR does not actually have a suitable contrast unless it has a high CNR, particularly where a sufficient distinction between the pathology and healthy tissue is necessary (Smith & Webb, 2011). However, within the literature review, most studies evaluate image quality using CNR in abdominal CT based on comparisons between tube voltage with iterative reconstruction, using contrast agent enhancement for the patient-to-evaluation balance between image quality and the amount of iodine injected (Buls et al., 2015). In addition, image quality assessment often uses CNR in routine abdominal CT for the evaluation of small lesions such as liver, spleen, pancreas or kidneys when using ATCM. ATCM based on CNR considers lesion-to-background contrast and is a good method for assessing image quality with lesion detection in mind (Funama et al., 2013).

4.2.1.4 Signal to noise ratio (SNR)

SNR is employed broadly to assess image quality from CT scans. This is due to the fact that, within CT scanning, a key determinant of image quality is noise. SNR's association with human observer detectability was initially scrutinised in 1948 by Albert Rose (Rose, 1973). He attempted to discover the smallest noise level required for an image to be perceived by the human eye. He discovered that a ratio of ≥5 is necessary (Båth, 2010). Therefore, for many years, SNR has been used to give an indication of quality image along with a notion of how visible an object (e.g. pathology) might be within an image (Månsson, 2000; Zarb et al., 2010).

SNR explains the relationship between signal and noise levels in an image. Within this context, SNR comprises a simplistic method to describe the visibility of an object in the image (Lança & Silva, 2008). It comprises of the mean of the linearised signal intensity over the selected ROI divided by the SD from an area exterior to the background noise of the image. High SNR indicates that actual information (signal) surpasses noise. (Rahim et al., 2010). SNR can be determined by the following **Equation 4-3**:

$$SNR_A = \frac{S_{mean\ A}}{N_{SD\ A}} \quad \text{.....Equation (4-3)}$$

Where $S_{mean\ A}$ =is the mean signal from organ A,

$N_{SD\ A}$ =is the standard deviation (SD) of background noise from organ A

Several issues relate to the use of SNR which could impact its dependability and validity for both FTC and ATCM. For instance, the SNR does not take into consideration the size of the imaged object and consequently its correlation with observer performance can be poor. The noise description (i.e. SD of pixel value) utilised in this method is often too simplistic for an observer who is sensitive to the noise (Zarb et al., 2010).

In order to demonstrate this, the SNR model is established on quantum noise which is associated with the photon density at the detector. By contrast the human observer is conversant with the background quality of an image which could be influenced by other noise types like anatomical noise. In order to acquire comparable imaging features (with comparable SNR values), images with a small pixel size require a large number of photons in contrast to those comprising of a higher pixel size. Finally, concerning the ROI location in estimating the level of noise, positioning it in a non-homogenous region of the image would lead to differences

within the pixel values due to anatomical differences, and thus would adversely affect SNR measurements (Båth, 2010). Within the literature, the assessment of physical image quality using SNR method is seen as a very important method for evaluating the relationship between signal and noise for CT scan examinations image quality. In the last five years, most literature has concentrated on calculating SNR values for evaluating physical image quality for CT scan examinations when comparing between different tube potentials (kVp) using ATCM techniques. **Table 4-1** shows recent examples of comparison studies which have compared SNR between different CT scan examinations.

Table 4- 1:Example of studies which have compared SNR between different CT scan examinations

Authors	Year	CT body part	SNR comparison
Scholtz et al	2015	portal venous–phase thoracoabdominal	tube voltage with advanced iterative reconstruction
Luo et al	2014	cerebral CT angiography	low kVp with low contrast material volume
Kanematsu et al	2014	CT angiography	Low-tube-voltage with low-concentration iodinated contrast material.
Weis et al	2017	Chest Computed Tomography	Comparison Between 70 kVp and 100 kVp
Takahashi et al	2018	adrenal vein imaging	Low kV, and low kV with reduced contrast medium protocols.

Only two studies have been identified comparing SNR between FTC and ATCM. Sookpeng & Budde (2017) compared SNR values between FTC and ATCM for the lens of the eye from CT brain examinations. The results demonstrated no statistically significant differences for SNR between FTC and ATCM images. However, SNR did significantly decrease while tilting the gantry using FTC during CT brain. However, work by Su et al. (2010) compared the SNR values between FTC and ATCM for the hepatic artery with contrast enhancement with two constant tube currents. The results show the mean SNR was found to be higher for FTC when compared with ATCM.

Comparisons have been made between SNR and CNR for CT scan examinations using ATCM. Ha, Hong, Kim, & Lee (2016) compared image quality using ATCM in abdominal organ image quality evaluation using SNR and CNR with two constants effective mAs and tube voltages and contrast medium. The SNR and CNR results for abdominal organs were similar for ACTM and FTC, with the difference between SNR and CNR being very small.

Other work by Feng, Tong, Liu, Zhao & Zhang (2017) evaluated image quality using SNR and CNR in high-pitch coronary CT angiography with medium contrast, with two patient groups (A and B) using ATCM. The SNR and CNR values for group A were higher than for group B; no image quality differences were identified between A and B for SNR and CNR.

Ultimately, when used correctly, SNR is an efficient and reliable physical measure of image quality and has a place in quality assurance as well as having utility in image optimisation studies (Abdulfatah et al., 2014). Therefore, it is widely accepted that SNR can be used as a predictor of physical image quality when comparing between CT techniques, such as FTC and ATCM for specific abdominal organs during abdominal CT scan examination with different parameters.

4.2.1.5 Contrast resolution

The contrast resolution (CR) of an imaging system determines the visible reproduction of contrast detail when there is some relative density difference between the structure and the surrounding area. This implies that more subtle objects can be seen on the image when high contrast resolution is present (Williams et al., 2007). CR is usually degraded by noise. A noisy or inhomogeneous background makes it difficult to distinguish between two lesions with minimal differences in density (Park et al., 2009). Therefore, in order to clearly identify a structure, CNR should be more than 5:1 (Starck et al., 1998). A reduction in this minimal threshold might be necessary especially for areas with high inherent contrast. For example, images of adipose and muscle tissue have been shown to be adequate despite a reduction in CR, which was accompanied with a 25% reduction in radiation dose (Zarba et al., 2010). Nagata et al. (2015) have also suggested an optimized radiation protocol for CT colonography in the detection of polyps. They suggested a reduction in dose with minimum slice thickness in order to achieve an acceptable CR. This, they proposed, will still enable a confident diagnosis to be made for lesions despite the degradation of contrast. Low dose protocols have also been suggested in the detection of pulmonary nodules using low mAs. This protocol is increasingly becoming acceptable for pulmonary screening despite the reduction in CR (Zarb, 2010).

Several factors, including tube collimation, radiation dose, noise, slice thickness, subject contrast, scatter radiation, beam filtration, detector properties (i.e. sensitivity), image display, and algorithmic reconstruction, affect contrast resolution (Goldman, 2007; Mahesh, 2009). SNR has been described as one the most suitable indicators of CR being relatively simple to estimate from ROIs within the test object and surrounding noise (Zarb, 2010).

4.2.2 Psychophysical method

Psychophysical measurements are based on signal detection theory (SDT) and are quantitative interpretations of an observer's decision. The concept and early methods were developed by radar researchers in the early 1950s and overall it is a technique that can be used to evaluate the sensitivity in decision-making (Peterson, Birdsall& Fox, 1954). Psychophysical measurements refer to the subjective response by an observer in relation to the influence of a physical stimulus on a test object being imaged. These test objects are usually simple, for example, line pairs which are utilised for the determination of spatial resolution, and discs made with holes of varying contrasts and diameters within an appropriate phantom containing cylinders of different attenuation coefficients. The image is evaluated according to the number of discs adequately demonstrated (Ciantar et al., 2000; Zarb et al., 2010). For line pairs, the test images are evaluated giving a quantitative measure of the spatial resolution. In order to obtain highly reliable results with this method, inter-observer variation and training should be considered. Findings from multiple readers can be averaged as an alternative method for taking into account variability (Månsson, 2000).

4.2.3 Diagnostic performance method

The diagnostic performance method is based on the observer's assessment of image quality. It involves the use of human volunteers to visualise structures on the displayed images and make a judgment. It is very important in medical imaging practice to optimize the radiation dose as best as practically attainable, while at the same time keeping the image quality acceptable for diagnostic purposes (Zhang, Leng, Yu, Carter, McCollough, 2014). Observer performance measures are obtained from images of patients in the clinical settings or on phantoms (Mansson, 2000). There are several established methods of evaluating the quality of images based on set criteria which have to be fulfilled. The two most common of these methods involves the use of Receiver Operating Characteristic-ROC and visual grading analysis (VGA).

4.2.3.1 Diagnostic performance Receiver Operating Characteristic (ROC)

For Receiver Operating Characteristic (ROC), observers are asked to say whether a lesion is present or not; some variants of ROC also allow for classification of the lesion. ROC measures have a major drawback in that they are highly dependent upon disease prevalence. Additionally, the images have to be divided into normal and abnormal, and often a large number of images are necessary. The ROC methodology does not work well for multiple lesions in one image. The localisation of the stated lesion is not considered and thus an image could be diagnosed as abnormal while still missing the actual lesion (Zarb et al., 2015).

With localisation ROC (LROC), an observer will mark the location of a suspicious region and then provide the confidence level of defect presence. If the mark is close enough to the true lesion, it is considered a correct localisation. A drawback of this method is that the definition of closeness is subjective (He and Frey, 2009). The improvement with free response ROC (FROC) is that in LROC the observer has to identify several lesions by indicating their locations. Additionally, for Jackknife Free-response ROC (JAFROC), the observer is required to rate their confidence level concerning the presence of the lesion usually in terms of its clinical significance (e.g. malignant or not, using a scale).

Assuming the right numbers of cases and observers are used, this method permits suitable statistical power (Samei & Krupinski, 2014; Wunderlich & Abbey, 2013). A further ROC improvement includes free-response forced error (FFE), within which if the observer detects a high percentage of abnormality prior to the occurrence of any false positive error for one modality, then this modality is perceived as improved. Ultimately, ROC methodologies can be used in clinical images when properly designed (Båth, 2010).

4.2.3.2 Observer performance (Visual Grading Analysis-VGA)

Visual grading analysis is used to assess how clearly structures are visualised by an observer. The observer is asked to rate the visibility of anatomical reproduction quality. This is said to be clinically pertinent and it is the preferred means of appraising the image quality by many researchers (Zarb et al., 2015). Additionally, the value of VGA for the detectability of pathology has been investigated; there is a strong association between the visibility of normal anatomy as well as the detectability of pathological structures on the image (Bath & Mansson 2007, Ludewig, Richter & Frame, 2010; Smedby, Fredrikson, 2010). There are two common types of VGA approaches which can be applied to assess an image absolute and relative:

4.2.3.2.1 Relative VGA

For relative VGA, the observer ranks image quality in comparison to a reference image. Relative VGA requires rating the visibility of anatomical structures against the same structures that are ideally based on published and validated criteria. Criteria tend to be written as 'statements' and the answers provided by the observer are on a rating scale (e.g. better than, equal to, worse than). The images for evaluation have to be displayed in a random order so as to minimise bias, and the viewing conditions should be similar to the conditions in which the clinical task is normally performed. The image quality criteria should be as specific as possible, but it is possible to ask more than one question in order to evaluate several aspects of the image (Verdun et al., 2015). The data collected from this method is then computed to provide the visual grading analysis scores ($VGAS_{rel}$) using the following **Equation 4-4**:

$$VGAS_{rel} = \frac{\sum_{o=1}^{O}\sum_{i=1}^{I}\sum_{c=1}^{C} Grel}{I \times S \times O} \quad \text{.....Equation (4-4)}$$

Where G_{rel} represents the relative rating for a given image (I), criterion (C), and observer (O). The letters I, S and O refer to the number of images, structures and observers, respectively

4.2.3.2.2 Absolute VGA

For absolute VGA the observers have no reference image and the images to be evaluated are displayed one by one. VGA is performed for one image at a time. It requires the observer to respond to statements about image quality. Similar to relative grading, a scale can be used to grade responses. The data collected from this method is then computed to provide the visual grading analysis scores ($VGAS_{abs}$) using the following **Equation 4-5**:

$$VGAS_{abs} = \frac{\sum_{1\,j=1}^{I}\sum_{s=1}^{s}\sum_{0=1}^{O} Gabs}{I \times S \times O} \quad \text{.....Equation (4-5)}$$

Where G_{abs} represents the absolute rating for a given image (i), structure (s), and observer (O). The letters I, S and O refer to the number of images, structures and observers, respectively.

An article by Bath (2010) describes the merits of visual grading. Firstly, the validity of studies utilising this method can be assumed to be high if the anatomical structures are selected based on their clinical relevance. Secondly, VGA approaches often agree with detection studies which utilise human observers or advanced calculations of image quality. Thirdly, compared with ROC studies, visual grading studies are relatively easier to perform. Ultimately fewer number images are necessary and fewer observers would be adequate compared with ROC. Furthermore, the time necessary to conduct VGA analysis is comparatively small, when the workload of the observers is taken into account.

Clinical and phantom based images can both be evaluated with the ROC paradigm. Other derivatives of ROC, such as localisation ROC and free-response ROC, can also be utilised. Although these methods are sufficiently controlled and accurate estimates of clinical images can be obtained, they are still subjective measurements owing to its reliance on human observers. It is also a time-consuming method which requires a large number of images in order to obtain accurate results. An advantage of this method is its utility by radiographers and radiologists when dealing with clinical images. Naïve observers also find the method useful when dealing with phantom images. Simpler methods have been developed in order to avoid the burden associated with ROC methods. An example of these is the previously described VGA methods, which can be utilised for relatively quick image quality assessment. VGA neither requires a task nor pathology.

Another alternative is the use of the two alternative forced choice (2-AFC) or Multi alternative forced choice (M-AFC) methods for phantom image assessment. Observer assessment is complementary to the physical measurements of image quality. Observer assessment is however a subjective way of evaluating image quality. Among the general principles that apply to subjective observer studies is the involvement of as many observers as possible and the coverage of the range of expected competencies in the field.

4.2.4 Alternative methods of performing visual image quality assessment

An alternative method of dealing with observer decision criteria is by using alternative forced choice (m-AFC) experiments. In these types of experiments, the observer is shown several alternatives and is forced to choose the m-alternative which is most likely to contain the signal. A choice has to be made in forced choice experiments wherein the observer has to make the decision on the presence of a signal between the alternatives that are offered, even if this means that they have to guess. The m-AFC experiments are faster and easier to perform than ROC studies. However, m-AFC experiments do not provide insight into the underlying distribution functions and the trade-off between sensitivity and specificity (Verdun et al., 2015).

Independent image combinations and single images can be used for m-AFC experiment designs. For m-AFC experiments, the number of images is based on the comparison of the expected difference between the computers of the settings under evaluation for which standard statistical approaches can be followed as well as signal-known-exactly (SKE) (Zhang et al., 2014). SKE suggests that clues about the signal and its position are provided. Ideally, the signal should be visualised alongside its m-alternatives. The possible position of the lesion should also be indicated (Yu et al., 2013). Simulated and phantom images can be utilised for m-AFC experiments, owing to the total control of ground truth and the SNR related to the task. The quality of CT images in both humans and model observers can be evaluated using the m-AFC paradigm (Rivetti, Lanconelli, Bertolini & Acchiappati, 2011). The next section will discuss the two types of forced choice experiments, 2AFC and four alternative forced choice (4AFC).

4.2.4.1 Two alternative forced choice (2AFC)

This method can be utilised for the estimation of both absolute thresholds in detection tasks and difference thresholds in discrimination tasks. For example, during a typical 2AFC experiment, the participant observes two datasets- one of which contains a signal (Ulrich & Miller, 2004). The participant is usually fully aware that there is only one signal. They will be asked to indicate which of the two datasets contained the signal. The probability that the subject's choice is a function of stimulus difference can be calculated using a psychometric function. A direct measure of the subject's discrimination threshold is the slope of the sigmoidal function. The subject's performance can be measured as the proportion of correct responses, which can vary from 0.5 (indicative of very weak signals) to 1.0 (indicative of very strong signals). A threshold of 0.75 is usually considered as the detection threshold (Verdun et al., 2015). Another variant of the method is the use of two stimuli (standard and control). These are presented successively to the subject at intervals in a random order. Stimuli are

usually different (e.g. in terms of physical dimension, such as object weight, light intensity), with the control being usually more extreme (Verdun et al., 2015). In another variant of the discrimination test, the stimuli can be presented simultaneously rather than successively.

One of the benefits of using the standard 2AFC method is its simplicity and the fact that it provides a threshold measure in physical units unlike scaling methods (Stevens, 1946). Unlike most methods of adjustment, the binary nature of the subject's response prevents any contamination of the measured perceptual thresholds with motor noise. The number of data points is large; therefore, better statistical analyses can be carried out. (Jogan & Stocker, 2014)

4.2.4.2 Four alternative forced choice (4AFC)

The four-alternative forced choice (4AFC) test is a psychophysical method that can be adopted for observer performance evaluation in radiological studies. It is a variant of the two-alternative forced choice (2AFC) test and was a psychophysical method originally developed by Gustav Theodor Fechner (Fechner, 1889). The prefixes 'four' and 'two' are indicative of the number of objects provided to the subject at each time to choose from. Thus the prefix N can be added in place of the numbers to indicate the number of stimuli. In radiology, the 2AFC, 4AFC, and 9AFC methods have all been utilised in signal detection studies (Gang et al., 2011). Among N-AFC, the 4AFC is considered to be adequate for most problems in practice (Jakel & Wichmann, 2006).

There is however a general difficulty with large datasets, especially with 3-dimensional imaging modalities such as CT, magnetic resonance (MR) and digital breast tomosynthesis (DBT). There is also the problem of susceptibility to sampling bias and the difficulty of keeping track of the choice made by the observer. Throughout the entire test, the accuracy of the choices made by the observer as well as the time taken to make the choices must be precisely monitored (Zhang, Cockmartin, & Bosmans, 2016). In addition, since the images are classified according to the definition of the test objective and randomly presented to the observer, an automated data management system with random sampling mechanism is required. In 4AFC, 4 samples are compared; therefore, the 4-AFC is more prone to the physiological and psychological effects such as adaptation and memory problems. Furthermore, the observer is required to be able to adjust the various image parameters on the display to search for lesion or predefined target related characteristics (Zhang et al., 2016)

4.3 European Abdominal Image Quality Criteria

There are currently no validated image quality criteria specifically for abdominal CT scans for comparing FTC and ATCM techniques. Therefore, visual image quality criteria based on the commission of the European Community computer tomography criteria for abdominal CT images (CEC, 2000) were utilised. These criteria were developed in such a manner as to allow for all of the variables considered to be significant in influencing the image quality to be included (Marin et al., 2010). As described later in the method, image quality in this thesis was assessed using a series of criteria for abdominal CT images with different abdominal axial images slice (CEC, 2000).

This most recent document by the European Commission has some similarities to the other two guidelines (Jurik et al., 2000). There are quality criteria for six main groups of examinations including sensitive organs/tissues such as the cranium, face and neck, spine, chest, abdomen and pelvis, and bones and joints (pelvis and shoulder). For every examination, the quality parameters such as diagnostic requirements, which specify anatomical/diagnostic image criteria and the criteria for radiation dose to the patients, are defined (Jessen, 2001).

There are two types of diagnostic criteria, namely, anatomical and physical criteria. The former may be defined in terms of visualisation or critical reproduction of anatomical features. However, the European guidelines define the degree of visibility as follows:

Visualisation — Ability to detect the organs and structures in the volume of investigation.
Critical reproduction — Ability to discriminate structures peculiar to a specific indication to a level essential for diagnosis. Critical reproduction includes the terms:
Reproduction — in which the anatomical structures may be visible but are not adequately defined.
Visually sharp reproduction — which implies well defined anatomical structures.
The clinical question for the intended CT examination needs to be properly formulated to enable a clear description of the required image quality. Image quality criteria for several CT examinations have been compiled by the European Commission. They have also provided guidelines for high-quality imaging procedures and the use of Diagnostic Reference Levels (DRLs) (Tsapaki et al., 2014). Over fifteen years ago, the Commission of the European Community (CEC) published the computed tomography image quality criteria (report EUR 16262 EN) (CEC, 2000).

This document comprised of detailed criteria for image quality for six important aspects of CT scanning. These include scans of sensitive organs/tissue, namely cranium, chest, face and neck, pelvis and abdomen, spine, and joints and the bones (shoulder and pelvis). Each aspect included the routine scans of specific organs or body parts. For example, for the abdominal CT, an overall scan is performed including a more detailed evaluation of the retroperitoneal space, spleen and liver, pancreas, kidneys and adrenal glands.

The CEC, (2000) offer an important measure which can be used to minimise the variability in observer assessments of image quality – the provision of visual quality criteria. The proposed image quality criteria suggested by the CEC were evaluated in both a brain and lumber spine CT study by Calzado, Rodríguez, & Muñoz, (2000). They reported more intraobserver disagreements with lumber CT than brain CT. Such a study may be required to evaluate the applicability of CEC image quality criteria for abdominal CT examinations as well. Jurik et al. (2000) appraised the CEC quality criteria for five classes of examinations: (1) sinuses and faces, (2) vertebral trauma, (3) lung high resolution HRCT, (4) spleen and liver, and (5) osseous pelvis. They suggested that the validity of the CEC image quality criteria are useful for optimising CT procedures in continuance of the principle that patient dose should be as low as is consistent with required diagnostic image quality.

The use of the quality criteria has its limitations because they have not been evaluated in daily clinical practice. Furthermore, it is difficult to use the criteria in cases wherein anatomical areas are missing. In addition, it may be difficult to fulfil all the different criteria because there are so many factors affecting the quality of the image. Using quality criteria is particularly an issue for patients with distortion of anatomical structures due to disease. It is also problematic when the interpretation of images is carried out on films, which makes it impossible to alter the window width and level settings to better demonstrate the listed structures (Zarb et al., 2010). Although the purpose of using quality criteria is to standardise practice and minimise variability in image quality assessment, intra-observer variability has been reported with lumber spine CT and brain CT images, with more variability observed for the former (Calzado et al., 2000). Therefore, in order to overcome these limitations, it may be necessary to use a VGA method with normal anatomical structures. Construction and validation of the image quality criteria was studied by De Crop et al., (2015); Marin et al., 2010; Jurik et al. (2000); Bhosale et al., (2015) also documented a similar conclusion. They reported that the CEC image quality criteria were useful for the assessment image quality.

4.4 Image quality comparison between FTC and ATCM using different evaluations VGA methods

The VGA method, based on observer scorings, can be used to assess image quality only after the image criteria are fulfilled. Several studies have described methods of maintaining the same levels of image quality between FTC and ATCM. A study by Kalra, Maher & Toth in 2004 compared image quality with ATCM and FTC for CT examinations of the abdomen and pelvis. Image quality from both techniques were compared for each of the 62 CT datasets by two subspecialty radiologists who independently evaluated the images using a VGA (absolute) using a five-point Likert scale (1 representing unacceptable and 5 excellent). The study showed that ATCM resulted in reduced tube current–time compared with FTC, with similar diagnostic acceptability and subjective image noise levels.

Namasivayam and colleagues, in 2006, carried out a study optimising ATCM protocols for CT examinations of the neck. ATCM datasets were compared with FTC examinations with respect to radiation dose exposure and image quality. In their study, the diagnostic suitability of images was assessed by two radiologists, again utilising the absolute VGA method. They reported that similar subjective noise and diagnostic acceptability were observed with both Z-axis ATCM and FTC. Similarly, a study by Rizzo et al. (2006), using the absolute VGA method with signal constant tube current, also reported similar image quality, artefacts and diagnostic suitability when the ATCM method was compared to FTC for pelvic and abdomen CT examinations. They reported no significant difference between the two techniques with acceptable image noise and diagnostic acceptability.

In another study by Lee et al. (2009), the difference in radiation dose and image quality between FTC and ATCM in patients undergoing craniocervical CT angiography using a 64 MDCT system was compared. No significant difference in visual image quality at the shoulder region was reported. However, higher noise values (physical method) were noted at the upper neck region with ATCM. They concluded that, while ATCM techniques for craniocervical CT angiography reduced radiation exposure, there was no difference in image quality. In their study, image quality was independently assessed by two neuroradiologists utilising an absolute VGA method. Physical image quality was compared between angular ATCM and FTC CT scans in a study by Sabri et al. (2015). Their experiments were carried out using a thoracic phantom and image quality was evaluated physically using region of interest (ROI) analysis. However, results for this study demonstrated that the ATCM had higher image noise when compared with FTC technique. A study by Su et al. (2010) compared the image quality between z-axis ATCM MDCT and FTC with two constant parameters. Using an absolute VGA image

quality evaluation method, no significant difference in the quality of images with either method was reported.

Peng et al. (2009), in a study involving young children undergoing 64-slice MDCT chest scans, evaluated the use of an ATCM with a view to maintaining consistent image quality. They showed a statistically significant decrease in the quality of CT images in the study group. However, all image outputs were of acceptable diagnostic quality. When an absolute VGA scale was used to evaluate image quality, they found no statistically significant difference between FTC and ATCM.

An experiment by Wang et al., (2013) evaluated image quality by comparing ATCM (with different noise index) with FTC. The experiment was carried out using an abdominal phantom specifically designed to replicate Chinese patients. Radiologists with at least five years of abdominal CT diagnosis experience, from three hospitals, independently carried out a visual evaluation of the images using an absolute VGA scoring method. In addition, the physical region of interest analysis method was also used to evaluate the image quality. The study reported no statistically significant difference between ATCM and FTC, when the noise index (NI) was less than 10 in study subgroups. However, there was a statistically significant difference between the ATCM and FTC when the NI was greater than 13. The study concluded that SD can be slightly larger than NI for abdominal CT examinations when using ATCM.

Lee et al. (2011b) also compared ATCM with FTC for pelvic and abdominal CT examinations. They assessed the noise level in the liver parenchyma using absolute VGA with a five-point scale. Their study showed similar image quality between ATCM and FTC. The results of these studies support the use of ATCM for normal abdominal and pelvic CT scans. To facilitate the comparison between the studies described above, **Table 4-2** shows example of studies which have used different image quality evaluation methods for comparing FTC and ATCM CT techniques. The image quality evaluations which used absolute VGA found it was the most superior form of image quality assessment with different methods for CT scan examinations.

Table 4- 2: Example of studies which have used different image quality evaluation methods for comparing FTC and ATCM CT techniques.

Authors	Year	Image quality evaluation method	Image quality (FTC and ATCM)
Kalra et al	**2004a**	Absolute VGA five point scale	Similar image noise and diagnostic acceptability at CT of abdomen and pelvis
Namasivayam, et al	**2006**	Absolute VGA five point scale	Similar subjective noise and diagnostic acceptability
Lee et al	**2009**	VGA absolute method 5-point scale	ATCM and FTC maintained diagnostic image quality.
Su et al	**2010**	VGA absolute method four-point	ATCM maintenance of the image quality of hepatic with FTC
Lee et al	**2011b**	VGA absolute method five-point scale at five anatomic levels	Image quality between FTC and ATC are maintaining diagnostic image quality.
Rizzo et al	**2006**	VGA absolute method four-points	Similar image quality between FTC and ATCM
Wang et al	**2013**	absolute VGA method	no statistically significant difference between both ATCM and FTC

4.5 Chapter Summary

From what has already been discussed regarding VGA methods of assessing image quality, physical measures and visual image quality have been deemed useful CT examination for comparing between FTC and ATCM and characterising the intrinsic performance of imaging both techniques. Nevertheless, both methods rely on generalisations or assumptions, and therefore their accuracy in determining clinical imaging performance is limited. The results of image quality evaluation must be confirmed empirically. In addition, they do not predict the behaviour of the human observer and therefore do not take into consideration the display and observation steps of the imaging process, resulting in little information regarding direct clinical implication (ICRU 2012).

VGA employs a visual/clinical method for measuring image quality and the outcome may be more pertinent to the clinical setting when compared to physical measures. Visual methods concentrate on how easily anatomical detail and can be visualised by an observer (Månsson, 2000 & Ludewig, 2010). VGA is therefore very relevant to the aims of this thesis because this thesis evaluates image quality from normal 'phantom' abdominal CT images without the presence of any pathology. VGA is, therefore, one of the methods used to assess image quality in this thesis, along with physical measures SNR and CNR. Also, VGA was used because it most closely represents what happens in clinical practice.

Finally, from reviewing the image quality literature there are a number of gaps in the knowledge base. There is no evidence that either the relative VGA method or the physical method have been used extensively to compare the image quality of abdominal CT scans between FTC and ATCM techniques with different acquisition parameters.

Chapter Five: Methods

5.1 Chapter Overview

In this chapter, the materials and methods used to compare radiation dose and image quality between FTC and ATCM CT examinations will be described. An anthropomorphic adult phantom was used for the assessment of image quality, and a CIRS Adult ATOM phantom was used for dosimetry purposes. It is important to highlight the difficulty of directly comparing FTC and ATCM techniques together. ATCM scanning, using a Toshiba Aquillion 16 CT scanner, requires the selection of a SureExposure 3D setting (low dose +, low dose, standard, etc.). In order to allow a fair comparison with the relevant FTC technique, a series of data correction steps were required for radiation dose data. To achieve this, the radiation dose from the ATCM (raw) data was corrected using an equation reported in Venkat et al. (2014). This provided an opportunity to mathematically correct the ATCM data in order to match as closely as possible the acquisition conditions from the relevant FTC examination (tube current). Throughout the study, measurements of ED were performed using three different methods: (i) direct dose measurement using MOSFET dosimeters within the CIRS Adult ATOM dosimetry phantom; (ii) mathematical assessment by DLP and k factors; and (iii) a simulation method using the ImPACT software. In addition, ER values were also established from direct dose measurements using the MOSFET dosimeters. ER was calculated using Brenner's equations from the BEIR VII 2006 report (Brenner, 2012).

Image quality assessment comparing between FTC and ATCM were made using physical (e.g. SNR) and relative visual grading analyses (Mraity, England, & Hogg, 2014). The physical image quality was calculated using SNR in order to compare between ACTM and FTC; this included five different abdominal organs (liver, spleen, pancreas, left kidney and right kidney). Relative VGA was used to compare between ATCM and FTC for five abdominal axial images.

Radiation dose and image quality were collected for 45 CT protocols, comprising five different tube currents for FTC and five different SD values for Sure Exposure 3D ATCM, each tube current / image noise setting was acquired with three different pitch factors and three different detector configurations. The acquisition parameters are detailed in **Appendix I**. All experiments were carried out in University of Salford University Susan Hall Imaging Facility using Toshiba 16 Aquilion CT scanner, CIRS Adult ATOM dosimetry phantom and an anthropomorphic adult phantom image quality phantom. **Figure 5-1** diagram illustrated the overall study design.

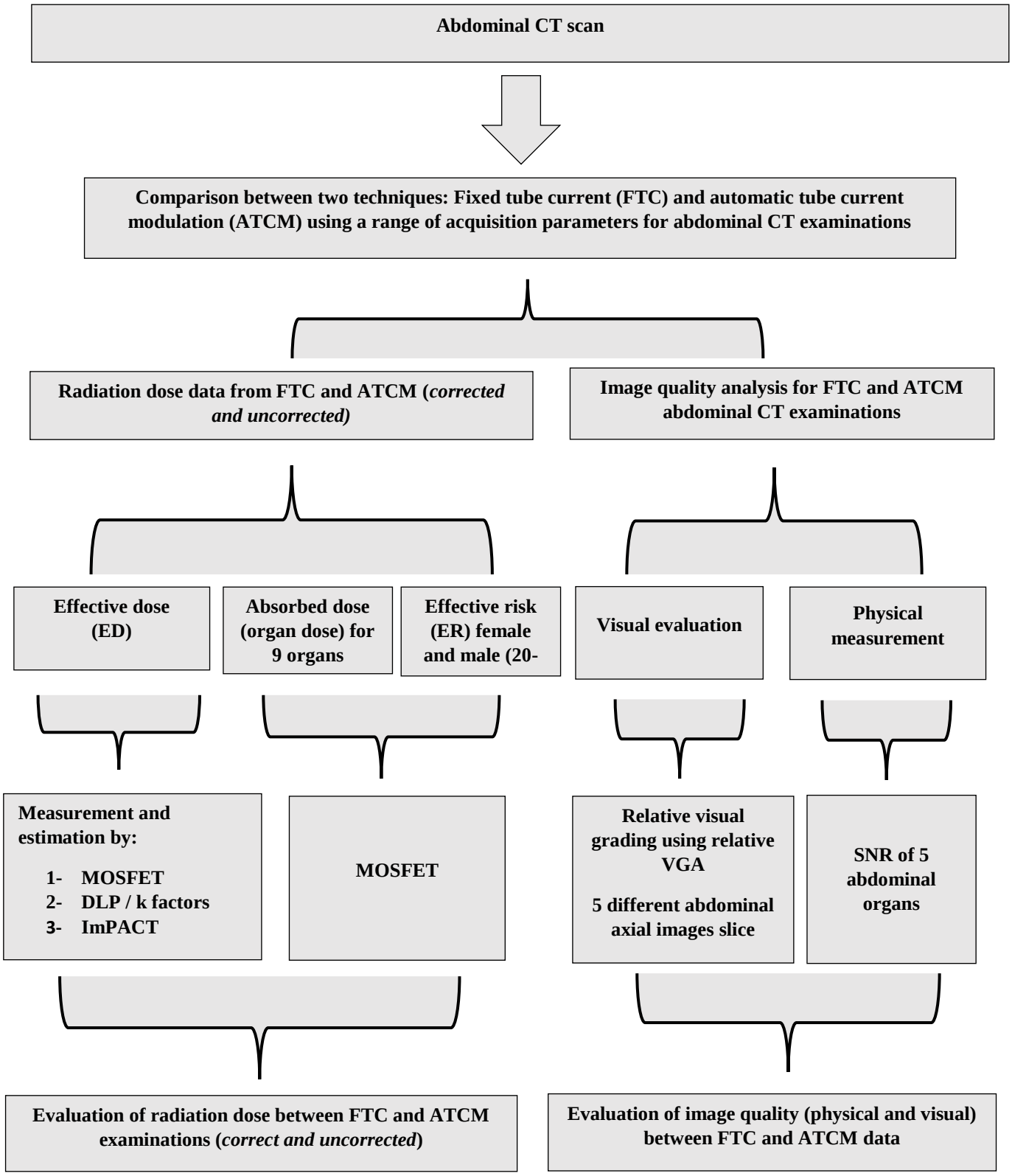

Figure 5- 1: This diagram illustrated the overall study design

5.2 Abdominal CT image acquisition and quality control testing

5.2.1 CT system

The CT scanner utilised was a Toshiba Aquilion 16, which is a third-generation multi-slice helical CT scanner. It has a 7.5-MHU tube and a 60 kW generator (Toshiba, 2014). Its gantry is standard design and based on traditional slip-ring technology. The scanner can carry out both 0.5-second and 0.32-second partial scans, thus it is capable of meeting the demands of helical and dynamic examinations. It can acquire 16 parallel data rows per rotation in the helical mode. These can be achieved with: collimation values of 16 x 0.5 mm, 16 x 1 mm, and 16 x 2 mm; multiple kV selections of 80, 100, 120 and 135 kV; and three pitch factors (detail-0.688, standard-0.938 and fast-1.438). **Figure 5-2** shows the Toshiba Aquilion 16 used in this thesis (Kulama, 2004 & Toshiba, 2014).

Figure 5- 2: Toshiba CT scan 16 slices (Toshiba Medical Systems, Tokyo, Japan)

The Toshiba scanner utilised Sure-Exposure 3D ATCM. This enables the operator to adjust image quality using a predefined standard deviation (SD) which provides an indication of the acceptable levels of noise permissible in the scan volume (Standard SD 5.00, Low dose+ SD 12.50, Low dose SD 7.50, Quality SD 3.00 and High Quality SD 1.00). This method depends on the SD of the pixel values measured. The operator is able to adjusted the SD value for image noise when ATCM has been selected; the tube current is adjusted manually for FTC. Once the

adjustments are made, an anterior and lateral CT localiser "scanogram" is acquired. Sure-exposure must be disabled in order to use the manual (fixed) tube current, which enables manual control of all the acquisition parameters (Söderberg, 2008 & Toshiba.2014).

5.2.2 Quality control (QC) Process

Routine QC was performed prior to utilising the CT scanner for experimental purposes. The QC procedure used was in accordance with the recommendations and guidelines set out by the American Association of Physicists in Medicine (AAPM) (2006), the Institute of Physics and Engineering in Medicine (IPEM) (Iball, Moore & Crawford, 2016) and the American College of Radiology (ACR) (ACR, 2015). Also the recommended ACR daily quality control checks (ACR, 2012), which involves the monitoring of image noise, CT number and image artefacts, were also conducted. The ACR recommendation is only possible with automatic evaluation methods, nevertheless it is a common practice in many radiology units around the world (Nowik et al., 2015).

The QC was carried out using Toshiba QC phantoms. These are cylindrical phantoms which are used for head and body scanning. Measurement of spatial resolution was performed using high contrast beads, wires or edges. This can be visualised with regular arrays of inserts of diminishing size and of high contrast. The insert has samples of different materials of specific CT numbers for specific radiation energies, which are utilised for low contrast detectability and the determination of the linearity of CT number (Franco & Tahoces, 2014; Nowik et al., 2015). The Toshiba CT scanner was serviced four times every year and has its performance evaluated by qualified medical physicists from. The Christie Hospital in the North West of England.

The results of all QC tests fell within the acceptable levels, as recommended by the radiation protection legislation by ICRP and the manufacturer (ICRP, 2007; Toshiba, 2014). All CT scan QC results were shown in **Appendix II**.

5.2.3 CIRS Adult ATOM dosimetry phantom

For dosimetry purposes, the human body was simulated using the CIRS adult ATOM dosimetry phantom (model 701 from CIRS, Inc, Norfolk, Virginia; see **Figure 5-3)**. The CIRS Adult ATOM phantom was made from epoxy resin and is 173 cm tall, weighs 75kg with a chest dimension of 23cm by 32cm. It has 39 cross-sectional slabs each of which is 25 mm thick. There are 5-mm pre-drilled holes within each slab to accommodate the dosimeters (TLD chips or MOSFETs). Assembling the phantom slabs forms the head and trunk of the body. The phantom has photon attenuation values which are within about 1% of bone and soft tissue and about 3% for lung tissue at photon energies between 30 keV and 20 MeV (Tootell et al., 2013).

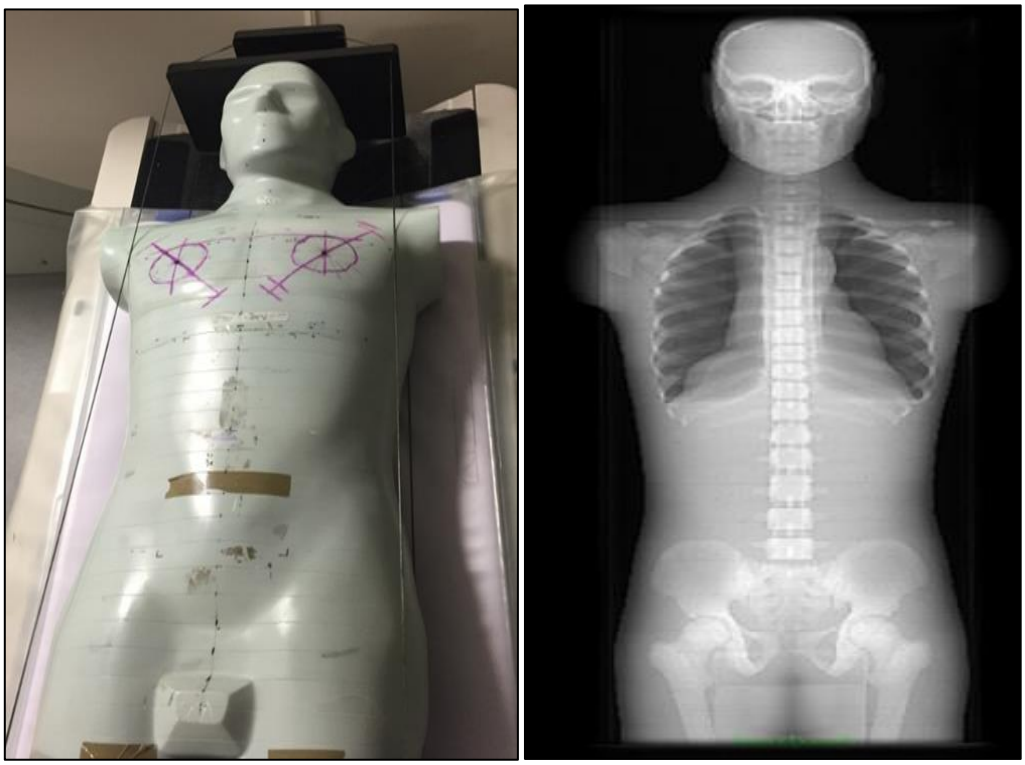

Figure 5- 3: CIRS 701 Adult ATOM dosimetry phantom used for radiation dosimetry within the study

The CIRS adult ATOM phantom comprises of 273 dosimeter locations in 23 internal organs to allow accurate estimation of radiation dose. When not in use, the holes within the slabs were plugged. This can be done with bone, tissue or lung equivalent materials, depending on the location. The position of the holes is determined using detailed anatomical information about the average location of the 23 organs. The internal organs were outlined on an organ map, which also details the locations of the holes (see **Figure 5-4**; CIRS, 2013). The choice of this phantom was based on the similarity of its attenuation properties to humans. CIRS Adult

ATOM phantoms are frequently used in medical physics and radiology and they have traditionally been considered as representative of the human anatomy (Hurwitz et al., 2007). A further reason for selecting the CIRS Adult ATOM phantom was that it is ethically unfeasible to conduct *in vivo* dosimetry on real subjects. However, a dosimetry phantom which simulates the human body can be used for this purpose, as supported from previous studies as (Zhang, et al., 2013b; Tootell et al., 2014a; Ali, England, Mcentee, & Hogg, 2015).

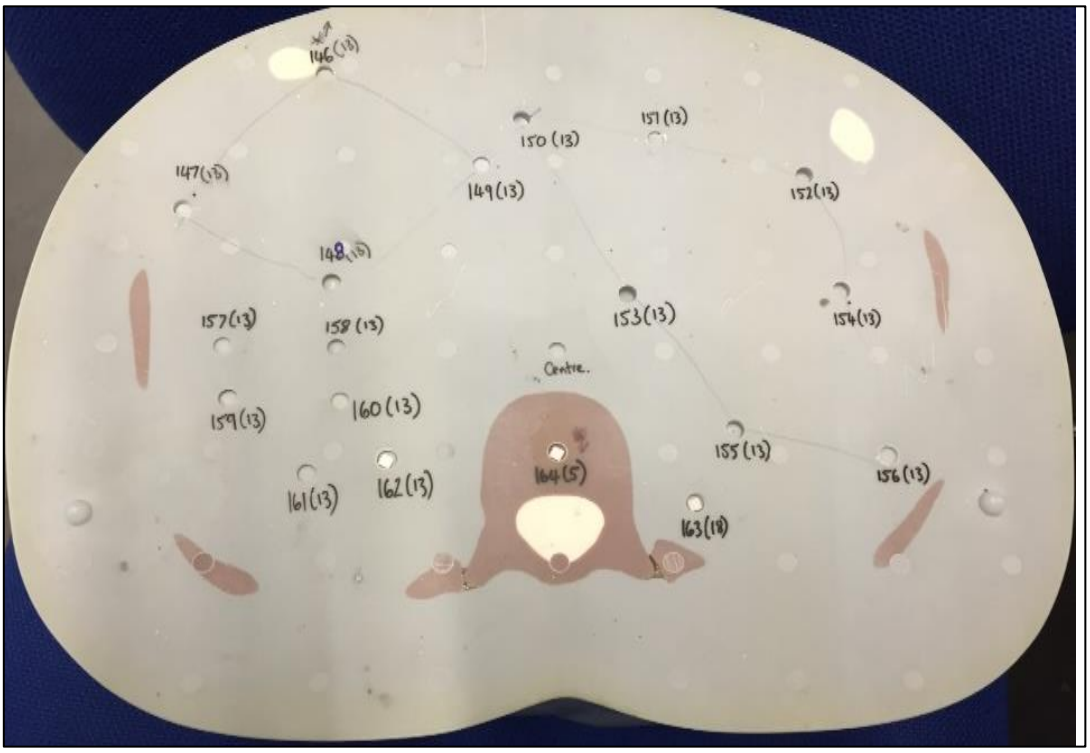

Figure 5- 4: Photograph displaying a cross sectional slab through the ATOM phantom; this shows the organ outlines and also the hole numbers where TLDs or MOSFETs can be located.

The organ map and look-up table were used to help the user optimise the quantity of TLDs or MOSFET detectors that were required for dosimetry. The look-up table indicates the number of TLDs or MOSFETs to be inserted as well as the hole number for each tissue and the corresponding depth they should be placed within each hole. To accommodate MOSFET detectors, the ATOM MOSFET Cartridge (which is available in bone and soft tissue formulations) is required as an accessory. **Figure 5-5** shows the standard solid tissue equivalent plugs, MOSFET cartridge and position. (CIRS, 2013; Xu & Eckerman, 2009).

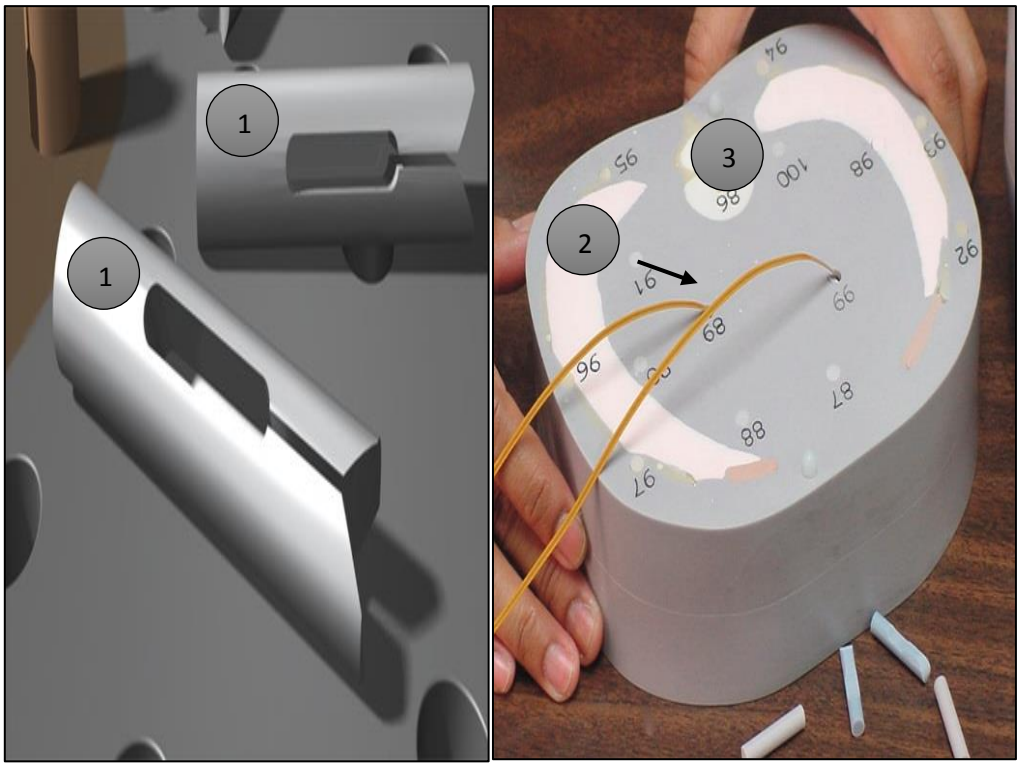

Figure 5- 5:(1) standard solid tissue equivalent MOSFET plugs,(2) MOSFET with plug in position and (3) CIRS adult ATOM phantom organ numbering (CIRS, 2013).

5.2.4 CT Adult Anthropomorphic Abdomen Phantom

The adult anthropomorphic abdominal phantom (PH-5 CT Abdomen Phantom, Kyoto Kagaku Company, Japan) was used for image quality assessment and is representative of different tissue densities found within the human abdomen. The phantom has a height of 30.5 cm and is 28.5 cm wide. Its axial (z-axis) length is 16 cm. (Lança et al., 2017). Organs and tissues, such as the liver, kidneys, pancreas, inferior vena cava, spleen, bile duct, hepatic artery, and hepatic vein, are represented within this phantom (see **Figure 5-6**).

The choice anthropomorphic phantom used in this thesis for image quality evaluation was made based on its being constructed from tissue-equivalent materials that represent various parts of the human body **(Table 5-1,** KYOTO KAGAKU CT, 2015**).** It has similar physical properties to human tissue, such as density and X-ray attenuation coefficients, and it has the advantage of being able to simulate clinical imaging conditions without irradiating humans. This means that, theoretically, an unlimited number of exposures can be undertaken for a more reliable comparison of the same anatomy under different imaging conditions, without any risk being incurred to a human.

Figure 5- 6: CT anthropomorphic image quality abdomen phantom used in this study

Table 5- 1:Comparison of abdominal organ HU values between humans and the anthropomorphic image quality phantom (Lim et al., 2014; Lamba et al., 2014; Bird, 2011;Vancauwenberghe et al., 2015)

Organs	HU values for human	HU values for anthropomorphic image quality phantom
Liver	**55-75**	**60 -78**
Spleen	**37- 49**	**40 -49**
Pancreas	**20-40**	**19 -36**
Kidneys	**15 -25**	**20-26**

5.2.5 Positioning of the CIRS Adult ATOM and Anthropomorphic phantoms for abdominal CT examinations

In order to simulate an abdominal CT examination, both phantoms were placed in a supine position, head first. A scan volume (205mm) with 41 slices was utilised, commencing at the level of the 11th thoracic spine vertebral level to the 4th lumbar spine vertebral level. Table height was 114mm for FTC and ATCM acquisition protocols which corresponded to the mid-axillary line. The scan range was checked using a scanogram before commencing scanning.

In order to avoid and reduce any random errors, careful positioning was undertaken during the CT scanning procedures with information available in pictorial and written formats (**see Figure 5-7 and Figure 5-8**).

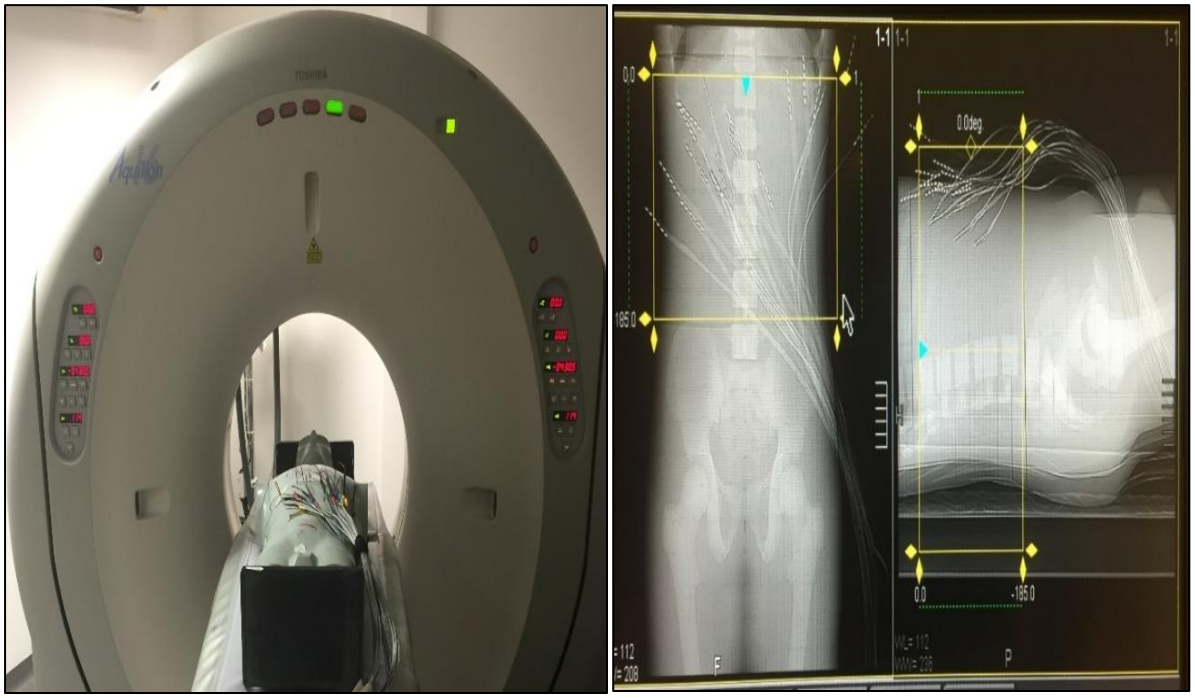

Figure 5- 7: Position of the CIRS adult ATOM dosimetry phantom and typical abdominal CT scanogram used in thesis

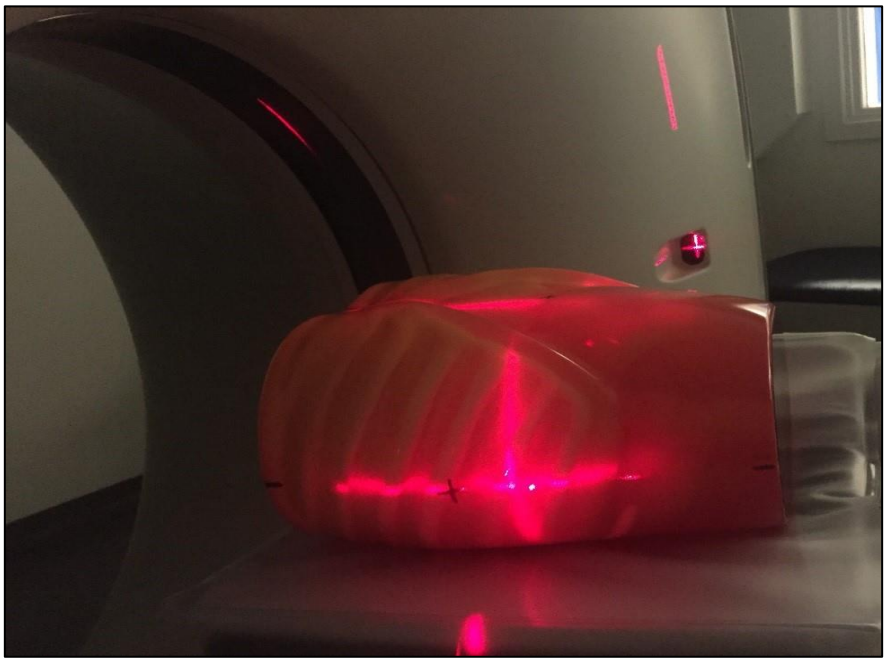

Figure 5- 8: Anthropomorphic abdomen phantom position, the CT laser lights were used as a positioning aid.

5.2.6 Abdominal CT acquisition protocols

Two different abdominal CT techniques (FTC and ATCM) were utilised in this thesis. Both techniques can be used in clinical practice, depending on the clinical indication. However, the ATCM technique was more frequently utilised due to its perceived dose reduction principles. The use of ATCM for abdominal CT scanning has been argued by Le et al. (2011) in that it can optimise image quality whilst reducing the radiation dose. As mentioned previously, the FTC and ATCM techniques were assessed whilst changing a number of scan parameters.

Full details of the CT protocol variations were shown in **Table 5-2** and **Table 5-3**. The reason for selecting the tube current range for FTC examinations (100 to 400 mA) was because this represents the range of tube currents employed by the ATCM software in order to achieve the different noise levels (SD values). As with the vast majority of abdominal CT examinations, a helical scan mode was utilised for both FTC and ATCM techniques. Acquisition parameters which stayed constant included: 120 KV, rotation time of 0.5 seconds, reconstructed slice thickness of 5 mm, large field of view and a small focal spot size. The minimum slice interval was 5 mm and the total scan time varied between 9.3 and 36.6 seconds.

Table 5- 2:Abdominal helical CT scan parameters used during FTC examinations

Tube current (m A)	Kvp	Image thickness (mm)	Rotation Time (seconds)	Detector configuration (mm)	Pitch factor
100 200 250 300 400	120	5	0.5	0.5 × 16 1.0 × 16 2.0 × 16	Detail (0.688) Standard (0.938) Fast(1.438)

Table 5- 3:Abdominal helical CT scan parameters used during ATCM examinations

Auto tube current Sure Exp. 3D		Kvp	Image thickness (mm)	Rotation time (second)	Detector configuration (mm)	Pitch factor
ATCM	SD					
Low dose+ Low dose Standard Quality High Quality	12.50 7.50 5.00 3.00 1.00	120	5	0.5	0.5 × 16 1.0 × 16 2.0 × 16	Detail (0.688) Standard (0.938) Fast(1.438)

5.3 MOSFET Dosimetry

Radiation dose measurements were carried out on the adult CRIS ATOM phantom used a MOSFET wireless system (Model TN-RD-70-W, Best Medical Canada Ltd., Ottawa, Canada). The MOSFET device TN-RD-70-W has a TN-RD-38 wireless Bluetooth transceiver, twenty high-sensitivity TN-1002RD-H dosimeters, four TN-RD-16 reader modules, and TN-RD-75M software, see **Figure 5-9**. The TN-RD-16 reader modules were capable of controlling five MOSFET dosimeters; these were operated using a high bias voltage of 30 mV/cGy in order to ensure good accuracy (Kumar et al., 2015). Communication between the personal computer and the TN-RD-16 reader modules was achieved using a TN-RD-38 wireless transceiver (Ottawa, Best Medical Canada Ltd.) (Koivisto et al., 2013). Each MOSFET was used to measure the difference in threshold voltage pre- and post-exposure. This voltage difference was proportional to the absorbed dose (Sharma et al., 2012). If necessary, four readers can be used simultaneously during each protocol. Twenty MOSFET dosimeters were used at a time in all experiments within this thesis.

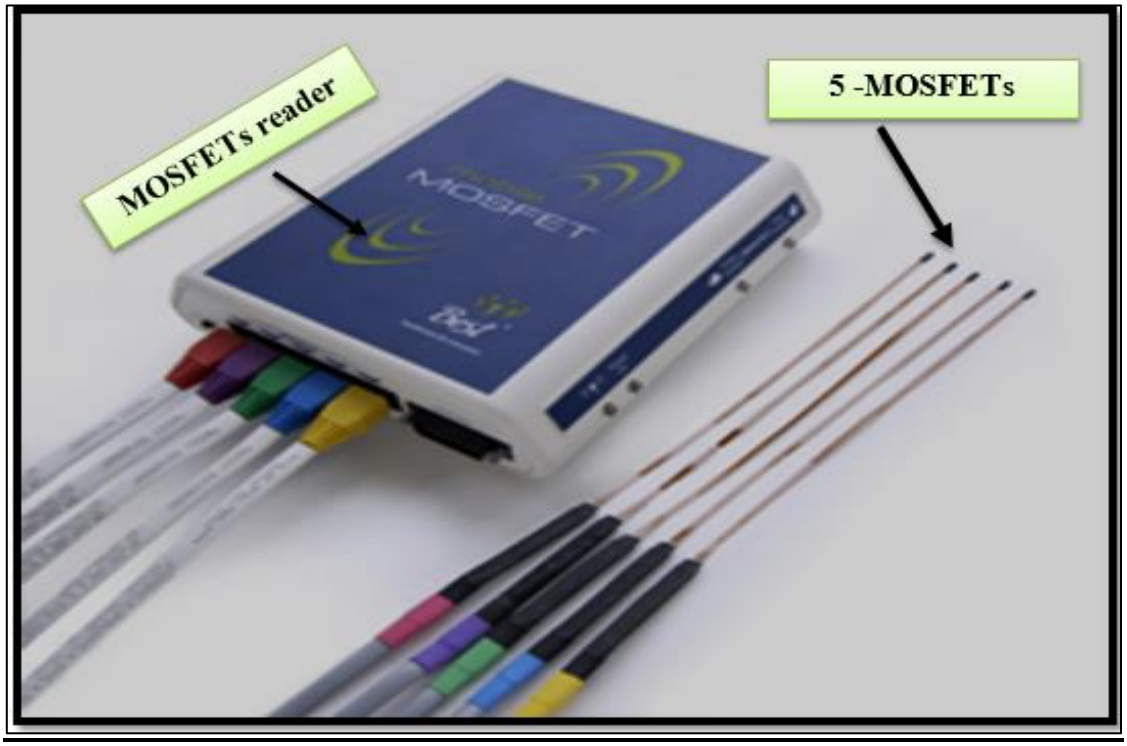

Figure 5- 9: MOSFET reader and five dosimeters.

5.3.1 MOSFET Calibration

The calibration of the MOSFET detectors was achieved using a conventional X-ray system (Arcoma, Annavägen, Sweden) - **see Figure 5-10**. The Arcoma Arco Ceil general radiography conventional x-ray tubes system has a high frequency generator and a VARIAN 130 HS X-ray tube (Mraity, England & Hogg, 2017). The MOSFET dosimeter was calibrated using 120 kVp and addition of a 1 mm Aluminium (AL) filter to x-ray tube to achieve the equivalent half-value layer of Toshiba Aquilion 16 (5-mm AL) which was consistent with the kVp and filter of the CT scanner (Jaffe et al., 2009). An Unfors 710L Mult-o-meter X-ray (Martin, 2007) was utilised. MOSFETs were exposed three times at 100, 160, 250, 360 and 450 mAs in order to minimise random error and mean and SD values were calculated. MOSFETs were placed at X-ray source which would replicate the source to detector distance in Toshiba Aquilion 16 scanner. For each MOSFET sensor, calibration factors (CF) were determined from detector response (mV) before normalisation to absorbed dose (mGy). CF calculation is based on the following **Equation 6-1**:

$$CF\left(\frac{\text{mV}}{\text{mGy}}\right) = \frac{\text{MOSFET mV resding}}{\text{Known radiation value (mGy)}} \quad \text{..... Equation (6-1)}$$

Lvall'ee et al., (2006) used a high sensitivity bias and reported a nonlinear reduction in the MOSFET CF at 150 kVp. Other studies have reported a reduction in calibration factor of 13.5% through the MOSFET lifetime. This suggests that MOSFETs are prone to error and steps need to be taken to minimise this. In this thesis, in order to minimise error arising from MOSFET readings, CFs were taken three times (before, during and after each radiation dose experiment). This was carried out for each of the 20 MOSFET dosimeters for both FTC and ATCM techniques. The average CFs for all the readers are summarised in **Table 5-4.**

Table 5- 4:Average calibration factors(CF) summarised across all four readers (1, 2, 3 & 4) for all 20 MOSFET dosimeters

Reader 1 (0735) Calibration Factors mV/mGy (average ± SD)	**MOSFET #1** 1.47±0.07	**MOSFET #2** 1.53±0.04	**MOSFET #3** 1.47±0.07	**MOSFET #4** 1.49±0.08	**MOSFET #5** 1.65±0.03
Reader 2 (0736) Calibration Factors mV/mGy (average ± SD)	1.46±0.06	1.47±0.05	1.48±0.07	1.46±0.04	1.51±0.04

Reader 3 (0737) Calibration Factors mV/mGy (average ± SD)	1.48±0.04	1.47±0.07	1.46±0.06	1.53±0.04	1.48±0.05
Reader 4 (0738) Calibration Factors mV/mGy (average ± SD)	1.45±0.08	1.45±0.08	1.48±0.07	1.53±0.06	1.59±0.06

The experimental setup for the MOSFET calibration process is shown in **Figure 5-10**. The bias sensitivity switch on the reader is set to high base sensitivity due to the likely relatively high radiation dose quantities expected during abdominal CT. Readings from 20 dose points were obtained per acquisition from the four readers, with each reader providing five dose measurements. The voltage obtained from each exposure was transformed into absorbed radiation dose based on the established calibration factors. Values from a solid-state dosimeter were entered in order to calculate the CFs.

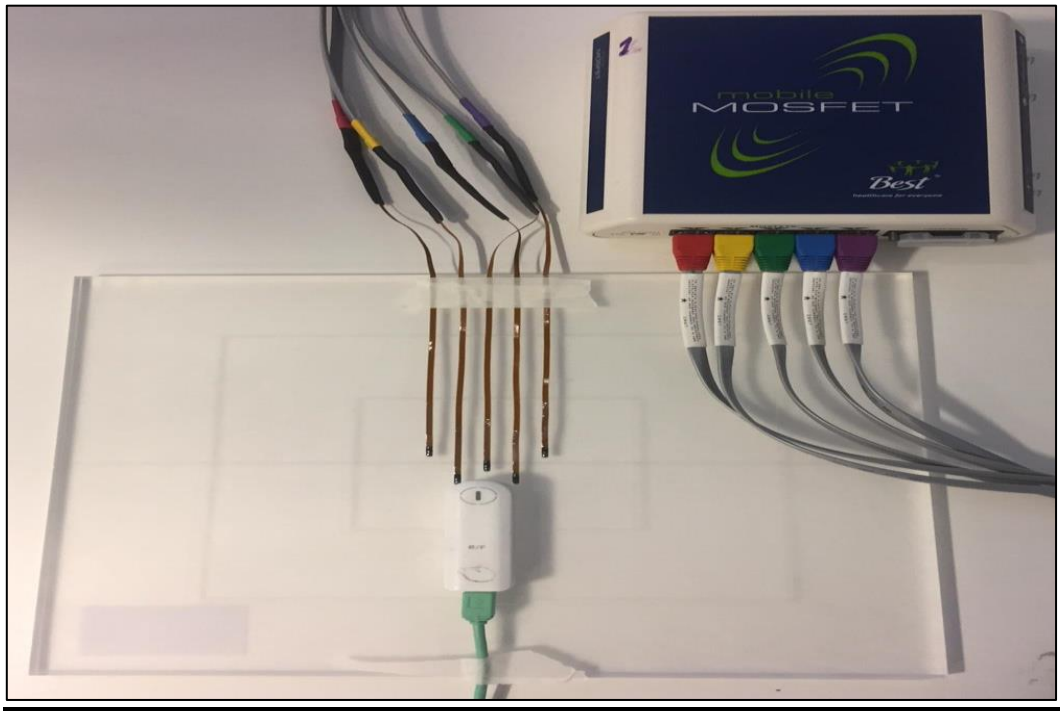

Figure 5- 10: Reader 1 and 5 MOSFET dosimeters in the calibration position alongside the solid-state dosimeter

5.4 Abdominal Radiation dose assessment

One of the main objectives of this study was to compare the radiation dose between FTC and ATCM acquisition methods **(see chapter 1 section 1.4 page 5)**. This would then allow identification of the acquisition conditions which produced the lowest radiation dose for an abdominal CT examination. However, comparison between FTC and ATCM techniques should be conducted with an unbiased methodology. A problem arises when deciding on the paired FTC / ATCM technique in terms of the tube current versus noise standard deviation. By way of an example of what FTC value would equate to a low dose + ATCM examination. In order to account for this mathematical correction of the ATCM data was undertaken. It should be noted that both corrected and uncorrected (raw) data have been presented throughout this thesis.

5.4.1 Mathematical correction of ATCM data

The average tube current for the ATCM protocols was higher than the closest comparable FTC setting in most cases (low dose + = 101mA, low dose = 205mA, standard = 366mA, quality = 422mA and high quality = 440mA). Therefore, to allow a fair comparison of the radiation dose between ATCM and FTC approaches, the ATCM data was corrected using the methodology described below.

Mathematical correction was applied in accordance with a mathematics equivalent fraction (EF) technique described by Venkat et al. (2014). The radiation dose corrected from the ATCM (raw-uncorrected) data used the following **Equation 6-2**:

$$\frac{R1}{R2} = \frac{T1}{T2} \quad \text{..... Equation (6-2)}$$

Where: **R1** = is the radiation dose (organ dose, ED and ER) *corrected from ATCM (raw) data*,

R2 = is the radiation dose results (organ dose, ED and ER) *from ATCM (raw).*

T1= is the tube current from the FTC examination (100, 200, 250, 300 and 400mA)

T2= is the average tube current from ATCM (raw) data (101, 205, 366, 422 and 440mA).

Overall, the correction intended to match as closely as possible the acquisition conditions for FTC and ATCM so that radiation dose could be appropriately compared. For the purpose of enabling clinically relevant comparisons between FTC and ATCM modalities, evaluations of the uncorrected ATCM and FTC are also presented. The radiation dose from the ATCM data

was corrected in accordance with Venkat et al. (2014), where FTC was corrected as follows: low dose+, equivalent to 100mA; low dose, equivalent to 200mA; standard, equivalent to 250mA; quality, equivalent to 300mA; and high quality, equivalent to 400mA- see **Table 5-5.**

Table 5- 5:Tube current for different FTC values and average tube current values from ATCM (raw) data after radiation dose results have been corrected to equivalent FTC values

Radiation dose from FTC (tube current)	Radiation dose from ATCM uncorrected (raw)data (tube current)	Radiation dose from ATCM corrected data (tube current)
100 mA	**Low dose+ (average mA~101)**	**100 mA**
200mA	**Low dose (average mA~205)**	**200mA**
250 mA	**Standard (average mA~366)**	**250 mA**
300 mA	**Quality(average mA~422)**	**300 mA**
400 mA	**High quality (average mA~440)**	**400 mA**

5.4.2 Measurement of organ dose, using MOSFETs

Twenty MOSFETs were used to measure the radiation dose for each abdominal CT exposure. This process was repeated multiple times until readings were obtained for all of the 273 dosimeter locations within the ATOM phantom **(see Appendix III).** Prior to each CT exposure, the MOSFET dosimeters were pre-loaded into different locations within the CIRS Adult ATOM phantom (**Figure 5-11**, Tootell et al., 2017). Owing to the availability of only 20 MOSFET dosimeters, the ATOM CRIS phantom was loaded and irradiated repeatedly in order to ensure coverage of all predrilled holes. Readings from the MOSFET dosimeters were transmitted via a wireless network to a computer where they were saved as an Excel file. In order to determine the absorbed dose, the readings were automatically divided by the respective average calibration factors (CF) **(Table 5-4 in section 5.3.1)** for each MOSFET dosimeter. To determine the doses for the 23 organs, MOSFET data from each organ were divided by the CF for each MOSFET dosimeter as follows **Equation 6-3**:

$$\text{Absorbed dose (mGy)} = \frac{\text{voltage (mV)}}{\text{CF}(\frac{\text{mV}}{\text{mGy}})} \quad \text{..... Equation (6-3)}$$

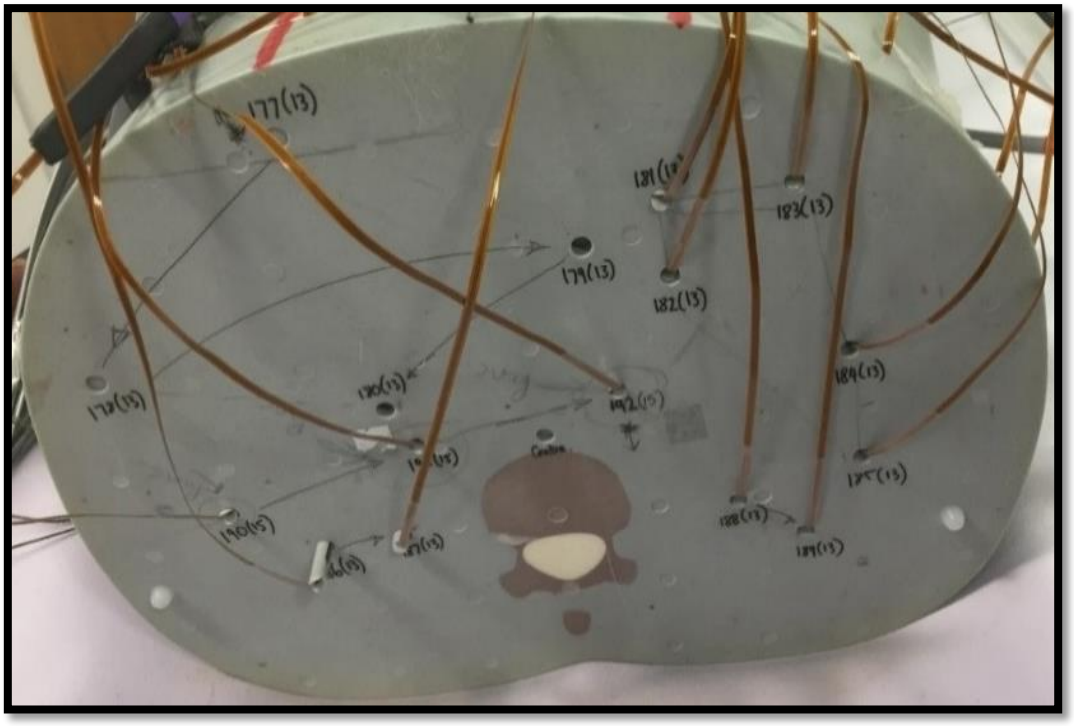

Figure 5- 11: CIRS Adult ATOM phantom with MOSFET dosimeters

5.4.2.1 Calculation of MOSFET organ doses

Absorbed dose calculations for large organs were often difficult because of the need to place MOSFET sensors in several locations within the phantom. A study by Scalzetti et al. (2008) suggested the use of 187 points of measurement in order to obtain the average absorbed dose by organs. 20 to 66 locations have been utilised in other studies (Hunold et al., 2003; Hurwitz et al., 2007b; Kawaura et al., 2006; Scalzetti et al., 2008). However, for this thesis, organ doses were obtained using 273 MOSFET dosimeter locations in order to minimise error, improve accuracy whilst at the same time making the measurements achievable in terms of the time available to conduct the study. The locations of the MOSFET dosimeters were indicated in **Table 5-6**. The MOSFET wires were fixed between the CIRS Adult ATOM phantom slabs with adhesive tape. However, the all Organ doses using the same scout projections were factored into the measurements of scan volume. DLP values were recorded when the exposures were made for MOSFETs, thereby ensuring that the scan conditions for both measured and modelled doses were the same.

Table 5- 6:Locations and number of MOSFET dosimeters in the organs and tissues			
Organs / Tissues	**Number of detectors**	**Organs / Tissues**	**Number of detectors**
Brain	**11**	**Kidneys**	**16**
Active Bone Marrow (ABM)	**75**	**Pancreas**	**5**
Eyes	**2**	**Gall bladder**	**5**
Thyroid	**6**	**Small Intestine**	**5**
Oesophagus	**3**	**Colon**	**11**
Lungs	**36**	**Salivary Glands**	**4**
Thymus	**4**	**Extrathoracic**	**2**
Breast	**2**	**Oral Mucosa**	**4**
Heart	**2**	**Bladder**	**16**
Spleen	**12**	**ovary's**	**2**
Adrenals	**2**	**Testes**	**2**
Liver	**29**	**Stomach**	**14**
Prostate	**3**	**Total**	**273**

Not all organs and tissues were modelled by the CIRS Adult ATOM dosimetry phantom. In some cases, approximate doses from other organs were used as a substitute (Brady, Cain, & Johnston, 2012). For example, the absorbed dose for active bone morrow (ABM) comprises of: cranium, mandible, vertebrae spine, clavicle, sternum, scapular, ribs, pelvis and femur). The method described by Hindorf, Glatting, Chiesa, Lindén & Flux., (2010) was used to determine the average of the absorbed radiation dose for each of the tissues from data for ages between 1 to 40 years. These were then multiplied by their corresponding percentages of ABM. The overall active ABM dose is subsequently summed before being multiplied by its respective tissue weighting factor. Finally, the oral mucosa and salivary glands have no specific location for dosimeters within the ATOM phantom, therefore, the mandible was used as a substitute. Similarly, the lack of specificity for the extrathoracic region necessitates the use of a location identified at the cervical spine (C2) and the superior margin of the oesophagus as surrogate locations. The ICRP 103 recommends the calculation of the mass-weighted mean of the upper large intestinal (DULI) absorbed dose and that of the lower large intestine (DLLI).

5.4.2.2 Reproducibility of organ dose measurements

As a further quality control step, the MOSFET dosimeters were assessed for reproducibility. This was carried out after obtaining the calibration factors for all 20 dosimeters, but before the main experiments were conducted.

The CIRS Adult ATOM phantom was scanned using the same CT scanner. The scan was repeated three times using the same acquisition factor to measurement the reliability of radiation dose measurements for FTC and ATCM examinations, before the start of the main

experiment. The average abdominal organ dose was then calculated. **Tables 5-7 and Table 5-8** show the results for abdominal organ dose from FTC and uncorrected ATCM (raw) data, respectively. Intra-class correlation coefficients (ICC) were used to assess the reliability between the three scans for each of the techniques (Rosner, 2010). This showed excellent reliability 0.999 (95%CI 0.966 to 0.999).

Table 5- 7: FTC organ dose reproducibility test results

TECH.	FTC(organs dose mGy)		
Organ	**scan1**	**scan2**	**scan3**
Liver	**20.112**	**20.474**	**20.354**
Gall Bladder	**28.980**	**29.180**	**28.980**
Pancreas	**24.780**	**24.700**	**23.800**
Spleen	**19.825**	**19.747**	**19.550**
Stomach	**25.843**	**26.021**	**25.407**
Kidneys	**23.575**	**23.331**	**24.206**
Adrenals	**12.135**	**13.685**	**12.695**
Small Intestine	**7.898**	**8.596**	**9.222**
Colon	**12.034**	**12.066**	**12.195**

Table 5- 8: ATCM (uncorrected) raw data organ dose reproducibility test results

TECH.	ATCM (raw)data (organs dose mGy)		
Organ	**scan1**	**scan2**	**scan3**
Liver	**24.708**	**24.774**	**24.975**
Gall Bladder	**41.840**	**42.420**	**40.560**
Pancreas	**34.660**	**35.580**	**34.740**
Spleen	**24.868**	**24.281**	**23.568**
Stomach	**34.336**	**34.243**	**33.371**
Kidneys	**33.719**	**34.681**	**33.875**
Adrenals	**14.905**	**13.310**	**13.535**
Small Intestine	**13.470**	**12.670**	**12.974**
Colon	**19.099**	**18.435**	**18.467**

5.4.3 Effective dose (ED)

As previously mentioned, the effective dose for FTC and ATCM were calculated using three methods: 1) direct measurement using MOSFETs, 2) mathematical estimation using DLP values and k factors and 3) mathematical simulation using the ImPACT software. For both the ImPACT and MOSFET methods, the effective doses were calculated using the ICRP 103 tissue weighting factors (ICRP, 2007; **see Chapter 3 Table 3-6 page 72**). For the DLP method, the DLP values were multiplied by the appropriate k-factors (for adult abdominal CT scans). However, the k- factors value based on also ICRP 103 (**see page 75, Chapter 3 Table 3-7).** The following subsection describes each method of estimating / calculating effective dose.

5.4.3.1 ED – MOSFET Method

MOSFET can be used to measure ED using weighted mean organ and tissue absorbed doses multiplied by the radiation organ or tissue factors. Radiation tissue weighting factors were provided by ICRP (ICRP, 2007). These were updated regularly in accordance with improved scientific understanding of the effects of radiation on the human body (**Chapter 3 Section 3.4.2).** In this thesis, the ED was determined according to ICRP 103 (ICRP, 2007) definitions by **Equation (3-5) page 72**. All tissues and organs, except the bone surface, skin, muscles and lymphatic nodes, contributed to the calculation of ED. In order to determine the contribution of each tissue to the ED, the absorbed doses for each of the tissues was multiplied by its tissue weighting factor. For marrow containing bones, the absorbed dose was multiplied with their corresponding percentages of active bone marrow.

5.4.3.2 ED- DLP k-factors method

Effective dose was calculated using the DLP and appropriate k factors. With FTC and ATCM techniques, the CTDIvol was calculated for every slice position. The CT scanner was able to automatically calculate the DLP by multiplying the CTDIvol by the scan length, based on the average effective mA for the complete length of the exposed volume (McCollough et al., 2011). The DLP value for each CRIS ATOM phantom CT exposure was recorded. Different values of DLP were recorded for the different adult abdominal CT protocols (FTC and ATCM-corrected and uncorrected (raw) data). To determine the ED, the DLP was converted using a standardised K factor for abdominal scanning (0.015 mSv/mGy×cm). This k factor was obtained from the American Association of Physics in Medicine (AAPM) report No. 96, (Deak, Smal, & Kalender, 2010; McCollough et al., 2008). Generally, the ED calculating from DLP is based on CTDIvol value using **Equation (3-6) page 74**. The ED reproducibility was assessed for the MOSFET method for both FTC and ATCM uncorrected (raw) data. **Table 5-9** shows the results for ED from FTC and ATCM-corrected and uncorrected data, respectively during the same acquisition factors (CT protocol).

Table 5- 9:DLP ED reproducibility test results

Techniques		**Scan 1 (mSv)**	**Scan 2 (mSv)**	**Scan 3 (mSv)**
FTC	**250 mA**	**8.861**	**8.861**	**8.861**
ATCM uncorrected (raw) data	**Standard(SD 5.00)**	**13.049**	**13.049**	**13.049**

5.4.3.3 ED - ImPACT simulation method

A commercial Monte Carlo simulation package (ImPACT) was also used to estimate abdominal CT ED for both FTC and ACTM techniques. Simulations were performed for adult patients only. The ImPACT software ensures rapid calculation of organ and ED. The results depend on the chosen image parameters and the model of the CT scanner **(see page 65, Chapter 3)**. The software used the ICRP 103 tissue weighting factors to estimate the ED. The average mA for every ATCM-uncorrected acquisition was determined by adding the mA for each slice together and then dividing this by the number of slices (n=41). This was done for each of the ATCM-uncorrected (raw) data protocols. **Table 5-10** shows the reproducibility results for ED estimations for FTC and ATCM techniques, respectively for the same acquisition factors.

Table 5- 10:ImPACT ED reproducibility test results

Techniques		**Scan 1 (mSv)**	**Scan 2 (mSv)**	**Scan 3 (mSv)**
FTC	**250 mA**	**12**	**12**	**12**
ATCM-uncorrected (raw) data	**Standard(SD 5.00)**	**16.972**	**16.972**	**16.972**

5.4.4 Effective risk (ER) estimations using MOSFET data

The ER was calculated using Brenner's equation (Brenner, 2007). This calculation is based on the attributable lifetime risk of cancer for different tissues. The attributable lifetime risk was obtained from BEIR VII – Phase 2 report of the National Academy of Sciences (2006 **see Chapter 3 Table 3-11 page 80)**. The life-time risk of fatal cancer inductions after standardized clinical FTC and ATCM adult protocols were calculated using the **Equation (3-7) page 79**. ER involves the collection of absorbed data for the different organs and tissues and the used of organ-specific radiation-induced cancer risk for 20 to 70 year old males and females. In this thesis, the ER was calculated for males and females of ages 20 to 70 years and comparisons were made between FTC and ATCM (corrected and uncorrected data) for both genders with different acquisition parameters.

5.5 Abdominal image quality assessment

Image quality assessment is essential in medical imaging **(see chapter 4 page 88)**. In this thesis, CT image quality was evaluated using physical and visual methods (Mraity et al., 2014). **Figure 5-12** summarises the processes involved in assessing image quality.

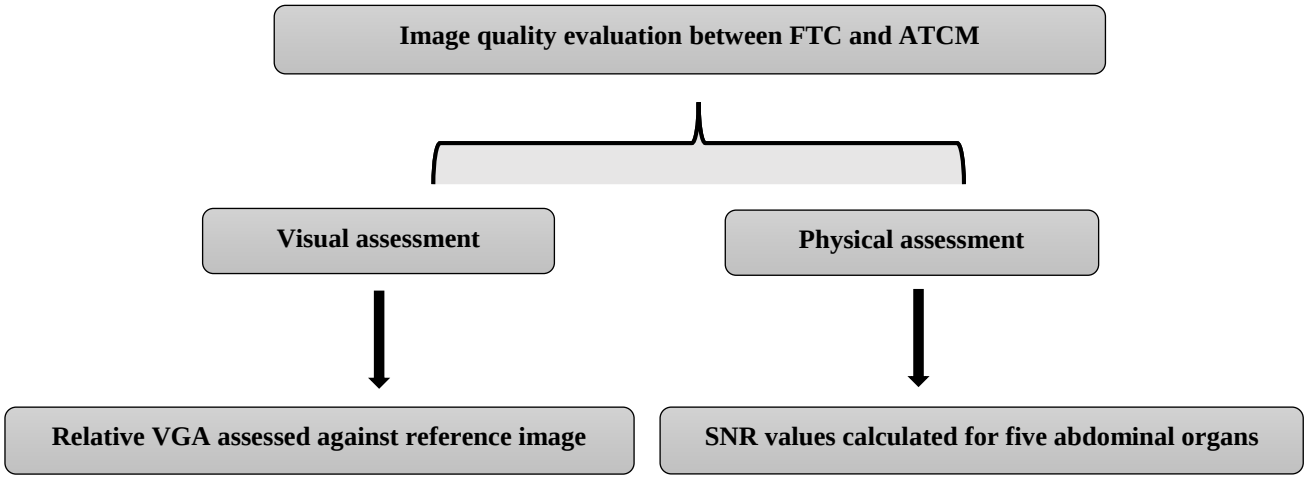

Figure 5- 12: This diagram illustrates an overview of how image quality was assessed

5.5.1 Physical assessment of image quality

Physical measures of image quality can be used to determine the technical performance of an imaging system. For this thesis, SNR was calculated as a physical measure of image quality. Image signal (S) is directly linked to the number of photons (N) and can be seen as the pixel's stochastic fluctuation around the mean value (Verdun et al., 2015). SNR has been discussed in **chapter 4 section 4.2.1**. The main reason for using SNR was that it is an efficient and reliable measure of image quality (Båth, 2010).

SNR was used to assess the level of correlation between signal and noise for the comparison between FTC and ATCM images. **Figure 5-13** shows the process of image quality assessment using SNR values. Five abdominal organs were selected for this analysis, as described in the European Guidelines (CEC, 2000) SNR values were recorded for each CT examination and for the five abdominal organs: liver, spleen, pancreas, left kidney and right kidney.

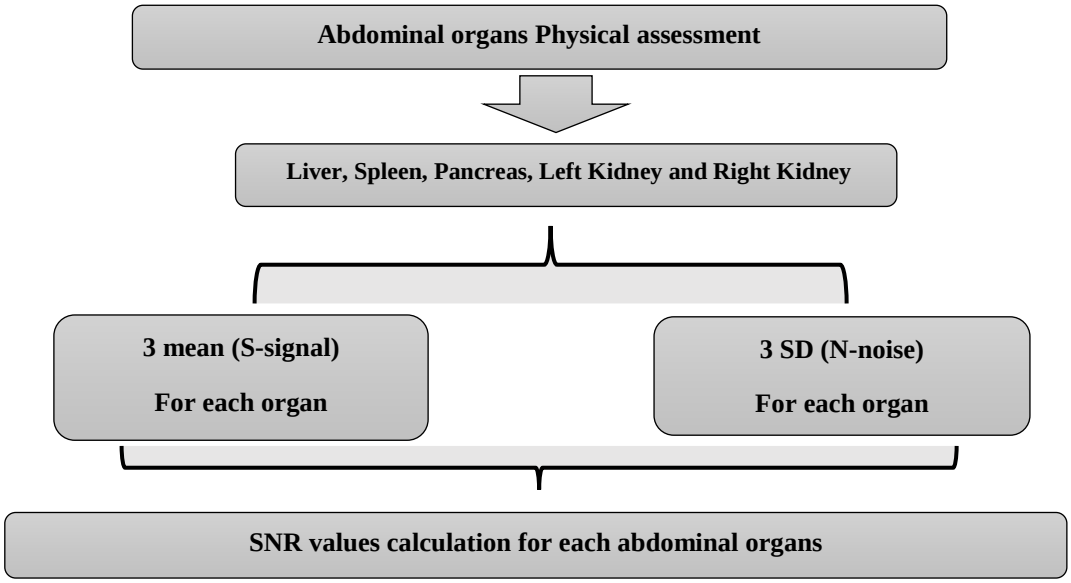

Figure 5- 13: This diagram illustrates the detailed physical assessment method using SNR within the thesis.

SNR was calculated using a standard **Equation (4-3) page 93** which provides physical image quality information regarding the comparison between FTC and ATCM. SNR is commonly defined as the ratio of mean to standard deviation of a signal. In this study, the SNR was calculated for three ROIs for each abdominal organ (Manson et al., 2016**). Figure 5-14** shows the signal (mean) and noise (SD) level of each abdominal organ and the overall SNR value. The reason for this method was to investigate how the local noise level of each ROI would affect the overall mean SNR value. This method of calculating SNR has been used by several authors (Lee et al., 2011a; Rizzo et al., 2006; Bhosale et al, 2015; De Crop et al., 2015 and Su et al., 2010).

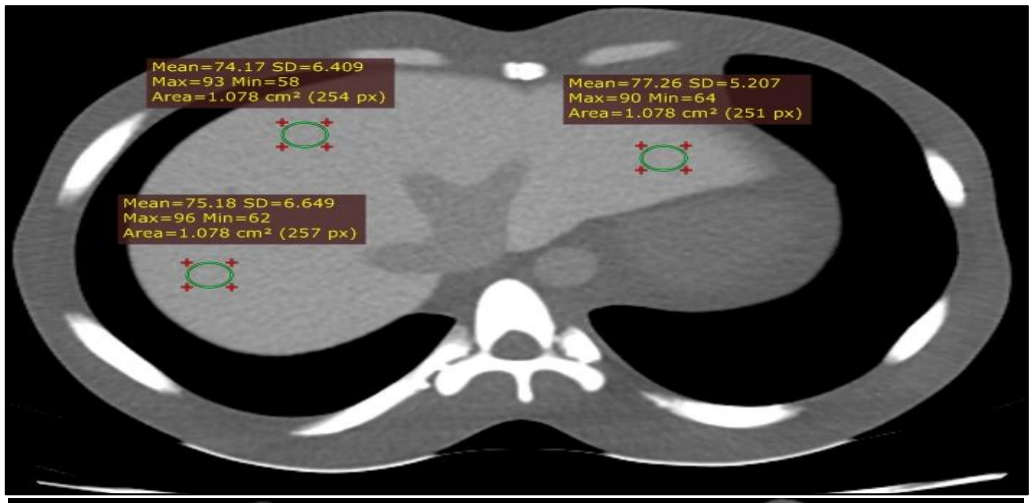
Mean=74.17 SD=6.409
Max=93 Min=58
Area=1.078 cm² (254 px)
Mean=77.26 SD=5.207
Max=90 Min=64
Area=1.078 cm² (251 px)
Mean=75.18 SD=6.649
Max=96 Min=62
Area=1.078 cm² (257 px)

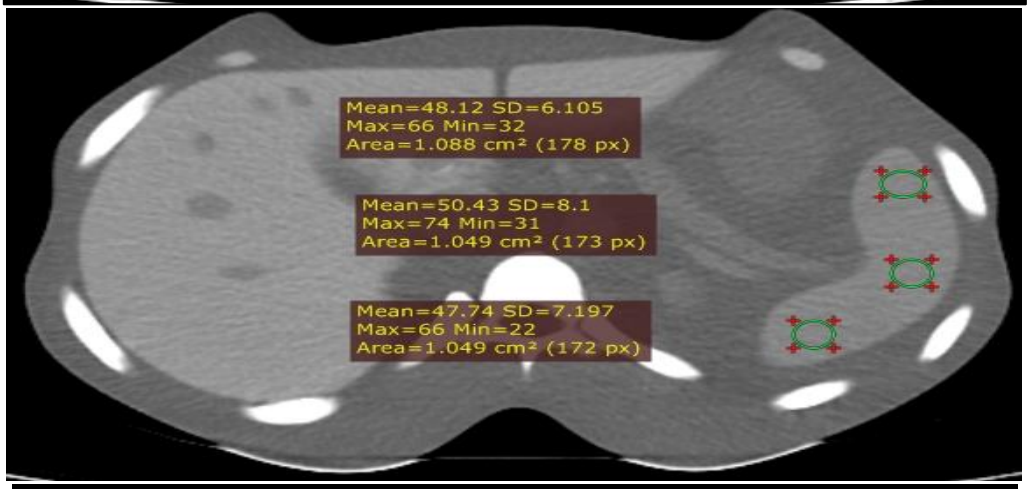
Mean=48.12 SD=6.105
Max=66 Min=32
Area=1.088 cm² (178 px)
Mean=50.43 SD=8.1
Max=74 Min=31
Area=1.049 cm² (173 px)
Mean=47.74 SD=7.197
Max=66 Min=22
Area=1.049 cm² (172 px)

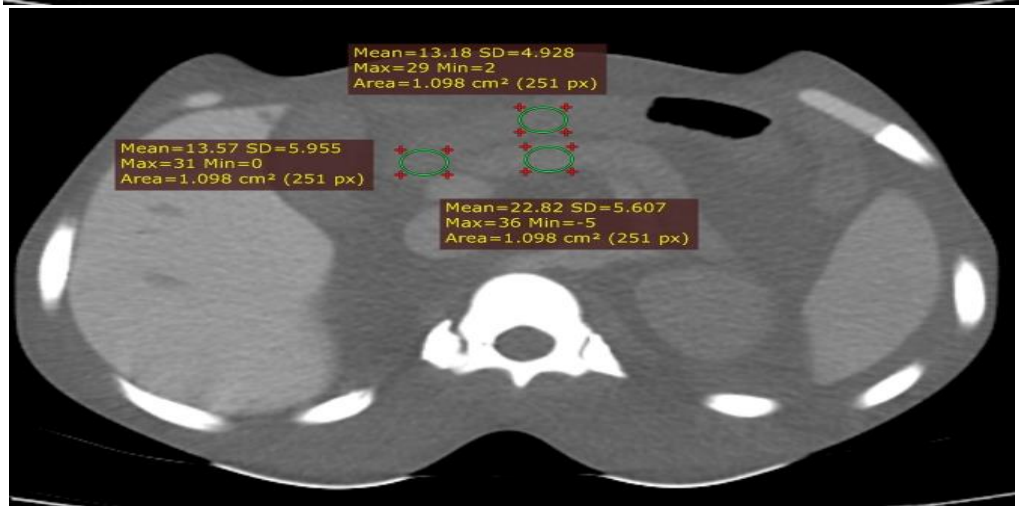
Mean=13.18 SD=4.928
Max=29 Min=2
Area=1.098 cm² (251 px)
Mean=13.57 SD=5.955
Max=31 Min=0
Area=1.098 cm² (251 px)
Mean=22.82 SD=5.607
Max=36 Min=-5
Area=1.098 cm² (251 px)

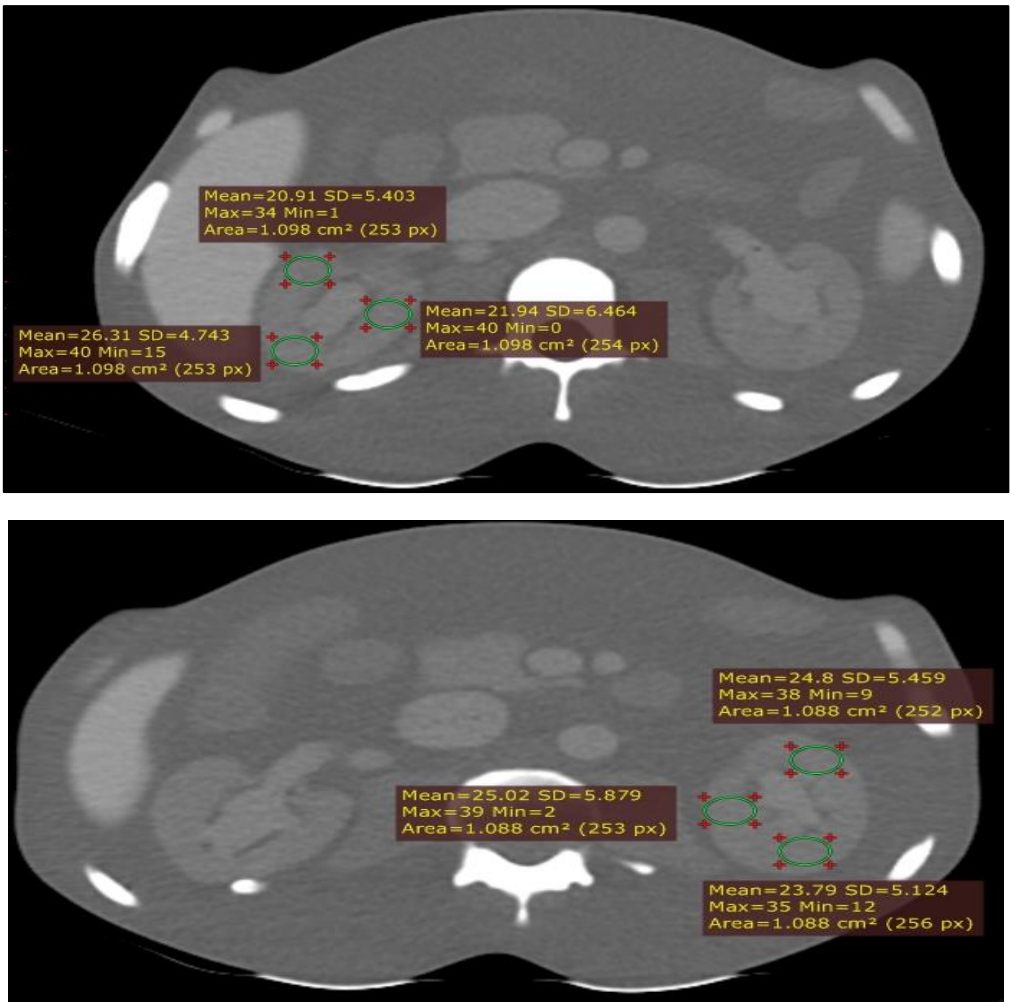

Figure 5- 14: This figure illustrates the 3 ROIs for each organ that were used to calculate SNR liver, spleen, pancreas, left kidney and right kidney, respectively.

Within this thesis, the ROIs size (1.00 cm^2) and position were kept constant for each acquisition protocol. This was done to improve accuracy when comparing between FTC and ATCM and to minimise random error. The three ROIs were selected to provide an overall objective measure for each abdominal organ. To facilitate calculations of SNR the RadiAnt DICOM Viewer software was used to calculate the mean pixel value and standard deviation for the respective ROIs. An ROI manager was used to save the location of ROIs in order to improve the reliability of results (Manson et al., 2016; Bhosale et al., 2015 and Lança et al., 2017).

The RadiAnti DICOM Viewer is a free software used for medical image processing and display. Image data import and display is in DICOM format (Digital Imaging and Communications in Medicine) (DICOM ,2013). This software can be downloaded from http://www.radiantviewer.com. (DICOM, 2016). RadiAnt DICOM Viewer has basic tools for data manipulation and measurement. It allows functions such as contrast adjustment, zooming, panning, and brightness and control. It also allows image rotation at 90 or 180 degrees and horizontal or vertical flipping, see **Figure 5-15.**

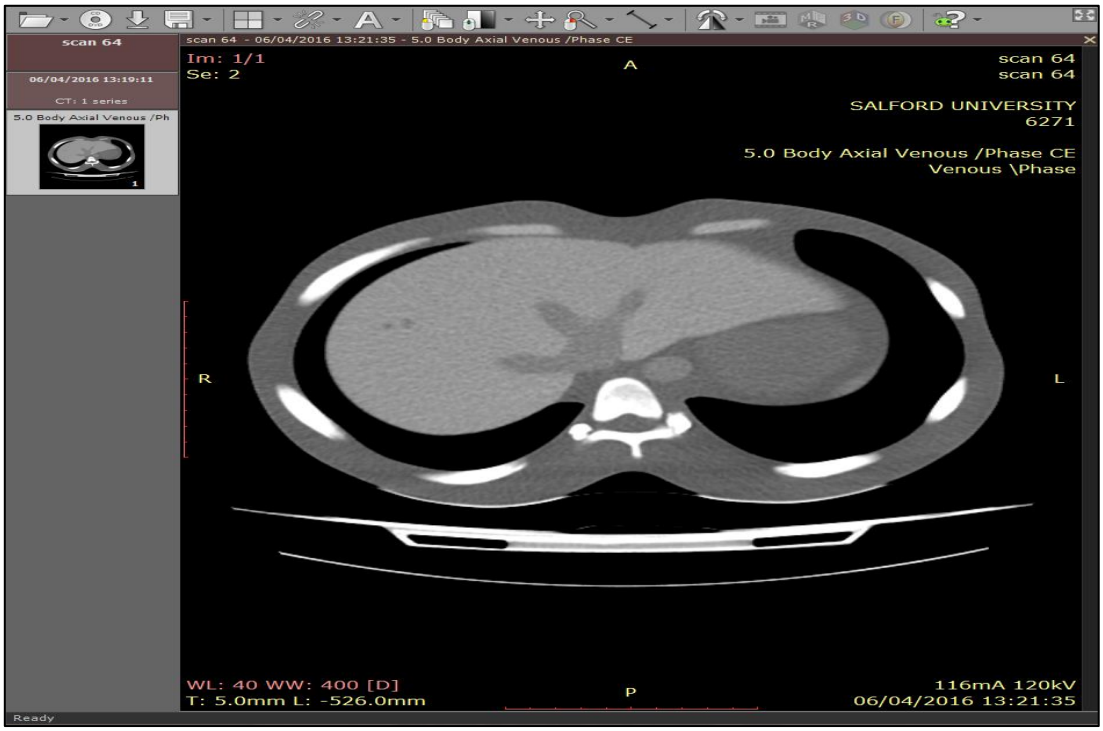

Figure 5- 15: RadiAnt DICOM Viewer displaying a study image

RadiAnt DICOM Viewer allows for ROIs measurements to be taken and the output data includes a range of metrics such as mean and SD values. It also allows concurrent browsing of several image data series on multiple split-screen panels, with automatic synchronization between the series and acquired images in the same plane (e.g. Computed Tomography series before and after contrast media administration) (DICOM, 2013). The RadiAnt DICOM Viewer has been used by a number of researchers and for similar purposes (Lança et al., 2017; Nunes, Pereira, Tomé, Silva & Fontes, 2016).

5.5.2 Visual assessment of image quality

Visual image quality assessment methods have been discussed in **chapter 4 section 4.2.3**. A relative visual grading (VGA) method was utilised for the assessment of image quality. Relative VGA is a technique that can provide information about clinical image quality as it takes into account a wider range of factors than just the physical methods (e.g. SNR).

However, this approach is subject to inter- and intra-observer variability which can occur from a range of factors that impact on human performance (Verdun et al., 2015). Relative VGA was utilised because of its high sensitivity and minimal bias (Zarb et al., 2015; Manning, Ethell, Donovan & Crawford, 2006). It provides much more consistent results and leads to less decision variability when compared to the absolute VGA method (Lança et al., 2014; Lee et al., 2011b; Rizzo et al., 2006). **Figure 5-16** summarises the visual assessment of the image quality using relative VGA method.

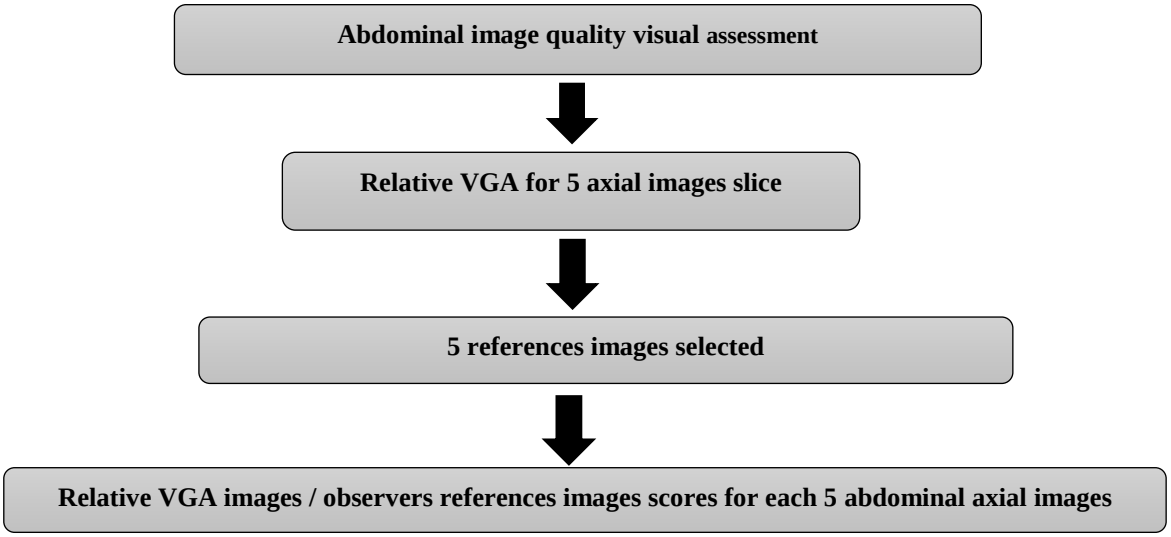

Figure 5- 16: This diagram illustrates the detailed image quality visual assessment method using relative VGA used within the thesis.

Five different axial CT images (anatomical level) were selected from 41 slices for each CT protocol (**see Table 5-11)**. These were consistent with the ones identified in the European CT Guidelines criteria (CEC, 2000). This resulted in 450 images from 90 different protocols (FTC =45 and ATCM =45). The choice of the five different axial CT images was deemed as sufficient for image quality evaluation after discussion and agreement by five expert radiographers. Discussions focused on how adequately the images demonstrated the respective organs, homogeneity and how they ensure comparison of inner structures within the phantom.

Table 5- 11:CT image locations selection for the visual assessment of image quality

Image numbers	Anatomical structures
Image # 1	**Liver parenchyma and aorta**
Image # 2	**Liver right and left lobe vessels and spleen**
Image # 3	**Liver, Gall blabber , splenic artery and pancreas**
Image # 4	**Kidneys, aorta and IVC**
Image # 5	**Renal artery, IVC and aorta**

Image #1 of the upper anterior abdomen, shows the liver size and shape. In this slice it is possible for the liver parenchyma and aorta to be seen. Image #2, of the upper abdomen, shows the complete liver size, shape (body right lobe and left lobe) and liver vessels. In Image #3, the image of the spleen and aorta are seen within the slice. In the third slice involving the middle section of the abdomen, there was visualisation of the liver size, shape (body right lobe and left lobe) and liver vessels, splenic artery, pancreas, gallbladder, aorta and IVC. Finally, Image #4 and #5 involved the lower abdomen, as seen in **Figure 5-17**. These images show the right and left kidneys, with the image of the renal artery, aorta and IVC.

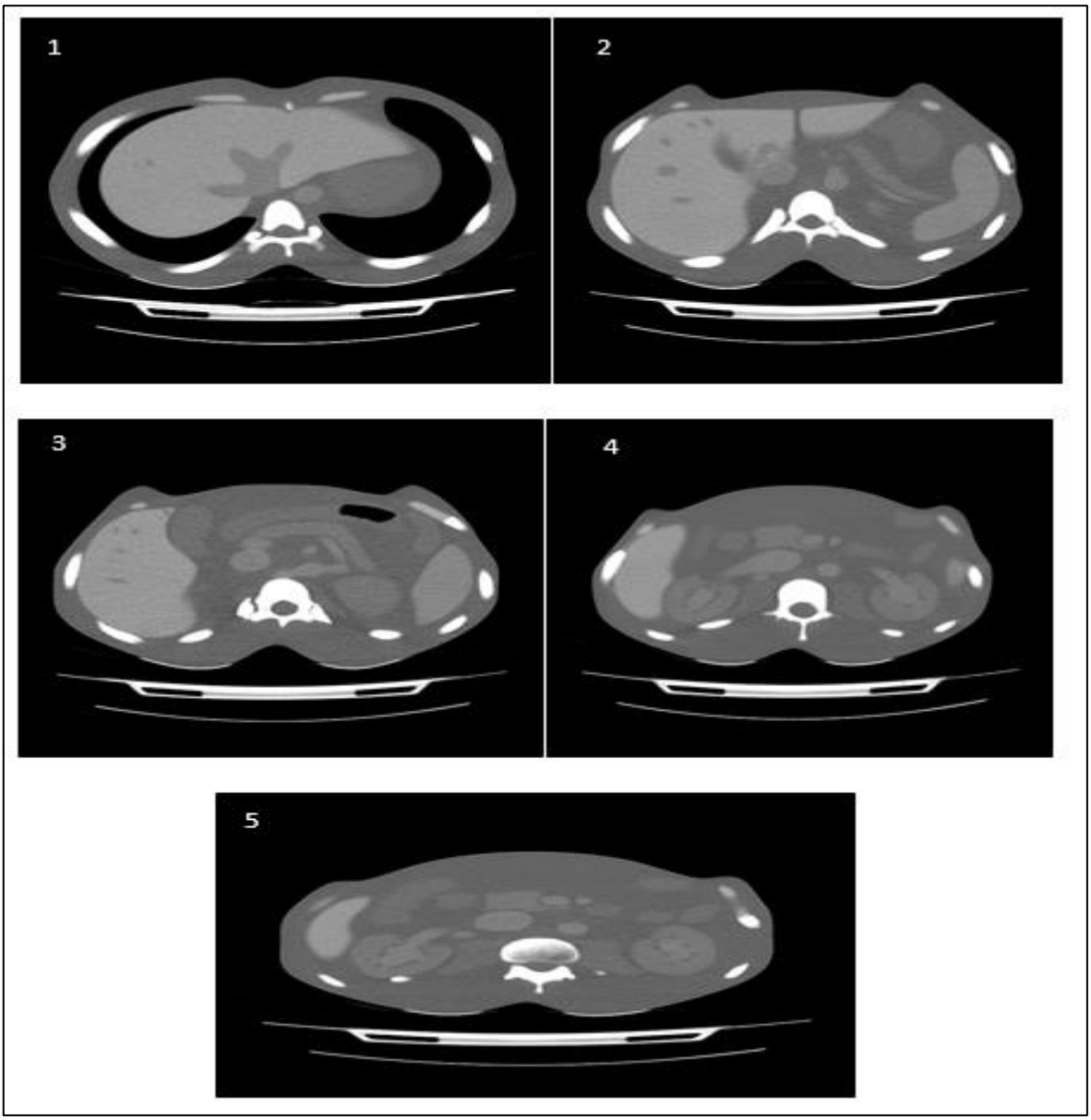

Figure 5- 17: Five different axial CT images slice acquired from an abdominal anthropomorphic phantom were used in this thesis for visual image quality analysis

Assessments for the FTC and ATCM images were carried out using the same fixed abdominal CT window width and levels (60 and 400 HU, respectively). This was based on the recommendations of the European Guidelines on Quality Criteria for Computed Tomography report 16262 (EUR, 1999). In this thesis, the five references images that were used in the relative VGA were selected using a mathematical SNR approach. The mathematical SNR approach involved the use of ROIs to calculate SNR values for each axial CT image. For example, three ROIs were created for the liver because of the high uniformity of the liver on abdominal CT scans (see **Figure 5-18)**. The images were ranked according to SNR from the

lowest to the highest. The image with the median SNR value was then selected as the reference image. This approach for selecting a reference image has been supported by Lança et al., 2017.

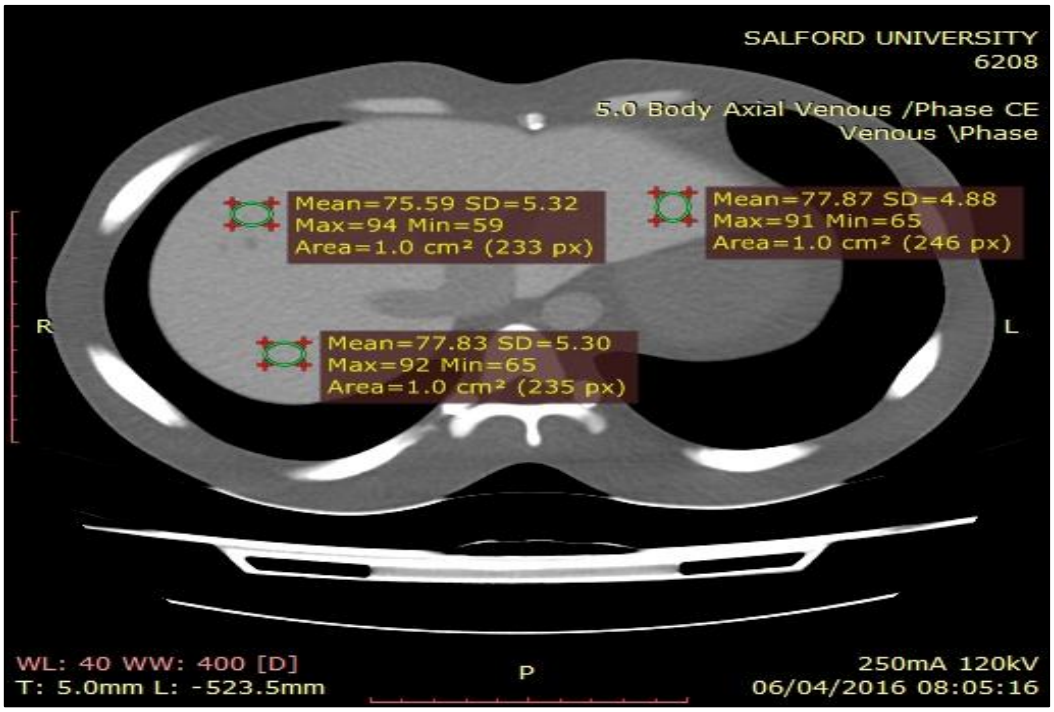

Figure 5- 18: Three ROIs placed across the whole of the liver region for calculating average SNR

For the relative VGA method, the images were displayed in a random order on two screens using bespoke software (Hogg & Blindell, 2012)**.** The software enables the observer's scores, for each image, to be captured and subsequently exported to Excel. The software prohibits the observers from adjusting window width/level or zooming, thereby reducing bias and variability. The above ensured that any differences in visual perception were due to the image acquisition parameters. The software has been used in similar study by Salamin et al., (2015).

The reference image was displayed on the same monitor throughout the course of the evaluation. Experimental images were evaluated using a 3-point Likert rating scale in order to minimise inter-observer variability from utilising a 5-point Likert scale (e.g. five-point Likert) (Abdulfatah ae al., 2014). Using a 3- instead of a 5-point Likert scale minimises the ambiguity/subjectivity which exists in a 5-point scale wherein the difference between 'worse' and 'much worse' or 'better' and 'much better' is often difficult for observers to distinguish (Phelps et al., 2015; Norman, 2010). For example, a score of 2 represents an image worse than the reference image, 3 represents equality with the reference image and 4 indicates an image that was better than the reference image. Scores of 3 and 4 were considered as acceptable image

qualities. The sum of all the visual scores for each criterion was compared between FTC and ATCM techniques for each of the five different abdominal axial CT images.

5.5.2.1 Image quality criteria

The relative VGA method relies on a series of items and statements regarding anatomical structures that should be visible on abdominal CT examinations. Providing observers with a set of criteria reduces bias, variability and subjectivity as it focuses their attention upon specific features within the image (Bath, 2010). To date, the Commission for European Countries report EUR 16262 EN (CEC, 200) has been the only body who has taken responsibility for the publication of visual image quality assessment criteria. Their criteria are used in clinical practice and as well as in research (Jessen, 2000; Jessen, 2001; Jurik et al. 2000; Zarb et al., 2010; Calzado et al., 2000; Crop et al., 2015; Bhosale et al., 2015; Ledenius, Svensson, Stålhammar, Wiklund & Thilander-Klang, 2010).

Within this thesis the criteria were extracted from CEC Guidelines and they were then evaluated for each axial CT slice by a panel of five experienced radiographers. They agreed the criteria were fit for purpose, and their decision was based on the adequacy of the organ visualisation from the anthropomorphic phantom and the ability to distinguish image quality differences for FTC and ATCM techniques **see Table 5-12**.

Table 5- 12:Image quality criteria used for the relative visual grading analysis	
Axial images slice	**Image criteria**
Image # 1	1- The liver right lobe edge is sharply defined.
	2- The liver left lobe edge is sharply defined.
	3- The liver parenchyma is adequately visualised.
	4- The aorta edge is sharply defined.
	5- Image noise is low.
	6- There is good contrast between the liver and the surrounding tissues / structures on the left of the liver.
Image # 2	1- The liver right lobe edge is sharply defined.
	2- The liver left lobe edge is sharply defined.
	3- The liver parenchyma is visualised clearly.
	4- The aorta edge is sharp.
	5- The vena cava edge is sharp.
	6- The splenic parenchyma is visualised clearly.
	7- The splenic artery is visualised clearly. (Add for slices 4 and 5).
	8- Image noise is low.
	9- There is good contrast between the liver and the surrounding tissues / structures on the left of the liver.
Image # 3	1- The liver right lobe edge is sharply defined.
	2- The liver left lobe edge is sharp (only slice 6).
	3- The liver parenchyma is well demonstrated.
	4- The gallbladder edge is sharply defined.
	5- The pancreatic contours are clearly visualised.
	6- The aorta edge is sharp.
	7- The vena cava edge is well visualised.
	8- The splenic parenchyma is clearly visualised.
	9- The splenic artery is clearly visualised.
	10- The image noise is low.
	11- There is good contrast between the liver and the surrounding tissues / structures on the left of the liver.
Image # 4	1- The liver edge is sharply defined.
	2- The pancreatic contours are well demonstrated.
	3- The aorta edge is sharp.
	4- The vena cava edge is demonstrated clearly.
	5- The right kidney parenchyma is demonstrated clearly.
	6- The left kidney parenchyma is demonstrated clearly.
	7- The right kidney pelvis and calices are clearly visualised.
	8- The left kidney pelvis and calices is demonstrated clearly.
	9- The renal vein tributaries to the vena cava are visualised clearly.
	10- Image noise is low.
	11- Contrast between right kidney and liver it good.
Image # 5	1- The aorta edge is sharply defined.
	2- The vena cava edge is sharp.
	3- The edge of the right kidney is sharp.
	4- The edge of the left kidney is sharp.
	5- Image noise is low.
	6- There is good contrast between right kidney and soft tissues on the left and right of the right kidney.

Finally, the scores images for each image were summed, based on the number of axial images slice criteria. For example, for image #1 the image quality scores would range from 12 to 24 (6 criteria 6×2=12, 6×3=18 and 6×4=24). A score of > 18 was considered an improvement in image quality and anything lower than 18 was considered a decrease in image quality.

5.5.2.2 Image viewing conditions

Two five mega-pixel computers with monochrome liquid crystal (LCD) monitors MODEL CA 95138 were used (NDS Surgical Imaging, 2014). Each computer monitor was calibrated to a DICOM grey scale standard display function. These monitors were high resolution and displayed high quality grayscale images and are routinely used to interpret clinical CT scan images (Park et al., 2011). The images were displayed in greyscale (Native resolution; 2560 x 2048 pixels). While carrying out the scoring, ambient light was dimmed to between 20-38 Lux

5.6 Relative VGA – Agreement between observers

A very large number of CT images were produced in this thesis; therefore, it was not possible for several observers to evaluate all the images. Hence, the PhD student (researcher) carried out image quality evaluation on all of the images. This was achieved on a blinded basis in which the acquisition parameters were hidden. The PhD student is a qualified radiographer with over 16 years' experience in CT scanning (as a radiographer). Given that one person scored all the images, a method was needed to assess their ability to score images using the relative VGA assessment method to ensure competency and reliability. This was achieved by assessing their performance against radiologists and radiographers prior to commencing the scoring of all the images. The method for testing observer variability and competency to score image quality is described in **Figure 5-19.**

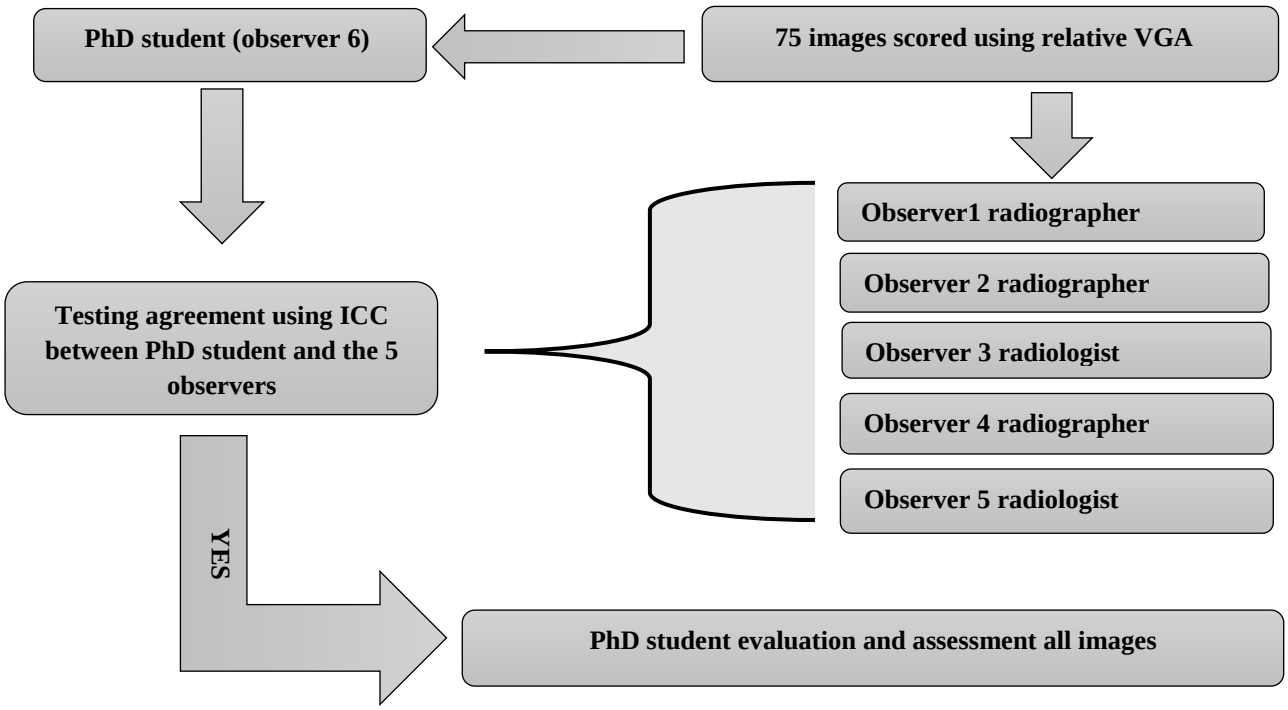

Figure 5- 19: Steps for testing observer competency and reliability in relative VGA

Five experienced observers' scores were compared against the PhD student's scores. The experienced observers included two radiologists and three radiographers. All observers had more than five years' experience in CT and this was similar to other studies (Nagatani et al., 2015). Fifteen images from five different axial images regions (15×5=75) were assessed. These images were selected objectively, depending on their SNR values, so as to acquire images with a range of different qualities (i.e. poor, moderate and good). The duration of each observation was between 60-120 minutes for each observer. When research requires human involvement, special care must be paid to volunteers' rights (EUROPEAN COMMISSION, 2016). Consequently, ethical approval was obtained for the visual grading agreement assessment between observers from the University of Salford (**Appendix IV**).

Before signing the consent form **Appendix V**, the PhD student provided each observer with a poster, a risk assessment sheet, an information sheet, a research observers training sheet and an invitation letter. This letter clearly defined the extent of the research and the manner in which the information acquired would be utilised. Once the observer agreed to participate in the study they signed a consent form to acknowledge that they fully understood what was required of them. The observers were blinded with regard to the all scanning parameters used.

Regression analysis was used for the test of agreement between the PhD student and the 5 other observers. Ordinal regression is useful in medical imaging because the data are recorded as ordered categories. The Mean Opinion Score analysis (MOS) and SD can be implemented using packages in statistical software as recommend by Keeble, Baxter, Gislason-Lee, Treadgold & Davies, (2016). In addition, intra-class correlation coefficients (ICC) were used for the assessment of inter-observer variability. ICC values of < 0.4 suggest poor agreement, values of 0.4 to 0.75 suggest good agreement and >0.75 is indicative of excellent agreement (Rosner, 2010). The observer variability (ICC) analyses were shown in **Table 5-13** below.

Table 5- 13:ICC values for the 6 observers		
Axial images slice	**No. of images**	**ICC mean (95%CI)**
Test agreement between observes 1 and 6		
Image # 1	**15**	**0.966(0.901-0.987)**
Image # 2	**15**	**0.987(0.963-0.995)**
Image # 3	**15**	**0.955(0.871-0.984))**
Image # 4	**15**	**0.973(0.922-0.991)**
Image # 5	**15**	**0.950(0.950-0.982)**
Test agreements between observes 2 and 6		
Image # 1	**15**	**0.949(0.853-0.982)**
Image # 2	**15**	**0.987(0.962-0.995)**
Image # 3	**15**	**0.960(0.884-0.986)**
Image # 4	**15**	**0.950(0.858-0.983)**
Image # 5	**15**	**0.957(0.877-0.985)**
Test agreements between observes 3 and 6		
Image # 1	**15**	**0.922(0.773-0.973)**
Image # 2	**15**	**0.961(0.888-0.986)**
Image # 3	**15**	**0.892(0.692-0.962)**
Image # 4	**15**	**0.955(0.870-0.984)**
Image # 5	**15**	**0.945(0.853-0.981)**
Test agreements between observes 4 and 6		
Image # 1	**15**	**0.786(0.387-0.925)**
Image # 2	**15**	**0.898(0.707-0.964)**
Image # 3	**15**	**0.8230.493-0.938)**
Image # 4	**15**	**0.890(0.686-0.962)**
Image # 5	**15**	**0.966(0.903-0.988)**
Test agreements between observes 5 and 6		
Image # 1	**15**	**0.888(0.679-0.961)**
Image # 2	**15**	**0.968(0.909-0.989)**
Image # 3	**15**	**0.940(0.828-0.979)**
Image # 4	**15**	**0.963(0.894-0.987)**
Image # 5	**15**	**0.960(0.886-0.986)**

The ICC between observer 1 and the PhD student (observer 6) shows excellent agreement. Overall image quality ICC varied between 95%CI 0.914 to 0.977. The resultant ICC values for the PhD student, when compared with observers 2, 3, 4 and 5, again showed excellent agreement 95% CI 0.917 to 0.975, 95% CI 0.807 to 0.922, 95% CI 0.838 to 0.952 and 95% CI 0.857 to 0.939, respectively. These findings indicate that the PhD student is competent in visually appraising the abdominal CT images using the method described within this thesis.

5.7 Statistical Analysis

Data were analysed using SPSS (version 22.0) and Excel (2013) in order to facilitate statistical data analysis. Entry mistakes and outliers were checked before computing any statistics. Mean and standard deviation (SD) were calculated to measure corresponding tendency and variation, for both radiation dose and image quality measures.

Normality testing was performed using the Shapiro-Wilk test. Radiation dose and physical measures of image quality (SNR) were normally distributed, but relative VGA data was not normal distributed; hence a non-parametric approach was used. For normally distributed data, the paired t –test was used, whilst the Wilcoxon test was used for non-normally distributed data. Tests were performed to compare the radiation dose including ED, abdominal organs dose and ER between FTC and ATCM-corrected and uncorrected data. Included in the comparison were physical SNR values for the five abdominal organs with different tube currents, pitch factors and detector configuration for all protocols. In addition, a linear correlation was used to measure the strength of the relationship between FTC and ATCM-corrected and uncorrected data for radiation dose and physical image quality measures. A regression line was also fitted to determine relationship trends for different acquisition parameters.

Relative VGA scores, for both FTC and ATCM, were compared using the Wilcoxon signed rank test for each abdominal axial images slice, pitch factor and detector configuration. P values of 0.05 were considered to be a significant result (Andy, 2013).

Chapter Six: Results

6.1 Chapter Overview

This chapter presents the radiation dose and image quality results for FTC and ATCM CT techniques using the anthropomorphic abdomen and CRIS ATOM phantoms. The presentation of the results is organised into two main themes.

The first theme focuses on the presentation of radiation dose data from MOSFET and the two mathematical/simulation methods (DLP/k factors and ImPACT). Radiation dose data is reported as 'corrected' and 'uncorrected', in accordance with the process described in the method **(Chapter 5, Section 5.4.1).** Effective dose and effective risk data are also presented after calculating the lifetime risk from abdominal CT scan protocols for a variety of ages and genders (ages from 20 to 70 for both females and males). The second theme focuses on the assessment and evaluation of image quality using physical (SNR) and visual grading (relative VGA) methods.

Given that there is a large amount of data, the results section contains summaries of the data in graphical, table and statistical formats. However, **Appendices VI-XXXIII** presents all the data, including radiation dose, SNR values and relative VGA scores in an unmodified/summarised format.

6.2 Abdominal organs dose - comparison between FTC and ATCM, corrected and uncorrected (raw) data

In this subsection, abdominal organ dose was calculated using MOSFET dosimetry. The mean of the MOSFET readings for each organ and tissue were calculated. MOSFET values were then divided by the calibration factor of each MOSFET reader in order to obtain a mean dose for each organ/tissue. In this subsection the nine abdominal organs within the primary scan volume were compared for FTC and ATCM techniques. Full details are provided in **appendix VI, VII and VIII.**

6.2.1 Tube current

The comparison of the mean abdominal organ dose for FTC and ATCM techniques are displayed in **Table 6-1** and **Table 6-2**. **Table 6-1** shows the mean abdominal organ dose for FTC and corrected ATCM; **Table 6-2** shows the mean abdominal organ dose for FTC and uncorrected ATCM (i.e. a comparison of FTC and ATCM approaches with different respective tube currents). The uncorrected ATCM (raw) data has been included to enable clinically relevant comparisons to be made between FTC and ATCM, whilst the corrected ATCM data has been included to enable fair comparison of organ dose data by normalising the tube currents between these modes **(as described in the methods chapter).**

6.2.1.1 Comparison of mean abdominal organ dose for FTC and corrected ATCM

As shown in **Figure 6-1**, there is a strong positive correlation between mean abdominal organ dose for FTC and corrected ATCM CT scans across the range of tube currents (R^2 = 0.986 to 0.999).

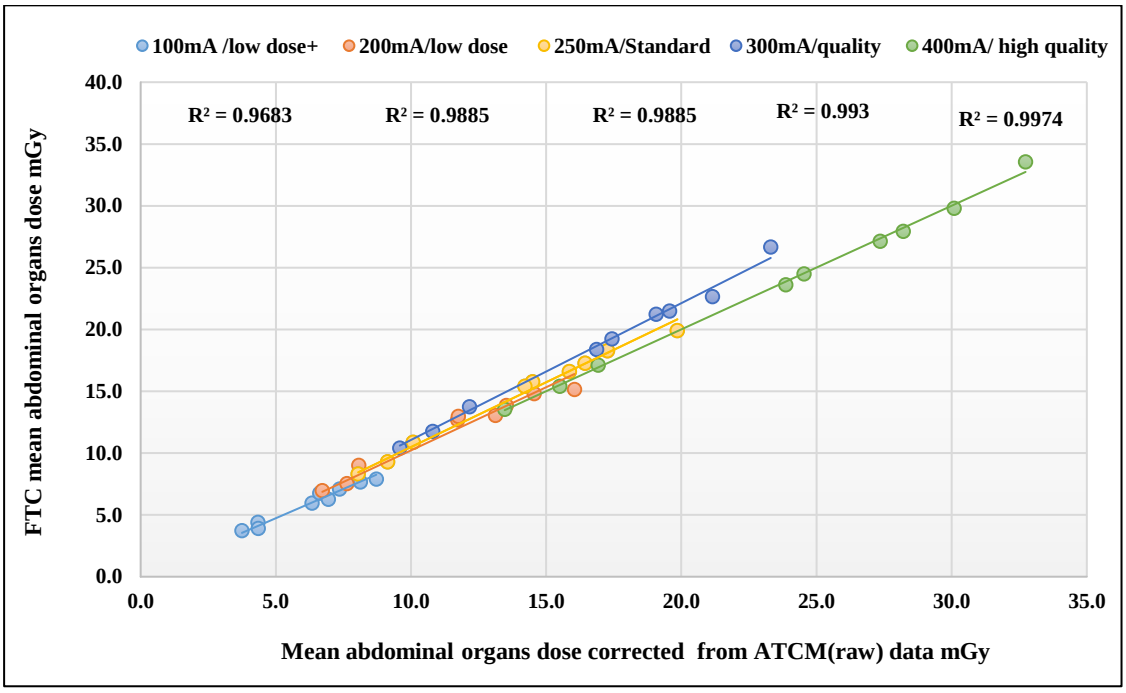

Figure 6- 1: A scatterplot illustrating the degree of linear correlation for abdominal mean organ dose between FTC and corrected ATCM using different tube currents.

Data in (**Table 6-1)** illustrates which tube currents had a high effect on abdominal organ dose. With a CT tube current of 100 mA /low dose+ (SD 12.50) the mean abdominal organ dose for FTC was slightly higher than mean for corrected ATCM for the liver (6.341 ± 1.518 and 5.970 ± 0.765 mGy), stomach (8.131 ± 1.848 and 7.659 ± 1.167 mGy), colon (4.353 ± 1.001 and 3.917 ± 0.387 mGy), kidneys (6.941 ± 1.961 and 6.282 ± 1.074 mGy), pancreas (37.357 ± 1.721 and 7.112 ± 1.231 mGy), small intestine (3.746 ± 0.777 and 3.729 ± 0.286 mGy) and gall bladder(8.717 ± 2.604 and 7.897 ± 1.378 mGy, FTC and ATCM, respectively). In contrast, the mean abdominal organ dose of FTC was slightly lower than the mean abdominal organ dose corrected ATCM data for spleen (6.631 ± 1.253 and 6.777±0.949 mGy) and adrenal glands (8.717 ± 2.604 and 7.897 ± 1.378 mGy) for FTC and ATCM techniques, respectively). However, these differences were statistically not significant (P>0.05; **Table 6-1**).

When the tube current was increased to 200mA/ low dose (SD 7.50) for the same abdominal protocol, the mean abdominal organs dose for corrected ATCM was higher than FTC for liver (11.734 ± 2.914 and 2.685 ± 1.490 mGy), spleen (11.752 ± 2.893 and 12.992 ± 1.458 mGy),

stomach (14.554 ± 4.120 and 14.823±2.099 mGy), pancreas (13.53 ±3 .702 and 13.850 ± 1.925 mGy), adrenals (8.069 ± 1.894 and 9.018±0.815), and small intestine (6.718 ± 1.528 and 6.975 ± 0.658 mGy, FTC and ATCM, respectively). The mean abdominal organ dose corrected ATCM was lower than FTC for colon (7.637 ± 1.829 and 7.537 ± 0.866 mGy), kidneys (13.132 ± 3.811 and 13.063 ± 2.082 mGy), and gall bladder (16.046 ± 5.132 and 15.166 ± 2.775 mGy, FTC and ATCM, respectively). As for tube current of 100 mA/low dose+, all of the above mentioned differences between mean abdominal organs dose for the corrected ATCM and FTC were not statistically significant (p>0.05; **Table 6-1**).

Table 6- 1:Comparison between mean abdominal organ dose from FTC and mean abdominal organs dose for corrected ATCM using different tube currents

CT Technique	FTC	Corrected ATCM	P value
Organ	**100mA / low dose+ (SD 12.50) Mean ± SD (mGy) n=9**		
Liver	**6.341±1.518**	**5.970±0.765**	**0.241**
Gall Bladder	**8.717±2.604**	**7.897±1.378**	**0.116**
Pancreas	**7.357±1.721**	**7.112±1.231**	**0.275**
Spleen	**6.631±1.253**	**6.777±0.949**	**0.341**
Stomach	**8.131±1.848**	**7.659±1.167**	**0.134**
Kidneys	**6.941±1.961**	**6.282±1.074**	**0.096**
Adrenals	**4.347±0.9387**	**4.406±0.582**	**0.440**
Small Intestine	**3.746±0.777**	**3.729±0.286**	**0.474**
Colon	**4.353±1.001**	**3.917±0.387**	**0.101**
200mA/ low dose (SD 7.50)			
Liver	**11.734±2.914**	**12.685±1.490**	**0.186**
Gall Bladder	**16.046±5.132**	**15.166±2.775**	**0.306**
Pancreas	**13.53±3.702**	**13.850±1.925**	**0.388**
Spleen	**11.752±2.893**	**12.992±1.458**	**0.130**
Stomach	**14.554±4.120**	**14.823±2.099**	**0.415**
Kidneys	**13.132±3.811**	**13.063±2.082**	**0.477**
Adrenals	**8.069±1.894**	**9.018±0.815**	**0.103**
Small Intestine	**6.718±1.528**	**6.975±0.658**	**0.329**
Colon	**7.637±1.829**	**7.537±0.866**	**0.435**
250mA/ standard (SD 5.00)			
Liver	**14.503±3.819**	**15.768±3.279**	**0.012**
Gall Bladder	**19.853±6.083**	**19.929±4.947**	**0.465**
Pancreas	**16.442±4.754**	**17.265±4.276**	**0.085**
Spleen	**14.219±3.492**	**15.413±3.175**	**0.016**
Stomach	**17.270±5.014**	**18.284±4.116**	**0.065**
Kidneys	**15.861±4.796**	**16.597±4.121**	**0.098**
Adrenals	**10.085±2.475**	**10.874±1.939**	**0.044**
Small Intestine	**8.049±1.711**	**8.314±0.677**	**0.285**
Colon	**9.131±2.172**	**9.309±2.015**	**0.227**
300mA/ quality (SD 3.00)			
Liver	**17.44±4.477**	**19.254±5.308**	**<0.001**
Gall Bladder	**23.307±6.907**	**26.688±8.807**	**0.001**
Pancreas	**19.573±5.688**	**21.508±6.883**	**0.002**
Spleen	**16.869±4.362**	**18.401±4.869**	**0.000**
Stomach	**21.158±6.204**	**22.659±6.999**	**0.002**

Kidneys	**19.068±5.714**	**21.242±6.711**	**0.001**
Adrenals	**12.167±2.574**	**13.746±3.007**	**0.000**
Small Intestine	**9.586±2.294**	**10.420±1.965**	**0.009**
Colon	**10.806±2.776**	**11.772±3.036**	**0.003**
400mA/ high quality (SD 1.00)			
Liver	**24.545±6.947**	**24.499±7.007**	**0.412**
Gall Bladder	**32.733±10.791**	**33.557±10.948**	**0.081**
Pancreas	**28.213±8.695**	**27.947±8.525**	**0.099**
Spleen	**23.872±6.319**	**23.618±6.325**	**0.197**
Stomach	**30.096±9.415**	**29.818±8.845**	**0.280**
Kidneys	**27.359±8.631**	**27.155±8.591**	**0.039**
Adrenals	**16.930±4.013**	**17.131±3.927**	**0.149**
Small Intestine	**13.465±2.914**	**13.547±3.028**	**0.418**
Colon	**15.510±4.185**	**15.420±3.917**	**0.355**
FTC mA range (100-400) / corrected ATCM mA range (100-400)			

When the tube current was increased to 250mA/standard, the mean abdominal organ dose corrected ATCM was higher than FTC for all abdominal organs. However, the differences were only statistically significant for liver (14.503 ± 3.819 and 15.768 ± 3.279 mGy; p=0.012), spleen (14.219 ± 3.492 and 15.413 ± 3.175 mGy; p=0.016) and adrenals (10.085 ± 2.475 and 10.874±1.939 mGy; p=0.044, for FTC and ATCM, respectively).

Using a tube current of 300 mA /quality (SD 3.00), the mean abdominal organ dose corrected ATCM was significantly higher than FTC for all abdominal organs (**Table 6-1**). The mean abdominal organ dose (corrected ATCM) was around 13% higher when compared to FTC. When the tube current was increased to 400mA/high quality (SD 1.00), the mean absorbed dose was higher for FTC than the mean abdominal organ corrected ATCM for the liver (24.545 ± 6.947 and 24.499 ± 7.007 mGy), spleen (23.872 ± 6.319 and 23.618 ± 6.325 mGy), stomach (30.096 ± 9.415 and 29.818 ± 8.845 mGy), pancreas (28.213 ± 8.695 and 27.947 ± 8.525 mGy), adrenals (16.930 ± 4.013 and 17.131 ± 3.927 mGy) and colon (15.510 ± 4.185 and 15.420 ± 3.917 mGy), for FTC and ATCM, respectively (**Table 6-1**). The mean abdominal organ dose for FTC was lower than the mean abdominal organs dose for corrected ATCM data when considering the kidneys (27.359 ± 8.631 and 27.155 ± 8.591 mGy), small intestine (13.465 ± 2.914 and 13.547 ± 3.028 mGy) and gall bladder (32.733 ± 10.791 and 33.557 ± 10.948 mGy) for FTC and ATCM, respectively. However, all these differences were not statistically significant except for the kidney (27.359 ± 8.631 and 27.155 ± 8.591 mGy; p=0.039, FTC and ATCM, respectively). The results of this element of the comparison using MOSFET method are displayed in **Figure 6-2**.

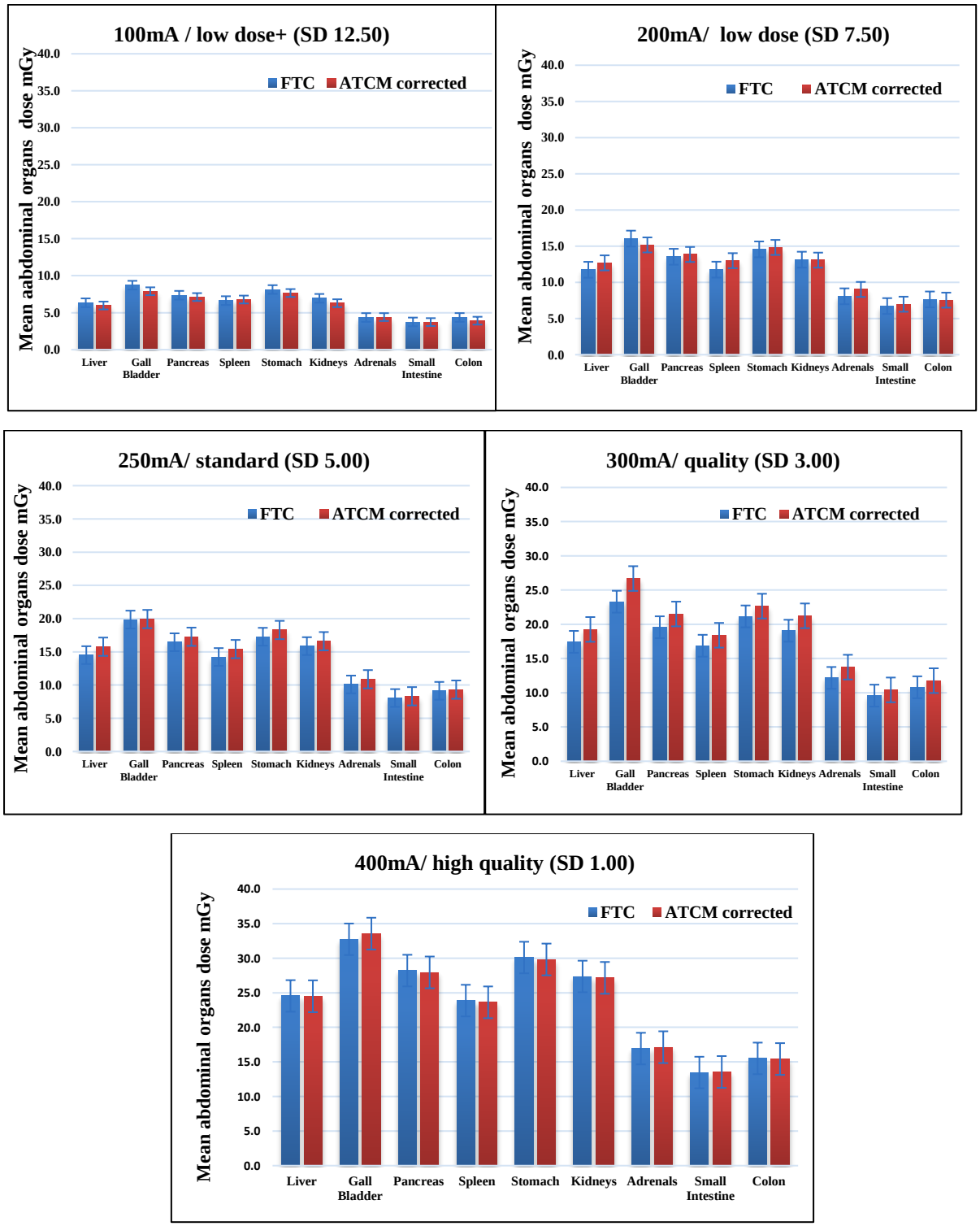

Figure 6- 2: Bar chart illustrating the difference in mean abdominal organ dose between FTC and corrected ATCM for a variety of tube currents/Sure Exposure 3D settings using MOSFET method

6.2.1.2 Comparison of mean abdominal organ dose for FTC and uncorrected ATCM techniques

Data presented in this section compares the mean abdominal organ dose associated with FTC (across a tube current range of 100-400mA) to the uncorrected ATCM with a tube current range of 49-440 mA **(Table 6-2)**. The mean abdominal organ doses for the uncorrected ATCM were significantly higher than FTC for all abdominal organs. All differences between mean abdominal organs doses for uncorrected ATCM and FTC were statistically significant ($p<0.001$). Mean abdominal organ dose was around 21% higher when compared to FTC.

Table 6- 2:Comparison between mean abdominal organ dose from FTC and uncorrected ATCM data using different tube currents

CT Technique	FTC	Uncorrected ATCM	P value
Organ	**Organs dose (mGy) Mean ± SD n= 45**		
Liver	**14.912±7.379**	**19.199±9.881**	**<0.001**
Gall Bladder	**20.131±10.355**	**25.395±14.449**	**<0.001**
Pancreas	**17.025±8.682**	**21.498±11.435**	**<0.001**
Spleen	**14.669±6.932**	**18.886±9.024**	**<0.001**
Stomach	**14.912±7.379**	**22.839±11.919**	**<0.001**
Kidneys	**16.473±8.577**	**20.726±11.442**	**<0.001**
Adrenals	**10.319±4.903**	**13.537±6.560**	**<0.001**
Small Intestine	**8.313±3.759**	**10.512±4.845**	**<0.001**
Colon	**9.488±4.487**	**11.749±5.949**	**<0.001**
FTC mA range (100-400) / uncorrected ATCM mean mA range (49-440)			

6.2.2 Pitch factors

6.2.2.1 Comparison of mean abdominal organ dose for FTC and corrected ATCM

There is a strong positive correlation between mean abdominal organ doses for FTC and corrected ATCM using detail (0.688), standard (0.938), and fast (1.438) pitch factors (R^2 = 0.998 to 0.999; **Figure 6-3).**

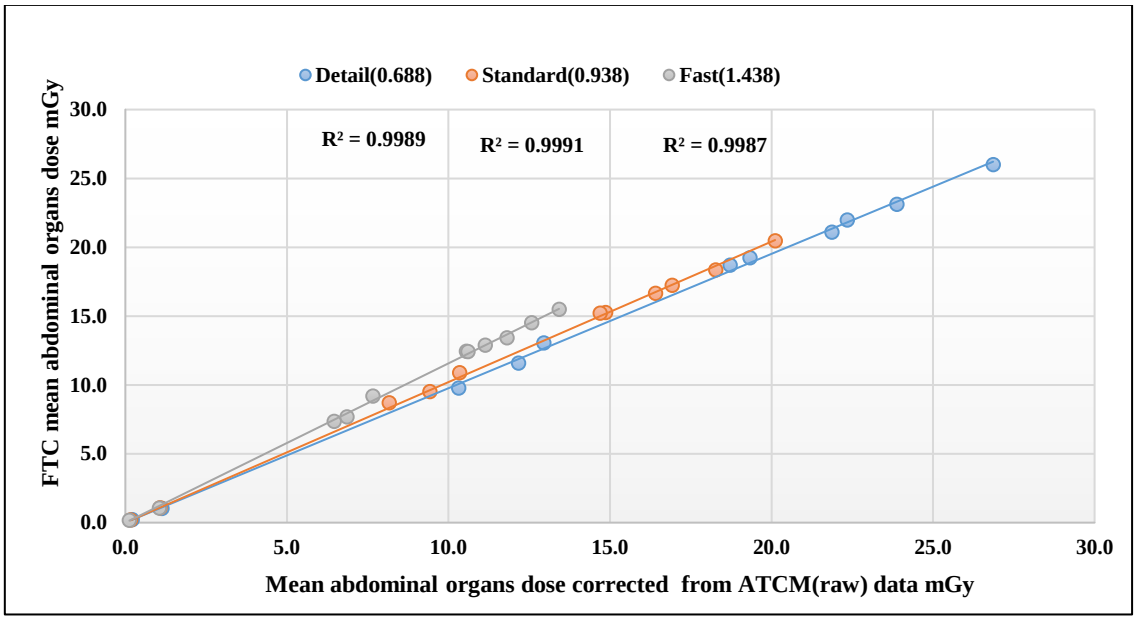

Figure 6- 3: Scatterplot illustrating the degree of linear correlation for mean abdominal organ dose between FTC and corrected ATCM using different pitch factors.

The mean abdominal organ doses for FTC techniques were slightly higher than mean abdominal organ dose for corrected ATCM for all organs within the scan volume detail pitch factor (0.688), except the adrenal glands (FTC 12.950 ± 5.602 and corrected ATCM 13.051 ± 6.149 mGy). The differences between mean FTC abdominal organ dose and corrected ATCM were not statistically significant for any abdominal organs, with the exception of colon (FTC 12.172 ± 0.357 and corrected ATCM 11.585 ± 5.805 mGy; p=0.044; **Table 6-3**).

The mean abdominal organ doses for FTC were marginally lower than mean abdominal organ dose for corrected ATCM for all abdominal organs within the scan volume when a standard pitch factor (0.938) was used. However, the difference between the mean abdominal organ doses for FTC and mean dose for corrected ATCM was statistically different for only the adrenal glands (FTC 10.344 ± 4.304 and corrected ATCM 10.868 ± 4.770 mGy; p=0.015) and small intestine (FTC 8.165 ± 3.125 and corrected ATCM 8.701 ± 3.414 mGy; p=0.015)

Table 6- 3:Comparison between the mean abdominal organ dose for FTC and corrected ATCM using different pitch factors

CT Technique	FTC	Corrected ATCM	P value
Organ	Detail(0.688) Mean ± SD (mGy) n=15		
Liver	19.328±8.495	19.220±9.650	0.417
Gall Bladder	26.859±11.472	25.986±14.129	0.222
Pancreas	22.340±10.073	21.959±10.959	0.247
Spleen	18.714±7.977	18.697±8.640	0.485
Stomach	23.880±10.704	23.097±11.602	0.089
Kidneys	21.866±9.747	21.088±11.143	0.118
Adrenals	12.950±5.602	13.051±6.149	0.394
Small Intestine	10.312±4.396	9.756±4.785	0.060
Colon	12.172±0.357	11.585±5.805	0.044
	Standard(0.938)		
Liver	14.861±6.249	15.249±6.644	0.132
Gall Bladder	20.111±8.706	20.465±9.986	0.262
Pancreas	16.926±7.177	17.232±7.782	0.211
Spleen	14.693±5.940	15.202±6.053	0.070
Stomach	18.271±7.803	18.335±8.106	0.414
Kidneys	16.408±7.228	16.643±7.868	0.257
Adrenals	10.344±4.304	10.868±4.770	0.015
Small Intestine	8.165±3.125	8.701±3.414	0.015
Colon	9.428±3.790	9.511±4.134	0.361
	Fast(1.438)		
Liver	10.548±4.313	12.436±3.783	<0.001
Gall Bladder	13.423±5.733	15.491±5.351	0.001
Pancreas	11.807±4.946	13.418±4.538	0.002
Spleen	10.599±4.102	12.421±3.483	0.001
Stomach	12.573±5.057	14.514±4.835	0.001
Kidneys	11.142±4.728	12.872±4.487	<0.001
Adrenals	7.664±4.728	9.186±2.754	<0.001
Small Intestine	6.461±2.707	7.334±2.269	0.001
Colon	6.861±2.722	7.678±2.499	<0.001
FTC mA range (100-400) / corrected ATCM mA range (100-400)			

From **Table 6-3,** when using fast pitch factor (1.438), the mean abdominal organ dose was higher for corrected ATCM in comparison with FTC for all abdominal organs and was statistically significant (P<0.001). The mean abdominal organ dose corrected ATCM was around 13% higher when compared to FTC. This suggests that the lowest organ doses were obtained when using MOSFET method with fast pitch factor (1.438) and the highest organ doses were produced with a detail (0.688) pitch **(See Figure 6-4)**.

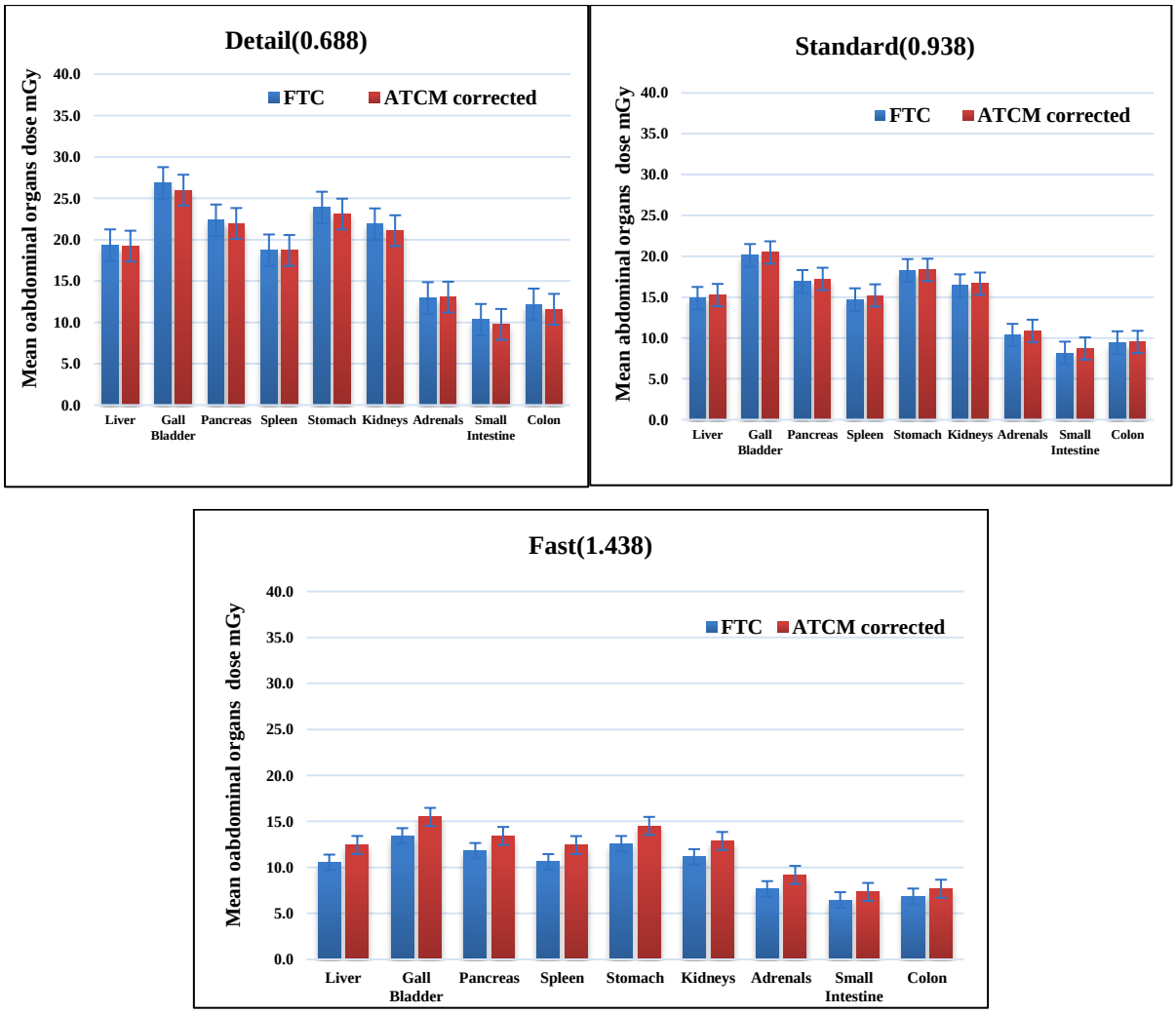

Figure 6- 4: Bar chart illustrating the difference in mean abdominal organ dose using MOSFET method between FTC and corrected ATCM using different pitch factors.

6.2.2.2 Comparison of mean abdominal organ dose for FTC and uncorrected ATCM

When different pitch factors are compared **(Table 6-4)** the mean abdominal organ dose was higher for uncorrected ATCM than FTC (e.g. gall bladder the higher dose using detail pitch factors ATCM 32.4156±18.336 and FTC 26.859 ±11.472 mGy). There was a highly significant statistical difference between the mean abdominal organ doses for FTC and mean abdominal organ dose for the uncorrected ATCM using detail (0.688), standard (0.938), and fast (1.438) pitch factors ($p<0.001$). There was a reduction in mean abdominal organ dose by around 17% from FTC techniques when compared to uncorrected ATCM.

Table 6- 4:Comparison between the mean abdominal organ dose from FTC and uncorrected ATCM using different pitch factors

CT Technique	FTC	Uncorrected-ATCM	P value
Organ	**Detail(0.688) Mean ± SD (mGy) n=15**		
Liver	**19.328±8.495**	**23.739±12.610**	**0.008**
Gall Bladder	**26.859±11.472**	**32.415±18.336**	**0.027**
Pancreas	**22.340±10.073**	**27.081±14.335**	**0.010**
Spleen	**18.714±7.977**	**23.018±11.456**	**0.005**
Stomach	**23.880±10.704**	**28.436±115.061**	**0.013**
Kidneys	**21.866±9.747**	**26.063±14.471**	**0.020**
Adrenals	**12.950±5.602**	**16.112±8.182**	**0.006**
Small Intestine	**10.312±4.396**	**11.958±6.081**	**0.022**
Colon	**12.172±0.357**	**14.280±7.516**	**0.023**
Standard(0.938)			
Liver	**14.861±6.249**	**18.764±8.919**	**0.002**
Gall Bladder	**20.111±8.706**	**25.199±13.090**	**0.005**
Pancreas	**16.926±7.177**	**21.152±10.285**	**0.003**
Spleen	**14.693±5.940**	**18.612±8.154**	**0.001**
Stomach	**18.271±7.803**	**22.475±10.674**	**0.003**
Kidneys	**16.408±7.228**	**20.457±10.315**	**0.004**
Adrenals	**10.344±4.304**	**13.715±6.843**	**0.002**
Small Intestine	**8.165±3.125**	**10.635±4.583**	**<0.001**
Colon	**9.428±3.790**	**11.675±5.515**	**0.004**
Fast(1.438)			
Liver	**10.548±4.313**	**15.097±5.286**	**<0.001**
Gall Bladder	**13.423±5.733**	**18.829±7.306**	**<0.001**
Pancreas	**11.807±4.946**	**16.259±6.061**	**<0.001**
Spleen	**10.599±4.102**	**15.030±4.884**	**<0.001**
Stomach	**12.573±5.057**	**17.606±6.534**	**<0.001**
Kidneys	**11.142±4.728**	**15.658±6.125**	**<0.001**
Adrenals	**7.664±4.728**	**11.151±3.886**	**<0.001**
Small Intestine	**6.461±2.707**	**8.946±3.307**	**<0.001**
Colon	**6.861±2.722**	**9.291±3.317**	**<0.001**
FTC mA range (100-400) / uncorrected ATCM mean mA range (49-440)			

6.2.3 Detector configuration.

6.2.3.1 Comparison mean abdominal organs dose of FTC and ATCM corrected data

As shown in **Figure 6-5** there is a strong positive relationship between the mean abdominal organ dose for FTC and corrected ATCM using different detector configurations (0.5×16mm, 1.0×16mm and 2.0×16mm; R^2 = 0.998-0.999).

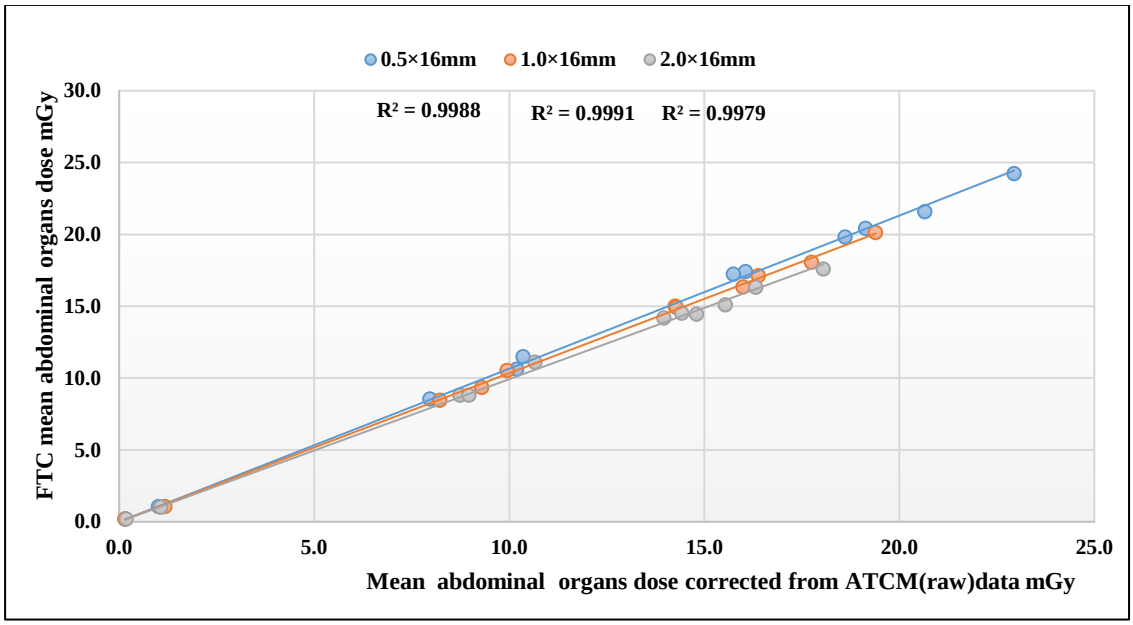

Figure 6- 5: Scatterplot illustrating the degree of linear correlation between mean abdominal organ dose for FTC and corrected ATCM using detector configurations

With a detector configuration of 0.5×16mm (**Table 6-5),** the mean abdominal organ dose for corrected ATCM was higher than FTC for all abdominal organs. These findings were statistically significant for all abdominal organs except the gall bladder (22.942 ± 12.269 and 24.234 ±12.500 mGy; p=0.08), stomach (20.657 ± 10.864 and 21.570 ± 10.534 mGy; p=0.063) and colon (10.195 ± 5.076 and 10.613 ± 5.046 mGy; p=0.075) for FTC and ATCM, respectively. The mean abdominal organ dose was around 13% higher for corrected ATCM techniques when compared to FTC. Also, from **Table 6-5**, the mean abdominal organ dose from corrected-ATCM data remained slightly higher than FTC for all abdominal organs within the scan volume when the detector configuration changed to 1.0×16mm. However, these findings were not significant (p>0.05).

Table 6- 5:Comparison between mean abdominal organ dose for FTC and corrected ATCM using different detector configurations			
CT Technique	**FTC**	**Corrected ATCM**	**P value**
Organ	**0.5×16mm Mean ± SD (mGy) n=15**		
Liver	**16.057±8.497**	**17.405±8.380**	**0.007**
Gall Bladder	**22.942±12.269**	**24.234±12.500**	**0.080**
Pancreas	**19.139±10.346**	**20.406±10.095**	**0.025**
Spleen	**15.748±8.018**	**17.218±7.605**	**0.003**
Stomach	**20.657±10.864**	**21.570±10.534**	**0.063**
Kidneys	**18.616±9.998**	**19.811±10.0164**	**0.040**
Adrenals	**10.353±5.452**	**11.480±5.338**	**0.002**
Small Intestine	**7.967±3.698**	**8.542±3.591**	**0.015**
Colon	**10.195±5.076**	**10.613±5.046**	**0.075**
1.0×16mm			
Liver	**14.253±7.081**	**14.991±6.970**	**0.058**
Gall Bladder	**19.394±9.860**	**20.126±10.757**	**0.190**
Pancreas	**16.391±8.159**	**17.117±8.207**	**0.048**
Spleen	**14.290±6.786**	**14.91±6.344**	**0.073**
Stomach	**17.747±8.947**	**18.058±8.336**	**0.296**
Kidneys	**15.998±8.243**	**16.343±8.343**	**0.232**
Adrenals	**9.943±4.672**	**10.524±4.741**	**0.055**
Small Intestine	**8.227±4.161**	**8.451±3.809**	**0.247**
Colon	**9.300±4.528**	**9.345±4.465**	**0.445**
2.0×16mm			
Liver	**14.427±6.831**	**14.509±7.246**	**0.433**
Gall Bladder	**18.057±8.692**	**17.583±9.536**	**0.272**
Pancreas	**15.543±7.463**	**15.086±7.468**	**0.133**
Spleen	**13.968±6.226**	**14.1849±6.416**	**0.317**
Stomach	**16.320±7.810**	**16.318±8.217**	**0.498**
Kidneys	**14.802±7.426**	**14.450±7.529**	**0.235**
Adrenals	**10.662±4.870**	**11.101±4.972**	**0.126**
Small Intestine	**8.744±3.616**	**8.798±3.923**	**0.440**
Colon	**8.967±4.015**	**8.815±4.242**	**0.292**
FTC mA range (100-400) / corrected ATCM mA range (100-400)			

The mean abdominal organ doses for FTC techniques and corrected-ATCM for all organs within the scan volume detector configuration value (2.0×16mm). The FTC and corrected ATCM data had nearly the same mean abdominal organ dose and consequently all the findings were not statistically significantly different ($p>0.05$). **(Table 6-5**). The results demonstrate that the lowest mean abdominal organ dose was generated when using direct measurement by MOSFET method with 2.0×16mm detector configuration and the highest organ dose was produced with 0.5×16mm detector configuration. **(Figure 6-6).**

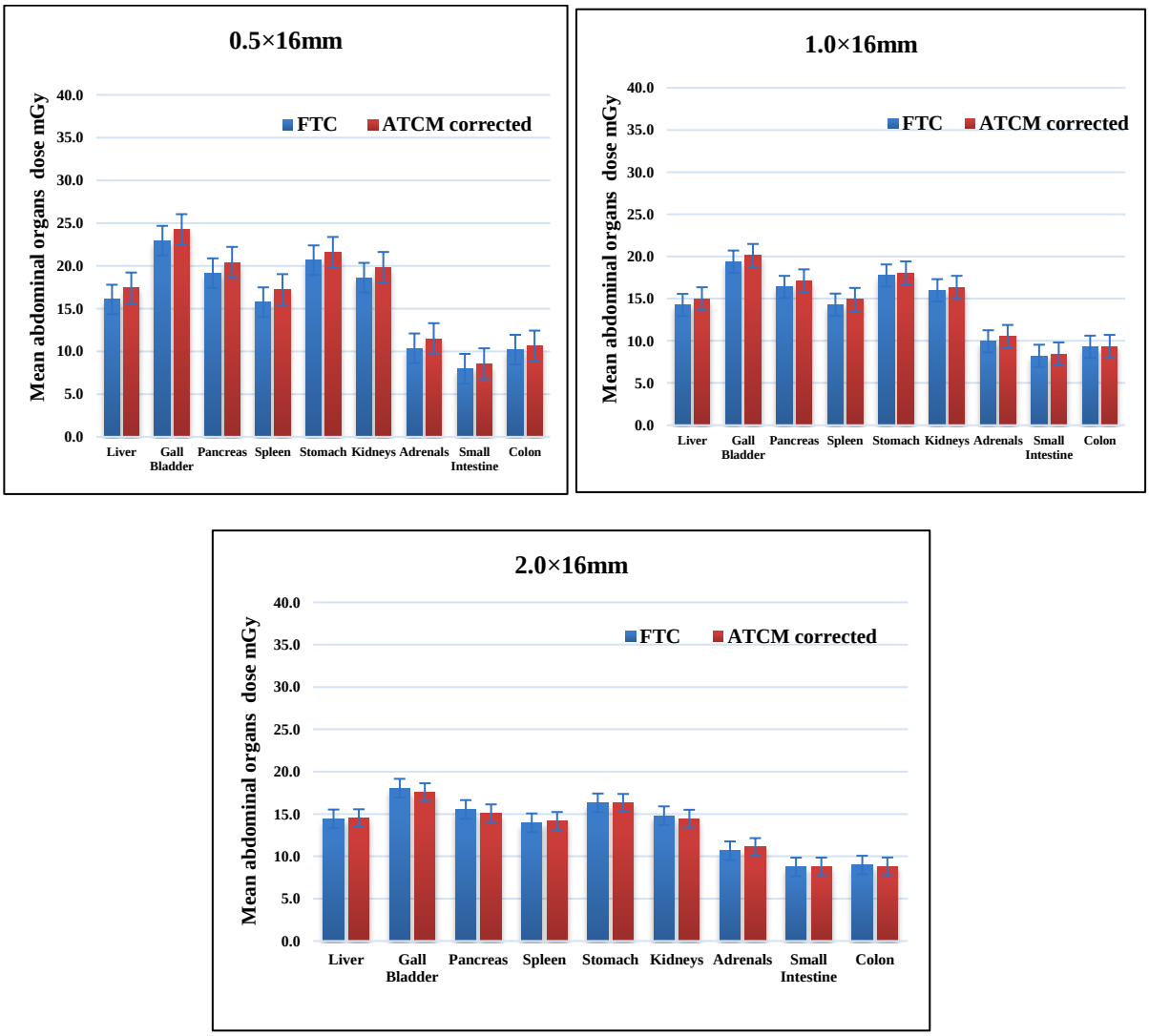

Figure 6- 6: Bar chart illustrating the difference in mean abdominal organ dose between FTC and corrected ATCM using different detector configurations using MOSFET method.

6.2.3.1 Comparison of mean abdominal organ dose for FTC and uncorrected-ATCM data

When different detector configurations are compared for FTC and uncorrected ATCM **(Table 6-6),** the mean abdominal organ dose was higher for the latter technique. There was a highly significant difference between the abdominal organ doses for FTC/uncorrected ATCM when using 0.5×16mm, 1.0×16mm, and 2.0×16mm detector configurations ($p<0.001$). There was a reduction in absorbed dose of around 23% when comparing FTC to uncorrected ATCM.

Table 6- 6:Comparison between mean abdominal organ dose for FTC and uncorrected ATCM using different detector configurations

CT Technique	FTC	Uncorrected-ATCM	P value
Organ	**0.5×16mm (mGy) Mean ± SD (mGy) n=15**		
Liver	**16.057±8.497**	**21.369±11.129**	**0.001**
Gall Bladder	**22.942±12.269**	**29.782±16.380**	**0.003**
Pancreas	**19.139±10.346**	**25.029±13.241**	**0.001**
Spleen	**15.748±8.018**	**21.053±10.193**	**<0.001**
Stomach	**20.657±10.864**	**26.429±13.781**	**0.001**
Kidneys	**18.616±9.998**	**24.346±13.162**	**0.002**
Adrenals	**10.353±5.452**	**14.093±7.095**	**<0.001**
Small Intestine	**7.967±3.698**	**10.460±4.776**	**0.001**
Colon	**10.195±5.076**	**13.003±6.618**	**0.002**
1.0×16mm			
Liver	**14.253±7.081**	**18.412±9.337**	**0.001**
Gall Bladder	**19.394±9.860**	**24.732±14.019**	**0.004**
Pancreas	**16.391±8.159**	**20.958±10.791**	**0.001**
Spleen	**14.290±6.786**	**18.252±8.534**	**0.001**
Stomach	**17.747±8.947**	**22.135±11.105**	**0.003**
Kidneys	**15.998±8.243**	**20.078±10.875**	**0.003**
Adrenals	**9.943±4.672**	**12.877±6.298**	**0.001**
Small Intestine	**8.227±4.161**	**10.306±4.907**	**0.002**
Colon	**9.300±4.528**	**11.465±5.916**	**0.007**
2.0×16mm			
Liver	**14.427±6.831**	**17.818±9.387**	**0.004**
Gall Bladder	**18.057±8.692**	**21.671±12.464**	**0.017**
Pancreas	**15.543±7.463**	**18.506±9.792**	**0.009**
Spleen	**13.968±6.226**	**17.356±8.438**	**0.002**
Stomach	**16.320±7.810**	**19.953±10.486**	**0.004**
Kidneys	**14.802±7.426**	**17.754±9.797**	**0.010**
Adrenals	**10.662±4.870**	**13.642±6.665**	**0.001**
Small Intestine	**8.744±3.616**	**10.772±5.176**	**0.003**
Colon	**8.967±4.015**	**10.778±5.447**	**0.004**
FTC mA range (100-400) / uncorrected ATCM mean mA range (49-440)			

6.3 Effective dose (ED) comparison between FTC and ATCM, including corrected and uncorrected (raw) data

In this subsection, the mean ED was calculated using MOSFET, DLP and ImPACT methods. To achieve this, the MOSFET readings for each organ and tissue were divided by each MOSFETs calibration factor to obtain a mean dose. Mean organ (weighted) doses were then multiplied by the relevant tissue weighting factor (**Table 6-7**). For estimations of ED from DLP and ImPACT methods, **see chapter 5 Section 5.4.3.** The mean EDs for when comparing FTC, corrected ATCM and uncorrected ATCM are outlined with further details in **Appendices IX to XIV.**

Table 6- 7:Example of mean MOSFETs readings for each organ and tissue using a FTC technique*

Organ	Weighted Dose(mGy)	Tissue Weighting Factor	Effective Dose mSv
Brain	**0.014**	**0.01**	**0.000**
ABM	**2.630**	**0.12**	**0.316**
Eyes	**0.003**	**0**	**0.000**
Thyroid	**0.173**	**0.04**	**0.007**
Oesophagus	**1.801**	**0.04**	**0.072**
Lungs	**2.998**	**0.12**	**0.360**
Breasts	**0.975**	**0.12**	**0.117**
Liver	**20.474**	**0.04**	**0.819**
Stomach	**26.021**	**0.12**	**3.123**
Bladder	**1.471**	**0.04**	**0.057**
Colon	**12.0657**	**0.12**	**1.448**
Salivary Glands	**0.071**	**0.01**	**0.001**
Testes	**0.8135**	**0.08**	**0.065**
Total			**6.383**
Remaining Organs		**Total ED from remaining organs**	
Thymus	**0.484**	**mean remaining organs × Tissue Weighting Factor = 11.185× 0.12**	**Total ED for radio sensitivity organs + Total ED from remaining organs = 6.383 +1.342**
Spleen	**19.747**		
Kidneys	**23.331**		
Adrenals	**13.685**		
Heart	**2.305**		
Pancreas	**24.700**		
Gall Bladder	**29.180**		
Prostate	**0.781**		
Oral Mucosa	**0.076**		
Small Intestine	**8.5960**		
Extrathoracic	**0.153**		
Total	**123.038**		
mean	**11.185**	**1.342**	**7.726 mSv**
*** parameters using/ 250mA, 0.5×16 detector configuration and 0.688 pitch factor**			

6.3.1 Tube current

The comparison of the mean ED for FTC and ATCM approaches can be viewed in **Table 6-8** and **Table 6-9** using three different CT dosimetry methods. **Table 6-8** shows mean ED from FTC and corrected ATCM data; **Table 6-9** shows mean ED from FTC and uncorrected ATCM (i.e. a comparison of FTC and ATCM approaches with different respective tube currents).

6.3.1.1 Comparison of ED for FTC and corrected-ATCM data

As illustrated in **Figure 6-7,** there is a strong positive correlation between MOSFET, DLP and ImPACT methods for ED estimation between the two techniques (R^2 =0.996, 0.998 and 0.997 for MOSFET, DLP and ImPACT, respectively).

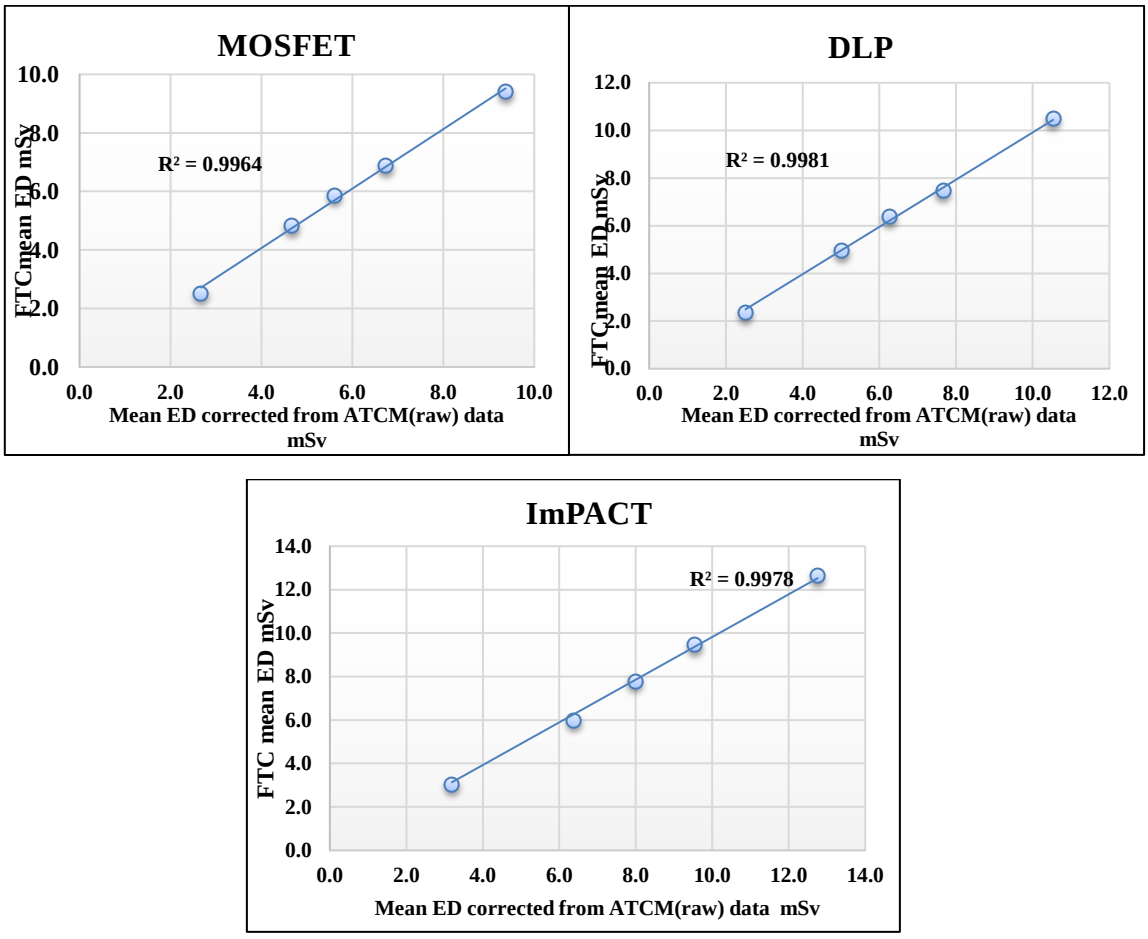

Figure 6- 7: Scatterplot illustrating the degree of linear correlation for MOSFET, DLP and ImPACT ED methods between FTC and corrected-ATCM data using different tube currents.

Data in **Table 6-8** illustrates FTC and corrected ATCM when using different tube currents. For 100mA/low dose+, the mean ED estimated by MOSFET for all FTC protocols was higher than the mean ED for the corrected ATCM (FTC 2.673 ± 0.526 and ATCM 2.520 ± 0.236 mSv). For 200mA/low dose, the mean ED, assessed using MOSFET, for all FTC protocols was lower than mean ED for the corrected ATCM (4.634 ± 1.116 and 4.838 ± 0.469 mSv). The results for this included 250mA/standard (5.602 ± 1.342 and 5.871 ± 1.102 mSv), 300mA/quality (6.742 ± 1.695 and 7.272 ± 1.896 mSv) and 400 mA/high quality (9.368 ± 2.500 and 9.402 ± 2.443 mSv, FTC and ATCM, respectively). However, the results were not statistically significant, except when using 300mA/quality (p=0.001). The mean ED corrected ATCM was around 7% higher when compared to FTC.

When using DLP and k factors, the mean ED, using tube currents/SureExposure 3D of 100mA/low dose+, was FTC 2.512 ± 0.675 and ATCM 2.350 ± 0.293 mSv. This resulted in 200mA/low dose (FTC 5.0245 ± 1.350 and ATCM 4.949 ± 0.580 mSv), 250mA/standard (FTC 6.458 ± 1.683 and ATCM 6.381 ± 1.225 mSv) and 400mA/high quality (FTC 10.533 ± 2.867 and ATCM 10.489 ± 3.001 mSv). The mean ED calculated using DLP was higher for all FTC protocols in comparison with corrected ATCM, however, these results were not statistically significant. With 300mA/quality the mean ED estimated using DLP for all protocols showed FTC to be lower than corrected ATCM (FTC 7.555 ± 2.233 and ATCM 8.252 ± 1.831 mSv). The mean corrected ATCM ED increased by around 8% when compared to FTC.

Table 6- 8:Comparison of ED for FTC and corrected ATCM using MOSFET, DLP and ImPACT methods

CT Technique	FTC	Corrected ATCM	P value
mA	ED (mSv)/MOSFET method (Mean ± SD) n=9		
100/low dose+	2.673±0.526	2.520±0.236	0.158
200/low dose	4.634±1.116	4.838±0.469	0.336
250/standard	5.602±1.342	5.871±1.102	0.078
300/quality	6.742±1.695	7.272±1.896	0.001
400/high quality	9.368±2.500	9.402±2.443	0.384
ED (mSv)/ DLP method			
100/low dose+	2.512±0.675	2.350±0.293	0.405
200/low dose	5.0245±1.350	4.949±0.580	0.435
250/standard	6.458±1.683	6.381±1.225	0.325
300/quality	7.555±2.233	8.252±1.831	0.000
400/high quality	10.533±2.867	10.489±3.001	0.311
ED (mSv)/ImPACT method			
100/low dose+	3.189±1.059	3.036±0.677	0.295
200/low dose	6.378±2.102	5.984±1.175	0.211
250/standard	7.978±2.610	7.789±1.995	0.264
300/quality	9.577±2.849	9.936±2.888	0.014
400/high quality	12.755±4.289	12.646±4.159	0.219
FTC mA range (100-400) / corrected ATCM mA range (100-400)			

Using ImPACT (**Table 6-8**), when using: 100mA/low dose+ (FTC 3.189 ± 1.059 and ATCM 3.036±0.677 mSv), 200mA/low dose (FTC 6.378±2.102 and ATCM 5.984±1.175 mSv), 250mA/standard (FTC 7.978 ±2.610 and ATCM 7.789±1.995 mSv) and 400mA/high quality (FTC 12.755 ± 4.289 and ATCM 12.646 ± 4.159 mSv), the mean ED for all FTC protocols was higher than mean ED for the corrected ATCM. However, these differences were not statistically significant. The mean ED estimated by the ImPACT method for FTC was lower than mean corrected ATCM ED data when 300mA/quality was selected (FTC 9.577 ± 2.849 and ATCM 9.936 ± 2.888 mSv). The mean corrected ATCM ED increased by around 4% when compared to FTC. Also, the mean ED using direct measurement by MOSFET method was lower than with others dosimetry methods, DLP and ImPACT for both FTC and corrected ATCM for all different tube currents (**See Figure 6-8).**

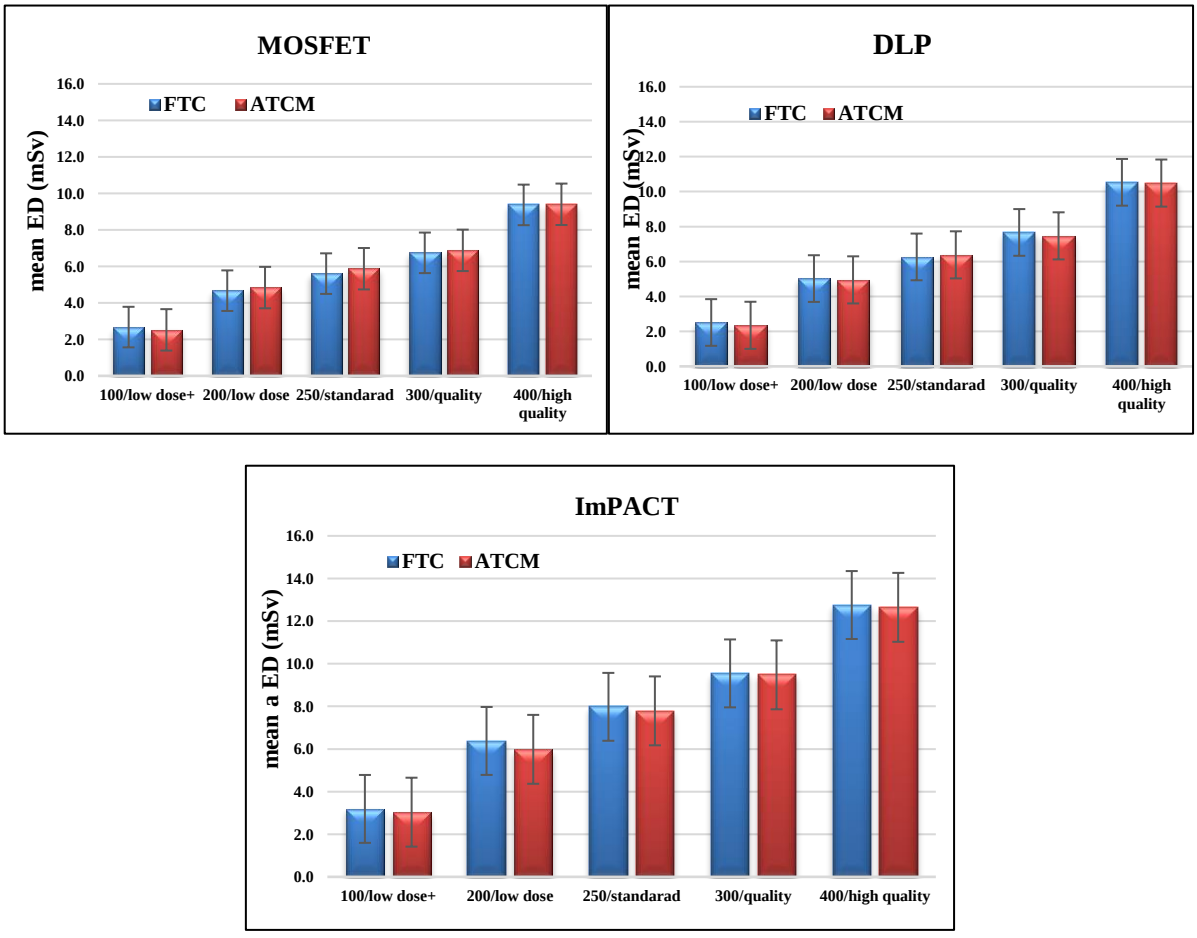

Figure 6- 8: Bar chart illustrating the difference in mean ED using MOSFET, DLP and ImPACT methods for FTC and corrected-ATCM data.

6.3.1.2 Comparison of mean ED for FTC and uncorrected-ATCM data

The data presented here compares the mean ED associated with FTC scans across a tube current range of 100-400mA against the uncorrected ATCM data with a tube current range of 49-440 mA **(Table 6-9)**. The mean ED using uncorrected ATCM (raw) data was significantly higher than FTC for the three dosimetry methods: MOSFET: (FTC 5.804 ± 2.711and ATCM 7.323 ± 3.598 mSv), DLP (FTC 6.468 ± 3.208 and ATCM 7.991 ± 3.265 mSv), and ImPACT: (FTC 7.976 ± 4.227 and ATCM 9.697 ± 5.452 mSv). All differences were statistically significant for the three dosimetry methods ($p<0.001$). The mean ED for uncorrected ATCM (raw) data was higher by approximately 21% (MOSFET), 19% (DLP) and 18% (ImPACT) when compared to FTC.

Table 6- 9:Comparison between mean ED using MOSFET, DLP and ImPACT methods for FTC and uncorrected ATCM

CT Technique	FTC	Uncorrected-ATCM	P value
Methods	**ED different mA mSv Mean ± SD n=45**		
MOSFET	**5.804±2.711**	**7.323±3.598**	**<0.001**
DLP	**6.468±3.208**	**7.991±3.265**	**<0.001**
Impact	**7.976±4.227**	**9.697±5.452**	**<0.001**
FTC mA range (100-400) / uncorrected ATCM mean mA range (49-440)			

6.3.2 Pitch factor

6.3.2.1 Comparison of mean ED of FTC and corrected-ATCM data

Figure 6-9 illustrates detail, standard and fast pitch factors which were used to demonstrate the degree of linear correlation of ED for MOSFET, DLP and ImPACT methods. There was a strong positive correlation between MOSFET, DLP and ImPACT methods. Furthermore, there was a good relationship between FTC and mean corrected ATCM ED when using the fast pitch factor (R^2 0.768 to 0.978).

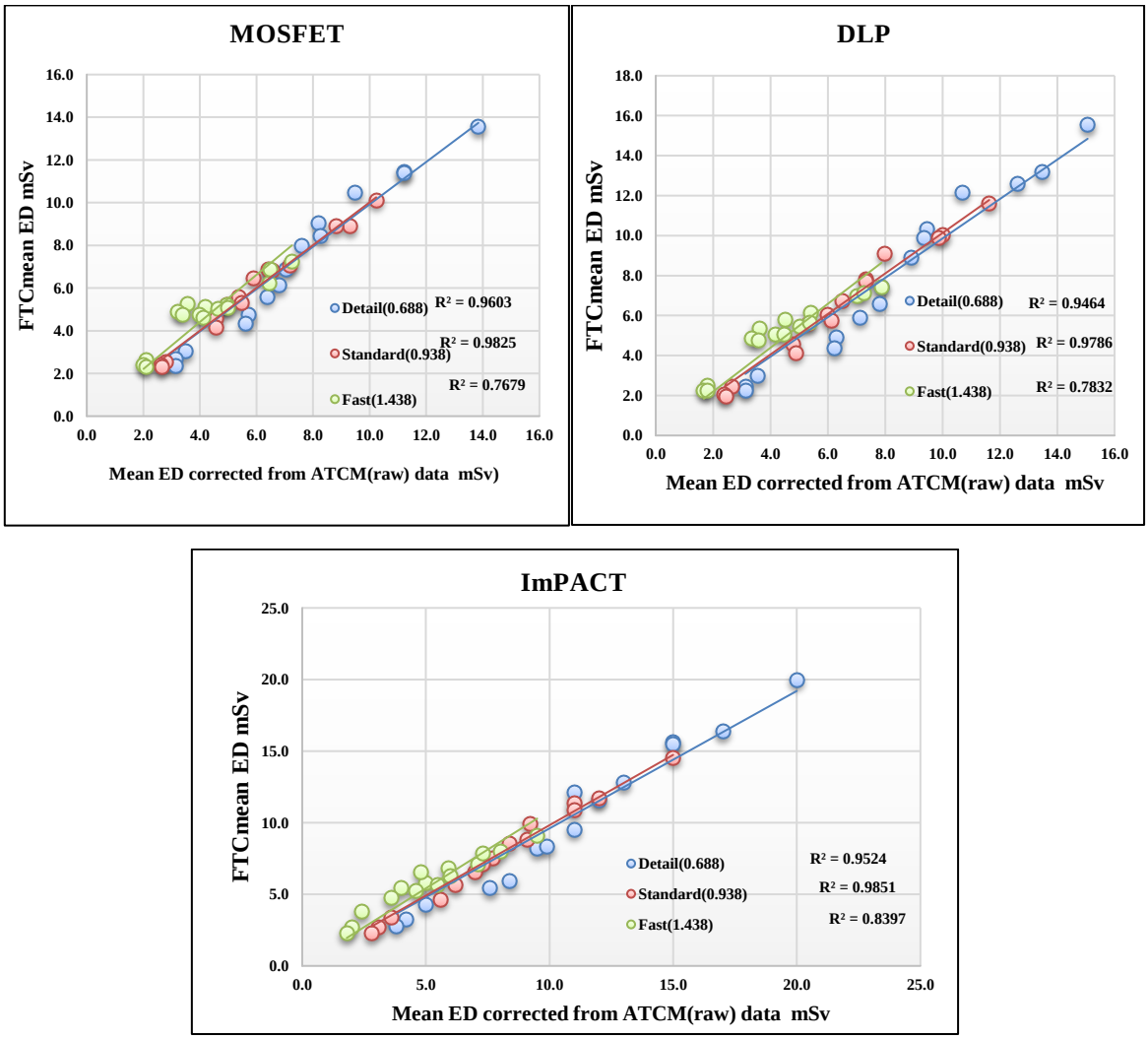

Figure 6- 9: Scatterplot illustrating the degree of linear correlation for ED using MOSFET, DLP and ImPACT methods between FTC and corrected ATCM using different pitch factors

From **Table 6-10**, the mean ED, as determined by the MOSFET method for FTC, was higher than the mean corrected ATCM ED when the detail (0.688) (FTC 7.410±3.109 and ATCM 7.207±3.406 mSv) and standard (0.938) (FTC 5.825±2.344 and ATCM5.820±2.409 mSv) pitch factors were used. However, these results were not statistically significant (p>0.05). The mean ED estimated by the MOSFET method for FTC was lower than the mean corrected ATCM ED when the fast (1.438) (FTC 4.231±1.617 and ATCM 4.822±1.452 mSv) pitch factors were used. This result was highly significant (p=0.001). The mean ED for the corrected ATCM data was around 12% higher when compared to FTC.

The mean ED using the DLP method is indicated in **Table 6-10**. The mean ED for FTC was higher than mean corrected ATCM ED data when using detail (0.688) (FTC 8.385±3.695 and ATCM 7.965±4.067 mSv). This result was not statistically significant (p>0.05). By increasing the pitch factor from detail to standard (0.938), the mean ED for FTC and corrected ATCM (raw) was almost equal (FTC 6.352 ± 2.786 and ATCM 6.370±2.907 mSv; P=0.065). By changing the pitch factor to the highest level, fast (1.438), the corrected-ATCM ED was around 13% higher (4.461 ± 1.939 mSv) than the FTC scans (5.118 ± 1.633 mSv; P=0.001).

Table 6- 10:Comparison of mean ED between MOSFET, DLP and ImPACT methods for FTC and corrected-ATCM (data using different pitch factors)

CT Technique	FTC	Corrected ATCM	P value
pitch factor	ED (mSv)/MOSFET method (Mean ± SD) n=15		
Detail(0.688)	7.410±3.109	7.207±3.406	0.131
Standard(0.938)	5.825±2.344	5.820±2.409	0.380
Fast(1.438)	4.231±1.617	4.822±1.452	0.001
ED (mSv)/ DLP method			
Detail(0.688)	8.385±3.695	7.965±4.067	0.079
Standard(0.938)	6.352±2.786	6.370±2.907	0.065
Fast(1.438)	4.461±1.939	5.118±1.633	0.001
ED (mSv)/ImPACT method			
Detail(0.688)	10.826±4.66	10.111±5.115	0.007
Standard(0.938)	7.933±3.451	7.713±3.579	0.021
Fast(1.438)	5.167±2.311	5.821±1.913	0.001
FTC mA range (100-400) / corrected ATCM mA range (100-400)			

When using the ImPACT method (**Table 6-10**), ED for FTC was higher than the mean corrected-ATCM ED but there was a reduction in ED of around 6% when using different pitch factors: detail (0.688) (10.826±4.66 and 10.111±5.115 mSv) and standard (0.938) (57.933±3.451 and 7.713±3.579 mSv, for FTC and ATCM, respectively).

The mean ED using the ImPACT method for all protocols indicated that the FTC ED was lower (13%) than the corrected ATCM dose when the fast (1.438) pitch factor (1.438) (5.167±2.311 and 5.821±1.913 mSv, FTC and ATCM, respectively) was used.

Figure 6-10 illustrates the difference in mean ED values using MOSFET, DLP and ImPACT methods for FTC and corrected ATCM data using different pitch factors. The mean ED using direct measurement by MOSFET method was lower than with other dosimetry methods: DLP and ImPACT for both FTC and ATCM for all different pitch factors.

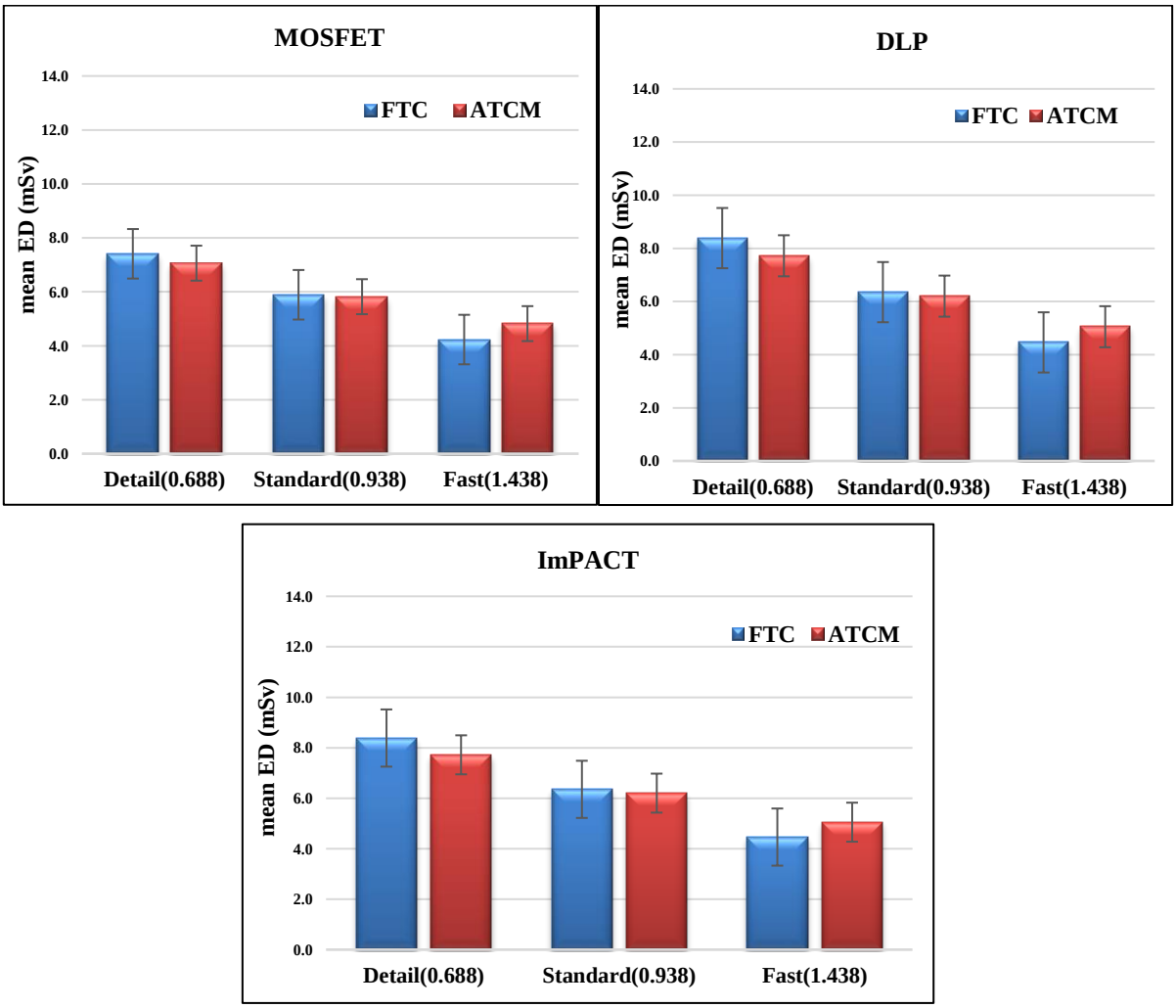

Figure 6- 10: Bar chart illustrating difference in mean ED values for MOSFET, DLP and ImPACT methods, between FTC and corrected ATCM using different pitch factors.

6.3.2.2 Comparison of mean ED for FTC and uncorrected-ATCM data

When comparing mean ED between FTC and uncorrected ATCM **(Table 6-11)**, the mean ED for all dosimetry methods was higher for uncorrected ATCM when compared to FTC. There was a highly significant difference between ED for FTC and uncorrected ATCM using detail (0.688), standard (0.938), and fast (1.438) pitch factors (p=0.001 to 0.028). This results in the mean ED increasing for uncorrected ATCM by around (13% to 16%) when compared to FTC.

Table 6- 11:illustrates a comparison between mean ED using MOSFET, DLP and ImPACT methods from FTC and uncorrected ATCM using different pitch factors

CT Technique	FTC	Uncorrected-ATCM	P value
pitch factor	ED (mSv)/ MOSFET Mean ± SD n=15		
Detail(0.688)	7.410±3.109	8.877±4.575	0.011
Standard(0.938)	5.825±2.344	7.218±3.294	0.003
Fast(1.438)	4.231±1.617	5.873±2.014	<0.001
ED (mSv)/ DLP			
Detail(0.688)	8.385±3.695	9.846±5.477	0.021
Standard(0.938)	6.352±2.786	7.838±3.938	0.003
Fast(1.438)	4.461±1.939	6.287±2.396	<0.001
ED (mSv)/ ImPACT			
Detail(0.688)	10.826±4.66	12.487±6.857	0.028
Standard(0.938)	7.933±3.451	9.573±4.855	0.004
Fast(1.438)	5.167±2.311	7.033±2.622	<0.001
FTC mA range (100-400) / uncorrected ATCM mean mA range (49-440)			

6.3.3 Detector configuration

6.3.3.1 Comparison mean ED for FTC and corrected-ATCM data

When using different detector configurations there were strong positive correlations between the MOSFET, DLP and ImPACT methods between FTC and corrected ATCM (R^2= 0.954-0.937; **Figure 6-11**).

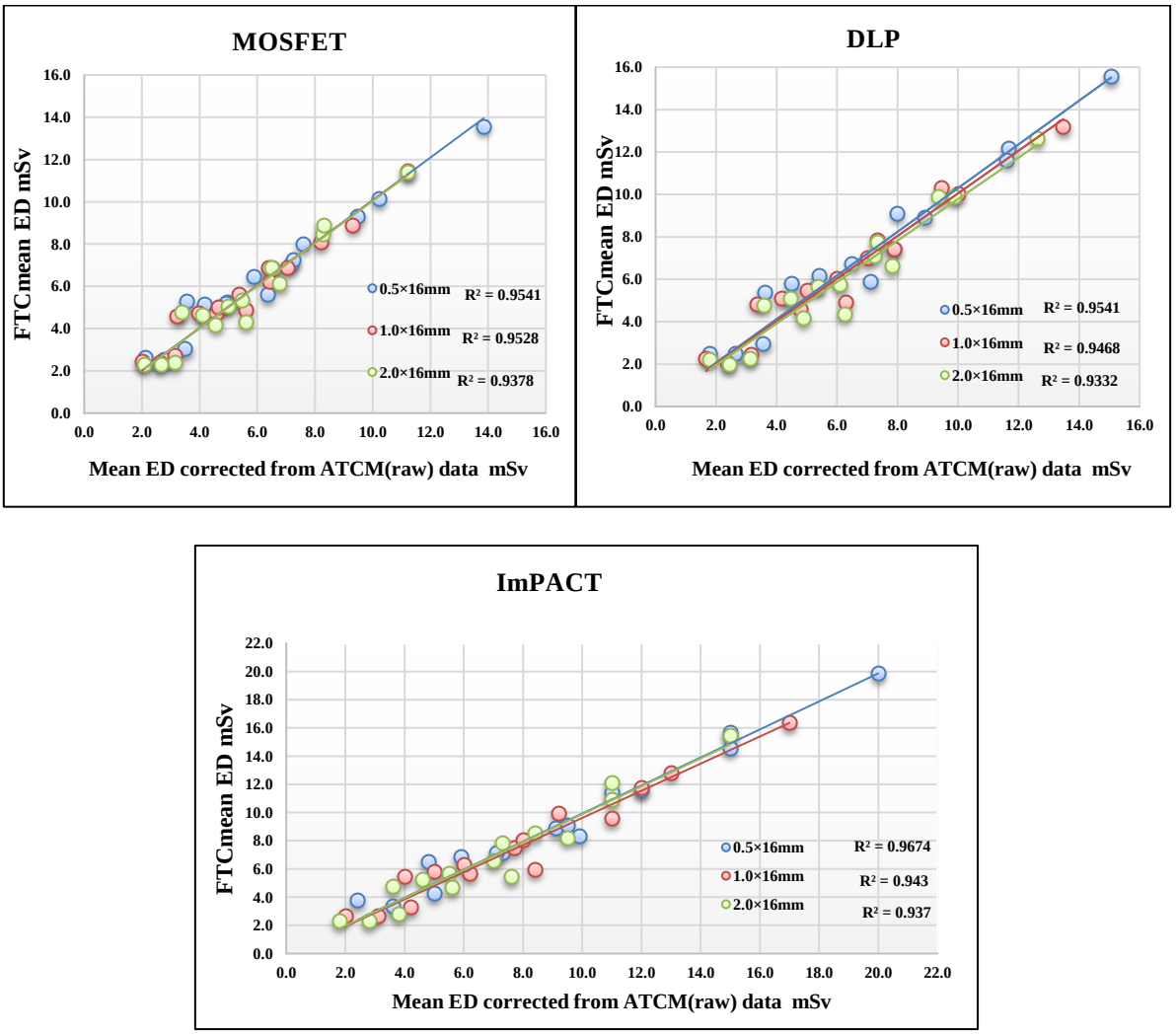

Figure 6- 11: Scatterplot illustrating the degree of linear correlation (MOSFET, DLP and ImPACT methods) for mean ED between FTC and corrected ATCM using different detector configurations

The mean ED in **Table 6-12** shows the effect of different detector configurations for the three dosimetry methods. The mean ED estimated by the MOSFET method for corrected ATCM was higher than FTC when using the detector configurations of 0.5×16mm (FTC 6.259 ± 3.155 and ATCM 6.429 2.978 mSv) and 1.0×16mm (FTC 5.587 ± 2.585 and ATCM 5.691±2.485 mSv). The mean ED for FTC and mean ED for corrected ATCM, when using the widest detector configuration (2.0×16 mm), were not statistically significant (p>0.05) (FTC 5.579 ± 2.456 and ATCM 5.584 ± 2.591 mSv).

Table **6-12** presents the mean ED estimated by the DLP method. The mean corrected ATCM ED was slightly higher than for FTC when using detector configurations of 0.5×16mm (FTC 6.910±3.727and ATCM 7.218±3.543 mSv) and 1.0×16mm (FTC 6.135±3.193 and ATCM 6.232±3.057 mSv). By contrast, the mean ED was slightly higher for FTC than corrected ATCM when the highest detector configuration 2.0×16mm was used (FTC 6.154±2.986 and ATCM 6.001±3.019 mSv. However, none of those results were statistically significant (p>0.05).

Table 6- 12:Comparison between mean ED using the MOSFET, DLP and ImPACT methods for FTC and corrected ATCM using different detector configurations

CT Technique	FTC	Corrected ATCM	P value
detector configuration	ED (mSv)/MOSFET method (Mean ± SD) n=15		
0.5×16mm	6.259±3.155	6.429±2.978	0.152
1.0×16mm	5.587±2.585	5.691±2.485	0.228
2.0×16mm	5.579±2.456	5.584±2.591	0.488
ED (mSv)/DLP method			
0.5×16mm	6.910±3.727	7.218±3.543	0.071
1.0×16mm	6.135±3.193	6.232±3.057	0.305
2.0×16mm	6.154±2.986	6.001±3.019	0.234
ED (mSv)/ImPACT method			
0.5×16mm	9.173±4.830	9.217±4.493	0.420
1.0×16mm	7.787±3.971	7.572±3.882	0.203
2.0×16mm	6.966±3.596	6.845±3.648	0.313
FTC mA range (100-400) / corrected ATCM mA range (100-400)			

Table 6-12 shows the mean ED estimated by the ImPACT method. FTC ED was slightly lower than the mean ED for the corrected ATCM using the detector configuration of 0.5×16mm (9.173 ± 4.830 and 9.217±4.493 mSv, FTC and ATCM, respectively). By increasing the detector configuration to 1.0×16mm, the mean ED was slightly higher for FTC than the mean ED for the corrected ATCM (7.787 ± 3.971 and 7.572 ± 3.882 mSv) and 2.0×16mm (6.966 ± 3.596 and 6.845 ± 3.648 mSv, FTC and ATCM, respectively). Nonetheless, these findings are not statistically significant (p>0.05).

Figure 6-12 illustrates no difference in mean ED for MOSFET, DLP and ImPACT methods between FTC and the mean ED corrected from ATCM when using different detector configurations. However, the mean ED with using direct measurement by MOSFET method was lower than with others dosimetry methods DLP and ImPACT for both FTC and ATCM for all different detector configurations.

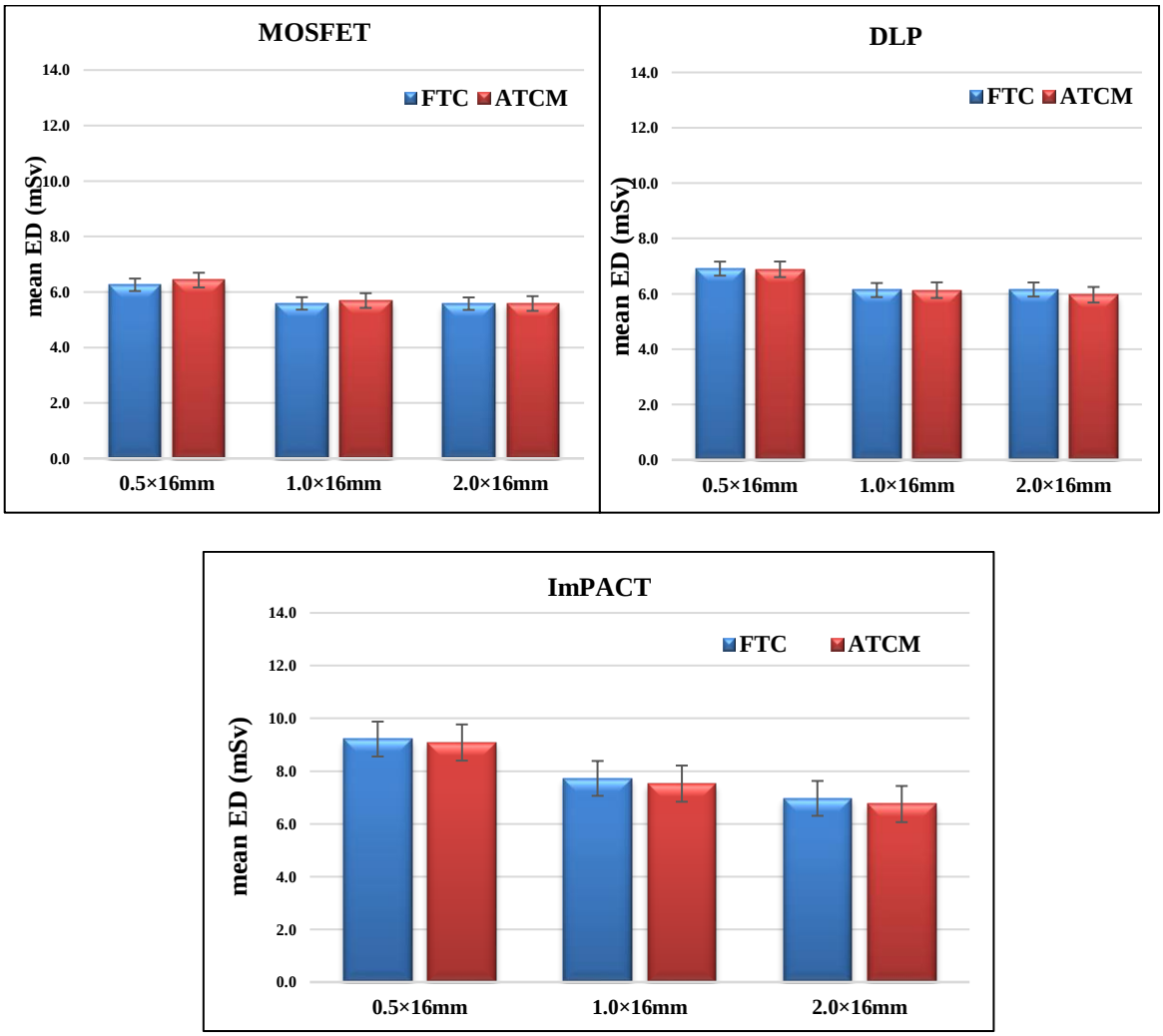

Figure 6- 12: Bar chart illustrating the difference in mean ED for MOSFET, DLP and ImPACT methods between FTC and corrected ATCM using detector configurations

6.3.3.2 Comparison of mean ED for FTC and uncorrected-ATCM data

Table 6-13 shows differences in the ED between different detector configurations for the FTC and uncorrected ATCM. As seen, the mean ED is higher for uncorrected ATCM when compared to FTC. There was a highly significant different between the three dosimetry methods for FTC and uncorrected ATCM when using different detector configurations ($p<0.001$). The mean ED for the uncorrected ATCM was higher than FTC by approximately MOSFET= 22%, DLP= 22% and ImPACT= 19% than when FTC was used (for all detector configurations).

Table 6- 13:Comparison of mean ED using MOSFET, DLP and ImPACT methods for FTC and uncorrected ATCM using different detector configurations

CT Technique	FTC	Uncorrected-ATCM	P value
detector configuration	ED (mSv)/MOSFET Mean ± SD n=15		
0.5×16mm	6.259±3.155(	8.086±4.082	0.001
1.0×16mm	5.587±2.585	7.052±3.428	0.002
2.0×16mm	5.579±2.456	6.830±3.363	0.003
ED (mSv)/DLP			
0.5×16mm	6.910±3.727	8.854±4.913	0.002
1.0×16mm	6.135±3.193	7.639±4.160	0.004
2.0×16mm	6.154±2.986	7.385±3.989	0.009
ED (mSv)/ ImPACT			
0.5×16mm	9.173±4.830	11.313±6.145	0.002
1.0×16mm	7.787±3.971	9.400±5.230	0.006
2.0×16mm	6.966±3.596	8.380±4.854	0.010
FTC mA range (100-400) / uncorrected ATCM mean mA range (49-440)			

6.4 Effective risk (ER) comparison between FTC and ATCM, including corrected and uncorrected (raw) data

In this subsection, ER data is presented using the MOSFET method with attributable lifetime cancer risk estimation using BEIR VII data modelling. Data are presented for both males and females aged from 20 to 70 years old. To achieve this, the MOSFET readings for each organ and tissue were averaged. MOSFET values were then divided by each detector's calibration factor to obtain a mean dose for all 45 protocols (FTC and ATCM) for the different ages and genders. A mean organ weighted dose was then multiplied by the relevant tissue Lifetime Attributable Risk Factors (LAR). The unit for effective risk is the 'number of cases per million for males and females', see **Table 6-14**. All ER raw data for FTC, ATCM corrected and uncorrected can be seen in **Appendix XV-XVII.**

Table 6- 14:Example of averaged MOSFET readings for a 20 year old female for each organ and tissue during an FTC CT examination* with details on the Lifetime Attributable Risk factors for each organ

Organ	Weighted Dose(mGy)	Lifetime Attributable Risk	Organ Effective risk case/10^6
Stomach	**25.843**	**0.52**	**13.438**
Colon	**12.034**	**1.14**	**13.719**
Lungs	**2.927**	**3.46**	**10.129**
Breasts	**0.975**	**4.29**	**4.181**
Uterus	**0.905**	**0.26**	**0.235**
Ovary	**2.685**	**0.5**	**1.343**
Thyroid	**0.133**	**1.13**	**0.151**
bladder	**0.905**	**1.09**	**0.987**
Liver	**20.112**	**0.14**	**2.816**
Total			**46.998**
Other organs		**Total ER other organs**	
Thymus	**0.356**	**mean other organs × LAR for other organ =11.132×3.23**	**Total ER organs + Total ER other organs =35.955+46.998**
Spleen	**19.825**		
Kidneys	**23.575**		
Adrenals	**12.135**		
Heart	**2.280**		
Pancreas	**24.780**		
Gall Bladder	**28.980**		
ABM	**2.472**		
Brain	**0.014**		
Small Intestine	**7.8980**		
Extrathoracic	**0.133**		
Total	**122.447**		
Mean Total	**11.132**	**35.955**	**82.953**
*** parameters using/ 250mA, 0.5×16 detector configuration and 0.688 pitch factor**			

6.4.1 Tube current

The comparison of the mean ER for FTC and ATCM approaches can be viewed in **Table 6-15** and **Table 6-16**. **Table 6-15** shows mean ER for FTC and corrected ATCM for males and females. **Table 6-16** shows the mean ER for FTC and uncorrected ATCM for males and females (i.e. a comparison of FTC and ATCM approaches with different respective tube currents). The uncorrected ATCM has been included to enable clinically relevant comparisons to be made between FTC and ATCM approaches, whilst the corrected ATCM data has been included to enable fair comparison of dose and risk data by normalising the tube currents between these modes as described in the methods chapter

6.4.1.1 Comparison of mean ER of FTC and ATCM corrected data

Table 6-15 shows the mean ER estimated for FTC and corrected ATCM for each age and gender group when using the 100 mA/low dose+ scan option. The mean ER for FTC was higher than for the corrected ATCM among females and males in any age group. Nonetheless, all these findings were not statistically significant ($p>0.05$). For example, the mean lifetime ER for a 20 year old female was 30.005 ± 5.675 and 28.594 ± 2.252 case/10^6; for a 20 year old male was 25.490 ± 5.329 and 23.961 ± 2.270 case/10^6; for a 70 year old female was 8.811 ± 0.681 and 8.3400 ± 0.599 case/10^6; and for a 70 year old male was 7.575 ± 1.534 and 7.084 ± 0.599 case/10^6, for FTC and ATCM, respectively.

When increasing tube current to 200mA/low dose, the mean ER for FTC was lower than for corrected ATCM among females and males in all age groups. All these findings were not statistically significant ($p>0.05$). For example, the mean lifetime ER for a 20 year old female was 52.475 ± 12.066 and 54.972 ± 4.452 case/10^6; a 20 year old male was 44.974 ± 10.673 and 46.245 ± 4.427 case/10^6; a 70 year old female was 15.366 ± 3.357 and 16.086 ± 1.274 case/10^6; and a 70 year old male was 13.199 ± 3.007 and 13.567 ± 1.210 case/10^6, FTC and ATCM, respectively.

When using a higher tube current at 250 mA/standard, the mean FTC ER was non-statistically ($P>0.05$) higher than the corrected ATCM among females and males in any age group. For example, the mean lifetime ER for a 20-year-old female was 67.262 ± 14.812 and 66.664 ± 10.866 case/10^6; for a 20 year old male was 57.500 ± 13.641 and 56.398 ± 10.581 case/10^6; for a 70 year old female was 19.6199 ± 4.296 and 19.373 ± 3.084 case/$10^{6;}$ and a 70 year old male was 116.781 ± 3.813 and 16.453±2.950 case/10^6, for FTC and ATCM, respectively.

Table 6- 15:Comparison between mean ER for male and females (FTC and corrected ATCM) using different tube currents

CT Technique	FTC female	ATCM female	P value	FTC male	ATCM male	P value
Age	100 mA /low dose+ Mean ± SD ER case/10^6 n=9					
20	30.005±5.675	28.594±2.252	0.200	25.490±5.329	23.961±2.270	0.179
30	20.165±3.82	19.191±1.486	0.196	17.494±3.646	16.429±1.537	0.176
40	18.411±3.519	17.490±1.332	0.198	16.402±3.402	15.392±1.416	0.173
50	16.055±3.077	15.230±1.138	0.198	14.655±3.019	13.745±1.235	0.171
60	12.866±2.462	12.190±0.892	0.197	11.522±2.351	10.794±0.937	0.167
70	8.811±0.681	8.3400±0.599	0.196	7.575±1.534	7.084±0.599	0.160
200mA/ low dose						
20	52.475±12.066	54.972±4.452	0.300	44.974±10.673	46.245±4.427	0.369
30	35.228±8.044	36.876±2.979	0.302	30.807±7.274	31.667±3.013	0.370
40	32.182±7.270	33.648±2.706	0.303	28.822±6.763	29.624±2.789	0.370
50	28.057±6.263	29.335±2.345	0.301	25.690±5.979	26.411±2.447	0.368
60	22.463±4.957	23.498±1.868	0.298	20.130±4.630	20.695±1.875	0.368
70	15.366±3.357	16.086±1.274	0.294	13.199±3.007	13.567±1.210	0.368
250 mA/standard						
20	67.262±14.812	66.664±10.866	0.098	57.500±13.641	56.398±10.581	0.121
30	45.114±9.929	44.677±7.275	0.102	39.351±9.285	38.595±7.216	0.122
40	41.177±9.123	40.696±6.649	0.113	36.780±8.621	36.071±6.701	0.125
50	35.870±7.942	35.420±5.755	0.120	32.747±7.610	32.120±5.909	0.127
60	28.699±6.325	28.332±4.557	0.125	25.620±5.876	25.126±4.557	0.133
70	19.6199±4.296	19.373±3.084	0.127	16.781±3.813	16.453±2.950	0.139
300 mA/ quality						
20	76.322±17.692	82.656±20.137	<0.001	64.840±15.959	70.427±18.130	<0.001
30	51.184±11.863	55.353±13.448	<0.001	44.392±10.898	48.164±12.361	<0.001
40	46.674±10.846	50.374±12.213	<0.001	41.512±10.154	44.982±11.496	<0.001
50	40.655±9.433	43.790±10.558	0.002	36.986±8.999	40.014±10.166	<0.001
60	32.539±7.523	34.979±8.375	0.002	28.960±6.992	31.271±7.870	<0.001
70	22.258±5.125	23.888±5.680	0.002	18.979±4.559	20.461±5.108	0.002
400 mA/ high quality						
20	106.527±25.870	105.757±25.790	0.155	91.267±24.081	90.711±23.206	0.223
30	71.424±17.343	70.874±17.219	0.142	62.468±16.438	62.067±15.821	0.218
40	65.132±15.903	64.594±15.632	0.126	58.391±15.304	57.990±14.708	0.211
50	56.7187±13.850	56.205±13.506	0.119	51.991±13.550	51.607±13.002	0.201
60	45.378±11.048	44.929±10.710	0.115	40.678±10.509	40.350±10.061	0.191
70	31.028±7.523	30.697±7.264	0.112	26.650±6.839	26.417±6.530	0.184
FTC mA range (100-400) / corrected ATCM mA range (100-400)						

Table 6-15 presents the mean ER estimated by using 300 mA/quality CT protocols. The mean corrected ATCM ER was decreased by around 8% when compared to FTC among females and males in any age group. These results did achieve statistical significance ($P<0.05$; **Table 6-15**). For example, the mean lifetime ER for a 20-year-old female was 76.322 ± 17.692 and 82.656 ± 20.137 case/10^6; for a 20-year-old male was 64.840 ± 15.959 and 70.427 ± 18.130 case/10^6; for a 70-year-old female was 22.258 ± 5.125 and 23.888 ±5 .680 case/10^6 ; and for a 70 year old male was 18.979 ± 4.559 and 20.461±5.108 case/10^6, for FTC and ATCM, respectively.

When using 400 mA/high quality CT protocols, FTC techniques had a higher mean ER than corrected ATCM among females and males in all age groups, these findings were not statistically significant ($P>0.05$). By way of an example, the mean lifetime ER for a 20 year old female was 106.527 ± 25.870 and 105.757 ± 25.790 case/10^6; for a 20 year old male was 91.267 ± 24.081 and 90.711±23.206 case/10^6; for a 70 year old female was 31.028 ± 7.523 and 30.697±7.264 case/10^6; and for a 70 year old male was 26.650 ± 6.839 and 26.417 ± 6.530 case/$10^{6,}$ for FTC and ATCM, respectively.

According to **Figures 6-13**, it can be concluded that, using direct measurement by MOSFET method, the mean ER for FTC and corrected ATCM increases when the tube current increases for any age group and any gender. Moreover, in all tube currents, the mean ER for FTC and corrected ATCM for males and females decreases with increasing the age. In all tube currents, the mean ER for FTC and corrected-ATCM (raw) data were higher for females than males in each age group.

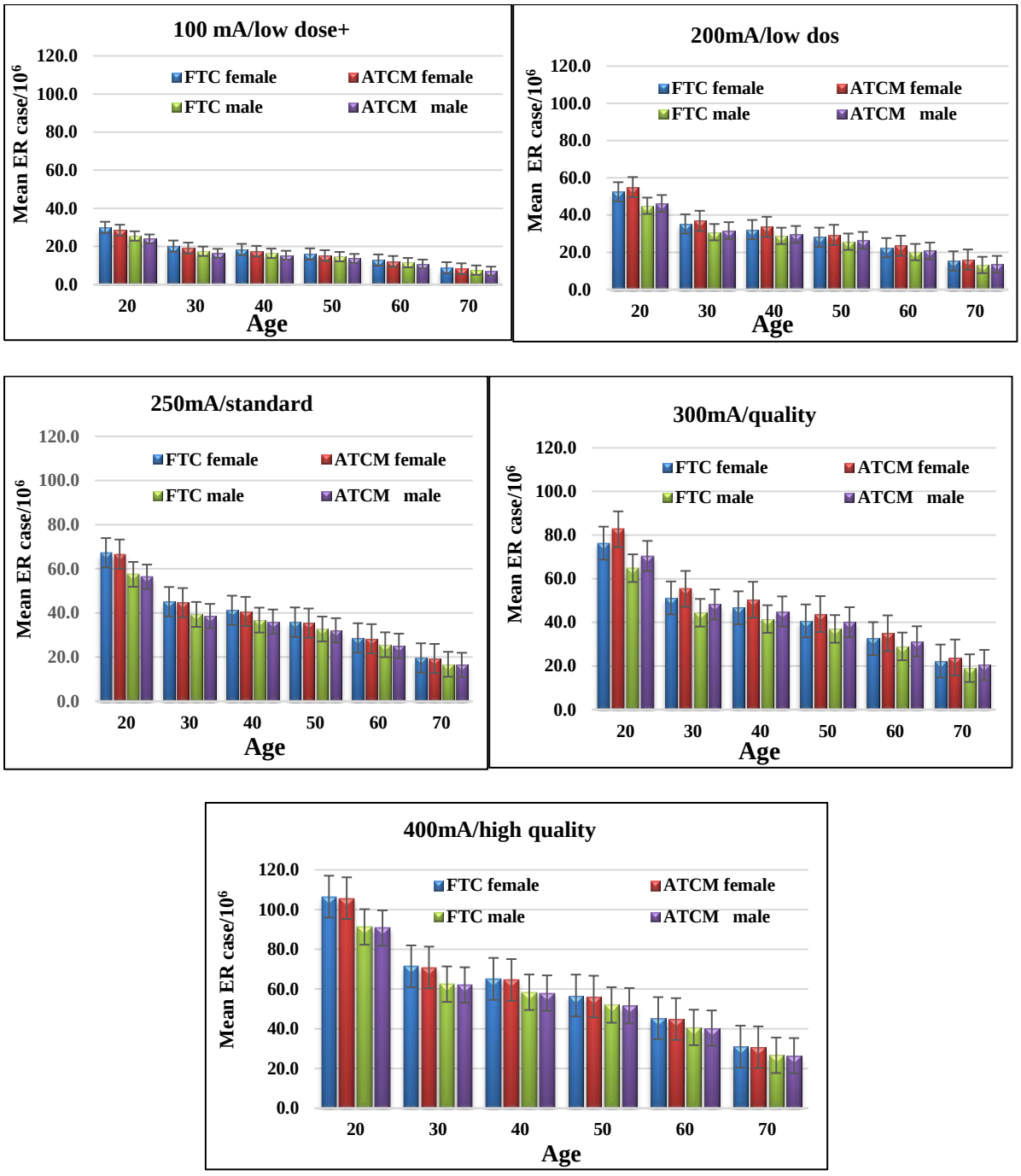

Figure 6- 13: Bar chart illustrating the mean ER from MOSFET method between FTC and corrected ATCM for both male and females, using different tube currents

6.4.1.2 Comparison of mean ER for FTC and uncorrected-ATCM data

The data presented here compares the ER associated with FTC across a tube current range of 100-400mA against the corresponding uncorrected-ATCM data with a tube current range of 49-440 mA **(Table 6-16)**. The mean ER from ATCM (raw) data was significantly higher than FTC for all ages and genders. For example, the mean lifetime ERs were: 20 year old female 65.521 ± 30.138 and 82.952 ± 39.934 case/10^6 , 20 year old male 56.163 ±26.348 and 70.493±34.816 case/10^6 ,70 year old female 19.218 ± 8.741 and 24.090±11.471case/10^6 and 70 year old male 16.458 ± 7.595 and 20.565 ± 10.005 case/10^6, FTC and ATCM (raw) data, respectively. All differences between mean ER from uncorrected ATCM and FTC were statistically significant (P<0.001) for all age and gender groups. The reduction in ER was around 20-21% when comparing FTC to uncorrected ATCM.

Table 6- 16:Comparison between mean ER for males and females, for FTC and uncorrected-ATCM (raw) data, using different tube currents

CT Technique	FTC	ATCM(raw) data	P value
Age	**Female ER case/10^6 Mean ± SD n=45**		
20	**65.521±30.138**	**82.952±39.934**	**<0.001**
30	**44.156±20.189**	**55.593±26.721**	**<0.001**
40	**40.287±18.418**	**50.648±24.313**	**<0.001**
50	**35.101±16.027**	**44.075±21.105**	**<0.001**
60	**28.096±12.804**	**35.244±16.827**	**<0.001**
70	**19.218±8.741**	**24.090±11.471**	**<0.001**
Male ER case/10^6 Mean ± SD n=45			
20	**56.163±26.348**	**70.493±34.816**	**<0.001**
30	**38.460±18.005**	**48.234±23.784**	**<0.001**
40	**35.972±16.796**	**45.086±22.175**	**<0.001**
50	**32.054±14.917**	**40.143±19.681**	**<0.001**
60	**25.106±11.626**	**31.405±15.328**	**<0.001**
70	**16.458±7.595**	**20.565±10.005**	**<0.001**
FTC mA range (100-400) / ATCM (raw) data mean mA range (49-440)			

6.4.2 Pitch factor

6.4.2.1 Comparison of mean ER for FTC and corrected-ATCM data

From **Table 6-17,** the mean ER for FTC was higher than mean corrected-ATCM ER in all age groups, for both males and females, when using the detail (0.688) pitch factor. However, these results were not statistically significant (P>0.05). For example, the mean lifetime ERs were: 20-year-old female 82.877 ± 34.450 and 80.576 ± 38.633case/10^6, 20 year old male 71.674 ± 30.224 and 69.277 ± 33.831case/10^6 ,70 year old female 24.156 ± 10.022 and 23.287±11.118case/10^6 and 70 year old male 20.880 ± 8.722 and 20.090 ± 9.718 case/10^6, for FTC and ATCM, respectively.

When the standard (0.938) pitch factor was used, the mean ER for FTC was slightly lower than corrected ATCM for males and females in any age group. Again, these results were not statistically significant (P>0.05). For example, the mean lifetime ERs were: 20 year old female 65.685 ± 26.325 and 66.646 ± 27.531 case/10^6, 20 year old male 55.979 ± 22.498 and 56.779 ± 23.984 case/10^6 ,70 year old female 19.147 ± 7.612 and 19.337±7.936 case/10^6 and 70 year old male 16.395 ± 6.513 and 16.564 ± 6.904 case/10^6, for FTC and ATCM, respectively.

Table 6- 17:Comparison between mean ER for male and female for FTC and corrected-ATCM data using different pitch factors

CT Technique	FTC female	ATCM female	P Value	FTC male	ATCM male	P Value
Age	**Detail(0.688) / ER case/10^6 Mean ± SD n=15**					
20	**82.877±34.450**	**80.576±38.633**	**0.135**	**71.674±30.224**	**69.277±33.831**	**0.098**
30	**55.589±23.085**	**53.975±25.857**	**0.123**	**49.049±20.658**	**47.380±23.112**	**0.094**
40	**50.751±21.083**	**49.158±23.553**	**0.103**	**45.834±19.275**	**44.244±21.548**	**0.089**
50	**44.203±18.359**	**42.729±19.762**	**0.088**	**40.792±17.122**	**39.346±19.123**	**0.083**
60	**35.350±14.676**	**34.117±16.311**	**0.077**	**31.893±13.348**	**30.724±14.891**	**0.075**
70	**24.156±10.022**	**23.287±11.118**	**0.070**	**20.880±8.722**	**20.090±9.718**	**0.068**
Standard(0.938)						
20	**65.685±26.325**	**66.646±27.531**	**0.213**	**55.979±22.498**	**56.779±23.984**	**0.228**
30	**44.054±17.620**	**44.663±18.420**	**0.225**	**38.331±15.378**	**38.856±16.383**	**0.236**
40	**40.172±16.034**	**40.683±16.770**	**0.241**	**35.848±14.353**	**36.317±15.277**	**0.246**
50	**34.986±13.941**	**35.395±14.078**	**0.258**	**31.940±12.759**	**32.335±13.561**	**0.257**
60	**27.997±11.142**	**28.2967±11.631**	**0.275**	**25.0136±9.958**	**25.298±10.569**	**0.273**
70	**19.147±7.612**	**19.337±7.936**	**0.289**	**16.395±6.513**	**16.564±6.904**	**0.292**
Fast (1.438						
20	**48.901±18.876**	**55.964±16.714**	**<0.001**	**40.833±15.892**	**46.590±14.108**	**<0.001**
30	**32.825±12.646**	**37.543±11.197**	**<0.001**	**27.998±10.871**	**31.917±9.656**	**<0.001**
40	**29.938±11.512**	**34.241±10.172**	**<0.001**	**26.231±10.158**	**29.875±9.024**	**<0.001**
50	**26.112±10.023**	**29.863±8.545**	**<0.001**	**23.427±9.042**	**26.657±8.033**	**<0.001**
60	**20.938±8.025**	**23.943±7.0784**	**<0.001**	**18.410±7.074**	**20.920±6.288**	**<0.001**
70	**14.350±5.493**	**16.406±4.845**	**<0.001**	**12.098±4.634**	**13.735±4.126**	**<0.001**
FTC mA range (100-400) / corrected ATCM mA range (100-400)						

When the pitch factor was increased to 1.438 (fast), the mean ER for FTC was considerably lower (by around 13%) than mean corrected ATCM for all ages and genders. For example, the mean lifetime ERs were: 20 year old female 48.901±18.876 and 55.964±16.714case/10^6 , 20 year old male 40.833 ± 15.892 and 46.590 ±14.108 case/10^6 ,70 year old female 14.350 ± 5.493 and 16.406 ± 4.845 case/10^6 and 70 year old male 12.098 ± 4.634 and 13.735 ± 4.126 case/10^6, for FTC and ATCM, respectively. Interestingly, all of these findings were statistically significant (P<0.05; **Table 6-17**).

From **Figures 6-14** it can be seen that the mean ER for FTC and corrected ATCM decreases when the pitch factor increases for any age group and gender using direct measurement by MOSFET method. Furthermore, for all pitch factors, the mean ER for FTC and corrected ATCM, for males and females, decreases with increasing age. Using any pitch factor, the mean ER for FTC and corrected ATCM techniques were higher for females than males in each age group.

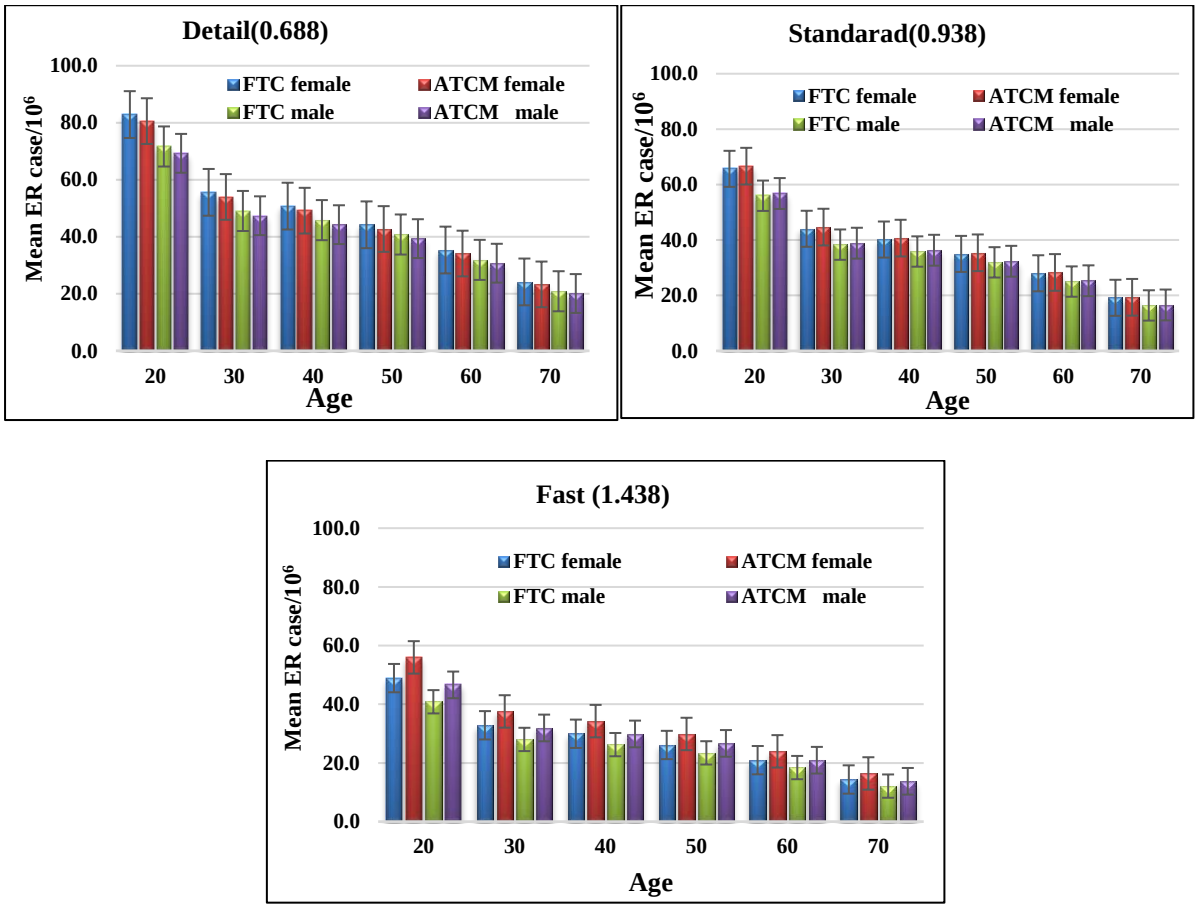

Figure 6- 14: Bar chart illustrating the mean ER using MOSFET method between FTC and corrected ATCM for both male and female using different pitch factors

6.4.2.2 Comparison of mean ER for FTC and uncorrected-ATCM data

When using uncorrected ATCM **(Table 6-18),** the mean ER was higher for ATCM techniques when compared to FTC for all ages and genders. For example, the mean lifetime ERs were: 20 year old female 82.877 ± 34.450 and 99.263 ± 50.684 case/10^6, 20 year old male 71.674 ± 30.224 and 85.370 ± 44.191 case/10^6 ,70 year old female 24.156 ± 10.022 and 28.682 ± 114.573 case/10^6 and 70 year old male 20.880 ± 8.722 and 24.747 ± 12.699 case/10^6, for FTC and ATCM data, respectively. All differences between were statistically significant (P<0.001). The reduction in FTC ER was around 17% (female) and 16% (male) when compared to uncorrected ATCM.

Table 6- 18:Comparison between mean ER for males and females for FTC and uncorrected-ATCM using different pitch factors

CT Technique	FTC female	ATCM female	P Value	FTC male	ATCM male	P Value
Age	**Detail(0.688) /ER case/10^5 Mean ± SD n=15**					
20	**82.877±34.450**	**99.263±50.684**	**0.012**	**71.674±30.224**	**85.370±44.191**	**0.014**
30	**55.589±23.085**	**66.490±33.919**	**0.012**	**49.049±20.658**	**58.384±30.189**	**0.015**
40	**50.751±21.083**	**60.553±30.879**	**0.013**	**45.834±19.275**	**54.515±28.149**	**0.015**
50	**44.203±18.359**	**52.932±26.812**	**0.013**	**40.792±17.122**	**48.476±124.984**	**0.015**
60	**35.350±14.676**	**42.023±121.378**	**0.014**	**31.893±13.348**	**37.850±119.458**	**0.015**
70	**24.156±10.022**	**28.682±114.573**	**0.014**	**20.880±8.722**	**24.747±12.699**	**0.016**
Standard(0.938)						
20	**65.685±26.325**	**81.778±37.065**	**0.002**	**55.979±22.498**	**69.655±32.097**	**0.003**
30	**44.054±17.620**	**54.802±24.828**	**0.002**	**38.331±15.378**	**47.667±121.934**	**0.003**
40	**40.172±16.034**	**49.912±22.599**	**0.002**	**35.848±14.353**	**44.550±20.463**	**0.003**
50	**34.986±13.941**	**43.422±119.641**	**0.002**	**31.940±12.759**	**39.663±18.177**	**0.003**
60	**27.997±11.142**	**34.712±115.683**	**0.002**	**25.0136±9.958**	**31.029±14.178**	**0.003**
70	**19.147±7.612**	**23.722±10.706**	**0.002**	**16.395±6.513**	**20.316±9.267**	**0.003**
Fast (1.438)						
20	**48.901±18.876**	**67.817±23.133**	**<0.001**	**40.833±15.892**	**56.453±119.427**	**<0.001**
30	**32.825±12.646**	**45.490±15.488**	**<0.001**	**27.998±10.871**	**38.669±13.288**	**<0.001**
40	**29.938±11.512**	**41.480±114.064**	**<0.001**	**26.231±10.158**	**36.192±12.412**	**<0.001**
50	**26.112±10.023**	**36.172±12.222**	**<0.001**	**23.427±9.042**	**32.290±11.044**	**<0.001**
60	**20.938±8.025**	**28.997±9.774**	**<0.001**	**18.410±7.074**	**25.337±8.638**	**<0.001**
70	**14.350±5.493**	**19.867±6.686**	**<0.001**	**12.098±4.634**	**16.633±5.662**	**<0.001**
FTC mA range (100-400) / uncorrected ATCM mean mA range (49-440)						

6.4.3 Detector configuration

6.4.3.1 Comparison of mean ER for FTC and corrected-ATCM data

From **Table 6-19,** corrected ATCM illustrates that the mean ER for FTC examinations was substantially lower (around 6%) than corrected ATCM examinations for any age group when using the detector configuration of 0.5×16mm. Moreover, all those findings were statistically significant (P<0.05). For example, the mean lifetime ERs were: 20 year old female 68.493 ± 34.031and 72.781 ± 33.805 case/10^6, 20 year old male 59.926 ± 30.175 and 63.254 ± 29.556 case/10^6 ,70 year old female 19.940 ± 9.88 and 21.021± 9.613 case/10^6 and 70 year old male 17.425 ± 8.655 and 18.298 ± 8.456 case/10^6, for FTC and ATCM, respectively.

Table 6- 19:Comparison between mean ER for males and females for FTC and corrected ATCM using different detector configurations

CT Technique	FTC female	ATCM female	P Value	FTC male	ATCM male	P Value
Age	**0.5×16mm/ ER case/10^6 Mean ± SD n=15**					
20	**68.493±34.031**	**72.781±33.805**	**0.023**	**59.926±30.175**	**63.254±29.556**	**0.035**
30	**45.951±22.804**	**48.761±22.593**	**0.025**	**41.012±20.607**	**43.253±20.182**	**0.036**
40	**41.974±20.849**	**44.441±20.515**	**0.029**	**38.320±19.209**	**40.377±18.806**	**0.038**
50	**36.545±18.149**	**38.624±17.163**	**0.033**	**34.094±17.044**	**35.889±16.676**	**0.040**
60	**29.205±14.491**	**30.821±14.132**	**0.036**	**26.637±13.264**	**28.002±12.969**	**0.043**
70	**19.940±9.881**	**21.021±9.613**	**0.039**	**17.425±8.655**	**18.298±8.456**	**0.046**
1.0×16mm						
20	**63.074±29.2789**	**64.866±28.689**	**0.176**	**54.172±25.805**	**55.483±25.332**	**0.213**
30	**42.301±19.605**	**43.454±19.188**	**0.186**	**37.096±17.640**	**37.965±17.300**	**0.220**
40	**38.563±17.863**	**39.550±17.440**	**0.199**	**34.690±16.458**	**35.476±16.122**	**0.228**
50	**33.565±15.526**	**34.377±14.603**	**0.211**	**30.899±14.616**	**31.573±14.297**	**0.237**
60	**26.8407±12.393**	**27.458±12.029**	**0.223**	**24.1902±11.394**	**24.686±11.126**	**0.250**
70	**18.345±8.455**	**18.751±8.187**	**0.232**	**15.852±7.445**	**16.154±7.256**	**0.266**
2.0×16mm						
20	**65.896±28.697**	**65.539±29.139**	**0.430**	**54.388±24.136**	**53.909±25.030**	**0.383**
30	**44.216±19.220**	**43.967±19.539**	**0.427**	**37.270±16.508**	**36.935±17.121**	**0.380**
40	**40.3241±17.498**	**40.0913±17.858**	**0.459**	**34.903±15.422**	**34.583±15.990**	**0.377**
50	**35.191±15.232**	**34.987±15.056**	**0.423**	**31.166±13.726**	**30.876±14.227**	**0.375**
60	**28.240±12.190**	**28.078±12.489**	**0.435**	**24.490±10.734**	**24.254±11.120**	**0.371**
70	**19.369±8.340**	**19.258±8.551**	**0.424**	**16.096±7.029**	**15.937±7.283**	**0.367**
FTC mA range (100-400) / corrected ATCM mA range (100-400)						

When the detector configuration was increased to 1.0×16mm, the mean ER for FTC was slightly lower than for corrected ATCM techniques, for any age or genders. For example, the mean lifetime ERs were: 20 year old female 63.074 ± 29.2789 and 64.866 ± 28.689 case/10^6 , 20 year old male 54.172 ± 25.805 and 55.483 ± 25.332 case/10^6 , 70 year old female 18.345 ± 8.455 and 18.751±8.187case/10^6 and 70 year old male 15.852 ± 7.445 and 16.154±7.256 case/10^6, for FTC and ATCM, respectively. These findings were, however, not statistically significant (see **Table 6-19)**. The same table demonstrates that the mean ER for FTC was slightly higher than the corrected ATCM for females and males in any age. When the detector configuration was changed to 2.0×16mm the results were again not statistically significant (P>0.05). For example, the mean lifetime ERs were: 20 year old female 65.896 ± 28.697 and 65.539±29.139 case/10^6 , 20 year old male 54.388 ± 24.136 and 53.909±25.030 case/10^6 , 70 year old female 19.369 ± 8.340 and 19.258 ± 8.551 case/10^6 and 70 year old male 16.096 ± 7.029 and 15.937 ± 7.283 case/10^6, for FTC and ATCM, respectively.

Based on the findings depicted in **Figures 6-15**, in any age group and for both genders, the mean ER for FTC and corrected ATCM, using the detector configuration of 0.5×16 mm, was the highest in comparison with other detector configurations. On the other hand, the mean ER for FTC and corrected ATCM, using the detector configuration of 1.0×16 mm, was the lowest for all ages across both genders. In all detector configurations, the mean ER using direct measurement by MOSFET method for FTC and corrected ATCM, for males and females, decreases with increasing the age. Further, in all detector configurations the mean ER for FTC and corrected ATCM techniques were higher for females than males in each age group.

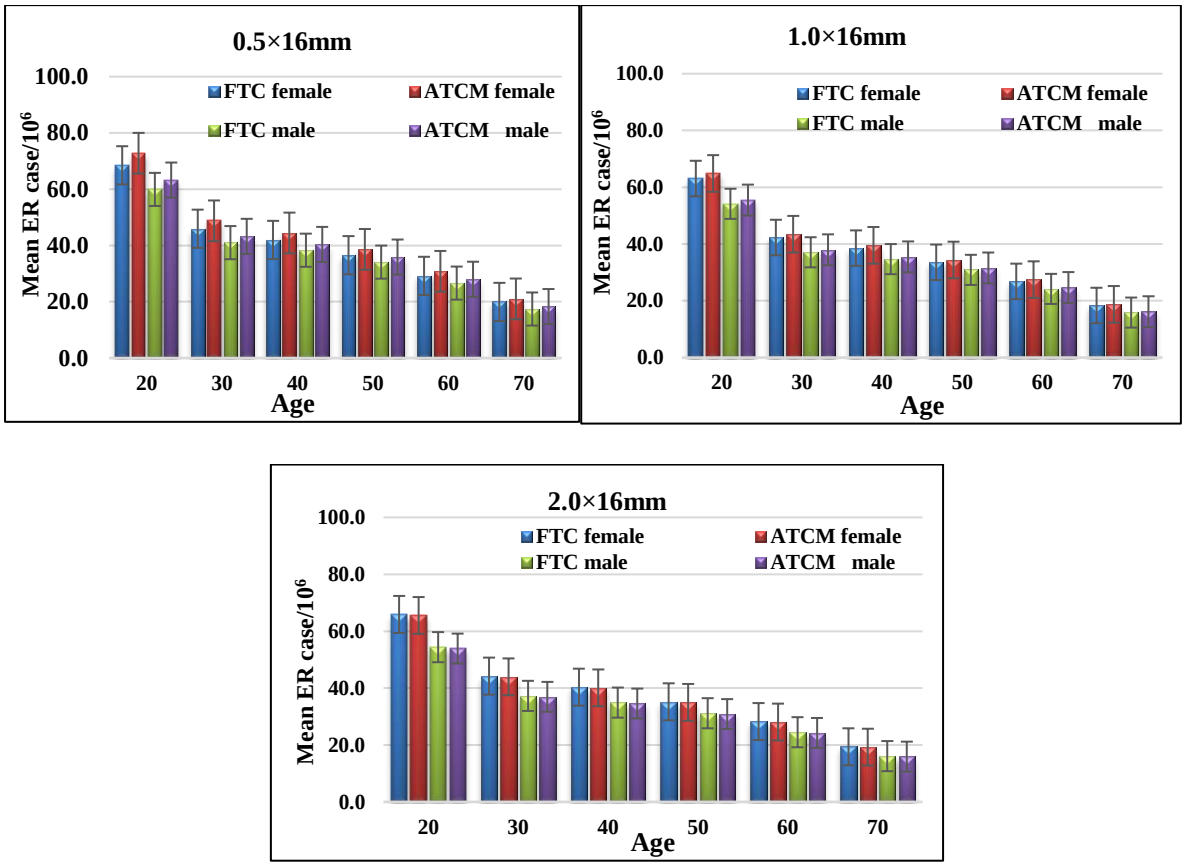

Figure 6- 15: Bar chart illustrating mean ER using MOSFET method for FTC corrected ATCM for both men and women using different detector configurations

6.4.3.2 Comparison of mean ER for FTC and uncorrected-ATCM data

When using uncorrected ATCM **(Table 6-20),** the mean ER was higher for uncorrected ATCM when compared to FTC, for the different detector configurations across all ages and gender groups. This leads to the mean ER increasing from uncorrected ATCM data by around 23% (female) and 23% (male) when compared to FTC. For example, the mean lifetime ERs were: 20 year old female 68.493 ± 34.031 and 89.220±44.845 case/$10^{6,}$ 20 year old male 59.926 ± 30.175 and 77.513 ± 39.097 case/10^6 ,70 year old female 19.940 ± 9.881 and 25.757 ± 12.785case/10^6 and 70 year old male 17.425 ± 8.655 and 22.415 ± 11.198 case/10^6, for FTC and ATCM, respectively. These differences were highly statistically significant (P<0.001).

Table 6- 20:Comparison between mean ER for males and females, for FTC and uncorrected ATCM, using different detectors configurations

CT Technique	FTC female	ATCM female	P Value	FTC male	ATCM male	P Value
Age	**0.5×16mm/ ER case/10^5 Mean ± SD n=15**					
20	**68.493±34.031**	**89.220±44.845**	**<0.001**	**59.926±30.175**	**77.513±39.097**	**<0.001**
30	**45.951±22.804**	**59.770±29.982**	**<0.001**	**41.012±20.607**	**53.000±26.699**	**<0.001**
40	**41.974±20.849**	**54.465±27.238**	**<0.001**	**38.320±19.209**	**49.474±124.209**	**<0.001**
50	**36.545±18.149**	**47.331±123.601**	**<0.001**	**34.094±17.044**	**43.971±122.044**	**<0.001**
60	**29.205±14.491**	**37.767±18.491**	**<0.001**	**26.637±13.264**	**34.305±117.176**	**<0.001**
70	**19.940±9.881**	**25.757±12.785**	**<0.001**	**17.425±8.655**	**22.415±11.198**	**<0.001**
1.0×16mm						
20	**63.074±29.278**	**79.485±38.234**	**0.002**	**54.172±25.805**	**67.961±33.634**	**0.002**
30	**42.301±19.605**	**53.250±25.576**	**0.002**	**37.096±17.640**	**46.503±22.981**	**0.002**
40	**38.563±17.863**	**48.481±23.233**	**0.002**	**34.690±16.458**	**43.452±21.428**	**0.002**
50	**33.565±15.526**	**42.146±20.137**	**0.002**	**30.899±14.616**	**38.670±19.014**	**0.003**
60	**26.840±12.393**	**33.663±16.032**	**0.002**	**24.190±11.394**	**30.233±14.809**	**0.003**
70	**18.345±8.455**	**22.987±10.917**	**0.002**	**15.852±7.445**	**19.784±9.664**	**0.003**
2.0×16mm						
20	**65.896±28.697**	**80.220±38.372**	**0.003**	**54.388±24.136**	**66.004±32.687**	**0.004**
30	**44.216±19.220**	**53.810±25.714**	**0.003**	**37.270±16.508**	**45.216±22.349**	**0.004**
40	**40.324±17.498**	**49.061±23.467**	**0.003**	**34.903±15.422**	**42.331±120.868**	**0.004**
50	**35.191±15.232**	**42.810±120.461**	**0.003**	**31.166±13.726**	**31.166±113.727**	**0.003**
60	**28.240±12.190**	**34.352±16.386**	**0.003**	**24.490±10.734**	**29.677±14.508**	**0.003**
70	**19.369±8.340**	**23.560±11.215**	**0.003**	**16.096±7.029**	**119.497±9.498**	**0.003**
FTC mA range (100-400) / uncorrected ATCM mean mA range (49-440)						

6.5 Image Quality - abdominal organs, comparing signal to noise ratio (SNR) between FTC and ATCM

In this subsection, the mean SNR was calculated from the five abdomen organs (Liver, Spleen, Pancreas, Left Kidney and Right Kidney) using the equation, indicated on **chapter 5 section 5.5.1**. SNR was calculated for the five abdomen organs for both FTC and ATCM, using three ROI for each organ. In this subsection SNR data from FTC and ATCM are outlined, with detailed data being provided in **Appendices XVIII to XXV.**

6.5.1 Comparing SNR values between FTC and ATCM using different tube currents

As shown in **Figure 6-16**, there is a strong positive correlation in SNR values between FTC and ATCM across the range of tube currents (R^2=0.98-1.0).

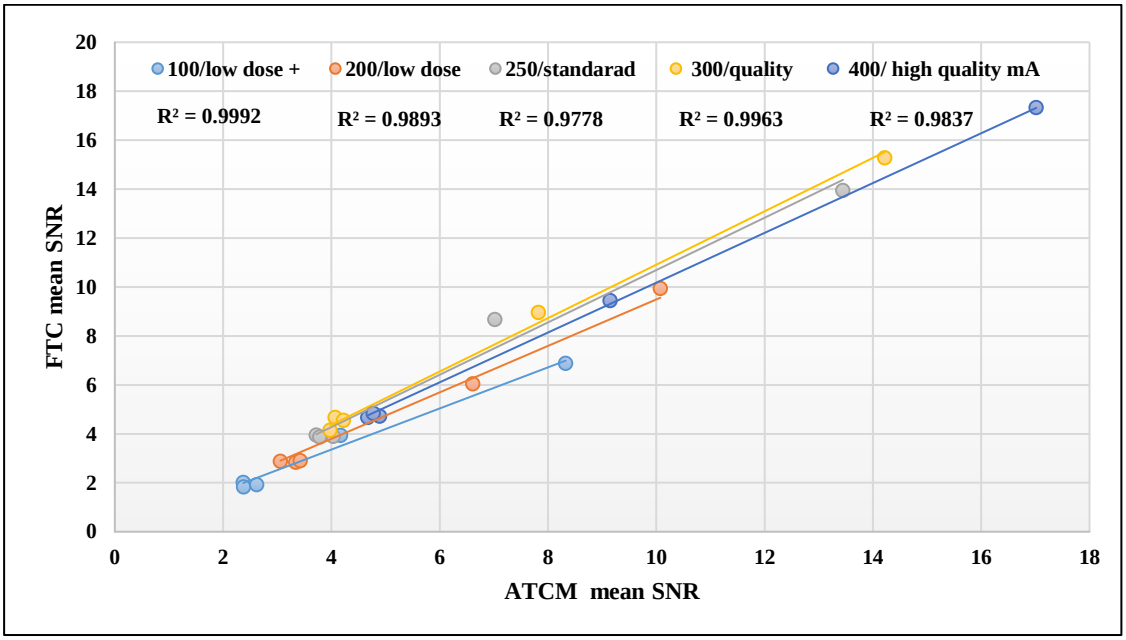

Figure 6- 16: Scatterplot illustrating the degree of SNR correlation between FTC and ATCM techniques, across different tube currents

When a tube current of 100mA/low dose + was used, the mean SNR value was higher for FTC than ATCM for all abdominal organs. However the differences between FTC and ATCM were statistically significant for only the pancreas (2.370 ± 0.487 and 2.025 ± 0.198; P=0.02), left kidney (2.381 ± 0.402 and 1.840 ± 0.170; P=0.002), and right kidney (2.619 ± 0.520 and 1.931 ± 0.155; P<0.001, FTC and ATCM, respectively) (**Table 6-21).**

Table 6- 21:Comparison of mean SNR values for FTC and ATCM techniques using different tube currents

CT Technique	FTC	ATCM	P value
Organ	**SNR 100mA/low dose + Mean ± SD n=9**		
Liver	**8.326±1.312**	**6.887±1.296**	**0.065**
Spleen	**4.170±0.758**	**3.947±0.178**	**0.189**
Pancreas	**2.370±0.487**	**2.025±0.198**	**0.020**
Lt. Kidney	**2.381±0.402**	**1.840±0.170**	**0.002**
Rt .Kidney	**2.619±0.520**	**1.931±0.155**	**0.001**
200 mA/ low dose			
Liver	**10.075±0.877**	**9.941±0.504**	**0.345**
Spleen	**6.608±1.451**	**6.048±0.529**	**0.153**
Pancreas	**3.060±0.516**	**2.882±0.192**	**0.119**
Lt. Kidney	**3.339±0.253**	**2.849±0.261**	**<0.001**
Rt .Kidney	**3.422±0.328**	**2.903±0.160**	**<0.001**
250mA/standard			
Liver	**13.447±2.337**	**13.944±1.322**	**0.204**
Spleen	**7.017±1.447**	**8.676±1.065**	**0.000**
Pancreas	**3.721±0.721**	**3.951±0.363**	**0.091**
Lt. Kidney	**3.785±0.746**	**3.880±0.255**	**0.331**
Rt .Kidney	**4.035±0.696**	**3.903±0.337**	**0.240**
300mA/quality			
Liver	**13.865±2.364**	**15.276±1.567**	**0.034**
Spleen	**7.823±1.523**	**8.969±1.501**	**0.003**
Pancreas	**4.066±0.833**	**4.677±0.647**	**0.017**
Lt. Kidney	**3.975±0.627**	**4.157±0.607**	**0.133**
Rt .Kidney	**4.224±0.417**	**4.551±0.544**	**0.091**
400mA/ high quality			
Liver	**17.016±3.111**	**17.331±3.215**	**0.207**
Spleen	**9.144±1.494**	**9.455±1.424**	**0.053**
Pancreas	**4.892±0.741**	**4.730±0.864**	**0.128**
Lt. Kidney	**4.670±0.505**	**4.671±0.434**	**0.497**
Rt .Kidney	**4.772±0.596**	**4.849±0.739**	**0.204**
FTC mA range (100-400) / ATCM mean mA range (49-440)			

Similarly, the mean SNR value for FTC was higher than ATCM for all abdominal organs when using the 200 mA/ low dose tube current. But, these findings were statistically significant for only left kidney (3.339 ± 0.253 and 2.849 ± 0.261; P<0.001), and right kidney (3.422 ± 0.328 and 2.903 ± 0.160; P<0.001, FTC and ATCM, respectively). By changing the tube current to 250mA/standard, the mean SNR value for FTC was lower than ATCM for all abdominal organs except the right kidney (4.035 ± 0.696 and 3.903 ± 0.337, FTC and ATCM, respectively). However, the results were not statistically significant for all abdominal organs except the spleen (7.017 ± 1.447 and 8.676 ± 1.065; P<0.001, FTC and ATCM, respectively).

In **Table 6-21,** the mean SNR value for FTC was lower than ATCM for all abdominal organs when using a tube current of 300mA/quality. However, only the liver (13.865 ± 2.364 and 15.276 ± 1.567; P=0.034), spleen (7.823 ± 1.523 and 8.969 ± 1.501; P=0.003), and pancreas (4.066 ± 0.833 and 4.677 ±0.647; P=0.003, FTC and ATCM, respectively) were statistically significant.

By increasing the tube current to the highest level, 400mA/ high quality, the mean SNR value for FTC was slightly lower than ATCM for the following abdominal organs: liver (17.016 ± 3.111 and 17.331 ± 3.215), spleen (9.144 ± 1.494 and 9.455 ± 1.424), and right kidneys (4.772 ± 0.596 and 4.849 ± 0.739, FTC and ATCM, respectively). The mean SNR value was slightly higher for FTC than ATCM for pancreas (4.892 ± 0.741 and 4.730 ± 0.864) whereas it was equal for both techniques for right kidney (4.670 ± 0.505 and 4.671 ± 0.434, FTC and ATCM, respectively). Nonetheless, none of these findings were statistically significant (P>0.05).

From **Figure 6-17**, it is clear that the mean SNR for both FTC and ATCM examinations, for all abdominal organs, increases as the tube current increases value for FTC and ATCM for each abdominal organ increases as the tube current increases.

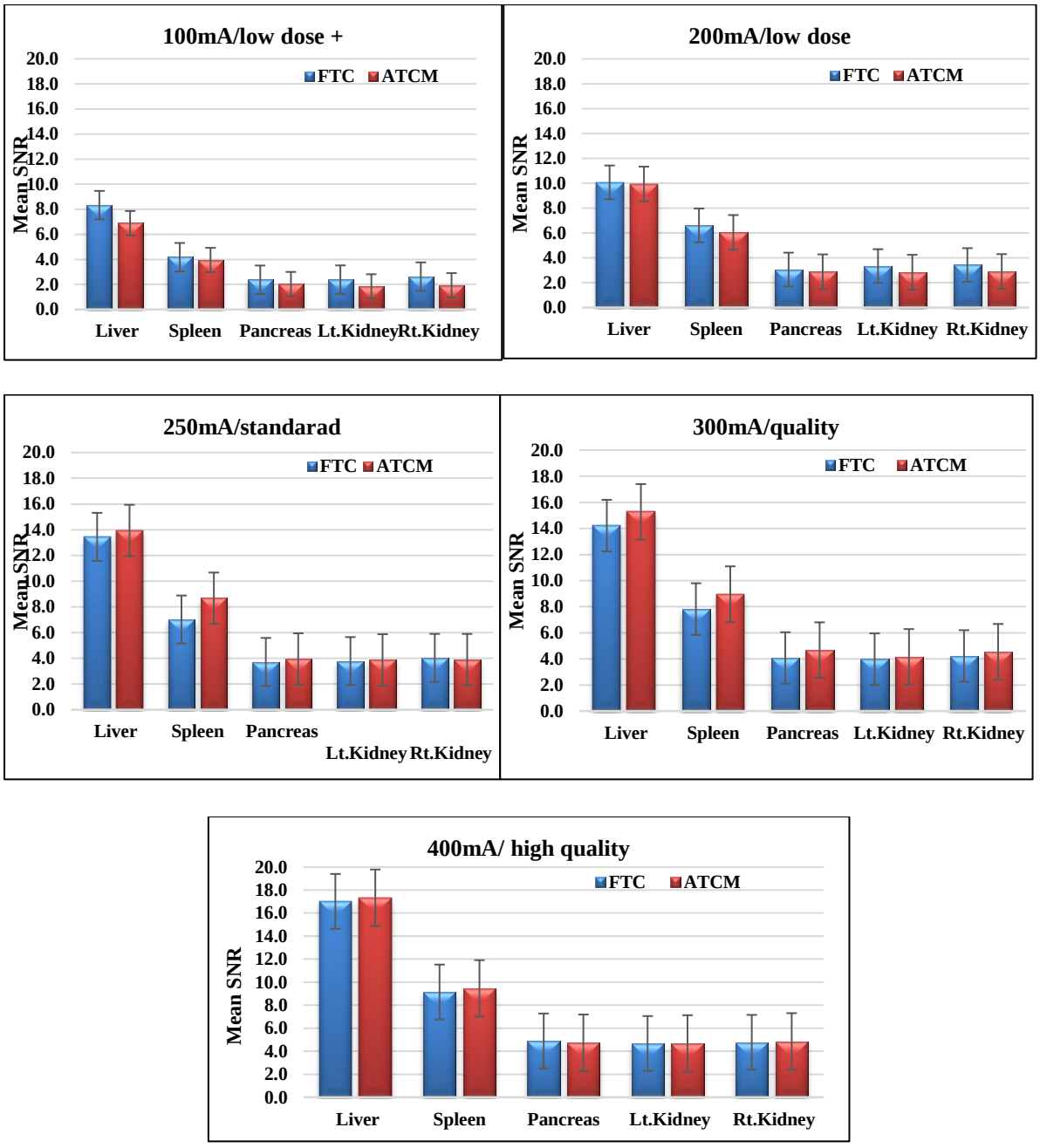

Figure 6- 17: Bar chart illustrating the mean SNR values for abdominal organs when comparing FTC and ATCM techniques

6.5.2 Comparing SNR values between FTC and ATCM with different pitch factors

As shown in **Figure 6-18**, there are strong positive associations between the mean SNR value for abdominal organs between FTC and ATCM techniques, using different pitch factors (R^2 > 0.993).

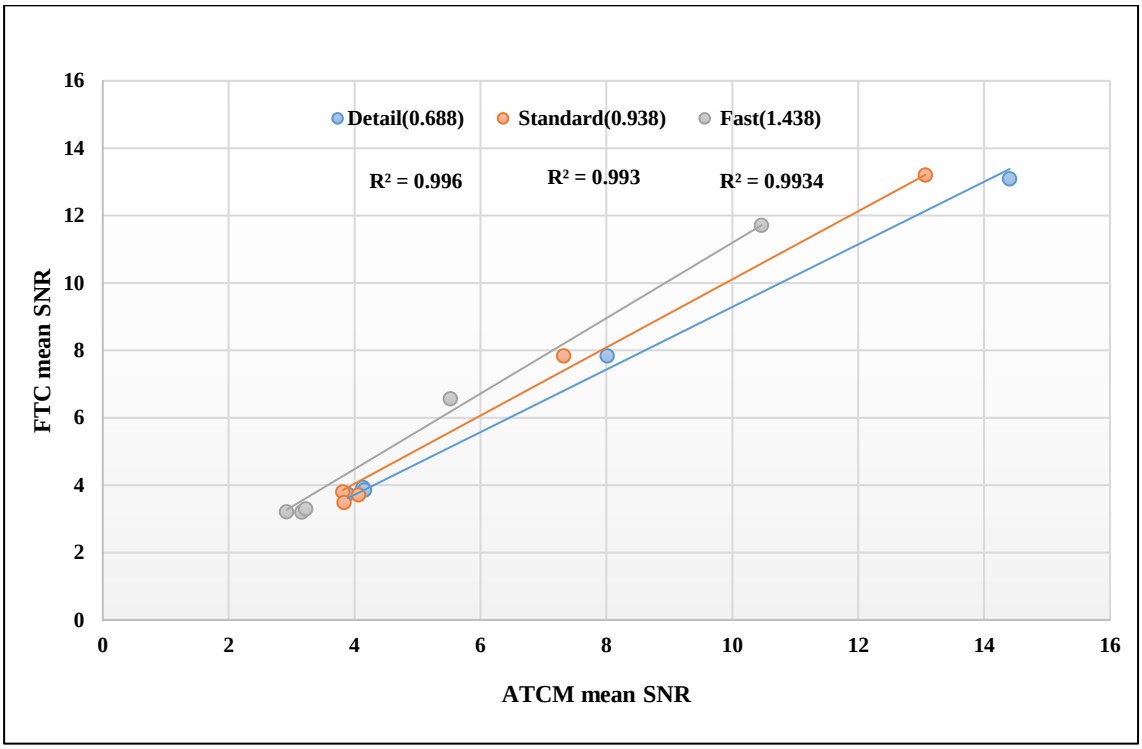

Figure 6- 18: Scatterplot illustrating the correlation in mean SNR values between FTC and ATCM techniques using different pitch factors.

Using the lowest pitch factor detail (0.688), the mean SNR value for FTC was higher than ATCM for all abdominal organs. However, the results were statistically significant for only liver (14.406 ± 3.795 and 13.098 ± 4.757; P=0.017) and right kidney (4.160 ± 0.752 and 3.863 ± 1.299; P= 0.049, FTC and ATCM, respectively; **Table 6-22**). Also, data from the same table demonstrates that the mean SNR value for FTC was slightly lower than ATCM for the liver (13.068 ± 3.696 and 13.211 ± 4.751) and spleen (7.32 ± 1.964 and 7.840 ± 2.655, FTC and ATCM, respectively) when a standard (0.938) pitch factor was used. By contrast, the mean SNR value for FTC was slightly higher than ATCM for left kidney (3.836 ± 0.899 and 3.489 ± 1.094) and right kidney (4.061 ± 0.938 and 3.720 ± 1.262, FTC and ATCM, respectively). However, findings regarding only left kidney (P=0.002) and right kidney (P= 0.013) were statistically significant (P<0.05) when using a standard (0.938) pitch factor.

Table 6- 22:Comparison of mean SNR values for FTC and ATCM techniques when using different pitch factors			
CT Technique	**FTC**	**ATCM**	**P value**
Organ	**SNR Detail (0.688) Mean ± SD n=15**		
Liver	**14.406±3.795**	**13.098±4.757**	**0.017**
Spleen	**8.012±2.090**	**7.844±2.605**	**0.302**
Pancreas	**4.132±1.136**	**3.936±1.314**	**0.101**
Lt. Kidney	**3.890±0.913**	**3.739±1.258**	**0.156**
Rt. Kidney	**4.160±0.752**	**3.863±1.299**	**0.049**
SNR Standard(0.938)			
Liver	**13.068±3.696**	**13.211±4.751**	**0.380**
Spleen	**7.32±1.964**	**7.840±2.655**	**0.077**
Pancreas	**3.813±0.969**	**3.806±1.238**	**0.481**
Lt. Kidney	**3.836±0.899**	**3.489±1.094**	**0.002**
Rt. Kidney	**4.061±0.938**	**3.720±1.262**	**0.013**
SNR Fast(1.438)			
Liver	**10.464±2.581**	**11.719±2.896**	**0.001**
Spleen	**5.522±1.480**	**6.572±1.570**	**<0.001**
Pancreas	**2.921±0.777**	**3.217±0.878**	**0.035**
Lt. Kidney	**3.165±0.818**	**3.209±0.879**	**0.374**
Rt. Kidney	**3.223±0.727**	**3.299±0.924**	**0.231**
FTC mA range (100-400) / ATCM mean mA range (49-440)			

By increasing the pitch factor to 1.438 (fast), the mean SNR for ATCM was slightly higher than FTC for all abdominal organs. However, the results regarding the liver (10.464 ± 2.581 and 11.719 ± 2.896 P=0.001), spleen (5.522 ± 1.480 and 6.572 ± 1.570; P<0.001) and pancreas (2.921 ± 0.777and 3.217 ± 0.878; P=0.035, for FTC and ATCM, respectively), were statistically significant. It is worth noting that the mean SNR values, for both techniques (FTC and ATCM) and for all abdominal organs, decreases when increasing the pitch factor (**Figure 6-19**).

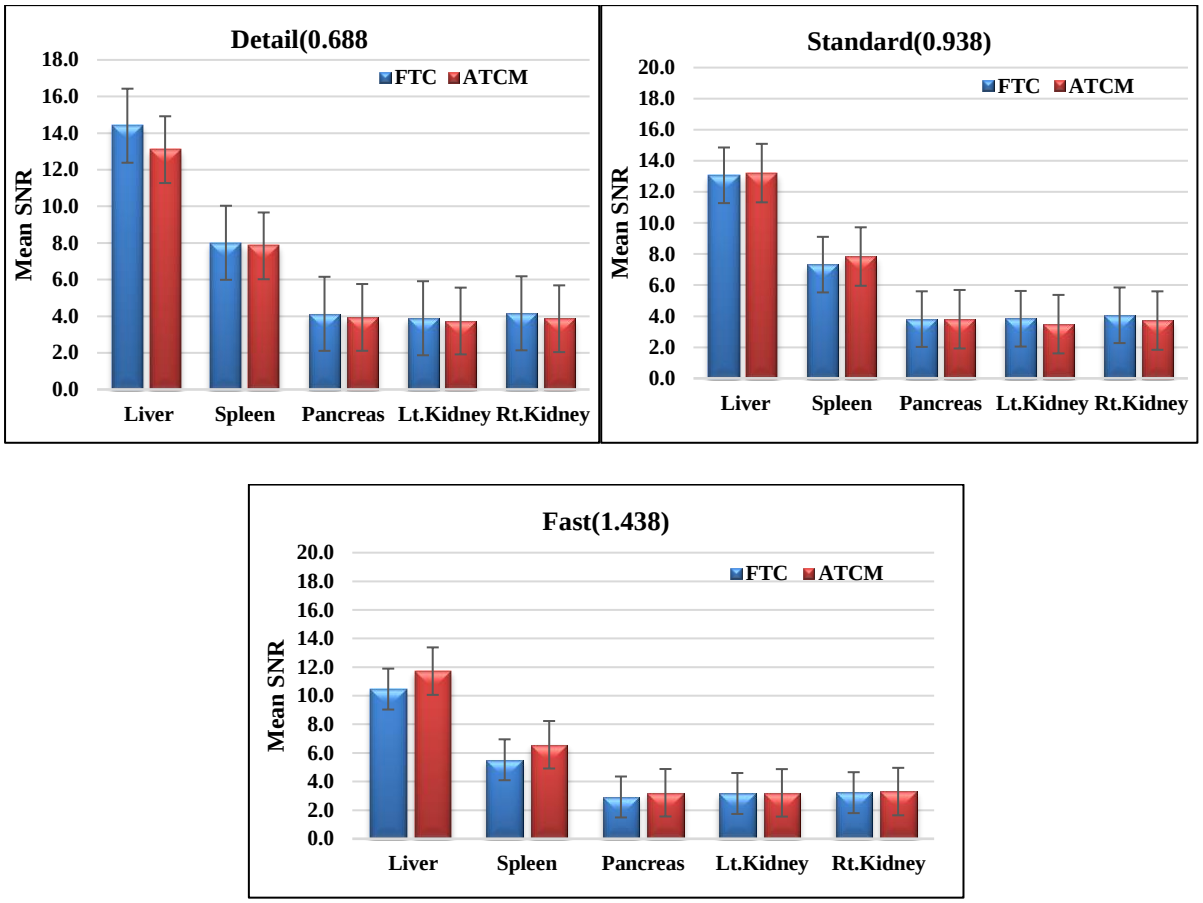

Figure 6- 19: Bar chart illustrating the mean SNR values for abdominal organs, when using FTC and ATCM techniques, for a range of pitch factors.

6.5.3 Comparing SNR values between FTC and ATCM with different detector configurations

Using different detector configurations, the mean SNR values for abdominal organs between FTC and ATCM are associated with strong positive correlations, as depicted in the regression line (R^2> 0.99; **Figure 6-20**).

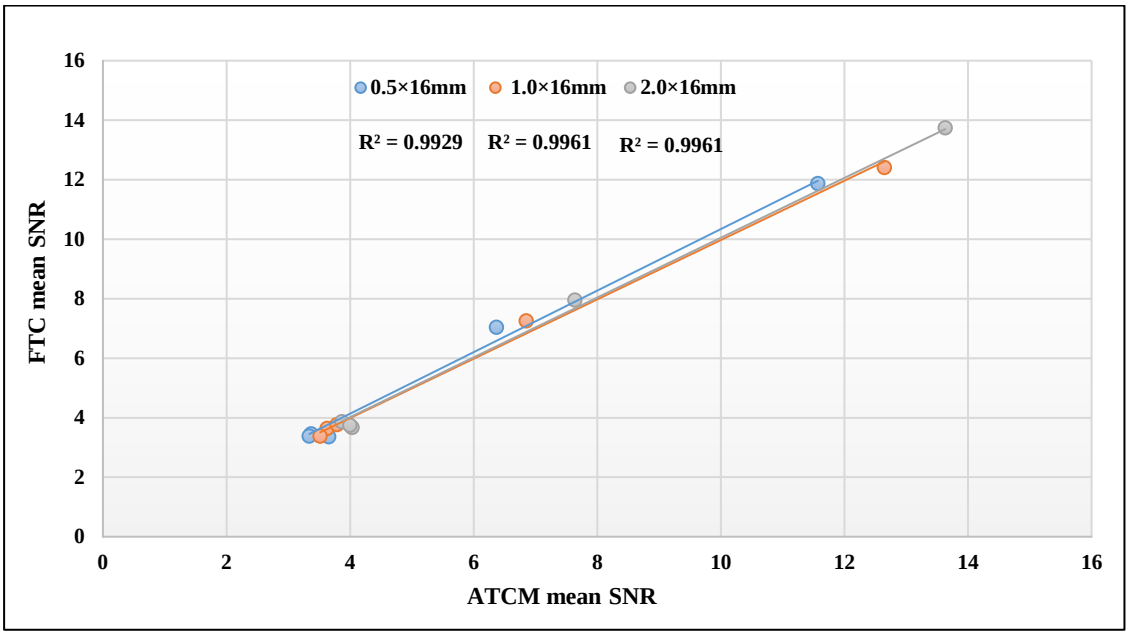

Figure 6- 20: Scatterplot illustrating the degree of correlation between mean SNR values for abdominal organs for FTC and ATCM techniques, using different detector configurations

From **Table 6-23,** when using a 0.5×16 mm detector configuration, the mean SNR value for FTC was slightly lower than ATCM for liver (11.572 ± 2.974 and 11.876 ± 4.022), spleen (6.370 ± 2.103 and 7.042 ± 2.227) and pancreas (3.370 ± 0.981 and 3.458 ± 1.172, FTC and ATCM, respectively). However, it was slightly higher for FTC when compared to ATCM for the right kidney (3.657 ± 0.816 and 3.433 ± 1.027, FTC and ATCM, respectively). For the left kidney (FTC 3.340 ± 0.795 and ATCM 3.380 ± 1.109), the mean SNR value were almost equal. Findings only relating to the spleen were statistically significant (P=0.022).

After changing the detector configuration to 1.0×16 mm, the mean SNR value was marginally higher for FTC than ATCM for the liver (12.646 ± 3.714 and 12.413 ± 4.083) and left kidney (3.516 ± 0.866 and 3.384 ± 1.013, for FTC and ATCM, respectively). It was slightly lower for FTC when compared to ATCM for the spleen (FTC 6.370 ± 2.103 and ATCM 7.042 ± 2.227. For the pancreas (3.627 ± 1.134 and 3.6394 ± 1.149) and right kidney (3.791 ± 0.998 and 3.7652 ± 1.268, for FTC and ATCM, respectively), the mean SNR values for FTC and ATCM were similar and none of these results achieved statistical significance (P>0.05).

Table 6- 23:Comparison of mean SNR values between FTC and ATCM techniques using different detector configurations			
CT Technique	**FTC**	**ATCM**	**P Value**
Organ	**SNR 0.5×16mm Mean ± SD n=15**		
Liver	**11.572±2.974**	**11.876±4.022**	**0.281**
Spleen	**6.370±2.103**	**7.042±2.227**	**0.022**
Pancreas	**3.370±0.981**	**3.458±1.172**	**0.260**
Lt. Kidney	**3.340±0.795**	**3.380±1.109**	**0.377**
Rt. Kidney	**3.657±0.816**	**3.433±1.027**	**0.059**
SNR 1.0×16mm			
Liver	**12.646±3.714**	**12.413±4.083**	**0.260**
Spleen	**6.852±1.818**	**7.256±2.293**	**0.109**
Pancreas	**3.627±1.134**	**3.6394±1.149**	**0.471**
Lt. Kidney	**3.516±0.866**	**3.384±1.013**	**0.118**
Rt. Kidney	**3.791±0.998**	**3.7652±1.268**	**0.436**
SNR 2.0×16mm			
Liver	**13.633±4.345**	**13.739±4.501**	**0.418**
Spleen	**7.636±2.313**	**7.959±2.595**	**0.195**
Pancreas	**3.869±1.138**	**3.862±1.251**	**0.484**
Lt. Kidney	**4.0351±0.999**	**3.673±1.179**	**0.014**
Rt. Kidney	**3.997±0.904**	**3.685±1.243**	**0.031**
FTC mA range (100-400) / ATCM mean mA range (49-440)			

When using a 2.0×16 mm detector configuration, the mean SNR value was slightly lower for FTC when compared to ATCM for the liver (13.633 ± 4.345 and 13.739 ± 4.501) and spleen (7.636 ± 2.313 and 7.959±2.595, FTC and ATCM, respectively). While it was slightly higher for FTC than ATCM for left kidney (4.0351 ± 0.999 and 3.673 ± 1.179) and right kidney (3.997 ± 0.904 and 3.685 ± 1.243, FTC and ATCM, respectively). For pancreas, the mean SNR value was almost equal for both FTC and ATCM. However, the results were statistically significant only for the left (P=0.014) and right kidneys (P=0.031; **Table 6-23**). According to **Figure 6-21**, the bar chart illustrates the mean SNR values for FTC and ATCM techniques using different detector configurations.

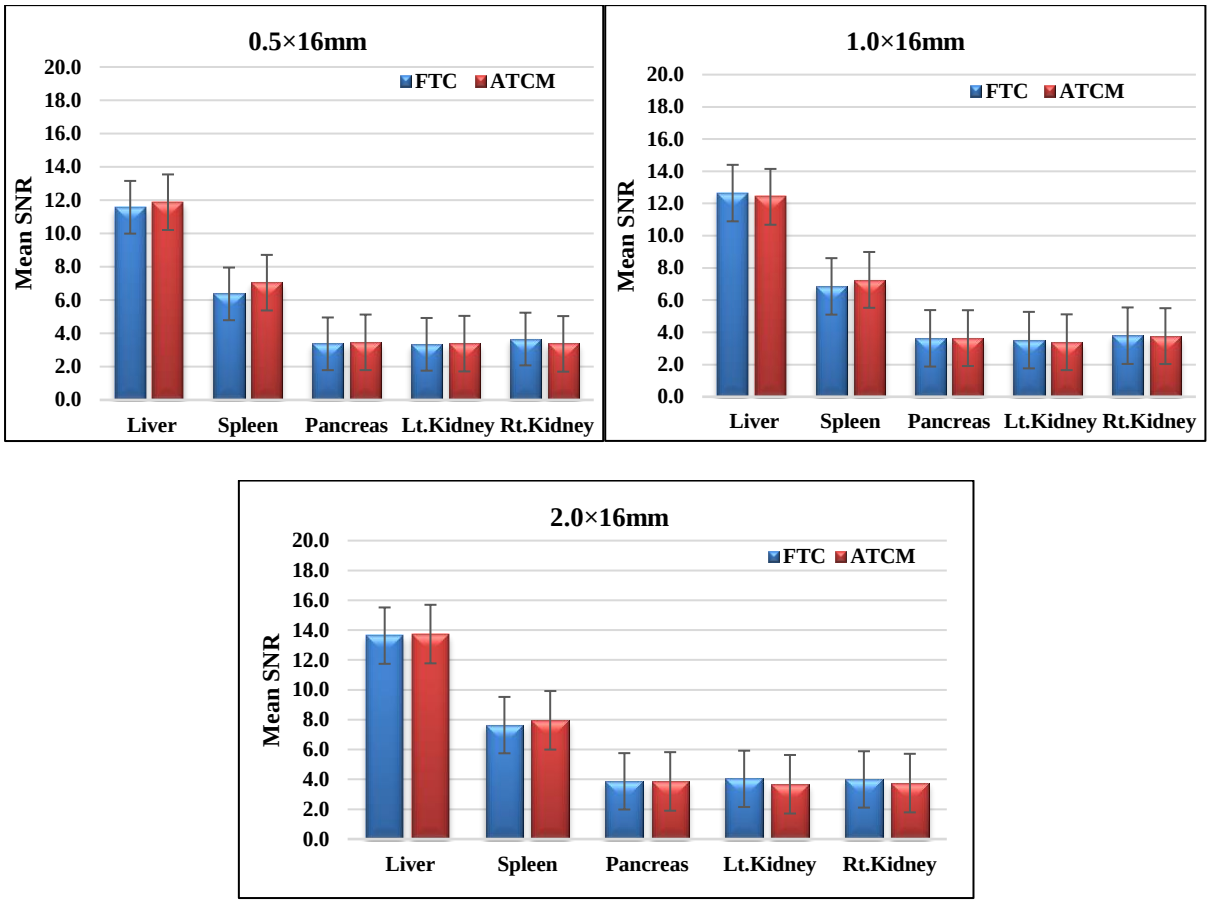

Figure 6- 21: Bar chart illustrating the mean SNR values for FTC and ATCM techniques using different detector configurations.

6.6 A comparison of relative visual grading analysis (VGA) between FTC and ATCM

In this subsection, **Table 6-24** shows the relative VGA scores for the five different axial CT images. The Likert scale response has 3 options: worse, equal, and better. Furthermore, because different visual grading scales are used for each anatomical area they each have differing numbers of criteria and this is reflected into the data illustrated in this subsection. Detailed data are provided in **Appendices XXVI to XXXIII.**

Table 6- 24:Information about the relative VGA criteria number used for each axial CT image along with score ranges*

Axial images slice	Criteria No.	Scale		
		2-Worse	3- Equals	4- Better
		Scores rang		
Image #1	6	12 -17	18-23	24
Image #2	9	18 -26	27-35	36
Image #3	11	22 -32	33-43	44
Image #4	11	22 -32	33-43	44
Image #5	6	12 -17	18-23	24
*Relative VGA criteria number used both FTC and ATCM				

6.6.1 Comparing relative VGA between FTC and ATCM with different tube currents

The mean relative VGA scores for FTC were slightly higher than ATCM for all slices when the 100mA/low dose + tube current was employed: image # 1 (12.2±0.441 and 12.0±0.0), image # 2 (18.6 ± 2.0 and 18.0 ± 0.0), image # 3(22.4 ± 1.3 and 22.0± 0.0), image # 4 (22.1 ± 0.3and 22.0± 0.0) and image # 5 (12.2 ± 0.6 and 12.0 ± 0.0, FTC and ATCM, respectively). However, these differences were not statistically significant (P>0.05). Using a higher tube current (200mA/low dose), the mean relative VGA scores for FTC were higher than ATCM for all abdominal slices except image #5 (13.7±1.1 and 13.888±1.8, FTC and ATCM, respectively), wherein it was slightly lower for FTC. Again, all these findings were not statistically significant (P>0.05; **Table 6-25**).

After increasing the tube current to 250mA/standard, the mean relative VGA scores for FTC became lower than ATCM for all abdominal axial images slice except image # 4 (35.2± 4.0 and 33.5 ± 2.1, FTC and ATCM, respectively). Where it was higher for FTC than ATCM, the results were only just statistically significant for image # 3 (34.3 ± 5.9and 36.7± 3.3, FTC and ATCM, respectively; P=0.049).

Table 6- 25:Comparison of mean relative VGA scores, between FTC and ATCM techniques, with different tube currents

CT Technique	FTC	ATCM	P Value
Axial images slice	**100mA/low dose + mA (Mean ± SD) n=9**		
Image #1	**12.222±0.441**	**12.000±0.000**	**0.157**
Image #2	**18.666±2.000**	**18.000±0.000**	**0.317**
Image #3	**22.444±1.333**	**22.000±0.000**	**0.317**
Image #4	**22.111±0.333**	**22.000±0.000**	**0.317**
Image #5	**12.222±0.667**	**12.000±0.000**	**0.317**
200mA/low dose			
Image #1	**15.111±1.536**	**13.333±1.936**	**0.050**
Image #2	**22.666±3.391**	**20.666±2.345**	**0.063**
Image #3	**26.444±3.678**	**24.111±2.571**	**0.074**
Image #4	**23.66±1.118**	**22.444±1.013**	**0.058**
Image #5	**13.770±1.092**	**13.888±1.793**	**0.785**
250mA/standard			
Image #1	**18.888±2.891**	**19.222±1.936**	**0.564**
Image #2	**28.666±3.968**	**30.222±2.818**	**0.071**
Image #3	**34.333±5.916**	**36.777±3.270**	**0.049**
Image #4	**35.222±4.024**	**33.555±2.127**	**0.233**
Image #5	**20.888±1.269**	**21.000±1.658**	**0.798**
300mA/quality			
Image #1	**21.333±1.936**	**22.444±2.351**	**0.040**
Image #2	**31.000±2.828**	**33.000±3.605**	**0.028**
Image #3	**37.777±5.068**	**40.333±3.840**	**0.067**
Image #4	**38.000±4.500**	**38.666±3.841**	**0.395**
Image #5	**22.111±1.833**	**23.222±1.201**	**0.066**
400mA/ high quality			
Image #1	**22.111±2.147**	**22.333±2.549**	**0.752**
Image #2	**33.111±3.407**	**33.666±2.598**	**0.750**
Image #3	**40.555±4.362**	**41.000±4.153**	**0.609**
Image #4	**39.888±5.011**	**42.000±3.162**	**0.043**
Image #5	**23.333±1.118**	**23.222±1.302**	**0.783**
FTC mA range (100-400) / ATCM mean mA range (49-440)			

From above table, the mean relative VGA scores for FTC were lower than ATCM for all CT images when the 300mA/quality tube current was used. The results were statistically significant only for image # 1 (21.3 ± 1.9 and 22.4 ± 2.3; P=0.04) and image # 2 (31.0 ± 2.8 and 33.0 ± 3.6; P=0.028, FTC and ATCM, respectively; **Table 6-25**).

Using the highest tube current (400mA/ high quality), the mean relative VGA scores for FTC were lower than ATCM across all CT slices: image # 5 (23.3 ± 1.1 and 23.2± 1.3, FTC and ATCM, respectively), where it was slightly higher for FTC than ATCM. Yet, only the result regarding image # 4 was statistically significant (FTC 39.8 ± 5.0 and ATCM 42.0 ± 3.1; P=0.043). According to **Figures 6-22**, it can be concluded that the mean relative VGA scores for FTC and ATCM for each CT image increased when increasing the tube currents.

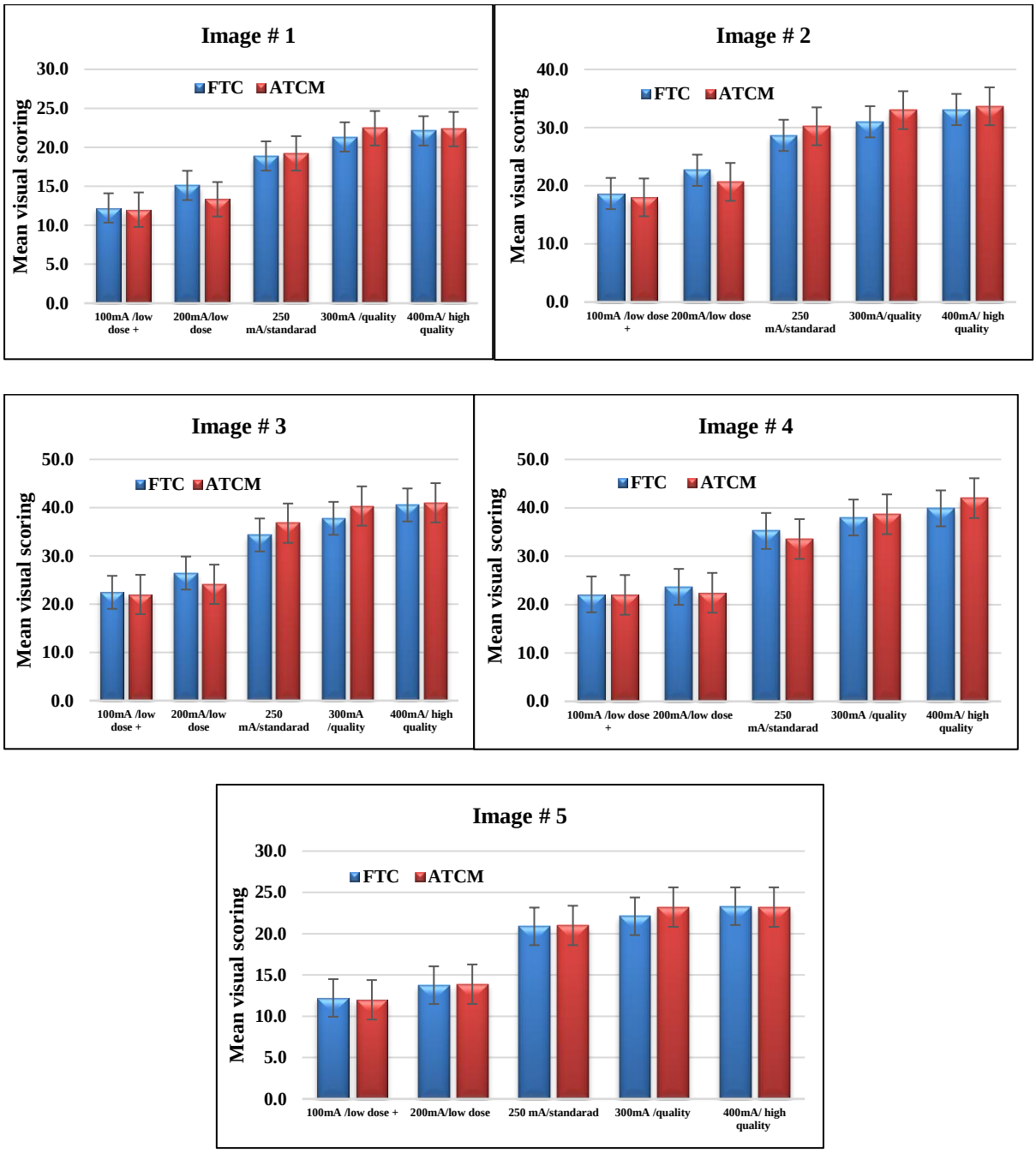

Figure 6- 22: Bar chart illustrating the mean relative VGA scores between FTC and ATCM for different tube currents

6.6.2 Comparing relative VGA between FTC and ATCM, with different pitch factors

When using the detail pitch factor, the mean relative VGA score for FTC was slightly higher than ATCM for all abdominal CT images: image # 1 (19.0 ± 4.456 and 18.9 ± 5.1), image # 2 (29.3 ± 6.1and 28.6 ±7.6), image # 3 (35.6±8.5 and 34.4 ±9.9), image # 4 (34.0 ± 9.4 and 32.6 ± 9.6) and image # 5 (19.1 ± 5.1 and 19.0 ± 5.4, FTC and ATCM, respectively). All differences between FTC and ATCM were not statistically significant (P>0.05; **Table 6-26**).

Table 6- 26:Provides a comparison of mean relative VGA scores between FTC and ATCM with different abdominal axial images slice using pitch factors

CT Technique	FTC	ATCM	P value
Axial images slice	**Detail(0.688) Mean ± SD n=15**		
Image #1	**19.000±4.456**	**18.933±5.188**	**1.000**
Image #2	**29.333±6.121**	**28.666±7.584**	**0.359**
Image #3	**35.600±8.483**	**34.400±9.883**	**0.090**
Image #4	**34.000±9.44**	**32.666±9.581**	**0.096**
Image #5	**19.133±5.054**	**19.000±5.358**	**0.581**
Standard(0.938)			
Image #1	**18.666±4.287**	**18.400±5.603**	**0.788**
Image #2	**27.400±6.467**	**27.733±7.591**	**0.592**
Image #3	**33.600±8.104**	**33.600±9.061**	**0.837**
Image #4	**32.600±8.724**	**32.666±9.461**	**0.949**
Image #5	**18.800±5.045**	**19.000±4.956**	**0.670**
Fast(1.438)			
Image #1	**16.133±3.583**	**16.266±3.731**	**0.719**
Image #2	**23.733±4.620**	**24.933±5.650**	**0.022**
Image #3	**27.733±5.573**	**30.533±7.268**	**0.006**
Image #4	**28.733±5.650**	**29.866±6.895**	**0.180**
Image #5	**17.466±4.307**	**18.000±4.956**	**0.251**
FTC mA range (100-400) / ATCM mean mA range (49-440)			

After increasing the pitch factor to 0.938 (standard), the mean relative VGA scores for FTC were slightly higher than the ATCM for image # 1(18.6 ± 4.2 and 18.4 ± 5.6, FTC and ATCM, respectively). It was lower for FTC than ATCM for image # 2 (27.400 ± 6.467 and 27.7 ± 7.5) and image # 5 (118.8 ± 5.0 and 19.0 ± 4.9) for FTC and ATCM, respectively. The same is true of image # 3 (33.6±8.1 and 33.6±9.1) and image #4 (32.600 ± 8.724 and 32.666 ± 9.461, FTC and ATCM, respectively).

Overall, the mean relative VGA scores for FTC and ATCM were equal and none of the findings were statistically significant (P>0.05). As illustrated in **Table 6-26**, by increasing the pitch fast to 1.438 (fast), the mean relative VGA score for FTC was slightly lower than ATCM for all acquired images. Results regarding only image # 2 (23.7 ± 4.6 and 24.9 ± 5.650) and image # 3 (27.7± 5.573 and 30.5± 7.2, FTC and ATCM, respectively) were statistically significant

(P<0.05). **Figures 6-23** show that the relative VGA scores for FTC and ATCM decreases when increasing the pitch factor.

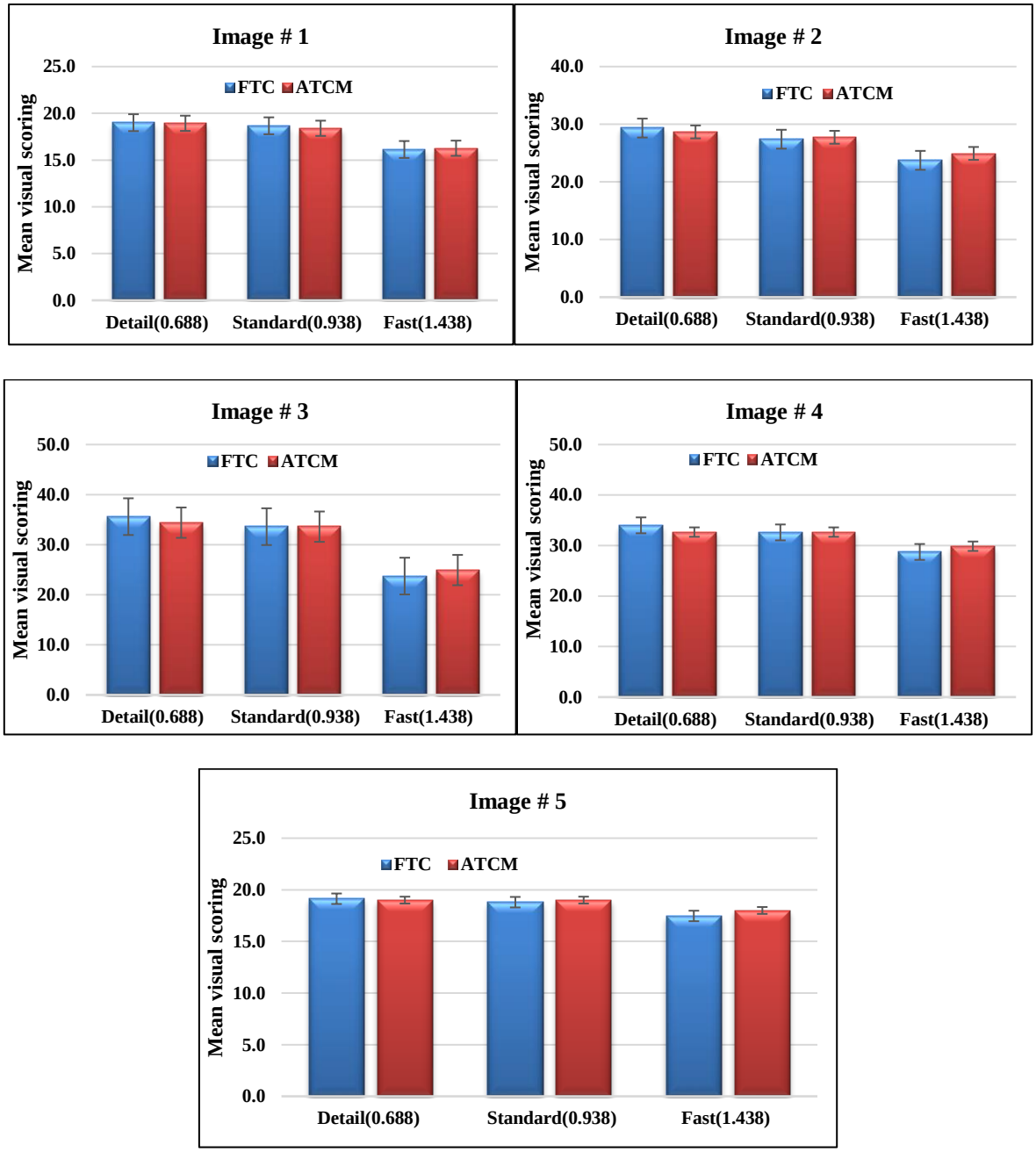

Figure 6- 23: Bar chart illustrating the mean relative VGA scores between FTC and ATCM for different pitch factors.

6.6.3 Comparing relative VGA between FTC and ATCM with different detector configurations

When the detector configuration of 0.5×16 mm was used, the mean relative VGA scores for FTC were slightly higher than ATCM for image # 3 (31.6 ± 7.9 and 31.1 ± 8.3, FTC and ATCM, respectively). It was lower for FTC than ATCM for image # 1 (17.1 ± 4.0 and 17.2± 4.9), image # 2 (25.5 ± 6.0 and 26.4 ± 7.1), and image # 4 (30.9 ± 7.7 and 31.3 ± 8.4, FTC and ATCM, respectively). For image # 5 (18.1 ± 4.9 and 18.0 ± 4.8, FTC and ATCM, respectively), the mean relative VGA scores for FTC and ATCM were almost equivalent. However, none of these findings achieved statistical significance (P>0.05; **Table 6-27**).

Table 6- 27:Comparison of mean relative VGA scores, between FTC and ATCM, with different detectors configurations

CT Technique	FTC	ATCM	P value
Axial images slice	**0.5×16mm Mean ± SD n=15**		
Image #1	**17.133±4.015**	**17.266±4.920**	**0.672**
Image #2	**25.533±6.034**	**26.400±7.109**	**0.395**
Image #3	**31.600±7.908**	**31.133±8.322**	**0.655**
Image #4	**30.866±7.670**	**31.266±8.404**	**0.271**
Image #5	**18.066±4.891**	**18.000±4.825**	**0.861**
1.0×16mm			
Image #1	**18.000±4.472**	**18.000±5.250**	**1.000**
Image #2	**27.000±6.253**	**27.133±7.019**	**0.605**
Image #3	**31.600±7.826**	**32.733±9.223**	**0.167**
Image #4	**31.933±8.688**	**31.466±8.688**	**0.672**
Image #5	**18.533±4.718**	**18.733±5.318**	**0.887**
2.0×16mm			
Image #1	**18.666±4.353**	**18.333±4.908**	**0.650**
Image #2	**27.933±6.397**	**27.800±7.367**	**0.789**
Image #3	**33.733±8.803**	**34.666±8.973**	**0.513**
Image #4	**32.466±8.871**	**32.466±9.417**	**0.634**
Image #5	**18.800±4.974**	**19.266±5.119**	**0.384**
FTC mA range (100-400) / ATCM mean mA range (49-440)			

Using a higher detector configuration (1.0×16 mm), the mean relative VGA scores for FTC were slightly higher than ATCM for image # 4 (31.9 ± 8.7 and 31.5 ± 8.7, FTC and ATCM respectively). It was lower for FTC than ATCM for image # 2 (27.0 ± 6.2 and 27.1 ± 7.0), image # 3 (31.6 ± 7.8and 32.7± 9.2) and image # 5 (18.5 ± 4.7 and 18.7 ± 5.3, FTC and ATCM, respectively). For image # 1 (18.0 ± 4.4 and 18.0 ± 5.2, FTC and ATCM, respectively), the mean relative VGA scores for FTC and ATCM were equal. All findings were not statistically significant (P>0.05)

When the detector configuration was increased to 2.0×16 mm, the mean relative VGA score for FTC was slightly higher than ATCM for image # 1 (18.7 ± 4.4 and 18.3 ± 4.9) and image # 2 (27.9 ± 6.3 and 27.8 ± 7.4, FTC and ATCM, respectively). The mean relative VGA score for FTC was slightly lower than ATCM for image # 3 (33.7 ± 8.8 and 34.6 ± 8.9) and image # 5 (18.8± 4.9 and 19.3 ± 5.1, FTC and ATCM, respectively). With regard to image # 4 (32.5 ± 8.9 and 32.5 ± 9.4, FTC and ATCM, respectively), the mean relative VGA score for FTC and ATCM was equivalent. However, these results were statistically insignificant (P>0.05). According to **Figures 6-24**, it can be concluded that when the detector configuration increases, the mean relative VGA score for FTC and ATCM, for each anatomical area, increases.

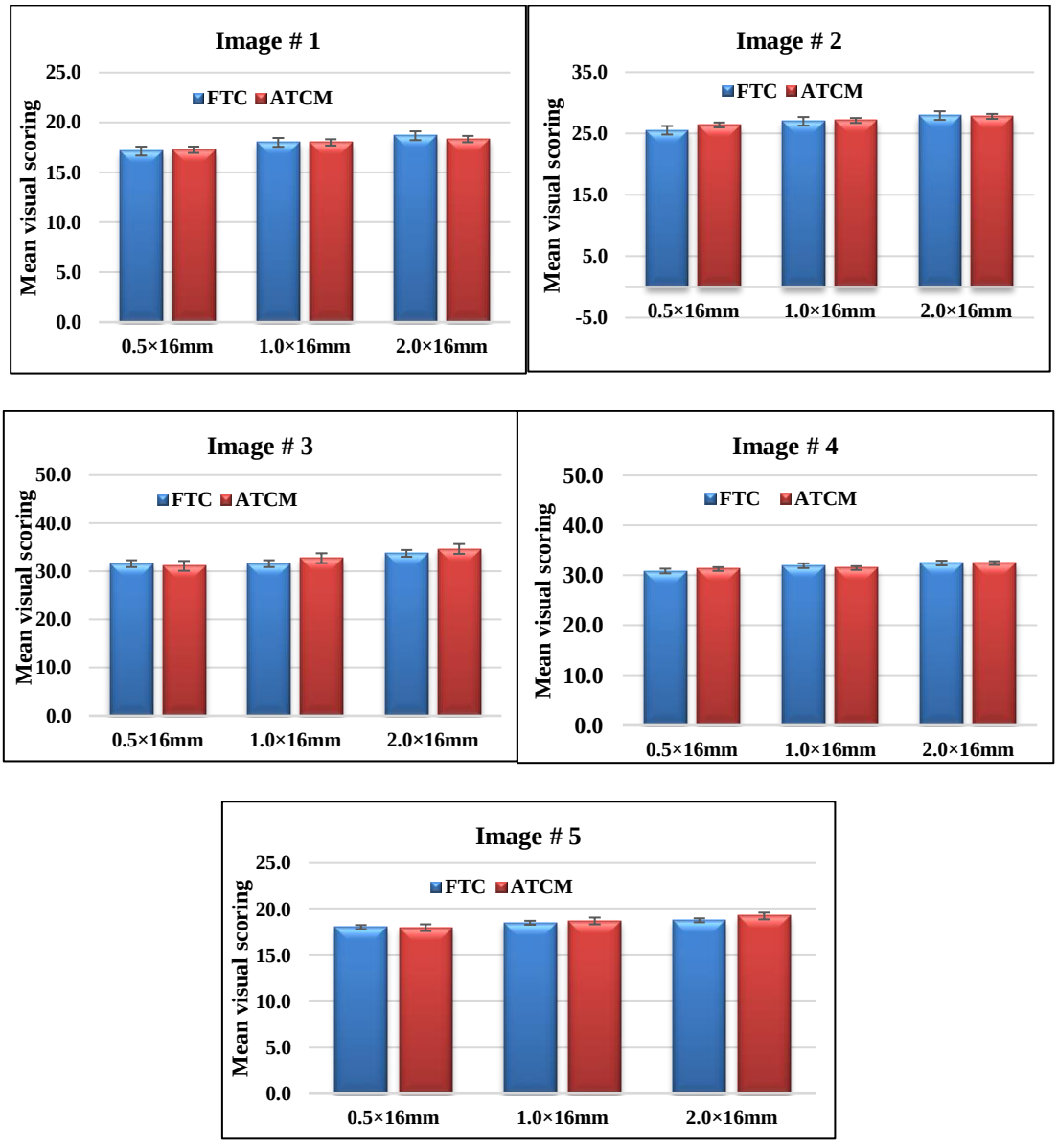

Figure 6- 24: Bar chart illustrating the mean relative VGA scores between FTC and ATCM for different detector configurations

6.7 Chapter Summary

Overall, the results for the radiation and image quality comparison are summarised below. **Table 7-28** and **Table 7-29** provide a summary of the radiation dose and image quality comparisons between FTC and ATCM techniques with different dosimetry methods and acquisition parameters. A full discussion of the data presented in the results chapter will follow in the Discussion Chapter.

Table 6- 28:Summary - Comparison radiation dose between FTC and ATCM (corrected and uncorrected), with different dosimetry methods and acquisition parameters

Radiation dose	Dosimetry method	Abdominal CT scan acquisition parameters*
		Tube currents
Abdominal organs dose (mGy)	MOSFET	300mA/quality FTC ↓ ATCM-corrected 13%
Effective dose(mSv)	MOSFET	300mA/quality FTC ↓ ATCM-corrected 7%
	DLP	300mA/quality FTC ↓ ATCM-corrected 8%
	ImPACT	300mA/quality FTC ↓ ATCM-corrected 4%
Effective Risk (case /10^6)	MOSFET	300mA/quality FTC ↓ ATCM-corrected 8%
		Pitch factors
Abdominal organs dose (mGy)	MOSFET	Fast (1.438) FTC ↓ ATCM-corrected 13%
Effective dose(mSv)	MOSFET	Fast (1.438) FTC ↓ ATCM-corrected 12%
	DLP	Fast (1.438) FTC ↓ ATCM-corrected 13%
	ImPACT	Detail (0.688) FTC ↑ ATCM-corrected 6% Standard (0.938) FTC ↑ ATCM-corrected 6% Fast (1.438) FTC ↓ ATCM-corrected 13%
Effective Risk (case /10^6)	MOSFET	Fast (1.438) FTC ↓ ATCM-corrected 13%
		Detector configurations
Abdominal organs dose (mGy)	MOSFET	0.5×16mm FTC ↓ ATCM-corrected 13%
Effective dose (mSv)	MOSFET	NO different between FTC and ATCM corrected
	DLP	NO different between FTC and ATCM corrected
	ImPACT	NO different between FTC and ATCM corrected
Effective Risk (case /10^6)	MOSFET	0.5×16mm FTC ↓ ATCM-corrected 6%
*Radiation dose for uncorrected ATCM with all different parameters ↑ FTC 13%-23%		

Table 6- 29:Summary - Comparison of image quality between FTC and ATCM, with different image quality methods and acquisition parameters

Image quality evaluation	method	Abdominal CT scan acquisition parameters*
		Tube current
Physical	SNR	100mA/low dose + and 200 mA/ low dose FTC ↑ ATCM (pancreas and kidney)14%-26%
		300mA/quality FTC ↓ ATCM (liver and spleen) 9%-13%
Visual	Relative VGA	300mA/quality FTC ↓ ATCM (image # 1 and image # 2) 5%-6%
		Pitch factors
Physical	SNR	Detail (0.688) and Standard (0.938) FTC ↑ ATCM (Liver and kidney) 7%- 9% fast (1.438) FTC ↓ ATCM(liver , spleen and pancreas)6%-11%
Visual	Relative VGA	fast pitch factor (1.438) FTC ↓ ATCM(image # 2 and image # 3) 5%-9%
		Detector configurations
Physical	SNR	0.5×16 mm FTC ↓ ATCM (Spleen) 4% 2.0×16 mm FTC ↑ ATCM (both kidneys) 9%
*Image quality (Relative VGA with detector configurations no different between FTC and ATCM		

Chapter Seven: Discussion and conclusion

7.1 Chapter Overview

The objective of an abdominal CT scan is to detect and diagnose diseases whilst minimising the radiation dose to the patient. Within medical imaging the radiation dose from abdominal CT scans is relatively high and concern exists regarding its widespread use; see **Chapter 1 Section 1.2**. Over the past decade many technological developments have been implemented by CT vendors to reduce the radiation dose. Following the introduction of ATCM there has been great debate and mixed opinion regarding the radiation dose and image quality differences between automatic and fixed tube current CT techniques. To allow comparison between the radiation dose and image quality associated with abdominal CT examinations, many researchers have focused on estimating effective dose. For image quality, researchers have focused on evaluating image quality using an absolute VGA method. However, the majority of researchers have failed to sufficiently evaluate ATCM techniques by comparing the effective radiation risks and physical image quality (e.g. SNR) for abdominal CT examinations.

This PhD thesis comprises of two major themes. The first theme, the *novel* comparison of radiation dose between FTC and ATCM techniques, uses three different dosimetry methods (MOSFET, DLP and ImPACT). Within this evaluation, radiation dose data has been reported as 'corrected' and 'uncorrected'. Uncorrected ATCM data has been included to enable clinically relevant comparisons between FTC, whilst the corrected ATCM data has been included to enable a theoretical mathematical method for a fairer comparison of radiation dose and risk data by normalising the tube currents between these modes as described in the methods **(Chapter 5, Section 5.4.1)**. A further novel angle of this work was the reporting of effective risk (ER) by calculating the lifetime risk from abdominal CT scan protocols for different ages and genders. The second theme within this thesis was a systematic comparison of image quality differences, between FTC and ATCM, using physical (SNR) and visual (relative VGA) methods.

Within this chapter, the results, which were reported in **Chapter 6**, will be discussed within six major sections. The first three sections will discuss the dosimetry data including abdominal organ dose, effective dose and effective risk. The fourth section considers SNR and the differences between techniques for the five specific abdominal organs. The next section considers the relative VGA results, and finally the general conclusions of this thesis including the novelty, limitations and future work will be summarised.

7.2 Organ dose for abdominal CT scans

Only a few studies have provided information on organ and tissue absorbed doses for CT examinations (Angel et al., 2009, Aoyama, Koyama, & Kawaura, 2002, Ay et al., 2004, Brenner & Hall, 2007& Kawaguchi et al., 2014). Undertaking these types of studies is complex and the resources and time for carrying out such studies are often lacking. Furthermore, it is worth noting that usually it is difficult to make direct comparisons between studies owing to the differences in data collection methods; in turn, this has a considerable effect on radiation dose estimations. Examples of methodological differences include how the dosimetry was conducted (i.e. experimental or computational), the representative ages, the type of phantom utilised, the CT scanner model and the CT examination parameters (e.g. kVp, mA, and pitch and detectors configuration).

Unlike many of the publications highlighted in the literature chapters, a major advantage of this thesis is that it used one of the most accurate methods for comparing organ dose (direct dose measurements using MOSFET). The advantages of MOSFET have been described in **Chapter 3, Section 3.3.1.3**. In addition, the MOSFET dosimeter is a more suitable choice for routine dose verification during CT scans. This is because the MOSFET method is suitable for measuring high radiation doses from CT scan examinations using CRIS adult ATOM dosimetry phantom with different organs depths for each phantom slice, as described by Sharma et al. (2012); and Kumar et al. (2015). Two researcher groups, Padole et al. (2016) and Sabarudin et al. (2014), have compared abdominal/pelvic organ dose between FTC and uncorrected ATCM. In both instances, their approaches were different to the methods used within this thesis. Nine abdominal organs (liver, gallbladder, pancreas, spleen, stomach, kidneys, adrenals, small intestine and colon) were investigated because they are the most radiosensitive abdominal organs according to the ICRP 103 (2007) report and are within the primary scan volume during abdominal CT.

7.2.1 Abdominal organ dose – comparison of FTC and corrected ATCM data

Theoretically, the correlations between FTC and corrected ATCM show a strong positive correlation between all mean abdominal organ doses and the different acquisition parameters (tube currents, pitch factors and detector confirmations) - **see Chapter 6 Figure 6-1, Figure 6-3 and Figure 6-5**. In addition, the highest mean abdominal organ doses for FTC and corrected ATCM were received by the gallbladder and stomach tissues and the lowest were by the small intestine and colon. Variations in the mean abdominal organ dose for both techniques were between 25%-70%. This could be attributed to the anatomical location difference of the abdominal organs, organ depth, shape and diameter in the CRIS ATOM dosimetry phantom. For example, the gallbladder, liver and adrenal glands, are closer to the primary radiation beam than the other abdominal organs. The colon, on the other hand, is further away because of its more dispersed location, in the upper and lower abdominal areas (Brady et al., 2012; Sabarudin et al., 2013). In addition, the mean abdominal organ dose calculated for each organ was based on different numbers of MOSFET dosimeters, therefore, it is expected that there will be some variation in the calculated organ dose- **see Chapter 5 Table 5-6**.

7.2.1.1 Tube current

Tube current was directly proportional to the mean abdominal organ dose- **Figure 6-2 (Chapter 6).** The mean abdominal organ dose for both corrected ATCM and FTC can therefore be minimised by manipulating the tube current. This finding is consistent with previous work which reported a directly (linear) proportional relationship (Scindera et al 2007, Raman, Mahesh, Blasko, & Fishman, 2013 and Aoyama, Koyama, & Kawaura, 2002) between tube current and dose. The mean abdominal organ doses from **Chapter 6, Table 6-1** for 100mA/low dose +, 200 mA/low dose, 250 mA/standard and 400mA/high quality protocols were not significantly different ($P>0.05$) between FTC and corrected ATCM techniques. This is because the average tube current for corrected ATCM was similar to the tube current for the FTC technique; **see Chapter 5, Table 5-5**.

When the tube current was increased to 250mA/standard, the mean abdominal organ dose for corrected ATCM was higher than FTC for all abdominal organs, this difference was however not statistically significant (P>0.05). Differences were statistically significant for the gallbladder, liver and adrenal glands (P<0.05). For a tube current of 300mA/quality, the mean abdominal organ dose for the corrected ATCM was significantly higher (around 13%, P<0.05) than FTC for all abdominal organs; **Chapter 6, Table 6-1**. These differences could be due to the Toshiba SureExposure 3D ATCM technique, which resulted in an increase in tube current for each respective slice when compared to the FTC technique. This is because the abdominal region contains different organs with different densities and atomic numbers, which can result in a geometric dose increase in tube current adapted to the abdominal organs at low noise (e.g. liver) and a decrease for high noise abdominal organs (e.g. kidneys) (Lim et al., 2014). In addition, the radiation dose distribution for the corrected ATCM technique is variable for each slice with the CRIS adult ATOM dosimetry phantom, based on the depth and locations for abdominal organs in phantom (Brady et al., 2012; Sabarudin et al., 2013). By contrast, for the FTC technique the tube current (300mA) was constant along the entire abdominal scan range.

7.2.1.2 Pitch factors

For the detail pitch factor (0.688) and standard pitch factor (0.938), there were no significant differences in the mean abdominal organ doses (P>0.05) between techniques **(Chapter 6, Table 6-3)**. The mean abdominal organ dose for all nine abdominal organs with corrected ATCM (detail pitch factor (0.688)) was 19.2 ± 5.5 mGy and for a standard pitch factor (0.938) was 15.2 ± 4.1 mGy. These were similar to the mean abdominal organ dose for FTC (detail pitch factor (0.688), 19.3 ± 5.7 mGy) and standard pitch factor (0.938) was 14.8 ± 4.1 mGy. Generally, with lower pitch values (<1), differences in abdominal organs dose were not significant, whether using FTC or corrected ATCM. The cause of these similarities between detail and standard pitch factors should be the subject of further investigation.

In contrast, when using a fast (1.438) pitch factor, there were significantly higher mean abdominal organ doses for the corrected ATCM technique than FTC, for all abdominal organs (P<0.05**; Chapter 6, Table 6-3)**. The mean abdominal organ dose for corrected ATCM was about 13% higher when compared to FTC. Differences in the mean abdominal organ dose for corrected ATCM and FTC, with a fast (1.438) pitch factor, can be attributed to the higher mean dose (for all nine organs) with corrected ATCM (12.4 ± 2.9 mGy) when compared to FTC (10.5 ± 2.5 mGy). At this pitch setting, with the ATCM method, the scanner will simply increase the tube current to keep the radiation dose and noise constant. By contrast, with the FTC, changing

the pitch will have no effect on the radiation dose (Ranallo & Szczykutowicz, 2015; Hsieh, 2009). In addition, it could be attributed to other factors (depth and locations abdominal organs phantom) as discussed earlier in this **section on page 206.** Generally, with the fast pitch values >1, there was a reduction in all abdominal organ doses using FTC.

When using a small pitch factor 'detail' (0.688), with FTC and corrected ATCM, this resulted in an increased mean abdominal organ dose due to the increased overlap in anatomy; **Figure 6-4 Chapter 6**. However, for FTC and corrected ATCM, using the fast pitch factor (1.438) results in scanning gaps in the anatomy with a reduction in scan time and hence an overall lower radiation dose. As a result, if all other parameters remain unchanged, increasing the pitch factor reduces the organ dose in a linear fashion for both FTC and corrected ATCM techniques (Raman et al. (2015); Goldman (2008).

7.2.1.3 Detector configurations

The mean organ doses for FTC and corrected ATCM are inversely proportional to detector configurations. With a smaller detector area (0.5×16 mm), using FTC and corrected ATCM, the organ dose increases with a narrow X-ray beam and few active detector elements. However, organ dose decreases with a large 2.0×16mm or wider detector configuration (Dobeli et al., 2014; Nagel 2007; Cody & Mahesh, 2007)- **Figure 6-6, Chapter 6**. With a detector configuration of 0.5×16 mm, the mean abdominal organ dose for the corrected ATCM was higher than FTC for all abdominal organs. These findings were statistically significant for all abdominal organs ($P<0.05$), except the gallbladder and colon. In contrast, the mean abdominal organ dose, when the detector configuration was changed to 1.0×16mm and 2.0×16mm, were not significant ($P>0.05$) between corrected ATCM and FTC for all abdominal organs. This could be attributed to the slightly similar mean tube current with both techniques for these configurations.

The differences in the mean abdominal organ dose for the 0.5×16 mm detector configuration could be attributed to the numbers of photons received by detectors. The detector configuration size is inversely proportional to image noise. When using a corrected ATCM technique for small detectors, the tube current automatically increases to keep the dose and noise constant during each slice (Solomon et al., 2013). By contrast, with the FTC, changing the detector configuration will have no effect on the radiation dose, except for a reduced organ dose for detector configurations (0.5×16 mm).

7.2.2 Abdominal organ dose – comparison of FTC and uncorrected ATCM data

For the clinically relevant results, the mean abdominal organ dose with uncorrected ATCM was higher than FTC for all abdominal organs and all acquisition parameters ($P<0.05$). The mean abdominal organ dose reduced, for the FTC technique, by approximately 21% for tube current variations, 17% with different pitch factors and 23% with the different detector configurations when compared to uncorrected ATCM; **Chapter 6, Table 6-2, Table 6-4 and Table 6-6**. The main reason for these differences was that the data presented compares the abdominal organ dose associated with FTC across a tube current range of 100-400mA compared to the uncorrected ATCM data with a tube current range of 49-440mA.

Other factors affecting the abdominal organ dose, which could result in significant differences between FTC and ATCM (corrected and uncorrected), include: scan length, CRIS adult ATOM dosimetry phantom position, and size and organ depth. Furthermore, the locations and depth of the organs and the numbers of MOSFETs can result in differences in absorbed doses by the adrenals, pancreas and kidneys. This is because these structures are usually more deeply positioned when compared with other abdominal organs (Brady et al., 2012; Kalra et al., 2015). The ATCM increases the mA in areas of the body with the greatest attenuation and decreases the mA in other areas with lower attenuation. Other studies have also shown that doses received by organs were different between techniques depending on the anatomical locations, depth and distance from the primary beam radiation (Sabarudin at al., 2013; Brady et al., 2012).

When compared to previous studies, a literature review shows that no study has so far compared the difference in abdominal organ dose between FTC and corrected ATCM using MOSFET dosimeters. This thesis is likely to be the first study to have carried out such a comparison. However, two studies- Padole et al. (2016) and Sabarudin et al., (2014)- have compared abdomen-pelvic organ dose differences between FTC and uncorrected ATCM data. Recently, Padole et al. (2015) undertook a comparison between FTC and uncorrected ATCM using a human cadaver. The abdominal organ doses (liver, stomach, left kidney and colon) were estimated with the Monte Carlo simulation software (radiation dose-tracking (RDT) software) and by direct measurement using an ionising chamber. In their study, they used three different tube currents/times (100, 200 and 300mAs) for FTC and three different average tube currents/times (58-187mAs) for the uncorrected ATCM technique. Their study showed that, for abdominal organs, FTC doses were 28% to 54% higher than uncorrected ATCM. This is not consistent with the findings reported in this thesis, which showed the mean abdominal organ doses ATCM (uncorrected) to be higher than FTC. Padole et al. (2016) used direct dose

measurement, with an ionization chamber, and reported a 17% higher abdominal organ dose for uncorrected ATCM than FTC. These data are consistent with the figures reported in this thesis showing the mean abdominal organ doses (ATCM-uncorrected) to be higher than FTC. The differences between Padole et al. (2016) and the findings of this thesis may be attributed to many factors. The different CT scanner used in work by Padole et al. (2016) was one likely contributory factor. The geometrical limitation of the human body mathematical phantoms using Monte Carlo simulation is another. The results of organ dose overestimation by Monte Carlo compared to the measured dose by MOSFET, due to the geometrical limitation of the mathematical phantom, has previously been reported by Tootell, Szczepura, and Hogg (2014). Also, there are physical differences between the human cadaver and the abdominal CRIS adult ATOM dosimetry phantom used within this thesis.

Work by Sabarudin et al. (2014) compared, using TLDs, FTC and uncorrected ATCM techniques with phantom measurements of organ doses for thoracic and abdomen–pelvic CT scans. The abdominal organ doses measured the liver, stomach, kidneys and colon, with an average tube current /time of 192mAs for uncorrected ATCM and 300mAs for FTC. The mean organ dose was lower with uncorrected ATCM (11.9 ± 0.2 mGy) when compared to FTC (33.2 ± 0.1 mGy) and corresponds to a 63% difference. This is not consistent with the figures reported in this thesis, which demonstrated an uncorrected ATCM dose of 18.2 ± 5.1 mGy, which was 23% higher than FTC (14.0 ± 3.8 mGy); **see Chapter 6, Table 6-2**. The differences between Sabarudin et al. (2014) and those reported in this thesis may be attributed to different acquisition parameters, different ATCM techniques manufacturers and the differences in the number of direct dosimetry measurement locations. For this thesis, 273 locations were sampled using the CRIS adult ATOM phantom and MOSFETs (**See Chapter 5, Table 5-6**), with five different tube currents, compared with 50 TLDs based on a single constant tube current utilised by Sabarudin et al. (2014).

In summary, the abdominal organ dose measurements, using MOSFET, for comparing FTC, corrected-ATCM and uncorrected-ATCM are in itself novel work within this thesis. Therefore, in the theoretical comparison between FTC and corrected ATCM, the mean abdominal organ dose shows no statistically different difference between both techniques. There were some exceptions (300mA/quality tube current, fast (1.438) pitch factors and 0.5×16 mm detector configuration). In contrast, the clinically relevant results from the uncorrected ATCM data were higher for all abdominal organs when compared to FTC techniques. FTC reduced the mean abdominal organ dose when compared with uncorrected ATCM technique.

7.3 Effective dose (ED)

From the literature review, the typical effective dose for abdominal CT scanning varies between 2.4 to 34.6 mSv (Dougeni et al., 2012; Yeh et al., 2016; Wichmann et al., 2015; **See chapter 3 Table 3-10**). These data are largely based on an ED estimation method using DLP. In this thesis, three different methods of measuring ED were utilised: direct measurement with MOSFET, mathematical estimation with DLP and mathematical simulation with ImPACT software. The main reasons for using these three methods are that they represent the main methods for measuring and estimating ED. It is worth noting that this thesis is the first to compare mean ED using the three different dosimetry methods for FTC and ATCM techniques during abdominal CT procedures.

Most published studies compared ED between FTC and uncorrected ATCM using the mathematical DLP or k-factor method (Kim et al., 2013, Sabarudin et al., 2014 Su et al., 2010; Gharbi et al., 2017). Three studies compared abdominal/pelvis dose using DLP and/or CTDI for both FTC and uncorrected ATCM (Sabarudin et al., 2014; Maués et al., 2016; Su et al., 2010). Unlike many of the above publications, a major advantage of this thesis is that it used one of the most accurate novel methods (MOSFET) for comparing ED.

7.3.1 Effective dose comparison for FTC and corrected ATCM data

The highest means ED for FTC and corrected ATCM were estimated using the ImPACT method; while the lowest mean ED was estimated using the MOSFET method for the different acquisition parameters (tube currents, pitch factors and detector confirmations). Variations in the mean ED for both techniques was 37%-80% higher with the ImPACT method than MOSFET method.

This difference could be attributed to ED overestimations by the ImPACT method, owing to the differences in the physical dosimetry phantom modelling and the geometrical limitations of the human body mathematical phantom shapes, locations and size of the abdominal organs. For example, during abdominal CT with a physical dosimetry phantom, the colon is not exposed to primary beam radiation and thus the calculated colon dose would be lower. In contrast, the large shapes of the liver and spleen allow exposure to the scan volume, resulting in an increased ED calculation. In addition, the different tube currents for every slice (using the ATCM technique) results in error in the ED estimation, because the ImPACT software only allows a single tube current value to be used for the estimation of ED (Tootell et al., (2014a). It should be noted that the ImPACT software cannot take into account the overlap between slice sections for physical dosimetry phantom modelling to estimation organ specific doses, and that the ImPACT software used for the preparation of the Monte Carlo data sets was acquired when only old CT technology was available. Therefore, the ImPACT method in the wide scan range might result in the overestimation of ED (Matsunaga et al., 2017; Gu et al., 2012).

The doses reported in this thesis using MOSFET, for both techniques, agree with previous studies, which have used MOSFET and similar underestimations of radiation dose were noted (Sharma et al., 2012; Kumar et al., 2015; Mattison et al., 2016; **See Chapter 3, Table 3-2**). The MOSFET method uses individual organ doses measured by placing the dosimeters in specifically designed locations in the CRIS adult ATOM dosimetry phantom. These phantoms are available for a range of patient types- **see Chapter 5, Section 5.2.3**. They are made up of contiguous slices with different tissues represented by different densities. Each phantom has attenuation properties that are equivalent to real human shapes, locations and sizes of the abdominal organs. Within the slices are locations for placing the dosimeters. On the other hand, the MOSFET effective dose method used the CRIS adult ATOM dosimetry phantom, and estimation took into account the overlap between phantom slice sections for the desired scan range (Matsunaga et al., 2017).

7.3.1.1 Tube current

The mean ED for both corrected ATCM and FTC can be minimised by manipulating tube current, which is directly proportional to the mean ED. Thus, increasing the tube current to 400mA/high quality resulted in a comparable percentage increase in ED when using MOSFET, DLP and ImPACT methods (Tawfik et al., 2011; Kalra et al., 2015) - **Figure 6-8 (Chapter 6)**. However, the mean ED with DLP was lower than reported in some previous studies (Papadimitriou et al., (2003); Heggie, (2005); Origgi et al., (2006); Fujii et a.,l (2007); Tyan et al (2008); Mayer et al., (2014); Sabarudin et al., (2014); Yeh et al., (2016)- **See Chapter 3 Table 3-10**). This may be due to different acquisition parameters, scan range, patient size and CT scanners models that were used in various studies when compared to this thesis.

From the three different dosimetry methods (MOSFET, DLP and ImPACT) comparison between FTC and corrected ATCM technique with 100mA/low dose+, 200mA/low dose, 250mA/standard and 400mA /high quality, the mean ED showed no difference between FTC and corrected ATCM and was not statistically significant across all dosimetry methods ($P>0.05$). This is because the mean tube current for corrected ATCM was similar to the tube current for FTC techniques when using MOSFETs and the ImPACT software methods. However, for the DLP method the mean DLP values for each tube current were similar for the comparison between FTC and corrected-ATCM 100mA/low dose+ (FTC; 187.3 and corrected ATCM; 176.6 mGy×cm^2), 200mA/low dose (FCT; 335.5and corrected ATCM; 329.9 mGy×cm^2), 250mA/standard (FCT; 417.5 and corrected ATCM; 425.3 mGy×cm^2) and 400mA /high quality (FCT; 702.2 and corrected ATCM; 703.970 mGy×cm^2)- **See Chapter 6 Table 6-8**.

However, with 300mA/quality current, the mean ED for the corrected ATCM was significantly higher than FTC using MOSFET, DLP and ImPACT methods ($P<0.05$). The mean ED was 7% higher with the FTC technique (MOSFET method). The difference in ED for MOSFETs and the corrected-ATCM data was 7.2 ± 1.8 mSv and FTC 6.7 ± 1.6 mSv) and can be attributed to the image noise level for the ATCM protocol (quality; SD 3.00). As a result, the mA increases towards the thicker/more dense regions and decreases at less dense/thinner regions (Lee et al., 2010; Martin & Sookpeng, 2016; Soderberg &Gunnarsson, 2010). The mean corrected-ATCM tube current, for thicker anatomical regions, generally varied between 330 and 422mA, while the tube current for FTC was fixed at 300mA along the full scan range.

The mean ED reduced by around 8% with FTC techniques when using the DLP method (FTC 7.5 ± 2.2 mSv and corrected-ATCM 8.2 ± 1.8 mSv) with 300mA/quality. Differences could exist because the DLP value with corrected-ATCM (550.1 mGy×cm^2) was higher than DLP value for FTC (503.4 mGy×cm^2) by around 10%. The DLP value increased with increased tube current, scan range, and scan length for the corrected-ATCM technique and this led to an increased ED (McCollough et al., 2009; Christner et al., 2010; Tootell et al., 2013).

The mean ED for the corrected ATCM increased by around 4% when compared to FTC techniques using the ImPACT method (FTC 9.5 ± 2.8 mSv and corrected ATCM 9.9 ± 2.8 mSv) with 300mA/quality. However, the difference in measured mean ED using the ImPACT method for corrected-ATCM and FTC was a result of differences in mean tube current. For corrected ATCM (quality SD 3.00) the tube current was 422mA, higher than the constant tube current used with FTC (300mA).

7.3.1.2 Pitch factors

The mean ED for both corrected-ATCM and FTC can also be minimised by manipulating the pitch factors and are inversely proportional to the pitch factor. Thus, increasing the pitch factor resulted in a comparable percentage decrease in the mean ED (Goldman 2007; Verdun et al., 2015; Lell et al., 2009; Hetterich et al., 2013) - **Figure 6-10 (Chapter 6).**

When considering the mean ED for comparisons using MOSFET and DLP for detail (0.688) and standard (0.938) pitch factors. The mean EDs were not different between FTC and corrected-ATCM ($P>0.05$). The main reasons for the similarities between techniques was that the mean tube current using FTC was similar to that used for corrected-ATCM scans with detail (0.688) and standard pitch factors (MOSFET method). In addition, the mean ED, using DLP was once again, had similar mean DLP values for FTC (detail pitch factor (0.688) = 556.7 mGy× cm^2 and standard pitch factor (0.938) = 425.9 mGy× cm^2) and corrected-ATCM (detail pitch factor (0.688) =530.97 mGy× cm^2 and standard pitch factor (0.938) = 424.6 mGy × cm^2). However, the lower pitch values < 1 can provide the same mean ED, whether using FTC or corrected ATCM- see **Chapter 6 Table 6-10.**

The mean EDs, using fast (1.438) pitch factors for FTC techniques, were statistically lower than for corrected-ATCM using MOSFET and DLP methods ($P<0.05$). The mean ED reduced by around 12% for FTC using the MOSFET method (FTC 4.2 ± 1.6 mSv and corrected ATCM 4.8 ± 1.4 mSv). However, the different mean ED using the MOSFET method, between FTC and corrected ATCM techniques, could be attributed to the increased mean ED with fast (1.438) pitch factors. This is because the tube current (for ATCM) increases to keep the radiation dose and noise constant. In contrast with the FTC, changing the pitch will have no effect on the radiation dose (Ranallo & Szczykutowicz, 2015; Hsieh, 2009).

The mean ED was around 13% higher than the FTC technique using DLP (FTC; 4.4 ± 1.9 mSv and corrected ATCM; 5.1 ± 1.6 mSv) for fast (1.438) pitch factors. However, the difference in mean ED using DLP method, with a fast (1.438) pitch factor, could be attributed to the DLP values with corrected-ATCM (344.9 mGy× cm^2) being higher than FTC (305.1mGy× cm^2) techniques. This is likely to be the result of an increased DLP values from the increased tube current and scan length with corrected-ATCM in order to keep the image noise constant (Ranallo & Szczykutowicz, 2015; Hsieh, 2009).

The mean ED between FTC and corrected-ATCM with the ImPACT method demonstrated a significant difference between the scanning techniques ($P<0.05$) for all pitch factors, see **Chapter 6 Table 6-10**. However, the mean ED for FTC was higher than the corrected-ATCM dose by around 6% (detail (0.688), FTC 10.8 ± 4.6 mSv and corrected ATCM 10.1 ± 5.1 mSv)) and standard (0.938) (FTC 57.9 ± 3.4 mSv and corrected ATCM 7.7 ± 3.5 mSv). On the other hand, the mean FTC ED was around 13% lower than the corrected-ATCM dose when a fast pitch factor (1.438) (FTC 5.1 ± 2.3 and corrected ATCM 5.8 ± 1.9 mSv) was used.

The difference in mean ED when using the ImPACT method for detail (0.688), standard (0.938) and fast (1.438) pitch factors, for FTC, was higher than for corrected-ATCM scans. This is because the mean tube current for the corrected-ATCM was lower than FTC and this is a key parameter within the software calculations. For fast pitch factors, the mean tube current using ImPACT software, increased for the corrected-ATCM when compared with the FTC scans. This is because the increased tube current with different slices results from different ATCM attenuation by the relevant anatomical structures (Lee et al., 2010; Martin & Sookpeng, 2016). In contrast, the pitch factors will have no effect on the constant tube current used during FTC because this is the same for all slices (Tootell et al., 2014a).

7.3.1.3 Detector configurations

The mean ED for all dosimetry methods (MOSFET, DLP and ImPACT) showed no difference between FTC and corrected-ATCM techniques when using different detector configurations (P>0.05; **Chapter 6 Table 6-12).** When considering the MOSFET and ImPACT results, the similarities may be attributed to the similarity in the tube currents for both FTC and ATCM across all the detector configurations. This needs further investigating to determine the cause. In addition, DLP method mean values for both FTC and corrected ATCM were again similar for all detector configurations 0.5×16 mm (FTC=484.1 mGy× cm^2 and corrected ATCM =460.9 mGy× cm^2), 1.0×16mm (FTC =415.5 mGy× cm^2 and corrected ATCM=412.2 mGy× cm^2) and 2.0×16 mm (FTC= 484.1 mGy× cm^2 and corrected ATCM=460.9 mGy× cm^2).

7.3.2 Effective dose - comparing FTC and uncorrected ATCM data

When considering the clinically relevant results (uncorrected data), the mean ED across all dosimetry methods (MOSFET, DLP and ImPACT) and for all different acquisition parameters were significantly different for FTC and ATCM techniques ($p<0.05$). The mean ED for uncorrected ATCM was higher than for FTC techniques. The mean ED increased for uncorrected ATCM technique when compared to FTC technique (21% MOSFET, 19% DLP and 18% ImPACT), pitch factors (13% MOSFET, 13% DLP and 16% ImPACT) and detectors configurations (22% MOSFET, 22% DLP and 19% ImPACT). The differences between FTC and uncorrected ATCM can be attributed the increase in mean tube current which results from the ATCM (49-440mA) scans. This was higher than for FTC (100-400mA) - **Chapter 6 Table 6-9, Table 6-11** and **Table 6-13**.

When compared to previous studies, no study has compared abdominal CT organ dose differences between FTC and corrected ATCM using three dosimetry methods. All previous published studies have utilised the DLP method for comparing between FTC and uncorrected ATCM abdominal/pelvis CT protocols (Sabarudin, et al., 2014; Maués et al., 2016; Su et al 2010). Sabarudin, et al. (2014) reported that the estimated mean EDs during abdomen/pelvis CT with FTC were 17.30±0.41 mSv and 6.01±0.20 mSv for uncorrected ATCM using the DLP method. This represents a 65% decrease. Another study by Su et al. (2010) reported the estimated mean ED for abdomen contrast-enhanced CT with FTC to be 19.4±2.8mSv and that uncorrected ATCM was 12.4±5.8 mSv, representing a 36% decrease. Furthermore, Maués et al. (2016) estimated mean ED during abdomen/pelvis CT scan with uncorrected ATCM to be 79.5% lower than FTC using DLP method.

In this thesis the mean ED, measured with DLP, was only 19% lower (FTC being 6.47±3.21 mSv and uncorrected ATCM, 7.99±3.27 mSv). The differences between these findings may be due to the different acquisition parameters, contrast enhancement (in some studies) and the different CT scanners utilised in ATCM techniques from each manufacturer. Furthermore, as reported in the literature, clinical conditions cannot be replicated within phantom models, hence contributing to the differences in the results. **Table 7-1** provides a summary of the comparison of FTC and uncorrected ATCM using different effective dose measurement and estimation methods and data from this thesis and the literature.

Table 7- 1: Comparison between abdominal/pelvis CT scan ED from this thesis with different previously published studies for both FTC and uncorrected ATCM

Study	Year	Effective dose measurement and estimation methods	Effective dose (FTC and uncorrected ATCM)
Sabarudin, et al	**2014**	DLP	Uncorrected ATCM 65% lower than FTC
Su et al	**2010**	DLP	Uncorrected ATCM 35.9% lower than FTC
Maués et al	**2016**	DLP	Uncorrected ATCM 79.49% lower than FTC
This thesis	**2018**	MOSFET	FTC 21% lower than uncorrected ATCM
		DLP	FTC 19% lower than uncorrected ATCM
		ImPACT	FTC 18% lower than uncorrected ATCM

In summary, the mean ED measured and compared by three dosimetry methods is in itself novel work within this thesis. Therefore, when theoretically comparing between FTC and corrected ATCM the mean ED there was no statistical difference between both techniques, except for a limited few (300mA/quality tube current, fast (1.438), detail (0.688) and standard (0.938) with different dosimetry methods. In contrast, the clinically relevant results demonstrated that the mean effective dose for uncorrected ATCM was higher than the FTC for all different parameters and dosimetry methods. The FTC technique had a lower mean effective dose for abdominal CT scanning when compared with uncorrected ATCM.

7.4 Effective risk from abdominal CT examinations

As discussed earlier in **Chapter 3, Section 3.4.3**, the effective risk (ER) is not only a function of organ dose but also strongly depends on patient age and gender. Therefore, even if the radiation dose to the abdomen for some individuals was higher due to the greater body size, the average risk in younger people (20, 30, and 40 years of age) will be higher than older people (50, 60, and 70 years of age). The derived number of cancer incidence cases using the BEIR VII report indicates a substantially higher lifetime attributable risk (LAR) of cancer incidence in females compared to males and in younger people than in older people (Brenner & Hall, 2007). Radiation doses varied significantly between the different types of CT studies. Owing to the ease and speed of image acquisition linked to technological developments, proliferation of procedures has occurred and in turn has led to increased doses to patients. Ionizing radiation from CT has thus become a public health concern (Bernier et al., 2012). The estimated number of CT scans that will lead to the development of cancer varies widely depending on the specific type of CT examination and the patient's age and gender.

The lifetime attributable cancer risks, or effective risk, to females and males aged 20, 30, 40, 50, 60 and 70 from abdominal CT is discussed in this section. The ER reflects the combined detriment from the risk for each age and gender, while the ED reflects the combined detriment from the risk of stochastic effects in different organs and tissues averaged over all ages and in both genders. Unlike previous studies, (Huda and He, 2011a, Karim et al., 2016; Saltybaeva et al., 2016) who used simulation methods, the mean ER was calculated in this thesis using direct measurement by MOSFET method from **Table 12-1D** - BEIR VII 2006 report (BEIR VII report (NAS, 2006). The ER is easy to calculate and it takes the individuals' age and gender into account, and generates data that are likely to more understandable to the public. In other words, for the public, it is easier to understand the risk of abdominal CT scanning in terms of cancer cases per million.

No largescale epidemiologic study of the cancer risks for different ages or gender, with abdominal CT using FTC and ATCM (corrected and uncorrected) has been reported. In this thesis a comparison in the mean ER across a range of different CT parameters between FTC and ATCM (corrected and uncorrected) was undertaken. The mean ER is estimated as case per 10^6 units for females and males undergoing abdominal CT scans.

7.4.1 Effective risk – comparison of FTC and corrected ATCM data

The mean ER for 20-70-year-old females and males with different acquisition parameters (tube current, pitch factors and detector configurations) were compared between FTC and corrected ATCM. The mean ER decreases with increasing age and is higher for females than males (Brenner and Hall 2007; Brenner. 2012; Costello, Cecava, Tucker & Bau, 2013; Saltybaeva et al., 2016) - **Figure 6-13 (Chapter 6)**. The highest mean ER with the MOSFET method was for 20-year-old females and the lowest in 70-year-old males. This is because the ER calculation is dependent on lifetime attributable risks (LARs) and the risk coefficient factor for each tissue decreases with increasing age; furthermore, the risk coefficient factor for different tissues are higher for females than males- see **Chapter 3, Table 3-11**. In other words, this difference relates to the changes in tissue radiosensitivity with age and gender difference. For instance, the risk coefficient factor for the stomach tissue is 52 (case/10^6 persons /Gy) for a 20-year-old female and 19 (case/10^6 persons /Gy) for a 70-year-old female. In contrast, the risk coefficient factor for the stomach tissue is 40 (case/10^6 persons /Gy) for a 20-year-old males and 14 (case/10^6 persons /Gy) for a 70-year-old males (NAS, 2006).

7.4.1.1 Tube current

Theoretically, when the mean ERs for 20 to 70-year-old females and males were compared between FTC and corrected ATCM, with tube currents at 100mA/low dose+, 200mA/ low dose, 250 mA/standard and 400mA /high quality, the mean ER for FTC was not significantly different ($p>0.05$). This implies that both ATCM and FTC have similar lifetime attributable risk of cancer incidence among females and males of all age groups at these tube currents. This finding needs further investigation to determine the cause.

In contrast, the mean ER for the corrected ATCM was 8% higher than FTC at 300mA/quality ($P<0.05$). This implies that at 300mA/quality, the lifetime attributable risk of cancer incidence due to the complete abdominal CT is higher with corrected ATCM than FTC among females and males of all age groups. For example, the mean lifetime effective risk (20-year-old female 76.3 ± 17.6 and 82.6 ± 20.1 case/10^6, 20-year-old male 64. ± 15.9 and 70.4 ± 18.1 case/10^6, 70-year-old female 22.2 ± 5.1 and 23.8 ± 5 .6 case/10^6 and 70-year-old male 18.9 ± 4.5 and 20.4 ± 5.1 case/10^6, for FTC and ATCM, respectively) **Chapter 6 Table 6-15.**

Accordingly, to could be attributed to other factors (e.g. corrected ATCM increased with different attenuation abdominal regions, densities atomic numbers, depth and locations from phantom and radiation dose distribution variable) as earlier discussed in abdominal organs dose **Section 7.2.1.1, page 205**.

7.4.1.2 Pitch factors

With detail (0.688) and standard (0.938) pitch factors, the mean ER for FTC was not significantly different from ATCM ($P>0.05$) for all age groups and males and females. This implies similar lifetime attributable risk of cancer incidence due to the complete abdominal CT scan among females and males of all age groups. In contrast, the mean ER for the corrected ATCM was higher (by around 13%) than FTC using the MOSFET method with 1.438 (fast) pitch factor- **Chapter 6, Table 6-17**. This difference was statistically significant. ($P<0.05$). The different between FTC and corrected ATCM, with the fast pitch factors, could have resulted from the increased tube current needed to maintain a constant noise level. Other factors include organ depth and locations from phantom and variable radiation dose distribution as earlier discussed in **section 7.2.1.2. Page 206.** This leads to increased mean effective risk with corrected ATCM by up to 13% during abdominal CT scan. Generally, fast pitch values (>1) can result in a reduced lifetime attributable risk of cancer incidence using abdominal CT scan FTC technique.

7.4.1.3 Detector configurations

The mean ER for FTC was significantly lower than corrected ATCM, with approximately a 6% reduction for all age groups, with 0.5×16 mm detector configuration ($p<0.05$). This could be attributed to factors such as the increase in tube current with small detectors while using corrected ATCM, organ depth and locations from phantom, experimental error and variable radiation dose distribution as earlier discussed in **section 7.2.1.3. Page 207**. In contrast, when the detector configuration was changed to 1.0×16mm and 2.0×16mm, the mean ER for FTC was not statistically different ($P>0.05$). Generally, a detector configuration of 0.5×16 mm can reduce the lifetime attributable risk of cancer incidence using FTC during abdominal CT scan- **Chapter 6 Table 6-19**.

7.4.2 Effective risk comparing FTC and uncorrected ATCM data

When considering the clinically relevant results (uncorrected data). The mean ER for uncorrected ATCM protocols was higher than for FTC techniques when considering all the acquisition parameters (tube currents, pitch factors and detector configurations); the data was statistically significant ($P<0.001$). However, the reduction in mean ER was around 20% for females and 21% for men when comparing FTC to uncorrected ATCM using different tube currents- **Chapter 6 Table 6-16**. In addition, using different pitch factors, the mean ER reduced when using FTC techniques (female 17% and male 16%) when compared to uncorrected ATCM- **Chapter 6 Table 6-18**. For the different detector configurations, the mean ER reduced by around (23% for males and female) when comparing FTC to uncorrected ATCM- **Chapter 6 Table 6-20.** This is suggests that the mean ER, with all different acquisition parameters, reduces the lifetime attributable risk of cancer incidence when using FTC by around 17-23% for females and 16 to 23% for men. These differences can result from the increased mean tube currents with ATCM (49-440mA), which were higher when compared to FTC (100-400mA). This leads to the total effective risk increasing with uncorrected ATCM by up to 23% during abdominal CT scan.

No previous study has compared abdominal organ doses and ER between FTC and ATCM corrected and uncorrected in patients across all age groups undertaking abdominal CT examinations. Hence, in this thesis, a new method has been applied to calculate and compare the mean ER of abdominal CT scans for FTC and corrected and uncorrected ATCM based on the BEIR VII (2006). This thesis provides further understanding of the radiation risks associated with abdominal CT scan when using FTC and ATCM techniques by carrying out direct dose measurements using MOSFET, which is novel. Some of the advantages to the ER approach applied include the ease of calculation, incorporation of the individuals' ages and genders, and the ability to generate data that are more understandable to the general public and clinical healthcare professionals.

Generally, the results presented in this thesis show that for both FTC and ATCM, the mean ER for abdominal CT is inversely proportional to age, irrespective of gender. These findings are in broad agreement with previous studies (Brenner, 2012; Ali et al., 2015; Brenner & Hall, 2007). The lifetime effective risk is generally higher in females than males; hence, one can conclude that abdominal CT scan cancer risk is not only based on the organ dose but also on a patient's age and gender. These findings are also in agreement with previous studies (Saltybaeva et al., 2016; NRC, 2006). The mean ER for abdominal CT showed no statistically significant

difference between FTC and corrected ATCM, except for some parameters (300mA/quality tube current, fast (1.438) pitch factors and 0.5×16 mm detector configuration). The mean ER was higher for uncorrected ATCM when compared with FTC.

In summary, the mean ER measurement by MOSFET, for both males and females (20 to 70 years old), for comparison between FTC and ATCM is in itself novel work within this thesis. Therefore, the mean ER for abdominal CT scans, comparing FTC and corrected ATCM, shows no statistically significant differences between techniques, except for some parameters. In contrast, for the clinically relevant results, the mean ER for all age groups for both males and females (20-70 old year) for the uncorrected ATCM protocols was higher than for FTC techniques.

Finally, as discussed earlier in **Section 2.9 of Chapter 2**, all the studies utilising an uncorrected ATCM approach showed a reduction in the radiation dose when compared to FTC (Kim et al 2013; Sabarudin et al., 2014; Su et al 2010; Gharbi et al., 2017 ; Sabarudin, et al., 2014; Maués et al., 2016; Su et al., 2010). Moreover, there are yet no 'fair' methods for radiation dose and image quality comparisons between FTC and ATCM techniques. Within this thesis the direct comparison between FTC and uncorrected ATCM (clinically useful data) is difficult because of the variations in the mean tube current for both techniques. However, all radiation dose results with an uncorrected ATCM technique were higher than FTC, for all acquisitions parameters. This is because the SureExposure 3D ATCM system on the Toshiba CT is based on different spatial projections (x, y & z) and is determined by anatomical attenuation from the frontal and lateral scout views. The uncorrected ACTM increased the tube current (dose) in projections with greater attenuation and by contrast decreased for lower attenuating regions. FTC, however, used a constant tube current based on patient size and clinical indications.

To avoid variations in the mean tube current between FTC and ATCM techniques and allow for a fair comparison, radiation dose data for ATCM were corrected using a mathematical method (equivalent equation fractions). The mathematical correction method used takes into account all of the radiation dose comparisons between FTC and ATCM for the different acquisition parameters. This method should be adopted in practice and could be used to evaluate the ATCM technique for different manufactures before use in patients. This is because the method is easy and fast to use without the need for complex and time-consuming calculations. Such corrections may help to improve our understanding of the comparison between FTC and ATCM techniques. In addition, the main reason for the difference between

theoretically corrected ATCM and actual uncorrected ATCM is that the uncorrected ATCM profiles are often complex and do not strictly follow theoretical results (Li, Segars & Samei, 2014).

Unfortunately, the main limitation with mathematical correction (corrected ATCM data) is that the results do not truly reflect the corrected radiation dose for the patient. In addition, the mathematical correction method may only be useful in certain situations such as evaluating and comparing different techniques. Therefore, the theoretical mathematical correction method should be subject to further investigations for its accuracy in comparing radiation dose between FTC and ATCM for CT techniques.

7.5 Physical Image Quality

Owing to the concerns about increased radiation dose in patients undergoing abdominal CT examinations, several techniques have been developed to minimize radiation dose without compromising physical image quality for different techniques. In the literature, there are several studies investigating image quality using physical methods (e.g. SNR, CNR and image noise). These studies compared different volumetric detectors or different tube voltages for abdominal CT and other CT examinations in adult patients (Bhosale et al., 2015; Kahn et al., 2014; Goshima et al., 2011; Ha, Hong, Kim, & Lee, 2016; Wang et al., 2013; Lv et al., 2015; Marin et al., 2009; Padole et al., 2016).

Physical image quality evaluation for FTC and ATCM can be useful for the purpose of image noise reduction and image quality improvement. Unfortunately, in the literature there are no studies providing information on SNR for comparisons between FTC and ATCM for abdominal CT examinations. In this thesis, the first attempt with this approach compares mean SNR values for the main abdominal organs between FTC and ATCM techniques. In this section, physical image quality results (SNR values) for the five abdominal organs (liver, spleen, pancreas, left kidney and right kidney) will be discussed. A comparison will be made between FTC and ATCM, for different parameters and abdominal organs.

In this thesis, the physical method correlations between FTC and corrected ATCM showed strong positive correlation between all mean SNR values and all different acquisition parameters (tube currents, pitch factors and detector confirmations) **See Chapter 6, Figure 6-16, Figure 6-18 and Figure 6 -20.**

7.5.1 Comparing SNR values between FTC and ATCM using different tube currents

The highest mean SNR value for all abdominal organs was noted when using 400mA/high quality CT scanning. The highest mean SNR were for the liver and spleen with ATCM (17.331±3.215 and 9.455±1.424). However, the lowest mean SNR value was at 100mA/low dose+ and for the left and right kidneys with ATCM (1.840±0.170 and1.931±0.155) - **Chapter 6 Section 6.5.1, Table 6-21.** This is because the mean SNR value for both FTC and ATCM techniques can be increased by manipulating tube current. The mean SNR value for all abdominal organs, for both FTC and ATCM, was directly proportional to tube current. Thus, increases in the tube current result in decreases in image noise with a consequential increase in the SNR for all organs. Other studies have previously reported this linear directly proportional relationship (Zarb et al., 2010; Kahn et al., 2014; Raman et al., 2013 and Zarb et al., 2011 & Park et al., 2013) - **Figure 6-17 (Chapter 6).**

On the other hand, the mean SNR values for abdominal organs, when using 100mA/low dose+ and 200 mA/ low dose, were higher for FTC than ATCM for all abdominal organs, but not statistically significant ($P>0.05$). This was with the exception of the pancreas (2.3 ± 0.4 and 2.1 ± 0.2), left kidney (2.3 ± 0.4 and 1.8 ± 0.1, and right kidney (2.6 ± 0.5 and 1.9 ± 0.1, FTC and ATCM, respectively) using100mA/low dose+. In addition, left kidney (3.339 ± 0.253 and 2.849 ± 0.261 ;), and right kidney (3.4 ± 0.3 and 2.9 ± 0.1, FTC and ATCM, respectively) using 200 mA/ low dose. These findings were statistically significant ($p<0.05$), with the SNR values increasing by approximately 15-23% when using FTC- **Chapter 6, Table 6-21.**

The difference in mean SNR value for the kidneys and pancreas, using 100mA/low dose+ and 200 mA/ low dose, showed FTC to be higher and this could be attributed to the image noise with ATCM being higher than FTC. This is because the ATCM, for Toshiba scanners, is based on the selected image noise values defined by SD (low dose+ SD= 12.5 and low dose SD= 7.5). This resulted in a decrease in mean tube current for ATCM techniques and a subsequent increase in image noise. The calculations for ATCM are based on the inverse square root relationship between image noise and tube current, and also between image noise and SNR values. This is consistent with the findings of Peng et al. (2009); Merzan, Nowik, Poludniowski & Bujila (2016). In addition, for the kidneys and pancreas, the tube current decreased for lower attenuating levels of the phantom (smaller structures), leading to increased image noise with ATCM technique. By contrast, the FTC technique uses a constant tube current and this leads to the image noise remaining more constant across the scan range.

On the other hand, for a tube current increased to 250mA/standard and 300mA/quality, the mean SNR value abdominal organs for the FTC was lower than ATCM for all abdominal organs and not statistically significant ($p>0.05$). Only the liver (13.8 ± 2.3 and 15.2 ± 1.5) and spleen (7.8 ± 1.5 and 8.9± 1.5, FTC and ATCM, respectively) were statistically significant ($p<0.05$) between FTC and ATCM. The mean SNR with ATCM was approximately 3-9% higher for the liver 13-19% for the spleen than FTC techniques- **Chapter 6, Table 6-21**. The difference in mean SNR value for the liver and spleen, using 250mA/standard and 300mA/quality, could be attributed to the image noise selected with ATCM (standard SD= 5 and quality SD= 3), which was lower than FTC technique and as such the mean tube current with ATCM was higher than FTC, increasing image quality. Additionally, the liver and spleen are highly homogenous structures and low image noise attenuating portions of the phantom. This could also lead to a decrease in image noise with ATCM technique (Peng et al., 2009).

When increasing the tube current to the highest level, 400mA/ high quality, the mean SNR value for FTC was no different with ATCM for all abdominal organs. This is because the mean tube current using ATCM with (high quality) was similar to the FTC constant tube current (400mA).

7.5.2 Comparing SNR values between FTC and ATCM with different pitch factors

Within this thesis, higher mean SNR values were identified for FTC compared to ATCM when using detail (0.688) pitch factor for the liver and spleen (14.406±3.795 and 8.1±2.1, respectively). However, the lowest mean SNR value between FTC and ATCM for abdominal organs was noted when using a fast (1.438) pitch factor for the left kidney and right kidney with FTC (3.165±0.818 and 3.2±0.7, respectively) - **Chapter 6, Section 6.5.2, Table 6-22.** The mean SNR value for all abdominal organs for both FTC and ATCM are inversely proportional to pitch factors. Thus, an increase in pitch factor results an increase in image noise with a consequential decrease in the SNR across all abdominal organs (Tacelli, et al., 2010; Raman et al., 2013; Park et al., 2013; Zhang et al., 2015; Schindera et al., 2007; Merzan et al., 2016)- **Figure 6-19 (Chapter 6).**

There was no difference in mean SNR values, for abdominal organs using the detail (0.688) pitch factor, for FTC and ATCM ($p>0.05$). There were, however, statistically significant ($p<0.05$) differences in SNR for the liver. FTC was around 9% higher than ATCM (14.4 ± 3.7 and 13.1 ± 4.7, FTC and ATCM, respectively). The mean SNR value for FTC was no different to ATCM when a standard (0.938) pitch factor was used ($p>0.05$). This was with the exception

of the left kidney (3.836 ± 0.899 and 3.489 ± 1.094) and right kidney (4.1 ± 0.9 and 3.7 ± 1.2, FTC and ATCM, respectively) where SNR for FTC was slightly higher (around 7%) **Chapter 6 Table 6-22**.

The different mean SNR values for the liver and both kidneys when using detail (0.688) and standard (0.938) pitch factors showed FTC techniques to be higher. This could be attributed to the Toshiba ATCM techniques when using low pitch factors/ Tube current was automatically decreased when decreasing pitch factors to keep the effective mAs at a constant image noise level. This means decreased tube current causes an increased image noise and as a result a deceased SNR value for ATCM for all abdominal organs. In contrast, for the FTC technique, the tube current is constant and not affected by different pitch factors across the full scan range. (Ranallo& Szczykutowicz, 2015).

When increasing the pitch factor to 1.438 (fast), the mean SNR for ATCM showed no difference with FTC for all abdominal organs ($p>0.05$). This was with the exception of the liver (10.4 ± 2.5 and 11.7 ± 2.8), spleen (5.5 ± 1.4 and 6.5 ± 1.5) and pancreas (2.9 ± 0.7and 3.2 ± 0.8, for FTC and ATCM, respectively). The mean SNR values for ATCM were higher than with FTC for the liver, spleen and pancreas. These differences could be attributed to the higher pitch factors resulting in higher tube currents in order to keep a constant image noise when compared with the FTC technique for all abdominal organs. This means an increased tube current and a decreased image noise, with a resultant increased SNR values, when using ATCM. (Merzan et al., 2016). In addition, for ATCM when the tube current is high (high pitch), the image noise remains constant regardless phantom size (Funama et al., 2008).

7.5.3 Comparing SNR values between FTC and ATCM with different detector configurations

The highest mean SNR value for all abdominal organs was when using a 2.0×16 mm detector configuration. The higher mean SNR for the liver and spleen was with ATCM (13.739±4.501 versus 7.959±2.595). However, the lowest mean SNR value was at 0.5×16mm. The lowest mean SNR was for the left kidney and right kidney with ATCM (3.3 ± 1.1 and 3.4 ± 1.1)- **Chapter 6, Section 6.5.3, Table 6-23.**

The mean SNR value for abdominal organs when using a 0.5×16 mm detector configuration with FTC showed no difference with ATCM ($P>0.05$). This was with the exception of the spleen (FTC 6.3 ± 2.1 and ATCM 7.1 ± 2.2; $P<0.05$). After changing the detector configuration to 1.0×16 mm, the mean SNR value was no different between FTC and ATCM techniques for all abdominal organs ($P>0.05$). When using a 2.0×16 mm detector configuration, the mean SNR value was no different between FTC when compared to ATCM for all abdominal organs ($P>0.05$). The exception was for the left kidney (4.1 ± 0.9 and 3.6 ± 1.1) and right kidney (3.9 ± 0.9 and 3.6 ± 1.2, FTC and ATCM, respectively; $P<0.05$), wherein the mean SNR value was slightly higher for FTC than for the ATCM technique- **Chapter 6, Table 6-23.**

To explain the different SNR values between different detector configurations, the ATCM technique exhibits a directly proportional relationship between detector configuration and the mean SNR for all organs. Increasing the detector configuration increases the tube current and decreases the image noise, thereby increasing the mean SNR (Raman et al., 2013 and Goshima et al., 2011). In this thesis, the different mean SNR value between FTC and ATCM techniques, with different detector configurations, could be attributed to the highest tube currents. These resulted from small (0.5×16 mm) detector configurations with ATCM for some abdominal organs and decreased image noise, increasing SNR values when compared with FTC. By contrast, a large detector configuration (2.0×16mm) requires a decrease in tube current across the scan range and subsequently increased image noise when using ATCM (Merzan et al., 2016).

In reviewing the literature, one study compares hepatic artery SNR between FTC and ATCM (Su et al., 2010). The work by Su et al. (2010) calculated the SNR for hepatic artery using contrast enhancement with two constant tube currents. The mean SNR was found to be higher for FTC than for the ATCM technique (FTC 46.4 ± 9.9 and ATCM 41.8 ± 11.9). This was not consistent with the figures reported in this thesis when comparing the mean SNR for liver at

300mA/quality, wherein the ATCM was higher than the FTC (FTC 15.2± 1.5 and ATCM 13.8 ± 2.3). The differences between the two studies is that in this thesis an anthropomorphic abdominal phantom was used together with different CT parameters. There was also no contrast enhancement and the CT scanners were from different manufacturers.

Mean SNR is directly proportional to tube current and detector configurations. These findings are in broad agreement with previous studies (Molen et al., 2012; Kahn et al., 2014; Raman et al., 2013). In contrast, the mean SNR values for all adnominal organs during both FTC and ATCM are inversely proportional to the pitch factors. In the literature, increasing the pitch increases noise and lowers SNR- these findings are therefore also in agreement with previous studies (Tacelli et al., 2012; Zhang, et al., 2015).

In summary, the mean SNR values calculated for all abdominal organs, when comparing between FTC and ATCM for abdominal CT scans with different parameters, are in themselves novel work. Therefore, the mean SNR values when comparing between FTC and ATCM show no statistical difference between both techniques, except for some parameters for some abdominal organs. The mean SNR values for FTC were higher than ATCM at 100mA/low dose+ and 200mA/low dose, pitch factors <1 and 2.0×16 mm detector configuration for lower abdominal organs (both kidneys).

7.6 Image quality (relative-VGA)

The methods for patient dose evaluation are easily available, however the techniques for visual image quality optimisation are far more complicated. VGA and ROC studies are commonly used to assess clinical image quality (**see chapter 4 Section 4.2.3**). In VGA studies, a relative or absolute scoring can be performed based on the visibility of normal or abnormal anatomical structures (Miéville et al., 2011 and Bath, 2010). In this thesis, visual image quality comparisons between FTC and ATCM techniques used a relative VGA approach. Five different axial CT images were selected (image #1 upper anterior abdominal, image # 2 upper abdominal, image # 3 medial abdominal, image # 4 lower abdominal and image # 5 lower inferior abdominal), with five different image quality criteria for each axial slice based on European Guidelines on Quality Criteria for Computed Tomography (CEC, 2000). A three point Likert scale was used; worse, equal, and better together with five different reference images facilitate comparison.

There are a number of studies comparing visual image quality for FTC and ATCM using an absolute VGA method (Funama et al., 2008; Kalra et al., 2004a; Lee et al., 2009; Lee et al., 2011b; Namasivayam et al., 2006; Peng et al., 2009; Rizzo et al., 2006; Su et al., 2010; Wang et al., 2013; Park et al., 2013; Kim et al., 2013). However, all of these studies demonstrated results comparing FTC and ATCM and the visual image quality scores were similar for most CT scan examinations.

Repeatability and agreement between observers was ensured for the visual evaluation task. Prior to discussing the relative VGA method image quality assessment results, the level of inter-observer variation between five observers and the PhD student was determined. When images are compared against a reference image they provide much more consistent results if an SNR approach is used. This is because the SNR method involves the use of ROIs to calculate SNR values for each axial CT image and reduces the bias when selecting a reference image. These findings are supported by the literature (Lança et al., 2017; Mraity, 2015). The purpose of calculating relative VGA agreement between observers and the PhD student was to determine the competency of the student in visually appraising abdominal CT images, using the methods described within this thesis. It gave an indication of the homogeneity observers and the PhD student's scoring. The ICC results for the visual evaluation showed excellent agreement when compared amongst observers. Estimated ICC ranged from 0.786 to 0.987. (95%CI 0.686-0.987)- **see chapter 5 Table 5-13**. This level of agreement is comparable to another optimisation study (Mraity, 2015) which reported ICC values of 0.672 to 0.881.

In general, the mean relative VGA scores between FTC and ATCM for different acquisition parameters shows that the highest mean relative VGA scores for all abdominal axial images slices was at a tube current 400mA/ high quality, detailed (0.688) pitch factor and 2.0 x 16 mm detector configuration for both techniques. In addition, the lowest mean relative VGA scores between FTC and ATCM, for all abdominal axial images, was at tube current 100mA/low dose +, fast pitch factor (1.438) and 0.5×16mm detector configuration for both techniques.

7.6.1 Comparing relative (VGA) between FTC and ATCM with different tube currents

The mean relative VGA scores between FTC and ATCM were directly proportional to the tube current. Thus, increasing the tube current increases the mean relative VGA scores on all abdominal axial images; this is because the tube current is inversely proportional to the image noise. Conversely, relative VGA scores are degraded by lowering the tube current (Su et al., 2010; De Crop et al., 2015; Kalra et al., 2004a) - **Figure 6-22 (Chapter 6).**

The mean relative VGA scores for FTC showed no difference when compared with ATCM for all axial images with 100mA/low dose +, 200mA/low dose, 250mA/standard and 400mA/ high quality, and were not statistically significant ($P>0.05$). The exception is image #4 with 400mA/ high quality (FTC 39.8 ± 5.0 and ATCM 42.0 ± 3.1), where the mean relative VGA scores were slightly higher for ATCM than FTC ($P<0.05$) - **Chapter 6 Table 6-25.** This is because the mean tube current with ATCM was similar to FTC with different tube currents. This suggests the same mean tube current produces a constant image noise, which is similar for the ATCM and FTC technique. In turn, this leads to the same image quality scores across both techniques. This is consistent with previous work (Funama et al., 2008; Kalra et al., 2004a; Lee et al., 2009; Lee et al., 2011b; Namasivayam et al., 2006; Peng et al., 2009; Rizzo et al., 2006; Su et al., 2010)

By contrast, the mean relative VGA scores for FTC were lower than ATCM for all abdominal CT axial images when the 300mA/quality scanning was used. Image #1 (FTC 21.3 ± 1.9 and ATCM 22.4 ± 2.3) and image #2 (FTC 31.0 ± 2.8 and ATCM 33.0 ± 3.6) were statistically significant ($P<0.05$). ATCM VGA scores were higher than FTC because of the large variations in beam attenuation with ATCM, based on anatomical regions. This was founded on the principle that x-ray attenuation and the amount image noise are determined by the size of the phantom. The ATCM aim is to modify the tube current based on regional phantom anatomy for adjustment of x-ray beam characteristics to maintain constant image noise (Lee et al., 2009). In addition, the mean tube current (quality) with ATCM was higher than constant tube current

300mA with FTC. The marked tube current increase may also contribute to the decrease in image noise and increase in relative VGA scores with the ATCM technique while the FTC had a constant tube current for the phantom scan range (Su et al., 2010). The most important finding was in the upper abdominal different mean relative VGA scores between FTC and ATCM. This suggests that when using tube current (quality), the mean relative VGA scores for ATCM were higher than FTC (300mA) for upper abdominal images by around 5% to 6%.

7.6.2 Comparing relative (VGA) between FTC and ATCM with different pitch factors

The pitch factors were inversely proportional to the mean relative VGA scores between FTC and ATCM. Therefore, the image noise increased with increased pitch factors. In addition, the mean relative VGA scores with standard (0.938) and fast (1.438) were lower than detail (0.688) for both FTC and ATCM. This is in agreement with what has previously been reported in the literature, which suggests that perceptual image quality remains equivalent when using absolute VGA evaluation with different pitch values (Tacelli, et al 2010; Sun & Ng, 2010) - **Figure 6-23 (Chapter 6).** The mean relative VGA scores for detail (0.688) and standard (0.938) pitch factors showed no difference between FTC and ATCM ($P>0.05$). This is because the Toshiba ATCM with detail (0.688) and standard (0.938) pitch factors decreased tube current to keep a constant image noise. However, the amount of image noise was similar with FTC for detail (0.688) and standard (0.938) pitch factors. This means the amount of image noise between both techniques leads to the same image quality scores for both techniques (Ranallo& Szczykutowicz, 2015).

In contrast, the mean relative VGA scores for FTC were lower than ATCM for all abdominal axial images when using a fast (1.438) pitch factor. Comparisons were, however, not significant ($P>0.05$), except for image # 2 (FTC 23.7 ± 4.6 and ATCM 24.9 ± 5.650) and image # 3 (FTC 27.7± 5.573 and ATCM 30.5± 7.2; $P<0.05$). However, image #2 and #3 with ATCM showed increasing mean relative VGA scores when compared to FTC by around 5% and 10%, respectively- **Chapter 6 Table 6-26.** The difference in mean relative VGA scores for image #2 and #3 could be attributed to the increased tube current and low image noise levels when using the ATCM technique. When using a fast (1.438) pitch factor, the Toshiba ATCM technique increased the mean tube current to keep a constant image noise when compared with FTC. This means an increased mean tube current leads to decreased image noise with increased image quality scores for ATCM (Merzan et al., 2016). By contrast, the FTC technique tube current is constant and not affected by different pitch factors (Ranallo & Szczykutowicz, 2015).

A pitch factor <1 results in mean relative VGA scores being no different between FTC and ATCM techniques. However, with a pitch factor >1, the mean relative VGA ATCM was superior to FTC for upper and middle abdominal organs.

7.6.3 Comparing relative (VGA) between FTC and ATCM with different detector configurations

The relationship between FTC and ATCM during different detector configurations was directly proportional to the mean relative VGA scores for all slices- **Figure 6-24 (Chapter 6).** For the 0.5×16 mm and 1.0×16 mm and 2.0×16mm detector configurations, the mean relative VGA scores were indifferent between FTC and ATCM for all images and not statistically significant (P>0.05)- **Chapter 6 Table 6-27.** For the different detector configurations, 0.5×16 mm and 1.0×16 mm and 2.0×16 mm, the results of this thesis indicate the mean relative VGA scores between FTC and ATCM demonstrate that there are no image quality differences. In this thesis there is no difference in mean relative VGA scores between FTC and ATCM techniques with different detector configurations. This could be attributed to the mean tube current with ATCM, resulting from a small (0.5×16 mm) and large detector (2.0×16 mm) configurations being similar to the mean tube current used with FTC.

No previous report has included comparisons of image quality for abdominal CT scan at different detector configurations between FTC and ATCM. This thesis showed that the ATCM provided similarly acceptable image quality with FTC for different detector configurations. In reviewing the literature, no study has compared visual image quality assessment using a relative VGA method for abdominal CT examinations between FTC and ATCM. However, in this thesis, the results will be compared to four previous studies that used the absolute VGA method to compare FTC and ATCM. This includes all studies that considered the image quality for abdominal/pelvis CT scan examinations, since they all used the absolute VGA method (Kalra et al., 2004a; Rizzo et al., 2006; Su et al 2010; Lee et al., 2011b).

Work by Kalra et al. (2004a) used an absolute VGA method (5-point scale at five abdomen and pelvis levels) to evaluate acceptable image quality between FTC and ATCM for two constant tube currents. The visual image quality assessment scores between both techniques found no significant (P>0.05) difference between FTC and ATCM for all anatomical levels. Similarly, Rizzo et al. (2006) evaluated diagnostic acceptability of the liver parenchyma at different levels in the abdomen. Rizzo used an absolute VGA method with a 5-point scale and, again, two constant effective tube currents. The visual image quality evaluation between both techniques

found no significant difference in diagnostic acceptability with either ATCM or FTC techniques (P>0.05). Another study by Su et al. (2010) evaluated the liver with medium contrast using an absolute VGA method. The visual image quality assessment scores between both techniques again found no significant difference between FTC and ATCM. Similarly, for Lee et al. (2011b), who compared abdomen / pelvic CT image quality for FTC and ATCM using an absolute VGA method with a single constant tube current, no significant differences (P>0.05) between visual image quality between were reported between FTC and ATCM.

This thesis is consistent with published studies which showed that different detector configurations produce similar image quality between FTC and ATCM. However, in this thesis other parameters, such as different tube currents, found the ATCM scores higher than FTC with image #1, image #2 and image #2 and image #3 with fast (1.438) pitch factors. This is because the previous published studies used patients, different positioning, fields of view, acquisition parameters and CT scanners. These differences make comparisons between this thesis and previous studies difficult. **Table 7-2** provide summary comparison between FTC and ATCM with different visual image quality evaluation methods from this thesis and previous studies.

Table 7- 2: Summary comparison CT scan between FTC and ATCM with different visual image quality methods from this thesis with different previous studies

Study	Year	Visual image quality evaluation methods	Visual image quality (FTC and ATCM)
Kalra et al	**2004a**	Absolute VGA	ATCM and FTC similar
Rizzo et al.	**2006**	Absolute VGA	ATCM and FTC similar
Su et al	**2010**	Absolute VGA	ATCM and FTC similar
Lee et al	**2011b**	Absolute VGA	ATCM and FTC similar
This thesis	**2018**	Relative VGA	ATCM higher than FTC image #1 image #2 and image #4 with different tube current
			ATCM higher than FTC imag#2 and image #3 at fast (1.438) pitch factors

In summary, the mean relative VGA score comparison between FTC and ATCM is in itself novel work. The mean relative VGA scores between FTC and ATCM shows no statistically significant difference between both techniques for most acquisitions parameters. The mean relative VGA scores for ATCM were higher than FTC technique at 300mA/quality (image #1 and 2) and fast (1.438) pitch factor (image # 2 and 3). Therefore, the ATCM technique is suitable for upper abdominal CT scanning.

7.7 Conclusion

The aims of this thesis were to measure and estimate the radiation dose and evaluation image quality between FTC and ATCM for adult abdominal CT examinations using phantoms. In this section, an overall conclusion and recommendations regarding the comparison between FTC and ATCM, a statement of novelty, thesis limitations and future works are presented. The major objectives of this research were to investigate different methods for lowering radiation dose (according to the ALARA) and acceptable image quality when comparing between both techniques (FTC or ATCM). This would take into account the combined effect of the abdominal acquisition factors (tube current, pitch factors and detectors configuration). The first essential investigation was the measurement and estimation of radiation dose using different methods including: organ dose, effective dose and effective risk between FTC and ATCM (corrected and uncorrected). The second was to evaluate image quality, using the physical (SNR) method for five abdominal organs and visual image quality evaluation by relative VGA method for five different abdominal axial images.

The abdominal organ doses during abdominal CT scan is complex. The MOSFET method results that are presented in this thesis demonstrate no significant difference (P>0. 05) between mean abdominal organs dose for FTC and corrected ATCM, except for some acquisition parameters. These include using 300mA/quality, fast (1.438) pitch factor and 0.5×16mm detector configuration where the mean abdominal organ dose for FTC was 13% lower than the corrected ATCM technique. In contrast, using uncorrected dose data, the mean abdominal organ doses for ATCM were higher than FTC for all acquisition parameters. In addition, the FTC reduced the mean abdominal organs dose between 17% and 23% when compared with uncorrected ATCM.

In this thesis, the estimation of mean ED during abdominal CT was undertaken using three different methods (MOSFET, DLP and ImPACT). The mean ED comparison between FTC and corrected ATCM reported no significant difference (P>0.05) between both techniques except for some parameters (with all different dosimetry methods). When using 300mA/quality, fast

(1.438) pitch factor, the mean abdominal organ dose for FTC was lower than for a corrected ATCM technique with MOSFET=7% to 20%, DLP=8% to 13%, ImPACT=4% to 13%). In addition, the corrected ATCM was around 6% lower than FTC when using detail (0.688) and standard (0.938) pitch factors with the ImPACT method. However, for the clinically relevant dose results, the mean ED from uncorrected ATCM was higher than FTC for all acquisition parameters. The difference between the dosimetry methods ranged between both techniques: MOSFET 21%, DLP 19% and ImPACT 18%. The higher mean ED was estimated by ImPACT method and the lowest measurement was by MOSFET method for both techniques.

The mean ER was calculated from MOSFET data and results from this thesis showed it was not significantly different (P>0.05) between FTC and corrected ATCM. The exception was 300mA/quality tube current, fast (1.438) pitch factors and 0.5×16mm detector configuration wherein FTC was lower than corrected ATCM in all males and females across all age groups; this was significantly different. This means the lifetime attributable risk of cancer incidence can be reduced between 7%-13% when using FTC when compared with corrected ATCM. By contrast, the mean ER for uncorrected ATCM data was higher than FTC with all acquisition parameters. The mean ER increased with uncorrected ATCM by around 21% when compared with FTC technique for all males and females/all age groups.

This thesis also demonstrates a comparison in image quality (physical and visual) between the FTC and ATCM techniques. The mean abdominal organ SNR values were generally not significantly different (P>0.05) between FTC and ATCM, except for some acquisition parameters. For example, the liver, spleen and pancreas at 300/quality mA and fast pitch factor (1.483), wherein the mean SNR values for ATCM were higher than FTC. In contrast, for both kidneys at 100/low dose + mA, 200 mA/ low dose, standard (0.938) pitch factors and 2.0×16mm detector configuration; the FTC had higher mean SNR values than ATCM. However, from this thesis, the mean relative VGA scores for FTC and ATCM were not significantly different (P>0.05). Except for some parameters wherein the mean relative VGA scores for ATCM were higher than for the FTC technique at 300mA/quality (image #1 and 2), upper abdominal axial slices, and fast (1.438) pitch factor (image # 2 and 3) for upper and middle axial slices. Therefore, the abdominal CT scan selected suitable techniques (FTC and ATCM) should be carefully chosen because to avoid received higher radiation dose with abdominal CT scan and maintaining the image quality level.

7.7.1 Thesis novelty

The main novel contributions of this PhD thesis are summarised below:

1-This is the first study to successfully compare radiation dose between FTC and ATCM techniques for abdominal CT, using radiation dose data corrected from uncorrected ATCM data.

2-This is the first study to use direct radiation dose measurements by MOSFET and estimations from computer simulations (ImPACT method) to compare ED between FTC and ATCM for abdominal CT examinations.

3-This is the first study to estimate the lifetime cancer risks for patients undergoing abdominal CT examinations for ages 20 to 70 years, and for both male and female when comparing between FTC and ATCM CT techniques.

4- This is the first study which demonstrated that the radiations dose for FTC was lower than ATCM (uncorrected or the clinically relevant results) for abdominal CT examinations with different acquisitions parameters and different dosimetry methods.

5-This is the first study to calculate SNR values for the major abdominal organs and compare them between abdominal CT for FTC and ATCM techniques.

6-This is the first study to compare the visual image quality of abdominal CT images between FTC and ATCM using the relative VGA method with different abdominal CT images.

7-This was the first study, using physical and relative-VGA methods, to demonstrate that there were no significant differences in image quality between FTC and ATCM techniques for abdominal CT scans, excepting some parameters.

7.7.2 Thesis limitations

The following are the limitations of this study:

1. The ATOM phantom used in this thesis is a standard male adult size phantom. In addition, the organ doses measured in this thesis were only for abdominal organs; it may have been more practical for all body organ doses to be measured directly by MOSFET, and this may have clinical utility. Also, the anthropomorphic abdominal image quality phantom was also representative of a standard adult size. Comparison of lesion and contrast enhanced images for both techniques was not possible. In addition, the phantom lacks some abdominal organs, such as the stomach.

2. Although different acquisition factors (tube current, pitch factors and detectors configuration) were investigated to compare radiation dose and image quality between FTC and ATCM were utilised in this thesis, several others including slice thickness, kVp, rotation time, and iterative reconstruction were not investigated and should be considered in future works.

3. Comparison of radiation dose and image quality described in this thesis are for adult patients only; further studies investigating the effects of FTC and ATCM for paediatric patients are warranted.

4. The physical assessment of image quality was based on SNR values only. SNR is highly useful as a measure of image quality comparison between both techniques (FTC and ATCM). It would have been useful to include other metrics, such as CNR values. In addition, the relative VGA method assessment of image quality was based on normal abdominal CT scan examinations between FTC and ATCM techniques. Comparison of CT scans including pathological lesions and with contrast enhancement for both techniques would be important clinically.

7.7.3 Recommendations from the thesis and future work

Work within this thesis provides important information for clinical practice when considering the comparison of FTC and ATCM techniques for abdominal CT scans. Within this work it is important to emphasise that the goal of imaging is not necessarily to create the highest quality image but to identify the most suitable clinical technique to generate an acceptable quality image, using the lowest possible radiation dose. This study increases awareness regarding the significance of medical radiation exposure and methods used to acquire CT images from FTC or ATCM techniques.

Findings from this thesis indicate that in theory the FTC and corrected ATCM techniques were generally similar in terms of radiation dose, except for some acquisition parameters, i.e. 300mA/quality tube current and fast (1.483) pitch factor where FTC was lower than corrected ATCM. In practice, this may mean that the FTC technique is more appropriate for reducing the radiation dose when fast scans are required. This can be useful for emergency scans and those performed on unstable patients.

When comparing FTC and uncorrected ATCM (clinical protocols), FTC can lower radiation dose (organ dose, effective dose and effective risk) by approximately 13-23% when compared with uncorrected ATCM techniques. However, the ATCM technique has the potential to produce superior image quality within the upper and middle portions of the abdomen when using quality and high pitch factors. In contrast, the FTC techniques had higher SNR values for lower abdominal organs when using lower tube current and low pitch factors. Other than this, there seems to be no major difference in image quality between FTC and ATCM techniques for abdominal CT examinations. This information is particularly useful for radiology department staff who undertake CT examinations using a Toshiba CT system.

When using a FTC technique, consideration should be given to patient size and clinical indication for the examination when attempting to minimise the radiation dose. FTC techniques should also be reviewed regularly, for example monthly tests for tube current and image noise, using a QC phantom. Further investigations of radiation dose differences between FTC and uncorrected ATCM are warranted. Clinical centres should test the efficacy of their ATCM techniques before introducing them into widespread clinical practice. CT scanner manufactures should also consider re-evaluating ATCM techniques in order to minimise radiation dose and optimise image quality levels.

Finally, this thesis can be consolidated upon in the future by:

1. Undertaking further studies investigating the radiation dose difference between FTC and corrected / uncorrected ATCM for CT scan examinations using ATOM phantoms of different sizes.

2. Carrying out a similar study, comparing image quality and radiation dose (corrected and uncorrected) between FTC and ATCM, for paediatric abdominal CT examinations. The radiation dose in paediatrics is about three times higher than adults because children are more sensitive to ionising radiation.

3. Comparing the detection of pathologies and image quality between FTC and ATCM, using a ROC methodology. This could be achieved by inserting simulated lesions into the phantom and using the same acquisitions parameters to see how could might affect diagnostic performance for abdominal CT scan examinations.

4. Investigating the effect of image quality differences for studies involving contrast enhancement, alternative image reconstruction methods and filtered back projection across a range of different parameters (FTC and ATCM techniques).

5. Carrying out radiation dose and image quality comparisons between FTC and ATCM for other CT examinations on other anatomical areas (e.g. head, chest, cardiac, spine and pelvis) and CT vendors.

Appendix I: Adult CT abdominal protocols and parameters FTC and ATCM data

FTC 45 protocols					
Protocols NO.	**FTC/m A**	**Kvp**	**Detector configuration**	**Pitch factor/Helical Pitch**	**DLP (mGy.cm^2)**
1	**250**	**120**	**0.5× 16mm**	**Detail(0.688)/ 11.0**	**593.7**
2	**250**	**120**	**0.5× 16mm**	**Standard(0.938)/ 15.0**	**433.3**
3	**250**	**120**	**0.5× 16mm**	**Fast(1.438)/ 23.0**	**300.5**
4	**250**	**120**	**1.0× 16mm**	**Detail(0.688)/ 11.0**	**525.2**
5	**250**	**120**	**1.0× 16mm**	**Standard(0.938)/ 15.0**	**399.3**
6	**250**	**120**	**1.0× 16mm**	**Fast(1.438)/ 23.0**	**278.9**
7	**250**	**120**	**2.0× 16mm**	**Detail(0.688)/ 11.0**	**520.6**
8	**250**	**120**	**2.0× 16mm**	**Standard(0.938)/ 15.0**	**407.3**
9	**250**	**120**	**2.0× 16mm**	**Fast(1.438)/ 23.0**	**299**
10	**100**	**120**	**0.5× 16mm**	**Detail(0.688)/ 11.0**	**240.5**
11	**100**	**120**	**0.5× 16mm**	**Standard(0.938)/ 15.0**	**190.5**
12	**100**	**120**	**0.5× 16mm**	**Fast(1.438)/ 23.0**	**170.2**
13	**100**	**120**	**1.0× 16mm**	**Detail(0.688)/ 11.0**	**230.1**
14	**100**	**120**	**1.0× 16mm**	**Standard(0.938)/ 15.0**	**159.7**
15	**100**	**120**	**1.0× 16mm**	**Fast(1.438)/ 23.0**	**140.6**
16	**100**	**120**	**2.0× 16mm**	**Detail(0.688)/ 11.0**	**218.3**
17	**100**	**120**	**2.0× 16mm**	**Standard(0.938)/ 15.0**	**185.9**
18	**100**	**120**	**2.0× 16mm**	**Fast(1.438)/ 23.0**	**150.6**
19	**200**	**120**	**0.5× 16mm**	**Detail(0.688)/ 11.0**	**475**
20	**200**	**120**	**0.5× 16mm**	**Standard(0.938)/ 15.0**	**355.1**
21	**200**	**120**	**0.5× 16mm**	**Fast(1.438)/ 23.0**	**245.4**
22	**200**	**120**	**1.0× 16mm**	**Detail(0.688)/ 11.0**	**420.1**
23	**200**	**120**	**1.0× 16mm**	**Standard(0.938)/ 15.0**	**319.4**
24	**200**	**120**	**1.0× 16mm**	**Fast(1.438)/ 23.0**	**223.2**
25	**200**	**120**	**2.0× 16mm**	**Detail(0.688)/ 11.0**	**416.5**
26	**200**	**120**	**2.0× 16mm**	**Standard(0.938)/ 15.0**	**325.8**
27	**200**	**120**	**2.0× 16mm**	**Fast(1.438)/ 23.0**	**239.2**
28	**300**	**120**	**0.5× 16mm**	**Detail(0.688)/ 11.0**	**712.5**
29	**300**	**120**	**0.5× 16mm**	**Standard(0.938)/ 15.0**	**532.6**
30	**300**	**120**	**0.5× 16mm**	**Fast(1.438)/ 23.0**	**360.6**
31	**300**	**120**	**1.0× 16mm**	**Detail(0.688)/ 11.0**	**630.2**
32	**300**	**120**	**1.0× 16mm**	**Standard(0.938)/ 15.0**	**489.8**
33	**300**	**120**	**1.0× 16mm**	**Fast(1.438)/ 23.0**	**334.7**
34	**300**	**120**	**2.0× 16mm**	**Detail(0.688)/ 11.0**	**624.8**
35	**300**	**120**	**2.0× 16mm**	**Standard(0.938)/ 15.0**	**488.7**
36	**300**	**120**	**2.0× 16mm**	**Fast(1.438)/ 23.0**	**358.8**
37	**400**	**120**	**0.5× 16mm**	**Detail(0.688)/ 11.0**	**1004**
38	**400**	**120**	**0.5× 16mm**	**Standard(0.938)/ 15.0**	**775.2**
39	**400**	**120**	**0.5× 16mm**	**Fast(1.438)/ 23.0**	**524.8**
40	**400**	**120**	**1.0× 16mm**	**Detail(0.688)/ 11.0**	**898.7**
41	**400**	**120**	**1.0× 16mm**	**Standard(0.938)/ 15.0**	**667.9**
42	**400**	**120**	**1.0× 16mm**	**Fast(1.438)/ 23.0**	**466.6**
43	**400**	**120**	**2.0× 16mm**	**Detail(0.688)/ 11.0**	**841.4**
44	**400**	**120**	**2.0× 16mm**	**Standard(0.938)/ 15.0**	**658.2**
45	**400**	**120**	**2.0× 16mm**	**Fast(1.438)/ 23.0**	**483.2**

ATCM corrected /uncorrected data 45 protocols					
1	Standard(SD 5.00)	120	0.5× 16mm	Detail(0.688)/ 11.0	594.2 /871.4
2	Standard(SD 5.00)	120	0.5× 16mm	Standard(0.938)/ 15.0	449.1 /658.5
3	Standard(SD 5.00)	120	0.5× 16mm	Fast(1.438)/ 23.0	386.1 /566.2
4	Standard(SD 5.00)	120	1.0× 16mm	Detail(0.688)/ 11.0	496.1 /727.4
5	Standard(SD 5.00)	120	1.0× 16mm	Standard(0.938)/ 15.0	403.1 /591.2
6	Standard(SD 5.00)	120	1.0× 16mm	Fast(1.438)/ 23.0	338.7 /496.7
7	Standard(SD 5.00)	120	2.0× 16mm	Detail(0.688)/ 11.0	440.8 /646.4
8	Standard(SD 5.00)	120	2.0× 16mm	Standard(0.938)/ 15.0	382.1 /560.2
9	Standard(SD 5.00)	120	2.0× 16mm	Fast(1.438)/ 23.0	338.3 /496.1
10	Low dose+ (SD 12.50)	120	0.5× 16mm	Detail(0.688)/ 11.0	198.7 /200.7
11	Low dose+ (SD 12.50)	120	0.5× 16mm	Standard(0.938)/ 15.0	164.5 /166.2
12	Low dose+ (SD 12.50)	120	0.5× 16mm	Fast(1.438)/ 23.0	165.7 /167.4
13	Low dose+ (SD 12.50)	120	1.0× 16mm	Detail(0.688)/ 11.0	161.9 /163.6
14	Low dose+ (SD 12.50)	120	1.0× 16mm	Standard(0.938)/ 15.0	138.6 /140
15	Low dose+ (SD 12.50)	120	1.0× 16mm	Fast(1.438)/ 23.0	150.7 /152.3
16	Low dose+ (SD 12.50)	120	2.0× 16mm	Detail(0.688)/ 11.0	149.6 /151.1
17	Low dose+ (SD 12.50)	120	2.0× 16mm	Standard(0.938)/ 15.0	131.3 /132.7
18	Low dose+ (SD 12.50)	120	2.0× 16mm	Fast(1.438)/ 23.0	148.6 /150.1
19	Low dose (SD 7.50)	120	0.5× 16mm	Detail(0.688)/ 11.0	393.7 /397.7
20	Low dose (SD 7.50)	120	0.5× 16mm	Standard(0.938)/ 15.0	373.9 /377.7
21	Low dose (SD 7.50)	120	0.5× 16mm	Fast(1.438)/ 23.0	358.8 /362.4
22	Low dose (SD 7.50)	120	1.0× 16mm	Detail(0.688)/ 11.0	327.2 /330.5
23	Low dose (SD 7.50)	120	1.0× 16mm	Standard(0.938)/ 15.0	306.2 /309.3
24	Low dose (SD 7.50)	120	1.0× 16mm	Fast(1.438)/ 23.0	322.9 /326.2
25	Low dose (SD 7.50)	120	2.0× 16mm	Detail(0.688)/ 11.0	290.9 /293.9
26	Low dose (SD 7.50)	120	2.0× 16mm	Standard(0.938)/ 15.0	276.6 /279.4
27	Low dose (SD 7.50)	120	2.0× 16mm	Fast(1.438)/ 23.0	318.8 /322
28	Quality (SD 3.00)	120	0.5× 16mm	Detail(0.688)/ 11.0	810.4 /1140
29	Quality (SD 3.00)	120	0.5× 16mm	Standard(0.938)/ 15.0	606.1 /852.7
30	Quality (SD 3.00)	120	0.5× 16mm	Fast(1.438)/ 23.0	410.4 /577.3
31	Quality (SD 3.00)	120	1.0× 16mm	Detail(0.688)/ 11.0	686.9 /966.3
32	Quality (SD 3.00)	120	1.0× 16mm	Standard(0.938)/ 15.0	522.2 /734.7
33	Quality (SD 3.00)	120	1.0× 16mm	Fast(1.438)/ 23.0	364.8 /513.2
34	Quality (SD 3.00)	120	2.0× 16mm	Detail(0.688)/ 11.0	657.9 /925.5
35	Quality (SD 3.00)	120	2.0× 16mm	Standard(0.938)/ 15.0	514.7 /724.1
36	Quality (SD 3.00)	120	2.0× 16mm	Fast(1.438)/ 23.0	377.8 /531.5
37	High Quality (SD 1.00)	120	0.5× 16mm	Detail(0.688)/ 11.0	1036.3 /1140
38	High Quality (SD 1.00)	120	0.5× 16mm	Standard(0.938)/ 15.0	775.1 /852.7
39	High Quality (SD 1.00)	120	0.5× 16mm	Fast(1.438)/ 23.0	536.9 /590.6
40	High Quality (SD 1.00)	120	1.0× 16mm	Detail(0.688)/ 11.0	878.4 /966.3
41	High Quality (SD 1.00)	120	1.0× 16mm	Standard(0.938)/ 15.0	667.9 /734.7
42	High Quality (SD 1.00)	120	1.0× 16mm	Fast(1.438)/ 23.0	466.5 /513.2
43	High Quality (SD 1.00)	120	2.0× 16mm	Detail(0.688)/ 11.0	841.3 /925.5
44	High Quality (SD 1.00)	120	2.0× 16mm	Standard(0.938)/ 15.0	658.2 /724.1
45	High Quality (SD 1.00)	120	2.0× 16mm	Fast(1.438)/ 23.0	474.7 /522.2

Appendix II: CT scan Quality control method and sheet result (2015-2016)

1. Insert the adapter from the body-arm rest into the table end.
2. Slide the phantom holder into the adapter and then mount the TOS phantom on the tube side of the phantom holder.
3. Insert the phantom centrally within the gantry.
4. Use the positioning lights to center on the QC insert part of the phantom
5. Create a new patient on the workstation and select the protocol located in XXXX

Multi Slice (S&V)	
Beam Collimation	**4x5mm**
kV	**120**
mA	**300**
Scan time	**1s**
Scan field	**Medium (320mm)**
Recon Filter	**FC70**
Stacking	**Stack-2 (2x10mm)**

6. Once acquired use the ROI tool that will fit each of the inserts.
7. Measure the mean HU for each insert and also in the center of the phantom for both images and record on the spreadsheet.

A	**Air**
B	**Delrin**
C	**Acrylic resin**
D	**Nylon**
E	**Polypropylene**
F	**Water**

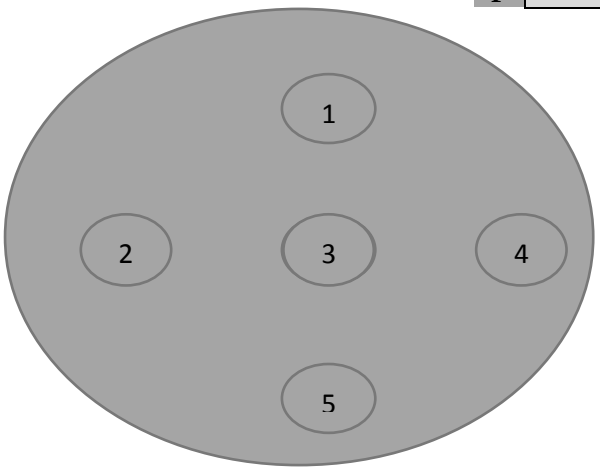

8. Position the medium water phantom centrally within the gantry aperture and acquire using the parameters above
9. Measure and record the standard deviation in the five positions.

The Christie NHS
NHS Foundation Trust

Christie Medical Physics & Engineering
The Christie NHS Foundation Trust
Withington, Manchester
M20 4BX, UK

Diagnostic X-Ray Equipment Performance and Radiation Safety Report

Report No: 743/SUSFU/16	Report Date: 9 October, 2016

Visit	
Establishment:	Salford University
Equipment location:	CT Suite, Mary Seacole Building
Equipment summary:	Toshiba TSX-101A/GC Aquillion S16
Date of tests:	22/09/2016
Performed by:	J. Czajka and D. Shaw
Reason:	Routine equipment performance measurements
Report	
Sent to:	Mr Andrew Tootell, RPS Chris Beaumont, RPS Dr Christie Theodorakou, CMPE
Previous relevant reports:	644/SUSFU/15
Areas needing attention	**Urgency**
None	
Additional notes:	
Follow-up	
Please report any action taken and outcome to the contact below	
Contact:	Dan Shaw on (0161) 446 3551 or e-mail daniel.shaw@christie.nhs.uk

Diagnostic Radiology and Radiation Protection Group
BSI registered - certificate number: FS 37543

1 List of Measurements Performed

Measurement	Tolerance	Outcome		
		Pass	Fail	Ref
General Radiation Safety				
Operation of controls and warning devices	Functioning as expected	Pass		
CT System				
Dosimetry CTDI	Baseline ±15%	Pass		2.1.1
Variation of output with helical pitch	Mean ±20%	Pass		
Image noise analysis	Inter slice mean ±10% Baseline ±10%	Pass		
CT number values	Baseline ±5HU(water) or ±10HU	Pass		
CT number uniformity	Difference between centre/periphery Body: Small ±10HU, Large ±20HU	Pass		
Artefacts	No visible artefacts	Pass		
Automatic Exposure Control/Dose Modulation	Functioning as expected	Pass		

2 Summary of Results and Recommendations

The results below are included for information or because there are recommendations concerning performance or safety. The results of all other measurements were satisfactory.

2.1 CT System

2.1.1 Computed Tomography Dose Index (CTDI)

The measured $CTDI_{100}$ at the isocentre in air were:

kV	Beam/detector collimation (mm)	Mode/SFOV	$CTDI_{100}$ (mGy/100 mAs)
120	12 (4x3)	Head/Small	28.7
"	2 (4x0.5)		71.5
"	4(1x4)		46.7
"	8 (4x2)		33.8
"	16 (4x4)		29.1
"	24 (4x6)		27.9
"	32 (4x8)		28.3
80	12 (4x3)		12.1
100	12 (4x3)		19.5
135	12 (4x3)		36.3
120	12 (4x3)	Body/Large	96.0
"	2 (4x0.5)		63.9
"	4(1x4)		46.2
"	8 (4x2)		43.3
"	16 (4x4)		39.8
"	24 (4x6)		40.7
"	32 (4x8)		38.5
80	12 (4x3)		21.7
100	12 (4x3)		32.2
135	12 (4x3)		53.4

These results are consistent with our previous measurements.

Doses in helical mode were within 5% of those in axial mode.

3 Conclusions

All our results were satisfactory and there are no recommendations to report.

AQUILION 16

Hospital:	SALFORD UNIVERSITY								
Serial No.	GCE0943448								
S-REF-No.	TSX-101A/GC.1510000925	Year 7				Year 8			
Test	Description:	A4	B4	C4	D4	A4	B4	C4	D4
	Date of Visit:	18.04.16	00.05.16	25.7.16	24.10.16	16.1.17	24.4.17		
GANTRY									
1.1	Anchor bolt check				✓				
1.2	Pillow block mounting bolt check				✓				
1.3	Rotation base mounting bolt check				✓				
1.4	Check of mounting plate of power cylinder mounting pin retaining plate				✓				
1.5	Power cylinder mounting bolt check				✓				
1.6	Tilt encoder gear setscrew check				✓				
1.7	Sector gear mounting bolt check				✓				
1.8	Encoder mounting plate check				✓				
1.9	LCSR brush assy. Mounting bolt check		✓				✓		
1.10	LCSR ring assy. Mounting bolt check		✓				✓		
1.11	ARM-L mounting bolt check				✓				
1.12	ARM-R mounting bolt check				✓				
1.13	Wedge slit Assy mounting bolt check				✓				
1.14	Oil cooler assy. Mounting bolt check				✓				
1.15	SRU-L-Assy mounting bolt check				✓				
1.16	SRU-H-Assy mounting bolt check				✓				
1.17	SRU-Power-Assy mounting bolt check				✓				
1.18	SRU-Power-Supply filter mounting bolt check				✓				
1.19	POWER-CONT-ASSY mounting bolt check				✓				
1.20	R.PSU-Assy mounting bolt check				✓				
1.21	PWB-Assy mounting bolt check				✓				
1.22	WEIGHT-Assy mounting bolt check				✓				
1.23	SSMD/DAS-Assy mounting nut and bolt check				✓				
1.24	X-ray tube mounting plate check				✓				
1.25	Photo-sensor cleaning				✓				
1.26	Check for abnormal sounds in the tilt power cylinder				✓				
1.27	Slit operation check & lubrication				✓				
1.28	Wedge slide mechanism check & lubrication				✓				
1.29	Large-current slip-ring cleaning	✓	✓	✓	✓	✓	✓		
1.30	Slipring brush abrasion check	✓	✓	✓	✓	✓	✓		
1.31	Tilt limit check & angle adjustment	✓	✓		✓				
1.32	Gantry rotation operation check	✓	✓	✓	✓	✓	✓		
1.33	Replacement, cleaning and operation check of positioning projector lamp		✓		✓		✓		
1.34	Cleaning the internal projector window of the dome section		✓		✓		✓		
1.35	Tilt cable routing check (cable movement)	✓	✓	✓	✓	✓	✓		
1.36a	Safety mechanism check: Emergency Function	✓	✓	✓	✓	✓	✓		
1.36b	Safety mechanism check: Tilt limit microswitch				✓				
1.37	Interlock check	✓	✓	✓	✓	✓	✓		
1.38	Operation check of the saftey circuit 1	✓	✓	✓	✓	✓	✓		
1.39	Operation check of the saftey circuit 2	✓	✓	✓	✓	✓	✓		
1.40	Operation check of the saftey circuit 3 (For TSX-101A/5)	✓	✓	✓	✓	✓	✓		
1.41	Gantry internal AC voltage check				✓				
1.42	Gantry internal DC voltage check				✓				
1.43	Operation check of fault-current protective breaker (NFB2)				✓				
1.44	Check for fan noise	✓	✓	✓	✓	✓	✓		
1.45	Filter cleaning	✓	✓	✓	✓	✓	✓		
1.46	Operating panel check	✓	✓	✓	✓	✓	✓		
1.47	Operating panel switch clearance check	✓	✓	✓	✓	✓	✓		
1.48	Off - Delay Timer		✓		✓		✓		
1.49	Check of the inside of the GTS unit	✓	✓	✓	✓	✓	✓		
1.50	Check of the inside of the rotation servo	✓	✓	✓	✓	✓	✓		
1.51	Couch height display check				✓				
1.52	Tilt angle display check				✓				
1.53	Rotation speed check				✓				
1.54	Couch movement speed check				✓				
1.55	Check for looseness of the terminal board of the gantry 200V input		✓		✓		✓		
1.56	Check for looseness of the screws & nuts on each terminal board								
1.57	Other - Visually check the gantry and couch cables								
1.58	Cleaning		✓		✓		✓		
COUCH									
2.1	Check of the bellows cover	✓	✓	✓	✓	✓	✓		
2.2	Check of the headrest	✓	✓	✓	✓	✓	✓		
2.3	Check for stains on the horizontal movement guide rails and rollers			✓					
2.4	Check for stains on the vertical movement rails			✓					
2.5	Check of the horizontal movement belt tension								

AQUILION 16

Hospital:	SALFORD UNIVERSITY								
Serial No.	GCE0943448								
S-REF-No.	TSX-101A/GC.1510000925	Year 7				Year 8			
Test	Description:	A4	B4	C4	D4	A4	B4	C4	D4
	Date of Visit:	3/8/16	8/8/16	25.7.16	31/10/16	16.1.17	24.2.17		
2.6	Check for interference & damage of couch internal cables	✓		✓	✓	✓			
2.7	Check of couch-top movement accuracy			✓					
2.8	Check for abnormal sounds from the patient couch during operation			✓					
2.9	Couch-top free movement operation check			✓					
2.10	Operation check of the gantry & patient couch interlocks	✓	✓	✓	✓	✓	✓		
2.11	Check of the limit mechanisms for couch vertical & horizontal movement	✓		✓		✓			
2.12	Check for oil leakage from the hydraulic circuit	✓		✓		✓			
2.13	Lubrication of the hydraulic cylinder rod			✓					
2.14	Check for cable disconnection & damage			✓					
2.15	Check of the tightening bolts			✓					
2.16	Anchor bolt tightening check			✓					
2.17	Measuring the natural fall rate			✓					
2.18	DC power supply check			✓					
2.19	Sensor check			✓					
X-RAY									
3.1	X-ray tube oil leakage check	✓	✓	✓	✓	✓	✓		
3.2	Heat exchanger oil leakage check	✓	✓	✓	✓	✓	✓		
3.3	Rubber hose oil leakage check	✓	✓	✓	✓	✓	✓		
3.4	X-ray tube rotor check	✓	✓	✓	✓	✓	✓		
3.5	X-ray tube receptacle check	✓	✓	✓	✓	✓	✓		
3.6	Heat exchanger fan and SRU fan check	✓	✓	✓	✓	✓	✓		
3.7	Heat exchanger operation (oil flow) check	✓	✓	✓	✓	✓	✓		
3.8	Coasting time check	✓	✓	✓	✓	✓	✓		
3.9	Check for loose screws due to vibration			✓					
3.10	X-ray tube voltage and current check	✓		✓		✓			
3.11	If check	✓		✓		✓			
3.12	X-ray exposure time check			✓					
3.13	Line voltage check during X-ray exposure			✓					
3.14	XC Battery replacement								
3.15	Charge/discharge check			✓					
3.16	Starter output check			✓					
3.17	Cable and connector check	✓	✓	✓	✓	✓	✓		
3.18	SRU molded connection check	✓	✓	✓	✓	✓	✓		
3.19	X-Ray tube bellows check	✓	✓	✓	✓	✓	✓		
DAS									
4.1	Main detector temperature measurement	✓	✓	✓	✓	✓	✓		
4.2	DAS unit connector looseness check	✓	✓	✓	✓	✓	✓		
4.3	Line voltage check	✓		✓		✓			
4.4	Fuse Check	✓		✓		✓			
4.5	Rotation check of the DAS cooling fans	✓	✓	✓	✓	✓	✓		
4.6	Main detector window cleaning	✓	✓	✓	✓	✓	✓		
MUDAT									
5.1	Operation check	✓	✓	✓	✓	✓	✓		
5.2	Cleaning & operation check			✓					
CONSOLE									
6.1	Monitor cleaning	✓	✓	✓	✓	✓	✓		
6.2	Air intake cleaning	✓	✓	✓	✓	✓	✓		
6.3	Air filter cleaning	✓	✓	✓	✓	✓	✓		
6.4	Air outlet cleaning	✓	✓	✓	✓	✓	✓		
6.5	Fan check	✓	✓	✓	✓	✓	✓		
6.6	Mouse cleaning	✓	✓	✓	✓	✓	✓		
6.7	PC (Power CONT) check	✓		✓	✓	✓			
6.8	Checking the emergency function	✓		✓		✓			
6.8	Check of the emergency function (OLP<30%)	✓		✓		✓			
6.9	Check of the intercom function	✓	✓	✓	✓	✓	✓		
6.10	Cleaning	✓	✓	✓	✓	✓	✓		
QA									
7.1	Image noise measurement	✓	✓	✓	✓	✓	✓		
7.2	CT number measurement using the TOS phantom	✓	✓	✓	✓	✓	✓		
7.3	Streak & Artifact test	✓		✓		✓			
7.4	Annual QA	✓				X			
	Engineer s Initials:	SP	SP	CK	SP	CK	CK		

Appendix III: All section for loaded and irradiated ATOM phantom MOSFETs method

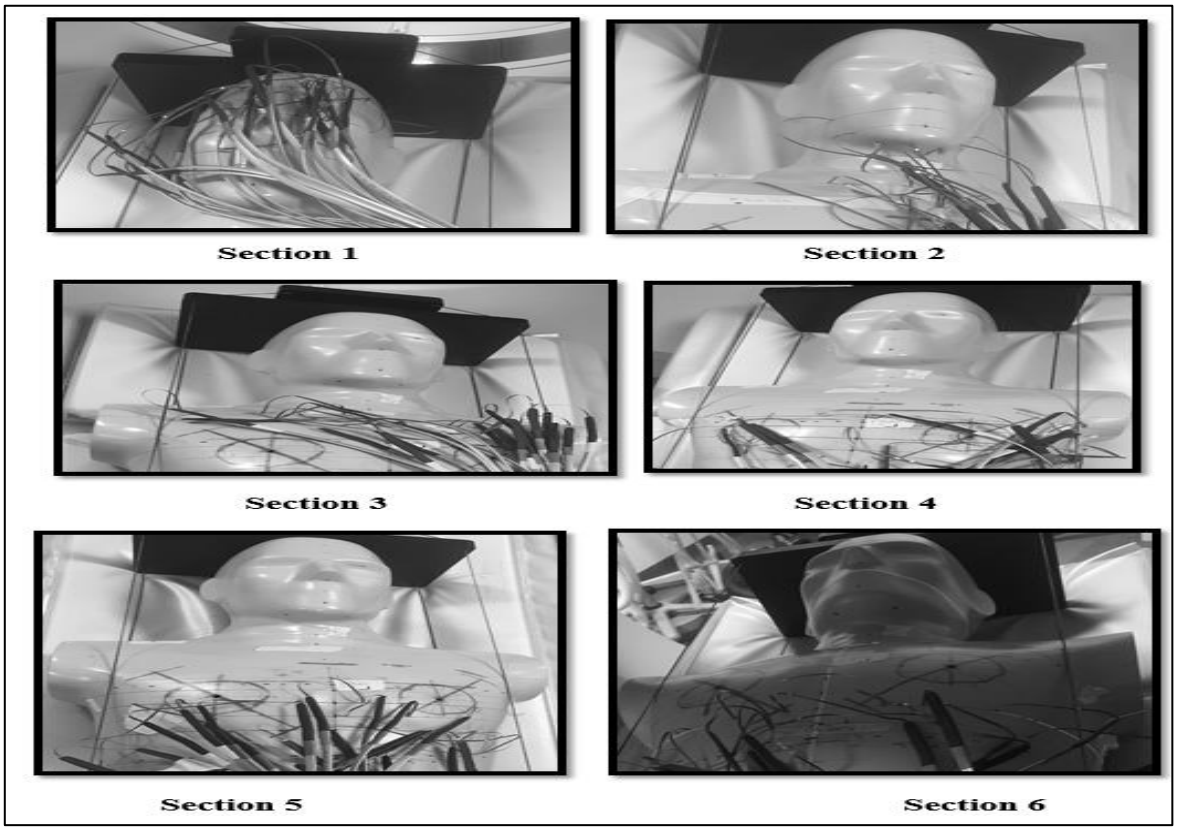

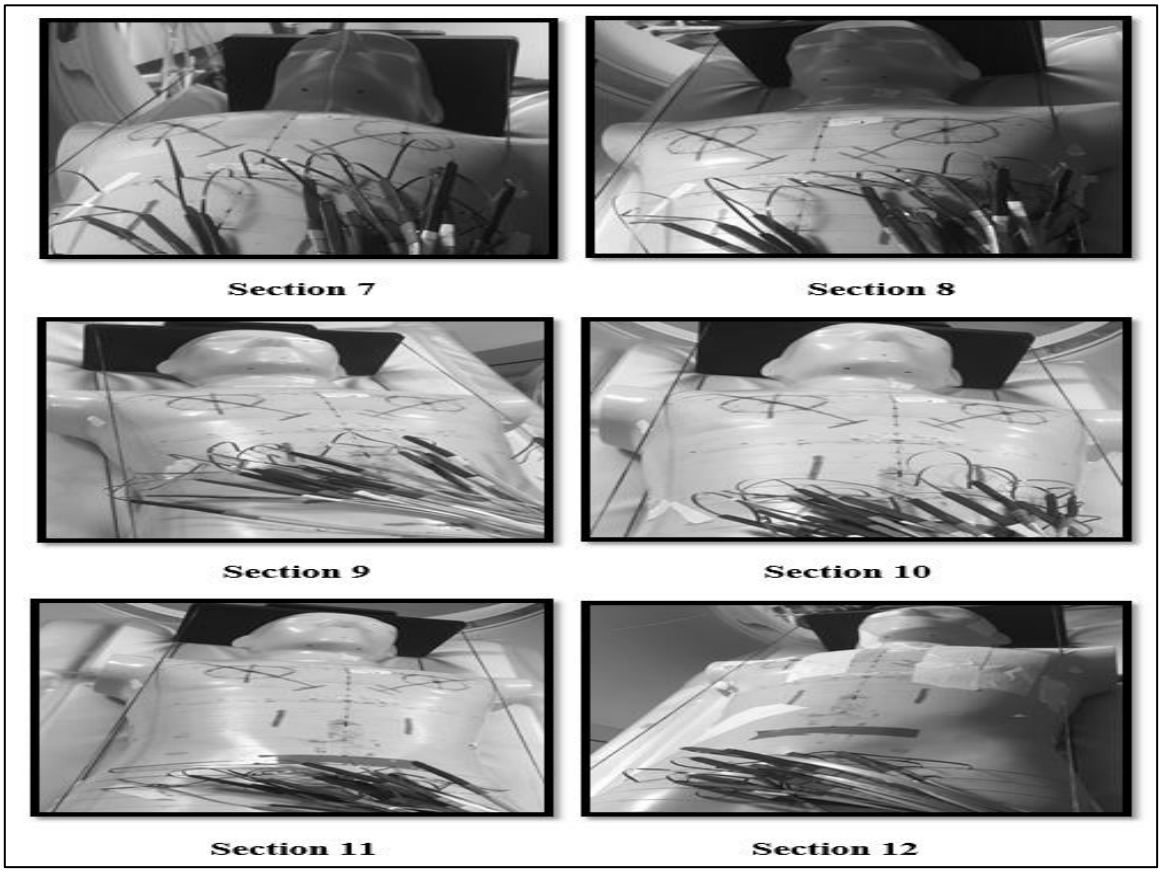

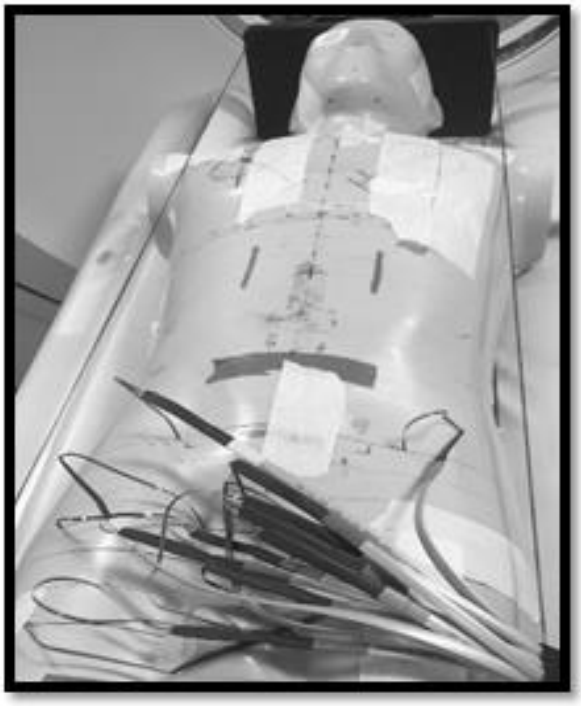

Section 13

Section 14

Section numbers	organs numbers
1	**1-20**
2	**21-40**
3	**41-60**
4	**61-80**
5	**81-100**
6	**101-120**
7	**121-140**
8	**141-160**
9	**161-180**
10	**181-200**
11	**201-220**
12	**221-240**
13	**241-260**
14	**261-273**

Appendix IV: University of Salford ethical approval

University of Salford MANCHESTER

Research, Innovation and Academic Engagement Ethical Approval Panel

Research Centres Support Team
G0.3 Joule House
University of Salford
M5 4WT

T +44(0)161 295 2280

www.salford.ac.uk/

2 September 2016

Dear Alrowily,

RE: ETHICS APPLICATION HSCR 16-89 – An investigation into observer variability when assessing abdominal CT image quality using CEC criteria.

Based on the information you provided, I am pleased to inform you that your application HSCR16-89 has been approved.

If there are any changes to the project and/ or its methodology, please inform the Panel as soon as possible by contacting Health-ResearchEthics@salford.ac.uk

Yours sincerely,

pp. Stephen Pearson (Deputy Chair)

On behalf of:

Appendix V: Research participant's consent form

Research Participant Consent Form

Title of the project: An investigation into observer variability when assessing abdominal CT image quality using CEC criteria.

Name of Researcher:	Maily Alrowily
Email Address:	M.Alrowily@edu.salford.ac.uk

Research Governance and Ethics Committee Approval (RGEC) Ref. NO: HSCR16-89

Name of observer:	

Please read the following statements carefully and put your initials in the in the box to show that you have read understood and agreed to each statement.

Please initial each box

1. I accept that I have read and comprehended the information sheet (**21/7/2016/V1**) regarding the above research. I have had a chance to contemplate the data, present queries and I have been given adequate responses to these. ☐
2. I am aware that my participation in this study is voluntary and that I am at liberty to leave at any point. I additionally understand that no financial benefit or otherwise will result from my participation in this study ☐
3. I am aware that the information documented in this research will be evaluated and employed in a doctoral thesis and later publications. My particulars will remain confidential and only the main researcher will be capable of recognizing my information. ☐
4. I am aware that the University 'of Salford Research Ethics Committee may demand to view all information obtained in this study project, and I hereby provide these suitable individuals my consent to acquire this data. ☐
5. **I agree to take part in the above study.** ☐

Name of participant	*Signature*	*Date*

Appendix VI: All abdominal CT scan organs dose(mGy) with different parameters MOSFET method FTC data

Protocols NO.	Brain	ABM	Thyroid	Oesophagus	Lungs	Breasts	Liver	Stomach	Bladder	Colon	Salivary Glands	Testes
1	0.031	2.654	0.249	2.135	2.682	0.659	20.354	25.407	1.481	12.195	0.048	0.759
2	0.000	2.127	0.201	1.362	2.352	0.788	15.193	18.929	1.306	10.002	0.052	0.707
3	0.002	1.520	0.085	1.022	1.674	0.709	10.716	13.107	0.972	7.070	0.029	1.090
4	0.025	2.537	0.227	1.934	2.633	0.862	18.383	22.950	1.370	11.569	0.084	0.795
5	0.045	1.976	0.145	1.477	2.450	0.806	13.493	16.907	1.245	8.533	0.083	1.400
6	0.048	1.570	0.159	1.385	2.188	0.759	9.606	11.430	1.182	6.629	0.075	1.325
7	0.023	2.864	0.308	2.298	3.833	1.120	18.038	19.886	1.687	10.880	0.029	0.819
8	0.017	2.373	0.074	2.019	3.408	0.852	14.117	15.829	1.375	8.952	0.083	0.982
9	0.076	2.048	0.208	1.936	3.019	1.070	10.634	10.986	1.326	6.355	0.026	0.931
10	0.017	1.243	0.078	0.742	1.313	0.483	8.471	11.506	1.031	5.703	0.050	0.915
11	0.055	1.022	0.017	0.701	1.077	0.336	6.682	9.062	0.934	4.407	0.066	0.945
12	0.042	0.853	0.027	0.636	0.870	0.323	4.608	6.414	0.969	3.417	0.020	1.160
13	0.032	1.188	0.018	1.033	1.297	0.398	7.623	9.440	0.952	5.358	0.015	1.375
14	0.053	1.043	0.094	0.736	1.081	0.373	6.101	7.983	0.944	4.442	0.007	1.254
15	0.045	0.815	0.031	0.767	0.997	0.485	4.520	6.159	0.874	2.838	0.032	1.275
16	0.035	1.409	0.056	0.864	1.645	0.571	7.961	9.046	1.183	5.278	0.031	0.914
17	0.043	1.230	0.075	0.771	1.444	0.500	6.521	7.794	1.014	4.447	0.096	0.621
18	0.019	1.112	0.097	0.946	1.352	0.457	4.577	5.772	0.907	3.289	0.045	1.035
19	0.012	2.213	0.119	1.505	2.337	0.769	16.109	21.364	1.326	10.312	0.043	0.798
20	0.026	1.733	0.108	1.129	1.823	0.750	12.771	16.021	1.203	7.960	0.041	1.234
21	0.023	1.341	0.087	1.106	1.391	0.329	8.786	11.240	1.101	6.188	0.039	1.009
22	0.052	2.000	0.140	1.481	2.129	0.724	14.306	18.507	1.195	9.888	0.051	1.100
23	0.011	1.829	0.169	1.036	1.918	0.839	11.227	14.587	1.119	7.506	0.067	0.835
24	0.046	1.373	0.075	0.836	1.762	0.488	8.269	9.559	1.059	5.351	0.007	0.870
25	0.062	2.328	0.214	1.572	2.884	1.006	14.468	17.121	1.210	9.039	0.095	0.821
26	0.033	2.098	0.076	1.936	2.598	0.921	11.489	13.279	1.189	7.042	0.050	1.320
27	0.004	1.888	0.118	1.705	2.369	0.357	8.180	9.311	1.151	5.451	0.102	0.912
28	0.020	3.145	0.176	2.559	3.414	1.305	24.663	32.221	1.744	14.941	0.113	1.530
29	0.034	2.530	0.266	2.118	2.687	0.938	18.412	24.407	1.362	11.155	0.087	0.967
30	0.029	1.722	0.167	0.920	2.017	0.793	12.772	15.997	1.262	8.205	0.028	0.605
31	0.042	2.887	0.174	2.174	3.310	1.340	21.433	26.321	1.477	13.320	0.086	1.310
32	0.003	2.379	0.140	1.846	2.685	0.895	16.656	20.186	1.259	10.449	0.063	1.245
33	0.031	1.885	0.110	1.312	2.556	0.834	12.403	13.766	1.174	7.538	0.033	0.943
34	0.042	3.394	0.276	2.306	4.593	1.310	21.400	24.657	1.817	13.798	0.053	1.165
35	0.045	2.948	0.149	2.399	4.281	1.271	17.041	18.579	1.480	10.428	0.123	1.145
36	0.060	2.387	0.202	2.346	3.670	1.184	12.178	14.284	1.494	7.417	0.083	1.032
37	0.067	4.504	0.390	3.209	4.982	1.495	36.400	46.629	2.040	22.695	0.226	1.220
38	0.056	3.525	0.315	2.443	3.804	1.275	26.740	34.357	1.761	16.363	0.142	1.150
39	0.068	2.543	0.115	1.753	2.847	1.145	18.187	23.200	1.437	12.325	0.068	1.063
40	0.067	4.139	0.415	3.256	4.635	1.560	30.562	38.371	1.814	19.915	0.223	1.562
41	0.024	3.145	0.204	2.423	3.858	1.700	23.387	30.043	1.584	15.566	0.132	1.520
42	0.041	2.521	0.165	1.914	3.320	1.255	15.825	20.007	1.325	10.598	0.025	0.793
43	0.035	4.380	0.274	3.868	5.733	2.025	29.755	34.786	2.101	17.696	0.178	1.840
44	0.054	3.740	0.394	3.237	5.351	1.805	23.090	26.114	1.664	14.183	0.074	0.672
45	0.045	3.322	0.231	3.180	4.582	1.120	16.962	17.364	1.866	10.257	0.046	1.760

Protocols NO.	Thymus	Spleen	Kidneys	Adrenals	Heart	Pancreas	Gall Bladder	Prostate	Oral Mucosa	Small Intestine	Extrathoracic
1	0.442	19.550	24.206	12.695	2.160	23.800	28.980	0.624	0.048	9.222	0.272
2	0.333	14.622	17.725	10.315	1.635	18.100	21.020	0.726	0.052	7.288	0.316
3	0.204	10.562	11.763	5.995	0.999	11.800	14.940	0.956	0.029	6.646	0.116
4	0.389	18.104	20.256	12.785	2.400	21.500	26.420	1.004	0.084	9.242	0.211
5	0.272	13.650	15.094	9.520	1.437	16.240	19.320	0.904	0.083	7.456	0.197
6	0.161	9.697	10.578	8.125	1.400	11.034	12.800	0.812	0.075	5.866	0.150
7	0.624	16.925	18.806	13.050	2.640	19.840	25.280	1.084	0.029	11.364	0.133
8	0.472	14.177	14.425	10.445	2.150	15.060	17.860	0.706	0.083	8.596	0.214
9	0.307	10.693	9.897	7.835	2.055	10.604	12.064	0.888	0.026	6.762	0.078
10	0.203	8.650	9.982	5.070	0.954	10.478	12.980	0.780	0.050	4.032	0.031
11	0.165	7.288	7.673	4.595	1.067	7.794	9.392	0.631	0.066	3.272	0.048
12	0.067	5.396	5.573	3.115	0.764	6.054	7.284	0.725	0.020	3.049	0.126
13	0.182	7.596	9.137	4.855	1.065	8.898	11.800	0.559	0.015	4.347	0.143
14	0.154	6.538	6.709	4.175	0.882	6.748	8.366	0.663	0.007	3.701	0.235
15	0.250	5.148	4.512	3.230	0.629	5.308	5.206	0.360	0.032	2.840	0.102
16	0.125	7.543	8.199	5.975	1.084	8.170	10.088	0.413	0.031	5.230	0.000
17	0.297	6.491	6.258	4.595	0.808	7.518	7.496	0.624	0.096	4.184	0.156
18	0.098	5.033	4.429	3.510	0.967	5.248	5.844	0.606	0.045	3.066	0.095
19	0.356	16.075	19.519	10.395	1.955	19.460	24.560	0.875	0.043	7.896	0.201
20	0.227	12.093	14.724	8.565	1.735	14.960	17.960	0.712	0.041	7.288	0.197

21	**0.090**	**9.018**	**9.847**	**5.545**	**1.176**	**9.886**	**11.240**	**0.879**	**0.039**	**4.818**	**0.051**
22	**0.260**	**14.434**	**16.431**	**9.285**	**1.249**	**17.260**	**20.840**	**0.768**	**0.051**	**8.178**	**0.207**
23	**0.174**	**11.565**	**12.668**	**7.960**	**1.375**	**13.600**	**15.980**	**0.676**	**0.067**	**6.616**	**0.167**
24	**0.141**	**8.340**	**9.089**	**5.865**	**1.185**	**9.002**	**9.546**	**0.524**	**0.007**	**4.462**	**0.092**
25	**0.299**	**14.472**	**15.950**	**10.705**	**1.935**	**15.760**	**19.360**	**0.955**	**0.095**	**8.926**	**0.207**
26	**0.425**	**11.824**	**11.833**	**8.075**	**2.165**	**12.760**	**14.660**	**1.060**	**0.050**	**6.688**	**0.187**
27	**0.264**	**7.952**	**8.131**	**6.230**	**1.750**	**9.152**	**10.268**	**0.662**	**0.102**	**5.590**	**0.333**
28	**0.607**	**23.667**	**28.400**	**15.495**	**2.605**	**29.300**	**34.700**	**0.970**	**0.113**	**10.366**	**0.235**
29	**0.418**	**17.738**	**21.069**	**11.995**	**2.120**	**21.660**	**26.100**	**1.059**	**0.087**	**8.784**	**0.459**
30	**0.374**	**12.190**	**14.006**	**8.745**	**1.635**	**14.780**	**17.360**	**1.089**	**0.028**	**6.808**	**0.116**
31	**0.356**	**21.308**	**24.663**	**14.440**	**2.440**	**24.500**	**29.740**	**1.022**	**0.086**	**11.022**	**0.408**
32	**0.334**	**16.542**	**18.481**	**10.860**	**2.550**	**18.680**	**22.720**	**1.100**	**0.063**	**10.368**	**0.248**
33	**0.221**	**12.058**	**12.614**	**9.200**	**1.860**	**12.680**	**15.320**	**1.007**	**0.033**	**7.002**	**0.003**
34	**0.499**	**20.600**	**23.081**	**15.150**	**3.360**	**23.860**	**27.700**	**1.216**	**0.053**	**13.974**	**0.207**
35	**0.651**	**15.908**	**17.488**	**13.450**	**2.935**	**17.620**	**21.860**	**0.971**	**0.123**	**10.356**	**0.293**
36	**0.536**	**11.812**	**11.810**	**10.170**	**2.215**	**13.080**	**14.260**	**0.899**	**0.083**	**7.594**	**0.245**
37	**0.699**	**35.283**	**42.500**	**23.550**	**4.060**	**44.360**	**52.580**	**1.560**	**0.226**	**17.038**	**0.418**
38	**0.553**	**25.875**	**31.463**	**16.820**	**3.105**	**32.080**	**38.420**	**1.013**	**0.142**	**12.070**	**0.527**
39	**0.455**	**18.214**	**20.800**	**12.400**	**2.030**	**22.580**	**26.620**	**1.096**	**0.068**	**10.928**	**0.197**
40	**0.535**	**29.358**	**35.344**	**19.650**	**3.825**	**34.840**	**41.540**	**0.864**	**0.223**	**18.842**	**0.245**
41	**0.667**	**23.583**	**26.375**	**16.800**	**2.950**	**26.980**	**31.720**	**1.123**	**0.132**	**12.898**	**0.323**
42	**0.418**	**16.442**	**18.025**	**12.400**	**2.195**	**18.600**	**19.600**	**1.045**	**0.025**	**10.572**	**0.214**
43	**0.872**	**27.150**	**31.519**	**21.150**	**3.800**	**33.080**	**36.320**	**1.087**	**0.178**	**15.014**	**0.469**
44	**0.639**	**22.508**	**24.144**	**17.000**	**3.145**	**24.100**	**28.800**	**1.513**	**0.074**	**12.910**	**0.459**
45	**0.604**	**16.442**	**16.069**	**12.600**	**3.550**	**17.300**	**19.000**	**1.123**	**0.046**	**10.916**	**0.238**

Appendix VII: All abdominal CT scan organs dose (mGy) with different parameters MOSFET method corrected ATCM

Protocols NO.	Brain	ABM	Thyroid	Oesophagus	Lungs	Breasts	Liver	Stomach	Bladder	Colon	Salivary Glands	Testes
1	0.021	2.563	0.136	1.945	3.099	1.091	22.100	26.381	0.892	12.847	0.115	1.108
2	0.052	2.126	0.132	1.810	2.627	0.999	17.469	20.614	1.180	10.491	0.106	1.135
3	0.025	1.856	0.143	1.379	2.176	0.890	13.537	16.362	1.046	8.105	0.049	0.815
4	0.063	2.380	0.224	1.820	2.784	1.023	18.683	21.822	1.056	11.461	0.121	0.866
5	0.004	2.012	0.150	1.585	2.461	0.962	14.532	18.067	1.028	8.878	0.033	0.982
6	0.008	1.854	0.156	1.383	2.625	1.036	12.484	14.613	1.028	7.133	0.075	1.043
7	0.027	2.428	0.198	1.862	3.271	1.033	16.771	18.247	1.166	9.820	0.079	1.020
8	0.022	2.337	0.107	1.967	3.537	1.320	14.344	15.202	1.040	8.225	0.010	0.617
9	0.052	2.207	0.123	2.429	3.460	0.665	11.997	13.254	1.208	6.829	0.056	0.716
10	0.011	1.185	0.102	0.412	1.158	0.540	7.447	9.765	1.076	4.643	0.082	0.879
11	0.029	1.028	0.028	0.719	1.061	0.253	6.145	8.178	0.746	3.904	0.010	1.105
12	0.009	1.006	0.069	0.774	1.047	0.276	6.540	8.159	0.894	4.369	0.026	0.778
13	0.055	1.019	0.038	0.767	1.003	0.530	6.309	8.725	0.739	4.092	0.047	1.153
14	0.014	0.926	0.077	0.744	1.056	0.450	5.421	7.296	1.019	3.830	0.010	1.255
15	0.015	1.072	0.093	0.681	1.308	0.466	6.158	7.028	0.780	3.769	0.062	0.862
16	0.025	0.989	0.029	0.721	1.239	0.574	5.411	7.170	0.959	3.575	0.032	0.746
17	0.005	1.087	0.007	0.742	1.237	0.599	4.991	6.750	0.890	3.601	0.029	1.033
18	0.071	1.406	0.143	1.105	1.855	0.256	5.312	5.868	0.776	3.476	0.054	1.284
19	0.038	1.924	0.097	1.262	2.127	0.685	14.906	18.380	1.102	9.139	0.056	1.029
20	0.056	1.888	0.113	1.540	2.123	0.729	14.358	16.358	1.231	8.276	0.087	1.186
21	0.084	1.890	0.256	1.478	2.357	0.647	13.769	16.832	1.120	8.386	0.045	1.441
22	0.012	1.822	0.181	1.320	2.025	0.840	12.682	15.127	0.985	7.163	0.046	1.038
23	0.049	1.757	0.108	1.286	2.003	0.596	11.759	14.526	1.096	7.225	0.029	1.149
24	0.061	2.078	0.147	1.673	2.900	1.023	12.758	14.400	1.129	7.350	0.094	1.554
25	0.024	1.795	0.131	1.340	2.531	0.616	11.308	13.141	1.040	6.823	0.016	0.840
26	0.042	1.935	0.154	1.699	2.619	0.788	10.228	11.811	1.134	6.494	0.034	1.194
27	0.030	2.303	0.120	2.552	3.812	1.203	12.402	12.835	1.355	6.980	0.066	1.267
28	0.070	3.491	0.348	2.476	3.771	1.578	28.382	35.047	1.593	16.380	0.215	1.148
29	0.064	2.716	0.295	1.885	3.182	1.201	21.150	26.014	1.344	13.364	0.087	1.077
30	0.025	1.904	0.137	1.562	2.186	0.794	14.286	18.153	1.048	9.006	0.085	1.098
31	0.010	3.137	0.206	1.985	3.399	1.600	24.354	29.177	1.554	14.999	0.067	0.783
32	0.022	2.506	0.186	1.621	2.611	1.031	17.939	21.423	1.242	11.927	0.048	1.049
33	0.005	2.293	0.202	1.713	2.593	0.755	13.233	15.051	1.061	8.046	0.028	0.807
34	0.018	3.322	0.310	2.628	4.474	1.440	22.526	25.770	1.533	13.423	0.082	0.809
35	0.039	3.054	0.233	2.171	4.158	1.152	18.351	20.052	1.402	10.831	0.061	0.995
36	0.018	2.519	0.179	2.560	3.651	1.400	13.066	13.248	1.348	7.974	0.044	0.903
37	0.035	4.307	0.441	3.166	4.670	2.073	36.182	45.435	1.764	22.252	0.106	1.013
38	0.016	3.454	0.326	2.219	3.475	1.364	26.060	34.084	1.780	16.348	0.096	0.977
39	0.035	2.498	0.174	1.957	2.736	1.145	18.753	23.799	1.348	11.698	0.066	1.109
40	0.058	3.986	0.327	2.741	4.249	1.836	30.339	36.247	1.900	19.204	0.136	1.273
41	0.016	3.111	0.366	2.479	3.624	1.405	22.681	28.675	1.364	14.693	0.077	0.786
42	0.033	2.445	0.151	1.779	3.267	0.772	15.548	18.701	1.533	10.411	0.067	1.186
43	0.055	4.641	0.356	3.487	5.807	1.482	30.915	36.026	1.956	17.956	0.046	1.509
44	0.032	3.768	0.351	3.295	5.142	1.700	23.317	25.974	1.787	14.583	0.076	1.459
45	0.059	3.281	0.267	3.372	4.671	1.441	16.699	19.422	1.649	11.640	0.097	0.734

Protocols NO.	Thymus	Spleen	Kidneys	Adrenals	Heart	Pancreas	Gall Bladder	Prostate	Oral Mucosa	Small Intestine	Extrathoracic
1	0.424	21.708	24.239	14.287	2.537	24.645	29.283	0.550	0.115	8.992	0.232
2	0.402	17.101	19.367	11.491	2.152	20.431	22.886	0.778	0.106	8.692	0.248
3	0.316	13.313	15.276	9.046	1.671	15.535	18.262	0.691	0.049	8.071	0.128
4	0.418	18.134	20.066	11.457	1.718	21.372	24.182	0.653	0.121	9.246	0.285
5	0.363	14.622	15.680	9.615	2.036	16.367	19.285	0.663	0.033	8.093	0.281
6	0.341	12.230	12.867	8.627	1.551	12.657	14.444	0.772	0.075	6.929	0.135
7	0.465	15.969	17.279	13.127	2.278	18.385	20.445	0.764	0.079	8.605	0.239
8	0.384	13.792	13.690	10.979	2.250	14.062	16.858	0.975	0.010	8.133	0.176
9	0.459	11.849	10.911	9.240	2.097	11.934	13.721	0.991	0.056	8.070	0.202
10	0.153	8.864	8.360	5.416	0.726	9.354	10.198	0.576	0.082	3.911	0.044
11	0.225	7.015	6.928	3.946	0.616	7.352	8.812	0.737	0.010	3.210	0.081
12	0.098	7.276	6.866	4.025	0.876	7.877	8.646	0.838	0.026	3.909	0.000
13	0.237	7.218	6.761	4.767	0.693	8.186	8.675	0.699	0.047	3.360	0.152
14	0.185	6.093	5.756	3.941	0.647	6.630	7.218	0.806	0.010	3.696	0.209
15	0.055	6.462	5.853	4.733	0.899	6.582	7.826	0.710	0.062	3.939	0.051
16	0.117	6.247	6.042	3.990	0.667	6.855	7.721	0.549	0.032	4.069	0.000
17	0.128	5.870	5.153	3.827	0.723	5.780	6.253	0.955	0.029	3.848	0.125
18	0.271	5.949	4.822	5.015	1.111	5.392	5.729	0.803	0.054	3.622	0.091

19	**0.318**	**15.388**	**16.163**	**9.941**	**2.045**	**16.693**	**18.931**	**0.517**	**0.056**	**7.446**	**0.091**
20	**0.340**	**14.578**	**15.501**	**10.015**	**1.842**	**15.980**	**18.733**	**0.631**	**0.087**	**7.242**	**0.216**
21	**0.357**	**14.210**	**15.124**	**8.738**	**1.683**	**15.287**	**17.762**	**0.809**	**0.045**	**6.505**	**0.101**
22	**0.389**	**12.406**	**13.323**	**8.262**	**1.359**	**14.693**	**15.644**	**0.955**	**0.046**	**6.337**	**0.178**
23	**0.354**	**12.708**	**12.098**	**8.104**	**1.574**	**13.604**	**13.446**	**0.902**	**0.029**	**8.303**	**0.051**
24	**0.336**	**12.786**	**12.488**	**9.361**	**1.762**	**12.970**	**15.030**	**0.833**	**0.094**	**6.778**	**0.168**
25	**0.312**	**11.405**	**11.034**	**8.896**	**1.569**	**12.416**	**11.881**	**0.911**	**0.016**	**6.270**	**0.340**
26	**0.408**	**10.989**	**10.564**	**7.965**	**2.069**	**11.071**	**12.277**	**0.946**	**0.034**	**7.301**	**0.178**
27	**0.431**	**12.461**	**11.278**	**9.886**	**2.802**	**11.941**	**12.792**	**0.828**	**0.066**	**6.596**	**0.145**
28	**0.654**	**27.150**	**33.315**	**17.808**	**3.117**	**33.711**	**41.360**	**0.964**	**0.215**	**11.163**	**0.297**
29	**0.364**	**19.775**	**24.757**	**13.898**	**2.396**	**24.924**	**31.123**	**0.803**	**0.087**	**11.124**	**0.116**
30	**0.305**	**13.867**	**16.688**	**10.681**	**1.795**	**16.493**	**20.588**	**0.580**	**0.085**	**8.443**	**0.247**
31	**0.494**	**22.453**	**26.850**	**17.346**	**2.893**	**27.583**	**35.062**	**1.049**	**0.067**	**12.202**	**0.121**
32	**0.346**	**17.654**	**20.345**	**12.547**	**2.023**	**20.687**	**26.303**	**0.586**	**0.048**	**10.311**	**0.285**
33	**0.317**	**13.169**	**13.991**	**9.704**	**2.243**	**14.019**	**16.180**	**0.722**	**0.028**	**7.392**	**0.218**
34	**0.591**	**21.623**	**24.508**	**16.386**	**3.480**	**24.867**	**31.365**	**0.872**	**0.082**	**13.700**	**0.288**
35	**0.474**	**17.441**	**18.266**	**14.467**	**3.007**	**18.782**	**23.047**	**1.048**	**0.061**	**10.686**	**0.206**
36	**0.586**	**12.482**	**12.459**	**10.877**	**2.872**	**12.512**	**15.171**	**0.732**	**0.044**	**8.760**	**0.293**
37	**0.954**	**34.250**	**41.943**	**23.500**	**3.641**	**43.291**	**51.455**	**1.066**	**0.106**	**17.144**	**0.346**
38	**0.507**	**25.894**	**31.545**	**17.182**	**2.582**	**32.036**	**40.055**	**1.315**	**0.096**	**11.733**	**0.297**
39	**0.378**	**17.892**	**21.097**	**12.232**	**2.036**	**22.491**	**25.418**	**0.765**	**0.066**	**10.549**	**0.306**
40	**0.862**	**29.053**	**35.449**	**20.136**	**3.664**	**35.273**	**44.564**	**1.288**	**0.136**	**17.200**	**0.309**
41	**0.709**	**22.076**	**26.023**	**16.818**	**2.918**	**27.309**	**32.582**	**1.179**	**0.077**	**13.753**	**0.523**
42	**0.507**	**16.705**	**17.597**	**12.455**	**2.223**	**18.836**	**21.455**	**1.083**	**0.067**	**9.229**	**0.318**
43	**0.799**	**28.598**	**31.000**	**20.455**	**3.423**	**32.073**	**39.036**	**0.910**	**0.046**	**16.707**	**0.377**
44	**0.568**	**22.424**	**23.972**	**18.227**	**3.414**	**23.473**	**28.109**	**1.284**	**0.076**	**14.395**	**0.312**
45	**0.537**	**15.674**	**15.778**	**13.182**	**3.195**	**16.745**	**19.345**	**1.048**	**0.097**	**11.220**	**0.393**

Appendix VIII: All abdominal CT scan organs dose (mGy) with different parameters MOSFET method from uncorrected ATCM (raw) data

protocols	Brain	ABM	Thyroid	Oesophagus	Lungs	Breasts	Liver	Stomach	Bladder	Colon	Salivary Glands	Testes
1	0.031	3.759	0.199	2.852	4.545	1.600	32.407	38.686	1.308	18.838	0.169	1.625
2	0.077	3.118	0.193	2.654	3.853	1.465	25.617	30.229	1.730	15.385	0.156	1.665
3	0.037	2.721	0.210	2.022	3.191	1.305	19.851	23.993	1.533	11.885	0.072	1.195
4	0.093	3.490	0.328	2.670	4.082	1.500	27.397	32.000	1.549	16.806	0.177	1.270
5	0.006	2.951	0.221	2.324	3.608	1.410	21.309	26.493	1.508	13.018	0.049	1.440
6	0.012	2.719	0.229	2.028	3.850	1.520	18.307	21.429	1.507	10.460	0.110	1.530
7	0.039	3.561	0.290	2.730	4.797	1.515	24.593	26.757	1.710	14.400	0.115	1.495
8	0.033	3.427	0.157	2.885	5.187	1.935	21.034	22.293	1.525	12.061	0.014	0.905
9	0.076	3.236	0.181	3.561	5.074	0.975	17.593	19.436	1.771	10.015	0.083	1.050
10	0.011	1.197	0.103	0.416	1.170	0.546	7.521	9.863	1.087	4.689	0.083	0.888
11	0.030	1.039	0.028	0.726	1.071	0.256	6.206	8.260	0.754	3.943	0.010	1.117
12	0.009	1.017	0.069	0.782	1.058	0.279	6.606	8.241	0.903	4.413	0.027	0.786
13	0.055	1.029	0.038	0.775	1.013	0.536	6.372	8.812	0.747	4.133	0.047	1.165
14	0.014	0.936	0.078	0.752	1.067	0.454	5.475	7.369	1.029	3.868	0.010	1.268
15	0.015	1.083	0.094	0.688	1.321	0.471	6.220	7.098	0.787	3.807	0.063	0.871
16	0.026	0.999	0.030	0.728	1.252	0.580	5.465	7.241	0.968	3.611	0.032	0.754
17	0.005	1.098	0.007	0.749	1.249	0.605	5.041	6.818	0.899	3.637	0.030	1.044
18	0.072	1.420	0.144	1.116	1.874	0.258	5.365	5.926	0.784	3.510	0.054	1.297
19	0.038	1.943	0.098	1.275	2.148	0.692	15.055	18.564	1.113	9.230	0.056	1.040
20	0.057	1.907	0.114	1.556	2.144	0.736	14.501	16.521	1.243	8.358	0.088	1.198
21	0.085	1.909	0.258	1.493	2.381	0.653	13.906	17.000	1.131	8.470	0.045	1.455
22	0.012	1.840	0.183	1.333	2.045	0.848	12.809	15.279	0.995	7.234	0.047	1.049
23	0.050	1.774	0.109	1.299	2.023	0.602	11.877	14.671	1.107	7.297	0.030	1.160
24	0.062	2.098	0.149	1.689	2.929	1.033	12.886	14.544	1.140	7.424	0.095	1.570
25	0.024	1.813	0.132	1.354	2.556	0.622	11.421	13.272	1.050	6.891	0.016	0.849
26	0.042	1.955	0.156	1.716	2.646	0.796	10.330	11.929	1.146	6.559	0.034	1.206
27	0.030	2.326	0.121	2.578	3.850	1.215	12.526	12.963	1.369	7.050	0.067	1.280
28	0.099	4.910	0.490	3.483	5.304	2.220	39.924	49.300	2.241	23.041	0.302	1.615
29	0.089	3.821	0.416	2.651	4.476	1.690	29.751	36.593	1.891	18.799	0.122	1.515
30	0.035	2.679	0.192	2.197	3.075	1.117	20.096	25.536	1.475	12.669	0.120	1.545
31	0.014	4.413	0.290	2.792	4.781	2.250	34.259	41.043	2.186	21.098	0.095	1.102
32	0.031	3.525	0.262	2.280	3.673	1.450	25.234	30.136	1.748	16.777	0.067	1.475
33	0.007	3.226	0.284	2.410	3.648	1.063	18.614	21.171	1.492	11.318	0.039	1.135
34	0.025	4.673	0.436	3.697	6.294	2.025	31.686	36.250	2.157	18.882	0.116	1.139
35	0.055	4.295	0.328	3.055	5.848	1.620	25.814	28.207	1.972	15.235	0.086	1.400
36	0.025	3.544	0.251	3.601	5.136	1.970	18.379	18.636	1.896	11.216	0.061	1.270
37	0.038	4.738	0.486	3.482	5.137	2.280	39.800	49.979	1.941	24.477	0.116	1.115
38	0.017	3.799	0.359	2.441	3.823	1.500	28.666	37.493	1.958	17.983	0.105	1.075
39	0.039	2.747	0.191	2.153	3.010	1.260	20.629	26.179	1.483	12.868	0.073	1.220
40	0.064	4.385	0.360	3.015	4.674	2.020	33.372	39.871	2.090	21.124	0.149	1.400
41	0.017	3.422	0.403	2.727	3.986	1.545	24.949	31.543	1.500	16.162	0.085	0.865
42	0.036	2.690	0.166	1.957	3.593	0.850	17.103	20.571	1.686	11.452	0.073	1.305
43	0.061	5.105	0.392	3.836	6.387	1.630	34.007	39.629	2.151	19.752	0.050	1.660
44	0.035	4.145	0.386	3.624	5.657	1.870	25.648	28.571	1.966	16.042	0.084	1.605
45	0.064	3.609	0.293	3.709	5.138	1.585	18.369	21.364	1.814	12.804	0.106	0.807

protocols	Thymus	Spleen	Kidneys	Adrenals	Heart	Pancreas	Gall Bladder	Prostate	Oral Mucosa	Small Intestine	Extrathoracic
1	0.622	31.833	35.544	20.950	3.720	36.140	42.940	0.806	0.169	13.186	0.340
2	0.589	25.078	28.400	16.850	3.155	29.960	33.560	1.141	0.156	12.746	0.364
3	0.463	19.522	22.400	13.265	2.450	22.780	26.780	1.013	0.072	11.836	0.187
4	0.613	26.592	29.425	16.800	2.520	31.340	35.460	0.957	0.177	13.558	0.418
5	0.532	21.442	22.994	14.100	2.985	24.000	28.280	0.972	0.049	11.868	0.412
6	0.501	17.934	18.869	12.650	2.275	18.560	21.180	1.131	0.110	10.160	0.197

7	**0.682**	**23.417**	**25.338**	**19.250**	**3.340**	**26.960**	**29.980**	**1.121**	**0.115**	**12.618**	**0.350**
8	**0.564**	**20.225**	**20.075**	**16.100**	**3.300**	**20.620**	**24.720**	**1.430**	**0.014**	**11.926**	**0.259**
9	**0.673**	**17.375**	**16.000**	**13.550**	**3.075**	**17.500**	**20.120**	**1.453**	**0.083**	**11.834**	**0.296**
10	**0.155**	**8.953**	**8.444**	**5.470**	**0.734**	**9.448**	**10.300**	**0.581**	**0.083**	**3.950**	**0.044**
11	**0.227**	**7.085**	**6.998**	**3.985**	**0.623**	**7.426**	**8.900**	**0.745**	**0.010**	**3.242**	**0.082**
12	**0.099**	**7.349**	**6.935**	**4.065**	**0.885**	**7.956**	**8.732**	**0.846**	**0.027**	**3.948**	**0.000**
13	**0.239**	**7.290**	**6.829**	**4.815**	**0.700**	**8.268**	**8.762**	**0.706**	**0.047**	**3.394**	**0.153**
14	**0.187**	**6.154**	**5.814**	**3.980**	**0.653**	**6.696**	**7.290**	**0.814**	**0.010**	**3.733**	**0.211**
15	**0.055**	**6.527**	**5.911**	**4.780**	**0.908**	**6.648**	**7.904**	**0.717**	**0.063**	**3.979**	**0.051**
16	**0.119**	**6.309**	**6.103**	**4.030**	**0.674**	**6.924**	**7.798**	**0.555**	**0.032**	**4.110**	**0.000**
17	**0.129**	**5.928**	**5.204**	**3.865**	**0.730**	**5.838**	**6.316**	**0.965**	**0.030**	**3.886**	**0.126**
18	**0.273**	**6.008**	**4.871**	**5.065**	**1.123**	**5.446**	**5.786**	**0.811**	**0.054**	**3.658**	**0.092**
19	**0.321**	**15.542**	**16.325**	**10.040**	**2.065**	**16.860**	**19.120**	**0.522**	**0.056**	**7.520**	**0.092**
20	**0.343**	**14.723**	**15.656**	**10.115**	**1.860**	**16.140**	**18.920**	**0.638**	**0.088**	**7.314**	**0.218**
21	**0.361**	**14.352**	**15.275**	**8.825**	**1.700**	**15.440**	**17.940**	**0.817**	**0.045**	**6.570**	**0.102**
22	**0.393**	**12.530**	**13.456**	**8.345**	**1.373**	**14.840**	**15.800**	**0.965**	**0.047**	**6.400**	**0.180**
23	**0.357**	**12.835**	**12.219**	**8.185**	**1.590**	**13.740**	**13.580**	**0.911**	**0.030**	**8.386**	**0.051**
24	**0.340**	**12.914**	**12.613**	**9.455**	**1.780**	**13.100**	**15.180**	**0.842**	**0.095**	**6.846**	**0.170**
25	**0.315**	**11.519**	**11.144**	**8.985**	**1.585**	**12.540**	**12.000**	**0.920**	**0.016**	**6.333**	**0.344**
26	**0.412**	**11.099**	**10.670**	**8.045**	**2.090**	**11.182**	**12.400**	**0.956**	**0.034**	**7.374**	**0.180**
27	**0.435**	**12.586**	**11.391**	**9.985**	**2.830**	**12.060**	**12.920**	**0.837**	**0.067**	**6.662**	**0.146**
28	**0.920**	**38.192**	**46.863**	**25.050**	**4.385**	**47.420**	**58.180**	**1.357**	**0.302**	**15.702**	**0.418**
29	**0.512**	**27.817**	**34.825**	**19.550**	**3.370**	**35.060**	**43.780**	**1.130**	**0.122**	**15.648**	**0.163**
30	**0.429**	**19.507**	**23.475**	**15.025**	**2.525**	**23.200**	**28.960**	**0.815**	**0.120**	**11.876**	**0.347**
31	**0.695**	**31.583**	**37.769**	**24.400**	**4.070**	**38.800**	**49.320**	**1.476**	**0.095**	**17.164**	**0.170**
32	**0.487**	**24.833**	**28.619**	**17.650**	**2.845**	**29.100**	**37.000**	**0.825**	**0.067**	**14.504**	**0.401**
33	**0.446**	**18.525**	**19.681**	**13.650**	**3.155**	**19.720**	**22.760**	**1.016**	**0.039**	**10.398**	**0.306**
34	**0.831**	**30.417**	**34.475**	**23.050**	**4.895**	**34.980**	**44.120**	**1.226**	**0.116**	**19.272**	**0.405**
35	**0.667**	**24.533**	**25.694**	**20.350**	**4.230**	**26.420**	**32.420**	**1.474**	**0.086**	**15.032**	**0.289**
36	**0.824**	**17.558**	**17.525**	**15.300**	**4.040**	**17.600**	**21.340**	**1.030**	**0.061**	**12.322**	**0.412**
37	**1.050**	**37.675**	**46.138**	**25.850**	**4.005**	**47.620**	**56.600**	**1.173**	**0.116**	**18.858**	**0.381**
38	**0.557**	**28.483**	**34.700**	**18.900**	**2.840**	**35.240**	**44.060**	**1.447**	**0.105**	**12.906**	**0.327**
39	**0.416**	**19.682**	**23.206**	**13.455**	**2.240**	**24.740**	**27.960**	**0.842**	**0.073**	**11.604**	**0.337**
40	**0.948**	**31.958**	**38.994**	**22.150**	**4.030**	**38.800**	**49.020**	**1.417**	**0.149**	**18.920**	**0.340**
41	**0.780**	**24.283**	**28.625**	**18.500**	**3.210**	**30.040**	**35.840**	**1.297**	**0.085**	**15.128**	**0.575**
42	**0.558**	**18.375**	**19.356**	**13.700**	**2.445**	**20.720**	**23.600**	**1.191**	**0.073**	**10.152**	**0.350**
43	**0.879**	**31.458**	**34.100**	**22.500**	**3.765**	**35.280**	**42.940**	**1.001**	**0.050**	**18.378**	**0.415**
44	**0.624**	**24.667**	**26.369**	**20.050**	**3.755**	**25.820**	**30.920**	**1.413**	**0.084**	**15.834**	**0.344**
45	**0.591**	**17.242**	**17.356**	**14.500**	**3.515**	**18.420**	**21.280**	**1.152**	**0.106**	**12.342**	**0.432**

Appendix IX: Abdominal CT scan ED (mSv) with different tube current MOSFET, DLP and ImPACT methods between ED from FTC and ED corrected ATCM

Protocols No.	FTC	ATCM	FTC	ATCM	FTC	ATCM
	ED (mSv)/MOSFET		ED (mSv)/DLP		ED (mSv)/ImPACT	
100 / low dos +mA						
10	3.497	3.028	3.563	2.981	5.000	4.257
11	2.777	2.550	2.663	2.468	3.600	3.366
12	2.119	2.618	1.803	2.486	2.400	3.762
13	3.147	2.697	3.152	2.430	4.200	3.267
14	2.623	2.402	2.396	2.079	3.100	2.673
15	2.007	2.421	1.674	2.262	2.000	2.673
16	3.141	2.366	3.125	2.244	3.800	2.772
17	2.656	2.298	2.444	2.971	2.800	2.277
18	2.098	2.299	1.794	2.229	1.800	2.277
200/ low dose mA						
19	6.372	5.604	7.125	5.906	9.900	8.317
20	4.959	5.240	5.327	5.609	7.300	7.129
21	3.253	5.274	3.681	5.382	4.800	6.535
22	5.734	4.731	6.302	4.908	8.400	5.941
23	4.584	4.572	4.791	4.594	6.200	5.644
24	3.230	4.876	3.348	4.845	4.000	5.446
25	5.618	4.319	6.248	4.365	7.600	5.446
26	4.567	4.158	4.887	4.150	5.600	4.653
27	3.395	4.770	3.588	4.782	3.600	4.422
250 / standard mA						
1	7.593	7.996	8.906	8.914	12.000	11.593
2	5.888	6.470	6.500	6.736	9.100	8.865
3	4.187	5.135	4.508	5.792	5.900	6.819
4	7.034	6.854	7.878	7.441	11.000	9.547
5	5.367	5.606	5.990	6.047	7.700	7.501
6	3.972	4.729	5.184	5.081	5.000	5.797
7	6.787	6.124	7.809	6.612	9.500	8.183
8	5.471	5.310	6.110	5.730	7.000	6.547
9	4.125	4.617	5.485	5.075	4.600	5.251
300 /quality mA						
28	9.490	10.491	10.688	12.156	15.000	15.640
29	7.187	8.063	7.989	9.093	11.000	11.374
30	4.943	5.595	5.409	6.156	7.100	7.109
31	8.196	9.059	9.453	10.304	13.000	12.796
32	6.400	6.877	7.347	7.834	9.200	9.953
33	4.651	5.013	5.021	5.473	6.000	6.256
34	8.271	8.460	9.372	9.869	11.000	12.085
35	6.546	6.849	7.331	7.721	8.400	8.531
36	4.999	5.052	5.382	5.668	5.500	5.687
400/ high quality mA						
37	13.843	13.568	15.060	15.545	20.000	19.865
38	10.231	10.123	11.628	11.628	15.000	14.545
39	7.252	7.239	7.872	7.422	9.500	9.091
40	11.225	11.429	13.481	13.177	17.000	16.364
41	9.310	8.891	10.019	10.019	12.000	11.727
42	6.443	6.224	6.999	6.998	8.000	8.000
43	11.205	11.392	12.621	12.620	15.000	15.455
44	8.310	8.895	9.873	9.874	11.000	10.909
45	6.497	6.855	7.248	7.121	7.300	7.860

Appendix X: Abdominal CT scan ED (mSv) with different tube current MOSFET, DLP and ImPACT methods from uncorrected ATCM (raw) data

protocols	ED/DLP (mSv)	ED (mSv)/MOSFT	ED/ ImPACT CT
1	13.071	11.726	17.000
2	9.878	9.487	13.000
3	8.493	7.530	10.000
4	10.911	10.050	14.000
5	8.868	8.220	11.000
6	7.451	6.934	8.500
7	9.696	8.980	12.000
8	8.403	7.786	9.600
9	7.442	6.770	7.700
10	3.011	3.058	4.300
11	2.493	2.575	3.400
12	2.511	2.644	3.800
13	2.454	2.724	3.300
14	2.100	2.426	2.700
15	2.285	2.445	2.700
16	2.267	2.390	2.800
17	1.991	2.321	2.300
18	2.252	2.322	2.300
19	5.966	5.660	8.400
20	5.666	5.292	7.200
21	5.436	5.327	6.600
22	4.958	4.778	6.000
23	4.640	4.618	5.700
24	4.893	4.925	5.500
25	4.409	4.362	5.500
26	4.191	4.200	4.700
27	4.830	4.818	4.800
28	17.100	14.757	22.000
29	12.791	11.342	16.000
30	8.660	7.870	10.000
31	14.495	12.743	18.000
32	11.021	9.673	14.000
33	7.698	7.051	8.800
34	13.883	11.900	17.000
35	10.862	9.634	12.000
36	7.973	7.106	8.000
37	17.100	14.925	22.000
38	12.791	11.135	16.000
39	8.859	7.963	10.000
40	14.495	12.572	18.000
41	11.021	9.780	14.000
42	7.698	6.846	8.800
43	13.883	12.531	17.000
44	10.862	9.784	12.000
45	7.833	7.540	8.000

Appendix XI: Abdominal CT scan ED (mSv) with different pitch factors MOSFET, DLP and ImPACT methods between FTC and ED corrected ATCM.

Protocols No.	FTC	ATCM	FTC	ATCM	FTC	ATCM
	ED (mSv)/MOSFET		ED (mSv)/DLP		ED (mSv)/ImPACT	
Detail(0.688)						
1	7.593	7.996	8.906	8.914	12.000	11.593
4	7.034	6.854	7.878	7.441	11.000	9.547
7	6.787	6.124	7.809	6.612	9.500	8.183
10	3.497	3.028	3.563	2.981	5.000	4.257
13	3.147	2.697	3.152	2.430	4.200	3.267
16	3.141	2.366	3.125	2.244	3.800	2.772
19	6.372	5.604	7.125	5.906	9.900	8.317
22	5.734	4.731	6.302	4.908	8.400	5.941
25	5.618	4.319	6.248	4.365	7.600	5.446
28	9.490	10.491	10.688	12.156	15.000	15.640
31	8.196	9.059	9.453	10.304	13.000	12.796
34	8.271	8.460	9.372	9.869	11.000	12.085
37	13.843	13.568	15.060	15.545	20.000	20.000
40	11.225	11.429	13.481	13.177	17.000	16.364
43	11.205	11.392	12.621	12.620	15.000	15.455
Standard(0.938)						
2	5.888	6.470	6.500	6.736	9.100	8.865
5	5.367	5.606	5.990	6.047	7.700	7.501
8	5.471	5.310	6.110	5.730	7.000	6.547
11	2.777	2.550	2.663	2.468	3.600	3.366
14	2.623	2.402	2.396	2.079	3.100	2.673
17	2.656	2.298	2.444	1.971	2.800	2.277
20	4.959	5.240	5.327	5.609	7.300	7.129
23	4.584	4.572	4.791	4.594	6.200	5.644
26	4.567	4.158	4.887	4.150	5.600	4.653
29	7.187	7.063	7.989	9.093	11.000	11.374
32	6.400	6.877	7.347	7.834	9.200	9.953
35	6.546	6.849	7.331	7.721	8.400	8.531
38	10.231	10.123	11.628	11.628	15.000	14.545
41	9.310	8.891	10.019	10.019	12.000	11.727
44	8.810	8.895	9.873	9.874	11.000	10.909
Fast(1.438)						
3	4.187	5.135	4.508	5.792	5.900	6.819
6	3.972	4.729	4.184	5.081	5.000	5.797
9	4.125	4.617	4.485	5.075	4.600	5.251
12	2.119	2.618	1.803	2.486	2.400	3.762
15	2.007	2.421	1.674	2.262	2.000	2.673
18	2.098	2.299	1.794	2.229	1.800	2.277
21	3.557	5.274	3.606	5.382	4.800	6.535
24	3.230	4.876	3.348	4.845	4.000	5.446
27	3.395	4.770	3.588	4.782	3.600	4.752
30	4.943	5.215	5.409	6.156	7.100	7.109
33	4.651	5.013	5.021	5.473	6.000	6.256
36	4.999	5.052	5.382	5.668	5.500	5.687
39	7.252	7.239	7.872	7.422	9.500	9.091
42	6.443	6.224	6.999	6.998	8.000	8.000
45	6.497	6.855	7.248	7.121	7.300	7.860

Appendix XII: Abdominal CT scan ED (mSv) with different pitch factors MOSFET, DLP and ImPACT methods between FTC and ED uncorrected ATCM (raw) data.

Protocols No.	FTC	ATCM	FTC	ATCM	FTC	ATCM
	ED (mSv)/MOSFET		ED (mSv)/DLP		ED (mSv)/ImPACT	
Detail(0.688)						
1	7.593	11.726	8.906	13.071	12.000	17.000
4	7.034	10.050	7.878	10.911	11.000	14.000
7	6.787	8.980	7.809	9.696	9.500	12.000
10	3.497	3.058	3.563	3.011	5.000	4.300
13	3.147	2.724	3.152	2.454	4.200	3.300
16	3.141	2.390	3.125	2.267	3.800	2.800
19	6.372	5.660	7.125	5.966	9.900	8.400
22	5.734	4.778	6.302	4.958	8.400	6.000
25	5.618	4.362	6.248	4.409	7.600	5.500
28	9.490	14.757	10.688	17.100	15.000	22.000
31	8.196	12.743	9.453	14.495	13.000	18.000
34	8.271	11.900	9.372	13.883	11.000	17.000
37	13.843	14.925	15.060	17.100	20.000	22.000
40	11.225	12.572	13.481	14.495	17.000	18.000
43	11.205	12.531	12.621	13.883	15.000	17.000
Standard(0.938)						
2	5.888	9.487	6.500	9.878	9.100	13.000
5	5.367	8.220	5.990	8.868	7.700	11.000
8	5.471	7.786	6.110	8.403	7.000	9.600
11	2.777	2.575	2.663	2.493	3.600	3.400
14	2.623	2.426	2.396	2.100	3.100	2.700
17	2.656	2.321	2.444	1.991	2.800	2.300
20	4.959	5.292	5.327	5.666	7.300	7.200
23	4.584	4.618	4.791	4.640	6.200	5.700
26	4.567	4.200	4.887	4.191	5.600	4.700
29	7.187	11.342	7.989	12.791	11.000	16.000
32	6.400	9.673	7.347	11.021	9.200	14.000
35	6.546	9.634	7.331	10.862	8.400	12.000
38	10.231	11.135	11.628	12.791	15.000	16.000
41	9.310	9.780	10.019	11.021	12.000	14.000
44	8.810	9.784	9.873	10.862	11.000	12.000
Fast(1.438)						
3	4.187	7.530	4.508	8.493	5.900	10.000
6	3.972	6.934	4.184	7.451	5.000	8.500
9	4.125	6.770	4.485	7.442	4.600	7.700
12	2.119	2.644	1.803	2.511	2.400	3.800
15	2.007	2.445	1.674	2.285	2.000	2.700
18	2.098	2.322	1.794	2.252	1.800	2.300
21	3.557	5.327	3.606	5.436	4.800	6.600
24	3.230	4.925	3.348	4.893	4.000	5.500
27	3.395	4.818	3.588	4.830	3.600	4.800
30	4.943	7.870	5.409	8.660	7.100	10.000
33	4.651	7.051	5.021	7.698	6.000	8.800
36	4.999	7.106	5.382	7.973	5.500	8.000
39	7.252	7.963	7.872	8.859	9.500	10.000
42	6.443	6.846	6.999	7.698	8.000	8.800
45	6.497	7.540	7.248	7.833	7.300	8.000

Appendix XIII: Abdominal CT scan ED (mSv) with different detector configurations MOSFET, DLP and ImPACT methods between FTC and ED corrected ATCM.

Protocols No.	FTC	ATCM	FTC	ATCM	FTC	ATCM
	ED (mSv)/MOSFET		ED (mSv)/DLP		ED (mSv)/ImPACT	
0.5×16mm						
1	7.593	7.996	8.906	8.914	12.000	11.593
2	5.888	6.470	6.500	6.736	9.100	8.865
3	4.187	5.135	4.508	5.792	5.900	6.819
10	3.497	3.028	3.563	2.981	5.000	4.257
11	2.777	2.550	2.663	2.468	3.600	3.366
12	2.119	2.618	1.803	2.486	2.400	3.762
19	6.372	5.604	7.125	5.906	9.900	8.317
20	4.959	5.240	5.327	5.609	7.300	7.129
21	3.557	5.274	3.606	5.382	4.800	6.535
28	9.490	9.321	11.688	12.156	15.000	15.640
29	7.187	7.063	7.989	9.093	11.000	11.374
30	4.943	5.215	5.409	6.156	7.100	7.109
37	13.843	13.568	15.060	15.545	20.000	19.865
38	10.231	10.123	11.628	11.628	15.000	14.545
39	7.252	7.239	7.872	7.422	9.500	9.091
1.0×16mm						
4	7.034	6.854	7.878	7.441	11.000	9.547
5	5.367	5.606	5.990	6.047	7.700	7.501
6	3.972	4.729	4.184	5.081	5.000	5.797
13	3.147	2.697	3.152	2.430	4.200	3.267
14	2.623	2.402	2.396	2.079	3.100	2.673
15	2.007	2.421	1.674	2.262	2.000	2.673
22	4.584	4.731	6.302	4.908	8.400	5.941
23	3.230	4.572	4.791	4.594	6.200	5.644
24	5.618	4.876	3.348	4.845	4.000	5.446
31	8.196	8.059	9.453	10.304	13.000	12.796
32	6.400	6.877	7.347	7.834	9.200	9.953
33	4.651	5.013	5.021	5.473	6.000	6.256
40	11.225	11.429	13.481	13.177	17.000	16.364
41	9.310	8.891	10.019	10.019	12.000	11.727
42	6.443	6.224	6.999	6.998	8.000	8.000
2.0×16mm						
7	6.787	6.124	7.809	6.612	9.500	8.183
8	5.471	5.310	6.110	5.730	7.000	6.547
9	4.125	4.617	4.485	5.075	4.600	5.251
16	3.141	2.366	3.125	2.244	3.800	2.772
17	2.656	2.298	2.444	1.971	2.800	2.277
18	2.098	2.299	1.794	2.229	1.800	2.277
25	5.618	4.319	6.248	4.365	7.600	5.446
26	4.567	4.158	4.887	4.150	5.600	4.653
27	3.395	4.770	3.588	4.782	3.600	4.752
34	8.271	8.460	9.372	9.869	11.000	12.085
35	6.546	6.849	7.331	7.721	8.400	8.531
36	4.999	5.052	5.382	5.668	5.500	5.687
43	11.205	11.392	12.621	12.620	15.000	15.455
44	8.310	8.895	9.873	9.874	11.000	10.909
45	6.497	6.855	7.248	7.121	7.300	7.860

Appendix XIV: Abdominal CT scan ED (mSv) with different detector configurations MOSFET, DLP and ImPACT methods between FTC and ED uncorrected ATCM (raw) data.

Protocols No.	FTC	ATCM	FTC	ATCM	FTC	ATCM
	ED (mSv)/MOSFET		ED (mSv)/DLP		ED (mSv)/ImPACT	
0.5×16mm						
1	7.593	11.726	8.906	13.071	12.000	17.000
2	5.888	9.487	6.500	9.878	9.100	13.000
3	4.187	7.530	4.508	8.493	5.900	10.000
10	3.497	3.058	3.563	3.011	5.000	4.300
11	2.777	2.575	2.663	2.493	3.600	3.400
12	2.119	2.644	1.803	2.511	2.400	3.800
19	6.372	5.660	7.125	5.666	9.900	8.400
20	4.959	5.292	5.327	5.436	7.300	7.200
21	3.557	5.327	3.606	4.958	4.800	6.600
28	9.490	14.757	11.688	17.100	15.000	22.000
29	7.187	11.342	7.989	12.791	11.000	16.000
30	4.943	7.870	5.409	8.660	7.100	10.000
37	13.843	14.925	15.060	17.100	20.000	22.000
38	10.231	11.135	11.628	12.791	15.000	16.000
39	7.252	7.963	7.872	8.859	9.500	10.000
1.0×16mm						
4	7.034	10.050	7.878	10.911	11.000	14.000
5	5.367	8.220	5.990	8.868	7.700	11.000
6	3.972	6.934	4.184	7.451	5.000	8.500
13	3.147	2.724	3.152	2.454	4.200	3.300
14	2.623	2.426	2.396	2.100	3.100	2.700
15	2.007	2.445	1.674	2.285	2.000	2.700
22	4.584	4.778	6.302	4.640	8.400	6.000
23	3.230	4.618	4.791	4.893	6.200	5.700
24	5.618	4.925	3.348	4.409	4.000	5.500
31	8.196	12.743	9.453	14.495	13.000	18.000
32	6.400	9.673	7.347	11.021	9.200	14.000
33	4.651	7.051	5.021	7.698	6.000	8.800
40	11.225	12.572	13.481	14.495	17.000	18.000
41	9.310	9.780	10.019	11.021	12.000	14.000
42	6.443	6.846	6.999	7.698	8.000	8.800
2.0×16mm						
7	6.787	8.980	7.809	9.696	9.500	12.000
8	5.471	7.786	6.110	8.403	7.000	9.600
9	4.125	6.770	4.485	7.442	4.600	7.700
16	3.141	2.390	3.125	2.267	3.800	2.800
17	2.656	2.321	2.444	1.991	2.800	2.300
18	2.098	2.322	1.794	2.252	1.800	2.300
25	5.618	4.362	6.248	4.409	7.600	5.500
26	4.567	4.200	4.887	4.191	5.600	4.700
27	3.395	4.818	3.588	4.830	3.600	4.800
34	8.271	11.900	9.372	13.883	11.000	17.000
35	6.546	9.634	7.331	10.862	8.400	12.000
36	4.999	7.106	5.382	7.973	5.500	8.000
43	11.205	12.531	12.621	13.883	15.000	17.000
44	8.310	9.784	9.873	10.862	11.000	12.000
45	6.497	7.540	7.248	7.833	7.300	8.000

Appendix XV: Abdominal CT scan ER (case / 10^6) female and male with different parameters age from 20 to 70 MOSFET method FTC data

Protocols NO.	20 FEMAL	20 MALE	30 FEMAL	30 MALE	40 FEMAL	40 MALE	50 FEMAL	50 MALE	60 FEMAL	60 MALE	70 FEMAL	70 MALE
1	82.953	72.167	55.620	49.316	50.813	46.009	44.219	40.866	35.312	31.851	24.087	20.811
2	65.290	57.174	43.814	39.157	40.035	36.610	34.889	32.598	27.912	25.507	19.079	16.710
3	46.292	40.199	31.047	27.563	28.255	25.800	24.560	22.998	19.623	18.013	13.408	11.796
4	77.06749	67.92538	51.68614	46.46502	47.23791	43.39106	41.13812	38.58019	32.87082	30.11782	22.43752	19.68429
5	60.4951	51.48158	40.57796	35.23156	37.03331	32.93421	32.24953	29.32901	25.79099	22.95216	17.62327	15.03306
6	46.64414	38.62452	31.28626	26.48565	28.47978	24.81645	24.8048	22.16652	19.87083	17.43188	13.61023	11.46248
7	80.215	67.077	53.767	45.890	49.050	42.897	42.766	38.220	34.256	29.946	23.448	19.626
8	64.116	53.559	43.127	36.712	39.522	34.390	34.610	30.714	27.837	24.148	19.120	15.886
9	50.913	39.959	34.093	27.413	30.898	25.715	26.903	23.022	21.594	18.159	14.831	11.966
10	38.401	33.342	25.793	22.856	23.567	21.394	20.525	19.074	16.411	14.943	11.211	9.794
11	30.068	26.342	20.232	18.061	18.547	16.912	16.199	15.084	12.980	11.824	8.880	7.753
12	23.626	20.314	15.884	13.939	14.507	13.070	12.644	11.676	10.121	9.179	6.922	6.027
13	34.6644	30.3836	23.3191	20.8292	21.3578	19.4989	18.6445	17.3843	14.9328	13.6321	10.216	8.94211
14	28.7098	24.942	19.3023	17.1315	17.6491	16.0689	15.4057	14.3612	12.3515	11.2946	8.46132	7.42518
15	22.8307	18.0795	15.3039	12.4108	13.8495	11.6453	12.0062	10.4209	9.59091	8.20782	6.55675	5.40953
16	36.473	30.562	24.515	20.982	22.366	19.677	19.510	17.589	15.644	13.845	10.725	9.115
17	30.687	25.707	20.628	17.670	18.819	16.593	16.433	14.857	13.199	11.715	9.062	7.719
18	24.589	19.739	16.515	13.573	15.036	12.763	13.135	11.454	10.567	9.065	7.268	5.993
19	69.908	61.212	46.919	41.868	42.910	39.100	37.365	34.767	29.847	27.142	20.362	17.748
20	54.926	47.472	36.812	32.479	33.525	30.337	29.111	26.980	23.211	21.070	15.820	13.775
21	38.278	34.267	25.803	23.538	23.753	22.073	20.815	19.716	16.720	15.486	11.464	10.169
22	62.7702	55.3109	42.1525	37.8893	38.5439	35.4309	33.585	31.5465	26.8567	24.6832	18.3478	16.1714
23	51.697	43.8803	34.6127	30.0435	31.4291	28.092	27.2773	25.0213	21.7727	19.5896	14.8632	12.8408
24	37.1719	31.3915	25.0106	21.5457	22.9107	20.202	20.0445	18.0576	16.1052	14.2074	11.0533	9.34899
25	64.744	54.534	43.366	37.321	39.464	34.893	34.345	31.086	27.482	24.346	18.799	15.953
26	53.025	43.600	35.552	29.869	32.331	27.964	28.139	24.957	22.530	19.590	15.425	12.854
27	39.756	33.098	26.823	22.712	24.774	21.312	21.836	19.081	17.649	15.058	12.162	9.935
28	102.316	89.257	68.614	61.065	62.613	57.033	54.460	50.716	43.488	39.581	29.672	25.883
29	77.867	67.721	52.189	46.317	47.649	43.253	41.467	38.466	33.128	30.023	22.608	19.626
30	55.375	48.015	37.127	32.901	33.823	30.781	29.423	27.430	23.520	21.474	16.072	14.061
31	91.3223	78.6893	61.1707	53.8258	55.6529	50.269	48.3298	44.7031	38.5626	34.9087	26.3079	22.8257
32	71.1229	61.8267	47.7046	42.3029	43.5531	39.5224	37.9209	35.1626	30.3091	27.4759	20.6999	17.9654
33	54.004	45.34	36.2412	31.0781	33.046	29.1006	28.8112	25.9707	23.0895	20.3803	15.8181	13.3684
34	96.085	81.249	64.498	55.652	58.940	52.078	51.473	46.447	41.298	36.442	28.309	23.925
35	78.093	63.910	52.401	43.774	47.782	40.983	41.714	36.587	33.492	28.749	22.982	18.897
36	60.719	47.556	40.712	32.614	37.015	30.595	32.303	27.395	25.973	21.613	17.853	14.261
37	149.819	133.305	100.503	91.135	91.995	85.049	80.177	75.556	64.082	58.908	43.738	38.476
38	111.317	97.673	74.627	66.778	68.180	62.329	59.358	55.392	47.423	43.208	32.364	28.240
39	80.971	70.443	54.287	48.217	49.440	45.061	42.968	40.096	34.305	31.347	23.414	20.517
40	129.388	113.55	86.7566	77.6938	79.227	72.5681	69.0057	64.5409	55.1788	50.423	37.6991	33.0086
41	103.649	88.914	69.4219	60.883	63.0553	56.9216	54.744	50.6816	43.7151	39.6516	29.8559	25.9821
42	74.5757	62.2467	49.9765	42.6325	45.4326	39.8925	39.5116	35.5717	31.6135	27.8971	21.6277	18.313
43	127.032	106.556	85.155	72.961	77.535	68.235	67.504	60.811	54.041	47.631	36.987	31.240
44	104.225	85.488	69.813	58.561	63.476	54.816	55.283	48.923	44.311	38.408	30.370	25.223
45	77.774	63.230	52.277	43.358	47.855	40.646	41.917	36.352	33.740	28.636	23.198	18.856

Appendix XVI: Abdominal CT scan ER (case / 10^6) female and male with different parameters age from 20 to 70 MOSFET method corrected ATCM

Protocols NO.	20 FEMAL	20 MALE	30 FEMAL	30 MALE	40 FEMAL	40 MALE	50 FEMAL	50 MALE	60 FEMAL	60 MALE	70 FEMAL	70 MALE
1	87.376	76.224	58.568	52.108	53.446	48.620	46.478	43.187	37.098	33.656	25.305	21.976
2	72.028	62.414	48.263	42.689	43.961	39.860	38.205	35.438	30.494	27.661	20.808	18.076
3	58.097	49.400	38.884	33.774	35.332	31.531	30.656	28.035	24.444	21.888	16.668	14.306
4	75.8674	66.0473	50.8421	45.2032	46.3403	42.2266	40.3059	37.5613	32.1982	29.3396	21.9893	19.1902
5	62.7097	53.2773	42.003	36.452	38.2088	34.0589	33.2002	30.312	26.5174	23.6951	18.108	15.5122
6	54.4593	44.5499	36.4547	30.5189	33.064	28.5655	28.7356	25.4899	22.9974	19.9922	15.7451	13.12
7	70.673	59.680	47.364	40.831	43.173	38.157	37.615	33.977	30.114	26.590	20.609	17.412
8	63.982	51.342	42.835	35.174	38.814	32.936	33.747	29.411	27.036	23.102	18.535	15.172
9	54.792	44.655	36.887	30.607	33.931	28.693	29.838	25.669	24.091	20.218	16.594	13.312
10	34.050	28.932	22.795	19.798	20.695	18.504	17.947	16.475	14.308	12.886	9.754	8.435
11	27.697	24.032	18.642	16.462	17.131	15.405	14.974	13.731	11.996	10.752	8.201	7.038
12	28.857	25.467	19.421	17.472	17.831	16.367	15.586	14.605	12.490	11.454	8.546	7.503
13	29.6132	24.968	19.821	17.0948	17.9527	15.987	15.5362	14.2387	12.3699	11.1374	8.42601	7.2865
14	26.7905	22.7222	17.9783	15.6039	16.3524	14.6403	14.2315	13.0922	11.3945	10.3022	7.80085	6.77099
15	28.077	23.3254	18.8194	15.9884	17.1186	14.9751	14.9008	13.3708	11.9293	10.4992	8.16654	6.88561
16	28.294	22.641	18.951	15.513	17.147	14.531	14.856	12.976	11.853	10.199	8.093	6.703
17	26.714	21.563	17.912	14.822	16.194	13.928	14.045	12.478	11.232	9.843	7.689	6.479
18	27.261	22.006	18.386	15.110	16.990	14.197	14.998	12.739	12.146	10.081	8.385	6.657
19	60.851	53.616	40.855	36.694	37.379	34.281	32.583	30.493	26.058	23.816	17.801	15.580
20	58.536	50.720	39.240	34.674	35.803	32.362	31.138	28.761	24.850	22.439	16.949	14.652
21	57.651	50.153	38.688	34.340	35.421	32.109	30.943	28.604	24.810	22.387	16.988	14.665
22	52.873	44.6866	35.3745	30.5696	32.1258	28.557	27.8687	25.4111	22.2243	19.8456	15.1579	12.9645
23	50.6673	43.7528	34.0214	29.9535	31.1281	28.0065	27.1507	24.9439	21.7319	19.5154	14.8568	12.7733
24	56.6529	45.9913	37.9631	31.5117	34.504	29.5054	30.0336	26.3431	24.0608	20.6835	16.4847	13.5835
25	49.293	41.637	33.144	28.549	30.396	26.748	26.630	23.894	21.425	18.772	14.717	12.332
26	49.385	40.194	33.127	27.536	30.198	25.789	26.344	23.034	21.134	18.110	14.490	11.903
27	58.840	45.456	39.472	31.184	35.883	29.264	31.324	26.217	25.196	20.694	17.331	13.655
28	115.200	100.058	77.052	68.336	70.072	63.709	60.775	56.542	48.409	44.016	32.965	28.707
29	89.877	78.013	60.188	53.344	54.817	49.797	47.635	44.262	38.017	34.550	25.936	22.589
30	61.664	53.673	41.319	36.688	37.673	34.243	32.763	30.431	26.160	23.748	17.849	15.525
31	101.581	87.7701	67.9645	60.0223	61.6725	56.0276	53.4307	49.7867	42.5466	38.8358	28.9841	25.3647
32	76.8369	67.2653	51.482	46.0146	46.8807	42.9653	40.727	38.1913	32.4913	29.8253	22.1625	19.5064
33	57.2143	48.3961	38.3767	33.1282	35.0527	30.9753	30.5738	27.5997	24.4915	21.618	16.7635	14.1683
34	98.452	82.729	65.923	56.538	60.037	52.786	52.257	46.958	41.798	36.712	28.575	24.031
35	80.379	66.797	53.924	45.724	49.249	42.770	43.006	38.140	34.508	29.911	23.658	19.623
36	62.701	49.150	41.948	33.685	37.920	31.565	32.945	28.219	26.397	22.225	18.107	14.636
37	149.077	130.000	99.740	88.846	90.677	82.872	78.617	73.577	62.607	57.318	42.632	37.418
38	110.813	97.206	74.210	66.433	67.636	61.981	58.746	55.047	46.836	42.904	31.909	28.010
39	79.951	68.904	53.561	47.139	48.742	44.026	42.316	39.152	33.750	30.570	23.013	19.995
40	128.4	111.626	85.916	76.2937	78.0698	71.1786	67.6825	63.2112	53.8987	49.2846	36.7083	32.1746
41	99.4496	86.2079	66.54	58.9242	60.5218	54.995	52.5697	48.8752	41.9588	38.1479	28.629	24.9352
42	71.8018	61.6621	48.2622	42.209	44.2626	39.4764	38.7159	35.1799	31.068	27.5783	21.2833	18.0881
43	127.045	108.544	85.328	74.310	78.191	69.479	68.364	61.905	54.861	48.464	37.595	31.778
44	103.827	86.183	69.595	59.048	63.356	55.271	55.209	49.319	44.254	38.714	30.329	25.425
45	81.452	66.073	54.717	45.400	49.894	42.639	43.629	38.206	35.128	30.176	24.176	19.938

Appendix XVII: Abdominal CT scan ER (case / 10^6) female and male with different parameters age from 20 to 70 MOSFET method from ATCM (raw) data.

Protocols NO.	20 FEMAL	20 MALE	30 FEMAL	30 MALE	40 FEMAL	40 MALE	50 FEMAL	50 MALE	60 FEMAL	60 MALE	70 FEMAL	70 MALE
1	128.128	111.775	85.884	76.411	78.373	71.296	68.156	63.329	54.400	49.353	37.107	32.225
2	105.622	91.524	70.772	62.599	64.464	58.451	56.025	51.967	44.717	40.563	30.512	26.506
3	85.193	72.441	57.019	49.526	51.811	46.238	44.954	41.111	35.845	32.096	24.441	20.978
4	111.252	96.852	74.555	66.286	67.953	61.921	59.105	55.080	47.215	43.024	32.245	28.141
5	91.957	78.126	61.593	53.453	56.029	49.944	48.685	44.450	38.885	34.747	26.554	22.747
6	79.859	65.328	53.457	44.753	48.485	41.888	42.138	37.378	33.723	29.317	23.089	19.239
7	103.635	87.514	69.454	59.875	63.309	55.953	55.159	49.824	44.160	38.992	30.220	25.534
8	93.823	75.288	62.813	51.579	56.916	48.297	49.487	43.128	39.646	33.876	27.180	22.248
9	80.346	65.483	54.092	44.882	49.756	42.075	43.755	37.642	35.327	29.647	24.334	19.520
10	34.391	29.221	23.022	19.996	20.902	18.689	18.127	16.639	14.451	13.015	9.852	8.519
11	27.974	24.273	18.828	16.627	17.303	15.559	15.124	13.869	12.116	10.859	8.283	7.108
12	29.146	25.722	19.616	17.646	18.009	16.531	15.742	14.751	12.615	11.568	8.631	7.578
13	29.909	25.218	20.019	17.266	18.132	16.147	15.692	14.381	12.494	11.249	8.510	7.359
14	27.058	22.949	18.158	15.760	16.516	14.787	14.374	13.223	11.508	10.405	7.879	6.839
15	28.358	23.559	19.008	16.148	17.290	15.125	15.050	13.505	12.049	10.604	8.248	6.954
16	28.577	22.867	19.140	15.668	17.319	14.677	15.004	13.106	11.972	10.301	8.174	6.770
17	26.981	21.779	18.091	14.970	16.356	14.067	14.185	12.603	11.344	9.941	7.766	6.544
18	27.534	22.226	18.570	15.261	17.160	14.339	15.148	12.866	12.267	10.181	8.468	6.723
19	61.459	54.152	41.263	37.061	37.753	34.623	32.909	30.798	26.318	24.054	17.979	15.736
20	59.121	51.227	39.632	35.020	36.161	32.686	31.449	29.049	25.099	22.664	17.119	14.799
21	58.228	50.654	39.074	34.684	35.775	32.430	31.252	28.891	25.058	22.611	17.158	14.812
22	53.402	45.133	35.728	30.875	32.447	28.843	28.147	25.665	22.447	20.044	15.310	13.094
23	51.174	44.190	34.362	30.253	31.439	28.287	27.422	25.193	21.949	19.711	15.005	12.901
24	57.219	46.451	38.343	31.827	34.849	29.800	30.334	26.607	24.301	20.890	16.650	13.719
25	49.786	42.054	33.476	28.834	30.700	27.015	26.897	24.132	21.639	18.960	14.864	12.455
26	49.878	40.596	33.458	27.811	30.500	26.047	26.607	23.265	21.346	18.291	14.635	12.022
27	59.429	45.910	39.866	31.496	36.241	29.556	31.637	26.479	25.448	20.901	17.504	13.792
28	162.048	140.749	108.387	96.127	98.568	89.618	85.490	79.536	68.095	61.915	46.370	40.381
29	126.427	109.738	84.664	75.038	77.109	70.048	67.006	62.262	53.477	48.600	36.483	31.775
30	86.741	75.500	58.122	51.608	52.994	48.168	46.086	42.806	36.799	33.406	25.108	21.838
31	142.891	123.463	95.603	84.431	86.753	78.812	75.159	70.033	59.849	54.629	40.771	35.680
32	108.084	94.620	72.418	64.727	65.946	60.438	57.289	53.722	45.704	41.954	31.175	27.439
33	80.481	68.077	53.983	46.600	49.307	43.572	43.007	38.824	34.451	30.409	23.581	19.930
34	138.489	116.372	92.732	79.530	84.452	74.252	73.508	66.054	58.796	51.641	40.196	33.803
35	113.066	93.961	75.853	64.318	69.276	60.163	60.495	53.651	48.541	42.075	33.279	27.604
36	88.199	69.137	59.007	47.384	53.340	44.401	46.343	39.695	37.132	31.264	25.471	20.588
37	163.985	143.000	109.714	97.731	99.745	91.159	86.478	80.935	68.868	63.050	46.895	41.159
38	121.894	106.926	81.631	73.076	74.400	68.179	64.621	60.552	51.520	47.194	35.100	30.812
39	87.946	75.794	58.917	51.853	53.616	48.428	46.548	43.067	37.124	33.627	25.314	21.994
40	141.240	122.788	94.508	83.923	85.877	78.296	74.451	69.532	59.289	54.213	40.379	35.392
41	109.395	94.829	73.194	64.817	66.574	60.494	57.827	53.763	46.155	41.963	31.492	27.429
42	78.982	67.828	53.088	46.430	48.689	43.424	42.588	38.698	34.175	30.336	23.412	19.897
43	139.749	119.399	93.861	81.741	86.010	76.427	75.200	68.095	60.347	53.310	41.354	34.955
44	114.210	94.801	76.554	64.953	69.691	60.799	60.729	54.250	48.679	42.586	33.362	27.967
45	89.597	72.680	60.189	49.940	54.883	46.903	47.992	42.027	38.641	33.194	26.594	21.931

Appendix XVIII: Abdominal CT scan SNR liver value calculation results from three ROIs for 90 images from FTC and ATCM protocols

Image NO.	FTC (liver 3 ROIs)								
	mean 1	mean 2	mean 3	average	SD 1	SD 2	SD 3	average	SNR value
1	78.660	74.810	77.270	76.913	4.410	5.860	5.430	5.233	14.697
2	76.640	75.660	76.840	76.380	6.930	6.650	5.650	6.410	11.916
3	80.170	75.900	78.460	78.177	8.500	7.500	7.640	7.880	9.921
4	78.110	75.960	77.770	77.280	4.940	5.120	4.740	4.933	15.665
5	76.450	75.700	76.350	76.167	5.030	5.680	6.200	5.637	13.513
6	76.120	73.060	76.390	75.190	6.210	6.320	7.240	6.590	11.410
7	78.480	74.810	76.370	76.553	4.870	4.710	4.040	4.540	16.862
8	78.780	74.230	71.770	74.927	5.050	4.630	4.970	4.883	15.343
9	75.250	76.090	77.450	76.263	6.400	6.500	6.650	6.517	11.703
10	76.080	76.220	77.650	76.650	7.340	9.450	7.760	8.183	9.367
11	77.490	76.050	78.220	77.253	8.470	10.260	9.060	9.263	8.340
12	80.560	73.590	75.080	76.410	12.500	10.790	13.170	12.153	6.287
13	76.330	74.920	75.250	75.500	7.340	7.880	8.240	7.820	9.655
14	76.040	75.900	77.780	76.573	7.620	8.830	8.680	8.377	9.141
15	75.340	71.650	76.720	74.570	10.790	12.510	11.760	11.687	6.381
16	76.790	73.920	76.440	75.717	6.390	7.610	6.970	6.990	10.832
17	75.190	70.410	76.120	73.907	8.320	8.340	8.670	8.443	8.753
18	76.460	75.450	75.600	75.837	10.550	9.350	10.490	10.130	7.486
19	76.730	75.630	77.280	76.547	6.140	8.050	7.490	7.227	10.592
20	77.250	75.820	76.920	76.663	7.530	8.960	6.980	7.823	9.799
21	79.780	74.970	76.550	77.100	8.470	10.350	8.140	8.987	8.579
22	78.230	74.710	74.370	75.770	6.060	7.620	7.580	7.087	10.692
23	75.740	75.710	75.630	75.693	6.020	8.660	6.190	6.957	10.881
24	77.870	72.840	74.640	75.117	7.770	9.240	7.640	8.217	9.142
25	75.260	75.080	75.630	75.323	6.260	7.430	6.270	6.653	11.321
26	77.050	72.970	77.050	75.690	7.850	8.430	6.560	7.613	9.942
27	76.720	74.340	78.880	76.647	7.350	8.100	8.170	7.873	9.735
28	77.150	74.630	75.760	75.847	5.070	4.940	5.540	5.183	14.633
29	76.220	74.860	76.300	75.793	5.120	5.680	6.660	5.820	13.023
30	76.810	75.190	75.450	75.817	6.300	7.340	6.480	6.707	11.305
31	76.680	73.550	76.250	75.493	4.320	4.780	4.780	4.627	16.317
32	75.910	74.880	75.560	75.450	4.850	5.330	4.860	5.013	15.050
33	78.040	73.470	75.330	75.613	8.030	5.920	7.040	6.997	10.807
34	74.560	74.020	75.490	74.690	3.530	4.680	4.530	4.247	17.588
35	75.110	75.010	76.760	75.627	5.110	4.930	3.800	4.613	16.393
36	76.590	73.630	75.380	75.200	5.520	6.110	5.900	5.843	12.869
37	77.580	75.960	76.920	76.820	4.420	4.800	4.370	4.530	16.958
38	78.220	75.290	77.460	76.990	5.060	5.410	4.890	5.120	15.037
39	76.620	76.090	77.180	76.630	5.480	5.760	6.270	5.837	13.129
40	76.310	74.300	74.040	74.883	4.050	3.620	3.840	3.837	19.518
41	76.360	74.690	74.080	75.043	3.400	4.820	4.090	4.103	18.288
42	78.240	72.540	75.040	75.273	5.970	4.830	6.250	5.683	13.245
43	75.560	74.480	76.170	75.403	3.230	3.110	4.230	3.523	21.401
44	75.470	70.270	76.190	73.977	3.550	3.490	3.730	3.590	20.606
45	77.130	72.640	73.710	74.493	4.750	5.090	5.090	4.977	14.969
Image NO.	ATCM (liver 3 ROIs)								
	mean 1	mean 2	mean 3	average	SD 1	SD 2	SD 3	average	SNR value
1	76.120	75.740	76.670	76.177	5.870	5.320	5.870	5.687	13.396
2	76.720	74.250	76.540	75.837	5.380	5.050	4.480	4.970	15.259
3	77.720	75.140	77.060	76.640	5.700	7.500	7.070	6.757	11.343
4	76.490	73.780	74.080	74.783	4.610	5.760	5.320	5.230	14.299
5	76.550	74.600	75.970	75.707	5.970	5.440	5.350	5.587	13.551

6	**78.240**	**73.000**	**76.140**	**75.793**	**5.290**	**6.130**	**5.870**	**5.763**	**13.151**
7	**76.090**	**75.600**	**76.280**	**75.990**	**4.800**	**4.440**	**5.300**	**4.847**	**15.679**
8	**76.400**	**75.300**	**74.070**	**75.257**	**4.090**	**5.330**	**5.570**	**4.997**	**15.061**
9	**78.640**	**71.700**	**75.700**	**75.347**	**5.330**	**5.470**	**5.620**	**5.473**	**13.766**
10	**76.650**	**74.640**	**75.730**	**75.673**	**11.840**	**12.020**	**12.920**	**12.260**	**6.172**
11	**76.330**	**74.380**	**75.020**	**75.243**	**12.460**	**15.640**	**13.800**	**13.967**	**5.387**
12	**76.460**	**77.660**	**75.350**	**76.490**	**11.420**	**12.670**	**10.100**	**11.397**	**6.712**
13	**75.620**	**74.630**	**75.510**	**75.253**	**9.500**	**10.650**	**12.720**	**10.957**	**6.868**
14	**75.050**	**75.960**	**76.510**	**75.840**	**10.380**	**11.310**	**10.920**	**10.870**	**6.977**
15	**74.850**	**73.040**	**72.810**	**73.567**	**10.270**	**11.240**	**12.920**	**11.477**	**6.410**
16	**76.410**	**75.920**	**73.830**	**75.387**	**10.610**	**13.240**	**13.320**	**12.390**	**6.084**
17	**75.830**	**75.190**	**75.140**	**75.387**	**9.020**	**11.670**	**9.860**	**10.183**	**7.403**
18	**77.060**	**73.980**	**72.830**	**74.623**	**7.570**	**8.600**	**6.280**	**7.483**	**9.972**
19	**76.800**	**76.000**	**76.660**	**76.487**	**8.520**	**7.900**	**7.370**	**7.930**	**9.645**
20	**76.380**	**74.920**	**77.070**	**76.123**	**7.350**	**8.860**	**7.620**	**7.943**	**9.583**
21	**75.690**	**76.590**	**76.930**	**76.403**	**7.410**	**8.430**	**7.930**	**7.923**	**9.643**
22	**76.780**	**75.230**	**75.420**	**75.810**	**7.460**	**7.640**	**7.630**	**7.577**	**10.006**
23	**75.950**	**72.520**	**75.480**	**74.650**	**7.310**	**7.510**	**8.790**	**7.870**	**9.485**
24	**76.360**	**72.040**	**76.580**	**74.993**	**7.590**	**8.520**	**6.960**	**7.690**	**9.752**
25	**74.340**	**76.490**	**75.300**	**75.377**	**5.950**	**7.670**	**8.340**	**7.320**	**10.297**
26	**73.730**	**72.580**	**75.850**	**74.053**	**7.220**	**8.470**	**6.630**	**7.440**	**9.953**
27	**78.580**	**73.840**	**75.780**	**76.067**	**7.330**	**7.050**	**6.170**	**6.850**	**11.105**
28	**77.370**	**75.410**	**76.220**	**76.333**	**5.970**	**4.280**	**6.030**	**5.427**	**14.066**
29	**76.330**	**74.160**	**77.290**	**75.927**	**4.560**	**4.530**	**4.920**	**4.670**	**16.258**
30	**76.420**	**74.360**	**75.060**	**75.280**	**5.110**	**6.600**	**5.610**	**5.773**	**13.039**
31	**76.200**	**73.420**	**75.790**	**75.137**	**4.220**	**5.430**	**4.500**	**4.717**	**15.930**
32	**75.180**	**74.110**	**74.730**	**74.673**	**4.650**	**4.260**	**5.350**	**4.753**	**15.710**
33	**74.410**	**75.000**	**75.320**	**74.910**	**4.470**	**6.360**	**6.180**	**5.670**	**13.212**
34	**75.310**	**74.890**	**75.670**	**75.290**	**4.370**	**5.980**	**4.670**	**5.007**	**15.038**
35	**74.760**	**75.650**	**75.250**	**75.220**	**4.310**	**4.870**	**3.630**	**4.270**	**17.616**
36	**79.700**	**72.350**	**74.020**	**75.357**	**4.520**	**4.570**	**4.510**	**4.533**	**16.623**
37	**76.980**	**74.430**	**76.350**	**75.920**	**4.220**	**4.200**	**3.730**	**4.050**	**18.746**
38	**77.010**	**75.550**	**76.710**	**76.423**	**3.970**	**4.820**	**4.940**	**4.577**	**16.698**
39	**75.300**	**76.640**	**76.240**	**76.060**	**6.000**	**6.920**	**5.780**	**6.233**	**12.202**
40	**75.750**	**74.700**	**75.840**	**75.430**	**4.450**	**3.530**	**3.300**	**3.760**	**20.061**
41	**74.330**	**76.770**	**75.800**	**75.633**	**4.610**	**4.210**	**4.040**	**4.287**	**17.644**
42	**78.130**	**73.850**	**75.800**	**75.927**	**5.040**	**6.300**	**5.990**	**5.777**	**13.144**
43	**74.820**	**75.750**	**75.540**	**75.370**	**3.270**	**3.870**	**4.060**	**3.733**	**20.188**
44	**76.970**	**75.410**	**75.160**	**75.847**	**2.940**	**3.820**	**3.780**	**3.513**	**21.588**
45	**72.320**	**79.540**	**77.730**	**76.530**	**4.550**	**4.790**	**5.270**	**4.870**	**15.715**

Appendix XIX: Abdominal CT scan SNR spleen value calculation results from three ROIs for 90 images from FTC and ATCM protocols

Image NO.	FTC (spleen 3 ROIs)								
	mean 1	mean 2	mean 3	average	SD 1	SD 2	SD 3	average	SNR value
1	49.190	49.790	48.570	49.183	5.602	5.828	6.001	5.810	8.465
2	48.370	50.270	47.590	48.743	7.339	6.866	7.836	7.347	6.634
3	49.520	49.240	47.110	48.623	10.020	9.617	10.510	10.049	4.839
4	49.130	50.400	47.000	48.843	5.214	4.990	7.377	5.860	8.335
5	48.400	51.250	46.920	48.857	7.386	8.178	7.775	7.780	6.280
6	48.910	48.330	46.450	47.897	7.597	7.455	8.640	7.897	6.065
7	47.670	48.790	46.650	47.703	5.208	5.842	5.101	5.384	8.861
8	46.540	49.340	47.400	47.760	5.096	5.864	6.750	5.903	8.090
9	46.730	50.640	46.540	47.970	9.292	7.828	8.632	8.584	5.588
10	48.840	51.830	47.440	49.370	10.550	14.030	10.680	11.753	4.201
11	47.970	48.820	48.160	48.317	13.160	10.760	12.720	12.213	3.956
12	46.710	45.930	49.410	47.350	17.200	14.870	16.940	16.337	2.898
13	47.740	49.960	46.240	47.980	10.580	9.691	10.510	10.260	4.676
14	47.000	49.370	45.450	47.273	10.990	10.780	10.890	10.887	4.342
15	49.070	49.370	46.230	48.223	13.010	15.540	14.050	14.200	3.396
16	47.350	47.980	46.320	47.217	9.167	9.350	9.505	9.341	5.055
17	45.860	48.270	45.600	46.577	8.104	7.802	10.830	8.912	5.226
18	47.660	49.950	46.200	47.937	12.120	10.160	15.730	12.670	3.783
19	48.360	49.790	47.790	48.647	7.694	6.407	6.228	6.776	7.179
20	50.490	49.390	47.100	48.993	7.147	8.045	8.861	8.018	6.111
21	46.700	49.070	47.240	47.670	11.890	11.460	11.440	11.597	4.111
22	48.870	50.780	46.110	48.587	5.042	5.692	8.876	6.537	7.433
23	48.900	50.940	48.850	49.563	6.374	6.995	6.767	6.712	7.384
24	48.390	49.420	47.100	48.303	7.130	7.663	10.280	8.358	5.780
25	47.960	50.100	47.120	48.393	5.202	5.006	6.471	5.560	8.704
26	47.520	50.130	44.980	47.543	4.988	6.778	6.692	6.153	7.727
27	47.600	49.890	45.680	47.723	8.612	10.140	9.600	9.451	5.050
28	48.850	50.030	47.020	48.633	7.030	5.175	6.184	6.130	7.934
29	49.600	50.150	49.040	49.597	6.437	6.824	8.444	7.235	6.855
30	48.330	51.510	48.580	49.473	8.363	8.505	7.925	8.264	5.986
31	47.680	48.990	46.720	47.797	5.483	6.897	6.298	6.226	7.677
32	46.560	49.550	46.780	47.630	6.077	5.289	6.252	5.873	8.110
33	48.130	50.510	45.770	48.137	6.970	6.712	7.840	7.174	6.710
34	47.400	49.700	46.850	47.983	4.824	4.514	4.227	4.522	10.612
35	44.290	51.230	45.620	47.047	5.329	4.452	4.618	4.800	9.802
36	45.150	50.280	46.950	47.460	7.646	6.552	6.964	7.054	6.728
37	49.720	50.800	48.860	49.793	5.147	5.099	4.825	5.024	9.912
38	47.600	50.850	48.210	48.887	5.588	4.824	4.672	5.028	9.723
39	49.110	49.800	47.350	48.753	7.881	7.126	6.661	7.223	6.750
40	47.660	50.000	47.320	48.327	4.861	4.938	4.690	4.830	10.006
41	47.710	49.790	47.680	48.393	5.287	5.294	5.035	5.205	9.297
42	48.500	49.560	47.860	48.640	6.165	6.057	7.789	6.670	7.292
43	47.060	50.270	48.450	48.593	4.414	4.170	4.502	4.362	11.140
44	48.400	52.070	47.730	49.400	5.044	4.360	4.955	4.786	10.321
45	48.890	51.240	47.840	49.323	6.435	6.060	6.322	6.272	7.864
Image NO.	ATCM (spleen 3 ROIs)								
	mean 1	mean 2	mean 3	average	SD 1	SD 2	SD 3	average	SNR value
1	48.820	50.290	47.100	48.737	4.939	4.895	5.092	4.975	9.796
2	49.190	50.640	47.010	48.947	5.411	6.112	6.715	6.079	8.051
3	48.350	49.280	46.680	48.103	7.454	5.835	6.345	6.545	7.350
4	46.130	49.900	47.100	47.710	5.274	5.142	4.897	5.104	9.347
5	46.290	49.880	46.300	47.490	4.859	4.767	5.746	5.124	9.268

6	**47.630**	**49.070**	**47.840**	**48.180**	**5.525**	**6.615**	**7.455**	**6.532**	**7.376**
7	**46.930**	**50.680**	**47.900**	**48.503**	**5.227**	**4.298**	**6.808**	**5.444**	**8.909**
8	**46.130**	**49.370**	**46.740**	**47.413**	**4.784**	**4.648**	**4.505**	**4.646**	**10.206**
9	**47.490**	**51.930**	**48.990**	**49.470**	**6.325**	**6.022**	**6.725**	**6.357**	**7.782**
10	**47.440**	**50.410**	**48.180**	**48.677**	**11.580**	**11.460**	**13.390**	**12.143**	**4.009**
11	**50.240**	**51.670**	**46.450**	**49.453**	**14.410**	**13.530**	**13.040**	**13.660**	**3.620**
12	**51.240**	**49.490**	**48.490**	**49.740**	**12.740**	**12.370**	**12.790**	**12.633**	**3.937**
13	**46.990**	**49.510**	**46.520**	**47.673**	**12.190**	**12.560**	**12.540**	**12.430**	**3.835**
14	**47.360**	**50.860**	**47.810**	**48.677**	**11.960**	**12.730**	**12.800**	**12.497**	**3.895**
15	**48.320**	**49.520**	**47.800**	**48.547**	**11.720**	**11.680**	**12.900**	**12.100**	**4.012**
16	**44.720**	**50.060**	**47.030**	**47.270**	**10.610**	**12.640**	**12.270**	**11.840**	**3.992**
17	**46.020**	**49.530**	**48.630**	**48.060**	**9.353**	**12.150**	**12.060**	**11.188**	**4.296**
18	**43.860**	**50.150**	**46.360**	**46.790**	**9.996**	**12.200**	**13.480**	**11.892**	**3.935**
19	**46.120**	**48.820**	**46.260**	**47.067**	**6.539**	**6.887**	**12.060**	**8.495**	**5.540**
20	**48.490**	**51.600**	**46.420**	**48.837**	**10.840**	**8.183**	**9.058**	**9.360**	**5.217**
21	**49.060**	**49.990**	**48.950**	**49.333**	**6.964**	**8.541**	**8.728**	**8.078**	**6.107**
22	**47.860**	**51.350**	**47.720**	**48.977**	**8.557**	**7.641**	**8.392**	**8.197**	**5.975**
23	**46.830**	**49.780**	**45.550**	**47.387**	**7.741**	**7.487**	**7.988**	**7.739**	**6.123**
24	**48.230**	**50.440**	**48.380**	**49.017**	**6.831**	**8.613**	**10.350**	**8.598**	**5.701**
25	**47.580**	**50.480**	**45.640**	**47.900**	**6.658**	**7.581**	**9.093**	**7.777**	**6.159**
26	**47.750**	**51.200**	**47.440**	**48.797**	**6.595**	**7.049**	**7.982**	**7.209**	**6.769**
27	**45.050**	**50.790**	**49.470**	**48.437**	**6.965**	**7.020**	**7.255**	**7.080**	**6.841**
28	**48.440**	**50.460**	**48.180**	**49.027**	**5.167**	**5.065**	**4.814**	**5.015**	**9.775**
29	**46.820**	**50.970**	**47.570**	**48.453**	**5.367**	**6.091**	**5.624**	**5.694**	**8.510**
30	**48.230**	**48.800**	**47.450**	**48.160**	**6.373**	**6.628**	**7.922**	**6.974**	**6.905**
31	**47.180**	**49.890**	**46.790**	**47.953**	**4.571**	**5.397**	**5.846**	**5.271**	**9.097**
32	**47.130**	**49.930**	**46.670**	**47.910**	**4.105**	**4.898**	**5.365**	**4.789**	**10.003**
33	**47.060**	**50.960**	**46.040**	**48.020**	**7.017**	**7.718**	**7.864**	**7.533**	**6.375**
34	**48.190**	**49.720**	**48.030**	**48.647**	**5.282**	**4.173**	**4.475**	**4.643**	**10.477**
35	**48.120**	**51.250**	**47.050**	**48.807**	**4.889**	**4.378**	**4.485**	**4.584**	**10.647**
36	**46.750**	**51.050**	**46.710**	**48.170**	**5.729**	**5.426**	**5.012**	**5.389**	**8.939**
37	**47.800**	**50.050**	**46.210**	**48.020**	**5.109**	**5.075**	**4.727**	**4.970**	**9.661**
38	**48.110**	**50.160**	**47.890**	**48.720**	**4.982**	**4.660**	**5.411**	**5.018**	**9.710**
39	**49.800**	**49.940**	**46.720**	**48.820**	**6.156**	**7.135**	**6.381**	**6.557**	**7.445**
40	**47.240**	**49.730**	**46.260**	**47.743**	**4.024**	**4.733**	**5.420**	**4.726**	**10.103**
41	**49.150**	**49.570**	**46.940**	**48.553**	**4.797**	**5.691**	**4.548**	**5.012**	**9.687**
42	**47.560**	**51.780**	**48.590**	**49.310**	**6.278**	**5.635**	**6.459**	**6.124**	**8.052**
43	**47.150**	**50.810**	**47.450**	**48.470**	**4.066**	**4.743**	**4.412**	**4.407**	**10.998**
44	**48.140**	**49.750**	**48.570**	**48.820**	**4.013**	**4.079**	**4.526**	**4.206**	**11.607**
45	**46.670**	**51.250**	**47.230**	**48.383**	**6.067**	**6.776**	**5.686**	**6.176**	**7.834**

Appendix XX: Abdominal CT scan SNR pancreas value calculation results from three ROIs for 90 images from FTC and ATCM protocols

Image NO.	FTC (pancreas 3 ROIs)								
	mean 1	mean 2	mean 3	average	SD 1	SD 2	SD 3	average	SNR value
1	22.290	24.380	24.350	23.673	6.500	5.510	5.420	5.810	4.075
2	24.530	25.530	22.240	24.100	5.560	5.930	8.910	6.800	3.544
3	24.290	25.020	22.400	23.903	8.030	8.500	10.480	9.003	2.655
4	24.050	25.940	22.210	24.067	5.850	4.860	5.230	5.313	4.529
5	24.780	24.690	21.650	23.707	5.560	4.420	7.470	5.817	4.076
6	24.510	26.270	21.260	24.013	8.250	6.630	10.320	8.400	2.859
7	21.540	25.300	21.000	22.613	4.950	4.680	4.990	4.873	4.640
8	23.330	22.990	20.100	22.140	5.190	5.160	6.120	5.490	4.033
9	22.920	25.310	21.310	23.180	7.830	5.840	8.900	7.523	3.081
10	24.260	25.580	22.070	23.970	9.640	8.680	11.610	9.977	2.403
11	24.670	26.090	23.890	24.883	10.510	9.210	11.540	10.420	2.388
12	23.660	26.710	22.870	24.413	12.430	11.930	14.980	13.113	1.862
13	24.090	26.140	21.090	23.773	10.630	8.520	10.840	9.997	2.378
14	23.450	25.240	23.050	23.913	8.900	7.120	10.080	8.700	2.749
15	23.190	25.550	22.110	23.617	13.540	12.850	19.400	15.263	1.547
16	24.500	25.630	22.840	24.323	7.500	7.130	9.310	7.980	3.048
17	24.470	24.170	22.260	23.633	7.620	7.290	9.610	8.173	2.892
18	24.630	26.890	21.010	24.177	10.900	10.270	13.950	11.707	2.065
19	23.400	25.960	22.210	23.857	8.450	5.720	9.010	7.727	3.088
20	23.150	25.220	22.160	23.510	7.250	6.670	10.280	8.067	2.914
21	23.400	27.810	22.670	24.627	10.510	7.820	12.850	10.393	2.369
22	24.650	26.770	21.640	24.353	5.480	6.300	9.730	7.170	3.397
23	24.230	25.380	20.230	23.280	7.420	5.230	9.420	7.357	3.164
24	23.190	23.460	21.550	22.733	8.290	6.710	9.690	8.230	2.762
25	23.810	25.480	22.940	24.077	6.610	5.220	5.350	5.727	4.204
26	21.410	23.070	19.160	21.213	7.110	6.210	8.960	7.427	2.856
27	20.250	24.710	20.220	21.727	7.060	6.710	9.610	7.793	2.788
28	24.930	25.460	21.490	23.960	4.760	4.360	8.020	5.713	4.194
29	25.180	25.420	22.800	24.467	6.670	6.000	6.580	6.417	3.813
30	23.480	25.580	24.140	24.400	7.230	7.310	8.410	7.650	3.190
31	22.170	23.700	20.510	22.127	6.120	4.490	6.850	5.820	3.802
32	25.550	26.650	23.400	25.200	4.830	4.880	5.810	5.173	4.871
33	24.770	24.460	20.490	23.240	5.940	6.390	9.420	7.250	3.206
34	25.640	25.890	21.470	24.333	4.110	3.990	5.420	4.507	5.399
35	24.350	25.750	22.890	24.330	4.990	4.490	5.350	4.943	4.922
36	23.700	27.520	20.970	24.063	8.870	5.730	7.930	7.510	3.204
37	25.010	25.550	23.170	24.577	4.540	4.980	4.830	4.783	5.138
38	24.740	25.670	22.810	24.407	4.580	4.430	5.650	4.887	4.995
39	25.000	25.130	22.640	24.257	5.900	6.160	6.480	6.180	3.925
40	24.360	25.270	22.970	24.200	4.340	4.430	4.340	4.370	5.538
41	24.940	25.310	22.320	24.190	4.010	4.650	4.860	4.507	5.368
42	23.850	26.660	21.910	24.140	5.750	5.710	5.910	5.790	4.169
43	25.000	25.610	21.760	24.123	3.750	3.510	4.510	3.923	6.149
44	22.280	23.010	22.020	22.437	4.810	4.250	5.520	4.860	4.617
45	23.590	26.220	20.490	23.433	5.940	4.690	6.360	5.663	4.138
Image NO.	ATCM (pancreas 3 ROIs)								
	mean 1	mean 2	mean 3	average	SD 1	SD 2	SD 3	average	SNR value
1	24.370	25.230	22.020	23.873	6.540	5.350	7.730	6.540	3.650
2	24.020	25.370	23.250	24.213	5.890	5.670	6.920	6.160	3.931
3	24.500	25.640	22.810	24.317	6.530	6.920	6.890	6.780	3.587
4	23.540	25.060	22.900	23.833	5.620	5.010	6.280	5.637	4.228
5	24.680	26.390	22.310	24.460	5.130	5.480	5.870	5.493	4.453

6	**23.420**	**24.930**	**22.410**	**23.587**	**7.890**	**5.450**	**6.670**	**6.670**	**3.536**
7	**24.310**	**25.090**	**22.250**	**23.883**	**5.240**	**4.730**	**6.320**	**5.430**	**4.398**
8	**24.280**	**25.330**	**22.130**	**23.913**	**5.380**	**5.540**	**6.400**	**5.773**	**4.142**
9	**24.560**	**26.080**	**22.790**	**24.477**	**7.690**	**5.320**	**7.160**	**6.723**	**3.641**
10	**24.060**	**25.830**	**22.020**	**23.970**	**11.470**	**10.790**	**13.480**	**11.913**	**2.012**
11	**24.760**	**25.790**	**22.370**	**24.307**	**11.780**	**13.830**	**15.540**	**13.717**	**1.772**
12	**24.070**	**26.440**	**22.770**	**24.427**	**13.020**	**11.940**	**13.500**	**12.820**	**1.905**
13	**25.420**	**26.180**	**21.590**	**24.397**	**10.780**	**10.310**	**10.290**	**10.460**	**2.332**
14	**24.130**	**25.600**	**22.370**	**24.033**	**11.780**	**9.640**	**16.140**	**12.520**	**1.920**
15	**24.860**	**25.670**	**21.100**	**23.877**	**12.930**	**11.170**	**14.760**	**12.953**	**1.843**
16	**24.880**	**25.310**	**21.110**	**23.767**	**10.470**	**10.840**	**12.110**	**11.140**	**2.133**
17	**23.480**	**25.380**	**21.340**	**23.400**	**10.240**	**9.680**	**10.340**	**10.087**	**2.320**
18	**24.700**	**26.360**	**21.270**	**24.110**	**11.250**	**13.740**	**11.270**	**12.087**	**1.995**
19	**24.630**	**25.060**	**21.150**	**23.613**	**8.310**	**6.920**	**10.860**	**8.697**	**2.715**
20	**24.080**	**26.800**	**22.160**	**24.347**	**9.550**	**7.150**	**9.530**	**8.743**	**2.785**
21	**24.440**	**25.130**	**22.950**	**24.173**	**9.500**	**8.560**	**9.110**	**9.057**	**2.669**
22	**24.880**	**26.050**	**21.170**	**24.033**	**6.790**	**8.080**	**8.560**	**7.810**	**3.077**
23	**24.900**	**25.290**	**21.400**	**23.863**	**9.180**	**8.230**	**6.890**	**8.100**	**2.946**
24	**23.390**	**25.870**	**22.750**	**24.003**	**9.850**	**8.810**	**8.940**	**9.200**	**2.609**
25	**24.670**	**25.080**	**21.810**	**23.853**	**7.400**	**7.040**	**8.520**	**7.653**	**3.117**
26	**24.550**	**25.760**	**21.070**	**23.793**	**6.890**	**6.960**	**10.400**	**8.083**	**2.944**
27	**24.460**	**26.800**	**21.010**	**24.090**	**7.380**	**6.920**	**9.170**	**7.823**	**3.079**
28	**24.980**	**25.890**	**22.790**	**24.553**	**4.170**	**5.140**	**6.450**	**5.253**	**4.674**
29	**24.880**	**25.680**	**22.700**	**24.420**	**4.880**	**4.320**	**5.240**	**4.813**	**5.073**
30	**24.610**	**26.530**	**21.770**	**24.303**	**7.010**	**6.790**	**9.350**	**7.717**	**3.149**
31	**24.770**	**26.130**	**22.410**	**24.437**	**4.290**	**4.460**	**5.500**	**4.750**	**5.145**
32	**24.760**	**25.660**	**22.940**	**24.453**	**4.430**	**4.150**	**5.880**	**4.820**	**5.073**
33	**24.870**	**25.430**	**22.830**	**24.377**	**5.230**	**5.420**	**6.890**	**5.847**	**4.169**
34	**24.250**	**25.720**	**22.560**	**24.177**	**5.440**	**3.130**	**5.720**	**4.763**	**5.076**
35	**25.100**	**27.560**	**21.810**	**24.823**	**4.090**	**4.080**	**7.140**	**5.103**	**4.864**
36	**23.880**	**24.050**	**21.940**	**23.290**	**4.550**	**4.040**	**5.740**	**4.777**	**4.876**
37	**24.850**	**25.100**	**22.240**	**24.063**	**4.480**	**3.510**	**6.030**	**4.673**	**5.149**
38	**24.920**	**26.070**	**22.590**	**24.527**	**4.110**	**4.500**	**5.640**	**4.750**	**5.164**
39	**25.660**	**25.750**	**22.680**	**24.697**	**6.120**	**5.620**	**8.570**	**6.770**	**3.648**
40	**24.640**	**25.440**	**22.480**	**24.187**	**4.020**	**4.020**	**6.150**	**4.730**	**5.113**
41	**24.080**	**25.180**	**20.970**	**23.410**	**4.920**	**3.880**	**6.430**	**5.077**	**4.611**
42	**24.080**	**24.730**	**21.190**	**23.333**	**7.260**	**5.290**	**7.250**	**6.600**	**3.535**
43	**23.870**	**25.100**	**21.660**	**23.543**	**3.540**	**3.290**	**4.520**	**3.783**	**6.223**
44	**24.120**	**24.800**	**21.220**	**23.380**	**4.140**	**3.990**	**5.620**	**4.583**	**5.101**
45	**24.360**	**26.560**	**21.600**	**24.173**	**6.570**	**5.420**	**6.020**	**6.003**	**4.027**

Appendix XXI : Abdominal CT scan SNR left kidney value calculation results from three ROIs for 90 images from FTC and ATCM protocols

Image NO.	FTC (Lt. kidney 3 ROIs)								
	mean 1	mean 2	mean 3	average	SD 1	SD 2	SD 3	average	SNR value
1	22.850	25.670	21.560	23.360	5.041	6.649	8.181	6.624	3.527
2	22.920	24.230	21.640	22.930	6.714	6.132	6.771	6.539	3.507
3	22.270	24.180	20.620	22.357	7.032	7.055	7.821	7.303	3.061
4	23.210	25.630	21.710	23.517	5.665	6.672	5.837	6.058	3.882
5	23.990	26.090	21.900	23.993	5.624	6.566	5.088	5.759	4.166
6	22.770	25.560	20.390	22.907	7.174	7.441	7.852	7.489	3.059
7	22.870	24.580	22.630	23.360	4.071	5.506	4.572	4.716	4.953
8	22.200	25.540	21.130	22.957	4.994	4.575	4.553	4.707	4.877
9	22.390	25.450	20.600	22.813	8.255	6.775	7.475	7.502	3.041
10	22.400	26.010	22.510	23.640	10.990	11.350	9.325	10.555	2.240
11	22.770	25.910	22.280	23.653	10.270	11.200	10.340	10.603	2.231
12	22.290	26.960	22.690	23.980	12.860	9.732	11.330	11.307	2.121
13	22.280	25.140	21.960	23.127	7.731	8.549	11.740	9.340	2.476
14	22.480	25.010	22.950	23.480	9.336	8.960	10.800	9.699	2.421
15	22.270	25.190	22.800	23.420	13.260	12.500	14.390	13.383	1.750
16	22.790	24.180	21.030	22.667	6.335	7.014	8.616	7.322	3.096
17	22.620	25.680	21.180	23.160	8.452	7.751	7.992	8.065	2.872
18	22.570	25.660	22.500	23.577	10.870	9.982	10.840	10.564	2.232
19	22.670	25.020	21.720	23.137	6.188	6.642	7.534	6.788	3.408
20	22.560	25.290	22.330	23.393	7.861	5.990	7.480	7.110	3.290
21	22.590	25.620	21.750	23.320	7.190	9.010	7.020	7.740	3.013
22	22.820	25.290	21.260	23.123	6.148	7.159	6.719	6.675	3.464
23	23.890	25.500	21.360	23.583	6.502	6.822	8.115	7.146	3.300
24	22.960	25.240	21.660	23.287	7.227	7.118	7.849	7.398	3.148
25	22.180	25.990	22.210	23.460	6.354	8.130	5.293	6.592	3.559
26	22.390	25.720	21.780	23.297	5.950	6.551	5.842	6.114	3.810
27	22.670	25.080	21.500	23.083	8.489	7.505	6.632	7.542	3.061
28	22.030	25.210	20.840	22.693	4.861	6.446	5.922	5.743	3.951
29	22.800	25.270	22.030	23.367	5.424	5.592	6.802	5.939	3.934
30	22.310	25.390	21.430	23.043	9.743	8.954	6.670	8.456	2.725
31	22.660	25.120	22.670	23.483	5.284	5.646	5.767	5.566	4.219
32	22.580	24.000	20.950	22.510	6.052	5.432	5.139	5.541	4.062
33	22.910	25.200	21.210	23.107	8.272	5.511	7.295	7.026	3.289
34	21.170	24.180	20.950	22.100	4.919	4.285	4.966	4.723	4.679
35	22.660	25.470	21.180	23.103	5.141	5.431	4.301	4.958	4.660
36	22.700	24.550	22.330	23.193	5.870	5.477	4.990	5.446	4.259
37	23.020	25.710	22.060	23.597	5.262	4.662	5.623	5.182	4.553
38	23.620	25.570	22.100	23.763	4.979	4.869	5.315	5.054	4.702
39	22.660	24.700	22.750	23.370	6.323	6.520	5.391	6.078	3.845
40	22.020	25.060	21.270	22.783	4.636	4.925	4.191	4.584	4.970
41	22.600	25.140	20.970	22.903	4.897	5.221	5.335	5.151	4.446
42	23.220	25.450	20.940	23.203	5.350	6.540	5.120	5.670	4.092
43	21.290	25.860	21.330	22.827	4.231	4.182	4.326	4.246	5.376
44	23.030	25.560	21.180	23.257	4.468	4.096	4.671	4.412	5.272
45	23.480	25.100	22.820	23.800	5.562	4.068	5.304	4.978	4.781
Image NO.	ATCM (Lt. kidney 3 ROIs)								
	mean 1	mean 2	mean 3	average	SD 1	SD 2	SD 3	average	SNR value
1	23.200	25.090	21.200	23.163	5.229	6.621	5.789	5.880	3.940
2	22.660	25.190	21.050	22.967	6.775	6.918	5.727	6.473	3.548
3	23.280	24.910	22.250	23.480	7.636	6.102	5.633	6.457	3.636
4	22.260	25.650	21.130	23.013	6.231	6.521	5.499	6.084	3.783
5	21.380	25.120	20.780	22.427	5.689	5.966	5.130	5.595	4.008

6	**23.040**	**24.020**	**21.090**	**22.717**	**6.495**	**6.138**	**5.628**	**6.087**	**3.732**
7	**23.580**	**24.380**	**20.720**	**22.893**	**5.058**	**5.589**	**4.910**	**5.186**	**4.415**
8	**22.180**	**25.520**	**21.870**	**23.190**	**6.434**	**5.604**	**5.963**	**6.000**	**3.865**
9	**22.640**	**25.910**	**22.630**	**23.727**	**7.496**	**4.985**	**5.325**	**5.935**	**3.998**
10	**23.490**	**24.160**	**22.040**	**23.230**	**14.380**	**15.100**	**14.260**	**14.580**	**1.593**
11	**22.150**	**25.690**	**22.410**	**23.417**	**14.430**	**12.200**	**12.700**	**13.110**	**1.786**
12	**22.200**	**24.730**	**20.790**	**22.573**	**13.750**	**12.300**	**11.860**	**12.637**	**1.786**
13	**22.710**	**24.700**	**22.110**	**23.173**	**12.090**	**10.390**	**10.330**	**10.937**	**2.119**
14	**22.020**	**25.960**	**20.180**	**22.720**	**14.290**	**13.810**	**12.400**	**13.500**	**1.683**
15	**23.630**	**25.170**	**21.610**	**23.470**	**14.300**	**14.660**	**10.220**	**13.060**	**1.797**
16	**23.580**	**25.400**	**21.020**	**23.333**	**15.030**	**11.510**	**12.850**	**13.130**	**1.777**
17	**22.350**	**25.930**	**22.200**	**23.493**	**13.990**	**10.400**	**10.810**	**11.733**	**2.002**
18	**23.620**	**24.590**	**21.960**	**23.390**	**11.680**	**12.200**	**10.920**	**11.600**	**2.016**
19	**23.370**	**25.040**	**22.130**	**23.513**	**7.285**	**8.148**	**7.918**	**7.784**	**3.021**
20	**22.560**	**24.480**	**21.950**	**22.997**	**8.900**	**9.180**	**8.014**	**8.698**	**2.644**
21	**22.031**	**25.880**	**22.290**	**23.400**	**8.734**	**8.930**	**9.147**	**8.937**	**2.618**
22	**22.270**	**25.620**	**21.370**	**23.087**	**8.137**	**8.925**	**8.123**	**8.395**	**2.750**
23	**23.650**	**25.080**	**20.090**	**22.940**	**8.642**	**8.782**	**7.333**	**8.252**	**2.780**
24	**23.090**	**25.400**	**20.640**	**23.043**	**7.968**	**8.650**	**8.752**	**8.457**	**2.725**
25	**23.410**	**25.160**	**21.110**	**23.227**	**7.605**	**6.065**	**7.923**	**7.198**	**3.227**
26	**23.680**	**24.940**	**23.660**	**24.093**	**8.090**	**7.417**	**6.522**	**7.343**	**3.281**
27	**23.520**	**25.140**	**21.110**	**23.257**	**8.108**	**8.007**	**10.750**	**8.955**	**2.597**
28	**23.560**	**24.190**	**22.770**	**23.507**	**5.409**	**5.410**	**4.161**	**4.993**	**4.708**
29	**22.700**	**24.870**	**21.760**	**23.110**	**5.205**	**6.823**	**4.778**	**5.602**	**4.125**
30	**23.840**	**24.190**	**21.100**	**23.043**	**6.194**	**7.867**	**6.336**	**6.799**	**3.389**
31	**23.240**	**24.790**	**21.230**	**23.087**	**4.998**	**5.895**	**4.235**	**5.043**	**4.578**
32	**22.580**	**25.130**	**20.330**	**22.680**	**5.434**	**6.732**	**6.208**	**6.125**	**3.703**
33	**23.630**	**24.880**	**20.250**	**22.920**	**5.750**	**7.542**	**5.898**	**6.397**	**3.583**
34	**22.100**	**24.330**	**21.950**	**22.793**	**4.476**	**4.653**	**4.199**	**4.443**	**5.131**
35	**22.380**	**25.330**	**20.910**	**22.873**	**5.015**	**5.036**	**5.047**	**5.033**	**4.545**
36	**23.000**	**25.180**	**20.130**	**22.770**	**5.163**	**6.526**	**6.990**	**6.226**	**3.657**
37	**22.730**	**25.264**	**20.640**	**22.878**	**4.710**	**4.264**	**5.010**	**4.661**	**4.908**
38	**23.460**	**24.960**	**21.950**	**23.457**	**4.890**	**5.974**	**3.982**	**4.949**	**4.740**
39	**23.650**	**24.490**	**21.480**	**23.207**	**5.102**	**5.274**	**5.941**	**5.439**	**4.267**
40	**22.110**	**24.530**	**20.400**	**22.347**	**4.337**	**5.524**	**4.512**	**4.791**	**4.664**
41	**23.780**	**24.620**	**21.480**	**23.293**	**5.461**	**4.653**	**5.003**	**5.039**	**4.623**
42	**22.600**	**24.800**	**21.610**	**23.003**	**5.301**	**5.665**	**5.287**	**5.418**	**4.246**
43	**23.120**	**24.430**	**21.550**	**23.033**	**4.066**	**4.523**	**4.008**	**4.199**	**5.485**
44	**23.490**	**24.640**	**21.350**	**23.160**	**4.332**	**5.320**	**4.213**	**4.622**	**5.011**
45	**23.760**	**24.630**	**21.990**	**23.460**	**6.246**	**4.952**	**5.968**	**5.722**	**4.100**

Appendix XXII: Abdominal CT scan SNR right kidney value calculation results from three ROIs for 90 images from FTC and ATCM protocols

Image NO.	FTC (Rt. kidney 3 ROIs)								
	mean 1	mean 2	mean 3	average	SD 1	SD 2	SD 3	average	SNR value
1	22.890	25.410	22.950	23.750	5.240	6.410	6.550	6.067	3.915
2	23.010	25.020	25.450	24.493	5.520	6.060	5.880	5.820	4.208
3	23.660	25.110	24.470	24.413	8.330	8.030	6.010	7.457	3.274
4	22.830	25.640	24.920	24.463	5.340	5.500	4.880	5.240	4.669
5	22.140	24.560	24.600	23.767	5.790	5.820	5.080	5.563	4.272
6	22.120	24.460	23.600	23.393	7.660	6.920	7.850	7.477	3.129
7	21.120	25.870	23.310	23.433	5.740	5.950	4.210	5.300	4.421
8	22.320	25.540	25.370	24.410	4.840	4.990	4.370	4.733	5.157
9	21.610	25.690	23.570	23.623	7.430	7.330	6.870	7.210	3.276
10	22.490	25.620	25.580	24.563	7.450	7.670	8.590	7.903	3.108
11	22.590	25.320	24.140	24.017	9.220	9.970	9.440	9.543	2.517
12	23.420	25.580	24.760	24.587	14.070	13.780	11.090	12.980	1.894
13	22.090	25.790	24.270	24.050	8.750	8.540	6.410	7.900	3.044
14	22.820	25.180	24.250	24.083	11.050	10.900	8.310	10.087	2.388
15	22.060	24.580	24.160	23.600	11.530	12.760	11.230	11.840	1.993
16	22.620	25.180	24.970	24.257	7.320	7.820	7.210	7.450	3.256
17	23.030	25.850	24.460	24.447	8.520	8.180	6.920	7.873	3.105
18	21.610	24.870	23.040	23.173	12.550	10.060	8.030	10.213	2.269
19	22.340	25.050	24.740	24.043	5.850	8.030	5.670	6.517	3.690
20	22.350	25.020	23.980	23.783	7.020	6.980	6.490	6.830	3.482
21	22.520	25.360	23.960	23.947	7.450	8.870	7.440	7.920	3.024
22	22.680	25.440	23.460	23.860	6.060	6.240	6.360	6.220	3.836
23	22.970	25.470	23.640	24.027	6.120	9.200	6.800	7.373	3.259
24	22.080	25.320	23.490	23.630	7.280	8.320	8.250	7.950	2.972
25	21.060	25.610	23.740	23.470	6.780	6.750	5.700	6.410	3.661
26	21.900	24.960	23.260	23.373	6.870	6.810	5.110	6.263	3.732
27	22.260	24.610	23.070	23.313	6.960	7.700	7.550	7.403	3.149
28	23.840	24.100	25.280	24.407	5.650	6.550	4.540	5.580	4.374
29	22.300	24.870	24.800	23.990	5.600	5.120	5.260	5.327	4.504
30	21.810	25.230	23.950	23.663	6.820	7.700	5.950	6.823	3.468
31	22.070	24.980	24.470	23.840	5.910	5.630	5.140	5.560	4.288
32	23.150	24.900	24.970	24.340	5.140	5.720	4.970	5.277	4.613
33	21.420	24.780	23.240	23.147	6.770	6.550	5.410	6.243	3.707
34	23.530	24.570	24.820	24.307	5.630	5.360	5.120	5.370	4.526
35	22.070	24.640	23.750	23.487	5.310	5.070	4.980	5.120	4.587
36	21.510	24.660	23.320	23.163	5.610	6.530	5.450	5.863	3.951
37	23.490	25.130	23.950	24.190	5.300	4.940	4.910	5.050	4.790
38	23.290	25.010	24.300	24.200	5.140	5.430	4.960	5.177	4.675
39	24.490	25.340	23.250	24.360	5.770	6.930	5.880	6.193	3.933
40	23.120	25.610	24.140	24.290	4.920	4.760	4.130	4.603	5.277
41	23.130	25.350	24.540	24.340	4.330	4.910	4.260	4.500	5.409
42	21.180	24.230	23.460	22.957	5.520	6.320	5.340	5.727	4.009
43	23.740	24.760	24.950	24.483	5.020	4.250	3.950	4.407	5.556
44	22.220	24.650	23.720	23.530	5.110	5.420	3.570	4.700	5.006
45	22.240	24.710	22.410	23.120	4.980	5.630	5.520	5.377	4.300
Protocols NO.	ATCM (Rt. kidney 3 ROIs)								
	mean 1	mean 2	mean 3	average	SD 1	SD 2	SD 3	average	SNR value
1	23.790	24.980	23.550	24.107	6.740	6.670	6.510	6.640	3.631
2	23.930	24.680	24.880	24.497	7.030	7.190	5.930	6.717	3.647
3	23.920	24.120	24.810	24.283	6.820	7.400	6.810	7.010	3.464
4	23.240	24.630	24.690	24.187	6.270	6.140	5.020	5.810	4.163
5	22.980	24.900	24.650	24.177	6.100	6.030	6.020	6.050	3.996

6	**21.840**	**24.430**	**23.660**	**23.310**	**6.930**	**6.110**	**6.090**	**6.377**	**3.656**
7	**23.640**	**24.530**	**24.690**	**24.287**	**5.420**	**5.610**	**5.090**	**5.373**	**4.520**
8	**22.330**	**24.710**	**22.930**	**23.323**	**5.830**	**6.240**	**4.800**	**5.623**	**4.148**
9	**21.550**	**23.830**	**23.130**	**22.837**	**5.890**	**6.460**	**5.190**	**5.847**	**3.906**
10	**23.670**	**24.530**	**24.790**	**24.330**	**13.720**	**12.020**	**12.800**	**12.847**	**1.894**
11	**23.520**	**24.170**	**24.280**	**23.990**	**13.500**	**14.230**	**13.710**	**13.813**	**1.737**
12	**23.360**	**24.900**	**24.140**	**24.133**	**13.230**	**14.630**	**12.520**	**13.460**	**1.793**
13	**23.470**	**24.970**	**24.830**	**24.423**	**13.280**	**13.250**	**11.900**	**12.810**	**1.907**
14	**23.120**	**24.050**	**24.090**	**23.753**	**12.520**	**11.250**	**11.090**	**11.620**	**2.044**
15	**23.220**	**24.630**	**24.120**	**23.990**	**12.390**	**10.500**	**12.650**	**11.847**	**2.025**
16	**23.630**	**24.130**	**23.170**	**23.643**	**10.150**	**12.320**	**9.740**	**10.737**	**2.202**
17	**22.330**	**24.640**	**24.210**	**23.727**	**11.070**	**12.540**	**11.530**	**11.713**	**2.026**
18	**21.250**	**24.900**	**23.780**	**23.310**	**13.700**	**13.190**	**12.910**	**13.267**	**1.757**
19	**23.540**	**24.550**	**24.860**	**24.317**	**8.930**	**7.240**	**7.280**	**7.817**	**3.111**
20	**22.770**	**24.720**	**24.690**	**24.060**	**7.920**	**11.600**	**6.960**	**8.827**	**2.726**
21	**23.350**	**24.110**	**24.910**	**24.123**	**8.730**	**8.880**	**8.350**	**8.653**	**2.788**
22	**23.170**	**24.630**	**24.160**	**23.987**	**8.540**	**9.660**	**7.560**	**8.587**	**2.793**
23	**22.130**	**25.580**	**24.830**	**24.180**	**9.020**	**7.420**	**6.980**	**7.807**	**3.097**
24	**22.120**	**24.060**	**24.550**	**23.577**	**8.370**	**9.080**	**7.890**	**8.447**	**2.791**
25	**23.640**	**24.780**	**24.820**	**24.413**	**8.140**	**8.540**	**7.240**	**7.973**	**3.062**
26	**22.480**	**24.250**	**23.640**	**23.457**	**7.130**	**9.110**	**7.220**	**7.820**	**3.000**
27	**23.110**	**24.140**	**23.480**	**23.577**	**9.150**	**8.020**	**8.460**	**8.543**	**2.760**
28	**23.350**	**24.410**	**24.270**	**24.010**	**5.290**	**4.960**	**5.120**	**5.123**	**4.686**
29	**22.100**	**24.690**	**24.060**	**23.617**	**5.880**	**5.870**	**5.900**	**5.883**	**4.014**
30	**23.620**	**24.300**	**24.800**	**24.240**	**6.350**	**6.900**	**6.140**	**6.463**	**3.750**
31	**23.530**	**24.520**	**24.500**	**24.183**	**4.550**	**5.300**	**4.012**	**4.621**	**5.234**
32	**24.820**	**24.450**	**24.360**	**24.543**	**4.270**	**5.470**	**3.950**	**4.563**	**5.378**
33	**23.390**	**24.410**	**24.670**	**24.157**	**6.070**	**5.340**	**5.120**	**5.510**	**4.384**
34	**23.230**	**24.720**	**24.640**	**24.197**	**5.650**	**4.740**	**4.500**	**4.963**	**4.875**
35	**23.630**	**24.720**	**24.580**	**24.310**	**5.280**	**6.050**	**6.080**	**5.803**	**4.189**
36	**21.520**	**23.840**	**23.580**	**22.980**	**6.220**	**5.160**	**4.090**	**5.157**	**4.456**
37	**23.720**	**24.980**	**24.540**	**24.413**	**5.400**	**5.150**	**4.780**	**5.110**	**4.778**
38	**23.570**	**24.570**	**24.250**	**24.130**	**4.290**	**5.600**	**5.110**	**5.000**	**4.826**
39	**23.160**	**24.380**	**24.410**	**23.983**	**6.560**	**6.850**	**6.310**	**6.573**	**3.649**
40	**23.760**	**24.730**	**24.210**	**24.233**	**4.550**	**4.980**	**4.250**	**4.593**	**5.276**
41	**23.860**	**24.330**	**24.970**	**24.387**	**4.100**	**4.920**	**4.420**	**4.480**	**5.443**
42	**22.250**	**24.090**	**23.420**	**23.253**	**6.280**	**5.650**	**4.330**	**5.420**	**4.290**
43	**23.880**	**24.560**	**24.850**	**24.430**	**4.330**	**3.910**	**4.350**	**4.197**	**5.821**
44	**21.370**	**24.790**	**24.200**	**23.453**	**4.320**	**4.280**	**4.120**	**4.240**	**5.531**
45	**23.720**	**24.590**	**24.930**	**24.413**	**6.540**	**6.880**	**4.760**	**6.060**	**4.029**

Appendix XXIII: Abdominal CT scan SNR value liver, spleen, pancreas ,Lt. kidney and Rt. kidney with different tube current comparing between FTC and ATCM

Protocols No.	FTC	ATCM	FTC	ATCM	FTC	ATCM	FTC	ATCM	FTC	ATCM
	liver		spleen		pancreas		Lt. Kidney		Rt. Kidney	
100/low dose + mA										
10	9.367	6.172	4.201	4.009	2.403	2.012	2.240	1.593	3.108	1.894
11	8.340	5.387	3.956	3.620	2.388	1.772	2.231	1.786	2.517	1.737
12	6.287	6.712	2.898	3.937	1.862	1.905	2.121	1.786	1.894	1.793
13	9.655	6.868	4.676	3.835	2.378	2.332	2.476	2.119	3.044	1.907
14	9.141	6.977	4.342	3.895	2.749	1.920	2.421	1.683	2.388	2.044
15	6.381	6.410	3.396	4.012	1.547	1.843	1.750	1.797	1.993	2.025
16	9.525	6.084	5.055	3.992	3.048	2.133	3.096	1.777	3.256	2.202
17	8.753	7.403	5.226	4.296	2.892	2.320	2.872	2.002	3.105	2.026
18	7.486	9.972	3.783	3.935	2.065	1.995	2.232	2.016	2.269	1.757
200/low dose mA										
19	10.592	9.645	7.179	5.540	3.088	2.715	3.408	3.021	3.690	3.111
20	9.799	9.583	6.111	5.217	2.914	2.785	3.290	2.644	3.482	2.726
21	8.579	9.643	4.111	6.107	2.369	2.669	3.013	2.618	3.024	2.788
22	10.692	10.006	7.433	5.975	3.397	3.077	3.464	2.750	3.836	2.793
23	10.881	9.485	7.384	6.123	3.164	2.946	3.300	2.780	3.259	3.097
24	9.142	9.752	5.780	5.701	2.762	2.609	3.148	2.725	2.972	2.791
25	11.321	10.297	8.704	6.159	4.204	3.117	3.559	3.227	3.661	3.062
26	9.942	9.953	7.727	6.769	2.856	2.944	3.810	3.281	3.732	3.000
27	9.735	11.105	5.050	6.841	2.788	3.079	3.061	2.597	3.149	2.760
250/standard mA										
1	14.697	13.396	8.465	9.796	4.075	3.650	3.527	3.940	3.915	3.631
2	11.916	15.259	6.634	8.051	3.544	3.931	3.507	3.548	4.208	3.647
3	9.921	11.343	4.839	7.350	2.655	3.587	3.061	3.636	3.274	3.464
4	15.665	14.299	8.335	9.347	4.529	4.228	3.882	3.783	4.669	4.163
5	13.513	13.551	6.280	9.268	4.076	4.453	4.166	4.008	4.272	3.996
6	11.410	13.151	6.065	7.376	2.859	3.536	3.059	3.732	3.129	3.656
7	16.862	15.679	8.861	8.909	4.640	4.398	4.953	4.415	4.421	4.520
8	15.343	15.061	8.090	10.206	4.033	4.142	4.877	3.865	5.157	4.148
9	11.703	13.766	5.588	7.782	3.081	3.641	3.041	3.998	3.276	3.906
300/quality mA										
28	14.633	14.066	7.934	9.775	4.194	4.674	3.951	4.708	4.374	4.686
29	13.023	16.258	6.855	8.510	3.813	5.073	3.934	4.125	4.504	4.014
30	11.305	13.039	5.986	6.905	3.190	3.149	2.725	3.389	3.468	3.750
31	13.317	15.930	7.677	9.097	3.802	5.145	4.219	4.578	5.288	5.234
32	15.050	15.710	8.110	10.003	4.871	5.073	4.062	3.703	4.613	5.378
33	10.807	13.212	6.710	6.375	3.206	4.169	3.289	3.583	3.707	4.384
34	17.588	15.038	10.612	10.477	5.399	5.076	4.679	5.131	4.526	4.875
35	16.393	17.616	9.802	10.647	4.922	4.864	4.660	4.545	4.587	4.189
36	12.869	16.623	6.728	8.939	3.204	4.876	4.259	3.657	3.951	4.456
400/ high quality mA										
37	16.958	18.746	9.912	9.661	5.138	5.149	4.553	4.908	4.790	4.778
38	15.037	16.698	9.723	9.710	4.995	5.164	4.702	4.740	4.675	4.826
39	13.129	12.202	6.750	7.445	3.925	3.648	3.845	4.267	3.933	3.649
40	19.518	20.061	10.006	10.103	5.538	5.113	4.970	4.664	5.277	5.276
41	18.288	17.644	9.297	9.687	5.368	4.611	4.446	4.623	5.409	5.443
42	13.245	13.144	7.292	8.052	4.169	3.535	4.092	4.246	4.009	4.290
43	21.401	20.188	11.140	10.998	6.149	6.223	5.376	5.485	5.556	5.821
44	20.606	21.588	10.321	11.607	4.617	5.101	5.272	5.011	5.006	5.531
45	14.969	15.715	7.864	7.834	4.138	4.027	4.781	4.100	4.300	4.029

Appendix XXIV : Abdominal CT scan SNR value liver, spleen, pancreas ,Lt. kidney and Rt. kidney with different pitch factors comparing between FTC and ATCM

Protocols No.	FTC	ATCM	FTC	ATCM	FTC	ATCM	FTC	ATCM	FTC	ATCM
	liver		spleen		pancreas		Lt. Kidney		Rt .Kidney	
Detail(0.688)										
1	14.697	13.396	8.465	9.796	4.075	3.650	3.527	3.940	3.915	3.631
4	15.665	14.299	8.335	9.347	4.529	4.228	3.882	3.783	4.669	4.163
7	16.862	15.679	8.861	8.909	4.640	4.398	4.953	4.415	4.421	4.520
10	9.367	6.172	4.201	4.009	2.403	2.012	2.240	1.593	3.108	1.894
13	9.655	6.868	4.676	3.835	2.378	2.332	2.476	2.119	3.044	3.907
16	9.525	6.084	5.055	3.992	3.048	2.133	3.096	1.777	3.256	2.202
19	10.592	9.645	7.179	5.540	3.088	2.715	3.408	3.021	3.690	3.111
22	10.692	10.006	7.433	5.975	3.397	3.077	3.464	2.750	3.836	2.793
25	11.321	10.297	8.704	6.159	4.204	3.117	3.559	3.227	3.661	3.062
28	14.633	14.066	7.934	9.775	4.194	4.674	3.951	4.708	4.374	4.686
31	13.317	15.930	7.677	9.097	3.802	5.145	4.219	4.578	4.288	5.234
34	17.588	15.038	10.612	10.477	5.399	5.076	4.679	5.131	4.526	4.875
37	16.958	18.746	9.912	9.661	5.138	5.149	4.553	4.908	4.790	4.778
40	19.518	20.061	10.006	10.103	5.538	5.113	4.970	4.664	5.277	5.276
43	21.401	20.188	11.140	10.998	6.149	6.223	5.376	5.485	5.556	5.821
Standard(0.938)										
2	11.916	15.259	6.634	8.051	3.544	3.931	3.507	3.548	4.208	3.647
5	13.513	13.551	6.280	9.268	4.076	4.453	4.166	4.008	4.272	3.996
8	15.343	15.061	8.090	10.206	4.033	4.142	4.877	3.865	5.157	4.148
11	8.340	5.387	3.956	3.620	2.388	1.772	2.231	1.786	2.517	1.737
14	9.141	6.977	4.342	3.895	2.749	1.920	2.421	1.683	2.388	2.044
17	8.753	7.403	5.226	4.296	2.892	2.320	2.872	2.002	3.105	2.026
20	9.799	9.583	6.111	5.217	2.914	2.785	3.290	2.644	3.482	2.726
23	10.881	9.485	7.384	6.123	3.164	2.946	3.300	2.780	3.259	3.097
26	9.942	9.953	7.727	6.769	2.856	2.944	3.810	3.281	3.732	3.000
29	13.023	16.258	6.855	8.510	3.813	5.073	3.934	4.125	4.504	4.014
32	15.050	15.710	8.110	10.003	4.871	5.073	4.062	3.703	4.613	5.378
35	16.393	17.616	9.802	10.647	4.922	4.864	4.660	4.545	4.587	4.189
38	15.037	16.698	9.723	9.710	4.995	5.164	4.702	4.740	4.675	4.826
41	18.288	17.644	9.297	9.687	5.368	4.611	4.446	4.623	5.409	5.443
44	20.606	21.588	10.321	11.607	4.617	5.101	5.272	5.011	5.006	5.531
Fast(1.438)										
3	9.921	11.343	4.839	7.350	2.655	3.587	3.061	3.636	3.274	3.464
6	11.410	13.151	6.065	7.376	2.859	3.536	3.059	3.732	3.129	3.656
9	11.703	13.766	5.588	7.782	3.081	3.641	3.041	3.998	3.276	3.906
12	6.287	6.712	2.898	3.937	1.862	1.905	2.121	1.786	1.894	1.793
15	6.381	6.410	3.396	4.012	1.547	1.843	1.750	1.797	1.993	2.025
18	7.486	9.972	3.783	3.935	2.065	1.995	2.232	2.016	2.269	1.757
21	8.579	9.643	4.111	6.107	2.369	2.669	3.013	2.618	3.024	2.788
24	9.142	9.752	5.780	5.701	2.762	2.609	3.148	2.725	2.972	2.791
27	9.735	11.105	5.050	6.841	2.788	3.079	3.061	2.597	3.149	2.760
30	11.305	13.039	5.986	6.905	3.190	3.149	2.725	3.389	3.468	3.750
33	10.807	13.212	6.710	6.375	3.206	4.169	3.289	3.583	3.707	4.384
36	12.869	16.623	6.728	8.939	3.204	4.876	4.259	3.657	3.951	4.456
39	13.129	12.202	6.750	7.445	3.925	3.648	3.845	4.267	3.933	3.649
42	13.245	13.144	7.292	8.052	4.169	3.535	4.092	4.246	4.009	4.290
45	14.969	15.715	7.864	7.834	4.138	4.027	4.781	4.100	4.300	4.029

Appendix XXV : Abdominal CT scan SNR value liver, spleen, pancreas ,Lt. kidney and Rt. kidney with different detector configuration comparing between FTC and ATCM

Protocols No.	FTC	ATCM	FTC	ATCM	FTC	ATCM	FTC	ATCM	FTC	ATCM
	liver		spleen		pancreas		Lt. Kidney		Rt. Kidney	
0.5×16mm										
1	14.697	13.396	8.465	9.796	4.075	3.650	3.527	3.940	3.915	3.631
2	11.916	15.259	6.634	8.051	3.544	3.931	3.507	3.548	4.208	3.647
3	9.921	11.343	4.839	7.350	2.655	3.587	3.061	3.636	3.274	3.464
10	9.367	6.172	4.201	4.009	2.403	2.012	2.240	1.593	3.108	1.894
11	8.340	5.387	3.956	3.620	2.388	1.772	2.231	1.786	2.517	1.737
12	6.287	6.712	2.898	3.937	1.862	1.905	2.121	1.786	1.894	1.793
19	10.592	9.645	7.179	5.540	3.088	2.715	3.408	3.021	3.690	3.111
20	9.799	9.583	6.111	5.217	2.914	2.785	3.290	2.644	3.482	2.726
21	8.579	9.643	4.111	6.107	2.369	2.669	3.013	2.618	3.024	3.788
28	14.633	14.066	7.934	9.775	4.194	4.674	3.951	4.708	4.374	4.686
29	13.023	16.258	6.855	8.510	3.813	5.073	3.934	4.125	4.504	4.014
30	11.305	13.039	5.986	6.905	3.190	3.149	2.725	3.389	3.468	3.750
37	16.958	18.746	9.912	9.661	5.138	5.149	4.553	4.908	4.790	4.778
38	15.037	16.698	9.723	9.710	4.995	5.164	4.702	4.740	4.675	4.826
39	13.129	12.202	6.750	7.445	3.925	3.648	3.845	4.267	3.933	3.649
1.0×16mm										
4	15.665	14.299	8.335	9.347	4.529	4.228	3.882	3.783	4.669	4.163
5	13.513	13.551	6.280	9.268	4.076	4.453	4.166	4.008	4.272	3.996
6	11.410	13.151	6.065	7.376	2.859	3.536	3.059	3.732	3.129	3.656
13	9.655	6.868	4.676	3.835	2.378	2.332	2.476	2.119	3.044	1.907
14	9.141	6.977	4.342	3.895	2.749	1.920	2.421	1.683	2.388	2.044
15	6.381	6.410	3.396	4.012	1.547	1.843	1.750	1.797	1.993	2.025
22	10.692	10.006	7.433	5.975	3.397	3.077	3.464	2.750	3.836	2.793
23	10.881	9.485	7.384	6.123	3.164	2.946	3.300	2.780	3.259	3.097
24	9.142	9.752	5.780	5.701	2.762	2.609	3.148	2.725	2.972	2.791
31	16.317	15.930	7.677	9.097	3.802	5.145	4.219	4.578	4.288	5.234
32	15.050	15.710	8.110	10.003	4.871	5.073	4.062	3.703	4.613	5.378
33	10.807	13.212	6.710	6.375	3.206	4.169	3.289	3.583	3.707	4.384
40	19.518	20.061	10.006	10.103	5.538	5.113	4.970	4.664	5.277	5.276
41	18.288	17.644	9.297	9.687	5.368	4.611	4.446	4.623	5.409	5.443
42	13.245	13.144	7.292	8.052	4.169	3.535	4.092	4.246	4.009	4.290
2.0×16mm										
7	16.862	15.679	8.861	8.909	4.640	4.398	4.953	4.415	4.421	4.520
8	15.343	15.061	8.090	10.206	4.033	4.142	4.877	3.865	5.157	4.148
9	11.703	13.766	5.588	7.782	3.081	3.641	3.041	3.998	3.276	3.906
16	9.525	6.084	5.055	3.992	3.048	2.133	3.096	3.777	3.256	2.202
17	8.753	7.403	5.226	4.296	2.892	2.320	2.872	2.002	3.105	2.026
18	7.486	9.972	3.783	3.935	2.065	1.995	2.232	2.016	2.269	1.757
25	11.321	10.297	8.704	6.159	4.204	3.117	3.559	3.227	3.661	3.062
26	9.942	9.953	7.727	6.769	2.856	2.944	3.810	3.281	3.732	3.000
27	9.735	11.105	5.050	6.841	2.788	3.079	3.061	2.597	3.149	2.760
34	17.588	15.038	10.612	10.477	5.399	5.076	4.679	5.131	4.526	4.875
35	16.393	17.616	9.802	10.647	4.922	4.864	4.660	4.545	4.587	4.189
36	12.869	16.623	6.728	8.939	3.204	4.876	4.259	3.657	3.951	4.456
43	21.401	20.188	11.140	10.998	6.149	6.223	5.376	5.485	5.556	4.821
44	20.606	21.588	10.321	11.607	4.617	5.101	5.272	5.011	5.006	5.531
45	14.969	15.715	7.864	7.834	4.138	4.027	4.781	4.100	4.300	4.029

Appendix XXVI: Abdominal CT scan relative (VGA) image quality 6 criteria scores image # 1 (upper anterior abdominal) results for 90 images from FTC and ATCM protocols

FTC image # 1 criteria number							
Image No.	**1**	**2**	**3**	**4**	**5**	**6**	**SUM**
1	4	3	3	4	3	3	20
2	3	3	3	3	3	3	18
3	2	2	3	2	2	2	13
4	3	3	4	3	4	4	21
5	3	3	4	3	3	3	19
6	3	3	3	3	3	2	17
7	3	3	4	3	4	4	21
8	4	3	4	4	4	4	23
9	3	3	3	3	3	3	18
10	2	2	2	2	2	2	12
11	2	2	2	2	2	2	12
12	2	2	2	2	2	2	12
13	2	2	2	2	2	2	12
14	2	2	2	3	2	2	13
15	2	2	2	2	2	2	12
16	2	3	2	2	2	2	13
17	2	2	2	2	2	2	12
18	2	2	2	2	2	2	12
19	3	3	3	2	3	2	16
20	2	3	3	2	3	3	16
21	2	2	2	2	3	2	13
22	2	2	3	3	3	3	16
23	2	3	3	2	3	3	16
24	2	2	2	2	2	2	12
25	2	2	3	3	3	3	16
26	3	2	3	2	3	3	16
27	3	3	3	2	2	2	15
28	4	3	3	4	3	4	21
29	4	4	3	3	3	4	21
30	3	3	3	3	3	3	18
31	4	4	4	4	4	4	24
32	4	3	4	3	4	4	22
33	3	3	3	3	4	4	20
34	4	4	4	4	4	4	24
35	4	3	4	3	4	4	22
36	3	3	4	4	3	3	20
37	3	4	4	3	3	4	21
38	4	4	4	4	4	4	24
39	3	4	4	3	3	3	20
40	4	4	4	4	4	4	24
41	4	4	4	4	4	4	24
42	3	3	3	3	3	3	18
43	4	4	4	4	4	4	24
44	3	4	4	3	4	4	22
45	4	3	4	3	4	4	22
ATCM image # 1 criteria number							
Image No.	**1**	**2**	**3**	**4**	**5**	**6**	**SUM**
1	4	3	3	4	4	4	22
2	3	3	3	3	3	3	18
3	3	2	2	2	2	2	13
4	4	3	3	4	3	3	20
5	4	3	3	4	4	4	22
6	3	3	3	3	3	3	18
7	3	4	3	3	3	3	19
8	4	4	3	3	4	4	22
9	3	3	3	3	3	4	19
10	2	2	2	2	2	2	12
11	2	2	2	2	2	2	12
12	2	2	2	2	2	2	12
13	2	2	2	2	2	2	12
14	2	2	2	2	2	2	12
15	2	2	2	2	2	2	12
16	2	2	2	2	2	2	12
17	2	2	2	2	2	2	12
18	2	2	2	2	2	2	12

19	**3**	**2**	**2**	**3**	**3**	**3**	**16**
20	**2**	**2**	**2**	**2**	**2**	**2**	**12**
21	**2**	**2**	**2**	**2**	**2**	**2**	**12**
22	**2**	**3**	**2**	**2**	**2**	**2**	**13**
23	**2**	**2**	**2**	**2**	**2**	**2**	**12**
24	**2**	**2**	**2**	**2**	**2**	**2**	**12**
25	**2**	**2**	**3**	**3**	**2**	**2**	**14**
26	**2**	**2**	**2**	**2**	**2**	**2**	**12**
27	**3**	**3**	**3**	**2**	**3**	**3**	**17**
28	**4**	**4**	**4**	**4**	**4**	**4**	**24**
29	**4**	**3**	**4**	**4**	**4**	**4**	**23**
30	**3**	**3**	**3**	**3**	**3**	**3**	**18**
31	**4**	**4**	**4**	**4**	**4**	**4**	**24**
32	**4**	**4**	**4**	**4**	**4**	**4**	**24**
33	**3**	**3**	**4**	**3**	**3**	**3**	**19**
34	**4**	**4**	**4**	**4**	**4**	**4**	**24**
35	**4**	**4**	**4**	**4**	**4**	**4**	**24**
36	**4**	**3**	**4**	**3**	**4**	**4**	**22**
37	**4**	**4**	**4**	**4**	**4**	**4**	**24**
38	**4**	**4**	**4**	**3**	**4**	**4**	**23**
39	**3**	**3**	**3**	**3**	**3**	**3**	**18**
40	**4**	**4**	**4**	**4**	**4**	**4**	**24**
41	**4**	**4**	**4**	**4**	**4**	**4**	**24**
42	**4**	**4**	**3**	**3**	**4**	**4**	**22**
43	**4**	**4**	**4**	**4**	**4**	**4**	**24**
44	**4**	**4**	**4**	**4**	**4**	**4**	**24**
45	**3**	**3**	**3**	**3**	**3**	**3**	**18**

Appendix XXVII: Abdominal CT scan relative (VGA) image quality 9 criteria scores image # 2 (upper abdominal) results for 90 images from FTC and ATCM protocols

FTC image # 2 criteria numbers										
Image No.	**1**	**2**	**3**	**4**	**5**	**6**	**7**	**8**	**9**	**SUM**
1	3	3	3	4	4	3	3	3	3	29
2	3	3	3	3	3	3	3	3	3	27
3	3	3	3	3	3	2	3	2	3	25
4	4	4	4	4	4	3	3	4	4	34
5	4	3	3	4	3	3	3	3	3	29
6	3	3	2	3	2	3	2	2	3	23
7	4	4	4	4	3	4	4	4	4	35
8	3	3	3	4	4	3	3	3	4	30
9	3	3	3	2	3	3	3	3	3	26
10	2	2	2	2	2	2	2	2	2	18
11	2	2	2	2	2	2	2	2	2	18
12	2	2	2	2	2	2	2	2	2	18
13	2	2	2	2	2	2	2	2	2	18
14	2	2	2	2	2	2	2	2	2	18
15	2	2	2	2	2	2	2	2	2	18
16	3	3	3	3	2	3	3	2	2	24
17	2	2	2	2	2	2	2	2	2	18
18	2	2	2	2	2	2	2	2	2	18
19	3	2	3	3	3	3	2	3	3	25
20	2	2	2	3	2	2	2	2	2	19
21	2	2	2	2	2	2	2	2	2	18
22	3	3	2	2	3	3	3	3	3	25
23	3	3	3	3	3	2	2	3	3	25
24	3	2	3	2	2	3	2	2	2	21
25	3	2	3	3	3	2	3	3	3	25
26	3	3	3	3	3	3	3	3	3	27
27	2	2	2	2	3	2	2	2	2	19
28	4	3	3	4	4	3	3	3	4	31
29	3	3	4	3	3	3	3	4	4	30
30	3	3	3	2	3	4	3	3	3	27
31	4	3	4	4	4	3	3	4	4	33
32	4	4	4	4	4	3	3	3	4	33
33	4	3	3	3	4	3	3	3	3	29
34	4	4	4	4	4	4	4	4	4	36
35	4	3	4	4	3	3	3	4	4	32
36	3	3	3	4	3	3	3	3	3	28
37	4	4	4	4	4	4	4	3	4	35
38	4	3	4	4	3	4	4	4	4	34
39	3	3	3	4	4	3	3	3	3	29
40	4	4	4	4	4	4	4	4	4	36
41	4	4	4	4	4	4	3	4	4	35
42	3	3	4	3	3	3	3	3	3	28
43	4	4	4	4	4	4	4	4	4	36
44	4	4	4	4	4	4	4	4	4	36
45	3	3	4	4	3	3	3	3	3	29
ATCM image # 2 criteria numbers										
Image No.	**1**	**2**	**3**	**4**	**5**	**6**	**7**	**8**	**9**	**SUM**
1	3	3	3	4	3	3	3	3	4	29
2	4	3	4	3	4	3	3	4	4	32
3	3	3	3	3	2	3	3	3	3	26
4	4	4	4	4	3	4	3	4	4	34
5	3	4	3	4	4	4	3	3	3	31
6	3	3	3	3	3	3	3	3	3	27

7	**3**	**4**	**4**	**3**	**3**	**4**	**4**	**4**	**4**	**33**
8	**3**	**3**	**4**	**4**	**3**	**4**	**4**	**3**	**4**	**32**
9	**3**	**3**	**3**	**4**	**3**	**3**	**3**	**3**	**3**	**28**
10	**2**	**2**	**2**	**2**	**2**	**2**	**2**	**2**	**2**	**18**
11	**2**	**2**	**2**	**2**	**2**	**2**	**2**	**2**	**2**	**18**
12	**2**	**2**	**2**	**2**	**2**	**2**	**2**	**2**	**2**	**18**
13	**2**	**2**	**2**	**2**	**2**	**2**	**2**	**2**	**2**	**18**
14	**2**	**2**	**2**	**2**	**2**	**2**	**2**	**2**	**2**	**18**
15	**2**	**2**	**2**	**2**	**2**	**2**	**2**	**2**	**2**	**18**
16	**2**	**2**	**2**	**2**	**2**	**2**	**2**	**2**	**2**	**18**
17	**2**	**2**	**2**	**2**	**2**	**2**	**2**	**2**	**2**	**18**
18	**2**	**2**	**2**	**2**	**2**	**2**	**2**	**2**	**2**	**18**
19	**2**	**2**	**2**	**3**	**3**	**3**	**2**	**3**	**2**	**22**
20	**2**	**2**	**2**	**2**	**2**	**2**	**2**	**2**	**2**	**18**
21	**2**	**2**	**2**	**2**	**2**	**2**	**2**	**2**	**2**	**18**
22	**3**	**3**	**2**	**2**	**3**	**3**	**3**	**3**	**3**	**25**
23	**2**	**3**	**2**	**2**	**2**	**2**	**2**	**2**	**2**	**19**
24	**2**	**3**	**3**	**2**	**2**	**2**	**2**	**2**	**2**	**20**
25	**2**	**3**	**2**	**3**	**2**	**2**	**2**	**2**	**2**	**20**
26	**2**	**3**	**3**	**2**	**2**	**3**	**2**	**3**	**3**	**23**
27	**2**	**3**	**2**	**3**	**2**	**3**	**2**	**2**	**2**	**21**
28	**4**	**4**	**4**	**4**	**4**	**4**	**4**	**4**	**4**	**36**
29	**4**	**4**	**4**	**4**	**3**	**4**	**3**	**4**	**4**	**34**
30	**3**	**3**	**3**	**4**	**3**	**3**	**3**	**3**	**3**	**28**
31	**4**	**4**	**4**	**4**	**4**	**4**	**4**	**4**	**4**	**36**
32	**3**	**4**	**4**	**4**	**4**	**3**	**4**	**4**	**4**	**34**
33	**3**	**3**	**4**	**3**	**3**	**3**	**3**	**3**	**3**	**28**
34	**4**	**4**	**4**	**4**	**4**	**4**	**4**	**4**	**4**	**36**
35	**4**	**4**	**4**	**4**	**4**	**4**	**4**	**4**	**4**	**36**
36	**4**	**3**	**3**	**3**	**3**	**3**	**3**	**3**	**4**	**29**
37	**4**	**4**	**4**	**4**	**4**	**4**	**3**	**4**	**4**	**35**
38	**4**	**4**	**4**	**4**	**3**	**3**	**4**	**4**	**4**	**34**
39	**3**	**4**	**4**	**3**	**3**	**3**	**3**	**3**	**4**	**30**
40	**4**	**4**	**2**	**4**	**4**	**4**	**4**	**4**	**4**	**34**
41	**4**	**4**	**4**	**4**	**4**	**4**	**4**	**4**	**4**	**36**
42	**3**	**3**	**4**	**4**	**3**	**3**	**3**	**3**	**3**	**29**
43	**4**	**4**	**4**	**4**	**4**	**4**	**4**	**4**	**4**	**36**
44	**4**	**3**	**3**	**4**	**4**	**3**	**4**	**4**	**4**	**33**
45	**4**	**4**	**4**	**4**	**4**	**4**	**4**	**4**	**4**	**36**

Appendix XXVIII : Abdominal CT scan relative (VGA) image quality 11 criteria scores image # 3 (medial abdominal) results for 90 images from FTC and ATCM protocols

FTC image # 3 criteria number												
Image No.	**1**	**2**	**3**	**4**	**5**	**6**	**7**	**8**	**9**	**10**	**11**	**SUM**
1	3	4	4	3	4	3	3	3	3	3	4	37
2	3	3	3	3	4	3	3	3	3	3	3	34
3	2	3	2	3	2	2	3	3	3	3	3	29
4	4	4	3	4	4	3	4	3	4	3	4	40
5	3	3	3	3	4	3	3	3	3	3	3	34
6	2	2	3	2	3	2	2	3	3	2	2	26
7	4	4	3	4	3	4	3	4	4	4	4	41
8	3	3	3	4	4	4	4	4	4	4	4	41
9	3	3	3	2	2	2	2	3	3	2	2	27
10	2	2	2	2	2	2	2	2	2	2	2	22
11	2	2	2	2	2	2	2	2	2	2	2	22
12	2	2	2	2	2	2	2	2	2	2	2	22
13	2	2	2	2	2	2	2	2	2	2	2	22
14	2	2	2	2	2	2	2	2	2	2	2	22
15	2	2	2	2	2	2	2	2	2	2	2	22
16	2	2	2	3	3	2	2	3	3	2	2	26
17	2	2	2	2	2	2	2	2	2	2	2	22
18	2	2	2	2	2	2	2	2	2	2	2	22
19	3	2	3	2	3	2	2	3	2	3	2	27
20	2	3	2	3	3	2	2	3	2	3	3	28
21	2	2	2	2	2	2	2	2	2	2	2	22
22	3	2	2	3	3	2	3	3	2	2	3	28
23	3	3	2	3	2	3	3	2	3	3	3	30
24	2	2	2	2	2	2	2	2	2	2	2	22
25	3	3	2	3	3	3	3	3	3	3	3	32
26	2	2	3	2	3	2	2	3	2	3	3	27
27	2	2	2	2	2	2	2	2	2	2	2	22
28	4	4	4	4	4	4	4	4	3	4	4	43
29	3	3	3	4	4	3	3	3	3	3	3	35
30	3	3	3	3	3	3	3	3	3	2	3	32
31	3	3	3	4	4	4	4	4	4	4	4	41
32	3	3	3	4	4	3	3	4	3	4	3	37
33	3	3	3	3	3	2	2	3	3	3	3	31
34	4	4	4	4	4	4	4	4	4	4	4	44
35	4	4	4	4	4	4	4	4	4	4	3	43
36	3	3	3	3	3	3	3	4	3	3	3	34
37	4	3	4	4	4	4	4	4	4	4	4	43
38	4	4	4	4	4	4	4	4	4	4	4	44
39	3	3	3	3	3	3	4	3	3	3	3	34
40	4	4	4	4	4	4	4	4	4	4	4	44
41	4	3	4	4	4	4	3	4	3	4	4	41
42	3	3	3	3	3	3	4	3	3	3	3	34
43	4	4	4	4	4	4	4	4	4	4	4	44
44	4	4	4	4	4	4	4	4	4	4	4	44
45	3	3	3	4	4	3	3	4	3	4	3	37
ATCM image # 3 criteria number												
Image No.	**1**	**2**	**3**	**4**	**5**	**6**	**7**	**8**	**9**	**10**	**11**	**SUM**
1	3	3	3	3	3	3	3	4	3	4	4	36
2	3	3	3	4	4	3	3	4	3	3	3	36
3	3	3	3	3	3	2	3	3	3	3	3	32
4	4	4	4	4	4	3	3	4	3	4	4	41
5	3	3	3	4	4	3	3	3	3	3	4	36
6	3	3	3	3	3	3	3	3	3	3	3	33

7	**4**	**3**	**4**	**4**	**4**	**3**	**3**	**4**	**3**	**4**	**4**	**40**
8	**3**	**3**	**3**	**4**	**4**	**4**	**4**	**4**	**4**	**4**	**4**	**41**
9	**3**	**3**	**3**	**4**	**4**	**3**	**3**	**4**	**3**	**3**	**3**	**36**
10	**2**	**2**	**2**	**2**	**2**	**2**	**2**	**2**	**2**	**2**	**2**	**22**
11	**2**	**2**	**2**	**2**	**2**	**2**	**2**	**2**	**2**	**2**	**2**	**22**
12	**2**	**2**	**2**	**2**	**2**	**2**	**2**	**2**	**2**	**2**	**2**	**22**
13	**2**	**2**	**2**	**2**	**2**	**2**	**2**	**2**	**2**	**2**	**2**	**22**
14	**2**	**2**	**2**	**2**	**2**	**2**	**2**	**2**	**2**	**2**	**2**	**22**
15	**2**	**2**	**2**	**2**	**2**	**2**	**2**	**2**	**2**	**2**	**2**	**22**
16	**2**	**2**	**2**	**2**	**2**	**2**	**2**	**2**	**2**	**2**	**2**	**22**
17	**2**	**2**	**2**	**2**	**2**	**2**	**2**	**2**	**2**	**2**	**2**	**22**
18	**2**	**2**	**2**	**2**	**2**	**2**	**2**	**2**	**2**	**2**	**2**	**22**
19	**2**	**2**	**2**	**2**	**2**	**2**	**2**	**2**	**2**	**2**	**2**	**22**
20	**2**	**2**	**2**	**2**	**2**	**2**	**2**	**2**	**2**	**2**	**2**	**22**
21	**2**	**2**	**2**	**2**	**2**	**2**	**2**	**2**	**2**	**2**	**2**	**22**
22	**2**	**2**	**2**	**2**	**2**	**2**	**2**	**2**	**2**	**2**	**2**	**22**
23	**2**	**2**	**2**	**2**	**2**	**2**	**3**	**3**	**3**	**2**	**2**	**25**
24	**3**	**2**	**2**	**2**	**2**	**2**	**2**	**2**	**2**	**2**	**2**	**23**
25	**3**	**2**	**3**	**2**	**2**	**2**	**3**	**3**	**3**	**3**	**3**	**29**
26	**3**	**2**	**2**	**3**	**3**	**2**	**2**	**3**	**3**	**2**	**2**	**27**
27	**2**	**3**	**2**	**2**	**2**	**2**	**2**	**3**	**3**	**2**	**2**	**25**
28	**4**	**3**	**4**	**4**	**4**	**3**	**3**	**4**	**3**	**4**	**4**	**40**
29	**3**	**3**	**4**	**4**	**4**	**3**	**3**	**3**	**3**	**4**	**4**	**38**
30	**3**	**3**	**3**	**3**	**3**	**3**	**4**	**3**	**3**	**3**	**3**	**34**
31	**4**	**4**	**4**	**4**	**4**	**4**	**4**	**4**	**4**	**4**	**4**	**44**
32	**4**	**4**	**4**	**4**	**4**	**4**	**4**	**4**	**3**	**4**	**4**	**43**
33	**3**	**3**	**3**	**3**	**4**	**3**	**3**	**4**	**3**	**3**	**3**	**35**
34	**4**	**4**	**4**	**4**	**4**	**4**	**4**	**4**	**4**	**4**	**4**	**44**
35	**4**	**4**	**4**	**4**	**4**	**4**	**3**	**4**	**3**	**4**	**4**	**42**
36	**4**	**4**	**4**	**4**	**4**	**3**	**4**	**4**	**4**	**4**	**4**	**43**
37	**4**	**4**	**4**	**4**	**4**	**4**	**4**	**4**	**4**	**4**	**4**	**44**
38	**4**	**4**	**4**	**4**	**4**	**4**	**3**	**4**	**4**	**3**	**4**	**42**
39	**3**	**3**	**3**	**3**	**3**	**3**	**3**	**3**	**3**	**3**	**3**	**33**
40	**4**	**4**	**4**	**4**	**4**	**4**	**4**	**4**	**4**	**4**	**4**	**44**
41	**4**	**4**	**4**	**4**	**4**	**4**	**4**	**4**	**4**	**4**	**4**	**44**
42	**3**	**3**	**4**	**4**	**3**	**3**	**3**	**3**	**3**	**3**	**3**	**35**
43	**4**	**4**	**4**	**4**	**4**	**4**	**4**	**4**	**4**	**4**	**4**	**44**
44	**4**	**4**	**4**	**4**	**4**	**4**	**3**	**4**	**4**	**3**	**4**	**42**
45	**4**	**3**	**4**	**4**	**4**	**4**	**3**	**4**	**3**	**4**	**4**	**41**

Appendix XXIX : Abdominal CT scan relative (VGA) image quality 11 criteria scores image # 4 (lower abdominal) results for 90 images from FTC and ATCM protocols

FTC image # 4 criteria number												
Image No.	1	2	3	4	5	6	7	8	9	10	11	SUM
1	3	3	3	3	3	3	3	3	3	3	3	33
2	3	3	3	3	3	3	3	3	3	3	4	34
3	3	3	3	4	3	4	3	3	3	3	3	35
4	4	4	4	4	4	4	4	4	4	4	3	43
5	3	3	3	3	3	3	3	3	3	3	3	33
6	3	3	3	2	3	3	3	4	3	3	3	33
7	4	4	3	3	3	4	4	4	4	4	4	41
8	3	3	3	3	4	3	3	3	3	3	3	34
9	3	3	3	2	3	3	3	3	2	3	3	31
10	2	2	2	2	2	2	2	2	2	2	2	22
11	2	2	2	2	2	2	2	2	2	2	2	22
12	2	2	2	2	2	2	2	2	2	2	2	22
13	2	2	2	2	2	2	2	2	2	2	2	22
14	2	2	2	2	2	2	2	2	2	2	2	22
15	2	2	2	2	2	2	2	2	2	2	2	22
16	2	2	3	2	2	2	2	2	2	2	2	23
17	2	2	2	2	2	2	2	2	2	2	2	22
18	2	2	2	2	2	2	2	2	2	2	2	22
19	2	2	2	3	2	2	2	2	2	2	3	24
20	3	2	3	2	2	2	2	2	2	2	2	24
21	2	2	2	2	2	2	2	2	2	2	2	22
22	2	2	2	2	2	2	2	3	2	2	3	24
23	3	2	2	2	3	2	2	2	2	2	2	24
24	2	3	2	2	2	2	2	2	2	2	2	23
25	2	2	2	3	3	3	2	2	2	2	2	25
26	3	2	2	3	2	2	2	2	2	2	3	25
27	2	2	2	2	2	2	2	2	2	2	2	22
28	3	3	4	4	4	3	4	4	4	4	4	41
29	4	4	3	3	3	3	3	3	3	3	4	36
30	2	2	3	3	3	3	3	3	3	3	3	31
31	4	4	3	3	3	3	3	3	4	4	4	38
32	3	3	4	4	4	4	4	4	4	4	4	42
33	3	3	4	3	3	3	3	3	3	2	4	34
34	4	4	4	4	4	4	4	4	4	4	4	44
35	3	3	4	4	4	4	4	4	4	4	4	42
36	3	3	3	3	3	3	4	3	3	3	3	34
37	4	3	4	4	4	4	4	4	4	4	4	43
38	3	4	4	3	4	4	4	4	4	3	4	41
39	3	3	3	3	3	3	3	3	3	3	3	33
40	4	3	4	4	4	4	4	4	4	4	4	43
41	4	4	4	4	4	4	4	4	4	4	4	44
42	3	3	3	3	3	3	3	3	3	3	3	33
43	4	4	4	4	4	4	4	4	4	4	4	44
44	4	4	4	4	4	4	4	4	4	4	4	44
45	3	3	3	3	3	3	3	3	3	3	4	34
ATCM image # 4 criteria number												
Image No.	1	2	3	4	5	6	7	8	9	10	11	SUM
1	3	3	3	3	3	3	3	3	3	3	3	33
2	3	3	4	4	3	3	3	3	4	3	3	36
3	3	3	3	3	3	3	3	3	3	3	3	33
4	3	3	3	3	3	3	3	3	3	3	4	34
5	3	3	3	3	3	3	3	3	3	3	3	33
6	3	3	3	3	2	2	2	2	3	3	3	29

7	**4**	**3**	**4**	**3**	**3**	**3**	**3**	**3**	**3**	**3**	**4**	**36**
8	**3**	**3**	**4**	**4**	**3**	**3**	**3**	**3**	**3**	**3**	**3**	**35**
9	**3**	**3**	**3**	**3**	**3**	**3**	**3**	**3**	**3**	**3**	**3**	**33**
10	**2**	**2**	**2**	**2**	**2**	**2**	**2**	**2**	**2**	**2**	**2**	**22**
11	**2**	**2**	**2**	**2**	**2**	**2**	**2**	**2**	**2**	**2**	**2**	**22**
12	**2**	**2**	**2**	**2**	**2**	**2**	**2**	**2**	**2**	**2**	**2**	**22**
13	**2**	**2**	**2**	**2**	**2**	**2**	**2**	**2**	**2**	**2**	**2**	**22**
14	**2**	**2**	**2**	**2**	**2**	**2**	**2**	**2**	**2**	**2**	**2**	**22**
15	**2**	**2**	**2**	**2**	**2**	**2**	**2**	**2**	**2**	**2**	**2**	**22**
16	**2**	**2**	**2**	**2**	**2**	**2**	**2**	**2**	**2**	**2**	**2**	**22**
17	**2**	**2**	**2**	**2**	**2**	**2**	**2**	**2**	**2**	**2**	**2**	**22**
18	**2**	**2**	**2**	**2**	**2**	**2**	**2**	**2**	**2**	**2**	**2**	**22**
19	**2**	**2**	**2**	**2**	**2**	**2**	**2**	**2**	**2**	**2**	**2**	**22**
20	**2**	**2**	**2**	**2**	**2**	**2**	**2**	**2**	**2**	**2**	**2**	**22**
21	**2**	**2**	**2**	**2**	**2**	**2**	**2**	**2**	**2**	**2**	**2**	**22**
22	**2**	**2**	**2**	**2**	**2**	**2**	**2**	**2**	**2**	**2**	**2**	**22**
23	**2**	**2**	**2**	**2**	**2**	**2**	**2**	**2**	**2**	**2**	**2**	**22**
24	**2**	**2**	**3**	**2**	**2**	**2**	**3**	**2**	**2**	**3**	**2**	**25**
25	**2**	**2**	**2**	**2**	**2**	**2**	**2**	**2**	**2**	**2**	**2**	**22**
26	**2**	**2**	**3**	**2**	**2**	**2**	**2**	**2**	**2**	**2**	**2**	**23**
27	**2**	**2**	**2**	**2**	**2**	**2**	**2**	**2**	**2**	**2**	**2**	**22**
28	**3**	**3**	**4**	**4**	**4**	**4**	**4**	**4**	**4**	**3**	**4**	**41**
29	**4**	**4**	**4**	**4**	**3**	**3**	**3**	**3**	**3**	**3**	**4**	**38**
30	**3**	**3**	**3**	**4**	**3**	**3**	**3**	**3**	**3**	**3**	**3**	**34**
31	**4**	**4**	**4**	**3**	**4**	**4**	**4**	**4**	**4**	**4**	**3**	**42**
32	**4**	**4**	**4**	**4**	**3**	**3**	**3**	**3**	**4**	**4**	**4**	**40**
33	**3**	**3**	**3**	**3**	**3**	**3**	**3**	**3**	**3**	**3**	**4**	**34**
34	**4**	**4**	**4**	**4**	**4**	**4**	**4**	**3**	**3**	**3**	**4**	**41**
35	**4**	**4**	**4**	**4**	**4**	**4**	**4**	**4**	**4**	**4**	**4**	**44**
36	**3**	**3**	**3**	**3**	**3**	**3**	**3**	**3**	**3**	**3**	**4**	**34**
37	**4**	**4**	**4**	**4**	**4**	**4**	**4**	**4**	**3**	**4**	**4**	**43**
38	**3**	**4**	**4**	**4**	**4**	**4**	**4**	**4**	**4**	**4**	**4**	**43**
39	**3**	**3**	**4**	**4**	**3**	**3**	**3**	**3**	**4**	**3**	**3**	**36**
40	**4**	**4**	**4**	**4**	**4**	**4**	**4**	**4**	**4**	**4**	**4**	**44**
41	**4**	**4**	**4**	**4**	**4**	**4**	**4**	**4**	**4**	**4**	**4**	**44**
42	**3**	**3**	**4**	**4**	**3**	**3**	**3**	**3**	**4**	**3**	**4**	**37**
43	**4**	**4**	**4**	**4**	**4**	**4**	**4**	**4**	**4**	**4**	**4**	**44**
44	**4**	**4**	**4**	**4**	**4**	**4**	**4**	**4**	**4**	**4**	**4**	**44**
45	**4**	**4**	**4**	**3**	**4**	**4**	**4**	**4**	**4**	**4**	**4**	**43**

Appendix XXX : Abdominal CT scan relative (VGA) image quality 6 criteria scores image # 5 (lower inferior abdominal) results for 90 images from FTC and ATCM protocols

FTC image # 5 criteria number							
Image No.	**1**	**2**	**3**	**4**	**5**	**6**	**SUM**
1	3	3	4	4	4	4	22
2	3	3	4	4	4	4	22
3	3	3	3	3	3	4	19
4	3	3	4	4	4	4	22
5	3	3	4	4	3	4	21
6	3	3	4	4	3	3	20
7	3	3	4	4	4	4	22
8	3	3	4	4	3	4	21
9	3	3	3	3	3	4	19
10	2	2	2	2	2	2	12
11	2	2	2	2	2	2	12
12	2	2	2	2	2	2	12
13	2	2	2	2	2	2	12
14	2	2	2	2	2	2	12
15	2	2	2	2	2	2	12
16	2	2	2	2	2	2	12
17	2	2	2	3	3	2	14
18	2	2	2	2	2	2	12
19	3	3	2	2	2	2	14
20	3	2	2	2	2	2	13
21	2	2	2	2	2	2	12
22	2	2	3	3	3	3	16
23	3	3	2	2	2	2	14
24	3	3	2	2	2	2	14
25	3	3	2	2	2	2	14
26	3	2	2	2	2	2	13
27	3	3	2	2	2	2	14
28	4	4	3	3	4	4	22
29	4	4	3	3	3	4	21
30	3	3	4	4	3	3	20
31	4	4	4	4	4	3	23
32	4	4	4	4	4	4	24
33	3	3	4	3	3	3	19
34	4	4	4	4	4	4	24
35	4	4	4	4	4	4	24
36	3	3	4	4	4	4	22
37	4	4	4	4	4	4	24
38	4	4	4	4	4	4	24
39	3	3	4	4	4	4	22
40	4	4	4	4	4	4	24
41	4	4	4	4	4	4	24
42	3	3	4	4	4	3	21
43	4	4	4	4	4	4	24
44	4	4	4	4	4	3	23
45	4	4	4	4	4	4	24
ATCM image # 5 criteria number							
Image No.	**1**	**2**	**3**	**4**	**5**	**6**	**SUM**
1	3	3	4	4	3	3	20
2	3	3	3	3	3	3	18
3	3	3	4	4	3	4	21
4	3	3	4	4	4	4	22
5	3	3	4	4	4	4	22
6	3	3	3	3	3	4	19

7	**3**	**3**	**4**	**4**	**4**	**4**	**22**
8	**3**	**4**	**4**	**4**	**4**	**4**	**23**
9	**3**	**3**	**4**	**4**	**4**	**4**	**22**
10	**2**	**2**	**2**	**2**	**2**	**2**	**12**
11	**2**	**2**	**2**	**2**	**2**	**2**	**12**
12	**2**	**2**	**2**	**2**	**2**	**2**	**12**
13	**2**	**2**	**2**	**2**	**2**	**2**	**12**
14	**2**	**2**	**2**	**2**	**2**	**2**	**12**
15	**2**	**2**	**2**	**2**	**2**	**2**	**12**
16	**2**	**2**	**2**	**2**	**2**	**2**	**12**
17	**2**	**2**	**2**	**2**	**2**	**2**	**12**
18	**2**	**2**	**2**	**2**	**2**	**2**	**12**
19	**3**	**3**	**2**	**2**	**2**	**2**	**14**
20	**3**	**3**	**2**	**2**	**2**	**2**	**14**
21	**2**	**2**	**2**	**2**	**2**	**2**	**12**
22	**3**	**3**	**2**	**2**	**2**	**2**	**14**
23	**3**	**3**	**2**	**2**	**2**	**2**	**14**
24	**2**	**2**	**2**	**2**	**2**	**2**	**12**
25	**3**	**2**	**2**	**2**	**2**	**2**	**13**
26	**3**	**3**	**3**	**3**	**3**	**3**	**18**
27	**3**	**3**	**2**	**2**	**2**	**2**	**14**
28	**4**	**4**	**4**	**4**	**4**	**4**	**24**
29	**3**	**3**	**4**	**4**	**4**	**3**	**21**
30	**3**	**3**	**4**	**4**	**4**	**4**	**22**
31	**4**	**4**	**4**	**4**	**4**	**4**	**24**
32	**4**	**4**	**4**	**4**	**4**	**4**	**24**
33	**4**	**4**	**4**	**4**	**4**	**4**	**24**
34	**4**	**4**	**4**	**4**	**4**	**4**	**24**
35	**4**	**4**	**4**	**4**	**4**	**4**	**24**
36	**3**	**3**	**4**	**4**	**4**	**4**	**22**
37	**4**	**4**	**4**	**4**	**4**	**4**	**24**
38	**4**	**4**	**4**	**4**	**4**	**4**	**24**
39	**3**	**3**	**3**	**4**	**3**	**4**	**20**
40	**4**	**4**	**4**	**4**	**4**	**4**	**24**
41	**4**	**4**	**4**	**4**	**4**	**3**	**23**
42	**4**	**4**	**4**	**4**	**4**	**3**	**23**
43	**4**	**4**	**4**	**4**	**4**	**4**	**24**
44	**4**	**4**	**4**	**4**	**4**	**4**	**24**
45	**4**	**4**	**4**	**4**	**4**	**3**	**23**

Appendix XXXI : Abdominal CT scan relative (VGA) image quality scores for image # 1,2,3,4 and 5 with different tube current comparing between FTC and ATCM

Protocols No.	FTC	ATCM	FTC	ATCM	FTC	ATCM	FTC	ATCM	FTC	ATCM
	Image #1		Image #2		Image #3		Image #4		Image #5	
100/low dose + mA										
10	12.000	12.000	18.000	18.000	22.000	22.000	22.000	22.000	12.000	12.000
11	12.000	12.000	18.000	18.000	22.000	22.000	22.000	22.000	12.000	12.000
12	12.000	12.000	18.000	18.000	22.000	22.000	22.000	22.000	12.000	12.000
13	12.000	12.000	18.000	18.000	22.000	22.000	22.000	22.000	12.000	12.000
14	13.000	12.000	18.000	18.000	22.000	22.000	22.000	22.000	12.000	12.000
15	12.000	12.000	18.000	18.000	22.000	22.000	22.000	22.000	12.000	12.000
16	13.000	12.000	24.000	18.000	26.000	22.000	23.000	22.000	12.000	12.000
17	12.000	12.000	18.000	18.000	22.000	22.000	22.000	22.000	14.000	12.000
18	12.000	12.000	18.000	18.000	22.000	22.000	22.000	22.000	12.000	12.000
200/low dose mA										
19	16.000	16.000	25.000	22.000	27.000	22.000	24.000	22.000	14.000	14.000
20	16.000	12.000	19.000	18.000	28.000	22.000	24.000	22.000	13.000	14.000
21	13.000	12.000	18.000	18.000	22.000	22.000	22.000	22.000	12.000	12.000
22	16.000	13.000	25.000	25.000	28.000	22.000	24.000	22.000	16.000	14.000
23	16.000	12.000	25.000	19.000	30.000	25.000	24.000	22.000	14.000	14.000
24	12.000	12.000	21.000	20.000	22.000	23.000	23.000	25.000	14.000	12.000
25	16.000	14.000	25.000	20.000	32.000	29.000	25.000	22.000	14.000	13.000
26	16.000	12.000	27.000	23.000	27.000	27.000	25.000	23.000	13.000	18.000
27	15.000	17.000	19.000	21.000	22.000	25.000	22.000	22.000	14.000	14.000
250/standard mA										
1	20.000	22.000	29.000	29.000	37.000	36.000	33.000	33.000	22.000	20.000
2	18.000	18.000	27.000	32.000	34.000	36.000	34.000	36.000	22.000	18.000
3	13.000	13.000	25.000	26.000	29.000	32.000	35.000	33.000	19.000	21.000
4	21.000	20.000	34.000	34.000	40.000	41.000	43.000	34.000	22.000	22.000
5	19.000	22.000	29.000	31.000	34.000	36.000	33.000	33.000	21.000	22.000
6	17.000	18.000	23.000	27.000	26.000	33.000	33.000	29.000	20.000	19.000
7	21.000	19.000	35.000	33.000	41.000	40.000	41.000	36.000	22.000	22.000
8	23.000	22.000	30.000	32.000	41.000	41.000	34.000	35.000	21.000	23.000
9	18.000	19.000	26.000	28.000	27.000	36.000	31.000	33.000	19.000	22.000
300/quality mA										
28	21.000	24.000	31.000	36.000	43.000	40.000	41.000	41.000	22.000	24.000
29	21.000	23.000	30.000	34.000	35.000	38.000	36.000	38.000	21.000	21.000
30	18.000	18.000	27.000	28.000	32.000	34.000	31.000	34.000	20.000	22.000
31	24.000	24.000	33.000	36.000	41.000	44.000	38.000	42.000	23.000	24.000
32	22.000	24.000	33.000	34.000	37.000	43.000	42.000	40.000	24.000	24.000
33	20.000	19.000	29.000	28.000	31.000	35.000	34.000	34.000	19.000	24.000
34	24.000	24.000	36.000	36.000	44.000	44.000	44.000	41.000	24.000	24.000
35	22.000	24.000	32.000	36.000	43.000	42.000	42.000	44.000	24.000	24.000
36	20.000	22.000	28.000	29.000	34.000	43.000	34.000	34.000	22.000	22.000
400/ high quality mA										
37	35.000	35.000	35.000	35.000	43.000	44.000	43.000	43.000	24.000	24.000
38	34.000	34.000	34.000	34.000	44.000	42.000	41.000	43.000	24.000	24.000
39	29.000	30.000	29.000	30.000	34.000	33.000	33.000	36.000	22.000	20.000
40	36.000	34.000	36.000	34.000	44.000	44.000	43.000	44.000	24.000	24.000
41	35.000	36.000	35.000	36.000	41.000	44.000	44.000	44.000	24.000	23.000
42	28.000	29.000	28.000	29.000	34.000	35.000	33.000	37.000	21.000	23.000
43	36.000	36.000	36.000	36.000	44.000	44.000	44.000	44.000	24.000	24.000
44	36.000	33.000	36.000	33.000	44.000	42.000	44.000	44.000	23.000	24.000
45	29.000	36.000	29.000	36.000	37.000	41.000	34.000	43.000	24.000	23.000

Appendix XXXII: Abdominal CT scan relative (VGA) image quality scores for image # 1,2,3,4 and 5 with different pitch factors comparing between FTC and ATCM

Protocols No.	FTC	ATCM	FTC	ATCM	FTC	ATCM	FTC	ATCM	FTC	ATCM
	Image #1		Image #2		Image #3		Image #4		Image #5	
Detail(0.688)										
1	20.000	22.000	29.000	29.000	37.000	36.000	33.000	33.000	22.000	20.000
4	21.000	20.000	34.000	34.000	40.000	41.000	43.000	34.000	22.000	22.000
7	21.000	19.000	35.000	33.000	41.000	40.000	41.000	36.000	22.000	22.000
10	12.000	12.000	18.000	18.000	22.000	22.000	22.000	22.000	12.000	12.000
13	12.000	12.000	18.000	18.000	22.000	22.000	22.000	22.000	12.000	12.000
16	13.000	12.000	24.000	18.000	26.000	22.000	23.000	22.000	12.000	12.000
19	16.000	16.000	25.000	22.000	27.000	22.000	24.000	22.000	14.000	14.000
22	16.000	13.000	25.000	25.000	28.000	22.000	24.000	22.000	16.000	14.000
25	16.000	14.000	25.000	20.000	32.000	29.000	25.000	22.000	14.000	13.000
28	21.000	24.000	31.000	36.000	43.000	40.000	41.000	41.000	22.000	24.000
31	24.000	24.000	33.000	36.000	41.000	44.000	38.000	42.000	23.000	24.000
34	24.000	24.000	36.000	36.000	44.000	44.000	44.000	41.000	24.000	24.000
37	21.000	24.000	35.000	35.000	43.000	44.000	43.000	43.000	24.000	24.000
40	24.000	24.000	36.000	34.000	44.000	44.000	43.000	44.000	24.000	24.000
43	24.000	24.000	36.000	36.000	44.000	44.000	44.000	44.000	24.000	24.000
Standard(0.938)										
2	18.000	18.000	27.000	32.000	34.000	36.000	34.000	36.000	22.000	18.000
5	19.000	22.000	29.000	31.000	34.000	36.000	33.000	33.000	21.000	22.000
8	23.000	22.000	30.000	32.000	41.000	41.000	34.000	35.000	21.000	23.000
11	12.000	12.000	18.000	18.000	22.000	22.000	22.000	22.000	12.000	12.000
14	13.000	12.000	18.000	18.000	22.000	22.000	22.000	22.000	12.000	12.000
17	12.000	12.000	18.000	18.000	22.000	22.000	22.000	22.000	14.000	12.000
20	16.000	12.000	19.000	18.000	28.000	22.000	24.000	22.000	13.000	14.000
23	16.000	12.000	25.000	19.000	30.000	25.000	24.000	22.000	14.000	14.000
26	16.000	12.000	27.000	23.000	27.000	27.000	25.000	23.000	13.000	18.000
29	21.000	23.000	30.000	34.000	35.000	38.000	36.000	38.000	21.000	21.000
32	22.000	24.000	33.000	34.000	37.000	43.000	42.000	40.000	24.000	24.000
35	22.000	24.000	32.000	36.000	43.000	42.000	42.000	44.000	24.000	24.000
38	24.000	23.000	34.000	34.000	44.000	42.000	41.000	43.000	24.000	24.000
41	24.000	24.000	35.000	36.000	41.000	44.000	44.000	44.000	24.000	23.000
44	22.000	24.000	36.000	33.000	44.000	42.000	44.000	44.000	23.000	24.000
Fast(1.438)										
3	13.000	13.000	25.000	26.000	29.000	32.000	35.000	33.000	19.000	21.000
6	17.000	18.000	23.000	27.000	26.000	33.000	33.000	29.000	20.000	19.000
9	18.000	19.000	26.000	28.000	27.000	36.000	31.000	33.000	19.000	22.000
12	12.000	12.000	18.000	18.000	22.000	22.000	22.000	22.000	12.000	12.000
15	12.000	12.000	18.000	18.000	22.000	22.000	22.000	22.000	12.000	12.000
18	12.000	12.000	18.000	18.000	22.000	22.000	22.000	22.000	12.000	12.000
21	13.000	12.000	18.000	18.000	22.000	22.000	22.000	22.000	12.000	12.000
24	12.000	12.000	21.000	20.000	22.000	23.000	23.000	25.000	14.000	12.000
27	15.000	17.000	19.000	21.000	22.000	25.000	22.000	22.000	14.000	14.000
30	18.000	18.000	27.000	28.000	32.000	34.000	31.000	34.000	20.000	22.000
33	20.000	19.000	29.000	28.000	31.000	35.000	34.000	34.000	19.000	24.000
36	20.000	22.000	28.000	29.000	34.000	43.000	34.000	34.000	22.000	22.000
39	20.000	18.000	29.000	30.000	34.000	33.000	33.000	36.000	22.000	20.000
42	18.000	22.000	28.000	29.000	34.000	35.000	33.000	37.000	21.000	23.000
45	22.000	18.000	29.000	36.000	37.000	41.000	34.000	43.000	24.000	23.000

Appendix XXXIII : Abdominal CT scan relative (VGA) image quality scores for image # 1,2,3,4 and 5 with different detector configuration comparing between FTC and ATCM

Protocols No.	FTC	ATCM	FTC	ATCM	FTC	ATCM	FTC	ATCM	FTC	ATCM
	Image #1		Image #2		Image #3		Image #4		Image #5	
0.5×16mm										
1	20.000	22.000	29.000	29.000	37.000	36.000	33.000	33.000	22.000	20.000
2	18.000	18.000	27.000	32.000	34.000	36.000	34.000	36.000	22.000	18.000
3	13.000	13.000	25.000	26.000	29.000	32.000	35.000	33.000	19.000	21.000
10	12.000	12.000	18.000	18.000	22.000	22.000	22.000	22.000	12.000	12.000
11	12.000	12.000	18.000	18.000	22.000	22.000	22.000	22.000	12.000	12.000
12	12.000	12.000	18.000	18.000	22.000	22.000	22.000	22.000	12.000	12.000
19	16.000	16.000	25.000	22.000	27.000	22.000	24.000	22.000	14.000	14.000
20	16.000	12.000	19.000	18.000	28.000	22.000	24.000	22.000	13.000	14.000
21	13.000	12.000	18.000	18.000	22.000	22.000	22.000	22.000	12.000	12.000
28	21.000	24.000	31.000	36.000	43.000	40.000	41.000	41.000	22.000	24.000
29	21.000	23.000	30.000	34.000	35.000	38.000	36.000	38.000	21.000	21.000
30	18.000	18.000	27.000	28.000	32.000	34.000	31.000	34.000	20.000	22.000
37	21.000	24.000	35.000	35.000	43.000	44.000	43.000	43.000	24.000	24.000
38	24.000	23.000	34.000	34.000	44.000	42.000	41.000	43.000	24.000	24.000
39	20.000	18.000	29.000	30.000	34.000	33.000	33.000	36.000	22.000	20.000
1.0×16mm										
4	21.000	20.000	34.000	34.000	40.000	41.000	43.000	34.000	22.000	22.000
5	19.000	22.000	29.000	31.000	34.000	36.000	33.000	33.000	21.000	22.000
6	17.000	18.000	23.000	27.000	26.000	33.000	33.000	29.000	20.000	19.000
13	12.000	12.000	18.000	18.000	22.000	22.000	22.000	22.000	12.000	12.000
14	13.000	12.000	18.000	18.000	22.000	22.000	22.000	22.000	12.000	12.000
15	12.000	12.000	18.000	18.000	22.000	22.000	22.000	22.000	12.000	12.000
22	16.000	13.000	25.000	25.000	28.000	22.000	22.000	22.000	16.000	14.000
23	16.000	12.000	25.000	19.000	30.000	25.000	24.000	22.000	14.000	14.000
24	12.000	12.000	21.000	20.000	22.000	23.000	24.000	25.000	14.000	12.000
31	24.000	24.000	33.000	36.000	41.000	44.000	38.000	42.000	23.000	24.000
32	22.000	24.000	33.000	34.000	37.000	43.000	42.000	40.000	24.000	24.000
33	20.000	19.000	29.000	28.000	31.000	35.000	34.000	34.000	19.000	24.000
40	24.000	24.000	36.000	34.000	44.000	44.000	43.000	44.000	24.000	24.000
41	24.000	24.000	35.000	36.000	41.000	44.000	44.000	44.000	24.000	23.000
42	18.000	22.000	28.000	29.000	34.000	35.000	33.000	37.000	21.000	23.000
2.0×16mm										
7	21.000	19.000	35.000	33.000	41.000	40.000	41.000	36.000	22.000	22.000
8	23.000	22.000	30.000	32.000	41.000	41.000	34.000	35.000	21.000	23.000
9	18.000	19.000	26.000	28.000	27.000	36.000	31.000	33.000	19.000	22.000
16	13.000	12.000	24.000	18.000	26.000	22.000	23.000	22.000	12.000	12.000
17	12.000	12.000	18.000	18.000	22.000	22.000	22.000	22.000	14.000	12.000
18	12.000	12.000	18.000	18.000	22.000	22.000	22.000	22.000	12.000	12.000
25	16.000	14.000	25.000	20.000	32.000	29.000	25.000	22.000	14.000	13.000
26	16.000	12.000	27.000	23.000	27.000	27.000	25.000	23.000	13.000	18.000
27	15.000	17.000	19.000	21.000	22.000	25.000	22.000	22.000	14.000	14.000
34	24.000	24.000	36.000	36.000	44.000	44.000	44.000	41.000	24.000	24.000
35	22.000	24.000	32.000	36.000	43.000	42.000	42.000	44.000	24.000	24.000
36	20.000	22.000	28.000	29.000	34.000	43.000	34.000	34.000	22.000	22.000
43	24.000	24.000	36.000	36.000	44.000	44.000	44.000	44.000	24.000	24.000
44	22.000	24.000	36.000	33.000	44.000	42.000	44.000	44.000	23.000	24.000
45	22.000	18.000	29.000	36.000	37.000	41.000	34.000	43.000	24.000	23.000

References

Abdallah, Y., & Salih, M. (2013). Appraisal of Radiation Dose Received in Abdominal Computed Tomography Patients. International Journal of Science and Research (IJSR) ISSN (Online Index Copernicus Value Impact Factor, 14(7), 2319–7064.

Abdulfatah, Garcia, A., Bakker, A., Tomkinson, D., Salamin, J., de Lange, R., Plasman, P. (2014). A comparison of Sinogram Affirmed Iterative Reconstruction and filtered back projection on image quality and dose reduction in paediatric head CT: a phantom study. In OPTIMAX (pp. 27–36).

Abou-Issa, A. H., Elganayni, F., & AL-Azzazy, M. Z. (2011). Effect of low tube kV on radiation dose and image quality in retrospective ECG-gated coronary CT angiography. The Egyptian Journal of Radiology and Nuclear Medicine, 42(3), 327-333.

Ali, R. M., Alrowily, M., Benhalim, M. R., & Tootell, A(2016a). METHODS FOR DIRECT MEASURMENT OF RADIATION DOSE: TLD and MOSFET. OPTIMAX 2016, 35.

Ali, R. M., England, A., Mcentee, M. F., & Hogg, P. (2015). Radiography A method for calculating effective lifetime risk of radiation-induced cancer from screening mammography. Radiography, 21(4), 298–303.

Alsleem, H., & Davidson, R. (2013). Factors affecting contrast-detail performance in computed tomography: A review. Journal of Medical Imaging and Radiation Sciences, 44(2), 62-70.

American Association for Physicist in Medicine (2008). The measurements, reporting and management of radiation dose in CT, AAPM Report 96.

American Association of Physicists in Medicine (AAPM) Report NO. 204. (2011). Size-Specific Dose Estimation (SSDE) in Pediatric and Adult Body CT Examinations. In Intergovernmental Panel on Climate Change (Ed.), Climate Change 2013 - The Physical Science Basis (pp. 1–30). Cambridge: Cambridge University Press.

American College of Radiology ACR. (2015). CT Accreditation Program. https://www.acr.org/~/media/ACR/Documents/PGTS/guidelines/CT_Abdomen_Pelvis.pdf

Andy, F, (2013). Exploring data with graphs chapter 4. From book Discovering Statistics Using SPSS. Sage, 81(1), 169–170 third edition.

Angel, E., & Zhang, D. (2012). TU- G- 217BCD- 06: Reducing CT Dose during Routine Brain CT Using Attenuation Based Tube Current Modulation (TCM). Medical Physics, 39(6), 3925-3925.

Angel, E., Yaghmai, N., Jude, C. M., DeMarco, J. J., Cagnon, C. H., Goldin, J. G., ... & McNitt-Gray, M. F. (2009). Dose to radiosensitive organs during routine chest CT: effects of tube current modulation. American Journal of Roentgenology, 193(5), 1340-1345.

Aweda, M. A., & Arogundade, R. A. (2007). Patient dose reduction methods in computerized tomography procedures: A review. International Journal of Physical Sciences, 2(1), 1-9.

Bahadori, A., Miglioretti, D., Kruger, R., Flynn, M., Weinmann, S., Smith-Bindman, R., & Lee, C. (2015). Calculation of organ doses for a large number of patients undergoing CT examinations. American Journal of Roentgenology, 205(4), 827-833.

Baliga, B. J. (2010). Fundamentals of power semiconductor devices. Springer Science & Business Media.

Bankier, A. A., & Kressel, H. Y. (2012). Through the Looking Glass revisited: the need for more meaning and less drama in the reporting of dose and dose reduction in CT 4-8.

Bath, M (2010), 'Evaluating imaging systems: Practical applications', Radiat Prot Dosimetry, vol. 139, no. 1-3 pp. 26-36.

Bath, M., & Mansson, L. G. (2007). Visual grading characteristics (VGC) analysis: a non-parametric rank-invariant statistical method for image quality evaluation. The British journal of radiology, 80(951), 169-176.

Bauhs, J. A., Vrieze, T. J., Primak, A. N., Bruesewitz, M. R., & McCollough, C. H. (2008). CT dosimetry: comparison of measurement techniques and devices. Radiographics, 28(1), 245-253.

Beeres, Martin, Brady, S. L., Mirro, A. E., Moore, B. M., Kaufman, R. A., Römer, M., Bodelle, B., … Bauer, R. W. (2014). Chest-abdomen-pelvis CT for staging in cancer patients: dose effectiveness and image quality using automated attenuation-based tube potential selection. AJR. American Journal of Roentgenology, 14(May), 28.

Berger, T., Reitz, G., Hajek, M., & Vana, N. (2006). Comparison of various techniques for the exact determination of absorbed dose in heavy ion fields using passive detectors. Advances in Space Research, 37(9), 1716-1721.

Bhosale, P. (2015). Comparing CNR, SNR, and Image Quality of CT Images Reconstructed with Soft Kernel, Standard Kernel, and Standard Kernel plus ASIR 30% Techniques. International Journal of Radiology, 2(2), 60-65.

Boone, J. M. (2007). The trouble with CTDI100. Medical physics, 34(4), 1364-1371.

Boone, J. M., Brink, J. A., Edyvean, S., Huda, W., Leitz, W., McCollough, C. H. ... & Brunberg, J. A. (2012). Radiation dose and image-quality assessment in computed tomography. Journal of the ICRU, 12(1), 9-149.

Borman, T., & Stoel, B. (2009). Review of the Uses of Computed Tomography for Analysing Instruments of the Violin Family with a Focus on the Future. J Violin Soc Am: VSA Papers, 22(1), 1-12.

Bostani, M., Mueller, J. W., McMillan, K., Cody, D. D., Cagnon, C. H., DeMarco, J. J., & McNitt-Gray, M. F. (2015). Accuracy of Monte Carlo simulations compared to in-vivo MDCT dosimetry. Medical physics, 42(2), 1080-1086.

Brady, Z., Cain, T. M., & Johnston, P. N. (2012). Comparison of organ dosimetry methods and effective dose calculation methods for paediatric CT. Australasian physical & engineering sciences in medicine, 35(2), 117-134.

Brenner, D. J. (2010). "Slowing the increase in the population dose resulting from CT scans." Radiat Res 174(6): 809-81.

Brenner, D. J. (2012). We can do better than effective dose for estimating or comparing low-dose radiation risks. Annals of the ICRP, 41(3), 124-128.

Brenner, D. J., & Hall, E. J. (2007). Computed tomography—an increasing source of radiation exposure. New England Journal of Medicine, 357(22), 2277-2284.

Brenner, D. J., Doll, R., Goodhead, D. T., Hall, E. J., Land, C. E., Little, J. B., Zaider, M. (2003). Cancer risks attributable to low doses of ionizing radiation: assessing what we really know. Proceedings of the National Academy of Sciences of the United States of America, 100(24), 13761–6.

Brenner, D., & Huda, W. (2008). Effective dose: A useful concept in diagnostic radiology. Radiation protection dosimetry, 128(4), 503-508.

Brix, G., Nissen-Meyer, S., Lechel, U., Nissen-Meyer, J., Griebel, J., Nekolla, E. A., Reiser, M., (2009). Radiation exposures of cancer patients from medical X- rays: How relevant are they for individual patients and population exposure. European Journal of Radiology, 72(2),342–347.

Buls, N., Van Gompel, G., Van Cauteren, T., Nieboer, K., Willekens, I., Verfaillie, G., & de Mey, J. (2015). Contrast agent and radiation dose reduction in abdominal CT by a combination of low tube voltage and advanced image reconstruction algorithms. European radiology, 25(4), 1023-1031.

Bushberg, J. T. (2002). Computed Tomography." The Essential Physics of Medical.

Bushong, S. C. (2013). Radiologic Science for Technologists-E-Book: Physics, Biology, and Protection. Elsevier Health Sciences.

Calzado, A., Rodriguez, R., & Munoz, A. (2000). Quality criteria implementation for brain and lumbar spine CT examinations. The British journal of radiology, 73(868), 384-395.

Chan, V. O., McDermott, S., Buckley, O., Allen, S., Casey, M., O'Laoide, R., & Torreggiani, W. C. (2012). The relationship of body mass index and abdominal fat on the radiation dose received during routine computed tomographic imaging of the abdomen and pelvis. Canadian Association of Radiologists Journal, 63(4), 260-266.

Christner, J. A., Kofler, & McCollough (2010). "Estimating effective dose for CT using dose-length product compared with using organ doses: consequences of adopting International Commission on Radiological Protection publication 103 or dual-energy scanning." AJR Am J Roentgenol 194(4): 881-889.

Ciantar D, Fitzgerald M, Cotterill D, Pettett A, Cook V, Beluffi G, et al (2000). Correlation between quantitative and subjective assessment of image quality in paediatric radiology. Radiat Prot Dosimetry; 90(1e2):185e8

Cierniak, Robert. (2011). "X-Ray Computed Tomography in Biomedical Engineering." X-Ray Computed Tomography in Biomedical Engineering, 1–319.

CIRS (2013), Computerized Imaging Reference Systems. ATOM Dosimetry Phantoms, User Guide and Technical Information Models: 701-706 ATOM PB 060514. 2428.

Cody, D. D., & Mahesh, M. (2007). Technologic advances in multidetector CT with a focus on cardiac imaging. Radiographics, 27(6), 1829-1837.

Cody, D. D., Pfeiffer, D., McNitt-Gray, M. F., Ruckdeschel, T. G., Strauss, K. J., & Wilcox, P. (2012). CT quality control manual. Reston, VA: American College of Radiology. ACR 2012

Commission of the European Community (CEC). (2000). European Guidelines on Quality Criteria for Computed Tomography European Guidelines on Quality Criteria, (EUR 16262 EN).

Committee to Assess Health Risks from Exposure to Low Levels of Ionizing Radiation. (2006). Health Risks from Exposure to Low Levels of Ionizing Radiation - BEIR VII Phase 2. Cancer.

Costa, P. R., Yoshimura, E. M., Nersissian, D. Y., & Melo, C. S. (2016). Correlation between effective dose and radiological risk: general concepts. Radiologia Brasileira, 49(3), 176-181.

Costello, J. E., Cecava, N. D., Tucker, J. E., & Bau, J. L. (2013). CT radiation dose: current controversies and dose reduction strategies. American Journal of Roentgenology, 201(6), 1283-1290.

Coursey, C. A., & Frush, D. P. (2008). CT and radiation: What radiologists should know. Applied radiology, 37(3), and 22.

Cunningham, I. A., & Judy, P. F. (2014). Computed Tomography chapter 2. In J Bronzino, J. D., & Peterson, D. R. (Eds.). (2014). Biomedical signals, imaging, and informatics. CRC Press.

De Crop, A., Smeets, P., Van Hoof, T., Vergauwen, M., Dewaele, T., Van Borsel, M., & Bacher, K. (2015). Correlation of clinical and physical-technical image quality in chest CT: a human cadaver study applied on iterative reconstruction. BMC medical imaging, 15(1), 32.

Deak, P. D., Smal, Y., & Kalender, W. A. (2010). Multisection CT protocols: sex-and age-specific conversion factors used to determine effective dose from dose-length product. Radiology, 257(1), 158-166.

Desouky, O., Ding, N., & Zhou, G. (2015). Targeted and non-targeted effects of ionizing radiation. Journal of Radiation Research and Applied Sciences, 8(2), 247-254.

Dhawan, A. P. (2011). Medical image analysis (2 Ed.). New Jersey: Wiley-IEEE Press.

DICOM (Digital Imaging and Communications in Medicine). (2013). RadiAnt DICOM Viewer User manual.

DICOM (Digital Imaging and Communications in Medicine). (2016). RadiAnt DICOM Viewer User manual. Retrieved from http://www.radiantviewer.com.

Dobeli, K. L., Lewis, S. J., Meikle, S. R., Thiele, D. L., & Brennan, P. C. (2014). Exposure (mAs) optimisation of a multi-detector CT protocol for hepatic lesion detection: Are thinner slices better? Journal of Medical Imaging and Radiation Oncology, 58(2), 137–143.

Dougeni, E., Faulkner, K., & Panayiotakis, G. (2012). A review of patient dose and optimisation methods in adult and paediatric CT scanning. European journal of radiology, 81(4), e665-e683.

EUROPEAN COMMISSION. (2016). Guidance How to complete your ethics self-assessment. Report H2020 Guidance version 5.2.

Feng, R., Tong, J., Liu, X., Zhao, Y., & Zhang, L. (2017). High-Pitch Coronary CT Angiography at 70 kVp Adopting a Protocol of Low Injection Speed and Low Volume of Contrast Medium. Korean journal of radiology, 18(5), 763-772.

Food and Drug Administration. (2006). Guidance for Industry, FDA Staff, and Third Parties Provision for Alternate Measure of the Computed Tomography Dose Index (CTDI) to Assure Compliance with the Dose Information Requirements of the Federal Performance Standard for Computed Tomography.

Franco, L., & Tahoces, P. G. (2014). Integrating quality control tests in a computed tomography system. From: http://www.impactscan.org.

Frey, G. D. (2014). Basic CT Parameters. American Journal of Roentgenology, 203(2), W126-W127.

Frush, D. P., & Yoshizumi, T. (2006). Conventional and CT angiography in children: dosimetry and dose comparisons. Pediatric radiology, 36(2), 154.

Fujii, K., Aoyama, T., Koyama, S., & Kawaura, C. (2007). Comparative evaluation of organ and effective doses for paediatric patients with those for adults in chest and abdominal CT examinations. The British journal of radiology, 80(956), 657-667.

Fujii, K., Aoyama, T., Yamauchi-Kawaura, C., Koyama, S., Yamauchi, M., Ko, S., & Nishizawa, K. (2009). Radiation dose evaluation in 64-slice CT examinations with adult and paediatric anthropomorphic phantoms. The British journal of radiology, 82(984), 1010-1018.

Funama, Y., Awai, K., Hatemura, M., Shimamura, M., Yanaga, Y., Oda, S., & Yamashita, Y. (2008). Automatic tube current modulation technique for multidetector CT: is it effective with a 64-detector CT? Radiological Physics and Technology, 1(1), 33–37.

Funama, Y., Sugaya, Y., Miyazaki, O., Utsunomiya, D., Yamashita, Y., & Awai, K. (2013). Automatic exposure control at MDCT based on the contrast-to-noise ratio: theoretical background and phantom study. Physical Medical, 29(1), 39-47.

Gang, G. J., Lee, J., Stayman, J. W., Tward, D. J., Zbijewski, W., Prince, J. L., & Siewerdsen, J. H. (2011). Analysis of Fourier- domain task- based detectability index in tomosynthesis and cone-beam CT in relation to human observer performance. Medical physics, 38(4), 1754-1768.

Gardner, E. A., Sumanaweera, T. S., Blanck, O., Iwamura, A. K., Steel, J. P., Dieterich, S., & Maguire, P. (2012). In vivo dose measurement using TLDs and MOSFET dosimeters for cardiac radiosurgery. Journal of Applied Clinical Medical Physics, 13(3), 190-203.

General Electric GE. (2008). GE Healthcare AutomA / SmartmA Theory TiP Training in Partnership AutomA off GE Healthcare AutomA On.

Gharbi, S., Labidi, S., Mars, M., Chelli, M., & Ladeb, F. (2017). Effective Dose and Size Specific Dose Estimation with and without Tube Current Modulation for Thoracic Computed Tomography Examinations: A Phantom Study. World Academy of Science, Engineering and Technology, International Journal of Medical, Health, Biomedical, Bioengineering and Pharmaceutical Engineering, 11(3), 81-85.

Gibson, D. A., Moorin, R. E., Semmens, J., & Holman, D. A. J. (2014). The disproportionate risk burden of CT scanning on females and younger adults in Australia: a retrospective cohort study. Australian and New Zealand journal of public health, 38(5), 441-448.

Goldman, L. W. (2007). Principles of CT and CT technology. Journal of nuclear medicine technology, 35(3), 115-128.

Goldman, L. W. (2008). Principles of CT: multislice CT. Journal of nuclear medicine technology, 36(2), 57-68.

González, A. B., Kim, K. P., Knudsen, A. B., Lansdorp-Vogelaar, I., Rutter, C. M., Smith-Bindman, R., ... & Berg, C. D. (2011). Radiation-related cancer risks from CT colonography screening: a risk-benefit analysis. American Journal of Roentgenology, 196(4), 816-823.

Goshima, S., Kanematsu, M., Nishibori, H., Sakurai, K., Miyazawa, D., Watanabe, H., & Bae, K. T. (2011). CT of the pancreas: comparison of anatomic structure depiction, image quality, and radiation exposure between 320-detector volumetric images and 64-detector helical images. Radiology, 260(1), 139-147.

Grant, K. L., Flohr, T. G., Krauss, B., Sedlmair, M., Thomas, C., & Schmidt, B. (2014). Assessment of an advanced image-based technique to calculate virtual monoenergetic computed tomographic images from a dual-energy examination to improve contrast-to-noise ratio in examinations using iodinated contrast media. Investigative radiology, 49(9), 586-592.

Groves, A. M., Owen, K. E., Courtney, H. M., Yates, S. J., Goldstone, K. E., Blake, G. M., & Dixon, A. K. (2004). 16-detector multislice CT: dosimetry estimation by TLD measurement compared with Monte Carlo simulation. The British journal of radiology, 77(920), 662-665.

Gu, J., Xu, X. G., Caracappa, P. F., & Liu, B. (2012). Fetal doses to pregnant patients from CT with tube current modulation calculated using Monte Carlo simulations and realistic phantoms. Radiation protection dosimetry, 155(1), 64-72.

Guimarães, L. S., Fletcher, J. G., Harmsen, W. S., Yu, L., Siddiki, H., Melton, Z., … McCollough, C. H. (2010). Appropriate Patient Selection at Abdominal Dual-Energy CT Using 80 kV: Relationship between Patient Size, Image Noise, and Image Quality. Radiology, 257(3), 732–742.

Gutierrez, D., Schmidt, S., Denys, A., Schnyder, P., Bochud, F. O., & Verdun, F. R. (2007). CT-automatic exposure control devices: What are their performances. Nuclear Instruments and Methods in Physics Research Section A: Accelerators, Spectrometers, Detectors and Associated Equipment, 580(2), 990-995.

Ha, H. I., Hong, S. S., Kim, M. J., & Lee, K. (2016). 100 kVp Low-Tube Voltage Abdominal CT in Adults: Radiation Dose Reduction and Image Quality Comparison of 120 kVp Abdominal CT. Journal of the Korean Society of Radiology, 75(4), 285-295.

Ha, H. I., Hong, S. S., Kim, M. J., & Lee, K. (2016). 100 kVp Low-Tube Voltage Abdominal CT in Adults: Radiation Dose Reduction and Image Quality Comparison of 120 kVp Abdominal CT. Journal of the Korean Society of Radiology, 75(4), 285-295.

Hall, E. J., and Brenner, D. J. (2008). Cancer risks from diagnostic radiology. British Journal of Radiology, 81(965), 362–378. http://doi.org/10.1259/bjr/019484541422740.

Hara, A. K., Wellnitz, C. V., Paden, R. G., Pavlicek, W., & Sahani, D. V. (2013). Reducing body CT radiation dose: Beyond just changing the numbers. American Journal of Roentgenology. 10.2214/AJR.13.10556.

Hart, D., Wall, B. F., Hillier, M. C., & Shrimpton, P. C. (2010). Frequency and collective dose for medical and dental X-ray examinations in the UK, 2008. Health Protection Agency.

Hasford, F., Van Wyk, B., Mabhengu, T., Vangu, M. D. T., Kyere, A. K., & Amuasi, J. H. (2015). Determination of dose delivery accuracy in CT examinations. Journal of Radiation Research and Applied Sciences, 8(4), 4–7.

He, X., & Frey, E. (2009). ROC, LROC, FROC, AFROC: An Alphabet Soup. Journal of the American College of Radiology, 6(9), 652-655.

Heggie, J. C. P. (2005). Patient doses in multi-slice CT and the importance of optimisation. Australasian Physics & Engineering Sciences in Medicine, 28(2), 86-96.

Hendee, W. (2010). The handbook of medical image perception and techniques (pp. 335-355). E. Samei, & E. A. Krupinski (Eds.). Cambridge: Cambridge University Press.

Hendee, W. R., & O'Connor, M. K. (2012). Radiation risks of medical imaging: separating fact from fantasy. Radiology, 264(2), 312-321.

Hetterich, H., Wirth, S., Johnson, T. R., & Bamberg, F. (2013). High-pitch dual spiral cardiovascular computed tomography. Current Cardiovascular Imaging Reports, 6(3), 251-258.

Hindorf, C., Glatting, G., Chiesa, C., Lindén, O., & Flux, G. (2010). EANM Dosimetry Committee guidelines for bone marrow and whole-body dosimetry. European journal of nuclear medicine and molecular imaging, 37(6), 1238-1250.

Hoang, J. K., Yoshizumi, T. T., Choudhury, K. R., Nguyen, G. B., Toncheva, G., Gafton, A. R., ... & Hurwitz, L. M. (2012). Organ-based dose current modulation and thyroid shields: techniques of radiation dose reduction for neck CT. American Journal of Roentgenology, 198(5), 1132-1138.

Hogg, P. & Blindell. (2012). Software for image quality evaluation using a forced choice comparison method Hogg. UKRC Manchester, 1(Figure 3), 25–27.

Hsieh, J 2009, Computed tomography: Principles, design, artifacts, and recent advances, 2nd end, SPIE, Bellingham.

Huda, W., & Mettler, F. A. (2011b). Volume CT dose index and dose-length product displayed during CT: what good are they. Radiology, 258(1), 236-242.

Huda, W., & He, W (2011a); Estimating cancer risks to adults undergoing body CT examinations. Radiation protection dosimetry, 150(2), 168-179.

Huda, W., Ogden, K. M., & Khorasani, M. R. (2008). Converting dose-length product to effective dose at CT. Radiology, 248(3), 995-1003.

Huda, W., Ravenel, J. G., & Scalzetti, E. M. (2002). How do radiographic techniques affect image quality and patient doses in CT. In Seminars in Ultrasound, CT and MRI (Vol. 23, No. 5, pp. 411-422). WB Saunders.

Huda, W., Sterzik, A., & Tipnis, S. (2009). X-ray beam filtration, dosimetry phantom size and CT patient dose conversion factors. Physics in medicine and biology, 55(2), 551.

Hurwitz, L. M., Reiman, R. E., Yoshizumi, T. T., Goodman, P. C., Toncheva, G., Nguyen, G., & Lowry, C. (2007a). Radiation dose from contemporary cardiothoracic multidetector CT protocols with an anthropomorphic female phantom: implications for cancer induction. Radiology, 245(3), 742-750.

Hurwitz, L. M., Yoshizumi, T. T., Goodman, P. C., Frush, D. P., Nguyen, G., Toncheva, G., and Lowry, C, (2007b). Effective dose determination using an anthropomorphic phantom and metal oxide semiconductor field effect transistor technology for clinical adult body multidetector array computed tomography protocols. Journal of Computer Assisted Tomography, 31(4): 544-9.

Hyer, D. E., Fisher, R. F., & Hintenlang, D. E. (2009). Characterization of a water- equivalent fiber-optic coupled dosimeter for use in diagnostic radiology. Medical physics, 36(5), 1711-1716.

Iball, G. R., Moore, A. C., & Crawford, E. J. (2016). A routine quality assurance test for CT automatic exposure control systems. Journal of applied clinical medical physics, 17(4), 291-306.

ICRP, International Commission on Radiological Protection. The (2007) Recommendations of the International Commission on Radiological Protection. ICRP Publication 103. Annals of the ICRP, 2007, 37(2-4):1-332.

International Atomic Energy Agency IAEA 1621. (2009). Dose Reduction in CT while Maintaining Diagnostic Confidence: A Feasibility/Demonstration StudyIAEA-TECDOC-1621.

International Electrotechnical Commission (IEC) (1994). Evaluation and routine testing in medical imaging departments. Part 2e6: constancy tests e X-ray equipment for computed tomography. IEC; (1223):2e6.

Jäkel, F., & Wichmann, F. A. (2006). Spatial four-alternative forced-choice method is the preferred psychophysical method for naïve observers. Journal of Vision, 6(11), 13-13.

Jessen, K. A. (2001). The quality criteria concept: an introduction and overview. Radiation protection dosimetry, 94(1-2), 29-32.

Jin, D. H., Lamberton, G. R., Broome, D. R., Saaty, H. P., Bhattacharya, S., Lindler, T. U., & Baldwin, D. D. (2010). Effect of reduced radiation CT protocols on the detection of renal calculi. Journal of Urology, 184(4), 1379–1380.

Jogan, M., & Stocker, A. A. (2014). A new two-alternative forced choice method for the unbiased characterization of perceptual bias and discriminability. Journal of Vision, 14(3), 20-20.

Jurik, A., Petersen, J., Jessen, K. A., Bongartz, G., Geleijns, J., Golding, S. J., & Tosi, G. (2000). Clinical use of image quality criteria in computed tomography: a pilot study. Radiation protection dosimetry, 90(1-2), 47-52.

Jursinic, P. A. (2007). Characterization of optically stimulated luminescent dosimeters, OSLDs, for clinical dosimetric measurements. Medical physics, 34(12), 4594-4604.

Kaasalainen, T., Palmu, K., Lampinen, A., Reijonen, V., Leikola, J., Kivisaari, R., & Kortesniemi, M. (2015). Limiting CT radiation dose in children with craniosynostosis: phantom study using model-based iterative reconstruction. Pediatric radiology, 45(10), 1544-1553.

Kachelrieß, M., & Noo, F. (2017). Advances and Trends in image formation in x-ray CT. Medical Physics, 44(9), e112–e112.

Kadir, A. B. A., Priharti, W., Samat, S. B., & Dolah, M. T. (2013, November). OSLD energy response performance and dose accuracy at 24-1250 keV: Comparison with TLD-100H and TLD-100. In AIP Conference Proceedings (Vol. 1571, No. 1, pp. 108-114). AIP.

Kahn, J., Grupp, U., Rotzinger, R., Kaul, D., Schäfer, M. L., & Streitparth, F. (2014). CT for evaluation of potential renal donors–How does iterative reconstruction influence image quality and dose. European journal of radiology, 83(8), 1332-1336.

Kalender, W. A. "Dose in x-ray computed tomography." Phys Med Biol (2014), 59: 129-150

Kalender, W. A. (2011). Computed tomography: fundamentals, system technology, image quality, applications. John Wiley & Sons.

Kalra, M. K., Maher, M. M., Toth, T. L., Hamberg, L. M., Blake, M. A., Shepard, J. A., & Saini, S. (2004b). Strategies for CT radiation dose optimization. Radiology, 230(3), 619-628.

Kalra, M. K., Maher, M. M., Toth, T. L., Kamath, R. S., Halpern, E. F., & Saini, S. (2004a). Comparison of Z-axis automatic tube current modulation technique with fixed tube current CT scanning of abdomen and pelvis. Radiology, 232(2), 347-353.

Kalra, M. K., Maher, M. M., Toth, T. L., Schmidt, B., Westerman, B. L., Morgan, H. T., & Saini, S. (2004c). Techniques and applications of automatic tube current modulation for CT. Radiology, 233(3), 649-657.

Kalra, M. K., Sodickson, A. D., & Mayo-Smith, W. W. (2015). CT radiation: key concepts for gentle and wise use. Radiographics, 35(6), 1706-1721.

Kalra, Mannudeep K, Stefania Rizzo, Michael M Maher, Elkan F Halpern, Thomas L Toth, Jo-Anne O Shepard, and Suzanne L Aquino. (2005). "Chest CT Performed with Z-Axis Modulation: Scanning Protocol and Radiation Dose." Radiology 237 (1): 303–8.

Kanematsu, M., Goshima, S., Miyoshi, T., Kondo, H., Watanabe, H., Noda, Y., & Bae, K. T. (2014). Whole-body CT angiography with low tube voltage and low-concentration contrast material to reduce radiation dose and iodine load. American Journal of Roentgenology, 202(1), W106-W116.

Kawaguchi, A., Matsunaga, Y., Kobayashi, M., Suzuki, S., Matsubara, K., & Chida, K. (2014). Effect of tube current modulation for dose estimation using a simulation tool on body CT examination. Radiation protection dosimetry, 167(4), 562-568.

Kaza, R. K., Platt, J. F., Goodsitt, M. M., Al-Hawary, M. M., Maturen, K. E., Wasnik, A. P., & Pandya, A. (2014). Emerging Techniques for Dose Optimization in Abdominal CT. RadioGraphics, 34(1), 4–17.

Keat, N. (2005). CT scanner automatic exposure control systems. MHRA Report 05016.

Keeble, C., Baxter, P. D., Gislason-Lee, A. J., Treadgold, L. A., & Davies, A. G. (2016). Methods for the analysis of ordinal response data in medical image quality assessment. The British Journal of Radiology, (January), 20160094.

Kelaranta, A., Mäkelä, T., Kaasalainen, T., & Kortesniemi, M. (2017). Fetal radiation dose in three common CT examinations during pregnancy–Monte Carlo study. Physical Medical: European Journal of Medical Physics, 43, 199-206.

Kharuzhyk, S. A., Matskevich, S. A., Filjustin, A. E., Bogushevich, E. V., & Ugolkova, S. A. (2010). Survey of computed tomography doses and establishment of national diagnostic reference levels in the Republic of Belarus. Radiation protection dosimetry, 139(1-3), 367-370.

Kim, S. M., Kim, Y. N., & Choe, Y. H. (2013). Adenosine-stress dynamic myocardial perfusion imaging using 128-slice dual-source CT: optimization of the CT protocol to reduce the radiation dose. The international journal of cardiovascular imaging, 29(4), 875-884.

Kim, S., Yoshizumi, T. T., Toncheva, G., Frush, D. P., & Yin, F. F. (2009). Estimation of absorbed doses from paediatric cone-beam CT scans: MOSFET measurements and Monte Carlo simulations. Radiation protection dosimetry, 138(3), 257-263.

Kishimoto, J., Sakou, T., & Ohta, Y. (2013). Evaluation of the individual tube current setting in electrocardiogram-gated cardiac computed tomography estimated from plain chest computed tomography using computed tomography automatic exposure control. Nihon Hoshasen Gijutsu Gakkai zasshi, 69(5), 508-513.

Koivisto, J. H., Wolff, J. E., Kiljunen, T., Schulze, D., & Kortesniemi, M. (2015). Characterization of MOSFET dosimeters for low- dose measurements in maxillofacial anthropomorphic phantoms. Journal of Applied Clinical Medical Physics, 16(4), 266-278.

Koivisto, J., Kiljunen, T., Tapiovaara, M., Wolff, J., & Kortesniemi, M. (2012). Assessment of radiation exposure in dental cone-beam computerized tomography with the use of metal-oxide semiconductor field-effect transistor (MOSFET) dosimeters and Monte Carlo simulations. Oral surgery, oral medicine, oral pathology and oral radiology, 114(3), 393-400.

Koivisto, J., Kiljunen, T., Wolff, J., & Kortesniemi, M. (2013). Characterization of MOSFET dosimeter angular dependence in three rotational axes measured free-in-air and in soft-tissue equivalent material. Journal of radiation research, 54(5), 943-949.

Koivisto, J., Schulze, D., Wolff, J., & Rottke, D. (2014). Effective dose assessment in the maxillofacial region using thermoluminescent (TLD) and metal oxide semiconductor field-effect transistor (MOSFET) dosimeters: a comparative study. Dentomaxillofacial Radiology, 43(8), 20140202.

Koral, K., Blackburn, T., Bailey, A. A., Koral, K. M., & Anderson, J. (2012). Strengthening the argument for rapid brain MR imaging: estimation of reduction in lifetime attributable risk of developing fatal cancer in children with shunted hydrocephalus by instituting a rapid brain MR imaging protocol in lieu of head CT. American Journal of Neuroradiology, 33(10), 1851-1854.

Kortesniemi, M., Salli, E., & Seuri, R. (2012). Organ dose calculation in CT based on scout image data and automatic image registration. Acta Radiological, 53(8), 908-913.

Kost, S. D., Fraser, N. D., Carver, D. E., Pickens, D. R., Price, R. R., Hernanz-Schulman, M., & Stabin, M. G. (2015). Patient-specific dose calculations for paediatric CT of the chest, abdomen and pelvis. Pediatric radiology, 45(12), 1771-1780.

Kulama, E. (2004). Scanning protocols for multislice CT scanners. The British journal of radiology, 77(suppl_1), S2-S9.

Kumar, A. S., Singh, I. R. R., Sharma, S. D., & Ravindran, B. P. (2015). Performance characteristics of mobile MOSFET dosimeter for kilovoltage X-rays used in image guided radiotherapy. Journal of Medical Physics/Association of Medical Physicists of India, 40(3), 123.

KYOTO KAGAKU CT, Medical Imaging abdomen and pelvis CT (2015) http://www.imagingsol.com.au/product/1812/CT-Abdomen-Phantom.html.

Laghi, A., & Paolantonio, P. (2006). The Right Scanner Parameters to Use. In Virtual Colonoscopy (pp. 61-71). Springer Berlin Heidelberg.

Lahham, A., ALMasri, H., & Kameel, S. (2017). ESTIMATION OF FEMALE RADIATION DOSES AND BREAST CANCER RISK FROM CHEST CT EXAMINATIONS. Radiation Protection Dosimetry.

Lamba, R., McGahan, J. P., Corwin, M. T., Li, C. S., Tran, T., Seibert, J. A., & Boone, J. M. (2014). CT Hounsfield numbers of soft tissues on unenhanced abdominal CT scans: Variability between two different manufacturers' MDCT scanners. American Journal of Roentgenology, 203(5), 1013–1020.

Lança, L., & Silva, A. (2008). Digital radiography detectors – A technical overview: Part 2. Radiography, 15(2), 134–138.

Lança, L., Franco, L., Ahmed, A., Harderwijk, M., Marti, C., Nasir, S., & Hogg, P. (2014). 10 kVp rule–an anthropomorphic pelvis phantom imaging study using a CR system: impact on image quality and effective dose using AEC and manual mode. Radiography, 20(4), 333-338.

Lança, L., Pietro Barros, Rodrigo D'Agostini Derech, Daniel Higgins, Marjolein Kleiker, Sébastien Liardet, Ine Michaela Løvlien, Kevin McNally, Manon Thévenaz, Peter Hogg (2017). The impact of pitch values on image quality and radiation dose in an abdominal adult phantom using CT page 105. From Hogg, P., Hogg, R., Thompson, –, & Buissink, C. (2017). Optimising image quality for medical imaging. Book -ISBN 978-1-907842-93-1.

Lavallée, D. A., Van Dam, T., Blewitt, G., & Clarke, P. J. (2006). Geocenter motions from GPS: A unified observation model. Journal of geophysical research: solid earth, 111(B5).

Lechel U, Becker C, Langenfeld-Jager G, Brix G (2009) Dose reduction by automatic exposure control in multidetector computed tomography: comparison between measurement and calculation. Eur Radiol 19(4):1027–1034

Ledenius, K., Svensson, E., Stålhammar, F., Wiklund, L. M., & Thilander-Klang, A. (2010). A method to analyse observer disagreement in visual grading studies: Example of assessed image quality in paediatric cerebral multidetector CT images. British Journal of Radiology, 83(991), 604–611.

Lee, C. H., Goo, J. M., Ye, H. J., Ye, S. J., Park, C. M., Chun, E. J., & Im, J. G. (2008). Radiation dose modulation techniques in the multidetector CT era: from basics to practice. Radiographics, 28(5), 1451-1459.

Lee, C., Kim, K. P., Long, D., Fisher, R., Tien, C., Simon, S. L. ... & Bloch, W. E. (2011a). Organ doses for reference adult male and female undergoing computed tomography estimated by Monte Carlo simulations. Medical physics, 38(3), 1196-1206.

Lee, E. J., Lee, S. K., Agid, R., Howard, P., & Bae, J. M. (2009). Comparison of image quality and radiation dose between fixed tube current and combined automatic tube current modulation in craniocervical CT angiography. American Journal of Neuroradiology, 30(9), 1754-1759.

Lee, S., Yoon, S.-W., Yoo, S.-M., Ji, Y. G., Kim, K. A., Kim, S. H., & Lee, J. T. (2011b). Comparison of image quality and radiation dose between combined automatic tube current modulation and fixed tube current technique in CT of abdomen and pelvis. Acta Radiological, 52(10), 1101–1106.

Lee, T. Y., & Chhem, R. K. (2010). Impact of new technologies on dose reduction in CT. European journal of radiology, 76(1), 28-35.

Lell, M. M., May, M., Deak, P., Alibek, S., Kuefner, M., Kuettner, A., & Radkow, T. (2011). High-pitch spiral computed tomography: effect on image quality and radiation dose in Pediatric chest computed tomography. Investigative radiology, 46(2), 116-123.

Lell, M., Hinkmann, F., Anders, K., Deak, P., Kalender, W. A., Uder, M., & Achenbach, S. (2009). High-pitch electrocardiogram-triggered computed tomography of the chest: initial results. Investigative radiology, 44(11), 728-733.

Lemoigne, Y., & Caner, A. (Eds.). (2010). Radiation protection in medical physics. Springer Science & Business Media.

Lewis, M. A., & Edyvean, S. (2005). Patient dose reduction in CT. The British journal of radiology, 78(934), 880-883.

Li, X., Segars, W. P., & Samei, E. (2014). The impact on CT dose of the variability in tube current modulation technology: a theoretical investigation. Physics in Medicine & Biology, 59(16), 4525.

Lim, S., Bae, J. H., Chun, E. J., Kim, H., Kim, S. Y., Kim, K. M., … Jang, H. C. (2014). Differences in pancreatic volume, fat content, and fat density measured by multidetector-row computed tomography according to the duration of diabetes. Springer, 51(5), 739–748.

Lin, E., & Alessio, A. (2016). What are the basic concepts of temporal, contrast, and spatial resolution in cardiac CT? PMC, 28(10), 1304–1314. http://doi.org/10.1002/nbm.3369.

Linet, M. S., Slovis, T. L., Miller, D. L., Kleinerman, R., Lee, C., Rajaraman, P., & Berrington de Gonzalez, A. (2012). Cancer risks associated with external radiation from diagnostic imaging procedures. CA: a cancer journal for clinicians, 62(2), 75-100.

Lira, D., Padole, A., Kalra, M. K., & Singh, S. (2015). Tube potential and CT radiation dose optimization. American Journal of Roentgenology, 204(1), W4-W10.

Lohan, R. (2015). Image Quality and Current Techniques for Dose Optimization in Abdominal CT: What Every Radiologist Should Know. Current Radiology Reports, 3(6), 17.

Ludewig, E., Richter, A., & Frame, M. (2010). Diagnostic imaging–evaluating image quality using visual grading characteristic (VGC) analysis. Veterinary research communications, 34(5), 473-479.

Luo, S., Zhang, L. J., Meinel, F. G., Zhou, C. S., Qi, L., McQuiston, A. D., ... & Lu, G. M. (2014). Low tube voltage and low contrast material volume cerebral CT angiography. European radiology, 24(7), 1677-1685.

Lv, P., Liu, J., Zhang, R., Jia, Y., & Gao, J. (2015). Combined use of automatic tube voltage selection and current modulation with iterative reconstruction for CT evaluation of small hypervascular hepatocellular carcinomas: effect on lesion conspicuity and image quality. Korean journal of radiology, 16(3), 531-540.

Mahesh, M. (2009). MDCT Physics: The Basics--Technology, Image Quality and Radiation Dose.

Manninen, A. L., Kotiaho, A., Nikkinen, J., & Nieminen, M. T. (2014). Validation of a MOSFET dosemeter system for determining the absorbed and effective radiation doses in diagnostic radiology. Radiation protection dosimetry, 164(3), 361-367.

Manning, D., Ethell, S., Donovan, T., & Crawford, T. (2006). How do radiologists do it? The influence of experience and training on searching for chest nodules. Radiography, 12(2), 134-142.

Manning-Stanley, A. S., Ward, A. J., & England, A. (2012). Options for radiation dose optimisation in pelvic digital radiography: a phantom study. Radiography, 18(4), 256-263.

Manson, E. N., Fletcher, J. J., Della Atuwo-Ampoh, V., Addison, E. K., Schandorf, C., & Bambara, L. (2016). Assessment of some image quality tests on a 128 slice computed tomography scanner using a Catphan700 phantom. Journal of Medical Physics/Association of Medical Physicists of India, 41(2), 153.

Månsson, L. G. (2000). Methods for the evaluation of image quality: a review. Radiat. Prot. Dosimetry, 90(1–2), 89–99.

Marin, D., Nelson, R. C., Schindera, S. T., Richard, S., Youngblood, R. S., Yoshizumi, T. T., & Samei, E. (2009). Low-tube-voltage, high-tube-current multidetector abdominal CT: improved image quality and decreased radiation dose with adaptive statistical iterative reconstruction algorithm—initial clinical experience. Radiology, 254(1), 145-153.

Martin, C. J. (2007). An evaluation of semiconductor and ionization chamber detectors for diagnostic x-ray dosimetry measurements. Physics in medicine and biology, 52(15), 4465.

Martin, C. J., & Sookpeng, S. (2016). Setting up computed tomography automatic tube current modulation systems. Journal of Radiological Protection, 36(3), R74.

Mathews, J. D., Forsythe, A. V., Brady, Z., Butler, M. W., Goergen, S. K., Byrnes, G. B., & McGale, P. (2013). Cancer risk in 680 000 people exposed to computed tomography scans in childhood or adolescence: data linkage study of 11 million Australians. Bmj, 346, f2360.

Matsunaga, Y., Kawaguchi, A., Kobayashi, M., Suzuki, S., Suzuki, S., & Chida, K. (2017). Radiation doses for pregnant women in the late pregnancy undergoing fetal-computed tomography: a comparison of dosimetry and Monte Carlo simulations. Radiological physics and technology, 10(2), 148-154.

Mattison, B. J., Nguyen, G. B., Januzis, N., Lowry, C., & Yoshizumi, T. T. (2016). A NOVEL APPROACH FOR EFFECTIVE DOSE MEASUREMENTS IN DUAL-ENERGY CT. Radiation protection dosimetry, 172(4), 416-421.

Maués, N. H., Alves, A. F., Neto, F. A. B., Rosa, M. E., de Oliveira, M., & Ribeiro, S. M. (2016). Dose optimization in computed tomography comparing automatic tube current modulation and fixed tube current techniques. Physical Medical, 32, 337.

Mayer, C., Meyer, M., Fink, C., Schmidt, B., Sedlmair, M., Schoenberg, S. O., & Henzler, T. (2014). Potential for radiation dose savings in abdominal and chest CT using automatic tube voltage selection in combination with automatic tube current modulation. American Journal of Roentgenology, 203(2), 292-299.

Mazonakis, M., Tzedakis, A., Damilakis, J., & Gourtsoyiannis, N. (2007). Thyroid dose from common head and neck CT examinations in children: is there an excess risk for thyroid cancer induction. European radiology, 17(5), 1352-1357.

McCollough, C. H., Bruesewitz, M. R., & Kofler Jr, J. M. (2006). CT dose reduction and dose management tools: overview of available options. Radiographics, 26(2), 503-512.

McCollough, C. H., Christner, J. A., & Kofler, J. M. (2010). How effective is effective dose as a predictor of radiation risk. American Journal of Roentgenology, 194(4), 890-896.

McCollough, C. H., Leng, S., Yu, L., Cody, D. D., Boone, J. M., & McNitt-Gray, M. F. (2011). CT dose index and patient dose: they are not the same thing. Radiology, 259(2), 311-316.

McCollough, C. H., Primak, A. N., Braun, N., Kofler, J., Yu, L., & Christner, J. (2009). Strategies for reducing radiation dose in CT. Radiologic Clinics of North America, 47(1), 27-40.

McCollough, C., Cody, D., Edyvean, S., Geise, R., Gould, B., Keat, N., & Morin, R. (2008). The measurement, reporting, and management of radiation dose in CT. Report of AAPM Task Group, 23(23), 1-28.

McCollough, Cynthia H., Shuai Leng, Lifeng Yu, Dianna D. Cody, John M. Boone, and Michael F. McNitt-Gray. "CT dose index and patient dose: they are not the same thing." Radiology 259, no. 2 (2011): 311-316.

McNitt- Gray, M. (2006). MO- A- ValB- 01: Tradeoffs in Image Quality and Radiation Dose for CT. Medical Physics, 33(6), 2154-2155.

Merzan, D., Nowik, P., Poludniowski, G., & Bujila, R. (2016). Evaluating the impact of scan settings on automatic tube current modulation in CT using a novel phantom. The British journal of radiology, 90(1069), 20160308.

Miéville, F. A., Gudinchet, F., Rizzo, E., Ou, P., Brunelle, F., Bochud, F. O., & Verdun, F. R. (2011). Paediatric cardiac CT examinations: Impact of the iterative reconstruction method ASIR on image quality - Preliminary findings. Pediatric Radiology, 41(9), 1154–1164.

Mohan, R., Singh, A., & Gundappa, M. (2011). Three-dimensional imaging in periodontal diagnosis–Utilization of cone beam computed tomography. Journal of Indian Society of Periodontology, 15(1), 11.

Mohan, R., Singh, A., & Gundappa, M. (2011). Three-dimensional imaging in periodontal diagnosis–Utilization of cone beam computed tomography. Journal of Indian Society of Periodontology, 15(1), 11.

Molen, A. J., Joemai, R. M., & Geleijns, J. (2012). Performance of longitudinal and volumetric tube current modulation in a 64-slice CT with different choices of acquisition and reconstruction parameters. Physical Medical, 28(4), 319-326.

Monnin, P., Marshall, N. W., Bosmans, H., Bochud, F. O., & Verdun, F. R. (2011). Image quality assessment in digital mammography: part II. NPWE as a validated alternative for contrast detail analysis. Physics in medicine and biology, 56(14), 4221.

Moore, C. L., Daniels, B., Ghita, M., Gunabushanam, G., Luty, S., Molinaro, A. M., Gross, C. P. (2015). Accuracy of reduced-dose computed tomography for ureteral stones in emergency department patients. Annals of Emergency Medicine, 65(2), 189–198.

Moore, K.L., Agur, A.M.R. & Dalley, A.F., 2010. Essential CLINICAL ANATOMY - Fourth Edition,

Moss, M., & McLean, D. (2006). Paediatric and adult computed tomography practice and patient dose in Australia. Journal of Medical Imaging and Radiation Oncology, 50(1), 33-40.

Mraity, H. A. A. (2015). Optimisation of radiation dose and image quality for AP pelvis radiographic examination (Doctoral dissertation, University of Salford).

Mraity, H. A., England, A., & Hogg, P. (2017). Gonad dose in AP pelvis radiography: impact of anode heel orientation. Radiography, 23(1), 14-18.

Mraity, H., England, A., & Hogg, P. (2014). Developing and validating a psychometric scale for image quality assessment. Radiography, 20(4), 306–311.

Mulkens, T. H., Bellinck, P., Baeyaert, M., Ghysen, D., Van Dijck, X., Mussen, E., & Termote, J. L. (2005). Use of an automatic exposure control mechanism for dose optimization in multi–detector row CT examinations: clinical evaluation. Radiology, 237(1), 213-223.

Nagarajappa, A. K., Dwivedi, N., & Tiwari, R. (2015). Artifacts: The downturn of CBCT image. Journal of International Society of Preventive & Community Dentistry, 5(6), 440.

Nagata, K., Fujiwara, M., Kanazawa, H., Mogi, T., Iida, N., Mitsushima, T., & Sugimoto, H. (2015). Evaluation of dose reduction and image quality in CT colonography: comparison of low-dose CT with iterative reconstruction and routine-dose CT with filtered back projection. European radiology, 25(1), 221-229.

Nagel, H. D. (2007). CT parameters that influence the radiation dose. Radiation dose from adult and Pediatric multidetector computed tomography, 51-79.

Namasivayam, S., Kalra, M. K., Pottala, K. M., Waldrop, S. M., & Hudgins, P. A. (2006). Optimization of Z-axis automatic exposure control for multidetector row CT evaluation of neck and comparison with fixed tube current technique for image quality and radiation dose. American Journal of Neuroradiology, 27(10), 2221-2225.

Namasivayam, S., Kalra, M. K., Pottala, K. M., Waldrop, S. M., & Hudgins, P. A. (2006). Optimization of Z- axis automatic exposure control for multidetector row CT evaluation of neck and comparison with fixed tube current technique for image quality and radiation dose. American Journal of Neuroradiology, 27(10), 2221-2225.

National Academy of Sciences (NAS) (2006). Health risks from exposure to low levels of ionizing radiation: BEIR VII phase 2 (Vol. 7). National Academies Press.

National Council on Radiation Protection and Measurements (2009). Ionizing radiation exposure of the population of the United States. NCRP Report No. 160. Bethesda, Md: National Council on Radiation Protection and Measurements.

NDS Surgical Imaging. (2014). DOME E5 5MP Diagnostic Grayscale Display. Retrieved from http://www.ndssi.com/data/uploads/pdf/Radiology/Dome_Graysacale/E5_Grayscale_Display/ds-NDS-Dome-E5.pdf.

Ngaile, J. E., Msaki, P., & Kazema, R. (2006). Current status of patient radiation doses from computed tomography examinations in Tanzania. Radiation protection dosimetry, 121(2), 128-135.

Nievelstein, R. A., van Dam, I. M., & van der Molen, A. J. (2010). Multidetector CT in children: current concepts and dose reduction strategies. Pediatric radiology, 40(8), 1324-1344.

Norman, G. (2010). Likert scales, levels of measurement and the "laws" of statistics. Advances in health sciences education, 15(5), 625-632.

Nowik, P., Bujila, R., Poludniowski, G., & Fransson, A. (2015). Quality control of CT systems by automated monitoring of key performance indicators: a two- year study. Journal of Applied Clinical Medical Physics, 16(4), 254-265.

Nunes, A., Pereira, H., Tomé, M., Silva, J., & Fontes, L. (2016). Tomography as a method to study umbrella pine (Pinus pinea) cones and nuts. Forest Systems, 25(2), 10.

Origgi, D., Vigorito, S., Villa, G., Bellomi, M., & Tosi, G. (2006). Survey of computed tomography techniques and absorbed dose in Italian hospitals: a comparison between two methods to estimate the dose–length product and the effective dose and to verify fulfilment of the diagnostic reference levels. European radiology, 16(1), 227-237.

Padole, A., Khawaja, R. D. A., Otrakji, A., Zhang, D., Liu, B., Xu, X. G., & Kalra, M. K. (2016). Comparison of Measured and Estimated CT Organ Doses for Modulated and Fixed Tube Current: A Human Cadaver Study. Academic radiology, 23(5), 634-642.

Papadakis, A. E., Perisinakis, K., & Damilakis, J. (2016). Development of a method to estimate organ doses for Pediatric CT examinations. Medical physics, 43(5), 2108-2117.

Papadimitriou, D., Perris, A., Manetou, A., Molfetas, M., Panagiotakis, N., Lyra-Georgosopoulou, M., & Vigorito, S. (2003). A survey of 14 computed tomography scanners in Greece and 32 scanners in Italy: Examination frequencies, dose reference values, effective dose and doses to organs. Radiation protection dosimetry, 104(1), 47-53.

Park, C. K., Choo, K. S., Jeon, U. B., Baik, S. K., Kim, Y. W., Kim, T. U., ... & Lim, S. J. (2013). Image quality and radiation dose of 128-slice dual-source CT venography using low kilovoltage combined with high-pitch scanning and automatic tube current modulation. The international journal of cardiovascular imaging, 29(1), 47-51.

Park, H, Jung, S, Lee, Y, Cho, W, Do, K, Kim, S & Kim, K (2009), 'The relationship between subjective and objective parameters in CT phantom image evaluation', Korean J Radiol, vol. 10, no. 5, pp. 490-5.

Park, Y. B., Jeon, H. S., Shim, J. S., Lee, K. W., & Moon, H. S. (2011). Analysis of the anatomy of the maxillary sinus septum using 3-dimensional computed tomography. Journal of Oral and Maxillofacial Surgery, 69(4), 1070-1078.

Paterson, A., & Frush, D. P. (2007). Dose reduction in paediatric MDCT: general principles. Clinical Radiology, 62(6), 507–517

Pejovic, M. M. (2016). P-Channel MOSFET as a sensor and dosimeter of ionizing radiation. Facta Universitatis, Series: Electronics and Energetics, 29(4), 509-541.

Peng, Y., Li, J., Ma, D., Zhang, Q., Liu, Y., Zeng, J., & Sun, G. (2009). Use of automatic tube current modulation with a standardized noise index in young children undergoing chest computed tomography scans with 64-slice multidetector computed tomography. Acta Radiological, 50(10), 1175-1181.

Peng, Y., Li, J., Ma, D., Zhang, Q., Liu, Y., Zeng, J., & Sun, G. (2009). Use of automatic tube current modulation with a standardized noise index in young children undergoing chest computed tomography scans with 64-slice multidetector computed tomography. Acta Radiological, 50(10), 1175-1181.

Peterson, W. W., Birdsall, T. G., and Fox, W. C. (1954). The theory of signal detectability. Trans. IRE Prof. Group Inf. Theory 4, 171–212.

Phelps, A. S., Naeger, D. M., Courtier, J. L., Lambert, J. W., Marcovici, P. A., Villanueva-Meyer, J. E., & MacKenzie, J. D. (2015). Pairwise comparison versus Likert scale for biomedical image assessment. American Journal of Roentgenology, 204(1), 8-14.

Pontone, G., Andreini, D., Baggiano, A., Bertella, E., Mushtaq, S., Conte, E., & Pepi, M. (2015). Functional relevance of coronary artery disease by cardiac magnetic resonance and cardiac computed tomography: myocardial perfusion and fractional flow reserve. BioMed research international, 2015.

Prokop, M., & Galanski, M. (2003). Spiral and multislice computed tomography of the body. Thieme.43, S4-10.

Puchalska, M., & Bilski, P. (2008). An improved method of estimating ionisation density using TLDs. Radiation Measurements, 43(2–6), 679–682.

Rahim, S., Anuar, K., Salleh, M., Azaman, N., Madiha, S., Amir, M., Hamzah, A. R. (2010). EFFECT OF EXPOSURE TIME REDUCTION TOWARDS SENSITIVITY AND SNR FOR COMPUTED RADIOGRAPHY (CR) APPLICATION IN NDT. In Malaysian Nuclear Agency (Nuclear (pp. 1–6).

Raman, S. P., Johnson, P. T., Deshmukh, S., Mahesh, M., Grant, K. L., & Fishman, E. K. (2013). CT dose reduction applications: Available tools on the latest generation of CT scanners. Journal of the American College of Radiology, 10(1), 37–41.

Raman, S. P., Reddy, S., Weiss, M. J., Manos, L. L., Cameron, J. L., Zheng, L., & Wolfgang, C. L. (2015). Impact of the time interval between MDCT imaging and surgery on the accuracy of identifying metastatic disease in patients with pancreatic cancer. American Journal of Roentgenology, 204(1), W37-W42.

Ramirez-Giraldo, J. C., Fuld, M., Grant, K., Primak, A. N., & Flohr, T. (2015). New approaches to reduce radiation while maintaining image quality in multi-detector-computed tomography. Current Radiology Reports, 3(2), 4.

Ramirez-Giraldo, J., Primak, A., Grant, K., Schmidt, B., & Fuld, M. (2014). Radiation dose optimization technologies in multidetector computed tomography: a review. Med Phys, 2(2), 420-30.

Ranallo, F. N., & Szczykutowicz, T. (2015). The correct selection of pitch for optimal CT scanning: avoiding common misconceptions. Journal of the American College of Radiology, 12(4), 423-424.Medicine, 42(3), 327-333.

Rivetti, S., Lanconelli, N., Bertolini, M., & Acchiappati, D. (2011). A new clinical unit for digital radiography based on a thick amorphous Selenium plate: Physical and psychophysical characterization. Medical physics, 38(8), 4480-4488.

Rizzo, S., Kalra, M., Schmidt, B., Dalal, T., Suess, C., Flohr, T., & Saini, S. (2006). Comparison of angular and combined automatic tube current modulation techniques with constant tube current CT of the abdomen and pelvis. American Journal of Roentgenology, 186(3), 673-679.

Rodrigues, S. I., Abrantes, A. F., Ribeiro, L. P., & Almeida, R. P. P. (2012). Dosimetry in abdominal imaging by 6-slice computed tomography. Radiologia Brasileira, 45(6), 326-333.

Rosner, B. (2010). Fundamentals of biostatistics (7 Ed.). Boston: Cengage Learning.

Rottke, D., Grossekettler, L., Sawada, K., Poxleitner, P., & Schulze, D. (2013). Influence of lead apron shielding on absorbed doses from panoramic radiography. Dentomaxillofacial Radiology, 42(10), 20130302.

Russell, M. T., Fink, J. R., Rebeles, F., Kanal, K., Ramos, M., & Anzai, Y. (2008). Balancing radiation dose and image quality: clinical applications of neck volume CT. American Journal of Neuroradiology, 29(4), 727-731.

Saba, L., & Suri, J. S. (Eds.). (2013). Multi-detector CT imaging: abdomen, pelvis, and CAD applications (Vol. 2). CRC Press.

Sabarudin, A., Mustafa, Z., Nassir, K. M., Hamid, H. A., & Sun, Z. (2014). Radiation dose reduction in thoracic and abdomen-pelvic CT using tube current modulation: a phantom study. Journal of Applied Clinical Medical Physics / American College of Medical Physics, 16(1), 5135.

Sabarudin, A., Yusof, M. Z., Mohamad, M., & Sun, Z. (2013). Radiation dose associated with cerebral CT angiography and CT perfusion: an experimental phantom study. Radiation protection dosimetry, 162(3), 316-321.

Sabri, A. H., Ali, A., Daud, N., Ha, M., and Nasir, F. (2015). Comparison of Image Quality and Radiation Dose between Angular Automatic Tube Current Modulation and Fixed Tube Current CT Scanning of Thorax: Phantom Study. Global Journal of Engineering Science and Researches, 2(7), 183–188

Salamin, J., Plasman, P., Bakker, A., Dominguez, A., Sohrabi, T., Ahmed, A., & Campeanu, C. (2015). Research article–A comparison of Sinogram Affirmed Iterative Reconstruction and filtered back projection on image quality and dose reduction in paediatric head CT: a phantom study. OPTIMAX 2014–radiation dose and image quality optimisation in medical imaging. -ISBN 9781907842603, 28-37.

Saltybaeva, N., Martini, K., Frauenfelder, T., & Alkadhi, H. (2016). Organ dose and attributable cancer risk in lung cancer screening with low-dose computed tomography. PloS one, 11(5), e0155722.

Saunders, J., & Ohlerth, S. (2011). CT physics and instrumentation–mechanical design. Veterinary Computed Tomography, 1-8.

Scalzetti, E. M., Huda, W., Bhatt, S., & Ogden, K. M. (2008). A method to obtain mean organ doses in a Rando phantom. Health physics, 95(2), 241-244.

Schindera, S. T., Nelson, R. C., Lee, E. R., DeLong, D. M., Ngyen, G., Toncheva, G., & Yoshizumi, T. T. (2007). Abdominal multislice CT for obese patients: effect on image quality and radiation dose in a phantom study. Academic radiology, 14(4), 486-494.

Schindera, S. T., Nelson, R. C., Lee, E. R., DeLong, D. M., Ngyen, G., Toncheva, G., & Yoshizumi, T. T. (2007). Abdominal multislice CT for obese patients: effect on image quality and radiation dose in a phantom study. Academic radiology, 14(4), 486-494.

Scholtz, J. E., Wichmann, J. L., Hüsers, K., Beeres, M., Nour-Eldin, N. E. A., Frellesen, C., & Lehnert, T. (2015). Automated tube voltage adaptation in combination with advanced modeled iterative reconstruction in thoracoabdominal third-generation 192-slice dual-source computed tomography: effects on image quality and radiation dose. Academic radiology, 22(9), 1081-1087.

Seeram, E. (2015). Computed Tomography-E-Book: Physical Principles, Clinical Applications, and Quality Control. Elsevier Health Sciences.

Sezdi, M. (2011). Dose optimization for the quality control tests of X-ray equipment. In Modern Approaches to Quality Control. InTech.

Sharma, S. D., Kumar, R., Akhilesh, P., Pendse, A. M., Deshpande, S., & Misra, B. K. (2012). Dose verification to cochlea during gamma knife radiosurgery of acoustic schwannoma using MOSFET dosimeter. Journal of cancer research and therapeutics, 8(4), 528.

Shirazu, I., Mensah, Y. B., Schandorf, C., & Mensah, S. Y. (2017). Using Age and Weight Specific CT Protocol to Estimate Reference Effective Dose to Patients Undergoing CT Examination.

Shrimpton, P. C., Hillier, M. C., Lewis, M. A., & Dunn, M. (2005). Doses from computed tomography (CT) examinations in the UK-2003 review (Vol. 67). NRPB.

Shrimpton, P. C., Hillier, M. C., Lewis, M. A., & Dunn, M. (2006). National survey of doses from CT in the UK: 2003. The British journal of radiology, 79(948), 968-980.

Shrimpton, P. C., Jansen, J. T., & Harrison, J. D. (2015). Updated estimates of typical effective doses for common CT examinations in the UK following the 2011 national review. The British journal of radiology, 89(1057), 20150346.

SIEMENS. SOMATOM Sensation 64 Application Guide. Siemens AG Medical Solutions, 2010.

Simkó, M., Nosske, D., & Kreyling, W. G. (2014). Metrics, dose, and dose concept: the need for a proper dose concept in the risk assessment of nanoparticles. International journal of environmental research and public health, 11(4), 4026-4048.

Singh, S., Kalra, M. K., Khawaja, R. D. A., Padole, A., Pourjabbar, S., Lira, D., ... & Digumarthy, S. R. (2014). Radiation dose optimization and thoracic computed tomography. Radiologic Clinics, 52(1), 1-15.

Singh, S., Kalra, M. K., Thrall, J. H., & Mahesh, M. (2011). Automatic exposure control in CT: applications and limitations. Journal of the American College of Radiology, 8(6), 446-449.

Smedby, Ö. & Fredrikson, M. (2010). Visual grading regression: analysing data from visual grading experiments with regression models. The British journal of radiology, 83(993), 767-775.

Smith, A. B., Dillon, W. P., Gould, R., & Wintermark, M. (2007). Radiation dose-reduction strategies for neuroradiology CT protocols. American Journal of Neuroradiology, 28(9), 1628-1632.

Smith, N. B., & Webb, A. (2011). Introduction to Medical Imaging Physics, Engineering and Clinical Applications. Cambridge: Cambridge university press.

Smith-Bindman, R., Moghadassi, M., Wilson, N., Nelson, T. R., Boone, J. M., Cagnon, C. H., & McNitt-Gray, M. (2015). Radiation doses in consecutive CT examinations from five University of California Medical Centers. Radiology, 277(1), 134-141.

Soderberg and M. Gunnarsson, (2010) "Automatic exposure control in computed Applications. Radiology, 233(2), 323–327.

Söderberg, M. (2008). Automatic exposure control in CT an investigation between different manufacturers considering radiation dose and image quality.

Söderberg, M. (2016). Overview, practical tips and potential pitfalls of using automatic exposure control in CT: Siemens Care Dose 4D. Radiation protection dosimetry, 169(1-4), 84-91.

Söderberg, M., & Gunnarsson, M. (2010). Automatic exposure control in computed tomography–an evaluation of systems from different manufacturers. Acta Radiological, 51(6), 625-634.

Sodickson, A. (2012). Strategies for reducing radiation exposure in multi-detector row CT. Radiologic Clinics of North America, 50(1),1–14.

Solomon, J. B., Li, X., & Samei, E. (2013). Relating noise to image quality indicators in CT examinations with tube current modulation. American Journal of Roentgenology, 200(3), 592-600.

Sookpeng, S., & Butdee, C. (2017). Signal-to-noise ratio and dose to the lens of the eye for computed tomography examination of the brain using an automatic tube current modulation system. Emergency radiology, 24(3), 233-239.

Sookpeng, S., Cheebsumon, P., Pengpan, T., & Martin, C. (2016). Comparison of computed tomography dose index in polymethyl methacrylate and nylon dosimetry phantoms. Journal of Medical Physics/Association of Medical Physicists of India, 41(1), 45.

Starck G, Lonn L, Cederblad A, Alpsten M, Sjostrom L, Ekholm S. Radiation dose reduction in CT: application to tissue area and volume determination. Radiology 1998; 209:397e403.

Strauss, K. J., & Goske, M. J. (2011). Estimated Pediatric radiation dose during CT. Pediatric radiology, 41(2), and 472.

Su, J. P., Jaw, T. S., Chen, C. Y., Kuo, Y. T., Hsieh, T. J., Lee, S. H., & Lin, C. C. (2010). Automatic tube current modulation versus fixed tube current in multi-detector row computed tomography of liver: Comparison of image quality and radiation dose. Chinese Journal of Radiology, 35(3), 131–142.

Suliman, I. I., Abdalla, S. E., Ahmed, N. A., Galal, M. A., & Salih, I. (2011). Survey of computed tomography technique and radiation dose in Sudanese hospitals. European journal of radiology, 80(3), e544-e551.

Suliman, I. I., Khamis, H. M., Ombada, T. H., Alzimami, K., Alkhorayef, M., & Sulieman, A. (2014). Radiation exposure during paediatric CT in Sudan: CT dose, organ and effective doses. Radiation protection dosimetry, 167(4), 513-518.

Sun, Z., & Ng, C. (2010). Dual-source CT angiography in aortic stent grafting: an in vitro aorta phantom study of image noise and radiation dose. Academic radiology, 17(7), 884-893.

Tacelli, N., Remy-Jardin, M., Flohr, T., Faivre, J. B., Delannoy, V., Duhamel, A., & Remy, J. (2010). Dual-source chest CT angiography with high temporal resolution and high pitch modes: evaluation of image quality in 140 patients. European radiology, 20(5), 1188-1196.

Takahashi, Y., Ota, H., Omura, K., Dendo, Y., Otani, K., Matsuura, T., & Ono, Y. (2018). Image quality and radiation dose of low-tube-voltage CT with reduced contrast media for right adrenal vein imaging. European journal of radiology, 98, 150-157.

Tamma, P. K. (2013). Selecting P-channel MOSFETs for Switching Applications. Retrieved from 13-11-25, V1.0

Tawfik, A. M., Kerl, J. M., Razek, a. a., Bauer, R. W., Nour-Eldin, N. E., Vogl, T. J., & Mack, M. G. (2011). Image quality and radiation dose of dual-energy CT of the head and neck compared with a standard 120-kVp acquisition. American Journal of Neuroradiology, 32(11), 1994–1999.

Teeuwisse, W., Geleijns, J., & Veldkamp, W. (2007). An inter-hospital comparison of patient dose based on clinical indications. European radiology, 17(7), 1795-1805.

Tobergte, D. R., & Curtis, S. (2006). The CT Physics of Diagnostic Imaging. In Dowsett, D., Kenny, P. A., & Johnston, R. E. (2006) the Physics of Diagnostic Imaging Second Edition. CRC Press. (Vol. 53).

Tootell, A. K., Szczepura, K. R., & Hogg, P. (2013). Optimising the number of thermoluminescent dosimeters required for the measurement of effective dose for computed tomography attenuation correction data in SPECT/CT myocardial perfusion imaging. Radiography, 19(1), 42–47.

Tootell, A. K., Szczepura, K., & Hogg, P. (2014b). Comparison of effective dose and lifetime risk of cancer incidence of CT attenuation correction acquisitions and radiopharmaceutical administration for myocardial perfusion imaging. Br J Radiol, 87(1041), 20140110.

Tootell, A., Szczepura, K., & Hogg, P. (2014a). An overview of measuring and modelling dose and risk from ionising radiation for medical exposures. Radiography, 20(4), 323-332.

Tootell, A., Szczepura, K., & Hogg, P. (2017). Analysis of effective and organ dose estimation in CT when using mA modulation: A single scanner pilot study. Radiography, 23(2), 159-166.

Toshiba medical groups (2017). Aquilion ONE™ / GENESIS Edition evolution of dynamic volume CT. Website linked https://medical.toshiba.com/products/computed-tomography/aquilion-one-genesis/.

Toshiba. (2014). Manual Toshiba Ct Aquilion One User.

Trattner, S., Cheng, B., Pieniazek, R. L., Hoffmann, U., Douglas, P. S., & Einstein, A. J. (2014). Sample size requirements for estimating effective dose from computed tomography using solid- state metal- oxide- semiconductor field- effect transistor dosimetry. Medical physics, 41(4).

Tsapaki, V., Tsalafoutas, I. A., Triantopoulou, C., Kolliakou, E., Maniatis, P., & Papailiou, J. (2014). Radiation dose in repeated CT guided radiofrequency ablations. Physical Medical, 30(1), 128-131.

Tyan, Y. S., Tsai, H. Y., Hung, Y. L., Lia, N. G., & Chen, C. P. (2008). In vivo dose assessment of multislice CT in abdominal examinations. Radiation Measurements, 43(2), 1012-1016.

Ulrich, R., & Miller, J. (2004). Threshold estimation in two-alternative forced-choice (2AFC) tasks: The Spearman-Kärber method. Attention, Perception, & Psychophysics, 66(3), 517-533.

Ulzheimer, S., & Flohr, T. (2009). Multislice CT: current technology and future developments. In Multislice CT (pp. 3-23). Springer Berlin Heidelberg.

United Nations Scientific Committee on the Effects of Atomic Radiation. UNSCEAR (2010). SOURCES AND EFFECTS OF IONIZING RADIATION United Nations Scientific Committee on the Effects of Atomic Radiation REPORT (Vol. I). ISBN: 978921

Vancauwenberghe, T., Snoeckx, A., Vanbeckevoort, D., Dymarkowski, S., & Vanhoenacker, F. M. (2015). Imaging of the spleen: what the clinician needs to know. Singapore medical journal, 56(3), 133.

Venkat, H., Rollnick, M., Loughran, J., & Askew, M. (Eds.). (2014). Exploring Mathematics and Science Teachers' Knowledge: Windows into Teacher Thinking. Routledge.

Verdun, F. R., Racine, D., Ott, J. G., Tapiovaara, M. J., Toroi, P., Bochud, F. O., & Marshall, N. W. (2015). Image quality in CT: From physical measurements to model observers. Physical Medical, 31(8), 823-843.

Vilar-Palop, J., Vilar, J., Hernández-Aguado, I., González-Álvarez, I., & Lumbreras, B. (2016). Updated effective doses in radiology. Journal of Radiological Protection, 36(4), 975.

Wang, Q., Zhao, X., Song, J., Guo, N., Zhu, Y., Liu, J., Hong, N. (2013). The application of automatic tube current modulation (ATCM) on image quality and radiation dose at abdominal computed tomography (CT): A phantom study. Journal of X-Ray Science and Technology, 21(4), 453–464.

Weis, M., Henzler, T., Nance Jr, J. W., Haubenreisser, H., Meyer, M., Sudarski, S., & Hagelstein, C. (2017). Radiation Dose Comparison Between 70 kvp and 100 kvp with Spectral Beam Shaping for Non–contrast-enhanced Pediatric Chest Computed Tomography: A Prospective Randomized Controlled Study. Investigative radiology, 52(3), 155-162.

Wichmann, J. L., Hardie, A. D., Schoepf, U. J., Felmly, L. M., Perry, J. D., Varga-Szemes, A., ... & De Cecco, C. N. (2017). Single-and dual-energy CT of the abdomen: comparison of radiation dose and image quality of 2nd and 3rd generation dual-source CT. European radiology, 27(2), 642-650.

Williams, B, Krupinski, A, Strauss, J, Breeden, K, Rzeszotarski, S, Applegate, K, Wyatt, M, Bjork, S & Seibert, a 2007, 'Digital radiography image quality: Image acquisition', J Am Coll Radiol, vol. 4, no. 6, pp. 371-88.

Wood, T. J., Moore, C. S., Stephens, A., Saunderson, J. R., & Beavis, A. W. (2015). A practical method to standardise and optimise the Philips DoseRight 2.0 CT automatic exposure control system. Journal of Radiological Protection, 35(3), 495.

Wunderlich, A., & Abbey, C. K. (2013). Utility as a rationale for choosing observer performance assessment paradigms for detection tasks in medical imaging. Medical physics, 40(11).

Wylie, J. D., Jenkins, P. A., Beckmann, J. T., Peters, C. L., Aoki, S. K., & Maak, T. G. (2018). Computed Tomography Scans in Patients with Young Adult Hip Pain Carry a Lifetime Risk of Malignancy. Arthroscopy: The Journal of Arthroscopic & Related Surgery.

Xu, X. G., & Eckerman, K. F. (Eds.). (2009). Handbook of anatomical models for radiation dosimetry. CRC press.

Yeh, D. M., Tsai, H. Y., Tyan, Y. S., Chang, Y. C., Pan, L. K., & Chen, T. R. (2016). The Population Effective Dose of Medical Computed Tomography Examinations in Taiwan for 2013. PloS one, 11(10), e0165526.

Yoshizumi, T. T., Goodman, P. C., Frush, D. P., Nguyen, G., Toncheva, G., Sarder, M., & Barnes, L. (2007). Validation of metal oxide semiconductor field effect transistor technology for organ dose assessment during CT: comparison with thermoluminescent dosimetry. American Journal of Roentgenology, 188(5), 1332-1336.

Yu, L., Leng, S., Chen, L., Kofler, J. M., Carter, R. E., & McCollough, C. H. (2013). Prediction of human observer performance in a 2- alternative forced choice low- contrast detection task using channelized Hotelling observer: Impact of radiation dose and reconstruction algorithms. Medical physics, 40(4).

Yu, L., Liu, X., Leng, S., Kofler, J. M., Ramirez-Giraldo, J. C., Qu, M., McCollough, C. H. (2009). Radiation dose reduction in computed tomography: techniques and future perspective. Imaging in Medicine, 1(1), 65–84.

Yu-Chun Lin, R. T., Ng, K. K., Tseng, J. H., Wong, M. C., Tung-Chung Lai, R. T., & Wan, Y. L. (2002). Helical Computed Tomography of the Abdomen: Evaluation of Image Quality Using 1.0, 1.3, and 1.5 Pitches. Chang Gung Med J, 25(2).

Zaehringer, C., Euler, A., Karwacki, G. M., Hohmann, J., Pansini, M., Szucs-Farkas, Z., & Schindera, S. T. (2016). Manual adjustment of tube voltage from 120 to 100 kVp during abdominal CT in patients with body weights≤ 75 kg: assessment of image quality and radiation dose in a prospective, randomised trial. Clinical radiology, 71(6), 615-e1.

Zarb, F., McEntee, M. F., & Rainford, L. (2015). Visual grading characteristics and ordinal regression analysis during optimisation of CT head examinations. Insights into imaging, 6(3), 393-401.

Zarb, F., Rainford, L., & McEntee, M. F. (2010). Image quality assessment tools for optimization of CT images. Radiography, 16(2), 147-153.

Zhang, D., Cagnon, C. H., Villablanca, J. P., McCollough, C. H., Cody, D. D., Zankl, M., ... & McNitt-Gray, M. F. (2013a). Estimating peak skin and eye lens dose from neuroperfusion examinations: Use of Monte Carlo based simulations and comparisons to CTDIvol, AAPM Report No. 111, and ImPACT dosimetry tool values. Medical physics, 40(9).

Zhang, D., Li, X., Gao, Y., Xu, X. G., & Liu, B. (2013b). A method to acquire CT organ dose map using OSL dosimeters and ATOM anthropomorphic phantoms. Medical Physics, 40(8), 81918.

Zhang, G., Cockmartin, L., & Bosmans, H. (2016, March). A four-alternative forced choice (4AFC) software for observer performance evaluation in radiology. In SPIE Medical Imaging (pp. 97871E-97871E). International Society for Optics and Photonics.

Zhang, L. J., Zhao, Y. E., Schoepf, U. J., Mangold, S., Felmly, L. M., Li, X., ... & Lu, G. M. (2015). Seventy–Peak Kilovoltage High-Pitch Thoracic Aortic CT Angiography without ECG Gating: Evaluation of Image Quality and Radiation Dose. Academic radiology, 22(7), 890-897.

Zhang, Y., Leng, S., Yu, L., Carter, R. E., & McCollough, C. H. (2014). Correlation between human and model observer performance for discrimination task in CT. Physics in medicine and biology, 59(13), 3389.

Zhao, M., Zhang, D., Zhou, Z., Li, T., & Wang, Z. (2015). Novel method for failure prognostics of power MOSFET. In Computational Intelligence and Virtual Environments for Measurement Systems and Applications (CIVEMSA), 2015 IEEE International Conference on (pp. 1-4). IEEE.